

Physicochemical
Problems
of Mineral Processing
41 (2007)

Instructions for preparation of manuscripts

It is recommended that the following guidelines be followed by the authors of the manuscripts:

- Original papers dealing with the principles of mineral processing and papers on technological aspects of mineral processing will be published in the journal which appears once a year
- The manuscript should be sent to the Editor for reviewing before February 15 each year
- The manuscript should be written in English. For publishing in other languages an approval of the editor is necessary
- Contributors whose first language is not the language of the manuscript are urged to have their manuscript competently edited prior to submission.
- The manuscript should not exceed 10 pages
- Two copies of the final manuscript along with an electronic version should be submitted for publication before April 15
- There is a 80 USD fee for printing the paper. No fee is required for the authors participating in the Annual Symposium on Physicochemical Problems on Mineral Processing
- Manuscripts and all correspondence regarding the symposium and journal should be sent to the editor.

Address of the Editorial Office

Wrocław University of Technology
Wybrzeże Wyspiańskiego 27, 50-370 Wrocław, Poland
Institute of Mining Engineering
Laboratory of Mineral Processing

Location of the Editorial Office:

pl. Teatralny 2, Wrocław, Poland
phone: (071) 320 68 79, (071) 320 68 78
fax: (071) 344 81 23

zygmunt.sadowski@pwr.wroc.pl
andrzej.luszczkiewicz@pwr.wroc.pl
jan.drzymala@pwr.wroc.pl

<http://www.ig.pwr.wroc.pl/minproc>

Physicochemical
Problems
of Mineral Processing
41 (2007)

www.ig.pwr.wroc.pl/minproc

WROCLAW 2007

Editors of the journal

Zygmunt Sadowski – editor-in-chief, Jan Drzymala, Andrzej Łuszczkiewicz

Editorial Board

Wiesław Blaschke, Marian Brożek, Stanisław Chibowski,
Witold Charewicz, Tomasz Chmielewski, Beata Cwalina, Janusz Girczys,
Andrzej Heim, Jan Hupka, Andrzej Krysztafkiewicz, Janusz Laskowski,
Kazimierz Małysa, Paweł Nowak,
Andrzej Pomianowski (honorary chairman), Stanisława Sanak-Rydlewska,
Jerzy Sablik, Kazimierz Sztaba (chairman)

Reviewers

W. Apostoluk, M.B. Bogacki, W. Charewicz, St. Chibowski, T. Chmielewski,
J. Drzymala, W. Janusz, T. Jesionowski, J. Hupka, A. Krysztafkiewicz, A. Lutyński,
K. Małysa, I. Maliszewska, P. Nowak, Z. Sadowski, W. Walkowiak

Technical assistance

Stefan Zawadzki

The papers published in *Physicochemical Problems of Mineral Processing* are abstracted
in *Chemical Abstracts*, *Metals Abstracts*, *Реферативный Журнал* and other sources

This publication was supported in different forms by:

Komitet Górnictwa PAN
(Sekcja Wykorzystania Surowców Mineralnych)
Akademia Górniczo-Hutnicza w Krakowie
Politechnika Śląska w Gliwicach
Politechnika Wrocławska
Scientific Network SURUZ
Bioshale

ISSN 0137-1282

OFICyna WYDAWNICZA POLITECHNIKI WROCLAWSKIEJ, WYBRZEZE WYSPIANSKIEGO 27
50-370 WROCLAW, POLAND

CONTENTS

J. Zawala J. Drzymala, K. Malysa, Natural hydrophobicity and flotation of fluorite.....	5
V.E. Vigdergauz, Evaluation of length of interaction between hydrophobic surfaces from the induction time measurement	13
J. Drzymala, Atlas of upgrading curves used in separation and mineral science and technology. Part II	27
J. Kim, B. Kim, Chemical and low-expansion treatments for purifying natural graphite powder	37
M. Brozek, A. Młynarczykowska, Analysis of kinetics models of batch flotation	51
J. Sablik, Energy characteristics of finest coal particles surfaces versus their upgrading using flotation	67
H.A.M. Ahmed, Optimization of desliming prior to phosphate ore upgrading by flotation	79
K.N. Sediak, A.M. Amer, Sedimentological and technical studies on the montmorillonitic clays of Abu Tartur Plateau, Western Desert, Egypt	89
T. Depci, G. Özbayoğlu, A. Yilmaz, The effect of different starting materials on the synthesis of lithium tetraborate	101
P. Nowak, K. Laajalehto, On the interpretation of the XPS spectra of adsorbed layers of flotation collectors – ethyl xanthate on metallic lead	107
M. Chojnacka D. Wawrzak, W. Mulak, A. Szymczycha-Madeja, Kinetics of pyrite oxidation in acidic potassium dichromate solutions	117
A. Szymczycha-Madeja, W. Mulak, A. Leśniewicz, Physicochemical study of spent hydrodesulphurization (HDS) catalyst	125
M. Ulewicz, K. Sadowska, J.F. Biernat, Selective transport of Pb(II) across polymer inclusion membrane using imidazole azocrown ethers as carriers	133
B. Gajda, M.B. Bogacki, The effect of tributyl phosphate on the extraction of nickel(II) and cobalt(II) ions with di(2-ethylhexyl)phosphoric acid	145
A. Boteva, M. Parashkevova, Processing of industrial pharmaceutical sediment	153
M. Janczarek, H. Kisch, J. Hupka, Photoelectrochemical characterization of nitrogen-modified TiO ₂	159
M. Pacholewska, A. Frąckowiak, J. Willner, Influence of physical and chemical factors on acid digestion of Zn-Pb flotation tailings	167
S. Chibowski, J. Patkowski, A research on stability of SiO ₂ in the presence of polyethylene oxide of different purities	177
F. Ciesielczyk, A. Krysztalkiewicz, T. Jesionowski, Adsorptive properties of synthetic magnesium silicates	185

B. Tepper, T. Jesionowski, A. Krysztafkiewicz, Colloidal silicas obtained via co-precipitation method using cyclohexane as an organic phase	195
K. Siwińska-Stefańska, A. Krysztafkiewicz, T. Jesionowski, Modification of hydrophilic/hydrophobic character of TiO ₂ surface using selected silane coupling agents	205
W. Janusz, E. Skwarek, V.I. Zarko, V. M. Gun'ko, The structure of the electrical double layer at the Al ₂ O ₃ -SiO ₂ /electrolyte solution interface	215
S. Wierzba, M. Nabrdalik, Biodegradation of cellulose in bottom sediments of Turawa Lake	227
P. Wodziński, Screens – classification and systematics. Single-plane screens	237
V.P. Nebera, Sai Kyaw Naing Oo, Biosorption of metals from geotechnology solutions	251
T. Grobelski, J. Farbiszewska-Kiczma, T. Farbiszewska, Bioleaching of Polish black shale	259
S. Groudev, I. Spasova, M. Nicolova, P. Georgiev, Acid mine drainage cleanup in a uranium deposit by means of a passive treatment system	265
Ż. Konopacka A. Łuszczkiewicz T. Chmielewski, Effect of non-oxidative leaching on flotation efficiency of Lubin concentrator middlings	275
J. Langwaldt, R. Kalapudas, Bio-beneficiation of multimetal black shale ore by flotation	291
I. Galfi, J. Aromaa, O. Forsén, Laboratory tool for electrochemical study of sulphide minerals	301
J. Aromaa, P. Pesonen, Leaching mechanisms and kinetics of complex low-grade sulfidic copper ores	313
T. Chmielewski, Non-oxidative leaching of black shale copper ore from Lubin mine	323
T. Chmielewski, Atmospheric leaching of shale by-product from Lubin concentrator.....	337
J, Wódka, T. Chmielewski, B. Ziółkowski, Pressure leaching of shale ore in oxygenated sulphuric acid	349
K. Rotuska, T. Chmielewski, Solvent extraction of valuable metals from pregnant leach solutions of cupriferous shale	365
P. d'Hugues, P.R. Norris, B. Johnson, A. Grotowski, T. Chmielewski, A. Łuszczkiewicz, Z. Sadowski, A. Skłodowska, T. Farbiszewska, Presentation of the FP6 European Project Bioshale. Exploitation of black shale ores using biotechnologies - Polish case studies	373
Z. Sadowski, A. Szubert, Comparison of kinetics of Black Shale bioleaching process using stationary and agitated systems	387
M. Brożek, A. Surowiak, Effect of particle shape on jig separation efficiency	397

Jan ZAWALA*, Jan. DRZYMALA**, Kazimierz. MALYSA*

NATURAL HYDROPHOBICITY AND FLOTATION OF FLUORITE

Received March 15, 2007; reviewed; accepted May 15, 2007

The free ascending bubble–fluorite surface collision test showed that the three phase contact (TPC) was formed and time of the TPC formation was strongly affected by the roughness of the fluorite surface. The time of the TPC formation varied by an order of magnitude, from ca. 20 to 200ms, depending on the fluorite origin and surface roughness. The fact that the TPC was formed shows that fluorite can be considered as a naturally hydrophobic material. The contact angle formed by the bubble attached to fluorite plate was found to be 40° in comparison to 10-25° measured by flotometry and 55° by sessile drop. Thus, the macroscopic contact angle of fluorite depends on the method of measurement as well as its origin and color since colorless fluorites float better. Hydrophobicity of fluorite and the time of the three phase contact formation influence its flotation. The best flotation is observed in Hallimond tubes while flotation is significantly reduced or absent in laboratory flotation machines. This is very likely a result of relatively long time of the TPC formation and/or low hydrophobicity of fluorite, which is not enough to withstand the detachment force during enhanced hydrodynamics of larger flotation devices.

Key words: fluorite, contact angle, bubble-particle attachment, induction time, three phase contact, hydrophobicity, hydrophilicity

INTRODUCTION

Natural flotation of minerals frequently interferes with collectors flotation of useful components of ores. Such difficulties may occur during upgrading by flotation of ores containing chalcopyrite, talc, and graphite. It was mentioned by Barskij (1984) that also fluorite may cause problems due to its native flotation.

Until sixties of the previous century fluorite was considered a hydrophilic mineral, that is material which forms in the water-air-fluorite system contact angle (θ) equal to zero. Gaudin and his coworkers (1957), in their classic paper on native floatability, did not include fluorite in the list of hydrophobic materials. As a result many researchers and technologists have been considering fluorite hydrophilic even today.

* Institute of Catalysis and Surface Chemistry Polish Academy of Sciences, Cracow, Poland.

** Wrocław University of Technology, Mining Engineering Department, Wrocław, Poland.

An information on native flotation of fluorite originates from Bakakin in 1960 (Barskij, 1984). They showed that fluorite samples from different sources floated in water, and the flotation of fluorite was reduced in the presence of water glass (Fig. 1a.). The extend of flotation was found to be dependent on the color of fluorite. Since then, there were only sporadic reports on the native hydrophobicity (Busscher et al., 1987; Janczuk et al., 1993) and collectorless flotation (Drzymala and Lekki, 1990; Drzymala, 1994a, 1994b (Fig.1b) of fluorite.

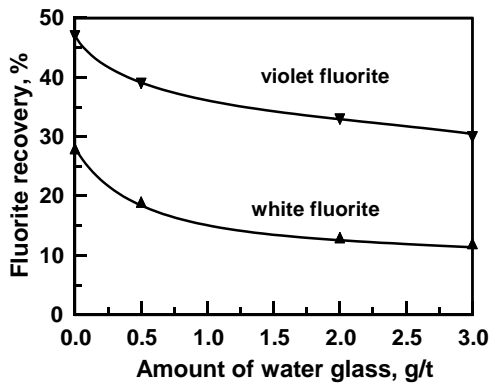


Fig. 1a. Flotation recovery of fluorite in water in presence of water glass (based on Barskij, 1984, original source - Bakakin, 1960)

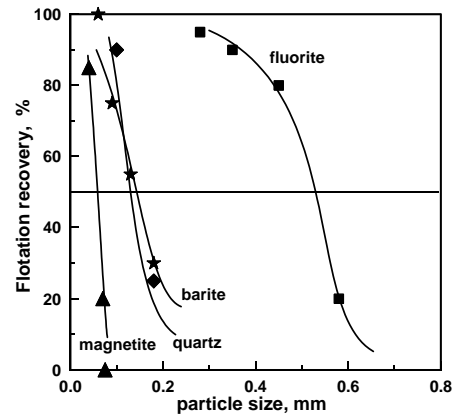


Fig. 1b. Recovery of fluorite and other minerals in water in a Hallimond tube (based on Drzymala and Lekki 1989 and Drzymala, 1994b). Flotation time 30 min. Flotation of each mineral and each fraction separately. Flotometric contact angles: quartz $\sim 0^\circ$, fluorite 25° , barite 5.0° , magnetite 0°

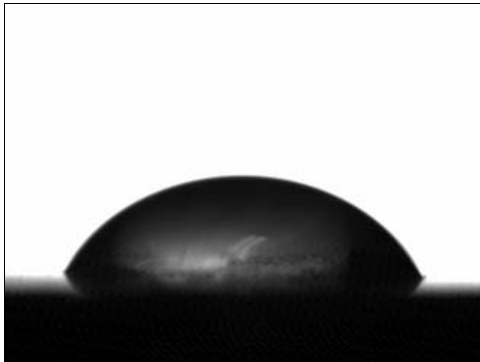


Fig. 1c. A drop of water on fluorite surface (polished with 1600 sand paper) forms contact angle equal to about 55° (Szyszka and Stepień, 2007)

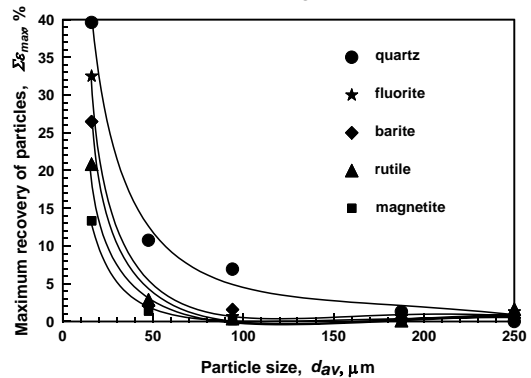


Fig. 1d. Entrainment of minerals in water in a Denver lab. flotation machine after long time of flotation in the presence of fuel oil (0.2 g/kg and 0.05 g/kg α -terpineol. pH natural. Each mineral was tested separately. Sequence of minerals flotation depends on their density (Konopacka, 2005)

Hydrophobicity of fluorite can be demonstrated by putting a drop of water on a polished fluorite surface. This creates non-zero contact angle (Fig. 1c). Most recently, Fa et al., 2006, during investigation of interaction of calcium dioleate colloidal particle and fluorite by atomic force microscope (AFM), found that the density of water at the fluorite surface is low and that fluorite surface is not strongly wetted. This also points to natural hydrophobicity of fluorite.

Micro-flotation tests performed by Drzymala and Lekki (1990) and Drzymala, 1994a,b in a small flotation device called Hallimond tube (Fig. 1b.) confirmed Bakakin's report on natural flotation of fluorite which depends on fluorite samples. Using flotometry, they showed that the contact angle of fluorite is between 10 and 25 degrees. However, trials to float naturally hydrophobic fluorite in laboratory mechanical Denver (5 dm³) flotation machine by Konopacka (2005) failed. Her investigations on mechanical entrainment of different minerals showed that fluorite does not float. Small amount of fluorite reporting to concentrate was due to mechanical carryover of particles as in the case of hydrophilic quartz or magnetite (Fig.1d).

The presented facts indicate that there is no a simple correlation between natural hydrophobicity and flotation of fluorite and that still more research is needed to understand the fluorite-water-gas system. The present study deals with dynamics of formation of the three phase contact at fluorite surface by a freely ascending bubble using the technique described in details elsewhere (Krasowska et al., 2004; Malysa et al., 2005; Krzan et al, 2006). The technique allows investigating phenomena occurring during bubble collisions with solid surface and time-scale of the three phase contact (TPC) formation. Geometry of the bubble–solid surface contact formed can be monitored as well.

EXPERIMENTAL

METHODS AND MATERIALS

The experimental set-up used in monitoring phenomena occurring during collisions of the rising bubble with fluorite surface was described in details elsewhere (Krasowska et al., 2004; Malysa et al., 2005; Krzan et al., 2006). The main elements of the set-up are the following: i) a square glass column (cross-section 50×50 mm), ii) glass capillary (inner diameter - 0.075 mm), iii) syringe pump with glass high precision syringes, iv) high-speed camera (Weinberger, SpeedCam 512+) and Moticam 2000 CCD camera. The fluorite samples studied were mounted at the distance either ca. 50 mm or 4 mm from the point of the bubble formation (capillary orifice). Distance 50 mm was long enough for the bubble to reach its terminal velocity 34.7 cm/s in water. When the fluorite was placed at the distance 4 mm then the bubble was still at the acceleration stage of its motion and the bubble impact velocity was ca. 17 cm/s (Zawala et al., 2007). For the sake of comparison the experiments were also

carried out using the freshly cleaved mica and Teflon plates. Further details about the experimental procedure were described by Krasowska and Malysa (2007).

Fluorite (calcium fluoride, CaF_2) was a fragment of natural high purity, checked by X-ray diffraction, mineral originated from East Germany. Fluorite samples were carefully washed with acetone and ethanol and finally rinsed with large quantity of the distilled water, before every experiment. The experiments were carried out at room temperature.

RESULTS AND DISCUSSION

In our tests of the bubble-mineral surface interactions, the free ascending bubble collides with the flat surface and the time of the three phase contact formation as well as bubble attachment is determined. As showed elsewhere (Malysa et al., 2005, Krasowska and Malysa, 2007) even in the case of such hydrophobic solid surface as Teflon, the bubble attachment did not need occur at first collision and in distilled water the bubble can bounce a few times without attachment. Simultaneously, after the first collision the bubble shape started to pulsate rapidly within time intervals of an order of fraction of millisecond. It was showed that roughness of the solid surface and presence of entrapped air at hydrophobic surface (Krasowska et al., 2007) are the factors of crucial importance for the kinetics of the bubble attachment. In the case of hydrophilic glass surface the bubble stayed “arrested” beneath the glass plate without formation of the three phase contact (Malysa et al., 2007). Thus, as a result of the collisions, the bubble either establishes the three phase contact with the solid surface, forming a characteristic constant angle when the surface is hydrophobic enough, or stays entrapped beneath the surface without forming the TPC, when the surface is more hydrophilic and there exists some forces stabilizing the wetting film. For instance repulsive electrostatics between both interfaces of the wetting film can assure its stability (Krasowska et al., 2007b).

Figure 2 presents a comparison of the sequences of photos illustrating phenomena occurring during collision of the rising bubble with freshly cleaved hydrophilic mica ($\theta = 0^\circ$) (Fig. 2a), highly hydrophobic Teflon ($\theta = 105^\circ$) (Fig. 2c) and fluorite (Fig. 2b). In the case of mica surface, after the complete dissipation of the kinetic energy, the bubble stayed “arrested” (motionless) beneath the mica plate without formation of the three phase contact (TPC). Thus, in this system the liquid film separating mica and bubble interfaces was stable and did not rupture. In the case of the bubble collision with fluorite surface, the TPC was formed and the bubble was attached to the fluorite surface forming $\theta = 40^\circ$, indicating its hydrophobicity. Results of quantitative analysis of the velocity variations during the collisions of bubble with mica and fluorite surfaces (sample B) showed that the velocity variations were very rapid and practically identical for the collisions with mica and fluorite surfaces. Moreover, there was at least five distinct “approach-bounce” cycles during which the bubble kinetic energy was dissipated and after sixth approach the bubble stayed practically motionless beneath the plates. Then, in the case of mica there was no TPC formation

and the bubble attachment to the mica surface (even after long time of the bubble being entrapped beneath the interface), while in the case of fluorite the TPC was formed at time $t_{\text{TPC}}=150$ ms (time between the first collision and TPC formation) and the bubble was attached. Similarly, the TPC formation was also observed for other fluorite samples (A and C). However, the time of the three phase contact formation and the bubble attachment was different for every of the fluorite samples, which is most probably due to differences in surface roughness and heterogeneity of the samples.

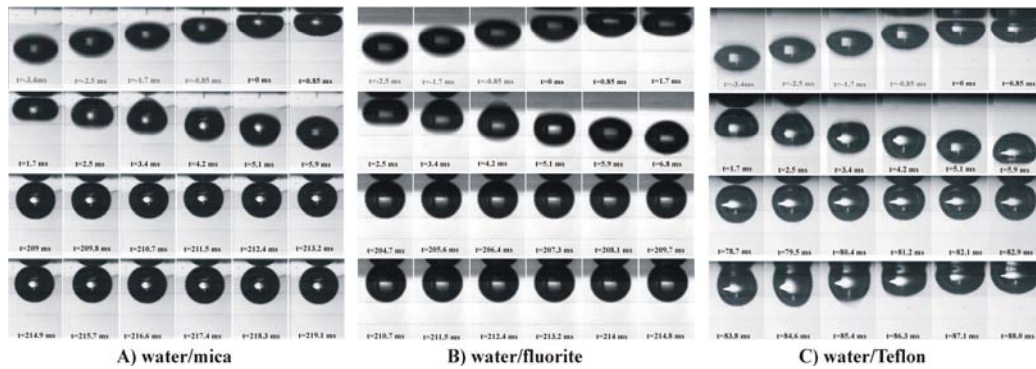


Fig. 2. Free ascending bubble and its collision with flat surfaces of different materials a) mica, b) fluorite, and c) Teflon. The photographs show that mica is hydrophilic ($\theta = 0^\circ$, Teflon is highly hydrophobic ($\theta = 105 \pm 2.5^\circ$) while fluorite is weakly hydrophobic ($\theta = 40 \pm 2^\circ$)

The fact that the surface roughness has a significant effect on the time of the colliding bubble attachment to fluorite can be attributed to the following: i) higher roughness means larger asperities (pillars) at the surface and higher probability that the rupture thickness of the thinning liquid film is locally faster attained, and/or ii) there are larger cavities at rougher surface and larger amount of gas can be present there leading to faster formation of a long enough perimeter of the TPC for the bubble attachment (Krasowska et al., 2007). However, in the case of fluorite we believe that the first factor is the predominant because air entrapment seems to be less important due to rather low hydrophobicity of the fluorite surface.

CONCLUSIONS

The free collision test showed that the three phase contact is formed at fluorite surface and the time of the TPC formation can vary by an order of magnitude (from ca. 20 to 200 ms). Increased roughness of the fluorite surface leads to shortening the time of the TPC formation. Fluorite surface shows some natural hydrophobicity and the measured contact angle values occur between 10 and 55 degrees, depending on the method of measurement. The contact angle is greater for water drops on the surface of fluorite and smaller for air bubble entrapped beneath the fluorite surface. The contact

angle of fluorite depends on its origin and the color of the specimen because more colorless fluorites are more hydrophobic. Since fluorite is inherently hydrophobic, it can float in water and aqueous solutions. The flotation of fluorite depends not only on the natural hydrophobicity of fluorite but also on the flotation devices used for flotation. The best flotation is observed for Hallimond tube while flotation is significantly reduced or absent in laboratory flotation machines. This is very likely a result of relatively long time of the TPC formation and/or low hydrophobicity of fluorite, which is not enough to withstand the detachment force during increased hydrodynamics of larger flotation units.

ACKNOWLEDGEMENTS

Partial financial support of the work by the project Scientific Network SURUZ - EC grant INCO-CT-2003-003355 - is gratefully acknowledged.

REFERENCES

- BAKAKIN V.V., 1960. *Questions on relation of structure of minerals and their flotation properties*, Journal of Structural Chemistry, v. 1(2), 89-97, in Russian.
- BARSKIJ L.A., *Principles of minerallurgy - theory and technology of separation of minerals*, Izd. Nauka, Moscow, 1984, in Russian.
- BUSSCHER H.J., DE JONG H.P., ARENDS J., 1987. *Surface free energy of hydroxyapatite, fluoroapatite and calcium fluoride*, Materials Chemistry and Physics, 17, 553-558.
- DRZYMAŁA J., 1994a. *Characterization of Materials by Hallimond Tube Flotation. Part 2: Maximum Size of Floating Particles and Contact Angle*, Int. J. Miner. Process., 42, 153-167(1994).
- DRZYMAŁA J., 1994b. *Hydrophobicity and Collectorless Flotation of Inorganic Materials*, Advances in Colloid and Interface Sci., 50, 143-186(1994).
- DRZYMAŁA J., LEKKI J., 1989. *Flotometry-Another Way of Characterizing Flotation*, J. Colloid Interface Sci., 130, 205-210.
- DRZYMAŁA, J., LEKKI J., 1990. *Fizykochemia procesów agregacyjnych przetwarzania surowców i odpadów nieorganicznych - V. Fotometryczne badania układu fluoryt oleinian oraz parafinowanych ziaren*, Raport I-11/S-114/90.
- Fa, Keqing; Nguyen, Anh V.; Miller, Jan D. 2006, *Interaction of calcium dioleate collector colloids with calcite and fluorite surfaces as revealed by AFM force measurements and molecular dynamics simulation*, Int. J. Miner. Process, 81 (3), 166-177.
- GAUDIN A.M., MIAW H.L., SPEDDEN H.R., 1957. *Native floatability and crystal structure*. In: *Electrical Phenomena and Solid/Liquid Interfaces*, Proc. 2nd Int. Congr. Surface Activity, London, Butterworths, pp. 202-219 .
- JANCZUK B.; BRUQUE J.M.; GONZALEZ-MARTIN M.L.; del POZO, J. MORENO, 1993. *Wettability and surface tension of fluorite*, Colloids Surf. Physicochem. Eng. Aspects, 75, 163-168
- KONOPACKA Z., 2005, *Flotacja mechaniczna*, Oficyna Wyd. PWr., 2005, Wrocław.
- KRASOWSKA M., KRZAN M., MALYSY K., 2004, *Frother inducement of the bubble attachment to hydrophobic solid surface*, Proceedings of the 5th UBC-McGill Bi-Annual International Symposium of Fundamentals of Mineral Processing, 2004, 121.
- KRASOWSKA M., MALYSY K., 2007. *Kinetics of Bubble Collision and Attachment to Hydrophobic Solids: I. Effect of Surface Roughness*, Intern. J. Mineral Process, 81, 205-216.
- KRASOWSKA, R. KRASSTEV, M. ROGALSKI, K. MALYSY, 2007. *Air facilitated three phase contact formation at hydrophobic solid surfaces under dynamic conditions*, Langmuir, 23 (2) 549-557.

- KRASOWSKA M., KOLASINSKA M., WARSZYNSKI P., MALYSA K., 2007b. *Influence of polyelectrolyte layers deposited on mica surface on wetting and bubble attachment*, J. Phys. Chem. C, 111, 5743-5749.
- KRZAN M., ZAWALA J., MALYSA K., 2006, *Development of steady state adsorption distribution over interface of the bubble rising in solutions of n-alkanols (C₅, C₈) and alkyltrimethylammonium bromides (C₈, C₁₂, C₁₆)*, Colloids & Surfaces A, 42-51, 298.
- MALYSA K., KRASOWSKA M., KRZAN M., 2005, *Influence of surface active substances on bubble motion and collision with various interfaces*, Advances Coll. Interface Sci., 205 114-115
- SZYSZKA D., STEPIEN P., 2007, unpublished data.
- VAGBERG L., STENIUS P., 1988. *ESCA and contact angle studies of the adsorption of aminosilanes on mica Herder, Peter*; Colloids and Surfaces, 34 (2), 117-132.
- ZAWALA J., KRASOWSKA M., DABROS T., MALYSA K., *Influence of the bubble kinetic energy on its bouncing during collisions with various interfaces*, Canad. J. Chem. Engin., 2007 (accepted).

Zawala J., Drzymala J., Malysa K., *Naturalna hydrofobowość i flotowalność fluorytu*, Physicochemical Problems of Mineral Processing, 41 (2007), 5-11 (w jęz. ang.).

Badania kolizji swobodnie wznoszącego się pęcherzyka z powierzchnią mineralną zanurzoną w wodzie wykazały, że czas tworzenia się kontaktu trójfazowego silnie zależy od chropowatości powierzchni fluorytu. W zależności od chropowatości powierzchni fluorytu, czas kontaktu wynosił od 20 do 200ms. Tworzenie się kontaktu trójfazowego świadczy o naturalnej hydrofobowości fluorytu. Kąt zwilżania tworzony pomiędzy pęcherzykiem powietrza a płaska płytką fluorytową zanurzoną w wodzie wynosił 40° w porównaniu do wartości 10-15° uzyskanych metodą fotometryczną i 55° uzyskaną metodą siedzącej kropli. Zatem makroskopowy kąt zwilżania dla fluorytu zależy od metody pomiaru oraz pochodzenia próbki, a nawet jego koloru, gdyż barwne odmiany flotują lepiej. Hydrofobowość fluorytu oraz czas tworzenia się kontaktu trójfazowego wpływają na flotację. Najlepszą flotację obserwuje się w celce Hallimond, podczas gdy flotacja w mechanicznej maszynie laboratoryjnej jest znacząco zredukowana z powodu względnie długiego czasu tworzenia się kontaktu trójfazowego i/lub słabą hydrofobowością fluorytu, który nie wytrzymuje zwiększonych sił odrywania występujących w większych maszynach flotacyjnych.

Vladimir E. VIGDERGAUZ*

EVALUATION OF LENGTH OF INTERACTION BETWEEN HYDROPHOBIC SURFACES FROM THE INDUCTION TIME MEASUREMENT

Received April 10, 2007; reviewed; accepted May 20, 2007

An approach, referred to here as the Scheludko-Malysa approximation has been used for the calculation of thickness of the rupturing film from the experimental values of air bubble – platinum, and air bubble – sulphide minerals, induction time (IT). The influence of applied potentials, pH, and flotation collectors on wettability is discussed. The results indicated a broad variation of IT. Calculated thickness of the rupturing film reaches some microns. It confirms a long-range character of the interactions between air bubbles and hydrophobic surfaces.

Key words: mineral flotation, hydrophobic interactions, rupturing film thickness

INTRODUCTION

Long-range attractive interaction between hydrophobic surfaces in water is well documented. Yoon (2000) clearly demonstrated how essential is to recognize the role of hydrophobic forces in flotation. A number of papers have been published that give a clear evidence that the electrostatic and van der Waals forces, neither of which are usually attractive (when both the bubbles and particles are charged negatively, that is the typical case in flotation practice), are not the only driving forces in a bubble-particle adhesion. All Derjaguin-Landau-Verwey-Overbeek (DLVO) forces (van der Waals and electrostatic forces) in the discussed systems are repulsive, but if the solid surface is hydrophobic, the wetting film ruptures, although there is no attractive interaction in the film. To find an explanation for this behaviour, a number of authors have postulated a “long-range hydrophobic force”, but in the past years, it turned out increasingly that the reason for the rupture is the occurrence of nanoscaled gas bubbles adhering to the solid surface.

* Institute of Complex Exploitation of Mineral Resources, Russian Academy of Sciences, IPKON RAS, 4 Kryukovskiy, 111020 Moscow, Russia, e-mail address: vigderg@mail.ru

The attachment of a solid particle to a gas bubble in flotation is the result of a complex process that is determined by hydrodynamic and surface effects and in an elementary flotation act it is possible to isolate the states before and after contact (Scheludko, 1967). For all types of proposed interactions the most important is how long and how strong they are.

Assuming that the thinning time of the liquid film between particle and bubble is equal to the induction time, an average thickness of the thin liquid film prior to its rupture at mineral surface could be calculated following the work of Malysa and his co-workers (Krasowska et al., 2003). To appreciate the impact of Scheludko and Malysa in the theoretical consideration of the problem and its implementation to IT experiments it will be called here the Scheludko-Malysa approximation. The Malysa-Scheludko approximation gives an opportunity to evaluate dependence of the critical distance for the rupture of the wetting film from the surface hydrophobicity.

In the present paper, experimental studies of wetting phenomena on platinum and sulphide minerals have been used. Thickness of the rupturing wetting films has been evaluated in the frame of the Malysa-Scheludko approximation by the air bubble induction time (IT) measurements. The paper contains studied electrochemical potential influence on IT. Results of the measurements of natural wettability and wettability induced by butyl-xanthate are reported. Also discussed potential dependence of the kinetics of dixanthogen layer formation on the surface of platinum and its influence on the thickness of the rupturing wetting films is presented.

EXPERIMENTAL

MINERALS

The minerals used in experiment were selected by hands. Their purity is shown in the Table 1.

Table 1. Sulphide minerals of IT experiments

Mineral	Formula	Principal mineral content, %	Mineral impurities
Pyrite	FeS ₂	98-99	not determined
Chalcocite	Cu ₂ S	97-98	not determined
Chalcopyrite	CuFeS ₂	94-97	pyrrhotite
Sphalerite	ZnS	95-96	galena, chalcopyrite
Molibdenite	MoS ₂	99	not determined
Galena	PbS	99	not determined

For IT study, cylinders of minerals with diameters near 5 mm were mounted in a fluoroplast holder. The working surface was dry-polished in stages using alumina down to 0.05 µm and rinsed with distilled water or sometimes with ethanol between polishing stages.

IT EXPERIMENTS

IT was defined as the minimum time necessary for the attachment of an air bubble to the platinum surface. Experimental details of the procedure of the measurements of IT were described earlier (Vigdergauz and Nedosekina, 1998). Air bubbles for measurements were deposited on the holder from a small diameter flat-nosed needle positioned below the holder. The bubble formation and size were controlled using a combination of plug and needle. The movement of the bubble was observed through the wall of the cell, the latter being illuminated by an electric lamp. Figures 1 and 2 show the device, that was used for IT measurements under electrochemical polarization, and also bubble images, before and after attachment.



Fig. 1. IT measurements in conditions of electrochemical polarization:
1- the Glembotskii device for IT measurements; 2 - three electrode electrochemical cell;
3 - potentiostat PI-50-1.1.; 4 - programmer PR-8

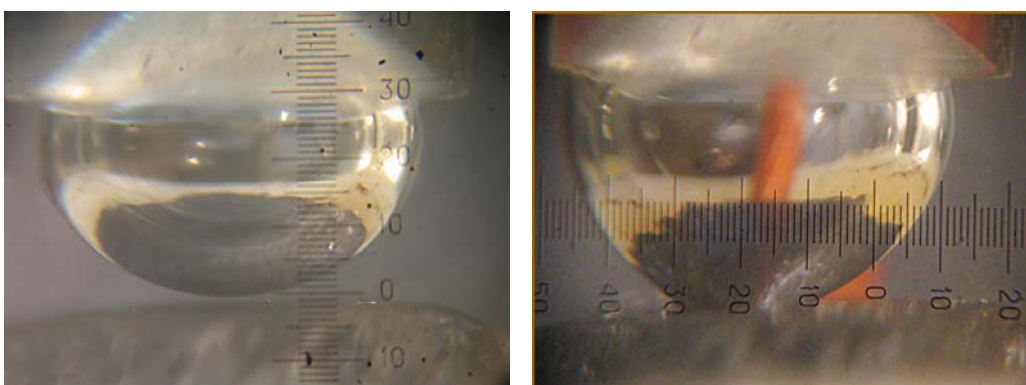


Fig. 2. The bubble before and after attachment during IT measurements

ELECTROCHEMICAL CELL

Electrochemical cell with a three-electrode system was used in potentially controlled IT experiments. Potentials were measured and were reported versus a silver-silver chloride reference electrode, which had a potential of +0.22V against the standard hydrogen electrode. The potential of mineral or platinum electrode was controlled by a potentiostat. A wire connected the working electrode to the external electrical circuit. The reference electrode was connected to the main compartment through a Lugging probe capillary. Current passed between the working platinum electrode and a platinum counter electrode, which was housed in the compartment, separated from the main cell by a sintered glass disc.

CALCULATION OF RUPTURING WETTING FILMS THICKNESS

For the evaluation of the thickness of the rupturing wetting films, the Malysa-Scheludko approximation (Krasowska et al., 2003). was used. According to Scheludko (1967), the thinning of the circular plane parallel film between a solid wall (non-slip conditions) and free surface (full mobility) can be described by the following relation:

$$d(1/h^2)/dt = 64\Delta P/3\eta a^2 \quad (1)$$

Where t is the time, η is the viscosity, a is the diameter of the film and ΔP is the difference between pressure inside the thin film and pressure in bulk phase. After integration one obtains:

$$1/h^2 = 64(\Delta P/3\eta a^2)t \quad (2)$$

Taking into account that:

$$\Delta P = 2\gamma_v/r, \quad (3)$$

where γ_v is the surface tension for the liquid and r is the bubble radius, one can obtain that:

$$1/h^2 = 128(\gamma_v/3\eta r a^2)t \quad (4)$$

For the case of experiment $r_b = 1$ mm, $\gamma_v = 72$ mN/m, $\eta = 0.001$ Ns/m². The mentioned value for the surface tension of bubble-water interface has been used because no xanthate possesses a noticeable surface activity on the water-air interface. In comparison with the water-air value, γ_v in 1 mM solutions of various xanthates does not decrease more than 2 mN/m (De Witt et al., 1935).

Calculations were done assuming constant average diameter of the baseline of the attached bubble $a=0.7$ mm in the experiments. The reasons for such assumption was

“rigid” form of the fixed on the holder bubble, that was used in the IT measurements (Drzymala and Vigdergauz, 2000). The calculations were performed under the assumption of the constant size of the thinning film. Symbol a denotes the diameter of the film (the average value in our experiments was 0.7mm) and this value was used in calculation as radius of the thinning film.

Obviously the obtained values of the critical length of the wetting film are very dependable on the base of the attached bubble that had been supposed to be critical for the rupture. Figure 3 illustrates $h=f(a)$ dependence for stabilized other parameters of the experiment and IT values for 1s and 10 ms.

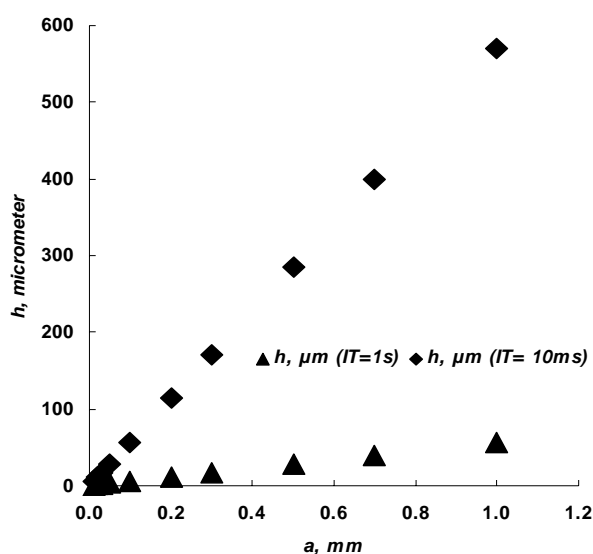


Fig. 3. Diameter of the rupturing film dependence of the critical thickness of the rupturing wetting film

A high-speed video sequence of the rupture of an aqueous wetting film on methylated glass shows that only one embryonic hole is sufficient to cause destabilization and dewetting of the entire film (Schulze et al., 2001). The mechanism of this rupture includes the presence of gas nuclei formed on heterogeneous surface sites.

Decrease of the IT values during repeated measurements (Drelich et al., 1997) and faster and easier flotation of the previously floated materials (Yoon, 2000) confirm in an indirect way the mechanism of strong long-range interactions as a result of the bubbles jump-in and jump-out. Possible transfer of reagents from bubble surface to the surface of mineral could not be the reason of the observed phenomena in the case of

xanthate-induced hydrophobicity. Xanthate ions have little effect on the gas-solution interface (De Witt et al., 1935).

Attard (2005) mentioned that the force has been measured by AFM between surfaces separated by $0.3\mu\text{m}$, which corresponds to about 1000 water molecules in width, and the idea that surfaces can induce order in liquids extending so far from the surfaces contradicts very fundamental theories of the liquid state.

Despite the limitations of the calculations by the Eq. 4 connected with parameter a , these limitations must not influence the evaluation of the trends and dependences of critical thickness of the rupturing film from pH, reagents consumptions and electrochemical polarization effects.

RESULTS AND DISCUSSION

PLATINUM ELECTRODE

Literature data on wettability of Pt-electrodes are controversial. Gardner and Woods (1974) had found that the surface of platinum electrode is hydrophilic. The reason was the observed contact angle that was below 10° at all potentials in the available region between hydrogen and oxygen evolution in 1M Na_2SO_4 and in 0.05M sodium tetraborate solution. This observation contradicts to the previous data of Gorodetskaya and Kabanov (1934) who found, that the surface of platinum was hydrophobic and angles up to 68° were shown.

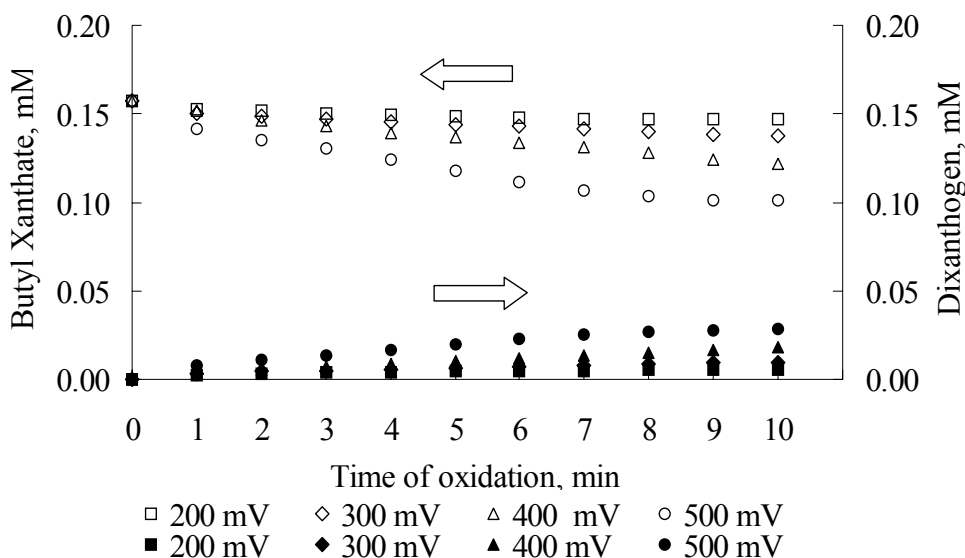


Fig. 4. Potential influence on the kinetics of xanthate electrochemical oxidation on platinum in neutral solutions: 1 – 150 mV; 2 – 200 mV; 3 – 300 mV

Cyclic voltammograms of Pt show that oxide formation begins near potentials of oxygen evolution and Pt surface is not oxidized in a wide area of potentials including potentials of the reported study (Chanturiya and Vigdergauz, 1993).

The study on xanthate oxidation and dixanthogen reduction kinetics shows the reversibility of the process. Figure 4 (Vigdergauz and Dorofeev, 2007) shows kinetics of xanthate oxidation and dixanthogen formation in neutral solution.

The study of the potential influence on the kinetics of xanthate oxidation on Pt shows its slowing down with increasing pH (Vigdergauz and Dorofeev, 2007). pH increasing slows down the formation of dixanthogen but its quantity is proportional to the charge in accordance with the Faraday law.

Table 2 summarizes results of the calculations of the thickness of the rupturing film based on the IT measurements in 20 mg/l xanthate solutions for various pH and potential values (Vigdergauz and Dorofeev, 2007).

Table 2. Time and potential of anodic polarization influence on the thickness of the rupturing film (nm) on Pt

pH 7.52					pH 9.18				
E_{Pt} , mV	Time of oxidation, min				E_{Pt} , mV	Time of oxidation, min			
	1.5	4.5	7.5	10		1.5	4.5	7.5	10
150	215	230	250	400	150	200	200	215	215
200	215	250	600	400	200	200	215	230	230
300	215	400	800	900	300	215	230	250	280
400	400	730	800	900	400	230	250	280	400
600	400	900	1030	1250	600	280	400	600	600
700	400	900	1030	1250	700	330	600	600	680

pH 12.4				
E_{Pt} , mV	Time of oxidation, min			
	1.5	4.5	7.5	10
150	NA*	NA	NA	NA
200	NA	NA	NA	NA
300	NA	NA	230	330
400	NA	250	330	400
600	280	280	330	400
700	280	400	400	400

NA* – no adhesion

Figure 5 shows dependence of the thickness of the rupturing film on the sorption density of dixanthogen which was produced by an electrooxidation at 700 mV for various pH values.

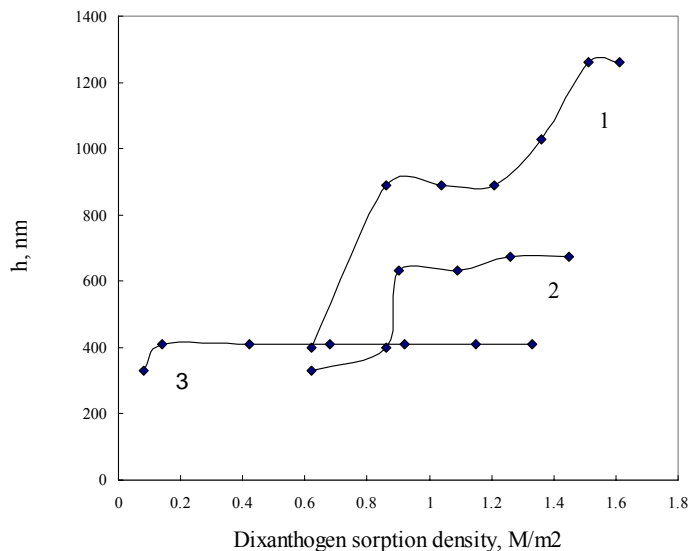


Fig. 5. pH influence on dependence of thickness of rupturing film and dioxanthogen quantity on Pt produced by electrochemical polarization at 700 mV: 1 – pH 7.5; 2 – pH 9.2; 3 – pH 12.5

There is some “critical values” of sorption density, which initiate the fast adhesion. For neutral and weak alkaline solutions, these values of sorption density are near 0.9 M/m^2 . Increasing pH leads to a slow down of adhesion and increases the critical thickness of the rupturing film due the hydrophilic hydroxyl-groups. The study of rupturing the wetting films on platinum indicates a broad variation of IT. The thickness of rupturing film that was calculated in the frame of the Malysa-Sheludko approximation reaches some microns and confirms a long-range character of the interactions between air bubble and hydrophobic platinum surface.

NATURAL WETTABILITY OF SULPHIDES

IT dependences on pH show hydrophilisation of sulphide minerals with increasing pH. Figure 6 (Vigdergauz et al., 2006) illustrates pH influence on the thickness of the rupturing film for sulphides without collector.

From the above results, it is seen that for more hydrophobic surfaces the film have been ruptured at longer distances. In the frame of the applied approximation under conditions of the experiment, average thicknesses of the thin liquid film prior to its rupture reaches 350 nm.

Calculations of the electrostatic repulsive forces show that they are negligibly small for such distances (Vigdergauz et al., 2006). The beginning of the rupture of the liquid film at such long distances shows the long-range character of the attractive forces. The nature of these forces is not quite clear until now, but in the past years it

turned out increasingly that the reason for the rupture is most probably the occurrence of nanoscaled bubbles adhered to the solid surface (Stockelhuber et al., 2004; Ishida et al., 2000).

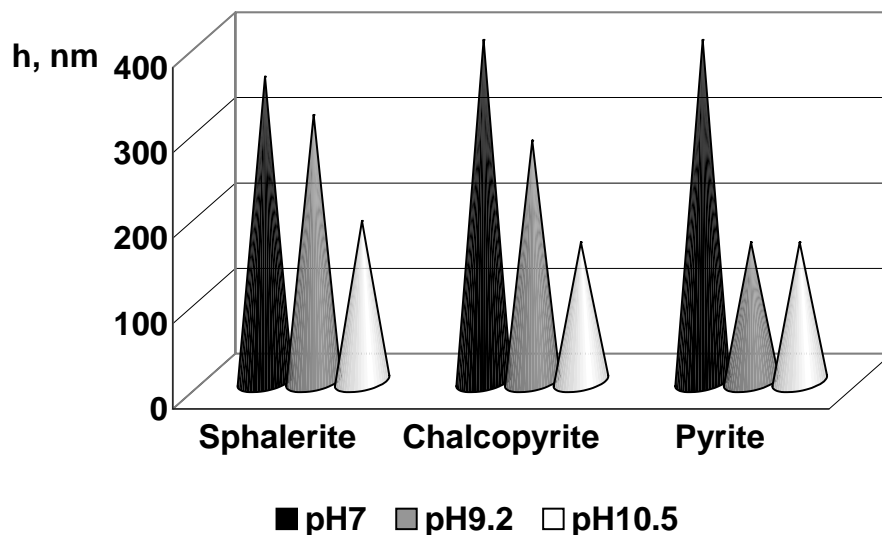


Fig. 6. pH dependence of the calculated thickness of rupturing film

Water structure changes near a hydrophobic surface facilitate formation of gaseous phase embryos. An approximate energy of the bubble-mineral interactions could be estimated basing on preposition that the detachment of an air bubble from the mineral surface is a reverse process to the bubble-mineral complex formation by jump-in of the nanobubbles on the solid hydrophobic surface with an air bubble. Detachment force values, after normalization to the contact area, give approximately an additional γ_v that supplements 72 mN/m to the energy change (Vigdergauz, 2005).

XANTHATE INDUCED WETTABILITY OF SULPHIDES

Previous experimental study (Vigdergauz and Nedosekina, 1998) showed that increasing carbon chain length mainly resulted in decreasing IT. These data are in accordance with the well-known fact that an increasing length of alkyl chain of xanthate collectors stimulates flotation (Sutherland and Wark, 1955).

Figure 7 shows the calculated average thickness of the rupturing film on sulphides for various xanthates in borate buffer solution.

For studied sulphides, there is a observed tendency of an increasing average thickness of the rupturing film with increasing length of the hydrocarbon chain.

Table 3 (Vigdergauz, 2005) presents the dependence of IT on the potential of electrochemical polarization in borate buffer solution.

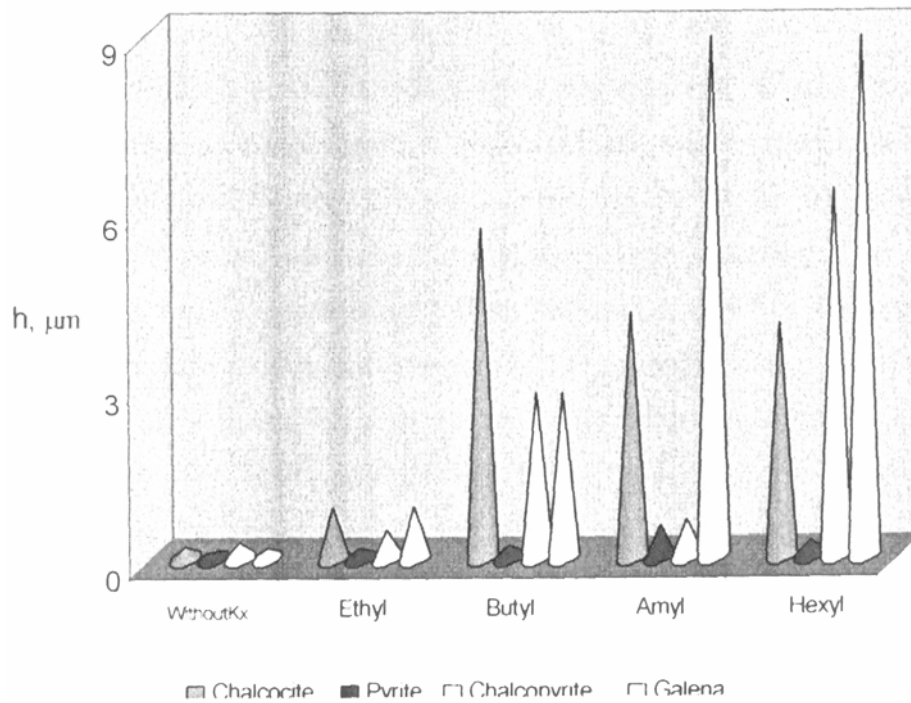


Fig. 7. Influence of carbon chain length of xanthate on the calculated thickness of the rupturing film

Table 3. Induction time for a gas bubble on sulphides at different potentials in 50 mg /dm³ or 265μM amyl xanthate aqueous solutions

Applied potential [V]	Induction time [ms]			
	Chalcocite	Pyrite	Chalcopyrite	Galena
-0.8				4500
-0.6				3500
-0.4	3500			600
-0.2	3500	3500	4000	90
0	70	3000	2000	7
0.2	150	500	2000	2
0.4	200	4000	1500	25
0.6	2000		2000	
0.8	20		400	
1.0	3000		1500	
1.2	9		1500	

The obtained results (Table 3) indicate a broad variation of IT from 2 ms to 4.5 s.

Molibdenite is the most hydrophobic sulphide mineral and using the effect of hydrophobic interactions could be of special interest to improve molibdenite flotation. Lost of molibdenite during beneficiation of Cu-Mo ores remains one of the main problems of flotation practice. At Erdenet concentrator, for a 95% disintegration of mineral complexes, milling to 70% of the $-74 \mu\text{m}$ fraction leads to increasing of the output of slimes. The design of the used scheme of milling and classification of Cu-Mo ores at the Erdenet plant gives output of the $-5 \mu\text{m}$ fraction at the 10% level (Vigdergauz, 2005). The most prominent path for decreasing molibdenite losses with fine particles could be an implementation of selective flocculation technology that has been one of significant advances in mineral processing in recent years. An effect of a hydrophobic interaction of a hydrophobic polymer with the surface of naturally hydrophobic slimes was positively used for molibdenite flotation (Castro et al., 1997).

Figure 8 illustrates high hydrophobicity of molibdenite. Data calculated on the experiments of IT measurements in borate buffer solution for various potentials (Sohorov and Vigdergauz, 2007).

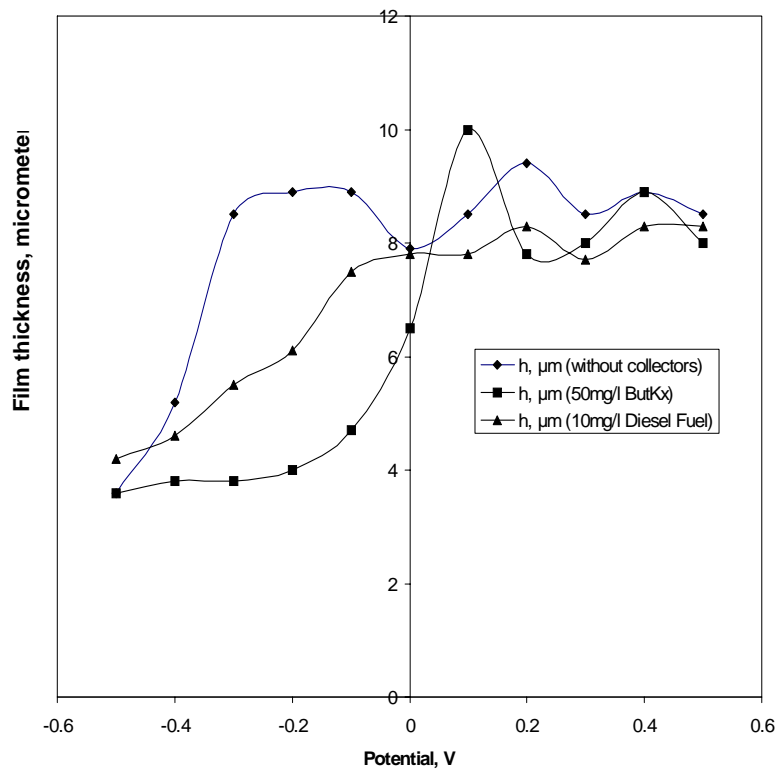


Fig. 8. Thickness of the rupturing film on molibdenite vs. potential of electrochemical polarization

Commonly used collectors, including diesel fuel or xanthate, do not increase hydrophobicity of this naturally highly hydrophobic mineral.

SUMMARY

Induction time measurements show that hydrophobic interactions are long-range. Calculated by the Sheludko-Malysa approximation values of the thickness of the rupturing films reach some hundreds of nanometers. The obtained values of the critical length of the wetting film are very dependable on the baseline of the attached bubble that had been supposed to be critical for the rupture.

ACKNOWLEDGEMENTS

The author thanks Dr. J. Drzymala for useful and thorough discussion on minerals' wettability and for making helpful comments.

The present work has been performed with the financial support of the Russian Foundation of Fundamental Researches (grant No 05-05-64050) and grant of the Mr. President of the Russian Federation (No NSh 4819.2006.6.).

REFERENCES

- ATTARD, P., (2005) <http://personal.chem.usyd.edu.au/Phil.Attard/nanobubble/nanob.htm>.
- CASTRO, S.H., STOCKER, R., LASKOWSKI, J.S., (1997) *The effect of hydrophobic agglomerant on the flotation of fine molybdenite particles*. In Proceedings, XX International Mineral Processing Congress, Aachen, Vol. 3, pp.559-569.
- CHANTURIYA, V.A., VIGDERGAUZ, V.E. (1993) *Electrochemistry of Sulfides: Theory and Practice of Flotation* (in Russian), Moscow: Nauka.
- DE WITT, C.C., MAKENS, R.F., HELZ, A.W., (1935) *The Surface Relations of the Xanthates*. The Journal of the American Chemical Society, 57, pp.796-801.
- DRELICH, J., MILLER, J.D., LI, J.-S., WAN, R.-Y., (1997) *Bubble attachment time measurements at a chalcopyrite surface using a high-speed video system*, Proc. XX International Mineral Processing Congress, Aachen, pp 53-64.
- DRZYMALA, J., VIGDERGAUZ, V., (2000) *Work and Force of Bubble-Particle Detachment as a Measure of Contact Angle in Flotation Systems*. Prace Naukowe Instytutu Gornictwa Politechniki Wrocławskiej, 87, C.3-11.
- GARDNER, J.R., WOODS, R., (1977) *An electrochemical investigation of contact angle and of flotation in the presence of alkylxanthates. II galena and pyrite surfaces*, Aust. J. Chem., 30, 981-991.
- GORODETSKAYA, A.V., KABANOV, B.N., (1934) *Kapillarelektische Erscheinungen und Benetzung von Metallen durch Elektrolytlosungen. II*. Physikalische Zeitschrift der Sowietunion, 3, 418-431.
- ISHIDA, N., SAKAMOTO, M., MIYAHARA, M., HIGASHITANI, K., (2000) *Attraction between hydrophobic surfaces with and without gas phase*. Langmuir, 16, 5681-5687.
- KRASOWSKA, M., KRZAN, M., MALYSA, K., (2003) *Bubble collisions with hydrophobic and hydrophilic surfaces in α -terpineol solutions*. Physicochemical Problems of Mineral Processing, 37, 37-50.
- SCHELUDKO. A., (1967) *Thin liquid films*, Advances Coll. Interface Sci., 1,391-464 (according to Krasowska, Krzan and Malysa, 2003).
- SCHULZE, H.J., STOCKELHUBER, K.W., WENGER, A., (2001) *The influence of acting forces on the rupture mechanism of wetting films – nucleation or capillary waves*, Colloids and Surfaces A, 192, 61-72.

- SOHOROV S.A., VIGDERGAUZ V.E., (2006) *Electrochemical Study of Adhesion Kinetics and Critical Thickness of Wetting Film on Molibdenite Surface (in Russian)*, Proc. 3^d Int. Conf. IPKON RAS, Moscow, pp. 220-225.
- STOCKELHUBER, K. W., RADOEV, B., WENGER, A., SCHULZE, H. J., (2004) *Rupture of wetting films caused by nanobubbles*. Langmuir, 20, 164-168.
- SUTHERLAND, K.L., WARK, I.W., (1955) *Principles of Flotation*, AIMM, Melbourne.
- VIGDERGAUZ, V.E. (2005) *Kinetics of Bubble-Particle Interaction, Surface Hydrophobicity and Interfacial Phenomena in Sulphide Mineral Flotation*, Proceedings, Centenary of Flotation, Brisbane: AusIMM, pp. 625-633.
- VIGDERGAUZ, V.E., DOROFEEV, A.I. (2007) *Electrochemical study of wettability of platinum electrode related to mineral flotation*, Proc. XII BMPC, Delphi, Greece.
- VIGDERGAUZ, V. E., NEDOSEKINA, T. V., (1998) *The wettability of electrodes made of natural metal sulphides*. J. Solid State Electrochem., 1, 50-57.
- VIGDERGAUZ, V.E., SCHRADER, E.A., SARKISOVA, L.M., KUZNETSOVA, I.N. (2006) *Wettability of sulfides in relation to mineral flotation and flocculation processes: strong long-range interactions between hydrophobic surfaces*, XXIII International Mineral Processing Congress, Istanbul, pp. 409-413.
- VIGDERGAUZ, V.E., (2005) *Interfacial Phenomena in Sulphide Mineral Flotation: IV Copper and Molibdenium Sulphides (in Russian)*, Proc. Int. Conf. 29-30 September, Mongolia, Erdenet.
- YOON, R.-H., (2000) *The role of surface forces in flotation kinetics*. In Proceedings XXI International Mineral Processing Congress, Rome, pp. B8a-1-7.

Vigdergauz V.E., *Ocena długości oddziaływań pomiędzy hydrofobowymi powierzchniami w oparciu o pomiary czasu indukcji*, Physicochemical Problems of Mineral Processing, 41, (2007), 13-25 (w jęz. ang.).

Użyto pewnej metody, w tej pracy nazwaną aproksymacją Scheludki i Malysy, do obliczenia grubości pękającego filmu. Oparto się na eksperymentalnych danych dotyczących czasu indukcji (IT) dla układu pęcherzyk powietrza – platyna oraz pęcherzyk powietrza - minerał siarczkowy. Przedyskutowano wpływ zastosowanego potencjału, pH i kolektora flotacyjnego na zwilżalność. Wyniki wskazują na dużą zmienność IT. Obliczona grubość pękającego filmu wynosi kilka mikrometrów. Potwierdza to długo zasięgowy charakter oddziaływań pomiędzy pęcherzykami powietrza i hydrofobową powierzchnią.

Jan DRZYMAŁA *

ATLAS OF UPGRADING CURVES USED IN SEPARATION AND MINERAL SCIENCE AND TECHNOLOGY Part II

Received March 15, 2007; reviewed; accepted June 6, 2007

The present Atlas (Part II) contains 12 new less known upgrading curves which relate quality and quantity of products of separation for a given feed quality α . Part II of the Atlas supplements the list of known upgrading curves presented in Part I. The classification of the upgrading curves used in this work is the same as previously. Group A_i covers upgrading α -insensitive curves with triangle or near triangle area accessible for plotting, A_o: α -insensitive curves, square area available for plotting, B_i: α -sensitive curves with triangle plotting area, B_o: α -sensitive curves, having square plotting area, C_i: α -insensitive curves for $\beta > \alpha$ triangle area, and C_o: α -insensitive curves for $\beta > \alpha$ or $\beta < \alpha$, square area, where β stands for content of a component in concentrate while α in the feed. It was emphasized in the paper that all upgrading curves contain the same information but in a different, specific for a given curve form. The use of upgrading curves depends on the needs and preferences of the user. An appropriate matching of upgrading plot with a set of separation results allows to approximate the curve with a suitable mathematical formula which can be used for characterizing separation. Additional curves will be present in Part III of the Atlas. The readers are kindly asked to report unmentioned upgrading curves to jan.drzymala@pwr.wroc.pl.

Key words: separation, upgrading, recovery, yield, efficiency

INTRODUCTION

Splitting an initial material (feed) into two or more portions in a real or virtual way is the essence of separation. The separation is possible due to ordering and splitting forces operating in the system. Depending on the character of forces, the separation can be real or virtual, selective or non-selective, etc.

The results of separation are usually presented in tabular and graphical forms. There is infinite number of separation curves. When quantity of separation products

* Wrocław University of Technology, Wybrzeże Wyspińskiego 27, 50-370 Wrocław, Poland,
jan.drzymala@pwr.wroc.pl.

and their quality are considered, such approach is called upgrading. There is infinite number of upgrading curves. They are based on three principal parameters: quantity of products (γ), quality (usually expressed as content of a component in a product (β), and the content of a component in the feed (α). Different combinations of α , β , and γ provide new parameters which equally well, as the original ones, characterize the separation process as upgrading. New parameters created with α , β , γ are for instance recovery ($\varepsilon = \gamma\beta/\alpha$) or enrichment ratio $K = \beta/\alpha$. Pairs of upgrading parameters provide upgrading curves which represent the same data but in a different esthetical and graphical form. The usefulness of a given upgrading curve depends, to a great extent, on personal preferences.

Eighteen upgrading curves were presented and discussed in Part I of Atlas of Upgrading Curves (Drzymala, 2006). The present paper continues the effort to present the most important and useful upgrading curve existing in literature. Some upgrading curves have never been used before. It is easy to create new upgrading curves because there are many selectivity indices in literature which can be combined into pairs and plotted as separation curves.

Complete plots with upgrading curves should contain lines (or points) of real, ideal, remixing, and no upgrading. When the shape of two curves is identical, they bear the same name but differ in Latin numerals.

UPGRADING BALANCE

For plotting upgrading curves, the same as in Atlas Part I (Drzymala, 2006) hypothetical results of separation were considered (Table 1). It was assumed that the feed contains only two components, that is component 1 and component 2 (rest of material). Only principal parameters, that is feed grade (α), yield of products (γ), content of component 1 (β_1), ($\beta_2 = 100\% - \beta_1$), and recoveries of both components are presented. Other parameters can be calculated using the formulas given in the axes of the upgrading curves. Details regarding calculation of parameters used for plotting the three MDTW upgrading curves are given in the appendix.

Table 1. Upgrading balance of a hypothetical separation. The data were used for calculation of upgrading curves

Product	Yield, γ (%)	Content of component 1 β_1 , %*	Recovery of component 1 $\varepsilon = \gamma\beta/\alpha$, %	Recovery of component 2 $\varepsilon = \gamma\beta/\alpha$, %
K_1	12.06	81.70	64.00	2.00
$K_1 + K_2$	20.14	60.40	79.01	9.43
$K_1 + K_2 + K_3$	42.27	32.44	89.07	33.71
$K_1 + K_2 + K_3 + K_4$	70.14	21.73	98.99	63.92
Tailing	29.86	0.52	1.01	36.08
Feed	100.00	15.40 = α	100.00	100.00

*content of component 2 (β_2 , %) is equal to: $\beta_2 = 100 - \beta_1$

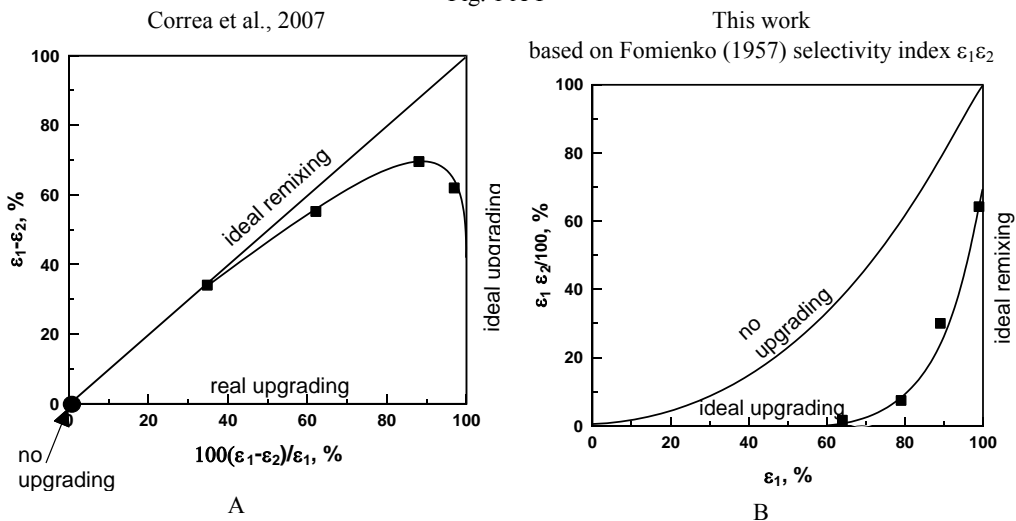
UPGRADING CURVES

In the previous paper the upgrading curves were classified into three categories: A (α -insensitive), B (α -sensitive), C (α -insensitive but covering limited range of variables). The same classification is shown in Table 2 along with names of upgrading curves discussed in the Atlas (Part I and II). The upgrading curves are shown in Figs 1-3.

Table 2. Upgrading curves considered in the Atlas (Part I and this work Atlas Part II)

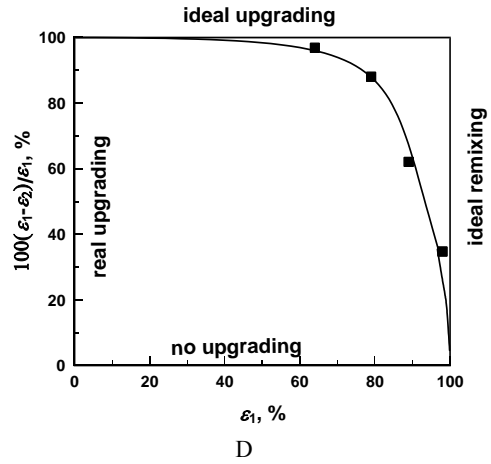
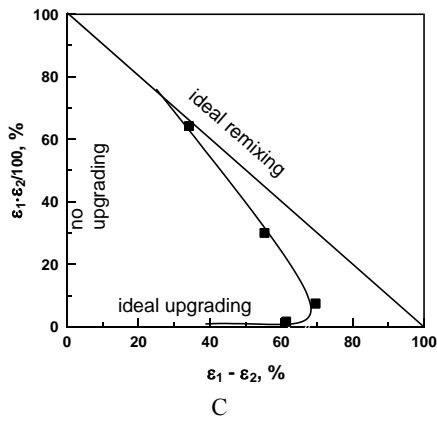
Group symbol	Description, sensitivity to variation of α and area available for plotting	Examples Atlas Part I	Examples Atlas Part II
A _l	α -insensitive curves, triangle area	Fuerstenau Luszczkiewicz	Correa et al. Fomienko 1 Fomienko 2
A _o	α -insensitive curves, square area	-	Correa Bieloglazov I, II
B _l	α -sensitive curves, triangle area	Henry I, II, III Mayer I, II, III (Dell) Holland-Batt β Holland-Batt H (Hancock) β - β	MDTW Hu Wei bai
B _o	α -sensitive curves, square area	Halbich, Stepinski I, II, III, IV,	Halbich II, III
C _l	α -insensitive curves, for $\beta > \alpha$, triangle area	not known	MDTWc
C _o	α -insensitive curves, for $\beta > \alpha$, square area	Drzymala (Stepinski V) Hall	MDTWr

Fig. 1 A-F



This work
based on Fomienko (1957) $\varepsilon_1\varepsilon_2$ and Hancock $\varepsilon_1 - \varepsilon_2$
selectivity index

Correa, 2007, unpublished



This work (Bieloglazov I)
based on selectivity index n (Bieloglazov, 1947;
Petrova and Boteva, 2006)

This work (Bieloglazov II)
based on selectivity index $\varepsilon_1/\varepsilon_2$ used by Ulewicz et
al., 2001

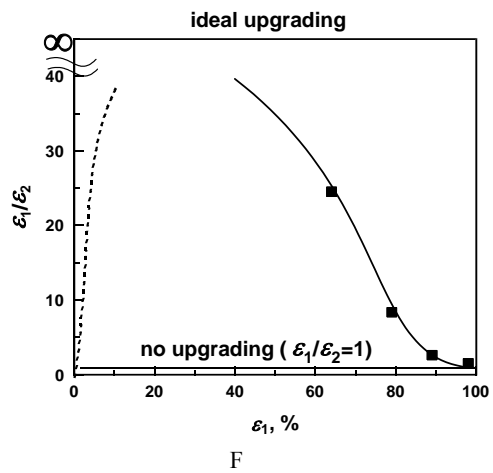
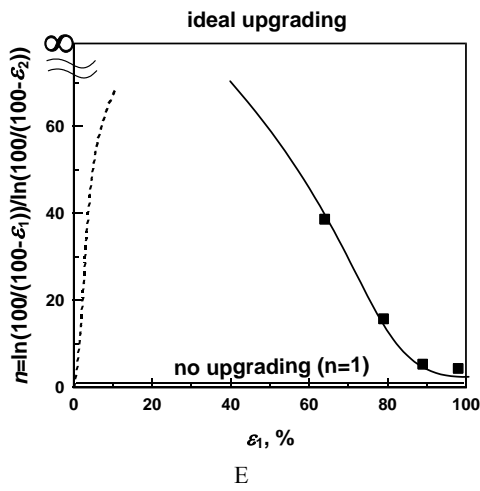


Fig. 1. Type A upgrading curves which are α -insensitive and offer either triangle-type (A, B, C) or square-type areas for plotting

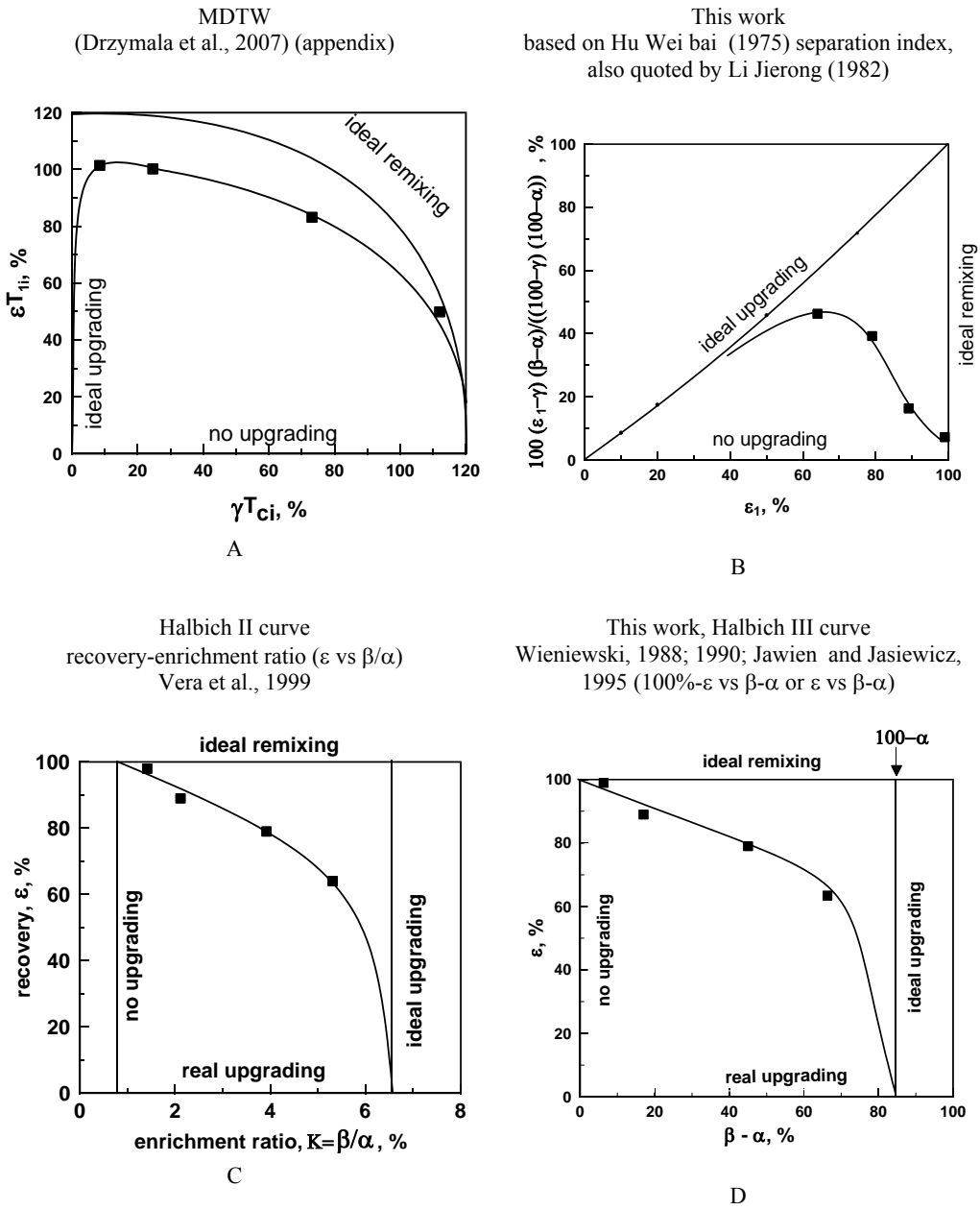


Fig. 2. Type B (α -sensitive with triangle (or near triangle) and square area available for plotting upgrading curves)

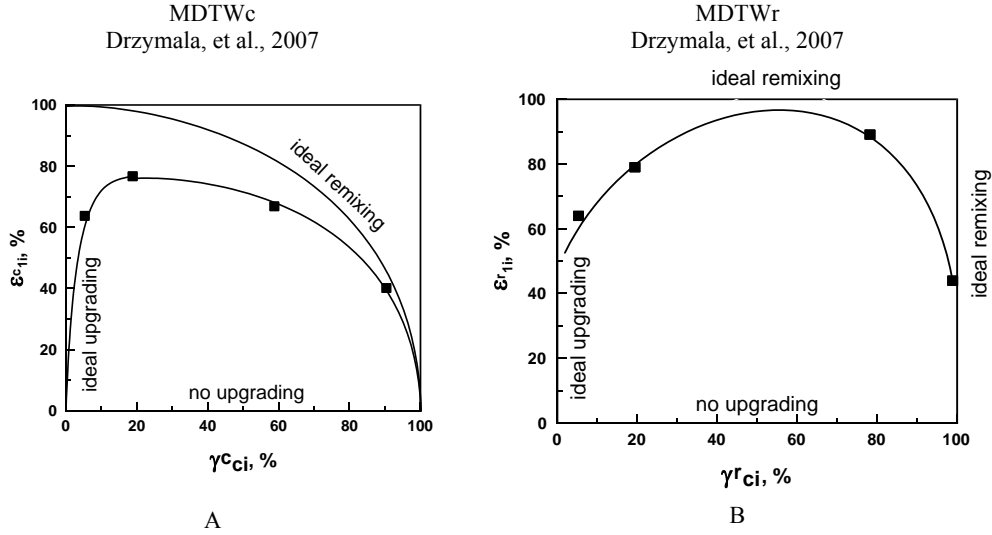


Fig. 3. C type of upgrading curve (α -insensitive curves, for $\beta > \alpha$, square or triangle area available for plotting)

CONCLUSIONS

Present Atlas of upgrading curves still represent a small number of possible upgrading curves. Therefore Part III of the Atlas will be prepared for publication in 2008. It will contain complex upgrading curves as well as other which exist in literature but have been so far mentioned, for many reasons, in the Atlas.

Appendix. Calculations of parameters needed for plotting MDTW (Mayer-Drzymala-Tyson-Wheelock) upgrading curves

All details regarding calculations of selectivity indices ε_{li}^T , ε_{li}^T , ε_{li}^r , γ_{ci}^T , γ_{ci}^c , and γ_{ci}^r can be found in the original paper by Drzymala et al. (2007). The needed equations are given in Table 3. Starting numbers are yield γ and recovery ε .

1. Use equation 4 to calculate θ_0 for each test.
2. Use $\tan \theta_i = \sum \varepsilon_{li} / \sum \gamma_{ci}$ to calculate θ_i for each experimental point.
3. Use equation 3 to calculate θ_i^T for each experimental point.
4. Use equations 1 and 2 to determine $\sum \gamma_{ci}^T$ and $\sum \varepsilon_{li}^T$, respectively.
5. Given $\sum \varepsilon_{li}^e = 100$, calculate $\sum \varepsilon_{li}^{eT}$ by using equation 9.

6. Calculate $\sum \gamma_{ci}^{eT}$ by using the following combination of equations 5, 7 and 8:

$$\sum \gamma_{ci}^{eT} = 100 \cos \theta_i^T / \sin \theta_i.$$
7. For circular normalization apply equations 10 and 11 to determine $\sum \varepsilon_{li}^c$ and $\sum \gamma_{ci}^c$, respectively.
8. For rectangular normalization and $\theta_i^T > 45^\circ$, use equations 12 and 13 to determine $\sum \varepsilon_{li}^r$ and $\sum \gamma_{ci}^r$, respectively.
9. For rectangular normalization and $\theta_i^T < 45^\circ$, use equations 14 and 15 to determine $\sum \gamma_{ci}^r$ and $\sum \varepsilon_{li}^r$, respectively.

Table 3. Equation needed for calculations of parameters for the MDTW, MDTWr and MDTWe upgrading curves. After Drzymala et al., 2007

$$\gamma_{ci}^T = \gamma_{ci} \frac{\cos \theta_i^T}{\cos \theta_i} \quad (1)$$

$$\varepsilon_{li}^T = \varepsilon_{li} \frac{\sin \theta_i^T}{\sin \theta_i} \quad (2)$$

$$\theta_i^T = \frac{90^\circ(\theta_i - 45^\circ)}{\theta_o} \quad (3)$$

$$\tan(\theta_o + 45^\circ) = \frac{100}{\alpha_1} \quad (4)$$

$$\gamma_{ci}^e = R_i^e \cos \theta_i \quad (5)$$

$$\varepsilon_{li}^e = R_i^e \sin \theta_i \quad (6)$$

$$R_i^e = \varepsilon_{li}^e / \sin \theta_i = 100 / \sin \theta_i \quad (7)$$

$$\gamma_{ci}^{eT} = \frac{\gamma_{ci}^e \cos \theta_i^T}{\cos \theta_i} \quad (8)$$

$$\varepsilon_{li}^{eT} = \frac{\varepsilon_{li}^e \sin \theta_i^T}{\sin \theta_i} \quad (9)$$

$$\varepsilon_{li}^c = \frac{R_i^c \sin \theta_i^T \varepsilon_{li}^T}{\varepsilon_{li}^{eT}} = \frac{100 \sin \theta_i^T \varepsilon_{li}^T}{\varepsilon_{li}^{eT}} \quad (10)$$

$$\gamma_{ci}^c = \frac{R_i^c \cos \theta_i^T \gamma_{ci}^T}{\gamma_{ci}^{eT}} = \frac{100 \cos \theta_i^T \gamma_{ci}^T}{\gamma_{ci}^{eT}} \quad (11)$$

$$\varepsilon_{li}^r = \varepsilon_{li}^{er} \frac{\varepsilon_{li}^T}{\varepsilon_{li}^{eT}} = 100 \frac{\varepsilon_{li}^T}{\varepsilon_{li}^{eT}} \quad (12)$$

$$\gamma_{ci}^r = \frac{\varepsilon_{li}^{er} (\gamma_{ci}^T)^2}{\varepsilon_{li}^T (\gamma_{ci}^{eT})} = \frac{100 (\gamma_{ci}^T)^2}{\varepsilon_{li}^T (\gamma_{ci}^{eT})} \quad (13)$$

$$\gamma_{ci}^r = \gamma_{ci}^{er} \frac{\gamma_{ci}^T}{\gamma_{ci}^{eT}} = 100 \frac{\gamma_{ci}^T}{\gamma_{ci}^{eT}} \quad (14)$$

$$\varepsilon_{li}^r = \frac{\gamma_{ci}^{er} (\varepsilon_{li}^T)^2}{\gamma_{ci}^T (\varepsilon_{li}^{eT})} = \frac{100 (\varepsilon_{li}^T)^2}{\gamma_{ci}^T (\varepsilon_{li}^{eT})} \quad (15)$$

Results of transformation and normalization for results of separation from Table 1 are given in Table 4. The data were used for plotting three upgrading curves: MDTW (Fig. 2A), circular MDTWc (Fig. 3A) and rectangular MDTWr (Fig. 3B)

Table 4. Results of transforming the coordinate system followed by either circular or rectangular normalization. $\alpha=15.40\%$

Product	$\sum \varepsilon_{li}$ (%)	$\sum \gamma_{ci}$ (%)	θ_i deg.	θ_i^T deg.	$\sum \varepsilon_{li}^T$ (%)	$\sum \gamma_{ci}^T$ (%)	$\sum \varepsilon_{li}^{eT}$ (%)	$\sum \gamma_{ci}^{eT}$ (%)	$\sum \varepsilon_{li}^c$ (%)	$\sum \gamma_{ci}^c$ (%)	$\sum \varepsilon_{li}^r$ (%)	$\sum \gamma_{ci}^r$ (%)
K ₁	64.0	12.1	79.3	85.2	64.9	5.4	101.4	8.4	63.8	5.3	64.0	5.3
K _{1,2}	79.0	20.1	75.7	76.2	79.2	19.4	100.2	24.6	76.7	18.8	79.0	19.4
K _{1,2,3}	89.1	42.3	64.6	48.7	74.1	65.0	83.2	73.1	66.9	58.8	89.1	78.2
K _{1,2,3,4}	98.9	70.1	54.7	24.0	49.3	110.7	49.9	112.0	40.2	90.4	44.0	98.9

REFERENCES

- BIELOGLAZOV, K. F., 1947. *Zakonomernosti flotacionnogo processa*, Metallurgizdat (in Russian)
 CORREA, A.F., 2006, unpublished.
 CORREA, A.F., DOMINGUEZ E., ALIOTTA, G., *The Holland-Batt method applied to a magnetic wollastonite purification*, XXII ENTMME/ VII MSHMT, Ouro Preto-MG, November 2007, Brasil.

- DRZYMALA, J., 2005, *Evaluation and comparison of separation performance for varying feed composition and scattered separation results*, Int. J. Miner. Process., 75, 189-196.
- DRZYMALA, J., 2006. *Atlas of upgrading curves used in separation and mineral science and technology*, Part I, Physicochemical Problems of Mineral Processing, 40, 19-29.
- DRZYMALA, J., TYSON, D. WHEELLOCK, T.D., *Presentation of particle beneficiation test results on an equal basis when yield and recovery are involved*, Minerals and Metallurgical Processes, in press.
- FOMIENKO T.G., 1957. *Opređenje optimalnych pokazateli obogashchenia*, Vsechsojuznyj Magadanskij NII 1, chapter IV, Obogashchenie i metalurgija, 24, Izd.-vo Severovastokzoloto.
- HU WEI BAI, 1975. *How to calculate separation efficiency*, Non-ferrous metal (Mineral processing), 6, 40-50.
- JAWIEŃ, M., JASIEWICZ, J, 1995. *Maksymalizacja zysku KGHM przez sterownie zawartością miedzi w koncentracie*, Konf. „Zastosowanie metod matematycznych w nauce i technice”, Kraków, 20-21.VI.1995, vol.1., 205-220.
- LI JIERONG, 1982, *The practice of concentration and the way to increase grade and recovery of the graphite concentration in Nanshu graphite Mine, Shandong, China*, XIV IMPC, Toronto, Canada, 1982, V-9.1 - V-9.10.
- PETROVA, H., BOTEVA, A., 2006. *Probable mechanism of the operation of the flotation pulp density on selective flotation of the sulphide minerals*, Górnictwo i geoinżynieria, v.30 (3/1), 295-300.
- ULEWICZ, M., WALKOWIAK, W., KOZŁOWSKI, C., 2001. *Selective flotation of zinc(II) and cadmium(II) ions from dilute aqueous solutions in the presence of halides*, Physicochemical Problems of Mineral Processing, 35, 21-29.
- VERA M.A., FRANZIDIS, J-P., MANLAPIG, E.V., 1999. *An empirical equation for the recovery – enrichment ration curve*, in: Mineral processing/ Environment, Health and Safety, B.A. Hancock and M.R.L. Pon editors, Proc. Copper 99-Cobre 99 Int. Conf. Vol. II, Oct. 10-13, Phoenix, Arizona USA.
- VERA, M.A., FRANZIDIS J-P., MANLAPIG, E.V., *An empirical equation for the recovery–enrichment ratio curve (AREV model)*, 1999, in: Mineral Processing/Environment, Health and Safety, Proc. COPPER 99 – COBRE 99 Int. Conf., V.II, Phoenix, USA, Hancock, B.A., Pon, M.R.L., Eds, The Minerals, Metals & Materials Society, 1999.
- WIENIEWSKI, A., IMN 4097/88 (1988) and 4463/II/90 Reports, Gliwice, Poland.

Drzymala J., *Atlas krzywych wzbogacania do opisu separacji stosowanych w nauce i w przemyśle mineralnym. Część II*, Physicochemical Problems of Mineral Processing, 41 (2007) 27-35 (w jęz. ang.).

Atlas przedstawia 12 różnych mniej znanych krzywych wzbogacania. Wiązą one jakość produktów separacji od ich ilości. Część II Atlasu uzupełnia listę znanych krzywych wzbogacania zawartą w części I Atlasu. Utrzymano klasyfikację krzywych wzbogacania na grupy: A_1 (nieczułe na zawartość składników w nadawie z trójkątnym obszarem dostępnym do kreślenia krzywych), A_0 (nieczułe na zawartość składników w nadawie z kwadratowym obszarem dostępnym do kreślenia), B_1 (czułe na zawartość składników w nadawie z trójkątnym obszarem dostępnym do kreślenia), B_0 (czułe na zawartość składników w nadawie z kwadratowym obszarem dostępnym do kreślenia), C_1 (nieczułe na zawartość składników w nadawie dla $\beta > \alpha$ oraz $\beta < \alpha$, obszar trójkątny), oraz C_0 (nieczułe na zawartość składników w nadawie α dla $\beta > \alpha$ oraz $\beta < \alpha$, obszar kwadratowy), gdzie β oznacza zawartość składnika w koncentracji a α w nadawie. W pracy podkreślono że wszystkie krzywe wzbogacania zawierają te same informacje lecz SO_4 podane w innej, specyficznej dla danej krzywej, formie graficznej. Ich stosowalność zależy od potrzeb użytkownika i osobistych preferencji. Odpowiednie skojarzenie krzywej wzbogacania z danymi pomiarowymi pozwala na aproksymacje krzywych odpowiednimi równaniami matematycznymi, użyteczne do opisu separacji. Dalsze krzywe będą podane w Części III Atlasu następnego wydania tego czasopisma. Autor prosi o nadsyłanie nieopisanych dotąd krzywych wzbogacania pod adres: jan.drzymala@pwr.wroc.pl

Jeongyun KIM* Byounggon KIM*

CHEMICAL AND LOW-EXPANSION TREATMENTS FOR PURIFYING NATURAL GRAPHITE POWDER

Received March 20, 2007; reviewed; accepted June 10, 2007

Fine natural graphite powder shows good properties in heat resistance, heat expansion and electric conductivity, and has been used as the materials for high-efficient secondary batteries, lubrication, etc. Graphite powder, as a high-tech material, is made through purifying and surface control processes. Developed countries produce high functional graphite powders by additional intercalation processes and sub-micronizing. This study is conducted to utilize low grade natural graphite powders as nano-material resources. Prior to production of the ultrafine graphite powder, studies on its pretreatments were performed. Typical acid/alkali treatments with expansion process were conducted. Expanding temperature for gasification process is set low compared to those of the traditional processes. This will make possible to give appropriate expansion ratio for effective chemical treatments and grinding processes. Expansion ratios were controlled as 20~30% of the original volume at 200~250 °C, since excessive expansion of graphite powder by traditional approach at high temperature leads to a low grinding efficiency.

Key words: graphite, purification, chemical treatment

INTRODUCTION

There are many methods of purification of graphite powders (KORES, 2007; Kim, 2001). Most of them involve acid or alkali treatments while several involve either expansion processes or physical treatments. There are many studies on the expansion of graphite powder at high temperatures under conventional expansion conditions (Lee, 2000; Jung et al., 1991). This could help purify graphite (Bouvard et al., 1988), but it does not help grind the powder. Graphite expanded at high temperatures has very low bulk density, indicating very large volume. Therefore, this is regarded as an inappropriate process for grinding the powder.

* Mineral Processing Group, Minerals and Materials Processing Division, Korea Institute of Geoscience and Mineral Resources, Gajeong-dong 30, Yuseong-gu, Daejeon 305-350, Korea,
e-mail: kooltz77@kigam.re.kr

The final objective of this study is to produce raw materials for making nano-sized graphite powder of high purity. In the literature, some experiments were conducted to determine the expansion conditions appropriate for removing impurities from the powder while maintaining or improving grinding characteristics of graphite powder (Bouvard et al., 1988).

EXPERIMENTAL

Figure 1 shows the graphite powders expand at high temperatures. As one can see in the pictures, the expanded graphite has string-like shape, expanding along c-axis. The SEM image shows the graphite powder expanded in a cluster range. It means that the expanded graphite powders could be ground effectively in cluster range compared to natural powders. Figure 2 provides the XRD patterns showing the changes in crystallinity of the expanded graphite powder. The graphite powders show different crystallinities, and various graphite samples having different crystallinities could be produced by the expanding procedure. The difference in crystallinity may affect the purifying property or grinding characteristics of the graphite powder.

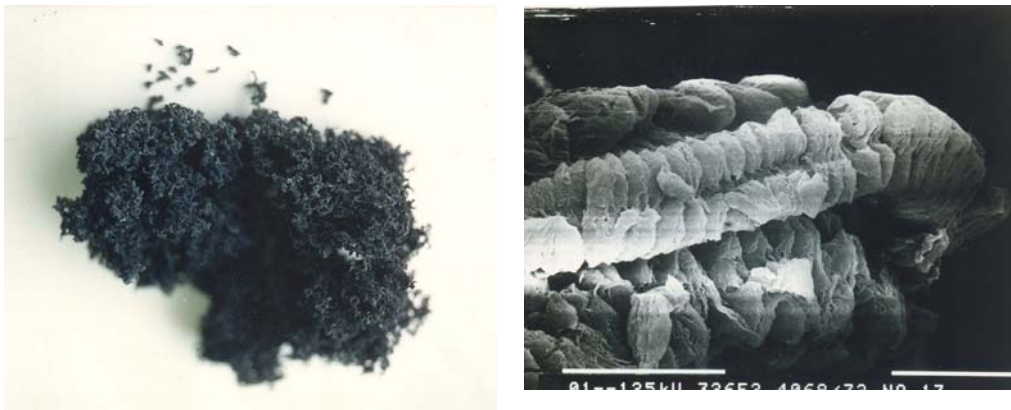


Fig. 1. Photos of expanded graphite powders: (a) optical image, (b) SEM image (x1,000)

In all experiments, two different sizes of graphite powder were used. One is the natural flake-shape graphite powder having a size ranging from 150 to 300 μm and a 90% fixed carbon content. This was used as the sample for preliminary tests to determine optimum expanding conditions. The other is also natural flake-shape graphite powder having an size of under 45 μm (average size of about 20 μm) and 85% fixed carbon. The latter was used in the main tests for purification with acid and alkali reagents and expansion by gasification.

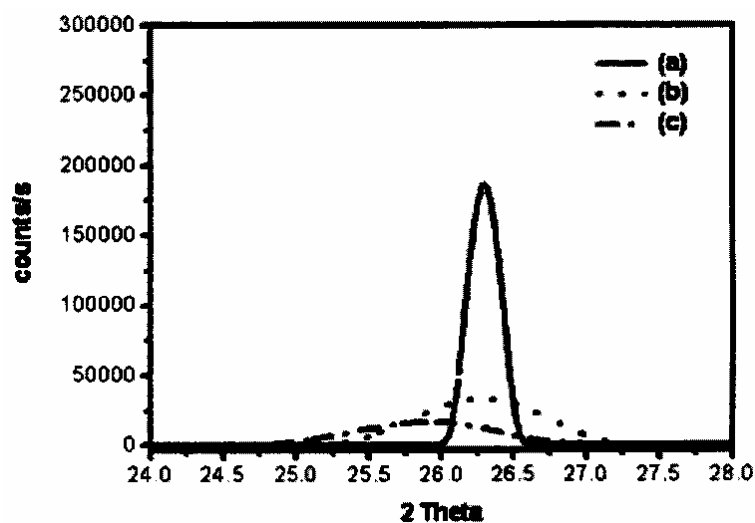


Fig. 2. XRD patterns for graphite powder: (a) raw material, (b) expanded in cluster range, and (c) expanded in layer, stack and cluster

Table 1. Acid treatment and gasification of 100-150 μm graphite powder for XRD pattern analysis

# of sample	Reagents	Expanding temp.	Treatment
13			Raw materials
3	H_2SO_4 600g+ H_2O_2 14g	Room temperature	Acid treatment
3-1			Duplicate of #3
4	H_2SO_4 1,200g+ H_2O_2 14g		H_2SO_4 added
5	H_2SO_4 600g+ H_2O_2 14g		Acid treatment
6			Duplicate of #5
10	H_2SO_4 267g+ CH_3COOH 133g	600 °C	Acid treatment
11	H_2SO_4 267g+ CH_3COOH 267g		CH_3COOH added
19	H_2SO_4 600g+ H_2O_2 14g	1,000 °C	Gasification
20		400 °C	
21		450 °C	
22		500 °C	
23		600 °C	
24		650 °C	

CHANGES IN CRYSTALLINITY OF GRAPHITE POWDER BY ACID TREATMENT AND GASIFICATION

General conditions in these tests were given in Table 1. After the acid treatment and gasification, samples were analyzed by XRD. All reagents used were a mixture of hydrogen peroxide and sulfuric acid, or sulfuric acid and acetic acid. In all the tests the amount of graphite sample was 100g and time of treatment was 3 hours. Samples

treated with acid mixture were rinsed with enough amount of clean warm deionized water, filtered and dried. These dried samples underwent gasification at various expanding temperatures. The gap between each layer of was analyzed by XRD pattern analyzer.

PREPARATION OF EXPANDED GRAPHITE SAMPLES AND PURIFYING PROCESS

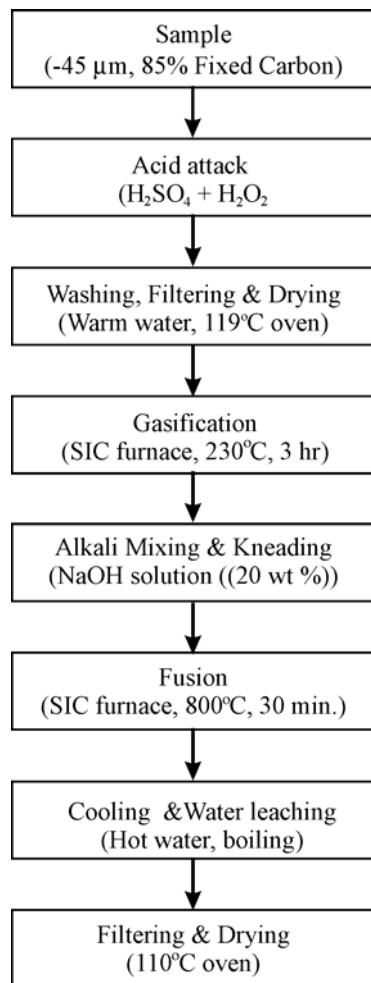


Fig. 3. Treatment procedure for processing graphite powder

In the tests samples smaller than $45\mu\text{m}$ were used. Reacting agents for acid treatments were the mixture of 600g of sulfuric acid and 14g of hydrogen peroxide. Reacting time was about 2 hours and reaction was performed at room temperature. After the acid treatment, samples were rinsed with 50°C clean water, filtered and dried. These samples were used as acid treated samples.

According to the result of preliminary experiments, expanding temperature was set at $200\sim 250^\circ\text{C}$. In this range, the samples showed about 30% of expansion ratio in volume. So various expanded graphite samples were produced at various temperature and expansion time.

Alkali treatments were also conducted for raw material, basic acid treated sample, and expanded sample with acid treatment. 5N sodium hydroxide solution (20 wt%) was used as the reagent for these tests. 10g of each graphite sample was mixed with 25g of alkali solution and kneaded during 12 hours. After that, the samples were dried about 10 hours and fusion process was followed at 800°C using a SiC furnace. Fused samples were cooled and rinsed several times with hot clean water. Final samples were obtained after neutralization with 12 wt% HCl solution, re-rinsing and drying. Overall procedure was given in Fig. 3.

ANALYSIS OF VARIOUS SAMPLES

Samples produced in each step underwent several analyzing procedures to establish such properties as ash content, expansion ratio, particle shape and size. Table 2 shows the major test conditions and properties analyzed by the test. Especially, expansion ratios were determined using samples produced at 230 °C with different treating times. According to the result of expanding tests at 210 °C, 230 °C and 250 °C, graphite powders expanded properly at 230 °C without excessive expansion.

Table 2. Acidic, gasification and alkaline treatment of -45 µm graphite powder at different times and temperatures

Treatment	Temp., °C	Sample No.	Time	Wt., g
Gasification	230	4	1 min	6 ~ 7
		5	2 min	
		6	4 min	
		7	8 min	
		8	15 min	
		9	30 min	
		10	60 min	
		11	120 min	
		12	240 min	
	210	13	240 min	60
	230	14		
	250	15		
Alkali	800	27	180 min	50
		28	180 min	

Analyses for ash contents were conducted basing on KSL 3412:2002 “Test methods for ash in graphite,” using SIC furnace and alumina crucibles (KSIC, 2002). SEM images were taken using JEOL JSM-6380 at 20kV of acceleration voltage. Expansion ratios were calculated by ‘tapping method’ based on volume.

RESULTS AND DISCUSSION

CHANGES IN CRYSTALLINITY OF GRAPHITE POWDER

Figure 4 shows the XRD patterns and gap of layer of treated graphite powder under various conditions, respectively. Sample numbers are based on Table 1. As shown in the figure, crystallinity of raw material was best with 3.37Å of layer gap. #3, #3-1 (repeated analysis of #3), #5, and #6 were the patterns of powder treated under the same conditions and so they show similar trend. On the other hand, #4 shows less

crystallinity and larger layer gap compared to other samples. #10 and #11 is the XRD patterns of samples treated with acetic acid mixture and show higher crystallinity and larger layer gap. It means that graphite powder could be treated with less damage in crystallinity when acetic acid is used as acid treatment reagent.

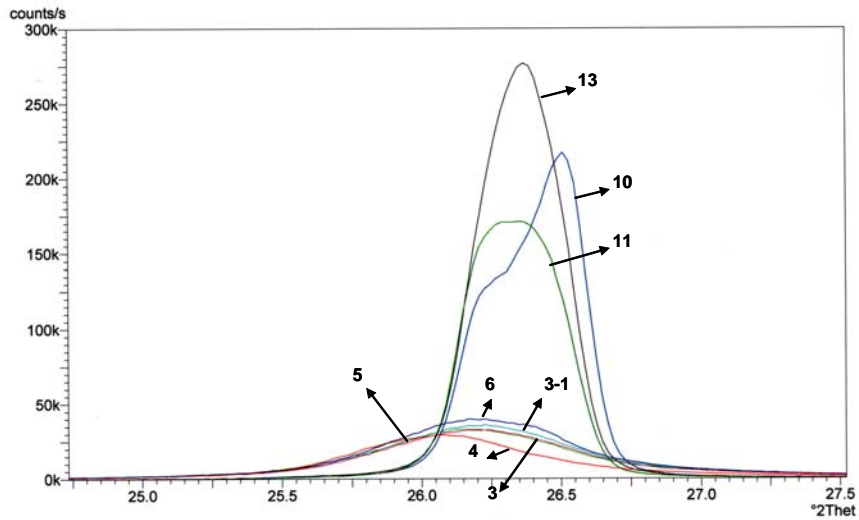


Fig. 4. XRD patterns of various graphite powders at various treating conditions (No. are based on Table 1)

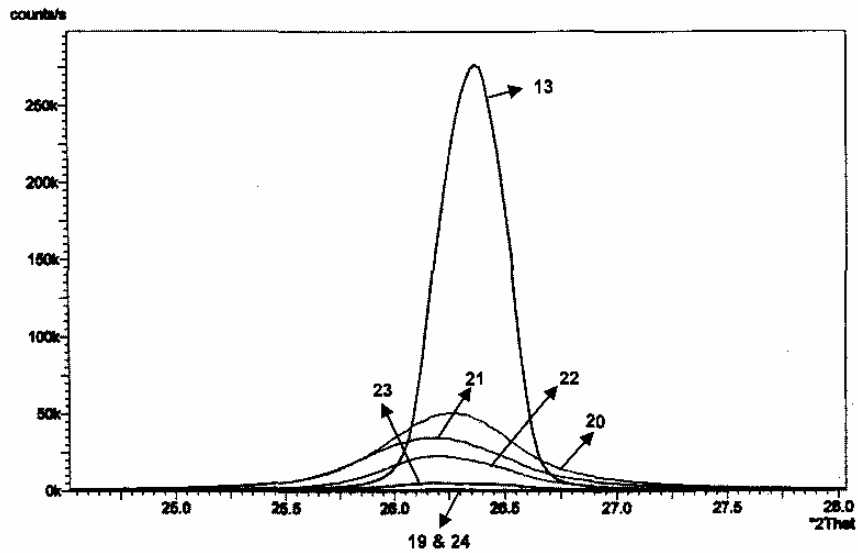


Fig 5. a)

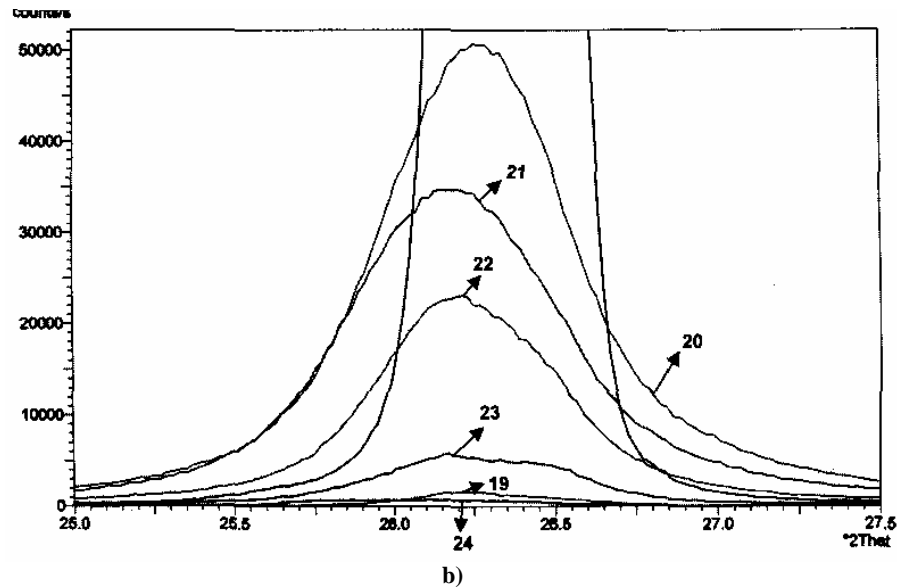


Fig. 5. XRD patterns of various graphite powders at various temperatures (No. are based on Table 1)

Figure 5 shows the XRD patterns of the graphite samples expanded after acid treatment. Sample numbers were based on Table 1, and Figure 5(b) is the image enlarging the major part of Figure 5(a). Crystallinity of graphite powders decreased significantly according to the increase of treating temperature and powders lost their crystalline properties at over 650 °C. On the other hand, the layer gaps were staying at 3.36~3.38Å. This implies that high expanding temperature makes the graphite powders losing their crystalline properties. So, it is important to search the optimum conditions for maintaining the crystallinity of graphite and improving the efficiency of purification or grinding simultaneously.

BULK DENSITIES AND EXPANSION RATIOS

Table 3 shows bulk densities and expansion ratio of -45µm graphite powders in various treating. Sample numbers were based on Table 2. The expansion ratio was calculated from the expanded volume percent compared to initial volume in %. The results show that expansion ratio changed from 9% to 28% with the increase of the treating time at 230 °C, and there were no changes of volume after 2 hours. At 210 °C and 250 °C, 31% and 26% of volume increases were observed. Decreasing from 31% to 26% according to the increase of temperature was because of the experimental errors or nonuniform expansions.

Sine excessive expansion generated by gasification at high temperature could cause lowering of the efficiency of grinding process, it was expected that about 30% of volume expansion could help improve the purifying and grinding efficiency.

Table 3. Bulk densities and expansion ratios of -45 μm graphite powders

Sample no.	Bulk density, g/cm^3				Expansion ratio, %
	test 1	test 2	average	variation	
1	0.375	0.349	0.362	7.1%	100.0
2	0.358	0.354	0.356	1.1%	101.5
4	0.334	0.330	0.332	1.3%	109.0
5	0.330	0.323	0.326	2.1%	110.9
6	0.302	0.310	0.306	2.6%	118.2
7	0.302	0.293	0.297	3.2%	121.7
8	0.295	0.296	0.295	0.3%	122.5
9	0.297	0.287	0.292	3.2%	124.0
10	0.286	0.290	0.288	1.3%	125.7
11	0.282	0.281	0.281	0.3%	128.6
12	0.287	0.283	0.285	1.5%	127.1
13	0.273	0.279	0.276	2.0%	131.2
14	0.265	0.299	0.282	13.1%	128.3
15	0.292	0.282	0.287	3.7%	126.1

Table 4. Ash contents of each graphite samples

Sample no. [†]	Ash content [‡]	Average ash content	Treatments
1	14.09%	14.15%	Raw materials
	14.20%		
2	11.02%	11.10%	Acid treated only
	11.19%		
27	23.58%	23.70%	Acid/alkali treated
	23.81%		
28	14.55%	14.54%	Acid/gasification/alkali treated
	14.54%		
27-2	16.94%	16.85%	Acid/alkali treated (2 nd rinsing)
	16.77%		
28-2	11.39%	11.43%	Acid/gasification/alkali treated (2 nd rinsing)
	11.48%		
27-3	4.30%	4.44%	Acid/alkali treated (3 rd rinsing with HCl)
	4.58%		
28-3	3.84%	3.91%	Acid/gasification/alkali treated (3 rd rinsing with HCl)
	3.99%		

Sample no.[†] is based on Table 2.

Ash content[‡] is determined according KS L 3412:2002

ANALYSES OF ASH CONTENTS FOR -45 μm SAMPLES

Table 4 shows the result of ash analyses for raw material (#1), basic acid treated sample (#2), acid and alkali treated sample (#27), and the sample treated by alkali after acid treatment and gasification (#28).

The ash content of raw material was about 14%, and after the acid treatment the ash content was about 11%, 20% lower than the raw material. It is believed that metallic impurities including iron were removed. The ash content of #27 and #28 appeared higher than #2 because of the incomplete removal of soluble silica formed by the alkali treatment. But the ash content of #27 and #28 proved that the gasification was helpful for removing the impurities by showing low ash content in #27. #27-2 and #28-2 were the samples rinsed 5 additional times with clean water. The ash contents achieved lower level, but not sufficient. In general, soluble silica could remain when alkali reagent was not removed completely. So, additional rinsing was performed using a small dose of hydrochloric acid aqueous solution. Finally, less than 5% of ash content was obtained.

ANALYSES OF SEM IMAGES OF GRAPHITE SAMPLES

Figure 6 shows the SEM images of raw graphite powders and powders after the acid treatment. Image of raw materials shows wide size range of particles showing flake-shape. Image of acid treated powders shows some aggregates created during rinsing and drying, and several particles show somewhat expanded shape in spite being prior to gasification process.

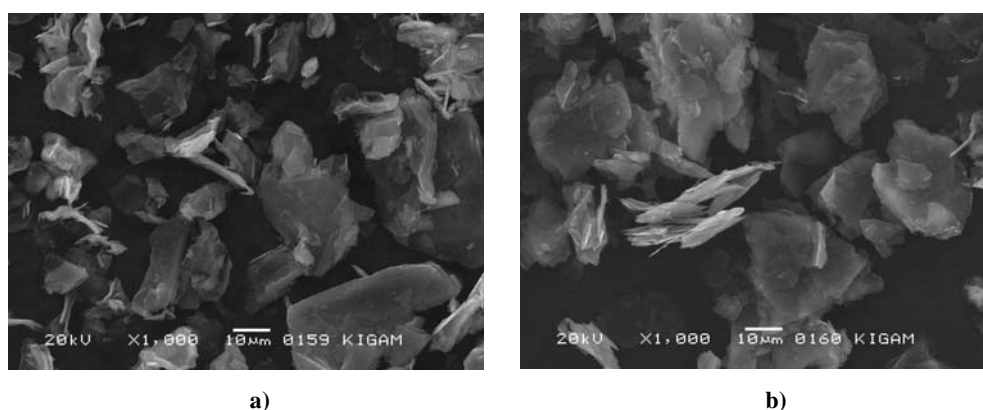


Fig. 6. SEM images of graphite powders; (a) raw materials (#1 in Table 2) and (b) acid treated (#2 in Table 2)

Figure 7 gives the SEM image of graphite powders treated in SIC furnace at 230 °C with various treating time. Expanded powders were observed more frequent in samples treated with long expanding time, but there was little difference in shape

between expanded particles. It was not observed the excessive expansion in this temperature condition. It implies that temperature is proper to produce the low-expanded powders.

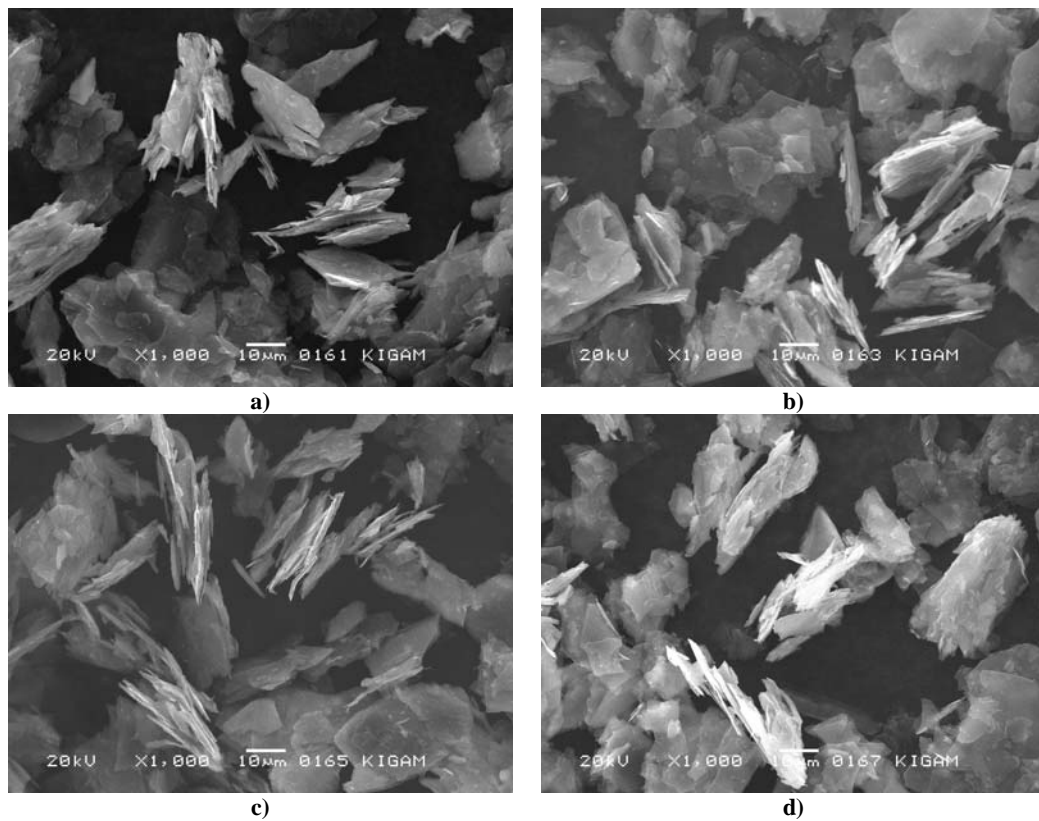


Fig. 7. SEM images of graphite samples expanded at 230°C for; (a) 1 min (#4), (b) 4 min (#6), (c) 15 min (#8), and (d) 1 hour (#10) (# are based on Table 2)

Figure 8 is the SEM images of graphite samples treated at 210, 230, and 250 °C for 3 hours. Similarly to the previous cases, there was little difference in shape between samples but some difference in expansion ratio. Especially, in spite of enough expanding time, there were not expanded particles. It implies that there are other factors affecting expansion of graphite powders, such as the shape of particle, structure of layer system or reagents.

Figure 9 shows the shape of graphite particles treated by alkali reagent. There also existed expanded particles and no expanded particles together, and some white particles having indeterminate form were observed on the surface of large particles, or between particles. These untypical particles are very likely silica particles

recrystallized by alkali treatment and drying. in Fig. 9(b) some peculiar shapes were observed. These are particles having damaged layer structures which might be caused by gasification and chemical treatments. This phenomenon was thought to be helpful to improve the efficiency of fine grinding process.

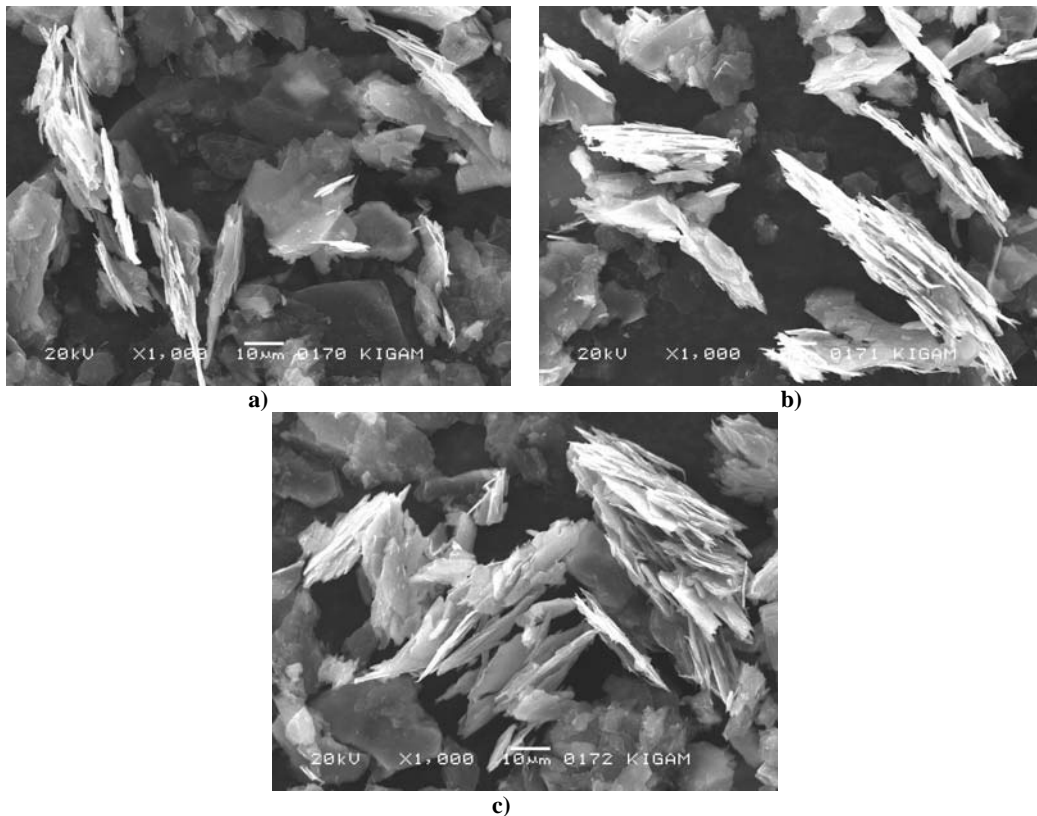


Fig. 8. SEM images of graphite samples expanded for 3 hours at; (a) 210 (#13), (b) 230 (#14) and (c) 250°C (#15) (No. are based on Table 2)

CONCLUSIONS

Several set of tests were conducted to make the high-grade graphite samples suitable for producing high-value fine graphite powders. To do this, typical acid/alkali treatment and low-expansion process were used. After the acid treatment and gasification at low temperature, the crystallinity of graphite particle decreased and only small change of the layer gap was observed. By acid treatment, using the mixture of sulfuric acid and hydrogen peroxide, about 20% of impurities, most likely metallic impurity, were removed. Gasification at low temperature (about 230°C) could help

produce low-expanded graphite powders. After the gasification, we observed about 30% volume increase for 3 hours heating. Despite more or less non-homogeneous expansion, there were not excessively expanded particles which were unfavorable to the grinding process. Final samples, produced by acid treatment, gasification and alkali treatment, showed 3.91% of ash contents, and some damaged-layer structures were observed.

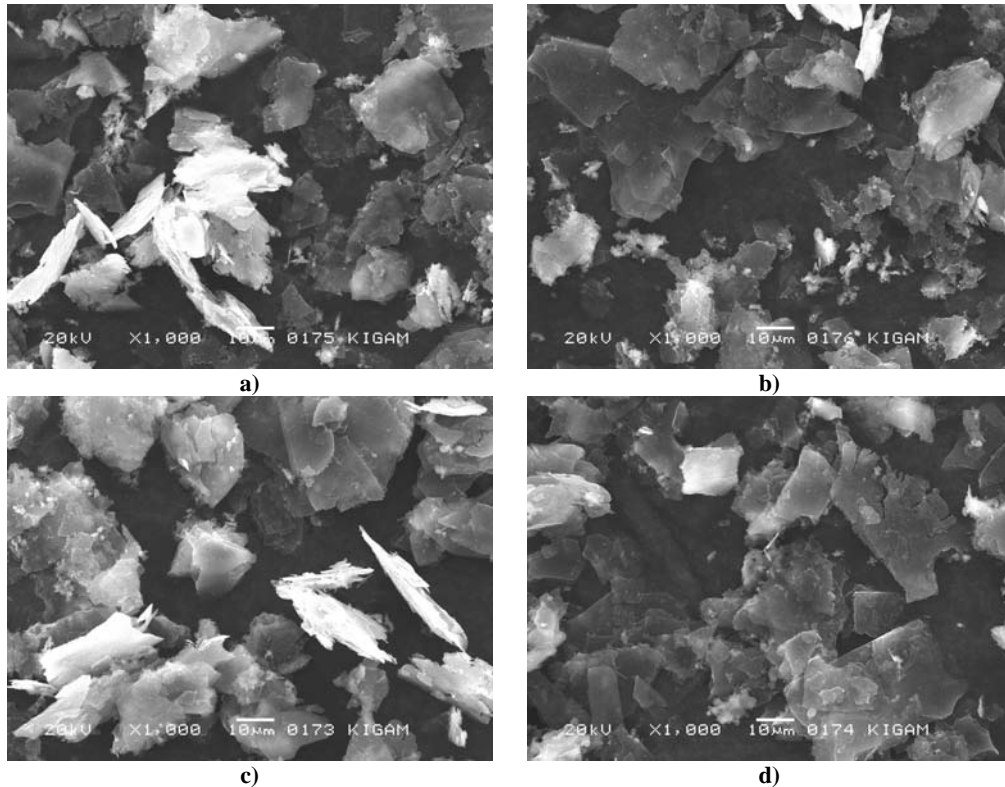


Fig. 9. SEM images of graphite samples; (a) treated with acid and alkali reagent without gasification (#27) and (b) treated with alkali reagent after acid treatment and expansion in SIC furnace for 3 hours at 230 C (#28) (No. are based on Table 2)

ACKNOWLEDGEMENT

This research was supported by the General Research Project of the Korea Institute of Geoscience and Mineral Resources (KIGAM) funded by the Ministry of Science and Technology (MOST) of Korea.

REFERENCES

- KORES, 2007, *Homepage of Korea Mineral Resources Information Service (KOMIS)*, <http://www.kores.net>.
 Kim, B., 2001, *Ultrafine Grinding and Surface Modification for High Performance Graphite Powder*, Ph.D Thesis, Kangwon National University, Korea.

- Lee, S., 2000, *The Classes of Graphite and their Usage*, Mineral & Industry, The Mineralogical Society of Korea, vol. 13, no. 2, pp. 40-50.
- Jung, J. et al, 1991, *Study on high purification of crystalline graphite with domestic products*, Studies on the technical development of metallurgy (KR-91-3B), Korea Institute of Geoscience and Mineral Resources (KIGAM), pp. 61-124.
- Bouvard, D., Lanier, J. and Stutz, P., 1988, *Mechanical Behaviour of Graphite Powder*, Powder Technology, vol. 54, pp. 175-181.
- KSIC, 2002, *Testing Method for Ash in Graphite*, Korean Industrial Standards (KS L 3412:2002), Korea Standards Information Center.

Jeongyun Kim, Byounggon Kim, *Oczyszczanie naturalnego grafitu metodami chemicznymi oraz ograniczonej ekspansji*, Physicochemical Problems of Mineral Processing, 41 (2007), 37-49 (w jęz. ang.).

Naturalny rozdrobniony grafit wykazuje dobrą odporność na ogrzewanie, niską rozszerzalność oraz małe przewodnictwo i jest używany do jako materiał wysoko wydajnych baterii, do smarowania, itd. Proszek grafitowy, aby mógł być zastosowany jako materiał zaawansowanych technologii, jest oczyszczany i modyfikowany powierzchniowo. Kraje rozwinięte produkują wysokiej jakości proszek grafitowy metodą interkalacji i sub-mikronowego rozdrabniania. Obecnie badania zostały przeprowadzone dla wykorzystania niskiej jakości naturalnego grafitu jako źródło nano-materiału. Dla produkcji ultradrobno proszku grafitowego przeprowadzono badania dotyczące wstępnej modyfikacji stosując typowy proces ekspansji i modyfikacji „kwas/zasad”. Zastosowano niską temperaturę gazyfikacji w porównaniu do tradycyjnego procesu, co pozwala uzyskać odpowiedni stopień ekspansji w celu efektywnej obróbki chemicznej i rozdrabniania. Proces ekspansji prowadzono w temperaturze 200~250°C dla uzyskania 20~30% wzrostu objętości ponieważ ekspansja proszku grafitowego, stosując tradycyjne podejście, tj. wysokie temperatury, prowadzi do słabej efektywności rozdrabniania.

Marian BROŻEK*, Anna MŁYNARCZYKOWSKA**

ANALYSIS OF KINETICS MODELS OF BATCH FLOTATION

Received March 15, 2007; reviewed; accepted June 8, 2007

Flotation as a kinetic and thermodynamic phenomenon is a random process. The random variable determining the number of particles in flotation, attached permanently to the bubble surface, and consequently also the recovery, depend on time. Numerous models of flotation kinetics have been worked out to describe this dependence. Each of these models covers in fact a separate aspect of the problem but they complement each other. The paper presents a detailed analysis of the models based on the kinetics of chemical reactions and on the model of chemical absorption. It results from analysis of these models that in the case of flotation of the feed which is non-homogeneous with respect to flotation properties in the initial moments of the process, the particles undergoing flotation have the highest flotation properties according to the equation of zero order and, next, according to the equation of 1/2 order. With time, the particles of decreasing ability to flotation undergo flotation and, simultaneously, the order of flotation kinetics increases. Narrow size-and-density coal fractions of intermediate floatability (type 33 of Polish classification) float according to the first order kinetic equation. From the theoretical point of view they can be assumed to be a homogenous material with respect to flotation properties.

Key words: flotation, chemical reaction, kinetics model, absorption model, flotation kinetics order

INTRODUCTION

Flotation as a process resulting from selective adhesion of mineral particles to air bubbles is both a thermodynamic and kinetic phenomenon. Kinetics, the course of the process in time, is affected by potential interactions of electromagnetic type between the mineral particle and the bubble. The interaction is necessary for adhesion. It is a random variable, and it also results from the successive inflow of the free surface in the form of air bubbles into the flotation system. The free surface is the place of adhesion of mineral particles and it limits, among others, the velocity of the process.

* AGH University of Science and Technology, Faculty of Mining and Geoinforming, Department of Mineral Processing and Environmental Protection, Al. Mickiewicza 30, 30-065 Kraków, Poland, tel/fax(48-12)617-21-98, e-mail: * brozek@agh.edu.pl; ** mindziu@agh.edu.pl.

The random character of interactions results from the fact that the particle surface properties determine the interaction and these properties change not only from one particle to another but they can also within the surface of the same particle.

To obtain a permanent adhesion of particle and bubble, the particle must overcome the energy barrier of the particle-bubble interaction. This phenomenon is of random character because of the random character of collision and the angle of collision of the particle with the bubble, as well as the random value of particle kinetic energy necessary to rupture of the thin film between particle and the air bubble. Apart from the above phenomena, the attached particle, especially the larger ones, can be detached from the bubble surface by external forces, present in the flotation chamber, the source of which originates from turbulences of the medium. This process is also of random character.

The process of bubble mineralization can be also considered as the adsorption process in which the role of adsorbent is played by the bubble surface while mineral particles fulfill the role of adsorbate. This is a selective adsorption whose selectivity depends on the interface energy, determined by surface properties of particles and the reagent system.

Due to the multi-topic character of problems determining the flotation course and affecting the process of mineralization of air bubbles, many authors dealt with the problem of flotation kinetics in the last several decades (Zuniga, 1935; Schuhmann, 1942; Sutherland, 1947; Pogorelyj, 1961ab, 1962, Melkich, 1963a, 1963b, 1964; Bogdanov et al., 1964; Volin and Swami, 1964; Bodziony, 1965; Zeidenberg et al., 1964; Harris and Rimmer, 1966; Loveday, 1966; Tille and Panou, 1968, Kapur and Mehrotra, 1973, 1974; Mehrotra and Kapur, 1974, 1975; Trahar and Warren, 1976; Collins and Jameson, 1976; Harris, 1978; Maksimov and Emelianov, 1983; Xu Changlian, 1985; Szatkowski and Freyberger, 1985a,b; Vanangamudi and Rao, 1986; Lasic and Calic, 2000; Brozek and Młynarczykowska, 2006). Many models of flotation kinetics were developed, from the deterministic and adsorption models to statistical and stochastic ones, out of which each dealt with another aspect.

This paper presents a critical analysis of the model based upon the model of kinetics of chemical reaction and the model of adsorption. This analysis has been supported by the example of flotation kinetics of narrow coal density fractions.

MODEL OF KINETICS OF CHEMICAL REACTION

The first kinetics model of batch flotation was proposed by Zuniga (1935). He applied the differential equation of kinetics of chemical reaction which, in its general form, can be written as:

$$\frac{dC}{dt} = -k C^n \quad (1)$$

where: $C(t)$ – concentration of floating particles remaining in the flotation chamber up to the moment t , k – flotation rate constant, n – constant characterizing the order character of the process (order of flotation kinetics).

Equation 1 represents flotation kinetics of particles which are homogeneous from the point of view of surface properties, the so-called equally well floating particles which have the same value of the flotation rate constant.

The solution of Eq. 1, with the initial condition: $C(t=0) = C_o$, is as follows:

$$C(t) = \left[(n-1) k t + C_o^{(1-n)} \right]^{\frac{1}{1-n}} \quad \text{for } n \neq 1 \quad (2)$$

where C_o denotes the initial concentration of particles under flotation in the flotation chamber.

The recovery of the particles in the froth product ε after time t is, from the recovery definition, equal to

$$\varepsilon = \frac{C_o - C}{C_o} = 1 - \frac{C}{C_o} \quad (3)$$

According to Eqs. 2 and 3, the term C/C_o and recovery ε are expressed by the formulas:

$$\frac{C}{C_o} = \left[1 + (n-1) C_o^{n-1} k t \right]^{\frac{1}{1-n}} \quad \text{for } n \neq 1, \quad (4)$$

$$\varepsilon(t) = 1 - \left[1 + (n-1) C_o^{n-1} k t \right]^{\frac{1}{1-n}} \quad \text{for } n \neq 1. \quad (5)$$

The limit values $\varepsilon(t)$ for $n > 1$ are

$$\lim_{t \rightarrow \infty} \varepsilon(t) = 1. \quad (6)$$

It means that after a long time of flotation all particles will have undergone flotation. In the general case, especially for larger and more difficult-to-float particles, it does not have to be so because despite the adhesion process of particles to air bubbles, a reverse process occurs (of lower intensity), i.e. detachment of the particles from the surface of bubbles into the pulp (Mika and Fuerstenau, 1968; Schulze, 1977; Woodburn et al., 1971; Stachurski, 1970; Schulze, 1992; Maksimov and Emelianov, 1983). Accordingly, in the state of equilibrium, the value of recovery after a long time of flotation is smaller than 1 and equals ε_{∞} . After imposing the following condition upon Eq. 5

$$\lim_{t \rightarrow \infty} \varepsilon(t) = \varepsilon_{\infty} \quad (7)$$

the dependence of recovery on time is:

$$\varepsilon(t) = \varepsilon_{\infty} \left\{ 1 - \frac{1}{\left[1 + (n-1) C_o^{n-1} k t \right]^{\frac{1}{n-1}}} \right\} \quad \text{for } n > 1 . \quad (8)$$

Equations 5 and 8 represent a general formula of flotation kinetics of n order, obtained from the solution the differential equation of chemical reaction kinetics.

ADSORPTION MODEL OF FLOTATION KINETICS

From the physical point of view, the process of flotation is closed to the process of adsorption (Pogorelyj, 1962). The role of adsorbent is played by air bubbles (bubbles surface) while the role of adsorbate by mineral particles. Analogically, as in the process of adsorption (Oscik, 1973), the time of contact of particle with air bubble, leading to the stable connection of a particle with a bubble (induction time), is very short.

Adsorption occurs on the bubble surface, and therefore the number of mineral particles attached (adsorbed) to bubbles is proportional to the free, still not mineralized, surface of bubbles. For the material, homogeneous from the point of view of flotation properties, the mass of particle attached to the bubbles surface in time $d\tau$ is:

$$dm = \lambda s C d\tau \quad (9)$$

where: λ - mineralization (adsorption) rate constant (mass of particles adsorbed for a bubble surface unit in a unit of time), s – free surface of bubbles coming to the flotation chamber in the unit time, τ - time of remaining of a bubble in the flotation chamber, C – volume concentration of particle in the flotation chamber.

As a result of mineralization, the free (not mineralized) surface of bubble decreases. The decrease of this surface in a unit of time is equal to:

$$-ds = \frac{1}{\alpha} dm \quad (10)$$

where: α -mass of particles adsorbed by the bubble surface unit. From Eqs. 9 and 10 we obtain:

$$ds = -\frac{\lambda s C}{\alpha} d\tau \quad (11)$$

After solving Eq. 11, at the initial condition $s(0) = s_o$ we obtain the dependence:

$$s = s_o \exp\left(-\frac{\lambda C}{\alpha} \tau\right). \quad (12)$$

The mineralized surface in a unit of time will be expressed by the formula:

$$s_o - s = s_o \left[1 - \exp\left(-\frac{\lambda C}{\alpha} \tau\right)\right]. \quad (13)$$

According to the above, the decrease of mineral mass from the flotation pulp in time dt is:

$$-dm = \alpha s_o \left[1 - \exp\left(-\frac{\lambda C}{\alpha} \tau\right)\right] dt. \quad (14)$$

If the volume of the flotation chamber is V then $dm = V dC$ and from expression (14), the following equation is obtained:

$$\frac{dC}{1 - \exp\left(-\frac{\lambda \tau}{\alpha} C\right)} = -\frac{\alpha s_o}{V} dt. \quad (15)$$

The integer on the left side of expression (15) is equal to (Gradstein and Ryzik 1971):

$$\int \frac{dC}{1 - \exp\left(-\frac{\lambda \tau}{\alpha} C\right)} = -\frac{\alpha}{\lambda \tau} \ln \left[\frac{\exp\left(-\frac{\lambda \tau}{\alpha} C\right)}{1 - \exp\left(-\frac{\lambda \tau}{\alpha} C\right)} \right]. \quad (16)$$

After integrating the entire expression (15) and transforming it, the following dependence is obtained:

$$\frac{\exp\left(-\frac{\lambda \tau}{\alpha} C\right)}{1 - \exp\left(-\frac{\lambda \tau}{\alpha} C\right)} = D \exp\left(\frac{\lambda \tau s_o}{V} t\right) \quad (17)$$

where D is the constant of integrating, calculated from the initial condition $C(0) = C_o$.

After calculating constant D and substituting into Eq.17, the following equation is obtained:

$$\exp\left(\frac{\lambda \tau}{\alpha} C\right) = \left\{ \left[\exp\left(\frac{\lambda \tau C_o}{\alpha}\right) - 1 \right] \exp\left(-\frac{\lambda \tau s_o}{V} t\right) + 1 \right\}. \quad (18)$$

From Eq.18 we obtain the dependence of volume concentration of particles in the flotation chamber upon time:

$$C(t) = \frac{\alpha}{\lambda \tau} \ln \left\{ \left[\exp\left(\frac{\lambda \tau C_o}{\alpha}\right) - 1 \right] \exp\left(-\frac{\lambda \tau s_o}{V} t\right) + 1 \right\}. \quad (19)$$

The recovery of the floated mineral in the froth product after flotation time t , according to Eq. 3 will be:

$$\varepsilon(t) = 1 - \frac{\alpha}{\lambda \tau C_o} \ln \left\{ \left[\exp\left(\frac{\lambda \tau C_o}{\alpha}\right) - 1 \right] \exp\left(-\frac{\lambda \tau s_o}{V} t\right) + 1 \right\}. \quad (20)$$

It results from Eq. 20 that the recovery depends on the volume concentration of particle in the flotation chamber C_o , flotation properties of particle measured by value λ , size of free surface of bubbles s_o , and flotation time t .

ANALYSIS OF FLOTATION KINETICS MODELS

KINETICS EQUATIONS OF ZERO AND $\frac{1}{2}$ ORDER

Particular cases of kinetics equations of zero and $\frac{1}{2}$ orders, based on the model of chemical reaction, can be obtain by means of formal setting the order of kinetics in Eq. 5 or by a series expansion of the general equation of flotation kinetics.

From Eq. (5) for $n = 0$ we obtain the following dependence:

$$\varepsilon(t) = \frac{k t}{C_o}. \quad (21)$$

Therefore, it is a rectilinear dependence. The rate constant in this case is:

$$k = C_o \frac{d\varepsilon}{dt}. \quad (22)$$

Subsequently, with the increase of the initial volume concentration of particle, the rate constant of flotation increases because $\frac{d\varepsilon}{dt} = const$. It results from Eq. 21 that the

recovery reaches the maximum value of 1, theoretically after the finite flotation time equal to $t_m = \frac{C_o}{k}$. It means that if the flotation of equally floating particles occurs according to the equation of zero order, there is no equilibrium detachment from air bubbles.

Equation 21 can be obtained from Eq. 5 in a different way. The expression in the square brackets of Eq. 5 is a binomial in relation to variable t . For small values of flotation time t , the second component of the binomial is small. The extension of binomial into a power series for $|x| < 1$ is as follows (Leja 1971):

$$(1+x)^m = 1 + mx + \frac{m(m-1)}{2!}x^2 + \dots + \frac{m(m-1)\dots(m-k+1)}{k!}x^k + \dots \quad (23)$$

Leaving two terms of extension in Eq. 5 we obtain:

$$\varepsilon(t) \cong C_o^{n-1} k t. \quad (24)$$

It is therefore possible, according to Eq. 24, to express an opinion that at initial moments of flotation, it always runs due to the rectilinear dependence. This equation for $n = 0$ is transformed into Eq. 24. Substituting the value $\frac{1}{2}$ for n in Eq.5 we obtain the following dependence of recovery on time:

$$\varepsilon(t) = \frac{k t}{\sqrt{C_o}} - \frac{k^2 t^2}{4 C_o}. \quad (25)$$

The dependence $\varepsilon(t)$, according to Eq. 25 is presented by a section of a parabola. Recovery reaches the maximum value after time $t_m = \frac{2\sqrt{C_o}}{k}$, equal $\varepsilon_{max} = \varepsilon(t_m) = 1$. Therefore, similarly to the kinetics of zero order, there is no detachment of particles in the sense of a stochastic process. The equation of kinetics of $\frac{1}{2}$ order, analogically to the former case, can be obtained from a general Eq. 5 by a series expansion. Expanding the expression included in the square bracket of Eq. 5 and considering three terms of expansion, the following dependence for $\varepsilon(t)$ is obtained:

$$\varepsilon(t) \cong C_o^{n-1} k t - \frac{1}{2} n C_o^{2(n-1)} k^2 t^2 \quad (26)$$

which for $n = 0.5$ can be transformed into dependence given by Eq. 25. It can be therefore said that for each flotation process there is a time range in which the recovery depends on time, according to the $\frac{1}{2}$ order kinetics equation. If, for obtaining

Eq. 26, the three term of expansion should be taken into consideration to get the required accuracy, it means that the interval of process duration in which flotation occurs according to the kinetics equation of $\frac{1}{2}$ order must be longer than in the kinetics of zero order. Hence, it can be concluded that after flotation according to the kinetics equation of zero order the process runs according to the equation of $\frac{1}{2}$ order.

Successively, the analysis of the kinetics model based on the process of adsorption leads to the following observations. In the initial moments of flotation, i.e. small value of time t , high volume concentration of particle in the flotation chamber C , not very much different from C_o , high value of λ since, first of all, the particles of the highest floatability are floating and at low of the surface accessible for adsorption in the time range τ , because the bubbles are quickly mineralized by the easily floating particles, Eq. 20 can be transformed as follows. For small values of s_o and t , $\exp\left(-\frac{\lambda \tau s_o}{V} t\right) \cong 1 - \frac{\lambda \tau s_o}{V} t$, and Eq. (20) transforms into the form:

$$\varepsilon(t) = 1 - \frac{\alpha}{\lambda \tau C_o} \left[\frac{\lambda \tau C_o}{\alpha} + \ln\left(1 - \frac{\lambda \tau s_o}{V} t\right) \right] \quad (27)$$

For small values s_o and t $\ln\left(1 - \frac{\lambda \tau s_o}{V} t\right) \cong -\frac{\lambda \tau s_o}{V} t$ (Leja, 1971) and the dependence of recovery upon the time of flotation is:

$$\varepsilon(t) = \frac{\alpha s_o}{V C_o} t = \frac{k t}{C_o} \quad (28)$$

where: $k = \frac{\alpha s_o}{V}$. Therefore we obtain the kinetics equation of zero order, analogical to Eq. 21. It can be said that according to the kinetics equation of zero order the particles which undergo flotation are the most easily floatable (of the highest λ values), which mineralize quickly the surface of the bubbles and consequently, the free surface of the bubble, accessible for the adsorption of consecutive particle in the time range τ , i.e. the time of the bubble remaining in the flotation chamber is small at large values of λ and C , according to Eq.12.

KINETICS EQUATION OF THE FIRST ORDER

The kinetics equation of the first order will be obtain from Eq. 8 by means of the transition with the order of equation n to 1. Denoting $\frac{1}{1-n} = m$, Eq.8 can be written as the following function sequence:

$$\varepsilon_m(t) = \varepsilon_\infty \left\{ 1 - \left[1 - C_o^{-1/m} \frac{k t}{m} \right]^m \right\}. \quad (29)$$

If n heads for 1, then m heads for infinity. Hence, the limit of the function sequence $\varepsilon_m(t)$ is:

$$\lim_{m \rightarrow \infty} \varepsilon_m(t) = \varepsilon(t) = \varepsilon_\infty (1 - e^{-k t}) \quad (30)$$

because the expression with square brackets in Eq. 29 heads for $e^{-k t}$ ($C_o^{-1/m} \rightarrow 1$). This is the form of the kinetics equation which is most often applied for investigation of flotation kinetics. As it can be seen from Eqs. 8 and 30, only in the case of flotation kinetics of the 1st order the course of dependence of recovery upon time does not depend on the initial concentration of particles in the flotation chamber. This is a criterion stating that for a given raw material, under given physicochemical conditions, flotation occurs according to the kinetics equation of the first order (Loveday, 1966). It results from the adsorption model of flotation kinetics that after a long flotation time t , i.e. low volume concentration of particles and low value of λ , the free surface, accessible for adsorption, is larger according to Eq. 12. Under these conditions $\exp\left(\frac{\lambda \tau C_o}{\alpha}\right) \cong 1 + \frac{\lambda \tau C_o}{\alpha}$ and Eq. 20 assumes the form:

$$\varepsilon(t) = 1 - \frac{\alpha}{\lambda \tau C_o} \ln \left[1 + \frac{\lambda \tau C_o}{\alpha} \exp\left(-\frac{\lambda \tau s_o}{V} t\right) \right] \quad (31)$$

Expanding the logarithmic expression into a series and considering the 1st component of expansion, Eq. 31 simplifies to the form:

$$\varepsilon(t) \cong 1 - \exp\left(-\frac{\lambda \tau s_o}{V} t\right). \quad (32)$$

The equation of kinetics of the first order is obtained. Therefore flotation according to the kinetics equation of the first order runs after a longer flotation time in the conditions of lower concentration of particles in the flotation chamber, larger free surface of the bubble in the time τ and lower values of λ .

EQUATIONS OF KINETICS OF HIGHER ORDERS

Higher orders of kinetics equations are obtained from the basic equation (Eq. 8) after substituting a proper value for n .

a) kinetics equation of the 1.5th order:

$$\varepsilon(t) = \varepsilon_{\infty} \left[1 - \frac{1}{\left(\frac{1}{2} \sqrt{C_o} k t + 1 \right)^2} \right] \quad (33)$$

b) kinetics equation of the 2nd order:

$$\varepsilon(t) = \varepsilon_{\infty} \frac{C_o k t}{1 + C_o k t} \quad (34)$$

c) kinetics equation of the 3rd order:

$$\varepsilon(t) = \varepsilon_{\infty} \left[1 - \frac{1}{\sqrt{1 + 2 C_o^2 k t}} \right] \quad (35)$$

d) kinetics equation of the 4th order:

$$\varepsilon(t) = \varepsilon_{\infty} \left[1 - \frac{1}{\sqrt[3]{1 + 3 C_o^3 k t}} \right] \quad (36)$$

e) kinetics equation of the 5th order:

$$\varepsilon(t) = \varepsilon_{\infty} \left[1 - \frac{1}{\sqrt[4]{1 + 4 C_o^4 k t}} \right] \quad (37)$$

f) kinetics equation of the 6th order:

$$\varepsilon(t) = \varepsilon_{\infty} \left[1 - \frac{1}{\sqrt[5]{1 + 5 C_o^5 k t}} \right] \quad (38)$$

Pictorial $\varepsilon(t)$ dependence for the above models are shown in Fig. 1.

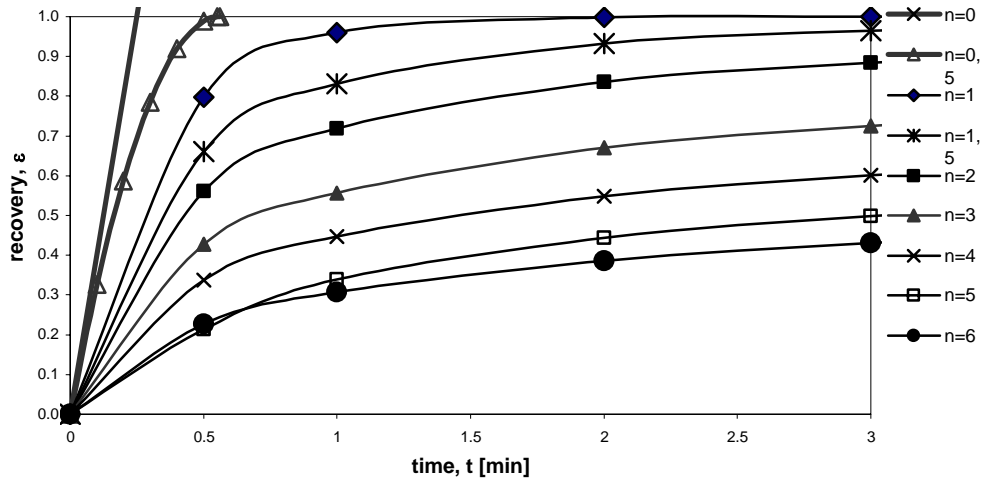


Fig. 1. Pictorial dependence of flotation recovery on time for kinetics orders from $n = 0$ to $n = 6$

ORDER OF FLOTATION KINETICS

In the model of flotation kinetics of the first order based upon the kinetics of chemical reaction the model parameters are the flotation rate constant and equilibrium recovery while in the stochastic model the parameters are the permanent adhesion rate constant and the detachment rate constant of the particle from the bubble (Brozek and Mlynarczykowska, 2006). In the stochastic model both the equilibrium recovery and the flotation rate constant (constant of resultant adhesion) are connected by function with the constants of adhesion and detachment. In both cases these are the two-parameter models. The constants of adhesion and detachment are expressed by probabilities of collision, adhesion and detachment of the particles from the bubble which, respectively, are connected with geometrical and surface properties of particles as well as physicochemical and hydrodynamic conditions in the flotation chamber. In the model of flotation kinetics of the n -th order (Eq. 8), apart from the flotation rate constant and equilibrium recovery, the third parameter occurs, i.e. the order of flotation kinetics. For the flotation carried out under conditions when the surface accessible for adsorption is large (free flotation) Pogorelyj (1962) presented the following expression for the order of flotation kinetics:

$$n = 1 + \frac{\lg \frac{\lambda}{\lambda_0}}{\lg C} \tag{39}$$

where: λ - average value of the adsorption rate constant of particles at the concentration of particles in the flotation chamber C , λ_0 - average value of the adsorption rate constant at the initial moment. Melkich (1964) worked out an

analogical expression for the order of flotation kinetics, starting from the statistical theory of flotation:

$$n = 1 + \frac{\sigma^2}{\lambda^2} \quad (40)$$

where: σ^2 – dispersion (variance) of flotation properties around the average value. It results from Eqs. 39 and 40 that only for the feed strictly homogeneous with respect to flotation properties, the order of flotation kinetics is equal to 1, since $\lambda = \lambda_0$ and $\sigma^2 = 0$. However, such a distribution of flotation properties of the feed is exclusively theoretical in character because even in the narrow size fraction of the pure mineral the distribution of induction time is connected with the statistical distribution of adsorption density of the reagent on the particle surface (Schulze, 1992) and also with the distribution of particle shape and size. Consequently, even for pure minerals, the adhesion rate constant, and also the order of flotation kinetics, will be characterized by fixed distributions. The investigations of flotation kinetics of pure minerals of narrow size fraction proved that under conditions of free flotation, i.e. when the surface of bubbles is not a limitation for their mineralization, the flotation results are consistent with the equations of the first order (Pogorelyj 1961 a,b; Tomlinson and Fleming, 1963).

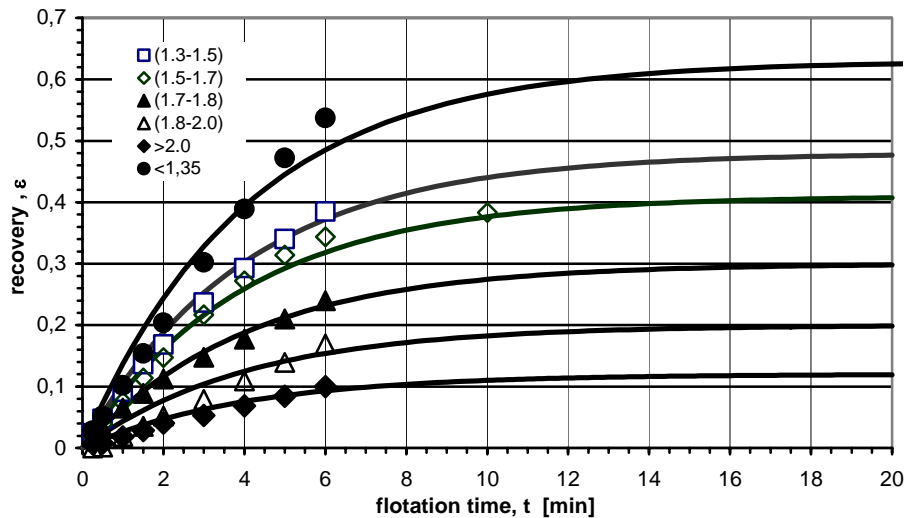


Fig.2. Flotation kinetics (Brozek and Młynarczykowska, 2006):

density fraction <1.35 [Mg/m^3], $A=1.06\%$, $\varepsilon=0.63(1-e^{-0.245t})$, $\lambda_0=0.154$ [1/min],
density fraction $(1.35-1.5)$ [Mg/m^3], $A=7.91\%$, $\varepsilon=0.48(1-e^{-0.249t})$, $\lambda_0=0.12$ [1/min],
density fraction $(1.5-1.7)$ [Mg/m^3], $A=23.18\%$, $\varepsilon=0.41(1-e^{-0.25t})$, $\lambda_0=0.102$ [1/min],
density fraction $(1.7-1.8)$ [Mg/m^3], $A=36.32\%$, $\varepsilon=0.30(1-e^{-0.246t})$, $\lambda_0=0.074$ [1/min],
density fraction $(1.8-2.0)$ [Mg/m^3], $A=48.71\%$, $\varepsilon=0.20(1-e^{-0.245t})$, $\lambda_0=0.079$ [1/min],
density fraction >2.0 [Mg/m^3], $A=77.63\%$, $\varepsilon=0.12(1-e^{-0.249t})$, $\lambda_0=0.03$ [1/min]

Also the investigations of flotation kinetics of narrow size-and-density fractions of intermediately floating coal type 33 proved that the result of flotation fulfill the equation of the first order. Figure 2 shows the curves of flotation kinetics of narrow size-and-density fractions of coal type 33 (Brozek and Mlynarczykowska, 2006). The index of curvilinear correlation, evaluating the rate of agreement of the model with the experiment is larger than 0.96. Therefore it can be said that according to Eq. 40 the rate of non-homogeneity of flotation properties of particle forming narrow size-and-density fractions is within the limit of experiment error and is negligibly little. If the feed is non-homogenous with respect to its flotation properties, as mentioned before, at first the particles of the highest floatability undergo flotation. Respectively, the average value of flotation properties of particle remaining in the flotation chamber decreases with time and also the concentration of floating particles changes.

Therefore, the order of flotation kinetics changes. According to Bogdanov (1959), the order of flotation kinetics changes during the process from 0 to 6 (Bogdanov 1959, according to Pogorelyj 1962). On the other hand, however, there are no theoretical premises stating that in a wide time range the flotation process of the non-homogeneous material will run according to the equation of a fixed order.

ACKNOWLEDGEMENTS

The paper has been written within the European Union grant “Scientific Network-Surfactant and Dispersed System in Theory and Practice”. Contract no INCO-CT-2003-003355, and supported by a grant of the National Research Committee no 4 T12A 035 30

REFERENCES

- BOGDANOV O.S., PODNIAK A.K., (1959), Rep. Invest. of Mechanobr Inst., vol.124 Leningrad (in Russian).
- BOGDANOV O.S., HAINMAN V.J., MAXIMOV I.I., (1964), *On certain physical – mechanical factors determining the rate of flotation*. Proc. VII IMPC, New York, Gordon & Breach, p.169 – 174.
- BODZIONY J., (1965), *On the analogy between a deterministic and a stochastic model of the kinetic of flotation*. Bull. Pol. Acad. Sci., 13, 485 – 490.
- BROŹEK M., MŁYNARCZYKOWSKA A., (2006), *Application of the stochastic model for analysis of flotation kinetics with coal as an example*. Physicochemical Problems of Mineral Processing, 40, 31-44.
- CHANGLIAN XU, (1985), *Kinetic models for batch and continuous flotation in a flotation column*. Proc. XV IMPC, Cannes, vol. III, p.16-27.
- COLLINS G.L., JAMESON G.J., (1976), *Experiments on the flotation of fine particles. The influence of particle size and charge*. Chem. Eng. Sci., 31, 985-991.
- GERSTENKORN T., SRODKA T., (1983) *Kombinatoryka i rachunek prawdopodobienstwa*, PWN, Warszawa.
- GRADSTEIN I.S., RYZIK I.M., (1971), *Tablicy integralow, summ, riadov i proizvedenij*.Izd. Nauka, Moskva.
- HARRIS C.C., RIMMER H.W., (1966) *Study of two-phase model of the flotation process*. Trans. IMM, 75, 153-162.
- HARRIS C.C., (1978) *Multiphase model of flotation machine behaviour*. Int. J. Miner. Process.,5, 107-129.

- KAPUR P.C., MEHROTRA S.P., (1973), *Phenomenological model for flotation kinetics*. Trans. IMM, 82, 229–234.
- KAPUR P.C., MEHROTRA S.P., (1974), *Estimation of the flotation rate distributions by numerical inversion of the Laplace transform*. Chem. Eng. Sci., 29, 411 – 415.
- LAZIC P., CALIC N., (2000), *Boltzman's model of flotation kinetics*. Proc. XXI IMPC (Rome), vol. B, p. B8a 87-93.
- LEJA F., (1971), *Rachunek różniczkowy i całkowy*. PWN, Warszawa.
- LOVEDAY B.K., (1966), *Analysis of froth flotation kinetics*. Trans. IMM, 75, 219-225.
- MAKSIMOV I.I., EMELJANOV I.I., (1983), *The effect of turbulence on detachment process in the flotation pulp*. Obogascenie rud, no 2, 16-19, (in Russian).
- MEHROTRA S.P., KAPUR P.C., (1974), *The effects of aeration rate, particle size and pulp density on the flotation rate distribution*. Powder Technology, 9, 213-219.
- MEHROTRA S.P., KAPUR P.C., (1975), *The effect of particle size and feed rate on the flotation rate distribution in a continuous cell*. Int. J. Miner. Process., 2, 15-28.
- MELKICH V.I., (1963a), *A statistical theory of the flotation process*. Obogascenie rud, no 6, 17–20 (in Russian).
- MELKICH V.I., (1963b), *The equation of statistical dynamic of the flotation process*. Obogascenie rud. no 4, 26 – 28 (in Russian).
- MELKICH V.I., (1964), *Experimental verification of statistical model of the flotation process*. Obogascenie rud, no 5, 42-43, (in Russian).
- MIKA T., FUERSTENAU D., (1968), *A microscopic model of the flotation process*. Proc. Proc. VIII IMPC, Leningrad, vol. II, pp.246-269.
- OSCIK J., 1973. *Adsorpcja*. PWN, Warszawa.
- POGORELYJ A.D., DEMIDO N.M., MATVEJEV I.I., (1961a), *The certain principles of performance of multi-cell flotation machine*. Izv. VUZ Tsvetnaja Metallurgia, no 6, 16-25, (in Russian).
- POGORELYJ A.D., (1961b), *On flotation characteristic of industrial pulp*. Izv. VUZ Tsvetnaja Metallurgia, no 5, 59-68, (in Russian).
- POGORELYJ A.D., (1962), *The range of application of Beloglazov equation of the kinetics*. Izv. VUZ Tsvetnaja Metallurgia, no 1, 33-40, (in Russian).
- SCHUHMANN R., (1942), *Flotation kinetics I. Methods for steady-state study of flotation problems*. J. Phys. Chem. 46, 891–902.
- SCHULZE H.J., (1977), *New theoretical and experimental investigations on stability of bubble particle aggregates in flotation: a theory on the upper particle size of floatability*. Int. J. Miner. Process., 4, 241-259.
- SCHULZE H.J., (1992), *Interface actions in mineral processes*. Aufber. Technik, 33, 434-443.
- STACHURSKI J., (1970), *The Mathematical Model for the Ion – Extraction Flotation Process*. Archiwum Górnictwa 15, 219 – 229.
- SUTHERLAND K.L., (1948), *Physical chemistry of flotation – XI kinetics of the flotation process*, J. Phys. Chem. 52, 394 – 425.
- SZATKOWSKI M., FREYBERGER W.L., (1985 a), *Kinetic of flotation with fine bubbles*. Trans. IMM, 94, 61-70.
- SZATKOWSKI M., FREYBERGER W.L., (1985 b), *Model describing mechanism of the flotation process*. Trans. IMM, 94, 129-135.
- TILLE R., PANU G., (1968), *Some considerations on flotation kinetics*. Proc. VIII IMPC, Leningrad, vol. II, p.487-499.
- TOMLINSON H.S., FLEMING M.G., (1963), *Flotation rate studies*. Proc. VI IMPC, Cannes, Pergamon Press, Oxford – New York, pp. 563-579.
- TRAHAR W.J., WARREN L.J., (1976), *The flotability of very fine particles – a review*. Int. J. Miner. Process., 3, 103-131.
- VANANGAMUDI M., RAO T.C., (1986), *Modelling of batch coal flotation*. Int. J. Miner. Process., 16, 231-243.

- VOLIN M.E., SWAMI D.V., (1964), *Flotation rates of iron oxides*. Proc. VII IMPC, New York, Gordon & Breach, p.193-206.
- WOODBURN E.T., KING R.P., COLBORN R.P., (1971), *The effect of particle size distribution on the performance of a phosphate flotation process*. Metall. Trans., 2, 3163-3174.
- ZAIDENBERG I. S., LISOVSKIJ D.I., BUROVOJ I.A., (1964), *On certain approach to mathematical modelling of the flotation process*. Tsvetnyje Metally, no 7, 24-29, (in Russian).
- ZUNIGA H.G., (1935), *Flotation recovery is an exponential function of its rate*. Bol. Soc. Nac. Min., Santiago 47, 83 – 86.

Brożek M., Młynarczykowska A., *Analiza modeli kinetyki flotacji cyklicznej*. Physicochemical Problems of Mineral Processing, 41 (2007) 51-65 (w jęz. ang.).

Flotacja jako zjawisko kinetyczne i termodynamiczne jest procesem losowym. Zmienna losowa oznaczająca liczbę ziaren flotujących, przyczepionych trwale do powierzchni pęcherzyka, a w konsekwencji i uzysk, są zależne od czasu. Dla opisu tej zależności opracowano szereg modeli kinetyki flotacji. Każdy z tych modeli ujmuje wprawdzie inny aspekt zagadnienia, lecz modele te się wzajemnie uzupełniają. W tym artykule podano szczegółową analizę modelu opartego na kinetyce reakcji chemicznej oraz na modelu absorpcji chemicznej. Z analizy równań tych modeli wynika, że w przypadku flotacji nadawy niejednorodnej pod względem własności flotacyjnych, w początkowych chwilach trwania procesu flotują ziarna o najwyższych własnościach flotacyjnych według równania rzędu zerowego a następnie według równania rzędu $\frac{1}{2}$. W miarę upływu czasu flotują ziarna o coraz niższych własnościach flotacyjnych i zwiększa się zarazem rząd kinetyki flotacji. Wąskie klaso-frakcje węgla o średnich własnościach flotacyjnych (typ 33) flotują według równania kinetyki rzędu I. Można więc z teoretycznego punktu widzenia uznać je za materiał jednorodny pod względem własności flotacyjnych.

Jerzy SABLİK*

ENERGY CHARACTERISTICS OF FINEST COAL PARTICLES SURFACES VERSUS THEIR UPGRADING USING FLOTATION

Received March 20, 2007; reviewed; accepted May 28, 2007

The paper presents selected results of investigations on energy properties of the fine coal particles, and methodological grounds for conducting such investigations. Using the discussed relationships, values of contact angle of coal particles with various degree of coalification in the range defined by the energy nonhomogeneity of the surfaces were computed. There have been determined the values of the contact angles of coal particles with hydrophobic and hydrophilic surfaces after coating with nonpolar and polar reagents. The energy state of the surfaces of coal particles in the feeds and products of industrial flotation were determined, which enabled to evaluate this process.

Key words: surface tension, surface energy, separation, coal, flotation

INTRODUCTION

As a consequence of coal mechanical mining and its transportation to the preparation plant as well as coal processing, a substantial part of coal is in the form of fine coal slurry. The coal slurry is contaminated with ash-generating minerals and other substances which contaminate the environment in the course of their utilisation. The coal slurry, to fulfil the principles of the “clean coal” programme [Sablik 2002], should be processed. The finest coal is basically prepared using physical-chemical methods, and most frequently the flotation method. The principal condition of flotation response of coal is low surface energy of the particles, which causes their surface to be hydrophobic. A measure of coal hydrophobic is the contact angle, and the surfaces of coal particles is considered hydrophobic when the contact angle is greater than zero. A measure of the energy state of the surface of coal particles can also be the critical surface tension of wetting, which can be determined using the film flotation method (Fuerstenau et al. 1991, Diao, Fuerstenau 1991). This is a parameter

* Central Mining Institute, Katowice, Poland.

enabling to give the surface energy characteristics of particles in the entire population, to draw up the probability curve of surface energy distribution and to determine the value of mean critical surface tension of wetting for a given collection of particles (Fuerstenau et al. 1991, Sablik, Wierzchowski 2001). The results of tests using this method enable also to determine the energy nonhomogeneity of particle surfaces in a specified population (Fuerstenau et al. 1991, Sablik 2000).

The film flotation method enables to determine the effect of chemical reagents on the state of surface energy of coal particles. The technique of particle surface coating outside the technological environment was developed by Sablik and Wierzchowski (1992, 1994, 1995), which made it possible to evaluate the effect of those reagents on the energy state of particle surface. It has been additionally shown that the particles that were upgraded within the flotation process have a similar surface energy to that of particles coated with a reagent outside the technological environment (Wierzchowski et al. 2000).

The development of research methods and determination of empirical relationships between some quantities characterising the surface of coal provide the possibility of a deeper analysis of the preparation process using physical-chemical methods.

METHODOLOGICAL GROUNDS FOR INVESTIGATION OF SURFACE ENERGY PROPERTIES OF FINEST SIZE PARTICLES

The information concerning the energy state of fine coal particles can be obtained using several methods (Sablik, 2007). To do this, one most often applies the measurement of the contact angle θ , while since the eighties of the last century, the measurement of the critical tension of wetting γ_c (Fuerstenau et al., 1991, Diao and Fuerstenau 1991). A relationship was found between the two parameters mentioned above describing the energy state of the surface of coal particles (Neumann and Good 1972; Neumann et al., 1972; Fuerstenau et al. 1970; Li and Neumann 1992; Sablik 2003). The empirical relationship $\cos \theta = f(\gamma_c)$, graphically presented in Fig.1, is described with the regression equation (Sablik 2003):

$$100 \cos \theta = 0,0012 \exp 0.1959 \bar{\gamma}_c \quad (1)$$

where θ – contact angle,

$\bar{\gamma}_c$ – mean critical surface tension of wetting,

while the correlation coefficient between these variables is 0.90.

In the case when $\cos \theta = 1$, the contact angle equals to zero, and the value of mean critical surface tension of wetting calculated with the use of Eq. 1, $\gamma_{c(\theta=0)}$, is equal to 57.83 mJ/m^2 . The particles whose surface tension of wetting is equal or greater than $\gamma_{c(\theta=0)}$ have hydrophilic surfaces. Such particles do not show any flotation response. This is proved by the results of tests on natural floatability F_n (Wierzchowski and

Sablik, 1993) and standard floatability (Sablik, 1998). The dependence on natural floatability F_n on the mean critical surface tension of wetting $\bar{\gamma}_c$ $\{F_n = f(\bar{\gamma}_c)\}$ can be described with the regression equation (Sablik, 2004):

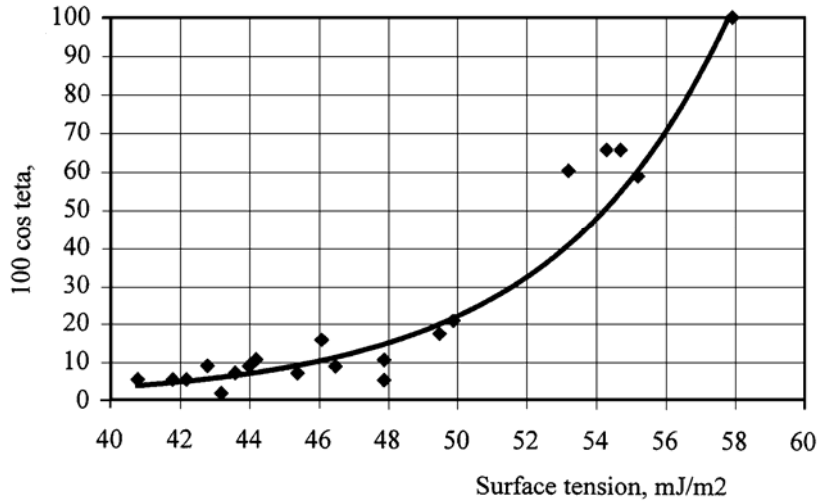


Fig. 1. Dependence between contact angle and mean critical surface tension of wetting for coals of different rank

$$F_n = 2 \cdot 10^7 \exp(-0.2903 \bar{\gamma}_c) \quad (2)$$

The correlation coefficient of these variables is - 0.92. The value of critical surface tension of wetting, when calculated using equation (2) $F_n=0$ is $\gamma_{c(F_n=0)} = 57.90 \text{ mJ/m}^2$. The standard floatability is the floatation response of various types of coal determined in identical experimental conditions. The measure of the standard floatability can be the yield of combustible in the concentrate ε , that is $\varepsilon = \gamma B_K/B_N$, where γ is the yield of the concentrate, B_K the content of combustible in concentrate, B_N the content of combustible in the feed. The relationship $\varepsilon = f(\bar{\gamma}_c)$ is described by the regression equation (Sablik, 2004):

$$\varepsilon = 3 \cdot 10^9 \exp(-0.3915 \bar{\gamma}_c) \quad (3)$$

and the coefficient of correlation between these variables is - 0.95. The value of critical surface tension of wetting calculated from equation (3) for $\varepsilon = 0$ is $\gamma_{c(\varepsilon=0)} = 55.73 \text{ mJ/m}^2$. The values $\gamma_{c(F_n=0)}$ and $\gamma_{c(\varepsilon=0)}$ prove the conclusion resulting from the relationship $\cos \theta = f(\bar{\gamma}_c)$ on the total disappearance of hydrophobicity of coal particles when $\bar{\gamma}_c \geq 57.83 \text{ mJ/m}^2$.

The value $\gamma_{c(\theta=0)}$ and that of the distribution function of critical surface tension of wetting of coal particles enable to determine the contents of hydrophilic particles in a

given collection of finest particles (Sablik, 2003, 2004, Sablik and Wierzchowski, 2004). Figure 2 shows the distribution functions of surface tension of wetting, determined using the film flotation method, obtained after disintegration of coal lump with the content of $C^{daf} = 77.46\%$ and of ash 3.42% , not covered and covered with an apolar reagent, while Fig. 3 those of coal with $C^{daf} = 82.80\%$ and ash content 2.30% not covered and covered with an nonpolar reagent or mixture of nonpolar (80 %) and polar (20%) reagents. In order to determine the content of hydrophilic particles in the analysed collections of particles, the point of intersection of the abscissa $\gamma_{c(\theta=0)} = 57.83 \text{ mJ/m}^2$ with the distribution function of the tension of wetting is projected on the axis of the content of lyophobic fraction.

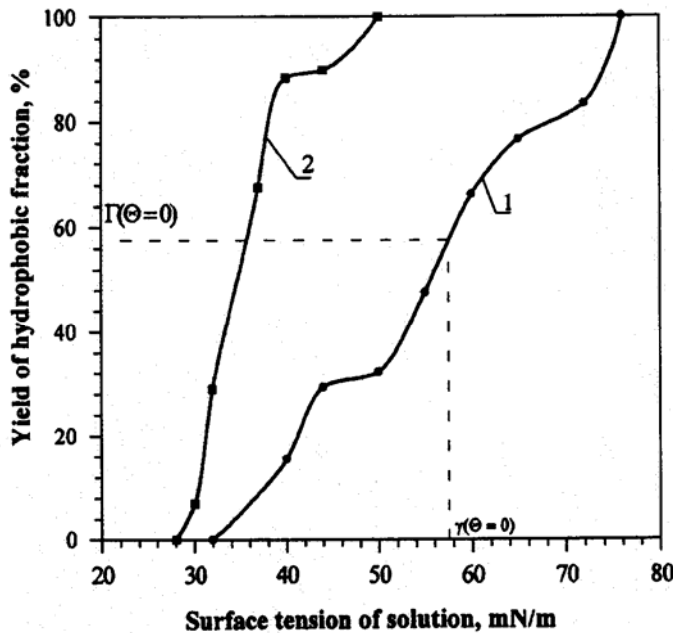


Fig. 2. Distribution functions of the surface tension of wetting of coal particles with a low degree of coalification, not coated (curve 1) and coated with a nonpolar reagent (curve 2). There has been marked the contribution of particles (ca. 42 %) whose value of the contact angle is zero degrees

The point $\Gamma_{(\theta=0)}$ found this way defines the content of particles with hydrophilic surfaces. This content is equal to $100 - \Gamma_{(\theta=0)}$. In the case of a very low coalification of coal (Fig.2), the content of hydrophilic particles in the collection obtained after disintegration of the coal lump with low ash content is about 42 %. In the population of particles obtained after disintegration of the lump of more coalificated coal (Fig.3), the content of hydrophilic particles is about 22 %. Because of a low content of ash-producing mineral substances (ash) in all tested lumps, one can draw a conclusion that the particles with hydrophilic surfaces are those of organic coal substance with a high content of reactive oxygen complexes. In the case of weakly coalificated coal, the content of such complexes is greater, which causes that the content of hydrophilic particles in the population is higher.

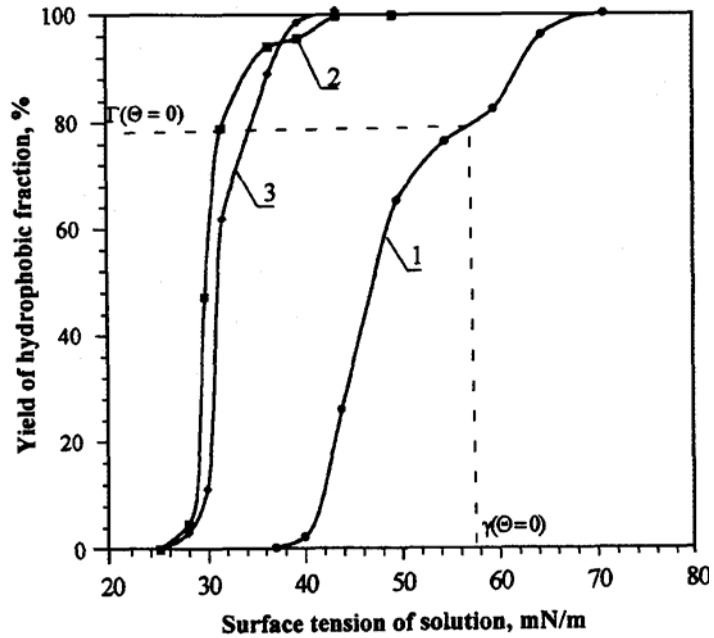


Fig. 3. Distribution functions of the surface tension of wetting of coal particles with medium degree of coalification not coated (curve 1) and coated with nonpolar reagent (curve 2) or reagent being a mixture of nonpolar (80 %) and polar (20 %) reagents (curve 3). There has been marked the contribution of particles (ca. 22 %) whose value of the contact angle is zero degrees

The surfaces of hydrophilic coal particles can be hydrophobised with an action of appropriate chemical reagents. Figures 2 and 3 present the curves of the distribution of surface tension of wetting of examined coals, after their surface has been coated outside the technological environment (Sablik and Wierzchowski, 1992, 1994, 1995) using a polar reagent or mixture of nonpolar and polar reagents.

Table 1. Surface tension of wetting (mJ/m²) of coal particle populations of non-coated with reagents, coated out of flotation environment and coated in flotation process

Carbon content C ^{daf} , %	Particles non-coated with reagents		Particles coated with reagents out of flotation environment		Particles coated with reagents in flotation process	
	Surface tension of wetting mJ/m ²	Energetic nonhomogeneity mJ/m ²	Surface tension of wetting mJ/m ²	Energetic nonhomogeneity mJ/m ²	Surface tension of wetting mJ/m ²	Energetic nonhomogeneity mJ/m ²
79.2	49.7	11.9	41.6	6.7	41.9	9.2
80.8	44.0	8.4	33.0	5.0	35.3	5.8
87.5	40.8	5.4	29.6	3.0	31.8	5.0

In the cases of both tested coals, coating of the particle surfaces with the reagents resulted in the hydrophobisation of all the particles in the populations. This means that surface tension of wetting of those particles is lower than $\gamma_{c(\theta=0)} = 57.83 \text{ mJ/m}^2$, and contact angle is greater than zero.

Using the film flotation method in the investigations, the hydrophobisation of the particles of different types of coal in the flotation process has been evaluated (Wierzchowski et al., 2000).

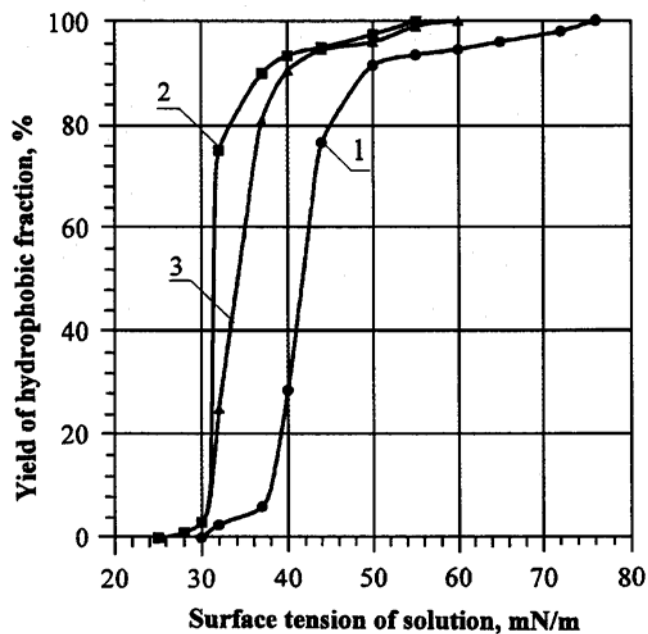


Fig. 4. Distribution functions of the surface tension of wetting of coal with $C^{daf} = 80.8 \%$; 1 - “clean” particles, 2 - particles coated outside the flotation environment, 3- particles coated in the flotation process

Presented in Table 1 and Fig. 4 are the results of tests of surface tension of wetting in the populations of coal particles not coated with a reagent, coated with a reagent outside the flotation environment, and those coated in the process of flotation. It has been experimentally shown that the particles of coal undergo hydrophobisation in the process of flotation, and the energy state of the surface, reached as a consequence of action of reagents, does not change in the course of dewatering and drying of those particles. The distribution of surface tension values of particles coated with reagents in the process of flotation is very close to the distribution on the surface of particles coated in ideal conditions outside the flotation environment (Fig.4). The differences in the values of evaluated energy parameters characterising the surfaces of particles result, first of all, from the differences in coalification of the investigated coals.

Table 2. Characteristics and selected properties of coals with the use of different relationships ($\cos\theta = f(\gamma_c)$) (1) and (Sablík and Wierzchowski 2001; Sablík, 2000, Sablík and Makula 1984), and minimal and maximal contact angles in the collection of fine coal particles, calculated on the basis of Eq. (1) and conditioned by energy nonhomogeneity of their surface

Carbon content, C^{daf} , %	Ash content A^a , %	Contact angle θ , deg	Mean critical surface tension, * $\bar{\gamma}_c$, mJ/m ²	Energetic surface nonhomogeneity ** σ_{γ_c} mJ/m ²	$\bar{\gamma}_c + \sigma_{\gamma_c}$ mJ/m ²	Minimal contact angle, deg	$\bar{\gamma}_c - \sigma_{\gamma_c}$ mJ/m ²	Maximal contact angle, deg
78.48	6.41	49	54.7	12.1	66.8	0	42.6	86
77.46	3.42	54	55.2	11.9	67.1	0	43.3	86
79.19	6.28	49	54.3	7.3	61.6	0	47.0	82
80.90	6.60	53	53.2	11.9	65.1	0	41.3	87
82.80	2.30	78	49.9	8.0	57.9	0	41.9	87
81.91	9.70	81	46.1	8.9	55.0	53	37.2	89
80.70	4.72	80	49.5	7.3	56.8	57	42.2	87
82.23	7.70	84	47.9	7.6	55.5	49	40.3	88
84.76	5.26	85	46.5	7.5	54.0	60	39.0	88
86.47	2.36	87	47.9	10.2	58.1	0	37.7	88
84.45	12.63	85	44.0	6.7	50.7	75	37.3	88
84.50	3.80	84	44.2	6.7	50.9	74	37.5	88
85.00	4.61	85	42.8	6.1	48.9	79	36.7	89
85.80	3.80	86	45.4	5.9	51.3	73	39.5	88
87.10	2.30	87	42.2	5.6	47.8	81	36.6	89
87.36	3.28	88	43.2	6.9	50.1	77	36.3	89
87.10	2.40	87	42.2	6.0	48.2	81	36.2	89
87.11	4.20	86	43.6	5.9	49.5	78	37.7	88
88.73	2.61	87	41.8	5.4	47.2	82	36.4	89
89.60	8.10	87	40.8	8.1	48.9	79	32.7	89

*Calculated according to relation

$$\bar{\gamma}_c = \int_{\gamma_{c \min}}^{\gamma_{c \max}} \gamma_c f(\gamma_c) d\gamma_c$$

** Calculated according to relation

$$\sigma_{\gamma_c} = \sqrt{\int_{\gamma_{c \min}}^{\gamma_{c \max}} (\gamma_c - \bar{\gamma}_c)^2 f(\gamma_c) d\gamma_c}$$

CONTACT ANGLES OF FINEST COAL PARTICLES

In the collections of finest coal particles with different coalification one observes the energetic nonhomogeneity of surface σ_{γ_c} (Sablík 2000). The values of the energy nonhomogeneity are, for all types of coal, confined in the range $\bar{\gamma}_c \pm \sigma_{\gamma_c}$. By using empirical relationship (1) and the values of energy nonhomogeneity of the surface of particles in a specified collection, one can determine the limits of the ranges corresponding with these values, in which the values of contact angles are confined (Sablík and Wierzchowski, 2004). Specified in Table 2 are the characteristics of coals with different degrees of coalification, and the limits of ranges within which the values

of contact angles of the surfaces of particles of a given population are confined. In the case of hard coals with the lowest coalification, the ranges of those values are very wide (0° - 87°), and the surfaces of a part of particles have the contact angle equal to zero (hydrophilic particles). With the increasing coalification of coal, the decrease of the ranges of contact angle values takes place, and in the case of hard coals with the highest coalification, up to several degrees (Table 2).

Table 3. Characteristics of tested coal samples and the influence of reagents on contact angles of slime particles

No.	Characteristics of coal samples				Characteristics of coal surfaces coated with reagents					
	Carbon content C^{daf} , %	Ash content A^a , %	$\bar{\gamma}_c$, mJ/m ²	Share of hydrophilic particlesn $\gamma_c(\theta=0)$, %	Reagent	$\bar{\gamma}_c$, mJ/m ²	σ_{γ_c} , mJ/m ²	Angle $\theta_{(\gamma_c)}$, deg	$\theta_{(\gamma_c + \sigma_{\gamma_c})}$, deg	$\theta_{(\gamma_c - \sigma_{\gamma_c})}$, deg
1	78.48	6.41	54.7	~ 55	A	48.3	9.5	81	7	88
					A +20%P	42.9	9.2	86	71	84
2	77.46	3.42	55.2	~ 35	A	38.1	5.8	88	86	89
					A +20%P	40.3	12.2	88	69	89
3	79.19	6.28	54.3	~ 23	A	39.3	9.4	88	80	89
					A +20%P	40.7	13.4	88	61	89(90)
4	80.90	6.60	53.2	~ 40	A	40.5	11.5	88	71	89(90)
					A +20%P	41.6	9.4	87	75	89
5	82.80	2.30	49.9	~ 15	A	31.1	3.4	89	89	90
					A +20%P	31.4	4.4	89	88	89(90)
6	80.70	4.72	49.5	~ 20	A	30.2	4.1	89	89(90)	90
					A +20%P	31.4	4.1	89	89	89(90)

A – nonpolar reagent, P – polar reagent

The particles built of the organic substance of coal, but containing numerous oxygen complexes and mineral intrusions can have hydrophilic surfaces, that is contact angles equal to zero. Such particles do not show the flotation response. The energy state of the surface of those particles can be changed by means of adequate chemical reagents. Presented in Table 3 is the effect of chemical reagents on the contact angles of six low- coalificated coals with low content of mineral substances (low ash content). The populations of finest particles of these coals contained a great number of particles with hydrophilic surfaces, having the surface tension values greater than $\gamma_{c(\theta=0)} = 57.83$ mJ/m², and contact angle equal to zero. After coating the surfaces of these particles with a nonpolar reagent or mixture of nonpolar (80%) and polar (20%) reagents, the surfaces of all particles revealed the hydrophobic properties that is the contact angle greater than zero. The results presented in Figures 2 and 3 and in Tables 1 and 3 prove that after contact with proper reagents, the hydrophilic surfaces of the particles of low-coalificated coals undergo hydrophobisation ($\theta > 0$, $\bar{\gamma}_c < 57.83$ mJ/m²), and coal should reveal flotation response.

ENERGY STATE OF THE SURFACES OF COAL PARTICLES IN THE FEED AND PRODUCTS OF INDUSTRIAL FLOTATION

In order to determine the energy state of the surface of coal particles in the course of industrial flotation, there were tested the feed and flotation products obtained in pneumatic-mechanical flotation machines type IZ with the capacity of 140 t/Mg (Sablik, 1998), concentrating under real conditions the slimes of coking and steam coals (Lenartowicz and Sablik, 2006; Lenartowicz 2007).

Table 4. Physicochemical characteristics of feed, concentrates and tailings of the tested coals and the share of particles with hydrophilic surfaces

Sample	Surface tension of wetting, $\bar{\gamma}_c$ mJ/m ²		Energetic nonhomogeneity, σ_{γ_c} , mJ/m ²		Ash content, %		Share of hydrophilic particles, %	
	Coking coal	Power coal	Coking coal	Power coal	Coking coal	Power coal	Coking coal	Power coal
Feed	48.90	62.40	13.69	17.37	15.88	33.87	~ 18	~ 65
Concentrate I	40.74	42.42	8.25	9.21	4.92	8.55	~ 3	~ 6.5
Concentrate II	40.90	47.26	8.27	12.03	5.63	16.02	~ 5	~ 16.5
Concentrate III	47.46	49.50	10.51	13.68	9.81	18.22	~ 19	~ 20
Tailings	67.34	65.58	17,25	17.87	63.02	52.28	~ 73.5	~ 70

The flotation machines were constructed of three two-impeller sections with two-sided collection of the concentrate. The concentrates were collected from each section, and the tailings from the tailings bin. The results of tests are compiled in Table 4, and graphically presented in Figs. 5 and 6. The use of the film flotation method to evaluate flotation concentration of coal slimes in the industrial conditions enables to obtain better understanding of this process in the IZ-type pneumatic-mechanical concentrators. The suspension of coking coal (feed) had relatively high surface tension of wetting (48.90 mJ/m²), and about 18% of the content of particles with hydrophilic surfaces, while the ash content was 15.88%. In successive impeller compartments, the concentrates containing 3%, 5% and 19% of hydrophilic particles were obtained, and the ashes in these compartments equalled 4.92, 5.63 and 9.81 %, respectively. The mean critical surface tension of wetting of particles in the concentrates is lower than the mean surface tension of wetting of particles in the feed, and much lower than this tension in the tailings (Fig. 6). A high content of hydrophobic particles in the tailings (26.5 %) indicates, however, that the analysed technology needs improving, aimed at decreasing the number of hydrophobic particles (combustible particles) that pass into tailings, and, consequently, increasing the ash content in the tailings.

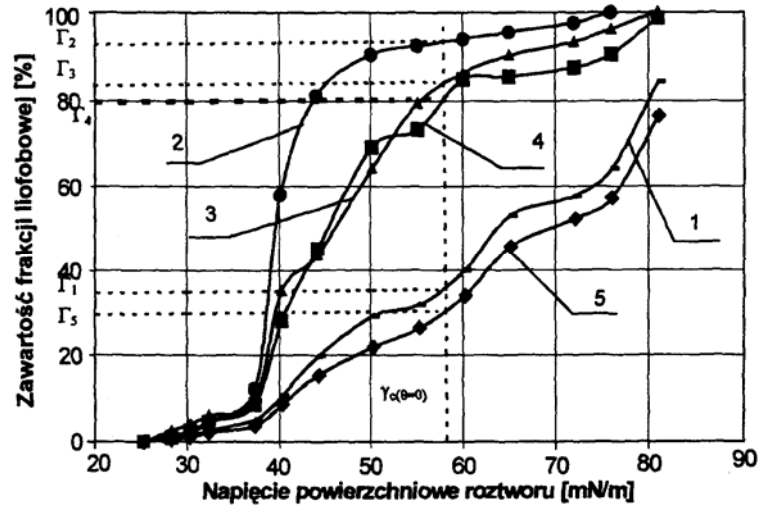


Fig. 5. Distribution curves of surface tension of wetting power coal particles in feed and products obtained in the IZ flotation machine, 1- feed, 2- concentrate I, 3 – concentrate II, 4 – concentrate III, 5 – tailings ($100 - \Gamma_n$) – yield of hydrophilic particles

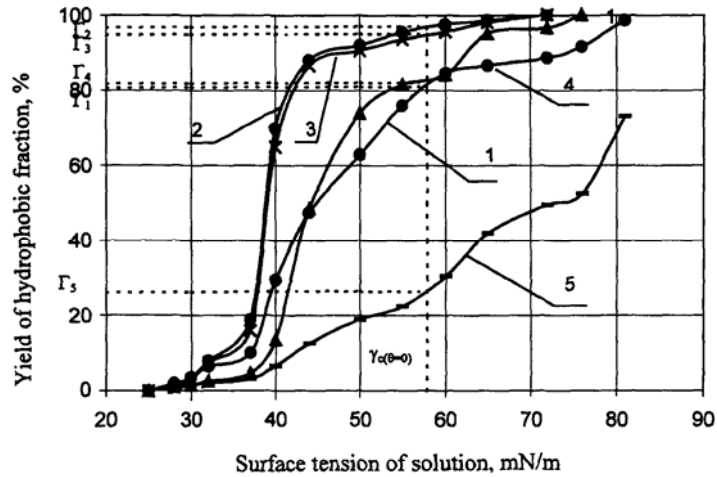


Fig. 6. Distribution curves of surface tension of wetting the coking coal particles in a feed and products obtained in the IZ flotation machine 1 - feed, 2- concentrate I, 3 – concentrate II, 4 – concentrate III, 5 – tailings ($100 - \Gamma_n$) – yield of hydrophilic particles

Steam coal has a substantially lower, as compared to coking coal, degree of coalification, and contains in its structure a relatively high number of oxygen-containing complexes, which causes that its surface is, to a great extent, hydrophilic. Such coal reveals a low flotation response. The mean critical surface tension of

wetting of slime particles of the analysed coal was high (64.4 %), and the proportion of hydrophilic particles was 65 % (Table 4, Fig. 5). Concentrating of coal slimes of such a type using the flotation method needs very accurate adjustment of technological parameters. The presented results prove that, particularly in this case, the technology needs improving. A considerable part of particles with hydrophilic surfaces in the feed was hydrophobised during the process of flotation and passed to the concentrate, while a considerable amount of hydrophobic particles (ca. 30%) passed into the tailings. This resulted in a too low ash content in the product and loss of combustible matter.

The imperfection, in this case, of the flotation process is illustrated by the distribution curves of surface energy of particles in the feed and in the tailings (Fig. 5, curves 1 and 5). The differences in surface tension of wetting of particles in the feed and tailings are too small for the process of concentration of steam slimes to be found correct.

From the considerations above, it follows that the energy characteristics of the surfaces of finest coal, including the particles in the feeds and flotation products, can be used to perform deepened assessment of the course of physical – chemical concentration (flotation) of coal slimes. The film flotation method is the one that enables to make energy characteristics of the surface for the population of the finest coal particles.

REFERENCES

- DIAO J., FUERSTENAU D.W., 1991: *Characterization of the wettability of solid particles by film flotation, Part II: Theoretical analysis*, Colloids and Surfaces, 60.
- FUERSTENAU D.W., DIAO J., HANSON J.S., 1990: *Estimation of the Distribution of Surface Sites and Contact Angles on Coal Particles from Film Flotation Data*, Energy and Fuels., 4, 34.
- FUERSTENAU D.W., DIAO J., WILLIAMS M.C. 1991: *Characterization of the wettability of solid particles by film flotation., Part I: Experimental investigation*, Colloids and Surfaces., 60.
- LENARTOWICZ M., SABLİK J., 2006: *The hydrophilic particles in washing products of trough pneumo – mechanical flotation machine*, 10th Conference on Environment and Mineral Processing, Part I, TSB-TU Ostrava, Czech Republik.
- LENARTOWICZ M., 2007: Praca doktorska, Główny Instytut Górnictwa, Katowice.
- LI D., NEUMANN A.W., 1992: *Contact angles on hydrophobic solid surfaces and their interpretation*, J. Colloid Interface Sci. 148 pp.190-200.
- NEUMANN A.W., GOOD R.J., 1972: J. Colloid Interface Sci., 38, 341–358.
- NEUMANN A.W., GOOD R.J., HOPE C.J., SEJPAL M., 1974: J. Colloid Interface Sci. 49 291– 04.
- SABLİK J., 1998: *Flotacja węgla kamiennych*, Wyd. Główny Instytut Górnictwa, Katowice.
- SABLİK J., 2000: *Niejednorodność krytycznego napięcia powierzchniowego zwilżania w zbiorze bardzo drobnych ziarn węglowych*, Inżynieria Mineralna, vol 1, 1.
- SABLİK J., 2002: *Przyroda go nie skąpi...*, Technologia czystego węgla-geneza i rozwój, Ekoprofit nr, (61).
- SABLİK J., 2003: *The relationship between contact angle and mean critical surface tension of coal of different rank*, Inżynieria Mineralna, vol. IV, nr 2 (11).
- SABLİK J., 2004: *Zero values of flotation resonance and contact angle of coals in the function of their critical surface tension of wetting*, Inżynieria Mineralna, vol. V, nr 1 (12).
- SABLİK J., 2007: *Fizykochemiczne właściwości powierzchniowe węgla kamiennych*, Monografia Wyd. Główny Instytut Górnictwa, Katowice.

- SABLIK J., MAKULA K., 1984: *Wyznaczanie granicznego kąta zwilżania węgla poprzez pomiar ciśnienia kapilarnego*, Aparatura Naukowo Dydaktyczna 6.
- SABLIK J., WIERZCHOWSKI K., 1992: *Evaluation of the influence of flotation reagents on the hydrophobicity of coal using the film flotation method*, Fuel 71, 4/474-475.
- SABLIK J., WIERZCHOWSKI K., 1994: *The Effect of Pre-wetting with Flotation Reagents on the Surface Energy of Coals*, Coal Preparation, vol 15, s. 1-10.
- SABLIK J., WIERZCHOWSKI K., 1995: *The film flotation method applied to determine surface energy of coal wetted with flotation reagents*, Archives of Mining Sciences, vol. 40 nr 1.
- SABLIK J., WIERZCHOWSKI K., 2001: *Characteristic of hard coals surface properties using film flotation*, Inżynieria Mineralna, II 2(4).
- SABLIK J., WIERZCHOWSKI K., 2004: *Wpływ odczynników technologicznych na wartości granicznych kątów zwilżania węgla w zbiorze ziaren młolowych*. *Górnictwo i Geoinżynieria*, Zeszyt 2/1, Wyd. AGH.
- WIERZCHOWSKI K., SABLIK J. 1993: *Energia powierzchniowa ziaren w młolach węgla o różnym stopniu zmetamorfizowania*, Prace naukowe GIG No 775 Katowice.
- WIERZCHOWSKI K., LENARTOWICZ M., SABLIK J., 2000: *Napięcie powierzchniowe zwilżania ziarn węglowych wzbogaconych w procesie flotacji*. *Fizykochemiczne Problemy Mineralurgii*, Prace Naukowe Instytutu Górnictwa Politechniki Wrocławskiej, nr 88.

Sablik J., *Energetyczna charakterystyka powierzchni ziaren w populacji węgla najdrobniej uziarnionych w aspekcie ich wzbogacania metodą flotacji*, Physicochemical Problems of Mineral Processing, 41 (2007) 67-78, (w jęz. ang.).

Przedstawiono wybrane wyniki badań energetycznych właściwości powierzchni ziaren węglowych w populacji węgla najdrobniej uziarnionych oraz metodologiczne podstawy prowadzenia takich badań. Informacje o stanie energetycznym powierzchni drobnych ziaren węglowych uzyskać można kilkoma metodami. Najczęściej w tym celu stosuje się pomiar kąta zwilżania θ , a od lat osiemdziesiątych ubiegłego stulecia pomiar krytycznego napięcia powierzchniowego zwilżania γ_c . Określona została zależność między powyższymi dwoma parametrami. Zależność ta jako funkcja ($\cos \theta = f(\gamma_c)$) przedstawiona została graficznie na rysunku 1 i opisana równaniem regresji (1). W przypadku kiedy $\cos \theta = 1$ graniczny kąt zwilżania θ równy jest zero, a wartość średniego krytycznego napięcia powierzchniowego zwilżania zerowego kąta zwilżania obliczona z wykorzystaniem równania (1) ($\gamma_{c(\theta=0)}$) wynosi 57,83 mJ/m². Ziarna, których napięcie powierzchniowe zwilżania jest równe lub większe od $\gamma_{c(\theta=0)}$, mają powierzchnie hydrofilowe. Ziarna takie nie wykazują aktywności flotacyjnej. Potwierdzają to wyniki badań flotowalności naturalnej F_n i flotowalności standardowej, której miarą może być uzysk substancji palnej w koncentracji ε . Obliczona z wykorzystaniem równania (2) wartość krytycznego napięcia powierzchniowego zwilżania kiedy $F_n = 0$ wynosi $\gamma_{c(F_n=0)} = 57,90$ mJ/m². Wartość krytycznego napięcia powierzchniowego zwilżania obliczona z równania (3) dla $\varepsilon = 0$, wynosi $\gamma_{c(\varepsilon=0)} = 55,73$ mJ/m². Wartości $\gamma_{c(F_n=0)}$ oraz $\gamma_{c(\varepsilon=0)}$ potwierdzają wniosek wynikający z zależności $\cos \theta = f(\gamma_c)$ o całkowitym zaniku hydrofobowości ziaren węglowych kiedy $\gamma_c \geq 57,83$ mJ/m². Wykorzystując omówione wyżej zależności obliczono kąty zwilżania ziaren węglowych o różnym stopniu uwęglenia w obszarze wyznaczonym przez niejednorodność energetyczną powierzchni w danym zbiorze. Przedstawiono sposób wyznaczania i określono wychód ziaren hydrofilowych w badanych zbiorach ziaren oraz zmiany wartości granicznych kątów zwilżania ziaren węglowych o powierzchniach hydrofobowych i hydrofilowych po zwilżeniu odczynnikami apolarnym i polarnym (rys. 2 i 3, tabele 2. i 3.). Wykazano, że rozkład napięć powierzchniowych zwilżonych odczynnikami w procesie flotacji jest bardzo zbliżony do rozkładu na powierzchni ziaren zwilżonych w warunkach idealnych poza środowiskiem flotacji. Przedstawiono wyniki badań procesu flotacji w korytowej pneumomechanicznej maszynie flotacyjnej typu IZ z zastosowaniem frakcjonowanej flotacji powierzchniowej. Określono stan energetyczny powierzchni ziaren węglowych w nadawach, koncentratkach z poszczególnych przedziałów wirokowych i odpadach (Rys. 5. i 6.), co umożliwiło analizę przebiegu i ocenę tego procesu.

Hussin A. M. AHMED*

OPTIMIZATION OF DESLIMING PRIOR TO PHOSPHATE ORE UPGRADING BY FLOTATION

Received March 27, 2007; reviewed; accepted June 6, 2007

Flotation is one of the most efficient techniques applied for phosphate upgrading. Desliming of flotation feed is a critical pre-request step for successful phosphate/gangue separation by flotation. Generally, the target of the desliming step is to minimize the feed fines to avoid their negative effects during flotation. However, such slimes normally contain phosphates which are considered as losses. An effective desliming should pay attention to minimizing the losses of phosphate bearing minerals in the removed slimes and, as a second target, to keep high phosphate recovery in the flotation feed. In this paper optimization of the desliming stage to achieve both targets at-a-time was studied using different techniques at different operating conditions. The applied slimes removal techniques included screening and hydrocycloning. It was found that desliming using hydrocyclone, at its optimum operating conditions, is better than desliming using screens. This is because the deslimed product contained small amount of phosphate slimes leading to efficient separation by flotation with an overall selectivity index $B=0.739$ defined by formula $\varepsilon_{1,c} = (100-\varepsilon_{2,t})^{(1-B)}/100^{(-B)}$ where $\varepsilon_{1,c} = P_2O_5$ recovery in flotation concentrate, %; $\varepsilon_{2,t} = MgO$ recovery in both slimes and flotation tail, % .

Key words: desliming, phosphate, flotation, selectivity index

INTRODUCTION

Phosphate rocks are important in different industries as phosphoric acid and fertilizers (80%), and elemental phosphorous production (15% of the phosphate utilizing in the world) (El-Mahdy, 2004). They are usually upgraded to minimize their gangues before introduced to any of the mentioned applications. Different upgrading techniques can be applied for phosphate concentration. A successful phosphate-upgrading technique depends on the ore type and its geological history in addition to nature of the phosphate-associated gangue. One of the most effective and widely applied techniques for phosphate upgrading is flotation (Houot, 1982; Abdel-Khalek

* Central Metallurgical Research and Development Institute (CMRDI), P.O. Box, 87, Helwan, Cairo, Egypt.

and Farrah, 2004, El-Mahdy, 2004). The technique proved its high effectiveness in upgrading siliceous phosphates when flotation is direct, reverse or in a combination of these two processes such as the Crago "Double Float" process (Yingxue et al., 1995) and its simplified reverse version (Patrick et al., 2000). In carbonaceous phosphate flotation, despite the difficulty of selective separation, yet it can be successfully achieved under strict conditions (Anazia and Hanna, 1987; Xiapeng et al., 2000).

One of the main disadvantages of phosphate upgrading by flotation is the high sensitivity of collectors to slimes. Therefore, for successful flotation, desliming is a necessary pre-request. Following this trend, the classical aim of desliming is removing fines (<37 μm or 400 mesh) from flotation feed. Unfortunately, in desliming, huge amounts of phosphate are lost in the slimes. The losses may lead to a rejection of up to 25% of the P_2O_5 mass content in some cases (Lawendy and Steven, 1993). For deeper visualization of the value of phosphate losses in the slimes, Patrick et al. (2001) showed that in Florida 180 gigagrams (Gg that is million tons) of P_2O_5 (an equivalent of 600 Gg (million tons) of phosphate rock with an average P_2O_5 content of 30%) discarded with the waste slimes in about 34 beneficiation years (1954-1987). In the year 2001 only, the losses in Florida district were evaluated to be 3.27 Gg of P_2O_5 which are equivalent to 10.9 Gg phosphate ore with an average P_2O_5 content of 27% (Patrick et al., 2001).

Keeping this in mind, research was devoted to recover the phosphate losses by re-treatment of such slimes (Patrick et al., 2001). In our opinion, it will be of more interest to minimize such losses from the beginning. Optimization of the desliming step is one of the proposed solutions to minimize phosphate losses in the slimes without effecting flotation performance. Therefore, this paper aims at studying the optimization of the desliming step to achieve two targets at-a-time, that is slimes removal with minimum phosphate disposal at constant flotation performance. The optimization will be carried out using different techniques set-to-work as classification tools. They include screens and hydrocyclones.

EXPERIMENTAL

SAMPLE CHARACTERIZATION AND PREPARATION

A low grade Egyptian phosphate sample from Abu-Tartur locality was used for this study. The run-of-mine was stepwise comminuted to 100% passing 0.25 mm screen. The prepared product was subjected to wet screening using a "Fritsch" shaker and a screen set. Each separated fraction of material was dried, weighed and its percent of total was recorded. Chemical analyses were run for both the run-of-mine and the different obtained size classes. Routine chemical analysis of samples was conducted using standard methods for phosphate analysis applying the "acid attack" method. Magnesium oxide was determined by atomic absorption technique (Ewing, 1975) using "Perkin-Elmer" Atomic Absorption model "Analyst 200". Phosphorous was

determined by spectrophotometric method (Scott, 1949) using “Perkin-Elmer” Spectrophotometer “model Lambda 3B”. The obtained product was deslimed at different operating conditions applying screening and hydrocycloning.

METHODS

Desliming using screening

In this series both wet and dry screening were tested for phosphate desliming. For all the investigated tests the same Fritsch shaker was used. The vibrating amplitude and screening time were kept constant at 50 Hz and 10 min respectively. Only the material flow rate was changed. The amount of material feed to the screen ranged from double layer to multiple layers of phosphate. The number of particle layers on the screen was calculated considering the average particle size of the feed and the total area of the screen. The screen products, oversize (flotation feed) and undersize (slimes) were calculated as percents on weight bases and analyzed for their P₂O₅ and MgO contents. The desliming step effectiveness was then evaluated on the bases of its flotation feed response to separation by flotation.

Desliming using hydrocyclone

A Mozely rig hydrocyclone was used for separating the fines (slimes) from the coarse phosphate. The tests conducted to evaluate the effect of cyclone parameters on the desliming of phosphate. They were run in two series. In the first series, the feed solid percent was verified stepwisely from 5-20% at a constant feeding pressure of 68.95 kPa (10 psi). While in the second series, the feeding pressure was investigated at an optimum previously determined solid percent of the feed. In each series, a feed batch was prepared to be enough for the whole run. In the first series, the cyclone was fed with the dense phosphate pulp (20% solids by weight) at constant pressure. Sampling for the first experiment was taken simultaneously from both the cyclone products for 30 s. Then, the same feed was diluted with the necessary amount of water for the second test, homogenized by circulating into the hydrocyclone. After homogenization the hydrocyclone products were sampled for the same 30 s. Both the underflow and overflow samples were analyzed for their solids content in addition to the cut size that was determined using Analysette 22 laser particle size analyzer. Finally, the underflow and overflow products were collected and prepared for chemical and mass balance analyses with underflow kept for further flotation investigation.

Evaluation of the desliming efficiency

The different deslimed products were considered as flotation feeds. All these feeds were subjected to flotation using a D-12 Denver flotation machine equipped with 0.5 dm³ cell. The flotation parameters were adjusted at their optimum values as previously determined for the same locality by El-Mahdy (2004). The used collector in this case

was sodium oleate of commercial grade of 75% obtained from Aldrich Chemicals, Germany. It was used without further purification. The collector dosage was maintained at a constant level of 1.5 kg/Mg. Analytical grade of NaOH, H₂SO₄, Na₂CO₃, and HCl were used as pH regulators. The overall separation efficiency due to desliming and flotation was evaluated using the Fuerstenau upgrading plot (Fig. 2) applying regression equation 1. This equation has a separation index B (Drzymala and Ahmed, 2005) and modified by Ahmed (2005)

$$\varepsilon_{1,c} = (100 - \varepsilon_{2,t})^{(1-B)} / 100^{(-B)} \quad (1)$$

where: $\varepsilon_{1,c}$ = P₂O₅ recovery in flotation concentrate, %; $\varepsilon_{2,t}$ = MgO recovery in both slimes and flotation tail, % and B is a separation index defined by Drzymala and Ahmed (2005). 0 < B < 1 means upgrading in concentrate, b=0 means no upgrading, and B= 1 means ideal upgrading.

RESULTS AND DISCUSSIONS

Figure 1 shows size distribution of the considered 100% -0.25 mm phosphate sample together with the P₂O₅ and MgO contents of the different fractions. It shows that the fine fractions (-0.075+0.045 and -0.045 mm) are characterized with their low P₂O₅ and high MgO contents. Thus, desliming using 0.075 mm screen can lead to 39% loss of the sample weight leading to rejection of 25.91% of the sample P₂O₅.

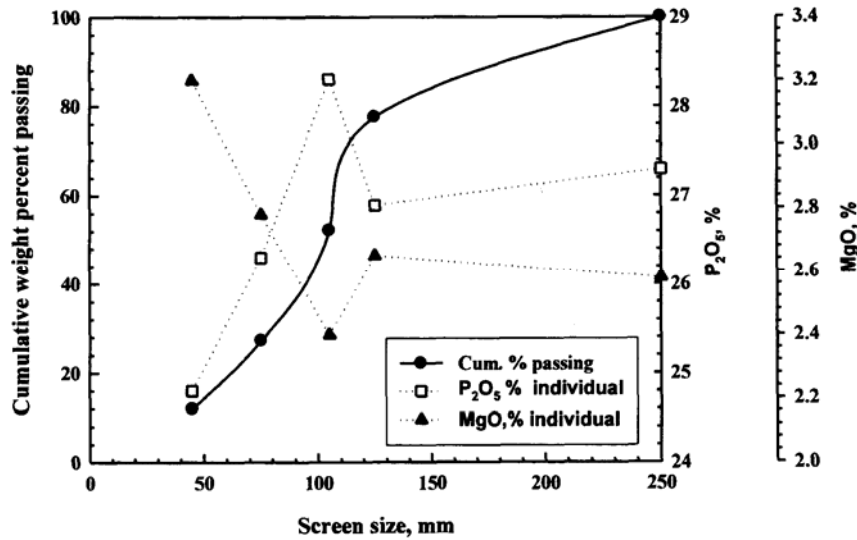


Fig. 1. Size distribution of the considered ground phosphate sample together with the individual fractions P₂O₅ and MgO contents

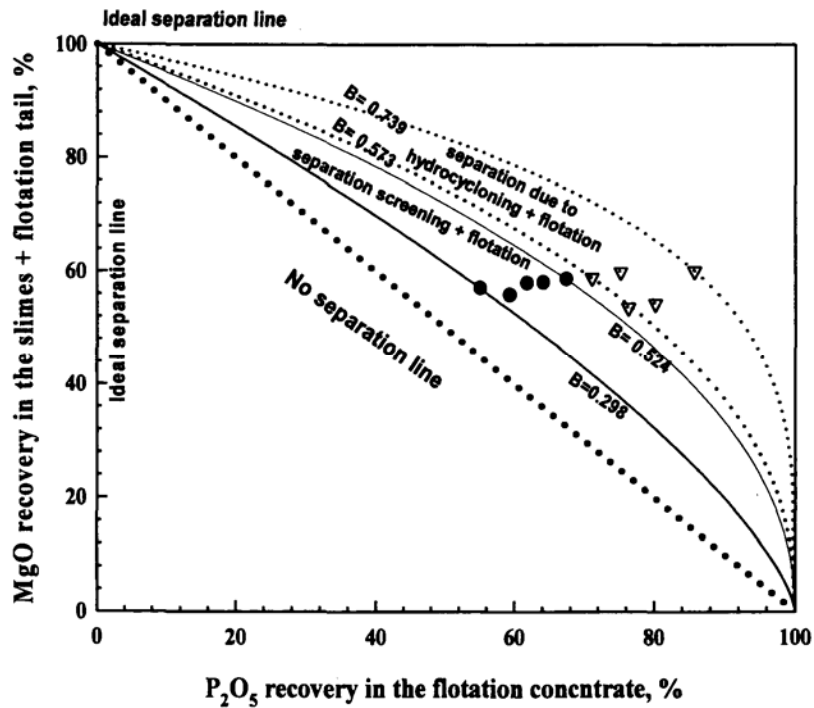


Fig. 2. Fuerstenau's plot showing effect of desliming technique on the separation efficiency of phosphate by flotation. Each point represents different desliming conditions. The results were approximated to get Drzymala-Ahmed selectivity index (parameter B in equation 1)

This loss will further increase considering the phosphate losses in the flotation tail. However, such desliming losses can be decreased to ~12 % of the sample weight with P₂O₅ rejection of 10.99 % when using a 0.045 mm screen. However, these findings reflect the importance of the cut size of the desliming stage.

SLIMES REMOVAL BY SCREENING

From the slimes phosphate content (losses) point of view, support can be given to desliming using the 0.045 mm screen. However, the screening efficiency with this fine screen depends mainly on the screening conditions. Table 1 shows the weight percent and chemical analyses of the slimes (-0.045 mm) and the flotation feed (-0.25+0.045 mm) under the investigated screening operating conditions.

In fact, the results shown in Table 1 are dangling because the phosphate losses in the slimes are minimum in some cases (exp. 5) but the flotation feed slimes seems to be still high. The relatively high fines content in the flotation feed may affect the flotation step performance. The high slimes contents of the flotation feed in the

mentioned case can be attributed to an inefficient dry screening. Therefore, to judge the best of the above results, the overall phosphate losses will be evaluated after running flotation test for all of the above shown flotation feeds (feeds from 1 to 5) as will be shown later in the flotation section.

Table 1. Results of phosphate desliming using 0.045 mm screen at different mass flow rates on the screen

ID	Screening conditions	Product	Wt., %	Assay, %		Recovery, %	
				P ₂ O ₅	MgO	P ₂ O ₅	MgO
1	Wet screening (double solid layer)	Flotation feed (OS)	88.07	27.17	2.60	89.00	85.66
		Slimes (US)	11.93	24.80	3.21	11.00	14.34
		Calculated head	100.00	26.89	2.67	100.00	100.00
2	Wet screening (four solid layers)	Flotation feed (OS)	89.65	27.18	2.59	90.47	87.20
		Slimes (US)	10.35	24.80	3.29	9.53	12.80
		Calculated head	100.00	26.93	2.66	100.00	100.00
3	Dry screening (single solid layer)	Flotation feed (OS)	89.90	27.26	2.60	91.06	86.78
		Slimes (US)	10.10	23.83	3.52	8.94	13.22
		Calculated head	100.00	26.91	2.69	100.00	100.00
4	Dry screening (double solid layer)	Flotation feed (OS)	90.75	27.33	2.59	91.94	87.45
		Slimes (US)	9.25	23.50	3.65	8.06	12.55
		Calculated head	100.00	26.98	2.69	100.00	100.00
5	Dry screening (triple solid layer)	Flotation feed (OS)	91.17	27.19	2.61	92.07	88.54
		Slimes (US)	8.83	24.20	3.49	7.93	11.46
		Calculated head	100.00	26.93	2.69	100.00	100.00

SLIMES REMOVAL USING HYDROCYCLONE

Table 2 shows hydrocyclone products, overflow named as slimes and underflow known as flotation feed, under variable operating conditions of feeding pressure and feed solid percent. Table 2 shows that depending on the hydrocyclone operating conditions the phosphate losses in the slimes can range from 6.16 to 14.63%. It can be also noticed that the MgO recovery in the flotation feed (74-79 %) is much less compared to that of the flotation feed obtained by screening desliming (85-88 %). In fact this may be attributed to separation effect of the hydrocyclone compared to the classification effect only of screening. This is in agreement with research findings that separation of fine gangues from phosphate could be partially achieved using hydrocyclones.

Table 2. Results of phosphate desliming using Mozley hydrocyclone under different operating conditions

ID	Hydrocyclone conditions	Product	Cut size, μm	Solid, %	Wt., %	Assay, %		Recovery, %	
						P ₂ O ₅	MgO	P ₂ O ₅	MgO
6	Pressure = 68.95 kPa (10 psi) Solid % = 20	Flotation feed (US)		21.48	80.35	28.68	2.45	85.37	73.46
		Slimes (OS)	65	15.60	19.65	20.09	3.62	14.63	26.54
		Calculated head		20.00	100.00	26.99	2.68	100.00	100.00
7	Pressure = 68.95 kPa (10 psi) Solid % = 10	Flotation feed (US)		12.08	83.05	28.82	2.43	88.87	74.92
		Slimes (OS)	52	5.42	16.95	17.69	3.98	11.13	25.08
		Calculated head		10.00	100.00	26.93	2.69	100.00	100.00
8	Pressure = 68.95 kPa (10 psi) Solid % = 5	Flotation feed (US)		6.54	87.19	28.98	2.46	93.84	79.76
		Slimes (OS)	48	1.92	12.81	12.96	4.25	6.16	20.24
		Calculated head		5.00	100.00	26.93	2.69	100.00	100.00
9	Pressure = 137.90 kPa (20 psi) Solid % = 5	Flotation feed (US)		7.13	85.07	29.27	2.45	92.47	77.77
		Slimes (OS)	53	1.85	14.93	13.59	3.99	7.53	22.23
		Calculated head		5.00	100.00	26.93	2.68	100.00	100.00
10	Pressure = 206.84 kPa (30 psi) Solid % = 5	Flotation feed (US)		8.01	84.37	29.23	2.47	91.41	77.78
		Slimes (OS)	59	1.65	15.63	14.83	3.81	8.59	22.22
		Calculated head		5.00	100.00	26.98	2.68	100.00	100.00

EVALUATION OF THE DESLIMING EFFICIENCY BY FLOTATION

Table 3 shows flotation response of the different deslimed products. It shows that applying screening as a desliming technique, the overall phosphate losses in both flotation tailings and slimes cannot be less than 32.4 % contained in a 40.4 % of the sample weight. In fact such losses may increase to approximately 45% contained in more than half of the sample weight if the screening step operating conditions were not appropriately selected. However, as a general rule one can confirm from the obtain results that wet screening is a better technique for phosphate desliming compared to dry screening. This can be attributed to two main reasons because wet screening is much more efficient in slimes removal in addition to the side effect of cleaning the flotation feed surface.

On the other hand, the flotation feeds deslimed using hydrocyclone at its optimum operating conditions lead to an overall-phosphate losses of 14.22% contained in approximately 27.5% of the sample weight. The worst losses in case of using hydrocyclones were also of acceptable values (29% of P₂O₅ in 39 % of the sample

Table 3. Results of phosphate flotation after desliming using screening and hydrocyclones

Flotation of screening deslimed product			Wt., %	Assay, %		Recovery, %	
				P ₂ O ₅	MgO	P ₂ O ₅	MgO
11	Wet screening (low solids rate)	Concentrate	59.57	30.50	1.86	67.57	41.50
		Tail	28.50	20.22	4.14	21.43	44.16
		Overall phosphate losses (slimes + tail)	40.43	21.57	3.86	32.43	58.50
12	Wet screening (double solid layer)	Concentrate	58.00	29.85	1.93	64.29	42.08
		Tail	31.65	22.28	3.79	26.18	45.12
		Overall phosphate losses (slimes + tail)	42.00	22.90	3.67	35.71	57.92
13	Wet screening (four solid layers)	Concentrate	55.40	30.08	2.05	61.93	42.22
		Tail	34.50	22.72	3.47	29.13	44.56
		Overall phosphate losses (slimes + tail)	44.60	22.97	3.48	38.07	57.78
14	Dry screening (single solid layer)	Concentrate	52.95	30.30	2.25	59.47	44.29
		Tail	37.80	23.18	3.07	32.48	43.16
		Overall phosphate losses (slimes + tail)	47.05	23.24	3.19	40.53	55.71
15	Dry screening (double solid layer)	Concentrate	49.32	30.15	2.35	55.22	43.09
		Tail	41.85	23.71	2.92	36.85	45.46
		Overall phosphate losses (slimes + tail)	50.68	23.80	3.02	44.78	56.91
Flotation of hydrocyclone deslimed product			Wt., %	Assay, %		Recovery, %	
				P ₂ O ₅	MgO	P ₂ O ₅	MgO
16	Pressure = 68.95 kPa (10 psi.) Solid % = 20	Concentrate	61.99	30.98	1.78	71.15	41.17
		Tail	18.36	20.90	4.71	14.22	32.29
		Overall phosphate losses (slimes + tail)	38.01	20.48	4.15	28.85	58.83
17	Pressure = 68.95 kPa (10 psi.) Solid % = 10	Concentrate	65.44	30.98	1.65	75.28	40.14
		Tail	17.61	20.77	5.31	13.58	34.78
		Overall phosphate losses (slimes + tail)	34.56	19.26	4.66	24.72	59.86
18	Pressure = 68.95 kPa (10 psi.) Solid % = 5	Concentrate	72.60	31.82	1.48	85.78	39.94
		Tail	14.59	14.86	7.34	8.05	39.82
		Overall phosphate losses (slimes + tail)	27.40	13.97	5.90	14.22	60.06
19	Pressure = 137.90 kPa (20 psi.) Solid % = 5	Concentrate	68.44	31.56	1.79	80.21	45.71
		Tail	16.63	19.85	5.17	12.26	32.06
		Overall phosphate losses (slimes + tail)	31.56	16.89	4.61	19.79	54.29
20	Pressure = 206.84 kPa (30 psi.) Solid % = 5	Concentrate	65.87	31.29	1.89	76.39	46.45
		Tail	18.50	21.90	4.54	15.02	31.33
		Overall phosphate losses (slimes + tail)	34.13	18.66	4.20	23.61	53.55

weight). Another important parameter to characterize the desliming step is the overall separation efficiency of the desliming and flotation steps. Figure 2 shows the Fuerstenau plot having the overall separation index for all the considered runs. It shows that flotation preceded by hydrocyclone desliming is more selective than flotation preceded by screening. The separation index B range was from 0.298-0.524 in case the flotation feed was deslimed by screening. On the other hand, desliming by hydrocyclone led to separation index of 0.573 at its worst case which is higher than that obtained in case of optimum screening parameters. However, at the optimum hydrocyclone operating conditions the separation index B jumped to 0.739 which is approximately three times improvement compared to that obtained in case of desliming by dry screening.

CONCLUSIONS

The work presented here has significantly showed that phosphate desliming is an important step from the phosphate losses and flotation performance point of views. The major findings of the present investigations and their potential contributions to obtaining optimum deslimed flotation feed are:

1. The performance of phosphate upgrading by flotation is sensitive to many parameters among which the desliming method of the considered feed.
2. Even with proper operating parameters, screening can never produce an optimum deslimed flotation feed.
3. The efficient screening decreases the content of flotation feed slimes but at the same time it increases the phosphate losses in such slimes.
4. Desliming on wet screening is much more efficient than desliming carried out on dry screening bases.
5. Desliming using hydrocyclone is generally better than desliming using screening.
6. The overall separation index after the desliming and flotation steps depends significantly on the desliming method. This index was found to be 0.298 at the worst case of desliming by screening, while it was as high as 0.739 at the optimum operating conditions of desliming using hydrocyclones.

REFERENCES

- ABDEL-KHALEK N.A., Farrah S., 2004, *Surface modification for advancing separation processes and environment protection*, US-Egypt joint project, Academy of Science Research & Technology, Cairo, Egypt.
- AHMED H. A. M., 2005, *Application of microemulsion for upgrading difficult-to-float materials*, Ph.D. thesis, Faculty of Mining Geoengineering and Geology, Wroclaw University of Technology, Poland.
- ANAZIA I.J., HANNA J., 1987, *New flotation approach for carbonate phosphate separation*, Minerals and Metallurgical Processing, November, pp. 196-202.
- DRZYMAŁA J., AHMED H.A.M., 2005, *Mathematical equations useful for approximation of separation results using the Fuerstenau upgrading curves*, International Mineral Processing Journal, 76, pp. 55-65.
- EL-MAHDY A., 2004, Ph. D. thesis, Faculty of Engineering, Cairo university, Egypt.

- EWING, G. W., 1975, *Instrumental methods of chemical analysis*.
- HOUOT R., 1982, *Beneficiation of phosphate ores through flotation: Review of industrial application and potential developments*, International Journal of Mineral Processing, Vol. 9, pp. 353-384.
- HUYNH L., FEILER A., MICHELMORE A., RALSTON J., JENKINS P., 2000, *Control of slime coatings by the use of anionic phosphates: a fundamental study*, Minerals Engineering, vol. 13, No. 10-11, pp. 1059-1069.
- LAWNDY A.B.T., STEVEN J.V., 1993, *Flotation of high-iron phosphate ores and phosphatic iron ores*, in *beneficiation of phosphate: theory and practice*; H. Elshall; B. M. Moudgill; and R. Wiegel (eds), pp. 29-43.
- PATRICK Z.; YU Y.; BOGAN M; 1996, *Challenging the CRAGO double float process. II. Amine-fatty acid flotation of siliceous phosphates*, Mineral Engineering '96 Conference, Brisbane, Aug. 26-29.
- PATRICK Z., ROBERT S., YINGXUE Y., Michael B., 2001, *Recovery of phosphate from Florida phosphatic clays*, Florida Institute of Phosphate Research (FIPR) project number: 93-02-096R, final report.
- Restarick C.J., 1989, *Classification with two-stage cylinder-cyclones in small-scale grinding and flotation circuits*, International Journal of Mineral Processing, Volume 26, Issues 3-4, Pages 165-179.
- SCOTT, W.W., 1949, *Standard method of chemical analysis*, Longman, London.
- XIAPENG ZHENG, ARPS P.J , SMITH R.W. , 2001, *Adhesion of two bacteria onto dolomite and apatite: their effect on dolomite depression in anionic flotation*, Int. J. Miner. Process. 62, 159-172.
- YINGXUE YU et al., 1995, *Amine-fatty acid flotation of siliceous phosphates, another challenge of the CRAGO double float process*, 10 th Annual Regional Phosphate Conference, Lakeland, Fla.

Ahmed H.A.M., *Optymalizacja odszlamiania poprzedzającego wzbogacanie fosforytów metodą flotacji*, Physicochemical Problems of Mineral Processing, 41 (2007) 79-88 (w jęz. ang.).

Flotacja jest jedną z najbardziej efektywnych technik stosowanych do wzbogacania fosforytów. Odszlamianie nadawy flotacyjnej jest ważnym warunkiem wstępnym dobrej separacji fosforytów od skały płonnej. Ogólnie, celem etapu odszlamiania jest minimalizacja ilości drobnych ziarn dla uniknięcia ich negatywnego wpływu na flotację. Jednakże szlamy zawierają także fosforany, które zostają tracone. Efektywne odszlamianie powinno brać pod uwagę minimalizację strat fosforanów w usuwanych drobnych ziarnach oraz pozwolić na utrzymywanie wysokiej zawartości fosforanów w nadawie flotacyjnej. W tej pracy optymalizowano etap odszlamiania dla uzyskania obu celów jednocześnie. Użyto różnych technik badawczych stosując zróżnicowane warunki technologiczne. Jako sposób usuwania drobnych ziarn zastosowano przesiewanie i klasyfikację w hydrocyklonach. Stwierdzono, że w optymalnych warunkach odszlamianie w hydrocyklonach jest lepsze niż na sitach. Odszlamiany materiał zawiera małe ilości fosforanów i dlatego prowadzi to do efektywnej separacji za pomocą flotacji a wskaźnik selektywności B, zdefiniowany jako $\varepsilon_{1,c} = (100 - \varepsilon_{2,t})^{(1-B)} / 100^{(-B)}$ osiąga wartość 0.739, gdzie $\varepsilon_{1,c}$ oznacza uzysk P_2O_5 w koncentracji flotacyjnym w %, podczas gdy $\varepsilon_{2,t}$ oznacza uzysk MgO w szlamach jak i w odpadzie flotacyjnym (w %).

Kadry N. SEDIEK*, Ashraf M. AMER**

SEDIMENTOLOGICAL AND TECHNICAL STUDIES ON THE MONTMORILLONITIC CLAYS OF ABU TARTUR PLATEAU, WESTERN DESERT, EGYPT

Received April 12, 2007; reviewed; accepted May 18, 2007

One of the most known sedimentary formation among Egyptian Upper Cretaceous rock units is named Duwi Formation (Lower Maastrichtian), an outcrop at the Abu Tartur plateau, Kharga Oasis, Western Desert, Egypt. This formation displays three montmorillonitic clayey layers. The investigations of these sediments provide information on the texture, constituents and type of clay minerals, which helps define and describe their physical and technical properties.

Granulometrically, the selected samples have siltstone, mudstone and claystone facies. Mineralogical analysis of the studied deposits proved that the clay minerals compose mainly of montmorillonite, in addition to small amount of glauconite, and traces of illite. Scanning electron microscopy revealed three main micro-structures, namely honeycomb, matrix, and turbulent.

Acid activation of eight samples was performed using hydrochloric acid. The efficiency of activation was examined by measuring their bleaching capacity to crude cotton seed oil, and changes in their surface areas. The acid treatment resulted in more than 4-fold increase in the activity of the pretreated bentonite samples. The extent of activation was found to be pronounced after the first 30 minutes of acid treatment.

Key words: clays, montmorillonite, acid activation, bleaching ability, drilling mud, Abu Tartur

INTRODUCION

The studied samples have been collected nearby the Abu Tartur mine, which is located at the intersection of longitude 30° E. and latitude 25°30'N. This area had attracted the attention of many researchers since the discovery of great phosphatic deposits in 1967 and is still under focus due to its strategic position as a source of raw

* Head of Environmental Science Department, Faculty of Science- Alex. University, Egypt,
e-mail: ashrafamer0408@yahoo.com.

** Geology Department, Faculty of Science, Alexandria University, Egypt, e-mail: kknسد@yahoo.com.

materials, especially the phosphates, clays and other rocks. Several lithologic, biostratigraphic, hydrological, geotechnical, and technological studies were carried out either on surface outcrop or subsurface. They were mentioned by Said (1990) and Sediek (1999).

Recently, the Kharga or New Valley government have new thoughts for encouraging scientists to carry out applied or technical studies on the exposed rocks to facilitate exploitation of claystone and mudstone as raw material for industry of ceramics, bricks and others industrial purposes. The most recent studies in this field were described by Sediek and Amer (2001) and Sediek (2005).

Bleaching and adsorption properties of bentonites towards oil and dyes are normally increased by acid treatment (Russu et al., 1979). Acid treatment of clay leads to removal of some ions from their frame structure, which cause an increase in their surface areas. However, caution should be taken during acid treatment of montmorillonite to avoid the formation of non-active hydrated silica. The efficiency of activation process of montmorillonite depends mainly on the nature of acid, its concentration, temperature of activation, and the nature of clay itself, especially the Al_2O_3 : SiO_2 ratio. The aim of the present work is the activation of montmorillonitic clays of Duwi Formation exposed at Abu Tartur plateau deposits to sustain its suitability to be used in drilling mud.

MATERIAL AND METHODS

Ten representative samples of surface exposed sediments on the Abu Tartur Plateau, Kharga Oasis were collected from the Duwi Formation. These samples have been exposed to megascopic investigation. Carbonate content, insoluble residue and organic matter content had been determined in the ten fine grained argillaceous samples. These samples were mechanically analyzed by wet method according to their grain-size following Carver (1971). The obtained data were illustrated in Table 1 and on a sand-silt-clay triangle (Braja, 1990) in Fig. 1.

The selected clayey samples were examined by X-Ray Diffraction (XRD) in Moscow State University using Dron 3-model instrument with CuK radiation. The resulted XRD diffractograms were interpreted using Krotova and Kazakova (1984) and Starkey et al. (1984) flow sheet to define the clay mineral type of these samples. The same samples were investigated by scanning electron microscope (SEM). These investigations were carried out at both Moscow State University and Alexandria University, Faculty of Science, Central Laboratory.

Acid activation was performed by treating these clayey samples with HCl having different concentrations between 1 and 6 M. The clay ratio was kept at 1:2.6. Treatment was carried out at 95°C and different leaching periods varying from 20 minutes up to 8 hours. A two-gram montmorillonite clay sample was added to 5 cm^3 of HCl in three-neck flask fitted with a thermometer, reflux condenser, and stirrer. A 0.25 g of the treated bentonite was added to 20 cm^3 of crude cotton seed oil in a wide

test tube immersed in an oil bath kept at 100° C for 30 min with stirring. The optical density of the bleached oil was measured by a Unicam Spectrophotometer SP 500 at 460 nm. The total surface area of activated solid products were determined using the ethylene glycol mono ethyl ether (EGME) method.

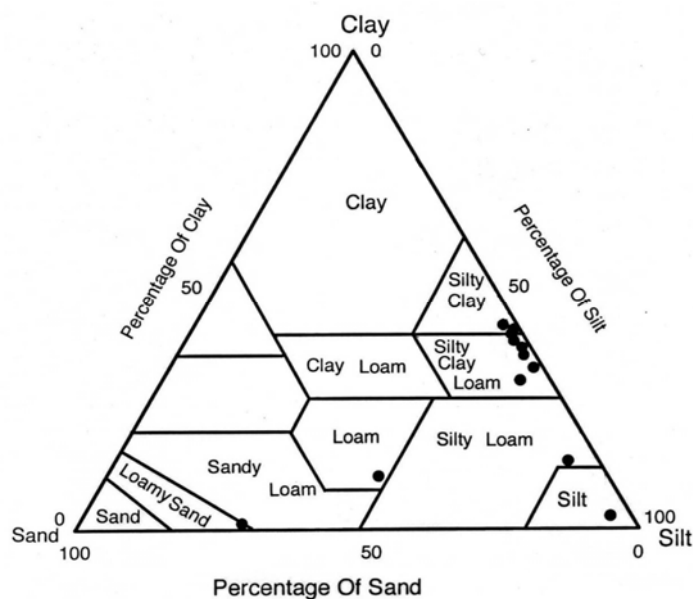


Fig. 1. Textural classification of the studied sediments (after U.S. Department of agriculture classification, Braja, 1990)

SEDIMENTOLOGICAL CHARACTERISTICS

GRANULOMETRIC INVESTIGATION

The studied fine sediments have subjected to granulometric analysis using the pipette or wet method. The obtained data are illustrated in Table 1. According to Shepard (1954) classification of fine-grained sediments, the Duwi Formation Sediments (DFS) lie in clayey siltstone, siltstone, silty mudstone and claystone in a decreasing order of abundance. It means that the common facies among these sediments is the siltstone, while the majority are represented by clayey siltstone and pure siltstone. The siltstones of Duwi Formation tend to be clayey in nature.

The granulometric analysis data revealed two main categories of rocks. The first and more common is the siltstone and the second is the mudstone and claystone. The investigated siltstones have clayey nature, occasionally exhibit glauconitic, phosphatic contents or even ferruginated tint. The first two materials were observed frequently in the DFS. Compositionally, the siltstone have a calcareous character, where the carbonate content ranges from 11.88 to 41.42 % in the DFS. Granulometrically, the

siltstones include three subfacies, namely pure siltstone, clayey siltstone, and sandy siltstone. The second subfacies is the most frequent one. In the case of mudstone and claystone, these rocks display the mentioned megascopic characters as in siltstones. According to the frequency distribution of clay fraction among the studied sediments, these facies are low in abundance (Table 1 and Fig.1).

The obtained data of the analyzed sediments were plotted on the triangle of textural classification of sediments (Braja, 1990). It had appeared that the samples fall into several zones (Fig. 1). The DFS samples lie in Silt, Silty loam, Silty clayey loam, and Loam.

Table 1. Granulometric analysis of the representative montmorillonitic sediments of Abu Tartur Plateau

Clastic constituents	Sample No.						
	Du. 27	Du. 26	Du. 25	Du. 23	Du. 21	Du. 17	Du. 16
Sand	0.84	0.38	0.08	0.40	0.76	12.52	3.39
Silt	58.21	60.21	50.78	58.49	60.32	71.14	82.63
Clay	40.95	39.40	49.12	42.05	38.92	16.34	13.43

MINERALOGICAL INVESTIGATION

The purpose of the present part is to describe the distribution and characteristics of mineral composition, especially the clay minerals of the fine sediments, and evaluate the clay mineral data in terms of environmental conditions and its effect on the technical properties. Six samples were analyzed using the X-Ray diffraction method. These samples were selected as good representative and cover the collected fine-grained sediments, which seem to be rich in montmorillonite clay mineral.

X-RAY ANALYSIS OF BULK SAMPLES

X-ray diffractogram of the investigated samples revealed the presence of two main mineral types, that is clayey and non-clayey. The detected clay minerals include smectite, illite, kaolinite, glauconite, while the non-clay minerals include quartz, feldspar, carbonate minerals (calcite and dolomite), evaporite (anhydrite or gypsum) and others as jarosite, pyrite and apatite. Analyzing the obtained data, two mineral associations were recognized. The first association includes high smectite (40 - 91 %), quartz (8.80 - 30.8 %), as well as traces of illite and kaolinite. The second association includes high glauconite (15.40 - 88.10 %), quartz (3.10 - 35 %), and traces of illite.

X-RAY ANALYSIS OF CLAY FRACTION

Ten samples of separated clay fraction were selected and investigated by the X-ray analysis. Three of them are illustrated in Fig. 2. Three runs of oriented clay particles (air dried untreated glycolated and heated to 550 °C) were carried out. The X-ray diffractograms of two selected samples of Duwi Formation (Du.27, 23) show a

uniformity in their recorded peaks and consequently refer to similar clay minerals, where the air dried untreated runs have 1.421 nm, this peak was expanded to 1.78 nm. By heating, this peak collapses to 1.0 nm with the appearance of weak 0.5 nm peak indicating montmorillonite clay mineral. The diffractogram of the third sample (Du.22) shows more or less different positions of the peaks, where the air dried untreated run shows 1.45 nm. Under glycolation this peak shifts to larger spacing 1.8 nm with increasing in its intensity and by heating this peak shifts to smaller spacing of 1.0 nm, indicating randomly interstratified smectite–chlorite. This diffractogram also shows 0.716 nm peak under air dried run, and remained at the same spacing through glycolation run, while destroyed during heated run, indicating kaolinite of disordered type.

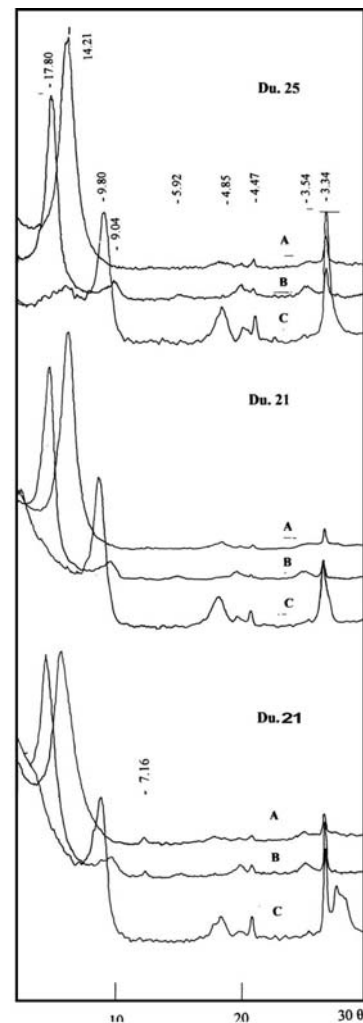


Fig. 2. Diffractogram of the representative clay fraction of the Upper Cretaceous sediments of Abu Tartur Plateau
 A: Oriented air dried run,
 B: Glycolated slide run,
 C: Heated slide run

Table 2. Mineralogical analysis of the representative montmorillonitic sediments of Abu Tartur Plateau

Sample No	Clay Minerals				Non-clay Minerals					
	Sm.	Illite	Ka	Gl	Q	F	D+C	An+G	J	O. M
Duwi Formation Sediments										
Du. 27	91.00	0.10	0.10		8.80					
Du. 26	61.50	0.70	1.10		30.80	5.90				
Du. 25				50.90	22.80			7.89	16.00	
Du. 23	89.10				9.20	1.60				
Du. 21	83.20		3.20		8.20	1.25	2.40			
Du. 17	73.40		0.60		17.30	2.60			3.80	P= 1.2
Du. 16				88.10	3.10			0.01	7.50	P=1.7
Du. 15	40.00	30.00			30.00					

Sm = smectite, Ka = kaolinite, Gl = glauconite, Ki = palygorskite, Q = quartz, F = feldspar, D = dolomite, C = calcite, An = anhydrite, G = gypsum, J = jarosite, P = pyrite, A = apatite, O. m = other minerals

MICRO-TEXTURES AND NANO-STRUCTURES

Depending on mineral composition, shape and degree of dispersion of primary clay particles as well as sedimentation conditions, micro-aggregates in clayey sediments may take different forms and may range in diameter from fractions to score of micrometers (Grabowska-Olszewska et al., 1984). The studied samples show broad ranges of form and size, they vary from sheet-like micro-aggregates and micro-blocks formed by illite (Figs. 3 b-e) and montmorillonite (Fig. 4a-c), occasionally show isometric forms.

The type of contacts of micro-grain or micro-crystal are face-to-edge or edge-to-edge (Fig. 3a) and face-to-face (parallel platelets) as in Fig. 3e.

The obtained microphotographs show a wide variation of sedimentary nano-structures, the first and most common microstructure is the honey comb microstructure. It is characterized by the presence of open nearly isometric cells 2-5 μm in size and the cells wall are mostly montmorillonite-illite (Fig. 3a,b). This structure is considered as a universal feature of marine sediments. Such structure reflects a certain conditions of formation, which express the difference in mineral composition (montmorillonite, illite, occasionally chlorite), temperature regime and salinity in their basin of sedimentation. A characteristic feature of honey comb microstructure in marine sediments is the presence of a great amount of organic residues (Grabowska-Olszewska et al., 1984).

The second microstructure is the matrix type, which is characterized by the presence of a continuous nanoriented clay mass (matrix), that contains irregularly arranged inclusions of silt (Fig. 3c). This microstructure indicates illite and mixed layer composition. It is most probably formed from reconstruction of the honey comb microstructure during compaction process (Grabowska-Olszewska et al., 1984).

The third recorded microstructure is the turbulent type (Fig. 3d,e) in which the orientation of clay material results in a pronounced anisotropy of physical and mechanical effects. This microstructure most probably occurred during compaction of clayey sediments containing both structure honey comb and matrix microstructures. The turbulent microstructures commonly occur in marine environment with medium degree of compaction.

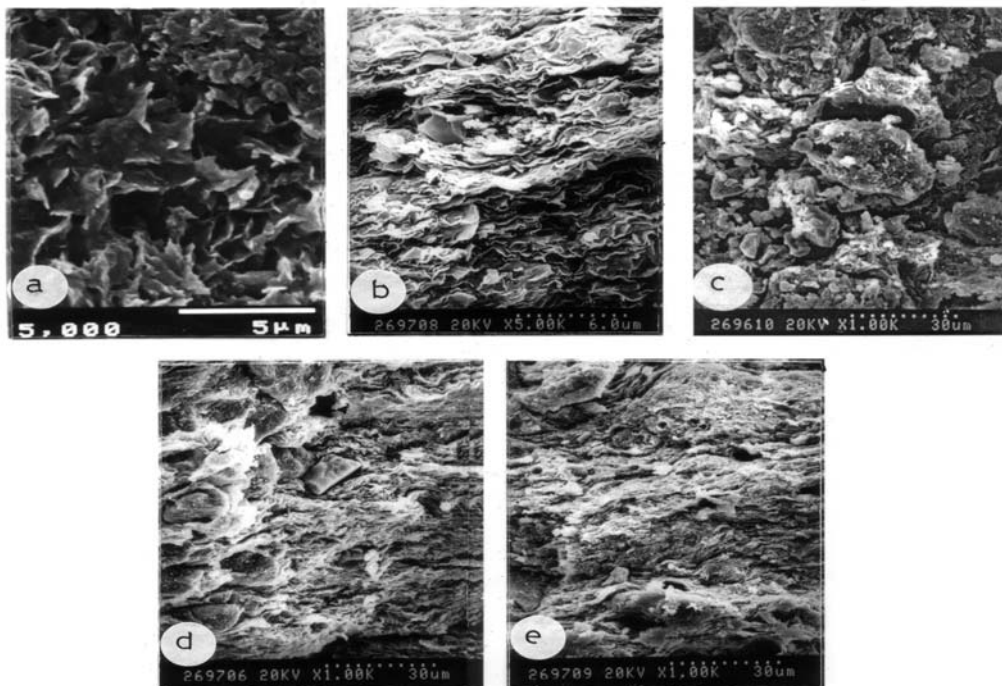


Fig. 3. Scanning Electron Microscope microphotographs of representative clayey sediments
a, b: honey comb microstructure with montmorillonite and illite cell walls, c: Matrix microstructure
with illite and mixed composition, d, e: turbulent microstructure type

According to the mutual grain-to-grain relationship, two main types of micropores were defined: inter-granular and intra-granular micropores. The first type is illustrated in Fig. 3a-e, which resulted in clayey sediments with silty grains. The second type is most probably due to diagenetic dissolution or leaching process (Fig. 3d), the pore here takes more or less an isometric form with several microns in diameter ($\approx 4\mu\text{m}$).

In reference to the Grabowska-Olszewska et al. (1984) classification, the recorded pores divided into two main types: ultrapore ($< 0.1 \mu\text{m}$ in size), which are completely filled with absorbed water and micropore ($0.1-10 \mu\text{m}$), in which capillary rise as well as filtration under gradient take place. The first type is not easy to observe, while the second one could be observed with isometric morphologic form (Fig. 3a-c).

ACTIVATION OF ABU TARTUR CLAYS

The montmorillonite type clays are usually subjected to some treatment in order to improve definite properties which make it suitable for the purposes of which the montmorillonite is required for. Some of these treatments include alkali activation, acid activation and thermal treatment which are of great importance in the industrial uses (Ross, 1964). Preliminary acid activation test were carried out on the investigated samples of Abu Tartur clays.

BLEACHING ABILITY

Acid activation was performed using HCl as an activation agent with different concentrations (1, 2, 4, and 6 M), at constant clay/acid ratio of 1:2.6 and constant temperature of 95° C for leaching period of 20 min - 10 hours. The activation extent was determined by measuring the external surface area of the activated samples using BET method. Furthermore, the bleaching was carried out on cotton seed oil using a clay oil ratio of 1:80 (g/cm³) at 100°C for 30 minutes.

Table 3. Bleaching ability of montmorillonitic clay samples of Abu Tartur Plateau

Sample No.	Leaching periods, min					
	Untreated	60	120	180	300	480
Du. 27	53.6	93.7	92.4	96.9	98.9	94.4
Du. 26	43.7	89.6	92.4	96.1	94.1	93.2
Du. 25	51.1	90.0	90.4	96.0	96.0	--
Du. 23	53.2	90.6	91.5	96.3	92.3	--
Du. 21	50.4	91.1	91.7	98.9	95.9	--
Du. 17	48.4	91.5	89.2	91.9	91.3	--
Du. 16	39.6	89.4	92.3	96.9	96.2	--
Du. 15	46.9	87.5	89.9	93.9	93.9	--

It was found that the bleaching ability and the external surface area of the acid treated samples were rapidly increased after the elapse of the first 20 minutes. They acquired limited values were of 3.5-fold and 5-fold respectively higher than those of the untreated sample. This may be attributed to the great ease with which a new active compound is formed as a result of the high reaction rate between smectite and hydrochloric acid. At leaching period longer than 20 minutes, a slight decrease in the bleaching ability was observed as a result of the complete destruction and collapse of smectite structure. At prolonged leaching periods, the bleaching ability was slightly increased due to the slow response of the clay minerals (e.g. kaolinite) to the action of hydrochloric acid. It is noticed that the bleaching ability does not appreciably

increased while the concentration of acid increase, where values of 85-100% were obtained at acid concentration range of 1-6 M respectively. Under the optimum leaching conditions, only 0.94g of the activated clays (using 6 M HCl) develop the same bleaching efficiency effect of 1 g of the standard bleaching material. The same effect is only remarked with 5.4 g of the unactivated samples.

SURFACE AREA

Changes in the total surface area of the studied montmorillonitic clay samples, as well as their respective activated products treated at 95° C with 6M HCl for different periods ranging from 1-5 hours. The results are shown in Table 4.

Table 4. Surface areas of montmorillonitic clay samples of Abu Tartur plateau

L.P./hours	Surface area (m ² /g)							
	Du. 15	Du. 16	Du. 17	Du. 21	Du. 23	Du. 25	Du. 26	Du. 27
Untreated	19.0	37.7	26.1	32.4	24.3	26.7	32.0	32.7
1	123	122	140	130	174	173	115	116
3	155	144	148	105	130	128	128	192
5	111	133	196	162	158	172	148	210

The obtained results in this Table illustrate that the starting surface areas are considerably different from one sample to another ranging from 19 to 37.7 m²/g. This may be attributed to the changes in the nature of the oxide components which are present in each sample, as well as its position as exposed sample or taken from the inside Abu Tartur mine. A sudden increase in the surface area was noticed after a short period of acid treatment (during the first hour), the increase ranges from 5 to 7-folds. There was a further gradual increase in the surface area with further acid treatment. A slight increase of the total surface area followed by a gradual decrease was observed upon increasing the leaching period. This increase is related to the destruction of the smectite structure. The sharp increase in the surface area could be interpreted due the dissolution of soluble salts, carbonates and some free oxides that lead to the creation of new space and pores accessible to adsorption, while the slight decrease of surface area, that happened after 3 hours, in some cases may be due slight collapse in the clayey flakes.

It can be noticed that the total surface area of the studied samples range from 115-210 m²/g indicating the presence of high internal surface area values which are mainly due to the presence of smectite minerals. Comparing the total surface areas obtained from the studied samples with those of pure montmorillonite (250m²/g) and kaolinite (70m²/g). It can be estimated that the studied clays contains a considerable amount of smectite minerals.

GEL INDEX

Determination of the gel index was carried out where 4.2 g clay, 7-8 g alumina and 0.6 g magnesium oxide were mixed with 100 cm³ of distilled water for 60 minute in a measuring cylinder. The mixture was allowed to stand for 24 hours and the volume of the suspension liquid is measured and subtracted from 100 cm³. This gives the value of gel index in percent. For comparison between the obtained values of yield test and gel index, it is clear that the activated Abu Tartur montmorillonite are of relatively high yield values (39 barrel/Mg). The plastic viscosity is relatively high (7 cP) and indicates that the studied samples can be used in preparation of drilling fluids for petroleum industry.

CONCLUSIONS

From the aforementioned studies, it is concluded that the fine-grained sediments of Upper Cretaceous of Abu Tartur Plateau are poorly fossiliferous and vary in color from gray, green to black in Duwi Formation sediments (abundance of black shale). According to the technical textural classification, the studied sediments lie in five zones, ordered according to their increasing in abundance, loam, silt, clay, silty clay, and silty clay loam. Based on the quantitative and qualitative estimation of mineral composition through the study of the X-ray diffractograms, two main mineral association were recognized: high smectite-quartz-traces of illite and kaolinite, high glauconite-quartz-trace of illite. Furthermore, the clay mineral has good crystallinity (high, intense peaks). With reference to the micro-texture and microstructure, three main micro-structures were defined namely, honey comb, matrix, and turbulent micro-structure, which refer to a vary paleo-condition of deposition. Experimentally, it has been noticed that the most effective condition of the bleaching efficiency of the studied samples were activation with 6 M HCl at 95 °C, and using clay to acid ratio (1 g : 2.5 ml) for 5 hours. The surface area of the studied montmorellonitic clay samples increased after short period of acid treatment (one hour) and the increase ranged between 5 to 7-folds. Displaying the main granulometric, mineralogical composition, nanostructure and other physical parameters after acid activation, shows that the studied Abu Tartur clays can be used in preparation of the drilling mud.

REFERENCES

- BRAJA M. (1990), *Principles of Geotechnical Engineering Geology*, PWS-KENT, publishing company- Boston, 665p.
- CARVER R.E. (1971), *Procedures in sedimentary petrology*, John Wiley and Sons Inc., New York, London, 663p.
- GRABOWSKA-OLSZEWSKA B., OSIPOV V., SKOLOV V. (1984), *Atlas of the microstructures of clay soils*, Panstwowe Wydawnictwo Naukowe, 414 p.
- KROTOVA G.E., V.E. KAZAKOVA (1984), *Directory for identification of clay minerals using X-ray diffraction method*, Univ. Patres Lomomba, Geol. Depart., Moscow, Paper N. 26, 52 p. (in Russian).

- MINGELGRIN U., KLINGER L., GAL M., SOLTZAM S., (1978), *Clays and clay minerals*, 26/4, 299-307.
- SAID R. (1990), *The Geology of Egypt*, A.A. Balkema, Rotterdam, Netherland, 734 p.
- SEDEIK K.N. (1999), *Contribution to the sedimentation of some glaucony deposits of the Kharga-Dakhla Stretch, Western Desert, Egypt*, *Egyptian Miner.* v. 11, 211-230.
- SEDEIK K.N., AMER A. M. (2001), *Sedimentological and technological studies of Abu Tartur Black shales, Western Desert, Egypt*, *Physicochemical Problems of Mineral Processing*, v. 34, 141-152, Wroclaw, Poland.
- SHEPARD F.P. (1954), *Nomenclature based on sand-silt-clay ratios*, *J. Sed. Petrology*, 24, 151-158.
- STARKEY H.C., BLACKMON P.D., HAUFF P.L (1984), *The routine mineralogical analysis of clay – bearing samples*. U.S geol. Surv., Bull. 1563.
- PATTERSON S.H., MURRAY H.H., (1975), *International minerals and rocks*, 4th Ed., Am. Industr. Min. Metall. & Petrol. Eng, New York.
- RASHED M.A., AMER A.M., (1997), *Geology, Mineralogy and beneficiation of south Alamein clays*, *Modeling, Measurements & control*. Tassan, France. v. 56, no. 1,2.
- ROSS J.S. (1964), *Bentonite in Canada*, *Miner. Branch Monograph 873*, Canada. Dept. nicefemale89@yahoo, Mines and Tech. Surveys.
- RUSSU V.I., OKOPNAYA N.T., STRATULAT G.V., ROPOT V.M. (1979), *Adsorpcionnyye Processy Adsorbentov*, Akad. Nauk Uzbeksoi SSR, Inst. Khimii, USSR, p. 257-259.

Sediek K.N., Amer A. M., *Sedymentologiczne i techniczne badania glin montmorylonitowych z Równiny Abu Tartur na Pustyni Zachodniej Egiptu*, *Physicochemical Problems of Mineral Processing*, 41 (2007) 89-99 (w jęz. ang.).

Jednym z najbardziej znanych utworów osadowych skał Egipskiego Górnego Cretaceous jest formacja Duwi w Dolnym Maastrichtianie wysadu Równiny Abu Tartur Oazy Charga na Egipskiej Pustyni Zachodniej. Formacja ta posiada trzy warstwy montmorylonitowe. Badania osadów dostarczyły informacji o teksturze, składnikach i typie minerałów gliniastych, co pomaga definiować i opisywać ich fizyczne oraz techniczne właściwości.

Badane próbki zawierały frakcje pyłowe, mułowe i gliniaste. Analiza mineralogiczna badanych osadów wykazała że minerały gliniaste zawierały głównie montmorylonit, a także małe ilości glaukonitu i ślady illitu. Skaningowa mikroskopia elektronowa wykazała trzy główne mikro-struktury, a mianowicie plastra miodu, matrycową i chaotyczną.

Przeprowadzono aktywację kwasową ośmiu próbek stosując kwas chlorowodorowy. Skuteczność aktywacji badano poprzez pomiar zdolności do wybielania surowego oleju z nasion bawełny oraz zmiany w ich obszarach powierzchniowych. Aktywacja kwasem prowadziła do czterokrotnego wzrostu aktywności próbek. Stopień aktywacji był znaczący po pierwszych 30 minut traktowania kwasem.

Tolga DEPCI*, Gülhan ÖZBAYOĞLU*, Ayşen YILMAZ**

THE EFFECT OF DIFFERENT STARTING MATERIALS ON THE SYNTHESIS OF LITHIUM TRIBORATE

Received April 15, 2007; reviewed; accepted May 7, 2007

Lithium triborate (LiB_3O_5) was synthesized using different starting materials. The effect of these materials on the phase purity of LiB_3O_5 was investigated in each case. Identification and characterizations of the products were carried out by powder X-ray diffraction (XRD) and infrared (IR) analyses. The present study showed that the starting materials play an important role in the synthesis of lithium triborate with respect to phase impurity.

Key words: lithium triborate, solid state, XRD analysis, IR analysis

INTRODUCTION

Lithium triborate, LiB_3O_5 , is a newly developed nonlinear optical crystal which is chemically stable, mechanically robust and not hygroscopic. It shows thermoluminescence properties. The synthesis and characterization of lithium triborate (LiB_3O_5) have been investigated and reported in the literature (Mazetti 1926; Rollet and Bouaziz 1955; Sastry and Hummel 1958; König and Hoppe 1978; Betourne and Touboul 1997; Massot et al., 1989; Zhong and Tang 1996; Morcyc and Ptak 1999; Almedia et al., 2001). It is difficult to obtain LiB_3O_5 as a pure compound. During the synthesis stage, some lithium borate compounds like tetraborate ($\text{Li}_2\text{B}_4\text{O}_7$), pentaborate (LiB_5O_8), lithium octaborate ($\text{Li}_2\text{B}_8\text{O}_{13}$) can be present in the lithium triborate phase (Sabharwal et al., 2003, 2004; Özdemir et al., 2004; Ardıçoğlu et al., 2006). The purity of lithium triborate is important in the usage of LiB_3O_5 as a thermoluminescent material, as the impurities may influence the intensity of glow curve.

* Department Mining Engineering, Middle East Technical University, 06531, Ankara, Turkey.

** Department of Chemistry, Middle East Technical University, 06531, Ankara, Turkey.

In recent years, Özdemir et al. (2004) and Ardiçoğlu et al. (2006) studied the synthesis of LiB_3O_5 starting from a stoichiometric mixture of the Li_2CO_3 and H_3BO_3 by heating at $750\text{ }^\circ\text{C}$ for 7, 14, and 21 hours. They found that LiB_3O_5 can be produced by solid state reaction method at $750\text{ }^\circ\text{C}$ for 14 hours, but they observed some impurities (e.g $\text{Li}_2\text{B}_4\text{O}_7$) in the XRD patterns.

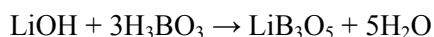
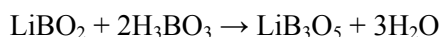
In this present study, the effect of different starting materials on synthesis of LiB_3O_5 was investigated with respect to phase impurity.

EXPERIMENTAL PROCEDURE

Li_2CO_3 and H_3BO_3 powders were used as starting materials for the synthesis of LiB_3O_5 . The powders, weighed in stoichiometric amounts, were ground in an agate mortar and pre-heated at $300\text{ }^\circ\text{C}$ for 4 hours to remove water. Obtained material was reground and heated in a crucible at $750\text{ }^\circ\text{C}$ for 14 hours. The procedure was based on the study carried out by Özdemir et al., (2004).

In the second series of tests, different starting materials were used for the synthesis of LiB_3O_5 to determine the possibility of its production without any impurity. The same synthesis conditions of previous test were applied during these tests. Four binary compounds, $\text{LiBO}_2 - \text{H}_3\text{BO}_3$, $\text{LiBO}_2 - \text{B}_2\text{O}_3$, $\text{LiOH} - \text{H}_3\text{BO}_3$, $\text{LiOH} - \text{B}_2\text{O}_3$ respectively were used in the preparation of LiB_3O_5 .

Typical reactions are given below:



In order to identify the phases of samples, a Rigaku MiniFlex X-ray Diffractometer was employed. All measurement were performed by using monochromatic $\text{Cu K}\alpha$ (30 kV, 15 mA, $\lambda=1.54051\text{ \AA}$) radiation at room temperature and XRD patterns were recorded from $5^\circ < 2\theta < 70^\circ$. The measurements were made with 0.05 degree steps and 1 degree/ minute rate.

In order to determine the structure of the produced compounds, the infrared spectra (IR) was measured, using KBr pellets made from a mixture of samples by using VARIAN 1000FTIR Spectrometer (from 400 to 2000 cm^{-1}).

RESULTS AND DISCUSSION

Lithium triborates, which were synthesized by using different starting materials, such as $\text{Li}_2\text{CO}_3 - \text{H}_3\text{BO}_3$, $\text{LiBO}_2 - \text{H}_3\text{BO}_3$, $\text{LiBO}_2 - \text{B}_2\text{O}_3$, $\text{LiOH} - \text{H}_3\text{BO}_3$, $\text{LiOH} - \text{B}_2\text{O}_3$ at 750°C for 14 hours, were evaluated by XRD and IR.

The phase identifications of the lithium triborates are shown in Fig. 1. Comparing these characteristic X-ray powder diffraction patterns of lithium triborates with each other, it was found that LiB_3O_5 obtained by a stoichiometric ratio of LiBO_2 and H_3BO_3 (Fig. 1b) was in a good agreement with the XRD pattern of LiB_3O_5 synthesized by using Li_2CO_3 and H_3BO_3 (Fig. 1a). Analysis of the powder X-ray diffraction data showed that the compounds contained LiB_3O_5 as a major phase (JCPDS File No 77-0774). The reflection at 21.8° , 25.55° , and 33.6° (2θ) confirmed the presence of $\text{Li}_2\text{B}_4\text{O}_7$ (JCPDS File No 18-717) and also, lithium triborate lines match exactly the peak values reported in the literatures (Betourne and Touboul 1997, Sabharwal et al., 2003, 2004, Özdemir et al., 2004, Ardiçoğlu et al., 2006).

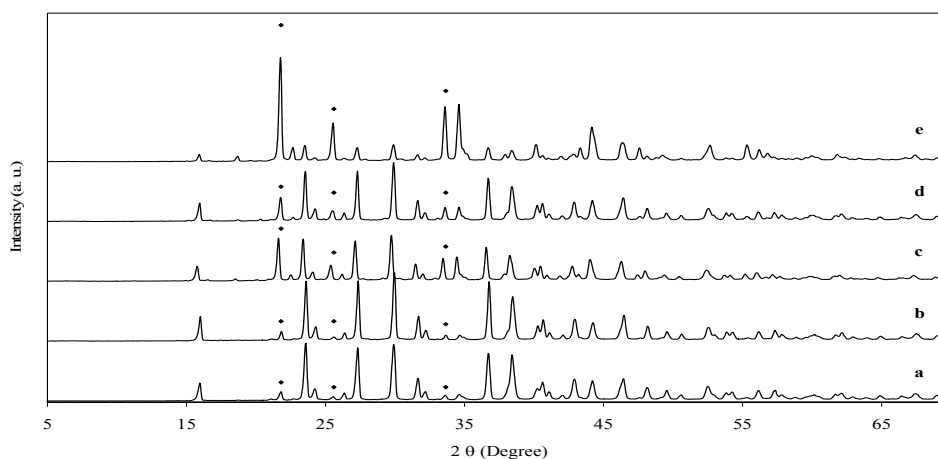


Fig. 1. Powder X-ray diffraction patterns recorded for the polycrystalline LiB_3O_5 materials obtained using different starting materials, a) Li_2CO_3 and H_3BO_3 , b) $\text{LiBO}_2 - \text{H}_3\text{BO}_3$, c) $\text{LiBO}_2 - \text{B}_2\text{O}_3$, d) $\text{LiOH} - \text{H}_3\text{BO}_3$, e) $\text{LiOH} - \text{B}_2\text{O}_3$. The reflections marked by (◆) have been identified as $\text{Li}_2\text{B}_4\text{O}_7$, the remaining reflections belong to LiB_3O_5

However, in the XRD patterns of LiB_3O_5 obtained from $\text{LiBO}_2 - \text{B}_2\text{O}_3$ (Fig. 1c), $\text{LiOH} - \text{H}_3\text{BO}_3$ (Fig. 1d) and $\text{LiOH} - \text{B}_2\text{O}_3$ (Fig. 1e), the intensities of lines belonging to LiB_3O_5 were lower and signal to noise ratios of $\text{Li}_2\text{B}_4\text{O}_7$ pattern were higher. Especially, in Fig. 1e ($\text{LiOH} - \text{B}_2\text{O}_3$ powders as starting materials), $\text{Li}_2\text{B}_4\text{O}_7$ appeared as a dominant phase.

The IR spectra of lithium triborates are shown in Fig. 2. In the literature, it was observed that $400 - 2000\text{ cm}^{-1}$ region was enough to determine the structure of lithium borates, because of existence of many clear intensive bands, sensitive to the boron

substitutions in this region (Morcy and Ptak 1999, Almedia et al., 2001). Therefore, in the present study, the IR spectra of lithium triborates were measured from 400 to 2000 cm^{-1} region.

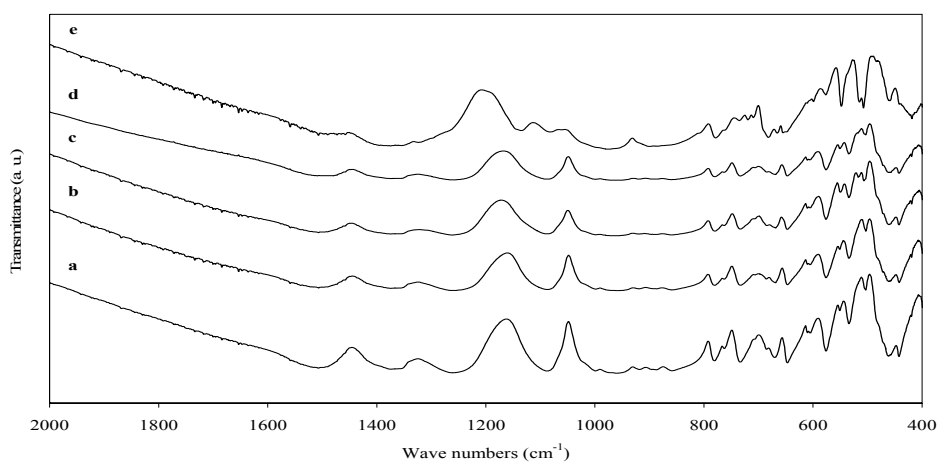


Fig. 2. IR spectra of LiB_3O_5 recorded for the polycrystalline LiB_3O_5 materials (a, b, c, d, e, are same as in Fig. 1)

When the IR spectra were compared, no major change was observed in the infrared bands except LiB_3O_5 synthesized by using $\text{LiOH-B}_2\text{O}_3$ as the starting materials. The strong bands observed in the frequency range of 1200–1600 cm^{-1} in the spectra were consistent with the existence of trigonal coordination, while the bands in the frequency range of 850–1100 cm^{-1} were characteristic of tetrahedral coordination. The weaker bands in the region 700–800 cm^{-1} attributed to scissor vibrations of B-O-B bridges in the boron oxygen network (Massot et al., 1989a, Zhong and Tang 1996, Morcy and Ptak 1999, Almedia et al., 2001).

Analysis of IR spectra of LiB_3O_5 synthesized using $\text{LiOH-B}_2\text{O}_3$ (Fig. 2e) showed that this combination caused changes in the absorption band. Its IR spectra showed a great similarity with that of $\text{Li}_2\text{B}_4\text{O}_7$ (Tsvetkova et al., 2006).

Under the light of XRD and IR analyses, it was found that none of the starting materials except $\text{LiBO}_2\text{-H}_3\text{BO}_3$ were superior over Li_2CO_3 and H_3BO_3 . However, LiBO_2 is much more expensive than Li_2CO_3 . Therefore, it was concluded that the combination of Li_2CO_3 and H_3BO_3 was good starting materials for LiB_3O_5 synthesis.

CONCLUSIONS

The starting materials play an important role in the synthesis of lithium triborate. Among the reagents used, the Li_2CO_3 and H_3BO_3 combination was found the most suitable for the synthesis of LiB_3O_5 in respect to phase impurity as well as their costs.

ACKNOWLEDGEMENTS

The financial support from OYP program (BAP-08-11-DPT2002120510) and National BORON Research Institute (2006-05-611-05) are gratefully acknowledged.

REFERENCES

- ALMEIDA A. F. L., THOMAZINI D., VASCONCELOS I. F., VALENTE M. A. and SOMBRA A. S. B., (2001), *Structural studies of lithium triborate (LBO–LiB₃O₅) in borophosphate glass-ceramics*, International Journal of Inorganic Materials, 3, 7, 829-838.
- ARDIÇOĞLU B., ÖZBAYOĞLU G., ÖZDEMİR Z., and YILMAZ A., (2006), *Production and identification of rare-earth doped lithium triborate*, J. Alloys and Compd. 418, 77-79.
- BÉTOURNÉ E., and TOUBOUL M., (1997), *Synthesis of lithium borates (B/Li≥3) as LiB₃O₅ by dehydration of hydrated precursors*, J. Alloys Compd. 255, 91.
- KÖNIG H., HOPPE R., (1978), *Zur Kenntnis von LiB₃O₅*, Zeitschrift für Anorganische und Allgemeine Chemie, 439, 71.
- MASSOT, M., HARO, E., OUESLATI, M., BALKANSKI, M., LEVASSEUR, A., MENETRIER, M., (1989), *Structural investigation of doped lithium borate glasses*, Mater. Scien. and Eng. B 3, 1-2, 57-63
- MAZZETTI C., CARLI F.D., (1926), *Borati anidri di litio, cadmio, piombo, manganese*, Gazzetta Chimica Italiana, 56:19–28.
- MORYC U., PTAK W.S., (1999), *Infrared spectra of β-BaB₂O₄ and LiB₃O₅: new nonlinear optical materials*, Journal of Molecular Structure, 511-512, 241-249.
- ÖZDEMİR Z., ÖZBAYOĞLU G., KIZILYALLI M., YILMAZ A., (2004), *Synthesis and characterization of lithium triborate*, Physicochem. Probl. Miner. Process. 38, 321.
- Powder diffraction file No. 77-0774 JCPDS-ICDD, USA.
- Powder diffraction file No. 18-717 JCPDS-ICDD, USA.
- ROLLET A. P., AND BOUAZIZ R., (1955), *Le Systeme Binaire Oxyde de Lithium-Anhydride Borique* (in Fr.), Acad. Sci., 20 [6] 2417–19
- SABHARWAL S.C., TIWARI B., SANGEETA, (2003), *Effect of highest temperature invoked on the crystallization of LiB₃O₅ from boron-rich solution*, J. Cryst. Growth 249, 502.
- SABHARWAL S.C., TIWARI B., SANGEETA, (2004), *Investigation on the growth of LiB₃O₅ crystal by top-seeded solution growth technique*, J. Cryst. Growth 263, 327.
- SASTRY B. S. R., AND HUMMEL F. A., (1958), *Studies in Lithium Oxide Systems: I, Li₂O.B₂O₃–B₂O₃*, J. Am. Ceram. Soc., 41 [1] 7–17.
- TSVETKOVA E.G., PYLNEVA N. A., DAVYDOV A.V., (2006), *Some aspects of lithium–boron melts structuring*, Journal of Crystal Growth 292, 358–363.
- ZHONG W., and TANG D., (1996), *Growth units and morphology of lithium triborate (LBO) crystals*, Journal of Crystal Growth, 166, 1-4, 91-98.

Depci T., Özbayoğlu G., Yılmaz A., *Wpływ różnych materiałów wyjściowych na syntezę trójboranu litu*, Physicochemical Problems of Mineral Processing, 41 (2007) 101-105 (w jęz. ang).

Synteżowano trójboran litu (LiB₃O₅) stosując różne materiały wyjściowe. Badano wpływ tych materiałów na końcową czystość LiB₃O₅. Identyfikowano i charakteryzowano produkty syntezy za pomocą dyfrakcji rentgenowskiej (XRD) oraz analizy spektroskopowej w podczerwieni (IR). Badania wykazały, że wyjściowe materiały grają ważną rolę w czystości syntezowanego trójboranu litu.

Paweł NOWAK*, Kari LAAJALEHTO**

ON THE INTERPRETATION OF THE XPS SPECTRA OF ADSORBED LAYERS OF FLOTATION COLLECTORS – ETHYL XANTHATE ON METALLIC LEAD

Received April 15, 2007; reviewed; accepted May 17, 2007

Ethyl xanthate adsorption on metallic lead was studied by X-ray photoelectron spectroscopy (XPS) after treatment of lead sample at different potentials in aqueous NaNO₃ solutions containing ethyl xanthate. Continuous increase of the amount of ethyl xanthate species on the lead surface was observed as the potential was raised from –400 mV to –340 mV at the ethyl xanthate concentration of 10^{–4} M. At the potential of –400 mV and the concentration of 10^{–4} M the amount of xanthate at the surface was at the detection limit. Lead oxide and lead carbonate were found as the main oxidation products of metallic lead. Ethyl xanthate layer was found to decompose to sulfide like species in a few hours of excitation with monochromatic AlK_α radiation, if XPS measurement was done at room temperature. Cooling the sample with liquid nitrogen down to T≈130 K prevented the decomposition.

Key words: X-ray photoelectron spectroscopy, xanthate, surface adsorption, lead

INTRODUCTION

Lead is one of those base metals existing mainly in the form of sulfides in the earth's crust. Lead sulfide (PbS, galena) is separated from the ore using a flotation process, where the surfaces of finely ground sulfide particles are made hydrophobic by adding suitable surface active reagents (collectors) to the process solution. Xanthates are the most popular collector reagents and there are a lot of papers published in the literature where the interaction between xanthate species and the lead sulfide surface is studied using, for example, different electrochemical, infrared and surface spectroscopic techniques (XPS, STM, SIMS etc.).

* Institute of Catalysis and Surface Chemistry, Polish Academy of Sciences, ul. Niezapominajek 8, 30 239 Cracow, Poland, ncnowak@cyf-kr.edu.pl.

** Laboratory of Physics, Helsinki Polytechnic, PO Box 40, FIN-00099 City of Helsinki, Finland.

In many surface analytical techniques, like in XPS, the measurement is carried out in ultra high vacuum (UHV) causing some limitations and problems when phenomena occurring at solid-liquid interfaces need to be studied. These difficulties and methods for minimizing the problems have been discussed several times in the literature (Kartio et al., 1992; McCarron et al., 1990; Smart, 1991). General conclusion is that to get relevant information with XPS, sample preparation procedures have to be carefully planned and often sample need to be cooled with liquid nitrogen even before introduction into the electron spectrometer and kept cool also during the measurement. Using proper procedures, XPS and other surface sensitive UHV techniques can still give valuable information from collector adsorption and the composition of the mineral surfaces under different conditions.

It is widely accepted that at early stages of interaction xanthate is bonded to lead sites in PbS therefore suggesting this interaction to be of primary importance. Although xanthate sulfurs have slightly different binding energies than sulfurs in PbS, low amounts of adsorbed xanthate is quite difficult to separate in XPS spectra from strong sulfur signal originating from the PbS substrate.

These observations in mind, we considered interesting to study the interaction of ethyl xanthate on metallic lead with XPS thus avoiding the problem of large background sulfur signal, but leaving the possibility to investigate the sulfur-lead interaction. Furthermore, only a few earlier studies of xanthate interaction with metallic lead have been published, but none of them include any surface spectroscopic technique. Tolun and Kitchener (1964) published the first electrochemical results, where they made a surprising observation that lead electrode covered with xanthate remained hydrophilic, although for a long time lead xanthate has been known to render the galena surface hydrophobic. They proposed this hydrophilicity to be due to excess xanthate ions in a layer. Later Woods (1972) reported his first electrochemical work and then Woods et al. (1997) recorded voltammograms at pH 9.2 and pH 6.8 using different concentrations of ethyl xanthate (10^{-2} , 10^{-3} or 10^{-4} M). On the basis of those measurements they calculated the Frumkin type isotherms for the system.

Our goal was to observe directly with XPS the surface composition of lead surface treated with ethyl xanthate solution at different electrode potentials. Questions of the role of oxidation products for hydrophilicity of the lead electrode reacted with xanthate and possible differences in sulfur binding in the case of monolayer and multilayer coverage were also addressed.

EXPERIMENTAL

The Perkin-Elmer PHI 5400 spectrometer equipped with monochromatized AlK_{α} X-ray source was used. The binding energy (BE) scale of the spectrometer was calibrated with the $Au4f_{7/2}$ (BE = 84.0 eV) and $Cu2p_{3/2}$ (BE = 932.6 eV) lines. With this calibration the BE for the $Pb4f_{7/2}$ line in the sample of metallic lead, abraded at the ultra high vacuum (neither carbon nor oxygen emission lines were observable in the

spectra) was 136.9 eV. Unless otherwise stated the spectra were recorded at the 45° take-off-angle. A slice of metallic lead (Goodfellow) was cut from the rod having the purity of 99.95% and used as an electrode. All reagents used were of “analytical reagent” grade. Water from Elgastat UHQ MKII apparatus (resistivity 18 MΩ) was used in experiments and to prepare the solutions. Ag/AgCl/saturated KCl electrode was used as a reference, but all potentials are, however, reported versus standard hydrogen electrode (SHE) assuming that Ag/AgCl/saturated KCl electrode has the potential +0.2 V versus SHE. Platinum wire was used as a counter electrode. The base electrolyte was 0.1 mol/dm³ NaNO₃ and the solutions were purged from oxygen by bubbling with 99.999% nitrogen gas before each electrochemical experiment. The fresh surface of the lead electrode was obtained by cutting with a steel blade. The electrode was first polarized to the potential -0.8 V in pure base electrolyte to reduce the oxidation products from the surface, then xanthate was added, the solution stirred quickly (the potential kept at -0.8 V all the time) and the sample immediately polarized to the required potential. Electrode was kept at that potential for 1 minute, withdrawn, rinsed with water and introduced to the spectrometer immediately. Sample pre-cooling was used (Kartio et al., 1992) and the spectra were recorded at sample temperature 130 K. For selected samples, the sample was let to warm up to room temperature after the acquisition and the spectrum re-measured to check the stability of the reaction product.

RESULTS AND DISCUSSION

METALLIC LEAD TREATED IN AQUEOUS SOLUTION WITHOUT XANTHATE

When metallic lead was treated in an electrolyte solution containing no xanthate at $E_h = -410$ mV, the surface was covered by a thick layer of oxidation products most of them probably formed during the transfer of lead sample from the electrochemical cell into the electron spectrometer. Although the transfer time was of the order of one minute, active metals like lead oxidizes immediately in contact with air (Nowak et al. 2000). According to O1s and C1s spectra, main species on a surface were lead oxide and lead carbonate. Only about 5 % of lead signal were from metallic lead suggesting the oxidized layer thickness of the order of 5 nm. This layer, especially the lead carbonate (lead oxide is a semiconductor) is also a poor electrical conductor causing surface charging observed in all samples. The amount of charging was estimated using C1s contamination line at 285.0 eV as a reference and it varied between 0.3 eV and 0.8 eV, the largest value found in this sample which was not treated with xanthate.

After charging correction of 0.8 eV (Table I), O1s binding energy 529.2 eV was determined which is typical for oxygen in lead oxide and binding energy 530.9 eV was found for lead carbonate. Carbon emission at 288.7 eV confirmed the existence of carbonate. By comparing the intensities of the carbonate peaks (288.7 eV and 530.9 eV) corrected with elemental sensitivity factors, very good agreement was found with

the lead carbonate stoichiometry. The broad O1s signal fitted at 532.7 eV (16 % of total oxygen) can be interpreted to be due to lead hydroxide, adsorbed water or some organic species as discussed in the literature (Nowak et al., 2000).

Table 1. Binding energies of measured photoemission lines from samples treated at different potentials in aqueous ethyl xanthate solutions at pH 6.7. Relative intensities of fitted components for each emission are given in parenthesis. All binding energies are corrected in respect to the measured value 136.9 eV for Pb4f_{7/2} binding energy in metallic lead

Xanthate conc. mol/l	Potential E _n /mV	Binding energy / eV				
		C1s	O1s	S2p	S2s	Pb4f _{7/2}
10 ⁻⁴	-340	289.6 (2) 287.7 (16) 286.6 (13) 285.3 (69)	533.7 (70) 531.8 (17) 529.9 (13)	162.5	226.8	136.9 (5) 138.4 (95)
10 ⁻⁴	- 360	289.7 (2) 287.9 (16) 286.7 (28) 285.5 (54)	533.9 (61) 531.8 (21) 530.0 (18)	162.7	226.9	136.9 (4) 138.5 (96)
10 ⁻⁴	- 380	289.1 (8) 287.8 (8) 286.9 (14) 285.6 (70)	533.9 (20) 531.4 (49) 529.7 (31)	162.6	226.9	136.9 (15) 138.3 (85)
10 ⁻⁴	- 400	289.1 (9) 286.5 (13) 285.7 (78)	533.8 (3) 531.9 (71) 530.1 (26)	(162.5) - (too weak)	-	136.9 (4) 138.5 (96)
10 ⁻³	-410	288.4 (6) 287.8 (19) 286.5 (27) 285.3 (58)	533.8 (59) (38) 530.0 (3)	162.5	226.8	136.9 (2) 138.6 (98)
0	- 610	289.4 (9) 286.6 (22) 285.8 (69)	533.5 (17) 531.7 (54) 530.0 (29)	-	-	136.9 (4) 138.5 (96)

Considering the lead oxidation products, lead hydroxide seems therefore be of minor importance, the main products being oxide (62 % of oxidized lead) and carbonate (38 % of oxidized lead). In the C1s spectrum the main component at 285.0 eV was due to hydrocarbon type contamination. Small amount of carbon-oxygen species was also detected in the region of 286 eV. This first experiment is not very informative, because the amount and type of oxidation species present when sample was still in electrolyte solution could not be concluded. However, this experiment can be used to estimate the uniformity and stability of xanthate covered surface against air oxidation by comparing the results with surface compositions of samples treated in xanthate solutions.

METALLIC LEAD TREATED IN AQUEOUS SOLUTION CONTAINING
10⁻⁴ M ETHYL XANTHATE

Four samples treated at potentials -400 mV, -380 mV, -360 mV and -340 mV and ethyl xanthate concentration 10⁻⁴ M were prepared. All samples were cooled inside the spectrometer to avoid decomposition of surface species during acquisition, which was observed when the samples were measured at room temperature. The decomposition will be discussed in more detail later in this paper. Only traces of xanthate (at the limit of detectability) were observed at potential of -400 mV but the amount of non-xanthate oxygen was almost the same as in the case of the sample treated in pure base electrolyte. This is in disagreement with the results by Woods et al (1997) who observed the chemisorption prewave in the region from -670 mV to -460 mV and concluded the formation of a full xanthate monolayer already at approximately -460 mV using xanthate concentration 10⁻⁴ M. The monolayer of chemisorbed xanthate on metal surface should be easily detected with XPS. This discrepancy may be explained if one assumes that xanthate species are not very strongly bonded to lead and in air are replaced or buried by such oxidation products as carbonate or oxide. Another possibility is that the end of the prewave does not indicate the formation of a full monolayer, but only some completion of the most favorable adsorption sites and therefore the potential -460 mV represents still under monolayer situation.

All spectra measured at different potentials were curve fitted to determine different chemical states of each element. Summary of the results is presented in Table 1, where all binding energies are given without charge correction, but corrected against the Pb4f_{7/2} binding energy of 136.9 eV in metallic lead. Charge correction with C1s contamination line is not automatically done, because there seems to be slight differences in charging between different species even in the same sample depending on the distribution and amount of different species in each case. By looking the BE of C1s contamination line, the charging decreases when xanthate treatment potential increases. This is an indication that larger amount of xanthate adsorbed at higher potentials reduces the oxidation and therefore works like an oxidation inhibitor as shown in Fig. 1 (curve A), where intensity ratio O_{ox}/Pb (O_{ox} is the total O1s intensity of oxidation products i.e. oxide+carbonate) is plotted at different potentials. Especially the formation of highly insulating carbonates is decreased as concluded from the C1s spectra of the -340 mV and -360 mV samples where carbonate component is hardly visible and shifted to higher binding energies as observed earlier at the early stages of oxidation (Laajalehto et al., 1993). When the amount of xanthate is lower on the surface, the carbonate signal intensity is significantly enhanced and its binding energy decreased.

Ethyl xanthate can be easily identified according to characteristic binding energies of S2p, S2s and O1s emissions for which we obtained average values of 162.2 eV, 226.4 eV and 533.4 eV after charge correction, respectively. The values obtained are

in good agreement with earlier studies of ethyl xanthate adsorption on PbS and the values presented for Pb(EX)₂ (Laajalehto et al., 1993). The relative amount of xanthate at different potentials was estimated using the measured intensity ratios O_{xant}/Pb (Fig. 1, curve B) and S/Pb (Fig. 1, curve C). They show continuous increase of the ratios as a function of the potential. The amount of xanthate at potential -340 mV represents definitely a multilayer situation.

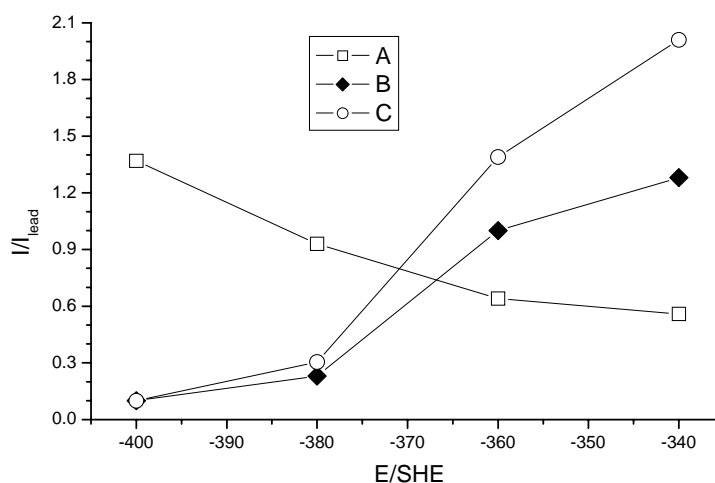


Fig. 1. Ratio of the intensity of the particular emissions to the total emission of lead for samples treated at different potentials and at the 10⁻⁴ M xanthate concentration. A – oxygen in oxidation products, B – xanthate oxygen, C – xanthate sulphur

In O1s spectra after xanthate treatment, three components are observed. In addition to xanthate oxygen at BE 533.4 eV, carbonate and oxide species are also detected in all spectra. Because metallic lead was first reduced at -800 mV before xanthate was added and then the potential increased to the final value, it can be assumed that lead surface was free of oxidation products in solution. Therefore most of the oxidation products were formed in air after the sample was taken out from the solution and dried, and before insertion to the spectrometer. This indicates that xanthate layer formed in solution is either not uniform or it does not totally protect the lead surface against air oxidation.

For a sample treated at -410 mV and ethyl xanthate concentration 10⁻³ M, O1s spectra at different electron take-off angles from 20° to 75° were recorded giving information about the layer structure on the surface region. These measurements show that on average carbonate species are on the top of xanthate therefore suggesting that they have formed in air by reaction of carbon dioxide with lead xanthate or lead diffused from the substrate. Removal of surface xanthate by carbonates cannot be excluded either.

Important observation is that sulfur binding energy does not significantly change (all changes are within 0.2 eV) when the conditions are changed from those for which monolayer formation might be expected to formation of lead xanthate. This supports our earlier measurements with bulk $\text{Pb}(\text{EX})_2$ where binding energy 162.2 eV was found (Laajalehto et al., 1993) and the SR-XPS measurements of a monolayer coverage of xanthate on PbS (Kartio et al., 1999), where S2p binding energy 162.0 eV was reported. Much larger shift, about 1 eV, proposed earlier by Buckley and Woods, is not consistent with our findings in this work and in the papers referred above.

One sample with higher ethyl xanthate concentration 10^{-3} M was also prepared at potential -410 mV i.e. at potential where xanthate was not observed with concentration 10^{-4} M. The measured spectra are very similar to those obtained at -340 mV and -360 mV and with concentration 10^{-4} M. This confirms the electrochemical nature of the process, which proposes that one order of magnitude increase in xanthate concentration would shift the reaction potential by 60 mV.

STABILITY OF THE XANTHATE LAYER IN EXPERIMENTAL CONDITIONS

It has been well documented that two types of damage can occur in XPS measurements. Firstly, in ultra high vacuum weakly bonded surface species can detach from the surface already during pumping down the sample chamber and those species will therefore be not detected in the subsequent XPS measurements. Well known flotation related system of this is the observation of physisorbed dixanthogen on pyrite or metallic gold surfaces, which is only possible using a specially designed pre-cooling method (Kartio et al., 1992). Secondly, X-ray radiation used to excite the photoelectron spectra can directly or indirectly cause decomposition or evaporation of surface species. It was observed by Johansson et al. (1986) that using a monochromatized AlK_α radiation instead of non-monochromatized MgK_α radiation prevented the decomposition and evaporation of xanthate bonded to metallic copper. It was also observed that cooling the sample during the measurement with liquid nitrogen significantly decreased the decomposition also in the case of non-monochromatized MgK_α radiation.

Although monochromatized AlK_α radiation was used in all measurements in this work, decomposition of xanthate was observed if measurements were done at room temperature. In Fig. 2, four sulfur 2p spectra are presented of the same sample originally treated in 10^{-3} xanthate solution at potential -340 mV. First measurement was done by keeping the sample at low temperature (130 K, spectrum a) and the spectrum shows the characteristic 2p doublet structure for a single chemical state of xanthate sulfur. Spectrum b was measured immediately after warming up the sample to room temperature corresponding to only 11 min irradiation time as warm, which was needed to record the spectrum. A weak shoulder at lower binding energy side of the xanthate peak is already visible indicating a new chemical state of sulfur. When irradiation time increased (3h in spectrum c and 10 h in spectrum d), the structure at

about 160.7 eV (after charging correction) continuously increased in intensity suggesting xanthate decomposition to lead sulfide like species at room temperature. Formation of PbS type species on the surface is further supported by the observation that Pb4f emission from oxidation products is shifted ≈ 0.3 eV towards lower binding energy. This shift is caused by the decrease of lead xanthate signal at higher BE side of that emission line and simultaneous increase in PbS type intensity at the other side of the peak. No separate components can be resolved, because all these three chemical states (lead xanthate, lead carbonate/oxide and lead sulfide) are within 1 eV. By comparing the sulfur and oxygen intensities for cool and warm sample, it is plausible to assume that the bond between CS₂ group and oxygen is broken and the hydrocarbon part, including the oxygen atom, is evaporated.

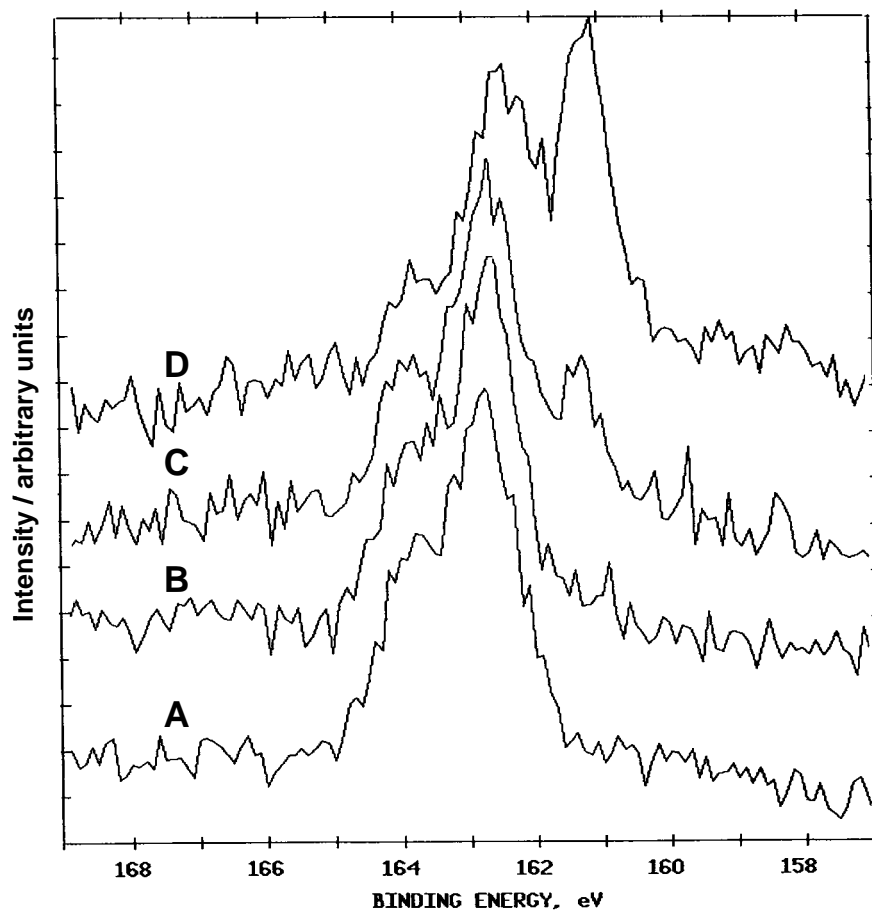


Fig. 2. S2p emission line for the sample treated at the potential of -410 mV in 10^{-3} M xanthate solution. A – measured cool, B – just after warming to room temperature, C – after 3 hours of irradiation, D – after 10 hours of irradiation

Decomposition has also been observed for adsorbed layer of ethyl xanthate on PbS surface after excitation with intensive synchrotron radiation (Kartio et al., 1999). It is interesting to note that decomposition products on PbS surface were identified as polysulfide type sulfur species having higher binding energy than xanthate sulfur whereas in metallic lead, decomposition product is sulfide type. Probable reason for this is that in the case of metallic lead there are lead atoms easily available to form sulfide, which suggests that decomposition takes place on the boundary between metal and xanthate. On PbS surface lead atoms are not so active and sulfur atoms start to form chain-like structures.

The reason for xanthate decomposition is evidently the high photoelectron and secondary electron yield in metallic lead. To explain the more serious damage observed with lead compared to that with copper substrate, the following phenomena can be considered: 1) the total cross section of photoelectron emission for AlK_{α} excitation in lead is much higher than in copper and, 2) the kinetic energy of photoelectrons in the most probable photoemission in lead (4f emission, $E_K \approx 1300$ eV) is significantly higher than for corresponding emission in copper (2p emission, $E_K \approx 550$ eV). Because of the about 50 % lower atomic density of lead atoms in PbS and much lower photoemission cross-section for S, the decomposition probability is much lower and practically not detected with conventional AlK_{α} radiation at room temperature. Our measurements show, however, that practically all damage also in this case can be avoided by using sample cooling during the excitation. No pre-cooling is needed because xanthate is either chemisorbed or lead xanthate is formed both species being not volatile and therefore not affected by the vacuum itself.

CONCLUSIONS

Xanthate adsorption on metallic lead was found to be potential dependant in a studied potential region between -410 mV and -340 mV. Using ethyl xanthate concentration 10^{-4} M, negligible amount of xanthate was detected at -400 mV, however the amount of xanthate grew with potential sharply attaining multilayer coverage at higher potentials. The binding energy of S2p electrons was within 0.2 eV at all xanthate coverage indicating that there is only a slight difference in sulfur chemical state. The adsorbed xanthate was always accompanied by lead oxidation products. Evidently the xanthate overlayer is either not compact or it is weakly bound to the surface and the surface covered by xanthate, either at monolayer or multilayer coverage may still react with atmospheric gases. This explains why Tolun and Kitchener found the surface of xanthate-covered lead hydrophilic. To avoid radiation damage during the XPS measurement, sample need to be cooled with liquid nitrogen. If the sample is at room temperature during the measurement, xanthate is decomposed to lead sulfide like species. Decomposition is caused by large amount of energetic photoelectrons from lead excited by AlK_{α} radiation and their interaction with adsorbed layer.

ACKNOWLEDGEMENTS

The authors will thank the Polish Academy of Sciences and the Academy of Finland for financial support in the framework of bilateral scientific research program between Poland and Finland.

REFERENCES

- JOHANSSON, L.S., JUHANOJA, J., LAAJALEHTO, K., SUONINEN, E. and MIELCZARSKI, J., 1986. *XPS studies of xanthate adsorption on metals and sulfides*, Surf. Interface Anal., 18: 501-505.
- KARTIO, I., LAAJALEHTO, K., SUONINEN, E., KARTHE, S. and SZARGAN, R., 1992. *Technique for XPS measurements of volatile adsorbed layers: application to studies of sulphide flotation*, Surf. Interface Sci., 18: 807-810.
- KARTIO, I., LAAJALEHTO, K. and SUONINEN, E., 1999. *Characterization of the ethyl xanthate adsorption layer on galena (PbS) by synchrotron radiation excited photoelectron spectroscopy*, Colloids Surf. A, 154: 97-101.
- LAAJALEHTO, K., NOWAK, P. and SUONINEN, E., 1993. *On the XPS and IR identification of the products of xanthate sorption at the surface of galena*, Int. J. Miner. Process., 37: 123-147.
- LAAJALEHTO, K., SMART, R.St.C, RALSTON, J. and SUONINEN, E., 1993. *STM and XPS investigation of reaction of galena in air*, Appl. Surf. Sci., 64: 29-39.
- McCARRON, J.J., WALKER, G.W. and BUCKLEY, A.N., 1990. *An X-ray photoelectron spectroscopic investigations of chalcopyrite and pyrite surfaces after conditioning in sodium sulfide solutions*, Int. J. Miner. Process., 30: 1-16.
- NOWAK, P., LAAJALEHTO, K. and KARTIO, I., 2000. *A flotation related X-ray photoelectron spectroscopic study of the oxidation of galena surface*, Colloids Surf. A, 161: 447-460.
- SMART, R.St.C., 1991. *Surface layers in base metal sulphide flotation*, Minerals Engineering, 4: 891-909.
- TOLUN, R. and KITCHENER, A., 1964. *Electrochemical study of the galena-xanthate-oxygen flotation system*, Trans. IMM, 73: 313-322.
- WOODS, R., 1972. *The anodic oxidation of ethyl xanthate on metal and galena electrodes*, Aust. J. Chem., 25:2329-2335.
- WOODS, R., CHEN, Z. and YOON, R.-H., 1997. *Isotherms for the chemisorption of ethyl xanthate on lead*, Int. J. Miner. Process., 50: 47-52.

Nowak P., Laajalehto K., *O interpretacji emisyjnych widm elektronowych (XPS) warstw adsorpcyjnych odczynników flotacyjnych – ksantogenu etylowego na powierzchni ołowiu*, Physicochemical Problems of Mineral Processing, 41 (2007) 107-116 (w jęz. ang.).

Adsorpcję ksantogenu etylowego na powierzchni metalicznego ołowiu z roztworów wodnych NaNO_3 badano metodą spektrometrii fotoelektronów generowanych promieniowaniem rentgenowskim (XPS, ESCA). W roztworze ksantogenu o stężeniu 10^{-4} mol dm^{-3} , wraz ze wzrostem potencjału od wartości -400 mV do -340 mV (względem standardowej elektrody wodorowej), ilość ksantogenu na powierzchni wrasta od wartości znikomo małej (na pograniczu możliwości detekcji) do pokrycia wielowarstwowego. Widmo produktu sorpcji jest identyczne z widmem ksantogenu ołowiu. We wszystkich widmach obserwowano produkty utlenienia ołowiu, produktu te zidentyfikowano jako mieszaninę węglanu i tlenku ołowiu (II), przy czym im wyższy potencjał polaryzacji próbki w roztworze ksantogenu tym mniej produktów utlenienia obserwowano na powierzchni. Produkty te powstawały w wyniku utlenienia ołowiu w trakcie kontaktu próbki z powietrzem atmosferycznym podczas przenoszenia próbki z roztworu do spektrometru, co świadczy o tym, że powstająca warstwa produktu sorpcji ksantogenu nie zabezpiecza powierzchni ołowiu przed utlenianiem. W wyniku naświetlania powierzchni promieniowaniem rentgenowskim w trakcie pomiaru, powstały na powierzchni ołowiu ksantogenu ołowiu rozkłada się do produktu, którego widmo jest identyczne z widmem siarczku ołowiu. Można temu zapobiec przeprowadzając pomiar w temperaturze ciekłego azotu.

Maria CHOJNACKA*, Dorota WAWRZAK**,
Władysława MULAŁ*, Anna SZYMCZYCHA-MADEJA*

KINETICS OF PYRITE OXIDATION IN ACIDIC POTASSIUM DICHROMATE SOLUTIONS

Received March 15, 2007; reviewed; accepted June 1, 2007

The kinetics of pyrite oxidation in potassium dichromate solution was investigated. The effect of stirring rate, temperature and particle size have been examined. In addition the solid phases before and after leaching were examined by SEM, electron microprobe and chemical analysis. The rate of pyrite oxidation was found to be independent of the stirring speed. The consumption of dichromate ions in the initial solutions showed that at all temperatures under consideration sulphide sulphur was oxidized to sulphate. The value of the apparent activation energy of $43.5 \pm 1.5 \text{ kJmol}^{-1}$, the independence of reaction rate on the stirring speed, the linear relationship between the rate constant, and the inverse of the initial particle diameter are in good agreement with a mechanism controlled by chemical reaction.

Key words: pyrite, oxidation, potassium dichromate, reaction kinetics

INTRODUCTION

Pyrite is the most abundant of all sulphide minerals. It occurs in most sulphide ore deposits, often as a major phase. It is also commonly associated with coal and gold deposits. Pyrite is one of the most refractory and difficult to leach minerals. Its exceptional stable electronic structure is responsible for this behaviour (Nowak, 2006). The literature data show that leaching of pyrite requires elevated temperatures and pressures in the presence of oxygen (Long and Dixon, 2004) or strong oxidizing agent such as nitric acid (Karaca et al., 2003)

Sulphuric acid containing dichromate ions is a powerful oxidizing agent with a pH-dependent oxidation potential. The first studies applying sulphuric acid solution of

* Wrocław University of Technology, Chemical Department, Wybrzeże Wyspiańskiego 27,
50-370 Wrocław, Poland, E-mail: wladyslawa.mulak@pwr.wroc.pl.

** Institute of Chemistry and Environmental Protection, Jan Długosz University of Częstochowa
Al. Armii Krajowej 13/15, 42-201 Częstochowa, Poland.

sodium dichromate were connected with copper concentrates (Shantz and Morris, 1974; Murr and Hiskey, 1981).

Our previous works dealt with the nickel sulphides leaching in acidic dichromate solutions (Mulak, 1983 and 1992). Another relevant papers on the leaching of sulphide minerals with dichromate are those on pyrite, molybdenite concentrates (Ruiz and Padilla, 1998) and copper converter slag (Altundogan et al., 2004).

In this paper the effect of stirring, temperature and particle size on the dissolution rate of pyrite have been examined.

EXPERIMENTAL

CHARACTERIZATION OF PYRITE SAMPLES

Pyrite used in the experimental work was obtained from *Smolnik* (Slovak Republic). The results of its semi-quantitative spectral analysis were as follows (in wt. % as the element): 10^1 Fe; 10^{-1} Si; 10^{-2} Al, Bi, Ca, Mg; 10^{-3} Co, Pb, Ti, Cu. The chemical analysis showed that it contained 45.0% iron, 42.1% sulphur as sulphide and 2.5% sulphur as sulphate (the iron and sulphur were determined gravimetrically as Fe_2O_3 and BaSO_4 , respectively). The X-ray diffraction patterns of the sample showed only pyrite lines.

LEACHING EXPERIMENTS

All experiments were performed with grains of the size <0.056 mm, except those relating to the effect of the particles size on the reaction kinetics. All reagents used were prepared from analytical grade chemicals and distilled water. In every experiment a flask containing 200 ml of acidic dichromate solution was submerged in a tank, the temperature of which was kept constant to within 0.1°C . When the required temperature had been reached, a charge of 0.2 g of pyrite was added and the stirring was started.

The leaching was carried out for 120 min during which seven 1 mL samples of the solution were taken for determination of the iron concentration by an atomic absorption method. The degree of dichromate reduction in the final solution was determined iodometrically.

RESULTS AND DISCUSSION

MORPHOLOGY OF UNREACTED PYRITE SAMPLE

SEM micrograph of unreacted pyrite particles presented in Fig.1 shows two different grain types (indicated by *a* and *b*). The first type (indicated by *a*) corresponds to a solid with a dense structure, smooth surfaces and sharp edges. In turn, the second type (marked by *b*) shows a solid with more round-shaped edges and porous surface. However, the inspection of cross-sections of the grains revealed the presence of micropores of various sizes beneath the surface (Fig.2.).

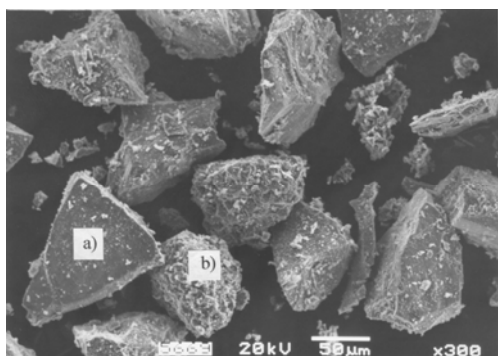


Fig. 1. SEM micrograph of unreacted pyrite sample

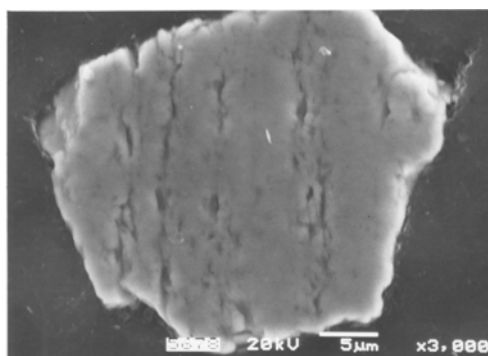


Fig. 2. SEM micrograph of unreacted pyrite grain cross-section

The electron microprobe analysis of the grain surface indicated by *a* in Fig.1 shows only iron and sulphur (Fig.3a), but the grain surface marked by *b* in Fig.1 indicates the presence of iron, sulphur and small peak of oxygen (Fig.3b).

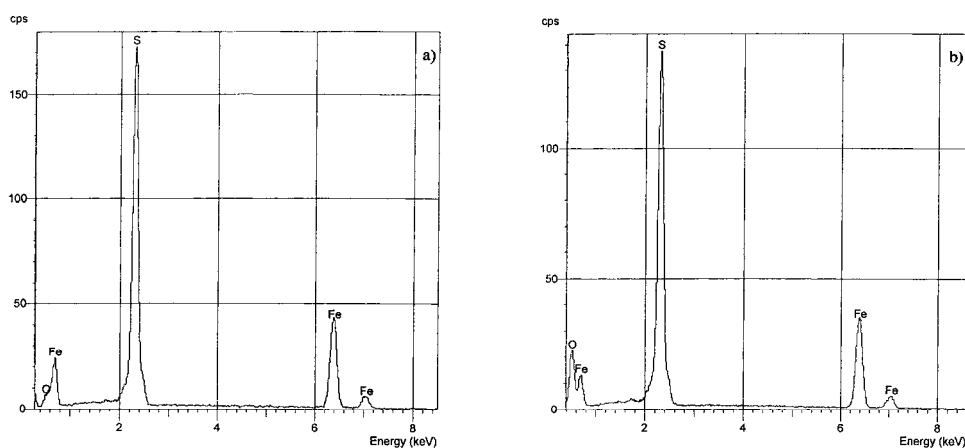


Fig. 3. Microprobe analyses of the grains marked by *a* and *b* in Fig.1

EFFECT OF STIRRING SPEED

The effect of stirring speed on the extraction of Fe from pyrite was investigated in a solution of 0.025 M $K_2Cr_2O_7$ and 0.5 M H_2SO_4 at 50°C. The variation of the stirring speed within the range 400–1200 min^{-1} had no effect on the rate. This indicates that the diffusion of the reactants from the solution toward the surface of the particle, and the products away from the particle, were fast, and hence did not control the leaching rate within the range of stirring speeds tested. All subsequent experiments were carried out at a stirring speed of 900 min^{-1} to assure invariance of this parameter.

EFFECT OF TEMPERATURE

The leaching was performed within the temperature range 30–90°C with an initial concentration of dichromate ions of 0.025 M and 0.5 M sulphuric acid at a constant stirring speed of 900 min⁻¹. The dissolution curves are shown in Fig.4. The high dissolution rate observed in the initial stage can be caused by soluble compounds already present in the raw material or oxides formed during grinding. The experimental data were analysed in terms of several models connecting the fraction reacted (α) and time (t) (Wadsworth, 1979).

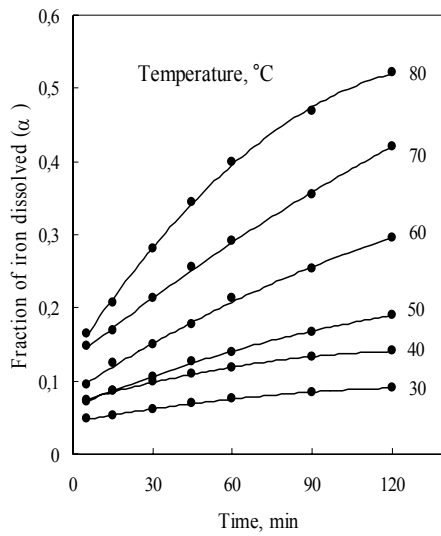


Fig. 4. Effect of temperature on the fraction of iron dissolved from pyrite in 0.025 M $K_2Cr_2O_7$ and 0.50 M H_2SO_4

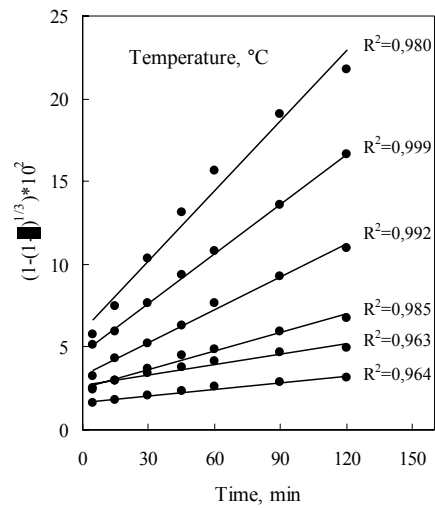


Fig. 5. A plot of the data in Fig.4 according to Eq. (1)

It seems that the model assuming chemical reaction on the surface of particles as the rate-limiting step of the process is correct. The following relationship $\alpha(t)$ is established:

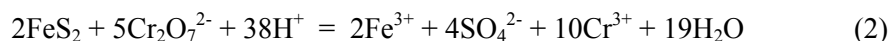
$$1 - (1 - \alpha)^{1/3} = kt, \quad (1)$$

where k [min⁻¹] = $\frac{const}{d_0}$ is the rate constant, d_0 denotes the initial particle diameter (Wadsworth, 1979).

It is evident from Eq.(1) that the left-hand side plotted vs. t should result in a straight line. A plot of the data from Fig.4 for temperature range 30–90°C, made according to Eq.(1), is shown in Fig.5. The apparent rate constant, k , obtained from the

slopes of the straight lines in Fig.5 was used to determine an activation energy of $43.5 \pm 1.5 \text{ kJmol}^{-1}$, as shown in Fig.6. This confirms that the chemical reaction on the surface of particles is the rate-limiting step of the dissolution process. The results of microprobe analysis of the cross-sections of partially leached pyrite in acidic dichromate solutions do not show any elemental sulphur layer on the pyrite surface.

The degree of dichromate ion reduction in the final solutions showed that at all temperatures sulphide sulphur was oxidized to sulphate according to the following reaction:



The influence of temperature on the consumption of the dichromate ions after 2 hours of pyrite dissolution is shown in Fig.7. A satisfactory agreement with the experimental data on the consumption of the dichromate ions and the theoretical ones calculated according to Eq.(2) is observed.

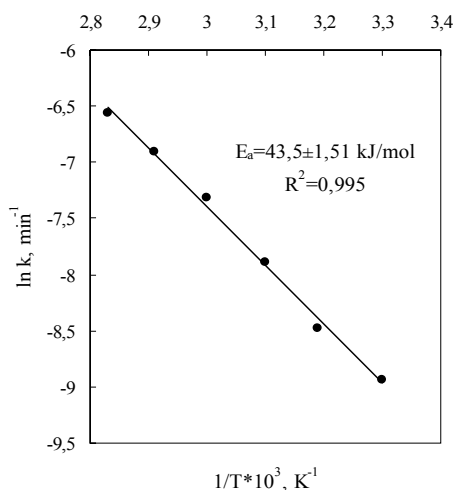


Fig. 6. Arrhenius plot for the dissolution of iron from pyrite in 0.025 M $\text{K}_2\text{Cr}_2\text{O}_7$ and 0.50 M H_2SO_4

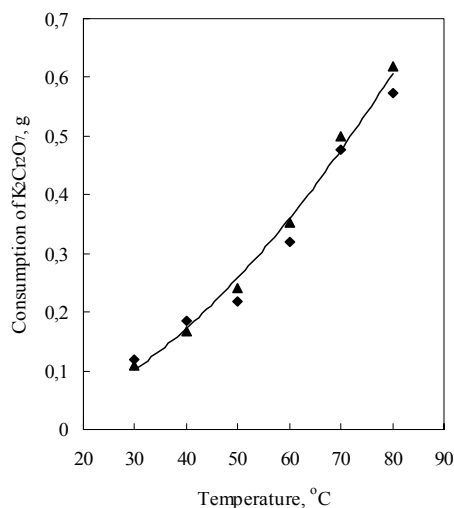


Fig. 7. Influence of temperature on the consumption of $\text{K}_2\text{Cr}_2\text{O}_7$, after 2 h of pyrite dissolution in 0.025 M $\text{K}_2\text{Cr}_2\text{O}_7$ and 0.5 M H_2SO_4 , \blacktriangle – experimental points, \blacksquare – according to equation (2)

The oxidation of pyrite in acidic dichromate solution leads to a creation of large pits (Fig. 8). These pits may exhibit defined geometry and orientation. For instance, the pyramidal pits characterize the intercept of dislocation with (001) planes of cubic crystals (Ciminelli and Osseo-Asare, 1995).

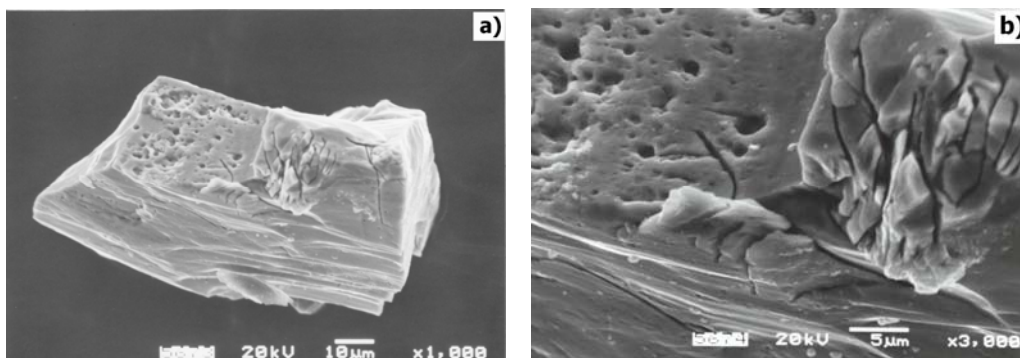


Fig. 8. SEM photograph of pyrite reacted in 0.5 M H_2SO_4 solution with 0.025 M $\text{K}_2\text{Cr}_2\text{O}_7$ addition at temperature 50°C ($\alpha = 21.2\%$): a) pyrite grain, b) fragment of the surface of this grain

EFFECT OF PARTICLE SIZE

The influence of particle diameter on the rate of iron extraction was examined by measuring the reaction rate for fractions of four sizes (in mm): <0.056 , $0.040 - 0.056$, $0.063 - 0.071$ and $0.071 - 0.080$, with 0.025 M $\text{K}_2\text{Cr}_2\text{O}_7$ in 0.5 M H_2SO_4 solution at 50°C .

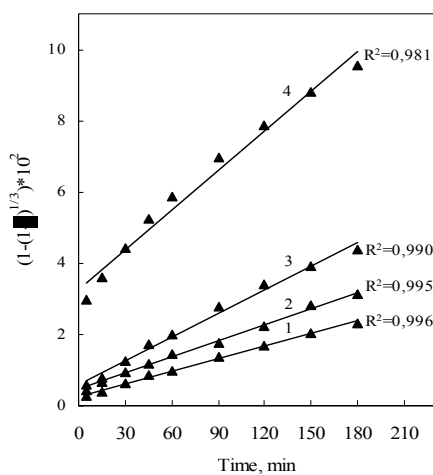


Fig. 9. The variation of $1 - (1 - \alpha)^{1/3}$ with time at various initial particle diameter d_0 of FeS_2

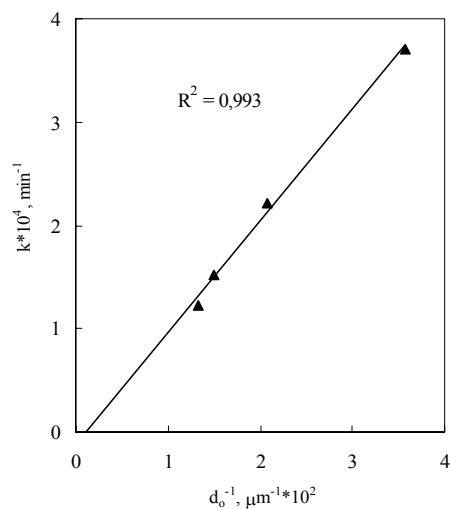


Fig. 10. A plot of the rate constant versus an initial particle diameter d_0 of FeS_2

The plot of $1-(1-\alpha)^{1/3}$ for various particle diameters is shown in Fig.9. As expected, the smaller is the particle size the faster the dissolution of pyrite is. Fig.10 shows the calculated apparent rate constants vs. the initial particle diameter d_0 . The linear relationship between the rate constant k and the inverse of d_0 indicates that the chemical reaction on the surface of particles is, indeed, the rate-limiting step of the dissolution process.

CONCLUSIONS

From the results of these examinations the following conclusions can be drawn.

1. The oxidation of pyrite in acidic dichromate ion solutions results in the formation of sulphate ions.
2. The rate of pyrite dissolution was found to be independent on the stirring speed.
3. A linear relationship between the rate constant k and the inverse of the initial particle diameter was established.
4. The value of the apparent activation energy of $43.5 \pm 1.5 \text{ kJ mol}^{-1}$ supports the conclusion that the rate of dissolution is limited by the chemical reaction on the surface of particles.

REFERENCES

- ALTUNDOGAN H.S., BOYRAZIL M., TUMEN F., 2004, *A study on the sulphuric acid leaching of copper converter slag in the presence of dichromate*, Mineral Engineering 17, 465-467.
- CIMINELLI V.S.T. AND OSSEO-ASARE K., 1995, *Kinetics of pyrite oxidation in sodium carbonate solutions*, Metallurgical and Materials Transactions B, 26B, 209-218.
- KARACA, S., AKYÜREK, M., BAYRAKÇEKEN, S., 2003, *The removal of pyritic sulphur from Aşkale lignite in aqueous suspension by nitric acid*, Fuel Processing Technology 80, 1-8.
- LONG, H., DIXON, D.G., 2004, *Pressure oxidation of pyrite in sulphuric acid media: a kinetic study*, Hydrometallurgy 73, 335-349.
- MULAK, W., 1983, *Kinetics of dissolution of synthetic millerite (β -NiS) in acidic potassium dichromate solutions*, Hydrometallurgy 11, 79-89.
- MULAK, W., 1992, *Kinetics of dissolution of Ni_3S_2 in acidic potassium dichromate solutions*, Hydrometallurgy 28, 309-322.
- MURR, L.E., HISKEY, J.B., 1981, *Kinetic effects of particle size and crystal dislocation density on the dichromate leaching of chalcopyrite*, Metall. Trans. 12B(2), 255-267.
- NOWAK, P., 2006, *Właściwości krystalochemiczne i struktura elektronowa a mechanizm utleniania siarezków metali*, Seria wyd. PAN, Instytut Katalizy i Chemii Powierzchni, Prace Habilitacyjne, Kraków.
- RUIZ, M.C., PADILLA, R., 1998, *Copper removal from molybdenite concentrate by sodium dichromate leaching*, Hydrometallurgy 48, 313-325.
- SHANTZ, R., MORRIS, T.M., 1974, *Dichromate process demonstrated for leaching of copper sulphide concentrates*, J. of Mineral Engineering. 175 (5), 71-72.
- WADSWORTH, M.E., 1979, *Hydrometallurgical processes*, In: Sohn, H.Y., Wadsworth, M.E., (Eds.), Rate Processes of Extractive Metallurgy, Plenum Press, New York, pp. 133-186.

Chojnacka M., Wawrzak D., Mulak W., Szymczycha-Madeja A., *Kinetyka ługowania pirytu w kwaśnym roztworze dichromianu potasu*, Physicochemical Problems of Mineral Processing, 41 (2007) 117-124 (w jęz. ang.).

Określono wpływ temperatury, wielkości ziaren oraz warunków hydrodynamicznych w roztworze na szybkość ługowania pirytu w kwaśnym roztworze $K_2Cr_2O_7$. W celu zbadania składu i morfologii powierzchni faz stałych przed i po ługowaniu wykonano analizy skaningowym mikroskopem elektronowym z mikrosondą rentgenowską. Na podstawie krzywych kinetycznych stosując zależność $f(\alpha)=1-(1-\alpha)^{1/3}$ od czasu obliczono stałe szybkości reakcji oraz energię aktywacji równą $43,5 \pm 1,5$ kJ/mol. Wartość energii aktywacji oraz liniowa zależność stałej szybkości reakcji od odwrotności średnicy ziaren wskazuje, że najwolniejszym etapem procesu jest reakcja chemiczna na powierzchni pirytu. Stwierdzono również, że w całym badanym zakresie temperatur (30-70°C) jony S^{2-} utleniają się do jonów SO_4^{2-} .

Anna SZYMCZYCHA-MADEJA*, Władysława MULAK*,
Anna LEŚNIEWICZ*

PHYSICOCHEMICAL STUDY OF SPENT HYDRODESULPHURIZATION (HDS) CATALYST

Received May 15, 2007; reviewed; accepted May 27, 2007

A spent hydrodesulphurization (HDS) catalyst Ni₂Mo/Al₂O₃ has been studied by means of X-ray diffraction, scanning electron microscope, electron microprobe and chemical analysis. Chemical analysis of catalyst confirmed its partial chemical composition as follows: Ni (5.26%), Mo (5.08%), Al (24.57%), V (5.36%), S (9.64%), C (17.63%), H (1.14%). Powder XRD analysis showed that the main phase of studied catalyst is γ -Al₂O₃ while V₅S₈ and Ni₃S₄ were also detected. SEM results confirmed that V and Ni sulphides are deposited on the surface. The surface area of the catalyst determined by nitrogen adsorption (BET method) was found equal to 80.1 m²/g. Leaching tests of the spent catalyst in solutions of sulphuric acid as well as oxalic acid with oxidizing agents such as NH₄NO₃, (NH₄)₂S₂O₈ and H₂O₂ have been carried out.

Key words: spent catalyst, critical metals, leaching

INTRODUCTION

Catalysts containing valuable metals such as nickel, cobalt and molybdenum are commonly used in the oil industry and especially for the hydrodesulphurization of petroleum fractions. This process results in generation of spent catalysts that contain S, C, V, Fe, Ni, Si and traces of As, P (Trim et al., 1989; Diez and Gattes, 1990; Furimsky and Massoth, 1990). Spent catalysts can be classified as hazardous materials (Loehr et al., 1993). Due to their toxic nature, the disposal of spent catalysts can pollute the environment since heavy metals are leached out. To avoid pollution in land disposal as well as to minimize landfill space, the spent catalysts are subjected to metal extraction by various solubilization processes and reused in variety of applications (Furimsky, 1996; Marafi and Stanislaus, 2003; Angelidis et al., 1995).

* Wrocław University of Technology, Chemical Department, Wybrzeże Wyspiańskiego 27,
50-370 Wrocław, Poland, E-mail: wladyslawa.mulak@pwr.wroc.pl.

Leached residue of a spent hydrodesulphurization catalyst has been combined for instance with ladle furnace slag for making of a high value added anorthite glass-ceramic materials (Sun et al., 2001).

In this investigation the spent hydrodesulphurization catalyst was characterized physically and chemically. Additional chemical leaching tests were also performed using solutions of sulphuric acid as well as oxalic acid with oxidizing agents: NH_4NO_3 , $(\text{NH}_4)_2\text{S}_2\text{O}_8$ and H_2O_2 .

EXPERIMENTAL

MATERIALS AND METHODS

The spent catalyst, as cylindrical extrudates of approximate diameter 0.3-0.4 mm and length 4-6 mm was studied. It contained residual oil which was washed out with hot toluene by Soxhlet process and then dried at 110°C before experiments. The surface area of the deoiled catalyst was determined by nitrogen adsorption (BET method). X-ray diffraction (XRD) analysis was performed on STOE model powder diffractometer. SEM-EDX analysis was made with scanning electron microscope (JEOL JSM 580 LV) coupled with the link ISIS 300 X-ray microanalysis system (Oxford Instrument). Prior to scanning electron microscopy (SEM) analysis samples were dried at room temperature, dispersed on a specimen holder, and coated with carbon film for SEM examination. Transmission electron microscopy (TEM) measurements were performed with CM 20 Philips instrument.

The concentrations of metals (V, Ni, Mo and Al) in the catalyst samples and leach liquids were measured by the atomic emission spectrometry with inductively coupled argon plasma as the excitation source. A Jobin-Yvon 38S spectrometer was equipped with a cross-flow nebuliser and Scott-type spray chamber. The high-pressure microwave sample decomposition was performed using Milestone digestion system (MLS-1200 MEGA). For CHNS analysis of the spent catalyst CHNS analyzer (VarioEl) was used.

LEACHING EXPERIMENTS

Leaching tests were carried out in a flask containing 200 ml of the leaching solution. The flask was submerged in a tank, temperature of which was kept constant to within 0.1°C. When the required temperature was reached, a 0.5g charge of spent catalyst was added and stirring started. Leaching lasted three hours, during which six 1 ml samples of the solution were taken to determine the metal concentration by ICP-OES.

RESULTS AND DISCUSSION

X-RAY DIFFRACTION (XRD)

X-ray diffractograms of the deoiled and oiled spent catalysts are given in Fig. 1. Both show that studied catalyst is amorphous. Its main phase is γ - Al_2O_3 , however V_5S_8 and Ni_3S_4 compounds were also visible. No additional peaks are observed. This indicates that molybdenum and nickel atoms are well dispersed over the alumina support.

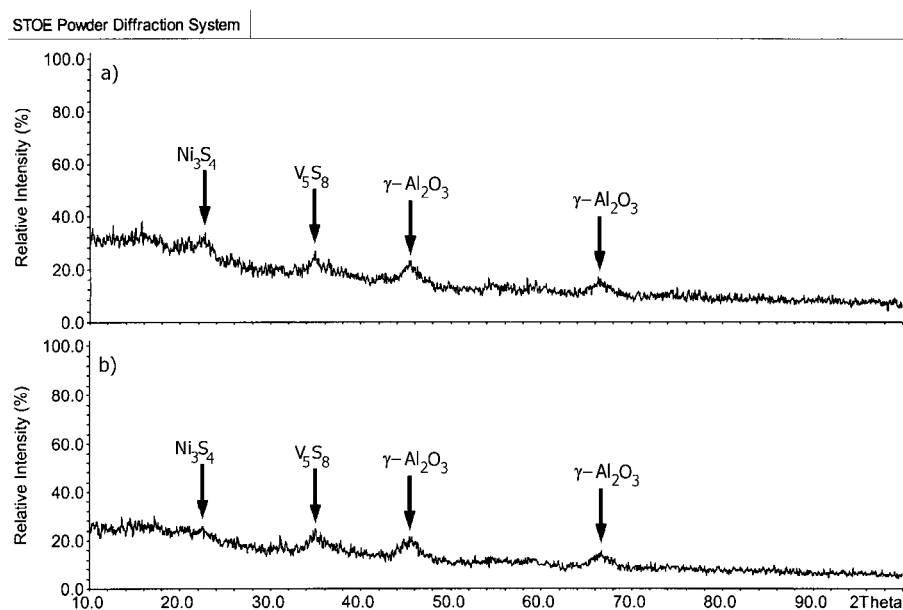


Fig. 1. X-ray diffractograms of the spent catalyst; a) deoiled, b) oiled

MISROSCOPIC ANALYSIS

Scanning electron micrograph of the spent catalyst extrudate is shown in Fig. 2. Fig. 2a presents the shape of the sample. Morphology of its surface (Fig. 2b) evidenced that it consists of aggregated small particles of diameter ranging from 0.4 to 1.7 μm .

The microprobe analysis of the surface of two different extrudates of the spent catalyst depicted in Fig. 3 (indicated by circle and square) resulted in comparable peaks of the elements.

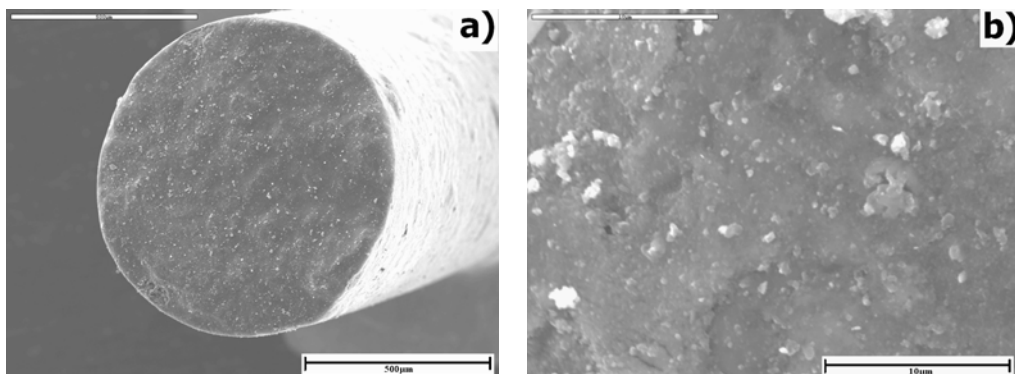


Fig. 2. Scanning electron micrograph of the spent catalyst;
a) shape of an extrudate, b) morphology of its surface

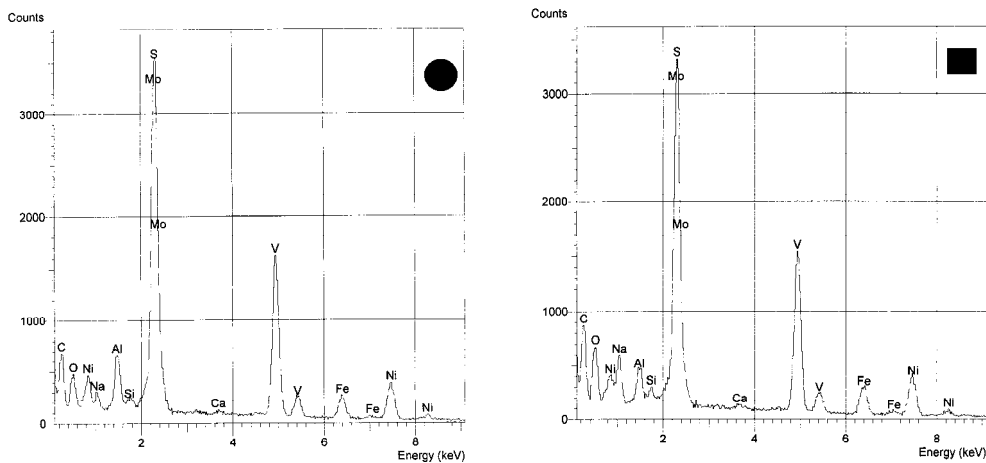


Fig. 3. Microprobe analysis of the surface of two different extrudates of the spent catalyst

The most interesting microscope evidence found in this study is provided by the cross-section of the spent catalyst extrudate shown in Fig. 4.

Microprobe analysis of the surface of edge extrudate cross-section (marked by circle in Fig. 4) proved high contents of V (19.35%), Ni (9.48%), Fe (4.20%), and sulphur (18.38%) but small amounts of Al (3.42%) and Mo (1.44%) (Fig. 5).

The middle part of the extrudate cross-section (indicated by square in Fig. 4) showed dominating contents of Al (32.39%), Mo (3.89%), S (7.01%) and Ni (2.25%), whereas practically no amounts of V and Fe were found. It is clearly shown that metal foulants such as vanadium, nickel and iron are concentrated near the outer surface of the catalyst extrudate, blocking the pore mouths and retarding the access of the

reactants to the active sites of the catalyst within pores. TEM analysis confirmed the existence of γ - Al_2O_3 , Ni_3S_4 , and V_5S_8 and revealed molybdenum sulphide (MoS_2). All metal sulphide deposits on a HDS catalyst are crystallites of 10 – 30 nm.

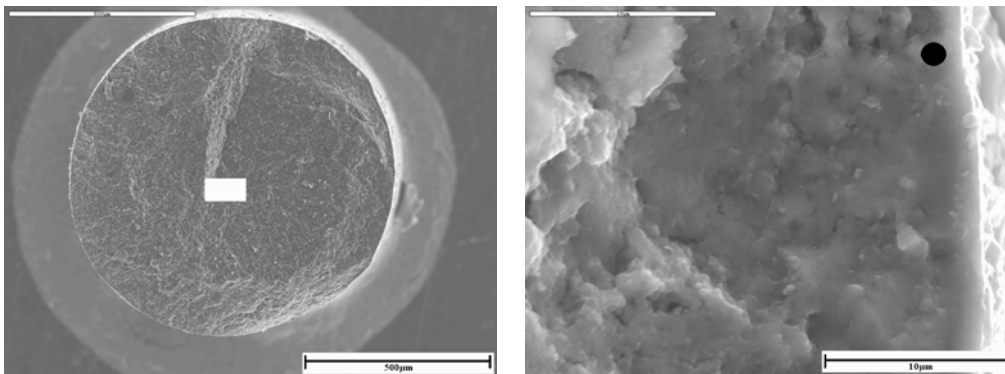


Fig. 4. SCM micrograph of the spent catalyst extrudate cross-section

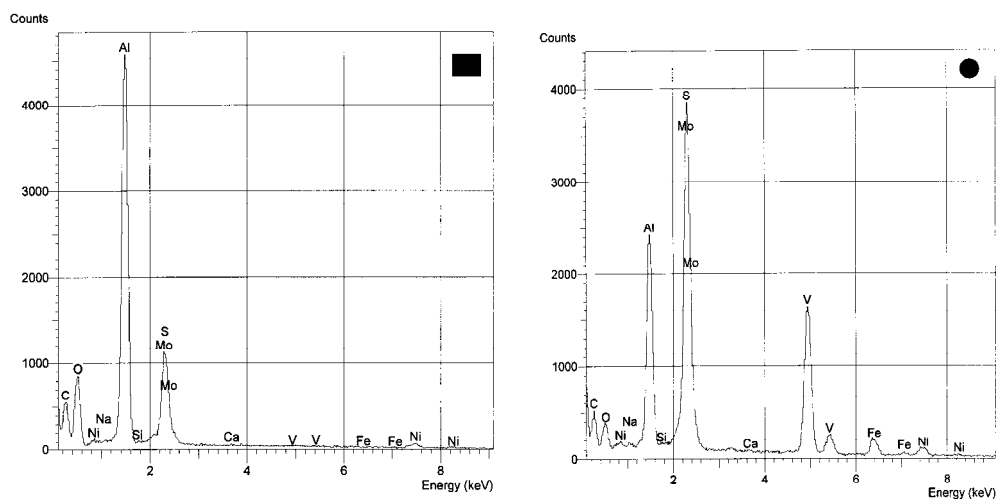


Fig. 5. Microprobe analysis of the surface cross-section showed in Fig. 4;
 ■ middle of the catalyst extrudate, ● edge of the catalyst extrudate

BET SURFACE AREA

The BET measurements were made in a conventional glass apparatus giving a base pressure of 10^{-6} Torr. The BET surface area of the deoiled, spent catalyst was measured by nitrogen adsorption at liquid nitrogen temperature, assuming 0.162 nm^2 as the area per one N_2 molecule. Prior to measurements the catalysts were degassed for 3h at 200°C . The surface area found is equal to $80.1 \text{ m}^2/\text{g}$.

CHEMICAL ANALYSIS

About 0.3 g of powdered spent catalyst was accurately weighted into a Teflon digestion vessel. Then 3 ml of concentrated hydrochloric acid, 7 ml of concentrated nitric acid and 3 ml of hydrogen peroxide (30 %) were added. Decomposition of the sample was carried out the next day with microwave digestion system. Samples microwave heated at maximum power of 500 W for 35 minutes. After cooling, the sample solution was quantitatively transferred into 100 ml volumetric flask and made up to the volume with distilled water. Before analysis all the solutions were filtered through the hard filter paper. The resulting solutions were diluted to the concentration range required for analysis. Results are as follows: 5.08 Mo, 5.36 V, 5.26 Ni and 24.57 Al (wt.%).

CHNS ANALYSIS

One to two milligrams of the spent catalyst was used to C, H, N and S analysis, following the procedure outlined in Aung and Ting (2004). The CHNS analysis showed that the spent catalyst contained (wt.%) carbon, 17.63; hydrogen, 1.14; nitrogen, 0.38 and sulphur, 9.64.

LEACHING TESTS

In order to choose a suitable leachant: sulphuric acid as well as oxalic acid without and with additional oxidants: NH_4NO_3 , $(\text{NH}_4)_2\text{S}_2\text{O}_8$ and H_2O_2 were tested.

The leaching was performed at 70°C for three hours. Reproducibility of leaching experiments was determined to be of order of $\pm 2\%$ by repeating selected experiments under identical conditions. Summarised results of extraction of metals with different reagents after 3 hours leaching at 70°C are given in Table 1.

Table 1. Metal extraction in various leaching solutions

Leaching solution	Metal extraction, %			
	Mo	Ni	V	Al
2 M H_2SO_4	2.1	40.4	5.1	12.4
2 M H_2SO_4 + 0.66 M H_2O_2	32.8	84.7	53.5	41.3
2 M H_2SO_4 + 0.5 M NH_4NO_3	38.1	83.5	58.3	67.1
2 M H_2SO_4 + 0.5 M NaNO_3	48.7	74.8	57.2	66.9
2 M H_2SO_4 + 0.1 M $\text{Na}_2\text{S}_2\text{O}_8$	31.1	70.8	39.1	59.0
2 M H_2SO_4 + 0.1 M $(\text{NH}_4)_2\text{S}_2\text{O}_8$	33.5	82.8	53.9	65.0
0,5 M $\text{H}_2\text{C}_2\text{O}_4$	11.9	33.1	12.8	18.7
0.4 M $\text{H}_2\text{C}_2\text{O}_4$ + 0.66 M H_2O_2	62.1	70.3	80.0	57.5
0.5 M $\text{H}_2\text{C}_2\text{O}_4$ + 0.5 M NH_4NO_3	7.4	36.1	11.7	12.9
0.5 M $\text{H}_2\text{C}_2\text{O}_4$ + 0.1 M $(\text{NH}_4)_2\text{S}_2\text{O}_8$	28.0	57.2	34.0	26.5

From Table 2 it comes that sulphuric and oxalic acids alone exhibit very poor efficiency for the leaching of metals from studied catalyst. The oxalic acid with H_2O_2 addition evidenced the highest leaching efficiency for vanadium (80.0%), molybdenum (62.1%) and nickel (70.3%). The oxalic acid, as a chelating agent, forms soluble metal complexes with molybdenum and vanadium (Marafi and Stanislaus, 1989), causing that the extraction of Mo and V is higher than that after leaching with H_2SO_4 in the presence of H_2O_2 . Leaching of the spent catalyst in oxalic acid as well as in sulphuric acid containing H_2O_2 resulted in the loss of the alumina catalyst support (about 40%). Leaching efficiency of nickel and vanadium in sulphuric acid solution with $(\text{NH}_4)_2\text{S}_2\text{O}_8$ and H_2O_2 is comparable for nickel (82.8%), vanadium (53.9%) and molybdenum (33.5%) but extraction of aluminium is of about 24% lower in the presence of H_2O_2 than $(\text{NH}_4)_2\text{S}_2\text{O}_8$.

CONCLUSIONS

1. Powder XRD analysis of the spent HDS catalyst showed that its main phase is $\gamma\text{-Al}_2\text{O}_3$ but V_5S_8 and Ni_3S_4 were also detected. No sharp peaks corresponding to nickel or molybdenum sulphides or other phases were observed.
2. SEM-EDX analysis of the spent catalyst extrudate cross-section illustrated that the metal foulants (vanadium, nickel and iron) are concentrated near the outer surface of the catalyst pellets.
3. Chemical analysis of the spent catalyst is as follows: Ni (5.26%), Mo (5.08%), V (5.36%) and Al (24.57%).
4. CHNS analysis revealed that the spent catalyst contained (wt.%): C (17.64), H (1.14%), N (0.38) and S (9.64).
5. Oxalic acid with H_2O_2 addition exhibited the highest leaching efficiency towards metals contained in the studied catalyst. After 3 hours of leaching at 70°C with solution of 0.4 M $\text{H}_2\text{C}_2\text{O}_4$ + 0.66 M H_2O_2 , extraction of metals from the spent catalyst were: 80.0% of V, 70.3% of Ni, 62.1% of Mo and 42.4% of Al.

ACKNOWLEDGEMENTS

The authors wish to thank the Polish Committee for Scientific Research for financial support (grant No 3T09B 05428).

REFERENCES

- ANGELIDIS T.N., TOURASANIDIS E., MARINO E., STALIDIS G.A., 1995, *Selective dissolution of critical metals from diesel and naphtha spent hydrodesulphurization catalysts*, Resources, Conservation and Recycling 13, 269-282.
- AUNG K.M.M., TING Y.P., 2005, *Biobleaching of spent fluid cracking catalyst using Aspergillus niger*, Journal of Biotechnology 116, 159-170.
- DIEZ F., GATTES B.C., 1990, *Deactivation of a Ni-Mo/ $\gamma\text{-Al}_2\text{O}_3$ Catalyst: Influence of coke on the hydroprocessing activity*, Ind. Eng. Chem. Res. 29, 1999-2004.
- FURIMSKY E., MASSOTH F.E., 1999, *Deactivation of hydroprocessing catalysts*, Catalysis Today 52, 381-495.

- FURIMSKY E., 1996, *Spent refinery catalysts: environment, safety and utilization*, Catalysis Today 30, 223-286, 1996.
- LOEHR R.C., ROGERS L.A., ERICKSON D.C., 1993, *Mobility of residues at petroleum industry hazardous waste land treatment sites*, Water Res. 27, 1127-1138.
- MARAFI M., STANISLAUS A., 1989, *Regeneration of spent hydroprocessing catalysts: metals removal*, Applied Catalysis 47, 85-96.
- MARAFI M., STANISLAUS A., 2003, *Options and processes for spent catalyst handling and utilization*, Journal of Hazardous Materials B101, 123-132.
- TRIM D.L., 1989, *Deactivation, regeneration and disposal of hydroprocessing catalyst*, in: Catalysts in Petroleum Refining. Trim D.L., Akasha S., Absi-Halabi M. and Bishara A. (Editors), Elsevier, Amsterdam, 1990, pp. 41-60.
- SUN D.D., TAY J.H., CHEONG H.K., LEUNG D.L.K., QIAN G., 2001, *Recovery of heavy metals and stabilization of spent hydrotreating catalyst using a glass-ceramic matrix*, Journal of Hazardous Materials B87, 213-223.

Szymczycha-Madeja A., Mulak W., Leśniewicz A., *Badania fizykochemiczne zużytego katalizatora hydroodsiarczania (HDS)*, Physicochemical Problems of Mineral Processing, 41 (2007) 125-132 (w jęz. ang.).

Charakterystykę fizykochemiczną zużytego katalizatora HDS wykonano stosując: analizę rentgenograficzną (XRD), skaningową mikroskopię elektronową z mikrosondą rentgenowską (SEM-EDX), transmisyjną mikroskopię elektronową (TEM) oraz analizę chemiczną i elementarną. Analiza XRD wykazała dużą amorficzność katalizatora i jako główną fazę określono γ - Al_2O_3 . Stwierdzono również słabe piki siarczku wanadu (V_5S_8) i niklu (Ni_3S_4). Analiza TEM potwierdziła fazę γ - Al_2O_3 oraz obecność V_5S_8 i Ni_3S_4 oraz wykazała zawartość MoS_2 w postaci cienkich płytek. Stwierdzono również, że siarczki metali występują w formie małych kryształków o wymiarach od 10 do 30 nm. Na podstawie wyników analizy SEM-EDX wykazano, że zanieczyszczenia katalizatora (V, Ni, Fe, S) osadzają się głównie na jego powierzchni w postaci siarczków. Analiza chemiczna i elementarna określiły następujące zawartości pierwiastków: 5.08% Mo; 5.36% V; 5.26% Ni; 24.87% Al oraz 17.63% C; 1.14% H; 0.38% N oraz 9.64% S. Przeprowadzono również ługowania testujące w roztworach kwasu siarkowego (VI) i szczawowego w obecności utleniaczy (NH_4NO_3 ; $(\text{NH}_4)_2\text{S}_2\text{O}_8$ i H_2O_2). Najwyższy stopień wylugowania metali uzyskano w roztworach kwasu szczawowego z dodatkiem H_2O_2 , po 3 godzinach ługowania do roztworu przechodziło: 62% Mo, 70% Ni, 80% V oraz 57% Al.

Małgorzata ULEWICZ*, Kamila SADOWSKA**, Jan F. BIERNAT**

SELECTIVE TRANSPORT OF Pb(II) ACROSS POLYMER INCLUSION MEMBRANE USING IMIDAZOLE AZOCROWN ETHERS AS CARRIERS

Received April 30, 2007; reviewed; accepted June 6, 2007

Transport of Pb(II) ions from equimolar aqueous solutions of Zn(II), Cd(II), and Pb(II) as well as from solutions containing only Pb(II) ions source phase ($c_{Me} = 0.001$ M) through polymer inclusion membranes (PIMs) containing imidazole azocrown ethers as carriers has been investigated. The polymer membranes consisting of cellulose triacetate (support), *o*-nitrophenyl pentyl ether (plasticizer) and imidazole crown ether derivatives (as ion carriers) were investigated. The influence of lipophilicity of macrocycles on the selectivity and efficiency of Pb(II) transport with azocrown **3** are higher than **1**, accordingly with the hydrophile-lipophile balance of imidazole azocrown ethers. The highest transport recovery for Pb(II) ions was observed for **3** (91.6%). The transport selectivity of the polymer inclusion membrane with **3** was: Pb(II) > Zn(II) > Cd(II) and the selectivity coefficient Pb(II)/Cd(II) and Pb(II)/Zn(II) equals 40.1 and 13.4, respectively. The stability of PIM with imidazole azocrown derivatives was confirmed by replicate experiments.

Keywords: polymer inclusion membrane, lead(II), zinc(II), cadmium(II), azocrown ethers

INTRODUCTION

The purifying of waste waters by removing transition/heavy metal ions is one of the major objectives of research in the hydrometallurgical processing. Liquid membranes (emulsion - ELMs or supported - SLMs), and recently, polymer inclusion membranes (PIMs) represent an attractive alternative to liquid-liquid extraction for the selective removal and concentration of metal ions such as Zn(II), Cd(II), and Pb(II) from aqueous solutions. The transport across liquid membrane is used for selective

* Department of Metal Extraction and Recirculation, Czestochowa University of Technology, 42-200 Czestochowa, Armii Krajowej 19 Street, e-mail: ulewicz@mim.pcz.czest.pl.

** Department of Chemical Technology, Gdańsk University of Technology, 80-952 Gdańsk.

separation and concentration of metal ions from source aqueous phase, in which the concentration of metal ionic species is above $1 \cdot 10^{-4}$ M (Bond et al., 1999).

During last years several neutral crown ethers and lariat ethers were successfully used for metal ions separation in solvent extraction, in ion exchange systems and transport across liquid membranes. Unfortunately, only few papers refer to heavy metals (Nghiem et al., 2006). In competitive transport of Zn(II) and Cd(II) ions across emulsion liquid membrane with dicyclohexane-18-crown-6, near quantitative selectivity for Cd(II) over Zn(II) and Hg(II) was achieved (Izatt et al., 1987). Hayashi et al. (2003) reported the selective proton-driven transport of lead(II) ions across polymer inclusion membranes with proton diionizable polyethers bearing alkyl chains of different length (from $-C_7H_{15}$ to $-C_{16}H_{33}$). The transport selectivity of PIM with polyether bearing $-C_8H_{17}$ alkyl chain was $Pb^{2+} > Cu^{2+} > Cd^{2+} > Zn^{2+} > Ni^{2+}$. Lead(II), cadmium(II) and zinc(II) cations can be effectively removed from aqueous nitrate solutions by polymer inclusion membrane transport with derivatives of ionizable dibenzo-16-crown-5 (DB-16C5) ethers as carriers. The type of group attached ($-H$, $-C_{10}H_{21}$, and $-C_6H_5$) to the DB-16C5 molecule has the influence on selectivity and efficiency of Zn(II), Cd(II), and Pb(II) transport through polymer inclusion membranes (Ulewicz et al., 2006).

Recently, the transport studies using the azacrown ethers have been reported. Cho et al. (1995) found that a single transport of Cd^{2+} across emulsion liquid membranes mediated by diaza-18-crown-6 (DA18C6) from 0.4 M SCN^- aqueous solutions is much more effective in comparison with Zn^{2+} . On the other hand, Dadfarnia and Shamsipur (1992) discovered quantitative transport of zinc(II) and only 1 % of cadmium(II) across bulk liquid membrane with DA18C6 and palmitic acid. Polymer inclusion membranes containing CTA and macrocyclic compounds such as DA18C6, dibenzo-18-crown-6 (DB18C6), hexathia-18-crown-6 and hexaaza-18-crown-6 were investigated by Gherrou et al. (2001, 2004, 2005). Pyrrole azocrown ethers in ordinary bulk membrane system were also found to preferentially transport lead(II) from equimolar mixture of Co^{2+} , Ni^{2+} , Cu^{2+} , Zn^{2+} , Cd^{2+} , Ag^+ and Pb^{2+} ions (Luboch et al., 2007). Comparison of carrier-facilitated transport of lead(II) across SLM and PIM has been reported by Aguilar et al. (2001). It was shown that ligands like diazadibenzo18-crown-6 had high selectivity for lead(II) over cadmium(II) and zinc(II) ions using a CTA/2-NPOE membrane of composition (w/w) 22 % CTA, 71,6 % 2-NPOE and 6,4 % carrier. On the other hand, Kim et al. (2001) observed selective transport of Ag(I) over Pb(II) and Cd(II) for a series of calix[4]azacrown ether derivatives immobilized in a CTA-based PIM plasticized with 2-NPOE and TBEP. Similarly, high transport selectivity for Ag(I) in the presence of Zn(II), Cd(II), Pb(II), Co(II), Ni(II) and Cu(II) ions was observed for transport across SLMs and PIMs using acyclic polyether ligands with diamide and diamine end-groups (Kim et al., 2001a).

Ulewicz et al. (2004) investigated competitive transport of Zn(II), Cd(II), and Cu(II) ions from aqueous chloride source phase across polymer inclusion membranes containing side-armed lariat ether-type derivatives of diphosphaza-16-crown-6 as ion

carrier. It was found, that the initial fluxes of all investigated cations increase with increase of the feed phase acidity and the selectivity order was Cd(II) > Zn(II) > Cu(II).

The present article deals with a competitive transport of lead(II) ions from a dilute aqueous solutions using PIM doped with imidazole azocrowns. The effects of structural modification of imidazole azocrown ether derivatives upon the efficiency and selectivity Pb(II) ions transport is reported. Also, the stability of PIMs with imidazole azocrown derivatives was confirmed by replication of experiments using the same membranes.

EXPERIMENTAL

REAGENTS

The inorganic chemicals, i.e. lead(II), zinc(II) and cadmium(II) nitrates, and hydrochloric acid were of analytical grade and were purchased from POCh (Gliwice, Poland). The aqueous solutions were prepared with double distilled water, which conductivity was 0.1 $\mu\text{S}/\text{m}$. The organic reagents, i.e. cellulose triacetate (CTA), *o*-nitrophenyl pentyl ether (*o*-NPPE) and dichloromethane were also of analytical grade and were purchased from Fluka and used without further purification. The density of plasticizer, i.e. *o*-nitrophenyl pentyl ether was 1.085 g/cm^3 . Azocrown ethers **1** ÷ **3** (Fig.1) were synthesized as described by Wagner-Wysiecka et al (Wagner-Wysiecka et al., 2003; Luboch et al., 2007).

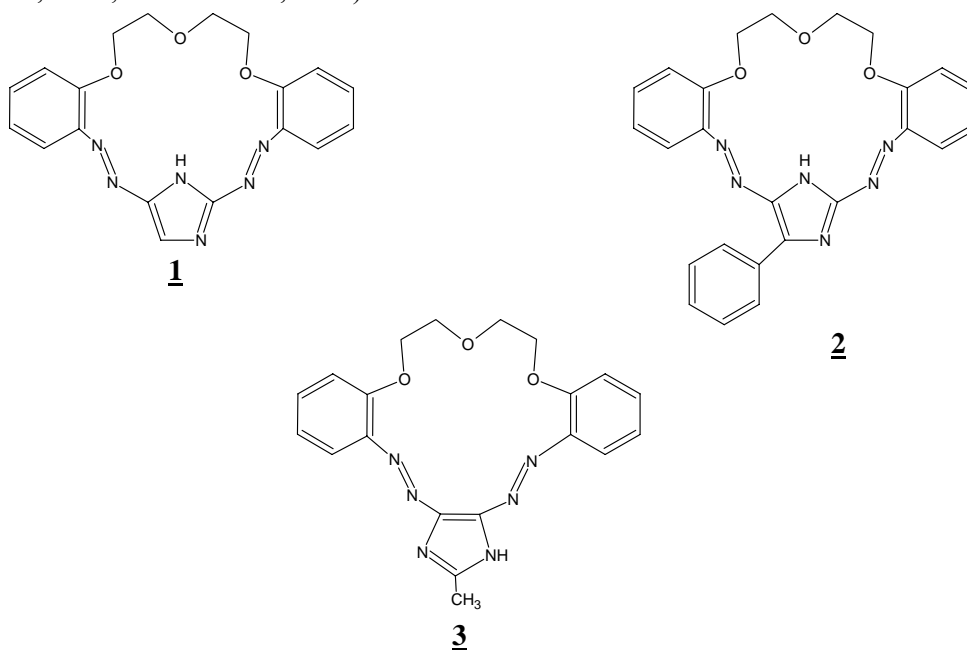


Fig. 1. Formulas of imidazole azocrown ethers

POLYMER INCLUSION MEMBRANE PREPARATION

A dichloromethane solution of cellulose triacetate, plasticizer (for example *o*-NPPE), and azocrown (**1** ÷ **3**) as the ion carrier was prepared. A specified portion of this solution was poured into a membrane mold comprised of a 9.0 cm diameter glass ring placed on a glass plate with cellulose triacetate - dichloromethane glue. After evaporation of the solvent overnight the resulting membrane was peeled off from the glass plate by immersion in cold water. Then the membrane was soaked for 12 hours in water. Two membrane samples were cut out from the same preparation for duplicate transport experiments. The membrane contained 2.6 cm³ *o*-NPPE /1g CTA, and 0.05 M azocrown based on plasticizer. The average PIM thickness was 30-35µm.

TRANSPORT STUDIES

Transport experiments were performed in a permeation cell in which the membrane film (surface area 4.9 cm²) was tightly clamped between two cell compartments. Both, source and receiving aqueous phases (50 cm³ each) were mechanically stirred at 600 rpm. 1.0 M HCl was used as a receiving phase. The PIM transport experiments were carried out at 20 ± 0.2°C. Small samples of the aqueous receiving phase were taken periodically *via* a sampling port equipped with a syringe and analyzed by atomic absorption spectroscopy (AAS Spectrometer, Solaar 939, Unicam) to determine lead(II), zinc(II), and cadmium(II) concentration. The source phase pH (equal 5.0) was kept constant and controlled by pH meter (CX-731 Elmetron, with combined pH electrode, ERH-126, Hydromet, Poland).

The transport across PIMs fits the first-order kinetics in relation to the metal-ion concentration (Danesi, 1984-85), which can be described by Equation 1:

$$\ln\left(\frac{c}{c_i}\right) = -kt \quad (1)$$

where c is the metal ions concentration (M) in the source aqueous phase at some given time, c_i is the initial metal ions concentration in the source phase, k is the rate constant (s⁻¹), and t is the time of transport (s).

To calculate the k value, a plot of $\ln(c/c_i)$ versus time was prepared. The rate constant value for the duplicate transport experiment was averaged and standard deviation was calculated. The permeability coefficient (P) was calculated as follows:

$$P = -\frac{V}{A}k, \quad [\text{m/s}] \quad (2)$$

where V is volume of the aqueous source phase, and A is an effective area of membrane.

The initial flux (J_i) was determined as equal to:

$$J_i = P \cdot c_i \quad [\text{mol/m}^2 \cdot \text{s}] \quad (3)$$

The selectivity coefficient (S) was defined as the ratio of initial fluxes for $M1$ and $M2$ metal ions, respectively:

$$S = J_{i,M1} / J_{i,M2} \quad (4)$$

To describe the efficiency of metal removal from the source phase, the recovery factor (RF) was calculated:

$$RF = \frac{c_i - c}{c_i} \cdot 100\% \quad [\%] \quad (5)$$

RESULTS AND DISCUSSION

In the first series of experiments, the transport of lead(II) from nitrate aqueous solutions containing metal ions at 0.001 M concentration through PIM with imidazole azocrown and *o*-NPPE as plasticizer into 1.0 M hydrochloric acid aqueous solutions was investigated. For blank experiment no transport was detected for more than 48 h of continuous running. The relationship between $\ln(c/c_i)$ and time for Pb(II) transport across PIM containing **1** or **3** azocrown is shown in Fig. 2. The kinetics parameters are summarized in Table 1. As shown in Fig. 2, the transport of Pb(II) ions across PIM with azocrowns can be described by first order kinetics in metal ion concentration changes. It is in accordance to the mathematical model proposed by Danesi (1984-85).

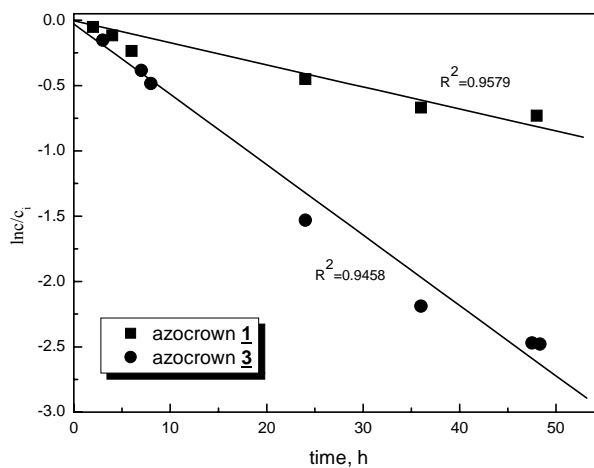


Fig. 2. Kinetics of Pb(II) ions transport across PIMs containing 0.05 M of azocrown ethers **1** or **3** from aqueous solutions. Source phase: $c_{\text{Pb(II)}} = 0.001$ M; pH = 5.0; receiving phase: 1.0 M HCl; membrane: 2.60 cm³ *o*-NPPE / 1 g CTA, 0.05 M of azocrown (based on plasticizer volume)

Table 1. Kinetics parameters, selectivity order and selectivity coefficients for competitive transport of metal ions across PIM with carriers **1** or **3**. Conditions as in Fig. 2

Azocrown	Metal ions	Permeability coefficient, J_i ($\mu\text{m/s}$)	Initial flux, J_i ($\mu\text{mol/m}^2\text{s}$)	RF, %
1	Pb(II)	46.30	0.397	51.8
3	Pb(II)	160.6	1.375	91.6

As can be seen from this table, higher value of permeability coefficient and initial fluxes for Pb(II) ions were obtained for compound **3**. Previously it was found (Ulewicz et al., 2007) that the initial fluxes of transported metal ions under competitive conditions depend on the hydrophile-lipophile balance (HLB) of azocrown ethers. At present, the similar dependence was obtained for solutions containing only Pb(II) ions. The initial fluxes of Pb(II) from aqueous solutions decrease with increase of hydrophile-lipophile balance value (HLB) for azocrown, i.e. **3** > **1**; HLB for these azocrowns are 10.9 and 11.4, respectively. In addition, the highest values of recovery factor of Pb(II) ions after 48 hours were obtained for compound **3**.

The transport of lead(II) from equimolar nitrate mixture of three metal ions, each at 0.001 M concentration through PIM with imidazole azocrown **3** was also investigated. The kinetics parameters and selectivity order are summarized in Table 2; the recovery factors of all investigated ions are shown in Fig. 3.

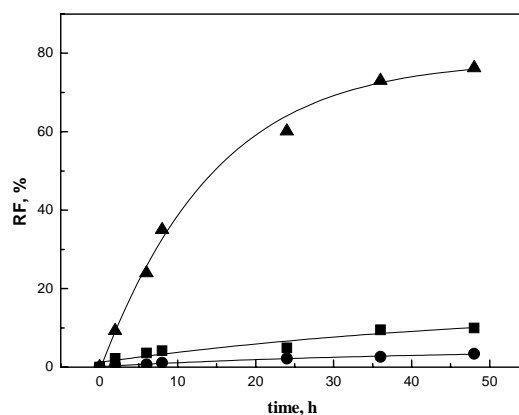


Fig. 3. Recovery of Zn(II), Cd(II), and Pb(II) ions from source phase from aqueous solutions in transport across PIM with azocrown ethers **3**. Source phase: $c_{\text{Me(II)}} = 0.001$ M each; pH = 5.0; receiving phase: 1.0 M HCl; membrane: 2.60 cm^3 *o*-NPPE / 1 g CTA, 0.05 M of azocrown (based on plasticizer volume)

As seen from this figure, the recovery factors of all investigated ions increase with time. The highest recovery factors 76.24 % (after 48 h) were obtained for Pb(II) ions, whereas for Zn(II) and Cd(II) the factors were 10.0 and 3.4 %, respectively. The transport selectivity of the polymer inclusion membranes with **3** were: Pb(II) > Zn(II) > Cd(II).

Table 2. Kinetics parameters, selectivity order and selectivity coefficients for competitive transport of metal ions across PIM with carriers **3**. Conditions as in Fig. 3

Metal ions	Permeability coefficient, J_i ($\mu\text{m/s}$)	Initial flux, J_i ($\mu\text{mol/m}^2\text{s}$)	Selectivity order and selectivity ratios
Zn(II)	6.02	0.060	Pb(II) > Zn(II) > Cd(II) 13.4 40.1
Cd(II)	2.08	0.020	
Pb(II)	93.40	0.801	

In order to examine the influence of the metal ions concentration in the source phase, the transport of metal ions from equimolar mixture of three ions was performed. The relationship between $\ln(c/c_i)$ and time for Pb(II), Cd(II) and Zn(II) transport across PIM is shown in Fig. 4, whereas the found kinetic parameters are summarized in Table 3. It is evident that metal ions are transported across PIMs with higher rate from solutions of lower concentration but initial fluxes are higher for solutions of higher metal concentration. For 0.01M concentration the selectivity coefficients Pb(II)/Zn(II) and Pb(II)/Cd(II) equal 11.3 and 53.6, respectively. For 0.001 M solutions the same parameters are 16.3 and 46.0, respectively. For both concentrations, the transport selectivity across the polymer inclusion membranes with **2** are: Pb(II) > Zn(II) > Cd(II) (Figure 4).

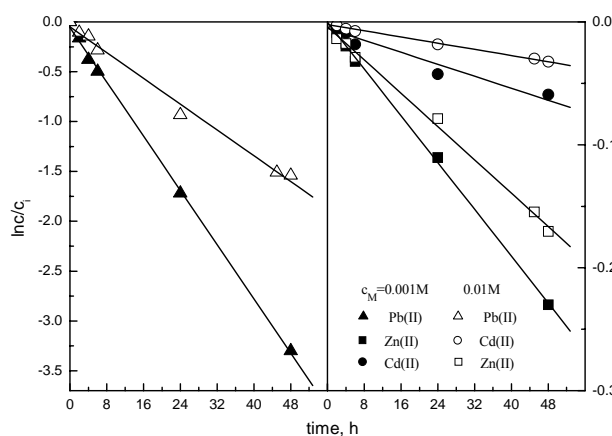


Fig. 4. Relationship of $\ln c/c_i$ vs. time for Pb(II), Cd(II) and Zn(II) transport across PIMs with **2** from source phase of different metal ions concentration; receiving phase: 1.0 M HCl; membrane: 2.60 cm^3 *o*-NPPE / 1 g CTA, 0.05 M of azocrown (based on plasticizer volume)

Recently, many papers deal with the membrane stability and lifetime. These factors determine the usefulness of membrane on large industrial scale. Kim et al. (2000, 2001) investigated the stability of SLMs and PIMs under similar experimental conditions. They reported small flux decline after 15 days of continuous transport

across PIMs containing CTA/2-NPOE and acyclic polyether carriers, and after 20 days using calix[4]arene derivatives as carrier. Ulewicz et al. (2005) also shown flux stability of Pb(II), Zn(II), and Cd(II) ions across PIMs with calix[4]-crown-6 derivative for 12 days. The higher stability of PIMs over SLMs was reported for membranes with Aliquat 336 as a carrier (Scindia et al., 2006).

Table 3. Kinetics parameters for competitive transport of metal ions across PIM with carrier 2. Conditions as in Fig. 4

Metal concentration	Metal ions	Rate constants, k (h^{-1})	Initial flux, J_i ($\mu\text{mol}/\text{m}^2\text{s}$)
0.001 M	Zn(II)	0.0048	0.1376
	Cd(II)	0.0012	0.0486
	Pb(II)	0.0681	2.2380
0.01 M	Zn(II)	0.0033	0.9400
	Cd(II)	0.0005	0.1986
	Pb(II)	0.0324	10.650

Stable performance of PIMs for 30 days was evidenced, while SLMs membrane worked well only for 7 days. Alguacil et al. (2005) showed that the percent extraction of Zn(II) in experiments with SLM with re-impregnated membrane decreased from 93.2 to 56.2 % after 12 h work (4 runs for 3 h). It demonstrates that the process with use of PIM type membranes show higher stability than with the use of SLM, although in both casus leaching of the carrier is observed.

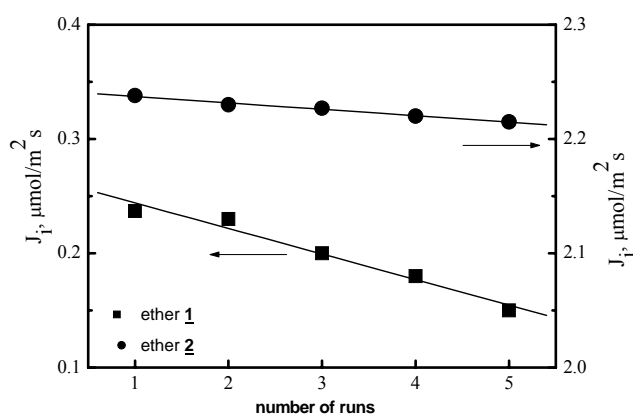


Fig. 5. Initial flux vs. number of run in repeated transport of Pb(II) ions across PIM with carriers 1 or 2; source phase: $[\text{Pb(II)}]=[\text{Cd(II)}]=[\text{Zn(II)}]=0.001\text{M}$ each, receiving phase: 1.0 M HCl; membrane: 2.60 cm^3 *o*-NPPE / 1 g CTA, 0.05 M of azocrown (based on plasticizer volume)

To examine the long-term stability of the PIMs with imidazole azocrown ethers, we reused the same membranes with azocrown **1** or **2** as ion carriers in successive metal ions transport experiments (48 h duration) from aqueous solutions at the same concentration. Fig. 5 shows that the initial flux of Pb(II) ions decrease with the number of runs of repeated transport across PIM. For azocrown **1** we observed that the initial flux decrease more than using azocrown **2**. The carrier leaching from membrane is associated with their hydrophilicity and water solubility. As can be seen from Fig. 6, the azocrown **1** is slightly soluble in water. Therefore, leaking of the ionophore **1** from the membrane is not the only reason of the initial fluxes decrease. It is considered, that it stays in connection with complex formation rate in the source phase (Wagner-Wysiecka et al., 2007, cf. Luboch et al., 2006).

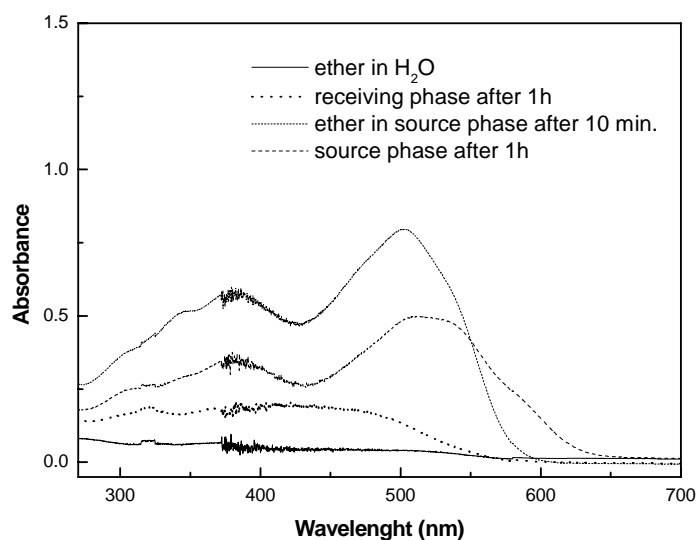


Fig. 6. Changes of absorbance for ether **1** in source and receiving phase

CONCLUSIONS

Lead(II) ions can be effectively removed from aqueous nitrate solutions using polymer inclusion membrane transport with derivatives of imidazole azocrown ethers as carriers. The initial fluxes of Pb(II) ions decrease with the increase of azocrown ethers hydrophile-lipophile balance, i.e. **3** > **1**. The selectivity order of metal ions fluxes for azocrown ether **3** is as follows: Pb(II) > Zn(II) > Cd(II), whereas the selectivity coefficients Pb(II)/Cd(II) and Pb(II)/Zn(II) equal 40.1 and 13.4, respectively. The selectivity coefficients of Pb(II)/Cd(II) decrease with increase of metal ions concentration in the source phase. The type of group attached to the imidazole azocrown molecule has the influence on long-term stability of the PIMs.

REFERENCES

- AGUILAR J.C., RODRIGUEZ E., GYVES J. De, BARTSCH R.A., KIM M. (2001), *Design, synthesis and evaluation of diazadibenzocrown ethers as Pb(II) extractants and carriers in plasticized cellulose triacetate membranes*, *Talanta*, 54, 1195-1204.
- ALGUACIL E. J., ALONSO M. (2005), *Separation of zinc(II) from cobalt(II) solutions using supported liquid membrane with DP-8R (di(2-ethylhexyl)phosphoric acid) as a carrier*, *Sep. Purification Technol.*, 41, 179-184.
- BOND H., DIETZ M. L., ROGERS R.D., Eds. (1999), *ASC Symposium Series 716*, Washington, DC.
- CHO M. H., CHUN H. S., KIM J. H., RHEE Ch. H., KIM S. J. (1991), *Study on separation of heavy metal ions in a natural macrocycle-mediated emulsion liquid membrane system*, *Bull. Korean Chem. Soc.*, 12, 474 - 477.
- CHO M.H., SHIN S. Ch. (1995), *Studies on the macrocycle-mediated transport of divalent metals ions in a supported liquid membrane system*, *Bull. Korean Chem. Soc.*, 16, 33 - 36.
- DADFARNIA S., SHAMSIPUR M. (1992), *Highly selective membrane transport of zinc(2+) ion by a cooperative carrier composed of 1,10-diaza-18-crown-6 and palmitic acid*, *Bull. Chem. Soc. Jpn.*, 65, 2779 - 2783.
- DANESI P.R. (1984-85) *Separation of metal species by supported liquid membranes*, *Sep. Sci. Technol.*, 19, 857-894.
- GHERROU A., KERDJOUJ H., MOLINARI R., DRIOLI E. (2001), *Facilitated transport of Ag(I), Cu(II) and Zn(II) ions by using DB18C6 and DA18C6 as carriers: Interface behavior on the ion transport*, *Sep. Sci. Technol.*, 36, 2289-2304.
- GHERROU A., KERDJOUJ H., MOLINARI R., SETA P., DRIOLI E. (2004), *Fixed sites plasticized cellulose triacetate membranes containing crown ethers for silver(I), copper(II) and gold(III) ions transport*, *J. Membr. Sci.*, 228, 194-157.
- GHERROU A., KERDJOUJ H., MOLINARI R., SETA P., (2005), *Preparation and characterization of polymeric plasticized membranes (PPM) embedding a crown ether carrier application to copper ions transport*, *Material Sci. Eng.*, C25, 436-443.
- HAYASHI R., HAYSHITA T., YASHIKAWA T., ARATANI K., BARTSCH R.A., TERAME N. (2003), *Design of a polymer inclusion membrane having proton ionizable polyether carriers and their separation function for lead ion*, *Bunseki Kagaku*, 52, 755-762.
- IZATT R. M., BONALD R. L., GENG W., CHO M. H., CHRISTENSEN J. J. (1987), *Separation of bivalent cadmium, mercury and zinc in a natural macrocyclic-mediated emulsion liquid membrane*, *Anal. Chem.*, 59, 2405 - 2409.
- KIM, J. K.; KIM, J. S.; SHIL, Y. G.; LEE, K. W.; OH, W. Z. (2001), *Selective extraction of cesium ion with calix[4]arene crown ether through thin sheet supported liquid membranes*, *J. Membr. Sci.*, 187, 3-11.
- KIM J.S.; KIM S.K.; CHO M.H.; LEE S.H.; KWON S.G.; LEE E.H. (2001a), *Permeation of silver ion through polymeric CTA membrane containing acyclic polyether bearing amide and amine end-group*, *Bull. Kor. Chem. Soc.* 22 (10), 1076-1080.
- LUBOCH E., WAGNER-WYSIECKA E., FAINERMAN-MELNIKOVA M, LINDOY L.F., BIERNAT J.F. (2006), *Pyrrole azocrown ethers. Synthesis, complexation, selective lead transport and ion-selective membrane electrode studies*, *Supramol. Chem.*, 18 (7), 593-601.
- NGHIEM L.D., MORNANE P., POTTER I.D., PERERA J.M., CATTRALL R.W., KOLEV S.D. (2006), *Extraction and transport of metal ions and small organic compounds using polymer inclusion membranes (PIMs)*, *J. Membr. Sci.*, 281, 7-41.
- SCINDIA Y.M., PANDEY A.K., REDDY A.V.R. (2005), *Coupled-diffusion transport of Cr(VI) across anion-exchange membranes prepared by physical and chemical immobilization methods*, *J. Membr. Sci.*, 249, 143-152.
- ULEWICZ M., KOZŁOWSKI C, WALKOWIAK W. (2004), *Removal of Zn(II), Cd(II) and Cu(II) ions by polymer inclusion membrane with side-armed diphosphaza-16-crown-6-ethers*, *Physicochemical Problems of Mineral Processing*, 38, 131-138.

- ULEWICZ M., WALKOWIAK W. (2006), *Removal of Zn(II), Cd(II) and Pb(II) ions in polymer inclusion membrane transport with ionizable dibenzo-lariat ethers*, Physicochemical Problems of Mineral Processing, 40, 185-194.
- ULEWICZ M., SADOWSKA K., BIERNAT J.F. (2007), *Facilitated transport of Zn(II), Cd(II) and Pb(II) across polymer inclusion membrane doped with imidazole azocrown ethers*, Desalination, in press.
- ULEWICZ M., BOCHEŃSKA M., LESIŃSKA U., WALKOWIAK W. (2005), *Studies on removal of Zn(II), Cd(II) and Pb(II) ions in polymer inclusion membrane transport with calix[4]-crown-6 derivatives*, Physicochemical Problems of Mineral Processing, 38, 107-116.
- WAGNER-WYSIECKA E., LUBOCH E., KOWALCZYK M., BIERNAT J.F. (2003), *Chromogenic macrocyclic derivatives of azoles – synthesis and properties*, Tetrahedron, 59, 4415-4420.
- WAGNER-WYSIECKA E., JAMRÓGIEWICZ M., FONARI M.S., BIERNAT J.F. (2007), *Azamacrocyclic derivatives of imidazole. Synthesis, structure and metal ion complexation properties*, Tetrahedron, in print.

Ulewicz M., Sadowska K., Biernat J.F., *Selektywny transport jonów Pb(II) przez polimerowe membrany inkluzyjne przy użyciu imidazolowych azokoron*, Physicochemical Problems of Mineral Processing, 41 (2007), 133-143 (w jęz. ang.).

Zbadano selektywność transportu jonów ołowiu(II) z równomolowych roztworów jonów Zn(II), Cd(II) i Pb(II) oraz z roztworów zawierających jony Pb(II) przez polimerowe membrany inkluzyjne (PIM) zawierające imidazolowe etery azokoronowe. Badania prowadzono dla azotanowych roztworów Pb(II) o stężeniu 0,001 M oraz dla roztworów zawierających równomolową mieszaninę jonów Pb(II), Cd(II) i Zn(II) ($c_{Me} = 0,001$ M każdego). Badane azokorony różniły się miejscem podstawienia imidazolu i rodzajem dołączonej do niego grupy (-H, -CH₃, -C₆H₅). Polimerowe membrany inkluzyjne otrzymywano z trójoctanu celulozy (nośnik), eteru *o*-nitrofenylopentylowego (pastyfikator) i jednego z eterów koronowych **1** ÷ **3** (przenośnik jonów); stężenie przenośnika jonów w przeliczeniu na objętość plastyfikatora wynosiło 0,05 M. Wykazano, że początkowe wartości strumienia transportu jonów ołowiu(II) maleją ze wzrostem balansu hydrofilowo-hydrofobowego (HLB) eteru koronowego, tj. **3** > **1**. Ponadto stwierdzono, że strumienie początkowe transportu jonów przy użyciu eterów **2** i **3** maleją w szeregu: Pb(II) > Zn(II) > Cd(II). Współczynniki separacji Pb(II)/Cd(II) i Pb(II)/Zn(II) przez PIM przy użyciu eteru **2** z 0,01M roztworu mieszaniny jonów wynosiły 11,3 i 53,6 natomiast z roztworów o stężeniu 0,001 M odpowiednio 16,3 i 46,0. Ponadto wykazano, że polimerowe membrany inkluzyjne z imidazolowymi azokoronami wykazują dużą stabilność, zależną w dużym stopniu od rodzaju jonoforu.

Bernadeta GAJDA*, Mariusz B. BOGACKI**

THE EFFECT OF TRIBUTYL PHOSPHATE ON THE EXTRACTION OF NICKEL(II) AND COBALT(II) IONS WITH DI(2-ETHYLHEXYL)PHOSPHORIC ACID

Received March 10, 2007; reviewed; accepted June 4, 2007

The paper presents the results of studies on the extraction of nickel(II) and cobalt(II) ions from sulphate solutions with di(2-ethylhexyl)phosphoric acid (D2EHPA). As the modifier of extracting capacity, tributyl phosphate (TBP) was used. The obtained experimental results indicate that a high excess of TBP in relation to D2EHPA reduces the extracting capacity of the latter, whereas its small amount (in a proportion of 1:1) improves the extraction of nickel(II) ions, while not affecting the extraction of cobalt(II) ions.

Key words: extraction, phosphoric acid derivatives, metal ions

INTRODUCTION

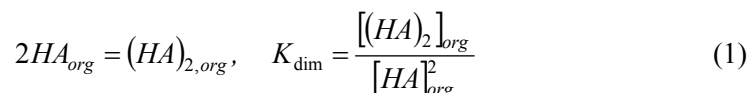
The use of nickel and cobalt has distinctly increased in recent years. This can be indicated, on the one hand, by the increase in the world's production of these metals, and by the appearance of increasingly large amounts of various wastes containing them, on the other. Considering the fact that nickel and cobalt ions are toxic to the natural environment, this adds to the problem of their disposal. One of the feasible solutions is to apply liquid extraction in combination with chemical reaction.

As typical extractants for the extraction of nickel(II) and cobalt(II) ions from aqueous solutions, organic derivatives of phosphoric acid are used. In this group, both typical acid extractants, such as di(2-ethylhexyl)phosphoric acid (D2EHPA) or di(2,4,4-trimethylpentyl)phosphinic acid (CYANEX 272), and Lewis bases can be distinguished, the most typical representatives of the latter being tributyl phosphate (TBP) and trioctylphosphine oxide (TOPO).

* Department of Metal Extraction and Recirculation, Częstochowa University of Technology, Armii Krajowej 19, 42-200 Częstochowa.

** Institute of Chemical Technology and Engineering, Poznań University of Technology, pl. M. Skłodowskiej-Curie 2, 60-965 Poznań.

Phosphoorganic extractants, having functional groups with strongly electron-donor oxygen atoms, can form complexes of a diverse structure (Rydberg, et al., 2004). In addition, these extractants have an ability to interact with one another, creating various associated molecules (Marcus and Kertes, 1969). Acid phosphoorganic extractants in solvents used for the extraction of metal ions occur in a dimer form:



Data collected in numerous publications indicate that the dimerization constant varies depending on the solvent used, for D2EHPA taking on the values of $\log(K_{dim})$ ranging from 3.95 to 4.89 (Kolarik, 1982). Taking into account such large values of the dimerization constant, it can be assumed that, in the organic phase, about 98% of extractant occurs in a dimer form, where two strong hydrogen bond $P(=O)OH...O=(OH)P$ is observed, with the single bond energy amounting to 4 – 5 kcal/mol (Figure 1).

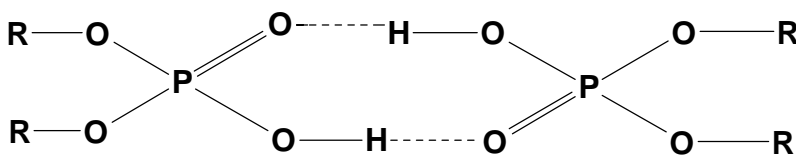
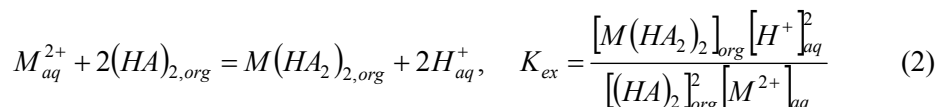


Fig. 1. Structure of the cyclic dimer of di(alkyl)phosphoric acid

On account of the dimerization of acid phosphoorganic extractants, it is adopted in scientific reports that in the formation of complexes with nickel(II) and cobalt(II) ions, these extractants take part in a monomer rather than dimer form (Swain, et al., 2006; Fu and Golding, 1987):



The complex formed in such reaction has a structure of an adduct, in which particular places in the coordination sphere of nickel(II) and cobalt(II) ions are occupied in total by four molecules of the extractant. At the same time, two of them, as acid anions, form polarized covalence bonds, and the other two, as non-dissociated molecules – coordinate bonds via the phosphoryl oxygen atom (Figure 2), (Marcus, and Kertes, 1969).

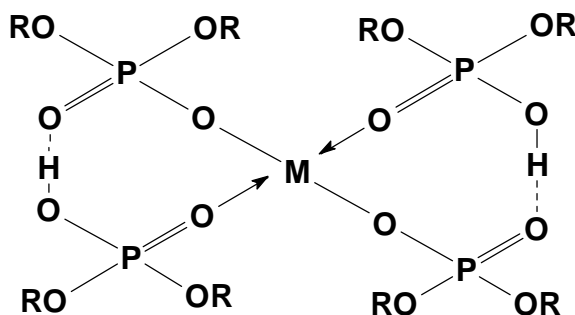
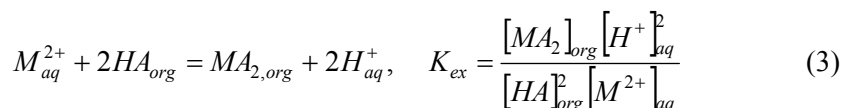


Fig. 2. Structure of the complex of the divalent metal ion with di(alkyl)phosphoric acid in the form of an $MA_2(HA)_2$ type adduct

The suggested structure of this complex is much more complicated than that of typical acid extractant complexes, which react with metal cations according to the reaction



to form chelate complexes, in which each extractant molecule occupies two coordinate places.

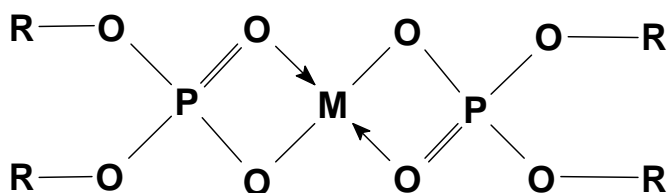


Fig. 3. Structure of the complex of the divalent metal ion with di(alkyl)phosphoric acid in the form of an MA_2 chelate complex

Complexes of nickel(II) and cobalt(II) ions, depending of loading have a face tetrahedral or octahedral structure (Sato and Nakamura, 1972; Van de Voorde et al. 2005). This means that, if the formation of a complex of the structure as shown in Figure (2) is assumed, the positioning of four large extractant molecules in the first coordination sphere should encounter problems associated with the spherical hindrance. Therefore, two of these molecules should be relatively easily exchanged for the molecules of another extractant of the properties of a Lewis base. Such an extractant, having a relatively smaller molecule and, at the same time, good extracting properties, is tributyl phosphate (TBP).

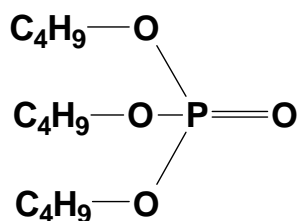
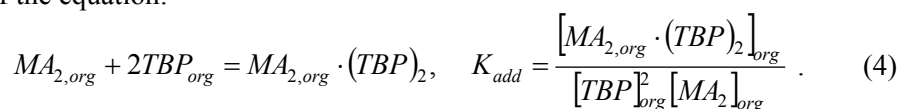
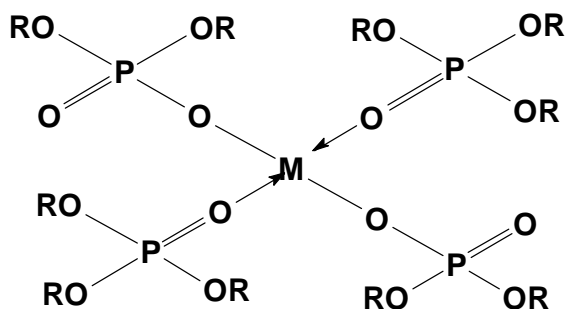


Fig. 4. Structure of tributyl phosphate (TBP)

TBP is often used in the extraction of metal ions as an additional solvating extractant, whose task is to form adducts with metal complexes existing in the solution. (Rydberg et al., 2004). The extraction process in this case can be written in the form of the equation:



The structure of adducts formed in this reaction is shown in Figure (5).

Figure 5. Structure of the complex of the divalent metal ion with di(alkyl)phosphoric acid and tributyl phosphate in the form of an $MA_2(HA)_2$ type adduct

The volume of the TBP molecule, as calculated from the van der Waals radii, is smaller than that of D2EHPA by about 50\AA (Z. Kolarik, 1982) (Table 1). Therefore, it should easier replace D2EHPA molecules in the forming complex. The greater dipole moment of the molecule of this extractant (TBP), indicating its greater polarity, is also an argument for the formation of adducts shown in Figure (5). The smaller charge (in terms of its absolute value) on the phosphoryl oxygen atom in TBP, on the other hand, points out to D2EHPA as a more favoured in the formation of associated molecules.

On the other hand, the presence in the organic phase of an additional compound of strongly solvating properties can give rise to the formation of associated molecules between the molecules of di(2-ethylhexyl)phosphoric acid and tributyl phosphate.

$$HA_{org} + TBP = HA \cdot TBP_{org}, \quad K_{dim} = \frac{[HA \cdot TBP]_{org}}{[HA]_{org} [TBP]_{org}} \quad (5)$$

Table 1. Physicochemical properties of di(2-ethylhexyl)phosphoric acid and tributyl phosphate. The volume calculated from the van der Waals radii

Extractant	Molecule volume, Å ³	Charge on the phosphoryl oxygen atom	Dipole moment, debye
D2EHPA	311.3	-0.873	2.74
TBP	263.7	-0.779	3.10

In such an associated molecule, the phosphoryl oxygen atom, owing to the two free electron pairs, form a hydrogen bond with the molecule of di(2-ethylhexyl)phosphoric acid (Figure 6).

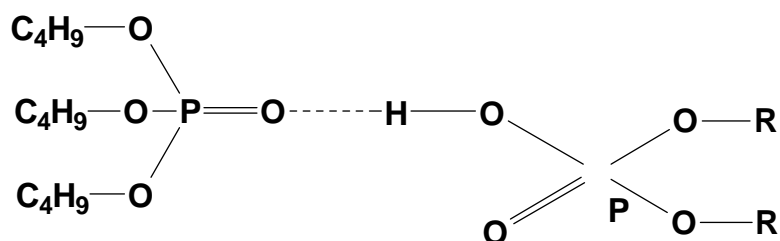


Fig. 6. Structure of the associated molecule of di(2-ethylhexyl)phosphoric acid with tributyl phosphate

As follows from the discussion above, the effect of a tributyl phosphate addition to the organic phase containing D2EHPA as an extractant is not unambiguous, because TBP can influence the extraction of nickel(II) and cobalt(II) ions either favourably or unfavourably.

The aim of the study is to examine the effect of TBP as a synergic addition in the extraction of nickel and cobalt with di(2-ethylhexyl)phosphoric acid from sulphate solutions.

REAGENTS

Hydrated sodium, nickel(II) and cobalt(II) sulphates(VI), as well as sodium hydroxide (supplied by POCh, Poland), were used for the tests. For the preparation of the organic phase solution, di(2-ethylhexyl)phosphoric acid (D2EHPA – 98 %, by Johnson Matthey GmbH, Germany), tributyl phosphate (TBP – 97%) and kerosene of a density of 0.85 g/dm³ (by ALDRICH) were used.

EXPERIMENTAL

A sulphate(VI) solution containing 0.01 mol/dm^3 of nickel(II) and cobalt(II) ions, each, formed a blank. The ionic strength of the initial solution was set at 0.10 M by adding an appropriate amount of sodium sulphate(VI). The pH of the solution was varied by adding 1 M NaOH . The organic phase was obtained by dissolving 0.05 M of the extractant (D2EHPA) in kerosene. As the modifier, TBP was added to the organic phase in a D2EHPA:TBP molar ratio of 1:1, 1:2 and 1:4, respectively. Flasks, each containing 10 cm^3 of the water phase and the organic phase, were shaken mechanically at a constant temperature of $21 \pm 1 \text{ }^\circ\text{C}$ for 15 minutes. After the separation of the phases, the concentration of metal ions in the water phase was assayed on an AAS Solaar 939 spectrophotometer (by Unicam), while pH was measured with a CX-731 pH meter (by Elmetron). The concentration of each sample was assayed three times, and the average value was taken for further consideration. The concentration of metal ions in the organic phase was calculated from the mass balance.

TESTING RESULTS AND DISCUSSION

Four series of experiments were carried out by testing the extraction of nickel(II) and cobalt(II) ions from sulphate solutions for different equilibrium pH values of the water phase. In the first series, D2EHPA in the concentration of 0.05 mol/dm^3 was used as the extractant. In subsequent series, TBP as the modifier of the extracting capacity of D2EHPA was added to the organic phase. TBP was added in the molar ratio to D2EHPA equal to 1:1, 1:2 and 1:4, respectively. The obtained results are shown in Figures 7 and 8.

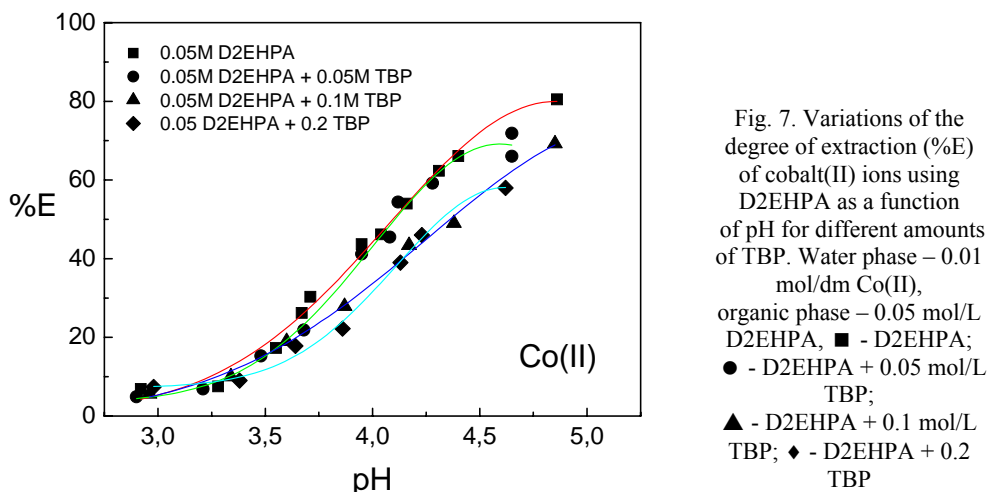


Fig. 7. Variations of the degree of extraction (%E) of cobalt(II) ions using D2EHPA as a function of pH for different amounts of TBP. Water phase – $0.01 \text{ mol/dm}^3 \text{ Co(II)}$, organic phase – $0.05 \text{ mol/L D2EHPA}$, ■ - D2EHPA; ● - D2EHPA + 0.05 mol/L TBP ; ▲ - D2EHPA + 0.1 mol/L TBP ; ◆ - D2EHPA + 0.2 mol/L TBP .

When comparing Figures 7 and 8 it can be noticed that the effect of TBP on extraction depends on the kind of metal being extracted. In the case of cobalt(II), the addition of TBP to the organic phase in the proportion of 1: 1 in relation to D2EHPA practically has no effect on the degree of extraction. A greater excess of TBP in relation to D2EHPA causes a decrease in the degree of extraction.

A different situation is observed for the extraction of nickel(II) ions. A small addition of TBP in the proportion of 1:1 in relation to D2EHPA in the organic phase causes an increase in the degree of extraction. Whereas, further increasing the amount of TBP in the solution results in its decrease.

The reduction of the degree of extraction for a high TBP excess in relation to D2EHPA suggests the formation of the associated molecules of TBP with D2EHPA (Figure 6). The formation of such associated molecules is possible, because the phosphoryl oxygen atom from the TBP molecule, having two free electron pairs, is able to form hydrogen bonds with D2EHPA molecules (Figure 6). Thus, the concentration of the monomer form of this extractant decreases (Equation 5), which causes the extraction equilibrium to shift to the right (Equations 2 and 3). This means the reduction of the degree of extraction of nickel(II) and cobalt(II) ions.

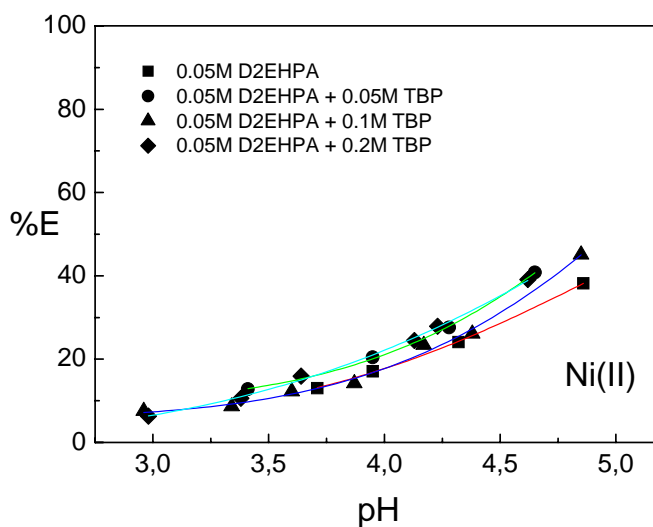


Fig. 8. Variations of the degree of extraction (%E) of nickel(II) ions using D2EHPA as a function of pH for different amounts of TBP. Water phase – 0.01 mol/dm Co(II), organic phase – 0.05 mol/L D2EHPA, ■ - D2EHPA; ● - D2EHPA + 0.05 mol/L TBP; ▲ - D2EHPA + 0.1 mol/L TBP; ◆ - D2EHPA + 0.2 TBP

A small TBP addition in the case of nickel(II) ions increases the extraction degree of nickel. This suggests a possibility of occurring adducts in the form of $NiA_2(TBP)_2$. In the case of cobalt(II) ion extraction, this effect is unnoticeable.

SUMMARY

The obtained experimental results show that a high excess of TBP in relation to D2EHPA reduces the extracting capacity of the latter towards nickel(II) and cobalt(II) ions, whereas its small amount (in the ratio of 1:1) improves the extraction of nickel(II) ions, while not affecting the extraction of cobalt(II) ions.

The work was carried out in part in the framework of Statutory Research 32-266/07-DS conducted at the University of Poznan.

REFERENCES

- RYDBERG J.; COX M., MUSIKAS C., CHOPPIN G. R., (2004), *Solvent Extraction Principles and Practise*; Marcel Dekker, Inc.: New York.
- MARCUS. Y., KERTES A.S., (1969), *Ion Exchange and Solvent Extraction of Metal Complexes*; John Wiley and Sons Ltd.: London.
- KOLARIK Z., (1982), *Critical Evaluation of Some Equilibrium Constants Involving Acidic Organophosphorus Extractants*, Pure & Appl. Chem, 54, 2593.
- SWAIN B., JEONG J., LEE J., LEE G.H., (2006), *Separation of Cobalt and Lithium from Mixed Sulphate Solution Using Na-CYANEX 272*. Hydrometallurgy, 84, 130.
- FU, X., GOLDING J. A., (1987), *Solvent Extraction of Cobalt and Nickel in Bis(2,4,4-tri-methylpentyl) Phosphinic Acid, "CYANEX 272"*, Solvent Extr. Ion Exch, 5, 205.
- SATO T., NAKAMURA T., (1972), *The Complexes Formed in the Divalent Transition Metal-Sulphuric Acid-Di-(2-Ethylhexyl) Phosphoric Acid Extraction Systems – Cobalt(III), Nickel(II) and Copper(II) Complexes*, J. inorg. Nucl. Chem., 34, 3721.
- VAN DE VOORDE I., PINOY L., COURTIJN E., VERPOORT F., (2005) *Influence of Acetate Ions and the Role of the Diluents on the Extraction of Copper(II), Nickel(II), Cobalt(II), Magnesium(II), and iron(II, III) with different Types of Extractants*, Hydrometallurgy, 78, 92.

Gajda B., Bogacki M.B., *Wpływ fosforanu tributylu na ekstrakcję jonów niklu(II) i kobaltu(II) za pomocą kwasu di(2-etyloheksylo) fosforowego*, Physicochemical Problems of Mineral Processing, 41 (2007) 145-152 (w jęz. ang.).

W pracy zaprezentowano wyniki badań dotyczących ekstrakcji jonów niklu(II) i kobaltu(II) z roztworów siarczanowych za pomocą kwasu di(2-etyloheksylo) fosforowego. Jako modyfikatora zdolności ekstrakcyjnej użyto fosforanu tributylu. Otrzymane wyniki badań wskazują, że duży nadmiar fosforanu tributylu w stosunku do kwasu di(2-etyloheksylo) fosforowego redukuje zdolności ekstrakcyjne kwasu di(2-etyloheksylo) fosforowego, podczas gdy jego małe ilości, w proporcji 1:1, zwiększają ekstrakcję jonów niklu(II), nie wpływając na ekstrakcję jonów kobaltu.

Antoaneta BOTEVA*, Mariela PARASHKEVOVA*

PROCESSING OF INDUSTRIAL PHARMACEUTICAL SEDIMENT

Received March 2, 2007; reviewed; accepted June 18, 2007

Separate sewerage collects waters that are being discharged from all technological lines in one of pharmaceutical factories in Bulgaria. The object of this study is slightly acidic waste water having pH=4-5 which is cleaned by neutralization. The water is neutralized in a radial settler equipped with peripheral device for collecting the waste water, where it is mixed and neutralized with $\text{Ca}(\text{OH})_2$. Necessary amount of $\text{Ca}(\text{OH})_2$ is added through a feeder and pump. The applied dosage is 10% higher than calculated. The mixture of $\text{Ca}(\text{OH})_2$ and waste water settles in a horizontal thickener, where the sludge is removed and final settling of the overflow is conducted. After the final settling, cleaned water (overflow) is being treated together with the household waste in a town waste water treatment plant. The remained sludge has pH=8-9 and 50 to 60% moisture. The extracted sludge from the settling/radial primary and secondary settler/through pumps enters a special sludge pond where the sludge is stored. It contains organic and inorganic compounds as well as various chemical elements. The treatment of the sludge is object of the present article.

Key words: wastes, neutralization, sewerage, sludge

INTRODUCTION

Two types of production waste waters are discharged by all pharmaceutical factories – polluted and the so-called conditionally clean waters. A common practice is to separate the industrial waste from the sewerage system of factories because the polluted industrial waste waters are used for circulation after cleaning.

The subject of this study is slightly acidic waste water (pH=4-5) cleaned by neutralization. This water is neutralized in a radial settler equipped with peripheral device for collecting the waste water, where it is mixed with neutralizing agent – $\text{Ca}(\text{OH})_2$. The necessary amount of $\text{Ca}(\text{OH})_2$ is added through a feeder and a pump. The chosen dosage is 10% higher than the calculated one. The mixture of $\text{Ca}(\text{OH})_2$ and waste water is subjected to settling in a horizontal thickener, where the sludge is

* University of Mining and Geology, Mineral Processing Department, Sofia-1700, Bulgaria

removed and final settling of the overflow is conducted. After the final settling, the already cleaned water (overflow) is treated together with the household waste in a town waste water treatment plant. The remained sludge has pH=8-9 and moisture of 50 to 60%. It is extracted from the radial (primary and secondary) settler through pumps, and then, directed to a special sludge pond where the sludge is stored. It contains series of organic and non-organic compounds as well as various chemical elements. Such elements as Ni and Zn have the highest concentration in the sludge and therefore their extraction is considered to be important. Not only sludge treatment is achieved by this process but also further concentration of extracted heavy metals is possible.

Elements content in the sludge and research methodology. The content of elements in the sludge is given in Table 1.

Table 1. Content of selected elements in the sludge

Element	Pb, %	Zn, %	Cu, %	Ni, %	S, %
Concentration	0.04	5.08	0.05	1.27	5.98

Several methods for extraction of Cu, Ni and Zn from the sludge have been investigated:

1. H₂SO₄ (5,10 and 15% solution) leaching (Table 2).
2. NaCN solid waste treatment (Table 3).
3. Stage leaching with 15% solution of H₂SO₄ (Table 4).
4. Stage leaching with heat treatment of the rests. (Table 5).

RESULTS AND DISCUSSION

Tables 2-5 show the results of experiments

Table 2. Sludge after leaching with H₂SO₄ solution

№	conditions	product	volume	Grade, mg/dm ³ , or %			Recovery,%		
				Cu	Ni	Zn	Cu	Ni	Zn
1.	1 dm ³ 5% H ₂ SO ₄ solution	filtrate	1.030 dm ³	3.7	105.8	1116	38.13	44.86	96.37
		hard rest	5.15g	0.12%	2.60%	0.84%	61.87	55.14	3.63
		input	26.80 g	0.037%	0.90%	4.44%	100.00	100.00	100.00
2.	1 dm ³ 10% H ₂ SO ₄ solution	filtrate	1.100 dm ³	1.9	1.9	1096	25.83	61.87	98.57
		hard rest	6.00g	0.10%	0.10%	0.29%	74.17	38.13	1.43
		input	26.80 g	0.029%	0.029%	4.48%	100.00	100.00	100.00
3.	1 dm ³ 15% H ₂ SO ₄ solution	filtrate	1.075 dm ³	3.1	123.1	1312	42.31	52.93	98.83
		hard rest	5.05g	0.09%	2.33%	0.33%	57.69	47.07	1.17
		input	26.80 g	0.026%	0.93%	5.32%	100.00	100.00	100.00

Table3. The results of NaCN solution leaching of the sludge after H₂SO₄ solution leaching

	Conditions	Product	Volume, dm ³	Containing, mg/d ³			Recovery%		
				Cu	Ni	Zn	Cu	Ni	Zn
1	0.400 dm ³	filtrate	0.425dm ³	<4	215,9	14,4	<5.46	30.83	8.32
2	5% NaCN and 0.5% CaO.	hard rest	12.25g	0.24%	1.68%	0.55%	95.54	69.17	91.68
3		input	16.50g	0.18%	1.80%	0.44%	100.00	100.00	100.00

Table4. Results after poly-stage leaching with 15% with H₂SO₄ solution

№	Conditions	Product	Volume, dm ³	Containing, mg/d ³			Recovery %		
				Cu	Ni	Zn	Cu	Ni	Zn
1	1 dm ³ 15% H ₂ SO ₄ solution one stage	filtrate	0.930dm ³	5	332.2	1467	50.27	86.75	98.50
		hard rest	11.50g	0.04%	0.41%	0.18%	49.73	13.25	1.50
		input	26.90g	0.034%	1.32%	5.16%	100.00	100.00	100.00
2	1 dm ³ 15% H ₂ SO ₄ solution two stages.	filtrate	0.580dm ³	4	930	3637	11.45	72.90	93.90
		hard rest1	6.55g	-	-	-	-	-	-
		hard rest2	9.75g	-	-	-	-	-	-
		common hard rest	16.30g	0.11%	1.23%	0.84%	88.55	27.10	6.10
		input	53.60g	0.037	1.38%	4.19%	100.00	100.00	100.00
3	1 dm ³ 15% H ₂ SO ₄ solution three stages	filtrate	0.420dm ³	21.36	1653	7666	29.48	76.39	92.02
		hard rest1	8,32g	-	-	-	-	-	-
		hard rest2	11,25g	-	-	-	-	-	-
		hard rest 3	11,25g	-	-	-	-	-	-
		common hard rest	30.65g	0.07%	0.70%	0.91%	70.52	23.61	7.98
		input	80.40g	1.13%	1.13%	4.35%	100.00	100.00	100.00

It is evident from Table 2 that the most appropriate concentration of H₂SO₄ solution is 10 and 15%. Nickel extraction from a solution with concentration of 10% gives better results than that of 15%, whereas copper extraction gives better results from a solution with concentration of 15% than that of 10%. Zinc extraction is constant. The differences in extraction results come from the increased concentration of the components. Due to the fact that decreased nickel extraction from a solution with concentration of 15% could not be attributed to passivation of solubility of nickel containing sludge components, we decided next experiments (sludge leaching) to be

conducted with 10% H₂SO₄ solution. The insoluble residues from the experiments were combined and the obtained material leached with 0.15% NaCN solution (Table 3) and 0.5% CaO solution. The pH of the solution during leaching was controlled, so that it was never below 9.5. The adjustment was performed with 10% Na₂CO₃ solution. The results in Table 3 show that after cyanation 30% of the nickel in the insoluble residue could be extracted.

The concentration of Ni and Zn in filtrate (Table 2) varies from 100 to 120 mg/dm³ for Ni and 1100-1300 mg/dm³ for Zn. A direct extraction by electrolysis is not possible due to the low concentrations of the metals. This is why the experiment was conducted with H₂SO₄ solution of 15% and one or two portions of fresh waste were added to the obtained filtrate. The results in Table 4 show that by applying three stages of leaching with nickel extraction ranging from 76%-80% and zinc from 90%-92%, the Ni and Zn levels in the solution increased to 1650 mg/dm³ and 7666 mg/dm³, respectively. The obtained solution from initial solutions of 76% nickel and 92% zinc could successfully be dissolved by usage of specific nickel and zinc agents (solvent extraction), thus increasing its concentration to the levels necessary for electro-winning. Thus, the solutions obtained by the three stage leaching process could be used as raw materials for nickel and zinc extraction. Organic residue was burnt at 800 °C in a hot air furnace. As a result, the extraction amount of final waste product was decreased by 65% (Table 5). The obtained product contains 2.17% Ni and 1.76% Zn and it can be used as raw material for nickel and zinc production as well. For instance, once cooled, the burnt product at 800°C was leached by 15% H₂SO₄ solution in the presence air enriched in O₂. The obtained sulfuric acid solution contained 12 g/dm³ zinc and 8 g/dm³ nickel.

Table 5. Results after temperature treatment of the rests

	Conditions	products	Yield γ,%	Content, %		Recovery, %	
				Ni	Zn	Ni	Zn
1.	Burning 800°C	Hard rest eliminated	34.98	2.17	1.79	97.33	97.85
2.		Eliminated proportion part	65.02	0.032	0.021	2.67	2.15
3.		input	100.00	0.78	0.64	100.00	100.00

CONCLUSIONS

Basing on the obtained results, the following diagram (Fig. 1) can be offered, which shows the processing of waste containing Ni and Zn. It shows three stages of leaching with 15% sulfur acid. The solution is removed after each stage and a new portion is added. The overflow (a product of three-stage leaching) is filtered and the obtained filtrate is then subjected to evaporation, cooling and crystallization of NiSO₄ and ZnSO₄.

The obtained sludge from the three-stage leaching and crystallization is then mixed and filtrated. Afterwards, the filter is returned to the first stage of leaching. After filtration, the hard residual material is burnt. The burnt residue is dissolved in 15% H_2SO_4 and the obtained solution, after settling and filtration, enters the evaporation stage. The hard residual material enters the drying stage. The product obtained from drying contains traces of Ni and Zn and can be used for modifying erosive soils.

REFERENCES

- BOTEVA A., 1975-76, *No-polar oil reagents oxidization in process of their emulsification*, Bull. Niproruda, 1976, 42-44.
- BOTEVA A., 1975-76, *No-ferrous metals ions flotoextraction by the no-polar oil reagents*, Annual reports, UMG volume XXII, part IV, 98-99.
- BOTEVA A., SECESENOV S., 1996., *Purification of waters containing oil drops*, 3rd Conference on Environment and Mineral Processing, Ostrava.
- BOTEVA A., 1996, *Treatment of slag from the waste-water purification plant at Asarel Mine.*, Mining and Environment Engineering, Bellgrade.
- BOTEVA A., 2000, *Oil extraction from waste water*, 9th International Symposium, "EKOLOGY"-2000, Bourgas, Bulgaria.
- BOTEVA A., 2000, *Flotation purification of effluents from sunflower oil refineries*. Processing of chemical and metallurgical industries wastes, Bhubaneswar, India.

Boteva A., Parashkevova M., *Przeróbka przemysłowego osadu farmaceutycznego*, Physicochemical Problems of Mineral Processing, 41 (2007) 153-158 (w jęz. ang.).

Oddzielna kanalizacja zbiera wody odprowadzane przez wszystkie linie technologiczne jednego z zakładów farmaceutycznych w Bułgarii. Przedmiotem obecnych badań są lekko kwaśne odpadowe muły, posiadające $pH=4-5$, które są otrzymane przez neutralizację. Wody są neutralizowane w odstożnikach promienistych wyposażonych w peryferyjne urządzenie do zbierania wody odpadowej, gdzie jest ona mieszana i neutralizowana za pomocą $Ca(OH)_2$. Niezbędna ilość wapna dodawana jest przez podajnik i pompy. Zużycie odczynnika wynosi około 10% więcej niż ilość obliczona. Mieszanina $Ca(OH)_2$ i wody odpadowej jest poddawana osadzeniu w horyzontalnych zagęszczaczach, gdzie usuwany jest szlam oraz przeprowadzany jest ostateczny oczyszczanie przelewu. Po końcowym osadzeniu, klarowna woda (przelew) jest mieszana z ściekami domowymi w miejskim zakładzie oczyszczania wody. Otrzymany muł posiada $pH=8-9$ oraz wilgotność od 50 do 60%. Wydzielony muł pobierany jest ze wstępnych radiacyjnych i wtórnych odstożników za pomocą pomp i przesyłane jest do specjalnego stawu, gdzie jest przechowywany. Zawiera on związki organiczne i nieorganiczne, jak również różne pierwiastki chemiczne. W pracy opisano przerób tych mułów.

Marcin JANCZAREK*, Horst KISCH**, Jan HUPKA*

PHOTOELECTROCHEMICAL CHARACTERIZATION OF NITROGEN-MODIFIED TiO₂

Received May 15, 2006; reviewed; accepted May 19, 2007

Modification of the chemical structure of titanium dioxide by non-metal elements (nitrogen) allows to move photocatalytic activity of titanium dioxide towards visible light. Three samples of photocatalysts with different nitrogen content and different photocatalytic properties were prepared for photoelectrochemical characterization. The positions of valence and conduction band edges of obtained semiconductors were calculated which enabled better understanding of the mechanism of visible light activity of the photocatalysts.

Key words: titanium dioxide, visible light, modification, photoelectrochemistry

INTRODUCTION

Heterogeneous photocatalysis using titanium dioxide represents efficient method for complete destruction of organic and inorganic compounds in liquid and gas phases which can successfully be degraded in this way. Pollutants containing carbon, hydrogen, nitrogen, sulphur and halogen atoms are mineralized to CO₂, H₂O, NO₃⁻, SO₄²⁻, and halide anions (Hoffmann, 1995). The number of papers and patents related to photocatalytic removal of toxic compounds is constantly on the rise. However, most of them pertain to artificial UV-light application. Photocatalytical methods based on TiO₂ were successfully used in some commercial applications, including water purification, air-cleaning units, antimicrobial coatings and self-cleaning glass (Anpo, 2000).

Although photocatalysis has been investigated for over 30 years, the number of successful commercial applications could be greater. First of all, practical application

* Department of Chemical Technology, Gdansk University of Technology, 80-952 Gdansk, ul. Narutowicza 11/12, Poland.

** Institute of Inorganic Chemistry, University of Erlangen-Nürnberg, 91054 Erlangen, Egerlandstr. 1, Germany.

of photocatalysis is limited by the fact that TiO₂ absorbs only UV light due to its high band gap energy (3.2 eV). Only 2 to 5 % of solar spectrum (UV fraction of solar light) can, therefore, be utilized by conventional TiO₂ photocatalysis (Anpo, 2000). UV lamps are needed to use the photocatalytical properties of TiO₂. Application of UV lamps poses a serious disadvantage because of high energy consumption, which increases the operating costs of the UV/TiO₂ system. Sensitization or modification of TiO₂ towards visible light photoactivity can allow to eliminate this limitation.

The most promising approach of activation of TiO₂ in the visible light region is modification of its chemical structure to shift absorption spectrum to the visible light region. This type of modification involves introduction (doping) of metal and non-metal species. To prepare an effective visible light-active photocatalyst doping should produce states in the band gap of TiO₂ that absorbs visible light. The conduction band minimum should be as high as that of TiO₂ or higher than the H₂/H₂O level to ensure its photoreduction activity. The states in the band gap should overlap sufficiently with the band states of TiO₂ to transfer photoexcited carriers to the reactive site at the photocatalyst surface within their lifetime (Asahi, 2001). It is necessary to use anionic species for the doping rather than metal cations, which can give localized *d* states deep in the band gap of TiO₂ and result in recombination centers of carriers (Asahi, 2001).

Recent investigation on titania modification has been mainly focused on applying non-metallic elements: nitrogen (Asahi, 2001; Gole, 2004; Janczarek, 2005; Mrowetz, 2004; Sakthivel, 2004), carbon (Sakthivel, 2003) and sulphur (Umebayashi, 2004). To propose mechanism of visible light activation, one needs to calculate the position of band edges (conduction and valence band) in titania semiconductor electronic structure. This paper presents results of photoelectrochemical investigations on nitrogen-modified titanium dioxide catalysts which were earlier prepared using thiourea and urea as precursors of nitrogen. These N-TiO₂ catalysts were active in visible light – a significant mineralization of 4-chlorophenol (4-CP) was observed (Sakthivel 2004; Janczarek, 2005).

EXPERIMENTAL

The band gap energy of photocatalysts was calculated from their diffuse reflectance spectra (DRS). DRS of the solids were recorded on a Shimadzu UV-2401PC UV-VIS spectrophotometer. Photocatalysts were diluted with BaSO₄ (50 mg TiO₂ and 2 g BaSO₄) and ground in an agate mortar. Subsequently, 10 mm pellets were prepared for the analysis. The background reflectance of BaSO₄ was measured first. Reflectance was converted by the instrument software to $F(R_{\infty})$ values according to the Kubelka-Munk theory. The band gap was obtained from a plot of $[F(R_{\infty}) \cdot E]^{1/2}$ versus energy of the exciting light (*E*) assuming that undoped titania and modified titanium dioxide are indirect crystalline semiconductors.

Quasi-Fermi level potentials were determined using optical train with XBO 150 W lamp and 100 cm³ Pyrex flask cell with electrodes (Fig. 1). Twenty mg of catalyst was

suspended in 50 cm³ of 0.1 M KNO₃. The concentration of methyl viologen (MV²⁺; 1,1'-dimethyl-4,4'-bipyridinium dichloride) was 1.0 mM. The suspension was stirred and sparged with N₂ before and during the measurement. The pH was adjusted with HNO₃ and NaOH solutions, and monitored with a pH-meter. A large surface platinum plate was the working electrode and Ag/AgCl – the reference electrode. The method was based on voltage measurements between these electrodes upon irradiation as a function of pH (Roy, 1995).

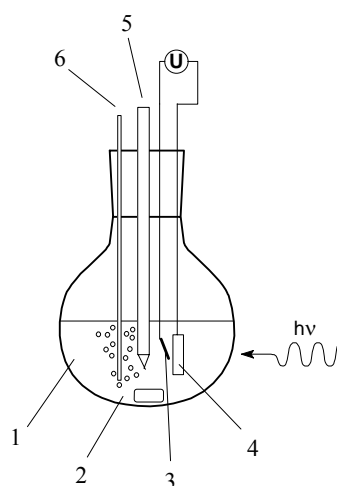


Fig. 1. Laboratory set-up for quasi-Fermi level potential determination: 1- suspension of catalyst, 2-magnetic stirrer, 3-reference electrode (Ag/AgCl), 4-working electrode (Pt), 5- pH electrode, 6-nitrogen inlet

MV²⁺ is used as an electron acceptor. pH-independent reversible reduction of MV²⁺ to MV^{•+} (blue solution) refers to $E^\circ_{MV^{2+/+•}} = -0.445$ V vs. NHE. Energy levels in semiconductors are generally dependent on pH. Assuming that TiO₂ is n-type semiconductor, three cases can be considered, see Fig. 2.

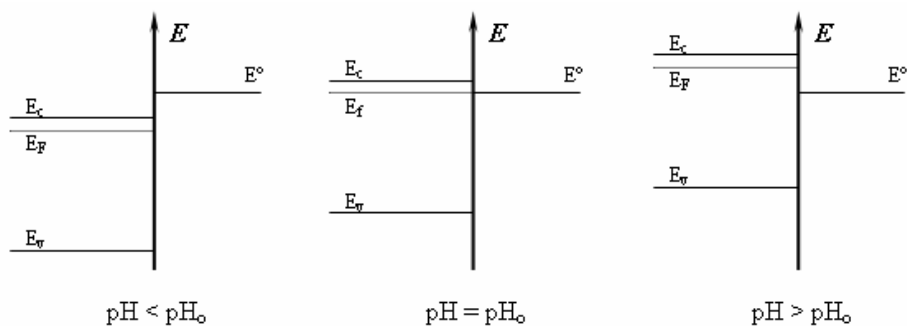


Fig. 2. Positions of energy levels in an *n*-type semiconductor at various pH [Roy, 1995]

At low pH the quasi-Fermi level potential is more positive than the redox potential of an electron acceptor (E^0). Then the excited electron from the conduction band is not able to reduce MV^{2+} what becomes possible at $pH \geq pH_0$, when ${}^*E_f \leq E^0$. The quasi-Fermi level potential depends on the pH [Roy, 1995]:

$${}^*E_f(pH) = {}^*E_f(pH = 0) - k \text{ pH} \quad (1)$$

At pH_0 the redox potential of $MV^{2+/+}$ couple equilibrates with $E_f(pH_0)$:

$$E^0 = {}^*E_f(pH = 0) - k \text{ pH}_0 \quad (2)$$

From equations 1 and 2:

$${}^*E_f(pH) = E^0_{MV^{2+/+}} + k (pH_0 - pH). \quad (3)$$

The obtained pH_0 values were converted to the quasi-Fermi level potential at $pH=7$ using the equation:

$${}^*E_f(pH=7) = -0.445 + 0.059 (pH_0 - 7). \quad (4)$$

The reproducibility of pH_0 measurements was better than 0.1 pH units.

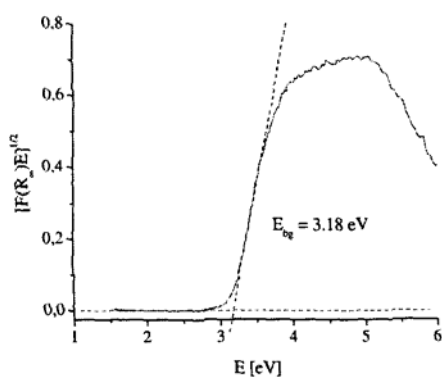
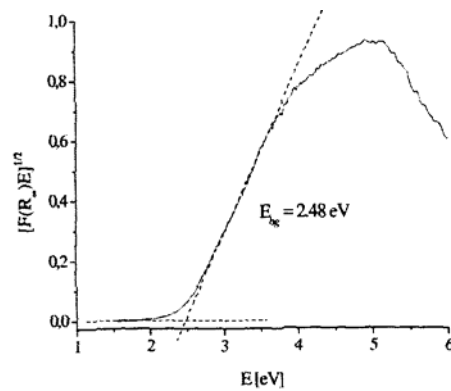
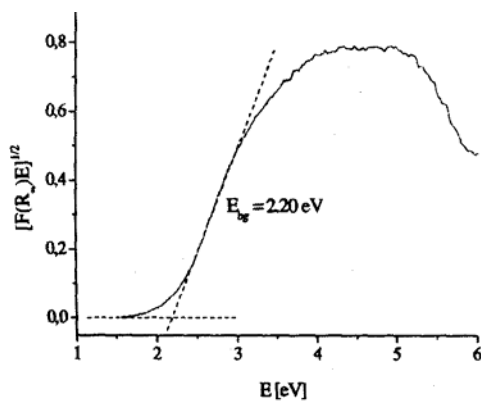
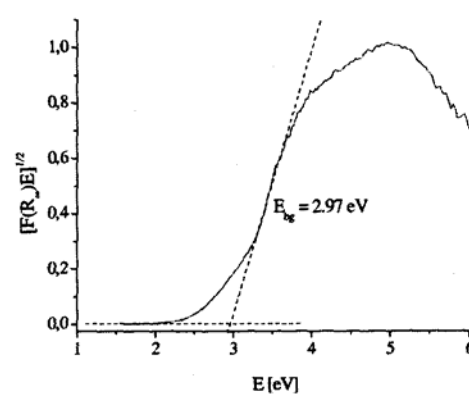
RESULTS AND DISCUSSION

BAND GAP ENERGIES

The determination of band gap energies is essential for identification of changes in the electronic structure of titania after doping with nitrogen. The reference sample of unmodified titania and three samples of surface-modified TiO_2 with nitrogen were considered. In comparison to the reference sample (Figure 3), the diffuse reflectance spectra show entire shift of the absorption spectra for TiO_2 -N/1 (1.4 wt.% N) (Figure 4) and TiO_2 -N/2 (12.7 wt.% N) (Figure 5). The corresponding calculated band gap energies are 2.48 eV and 2.20 eV, respectively. The presence of this shift and the value of the band gap energy are closely related to nitrogen content. In the case of TiO_2 -N/3 sample (0.6 % wt.% N) instead of the shift of the whole spectrum only an absorption shoulder in the 400-520 nm range was observed. The band gap energy for this sample was 2.97 eV (Figure 6). Thus, for high nitrogen-concentrated samples a significant band gap narrowing was observed.

Characterizing surface-modified samples, diffuse reflectance spectra exhibit an absorption shoulder at the range of 400 to 526 nm for TiO_2 -N/3 catalyst and complete shift of absorption spectrum for samples TiO_2 -N/1 and TiO_2 -N/2. Only one absorption edge was observed for each sample. This shift and the band gap energies are strictly

dependent on the nitrogen content. It is possible to control the band gap energy by varying nitrogen concentration through adjustment of calcination conditions. Such approach is more repeatable than varying the concentration of nitrogen precursor. Similar strong shift of absorption spectrum was observed by Yin et al. (Yin, 2003a; Yin, 2003b). They prepared nitrogen-doped yellowish rutile titania by high energy ball milling of P-25 titania with hexamethylenetetramine and reported two absorption edges at 400 nm and 520 nm resulting in 3.1 eV and 2.4 eV band gap energies, respectively. It is important to mention that the reflectance spectra were not transformed to Kubelka-Munk function, therefore it is impossible to indicate proper values of the band gap energies. The two band gap energies may not exist since authors did not show the calculation procedure and the reflectance vs. wavelength plot does not allow to determine these values. In the case of TiO₂-N/1 and TiO₂-N/2 samples a clear simultaneous shift for the valence and conduction bands was observed, which has not been shown for any N-TiO₂ yet. In case of TiO₂-N/2 the role of surface states is not so significant because of band gap narrowing.

Fig. 3. DRS spectrum for TiO₂Fig. 4. DRS spectrum for TiO₂-N/1Fig. 5. DRS spectrum for TiO₂-N/2Fig. 6. DRS spectrum for TiO₂-N/3

QUASI-FERMI LEVELS

Figures 7a-d show the dependences of photovoltage (V vs Ag/AgCl) on the pH value of electrolyte for the reference sample (TiO_2) and modified ones. In case of $\text{TiO}_2\text{-N}/2$, $\text{TiO}_2\text{-N}/1$ -0.47 V and -0.56 V quasi-Fermi levels were determined. The value of the quasi-Fermi levels was the same for unmodified titania (3.18 eV) and $\text{TiO}_2\text{-N}/3$ (2.97 eV).

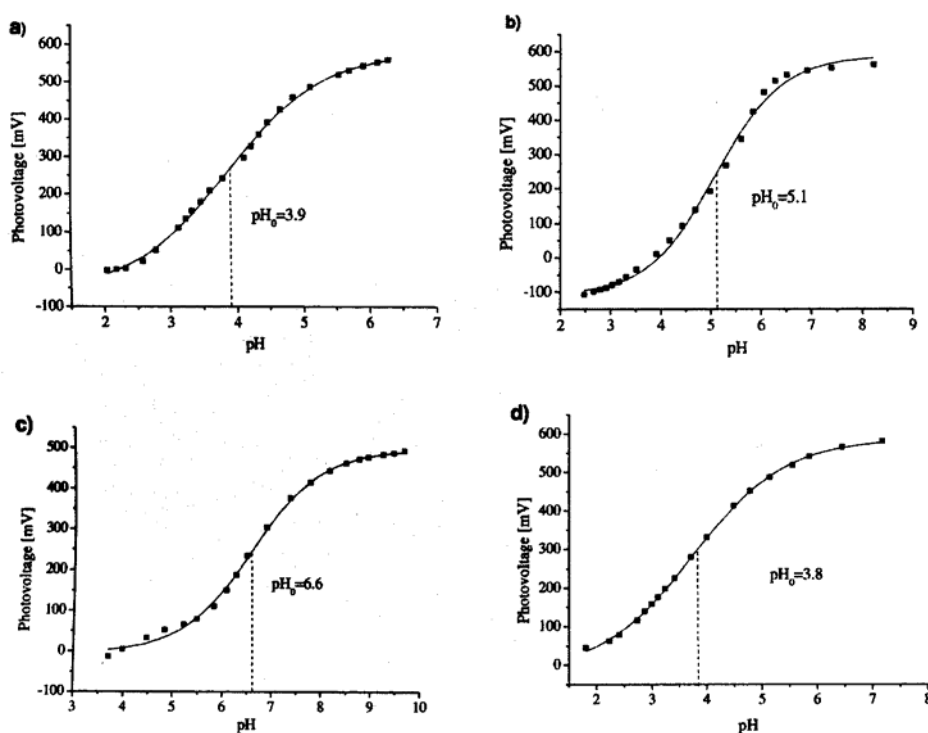


Fig. 7. Dependences of photovoltage (V vs Ag/AgCl) on pH value of electrolyte for: a) TiO_2 , b) $\text{TiO}_2\text{-N}/1$, c) $\text{TiO}_2\text{-N}/2$, d) $\text{TiO}_2\text{-N}/3$

ENERGY DIAGRAM

Calculated photoelectrochemical data are shown in Table 1. The positions of the conduction and valence bands for $\text{TiO}_2\text{-N}/1$ and $\text{N}/\text{TiO}_2\text{-N}/2$ samples are strongly shifted (especially cathodic shift of the valence band) - a significant band gap narrowing is observed (see Figure 8). Although, in this case the valence band edge is located at +2.34 V. Recalling that light absorbance starts already at 526 nm (2.39 eV), a manifold of surface states localized near the valence band must exist. It is consistent with the first of Asahi's postulates. Sample $\text{TiO}_2\text{-N}/2$ is not active but photocatalytic

activities of TiO₂-N/3 and TiO₂-N/1 are similar. Therefore, band gap narrowing is not directly responsible for the photocatalytic activity in visible light and the existence of surface states plays a crucial role in this phenomenon.

Table 1. Photoelectrochemical data

Sample name	Bandgap energy [eV]	Quasi-Fermi level [V]	Light absorption onset [nm]
TiO ₂	3.18	-0.63	380
TiO ₂ -N/3	2.97	-0.63	526
TiO ₂ -N/1	2.46	-0.56	534
TiO ₂ -N/2	2.20	-0.47	645

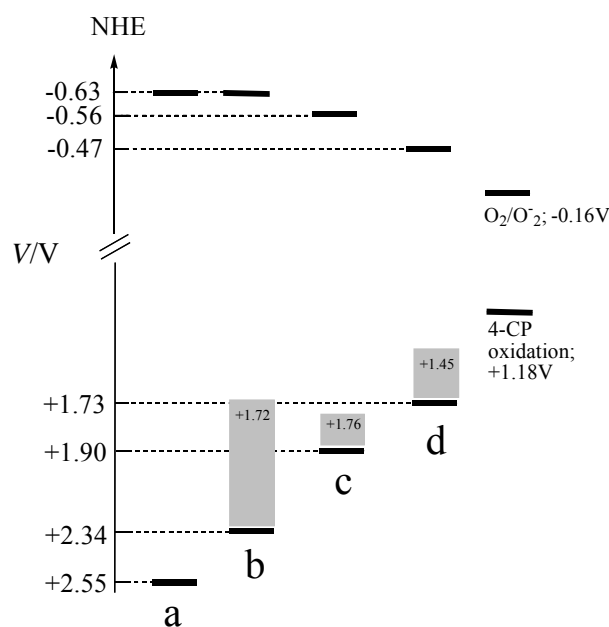


Fig. 8. Electrochemical potentials (vs. NHE) of band edges and surface states (shaded areas) at pH=7; (a) TiO₂, (b) TiO₂-N/3, (c) TiO₂-N/1, (d) N/TiO₂-N/2

CONCLUDING REMARKS

For the first time nitrogen content in titania catalyst was correlated with the band gap energy. An absorption shoulder (from 400 to 520 nm) corresponding to the band gap energy 2.97 eV was observed in the absorption spectrum of sample containing smallest amount of nitrogen. For other samples, the entire spectrum was shifted towards longer wavelengths resulting in an even lower band gap energy equal to 2.48 eV. However, nitrogen content of the catalyst exceeding 12 wt.% although

resulted in lowering the band gap energy below 2.20 eV, did not further enhanced the photocatalytic potential of titania. The positions of surface states localized near the valence band were calculated.

ACKNOWLEDGEMENTS

The investigation was financed by the Polish Committee for Scientific Research within the framework of grant No. 3 T09B 02427.

REFERENCES

- ANPO, M., (2000), *Utilization of TiO₂ photocatalysts in green chemistry*, Pure Appl. Chem., 72, 1265-1270.
- ASAHI, R.; MORIKAWA, T.; OWAKI, T.; AOKI, K.; TAGA, Y. (2001), *Visible-light photocatalysis in nitrogen-doped titanium oxides*, Science, 293, 269-271.
- GOLE, J.L.; STOUT, J.D.; BURDA, C.; LOU, Y.; CHEN, X. (2004), *Highly efficient formation of visible light tunable TiO_{2-x}N_x photocatalysts and their transformation at the nanoscale*, J. Phys. Chem. B., 108, 1230-1240.
- HOFFMANN, M.R.; MARTIN, S.T.; CHOI, W.; BAHNEMANN, D. (1995), *Environmental applications of semiconductor photocatalysis*, Chem. Rev., 95, 69-96.
- JANCZAREK, M.; HUPKA, J. (2005), Photocatalytic degradation using nitrogen-modified titanium dioxide, Proceedings of 4th International Conference Oils & Environment AUZO 2005, Gdansk, 356-360.
- MROWETZ, M.; BALCERSKI, W.; COLUSSI, A.J.; HOFFMANN, M.R. (2004), *Oxidative power of nitrogen-doped photocatalysts under visible illumination*, J. Phys. Chem. B., 108, 17269-17273.
- SAKTHIVEL, S.; JANCZAREK, M.; KISCH, H. (2004), *Visible light activity of nitrogen doped TiO₂*, J. Phys. Chem. B., 108, 19384-19387.
- SAKTHIVEL, S.; KISCH, H. (2003), *Daylight photocatalysis by carbon-modified titanium dioxide*, Angew. Chem. Int. Ed., 42, 4908-4911.
- ROY, A.M.; SASMAL, G.C.; BHATTACHARYYA, S.S. (1995), *Determination of the flatband potential of semiconductor particles in suspension by photovoltage measurement*, Int. J. Hydrogen Energy, 20, 627-630.
- UMEBAYASHI, T.; YAMAKI, T.; YAMAMOTO, S.; MIYASHITA, A.; TANAKA, S.; SUMITA, S.; ASAI, K. (2003), *Sulfur-doping of rutile-titanium dioxide by ion implantation: photocurrent spectroscopy and first-principles band calculation studies*, J. Appl. Phys., 93, 5156-5160.
- YIN, S.; ZHANG, Q.; SAITO, F.; SATO, T. (2003), *Preparation of visible light-activated titania photocatalyst by mechanochemical method*, Chem. Lett., 32 (4), 358-359.
- YIN, S.; YAMAKI, H.; KOMATSU, M.; ZHANG, Q.; WANG, J.; TANG, Q.; SAITO, F.; SATO, T. (2003), *Preparation of nitrogen-doped titania with high visible light induced photocatalytic activity by mechanochemical reaction of titania and hexamethylenetetramine*, J. Mater. Chem., 13, 2996-3001.

Janczarek, M., Kisch, H., Hupka J., *Fotoelektrochemiczna charakterystyka tlenku tytanu(IV) modyfikowanego azotem*, Physicochemical Problems of Mineral Processing, 41 (2007) 159-166 (w jęz. ang.).

Modyfikacja chemicznej struktury tlenku tytanu(IV) poprzez pierwiastki niemetaliczne (np. azot) jest jednym ze sposobów przesunięcia aktywności fotokatalitycznej tlenku tytanu(IV) w kierunku światła widzialnego. Trzy próbki katalizatorów o różnej zawartości azotu i różnych właściwościach fotokatalitycznych zostały wybrane do charakterystyki fotoelektrochemicznej, której efektem finalnym jest określenie położenia pasma wzbronionego i pasma przewodzenia w otrzymanych półprzewodnikach, co ma istotne znaczenie dla lepszego zrozumienia mechanizmu aktywności przygotowanych fotokatalizatorów w świetle widzialnym.

Małgorzata PACHOLEWSKA*, Aleksandra FRĄCKOWIAK*, Joanna WILLNER*

INFLUENCE OF PHYSICAL AND CHEMICAL FACTORS ON ACID DIGESTION OF Zn-Pb FLOTATION TAILINGS

Received April 15, 2007; reviewed; accepted May 15, 2007

The acid digestion of flotation tailings from Zn-Pb ore enrichment in the Boleslaw Mine and Metallurgical Plant was aimed at their initial chemical reusing by neutralization of alkaline components of gangue and potential recovery of magnesium compounds from filtrates after acid digestion. The nature of the research was explanatory and the obtained leaching residues will constitute a raw material in flotation tailings bioleaching in the presence of acidophilic microorganisms.

The article presents the results of the research regarding the influence of physicochemical factors (H_2SO_4 concentration, time, temperature, the ratio of solid phase to liquid phase) on the leaching rate of magnesium, zinc, cadmium, iron and lead by acid digestion of flotation tailings as well as the characteristics of solid leaching residues and magnesium compounds obtained by the concentration and crystallization of the filtrate.

Key words: Zn-Pb flotation tailing, digestion, magnesium recovery

INTRODUCTION

There are two zinc and lead ore processing plants in Poland. They belong to the Boleslaw Mine and Metallurgical Plant and the Trzebionka Mine Plant, where the process of ore enrichment produces a considerable amount of waste. Flotation tailings constitute around 60-70% of the ore processed for Zn concentrate production (Jarosiński and Natanek, 2005). At the current rate of ore processing at 2.6-2.7 teragrams (Tg) annually, around 1.5-1.6 Tg/y of flotation tailing is produced.

The subject of this research was the wastes storage area in the Boleslaw Mine and Metallurgical Plant situated in the Olkusz-Boleslaw region. This area contains sedimentation ponds, occupying the total area of approximately 110 ha. The current

* Silesian University of Technology, Faculty of Materials Engineering and Metallurgy,
40-019 Katowice, ul. Krasińskiego 8, e-mail: malgorzata.pacholewska@polsl.pl

mining-processing activities, being conducted there for over 50 years, have caused the accumulation of flotation tailings in the amount of about 38 Tg in them (Pajor, 2005). The waste is the tailing of the flotation enrichment process of non-ferrous metal ores containing hazardous substances marked with symbol 01 03 80* (Rozp.Min.Śr., 2001) according to the Minister of the Environment Order of 27 September 2001 concerning the catalogue of waste.

Flotation tailings are produced from lead and zinc ores in the exit section of the processing line in the Boleslaw Mine and Metallurgical Plant, where the following materials (given in approximate percentages) are obtained from the extracted ore (Pajor, 2005):

- 8% of metals in the form of Zn and Pb concentrates and a bulk concentrate,
- 35% of dolomite stone,
- 57% of flotation tailings.

The mineralogical composition of the discussed waste contains mainly dolomite (77%) and marcasite (17%). There are also certain quantities of heavy metals, i.e., Fe, Zn, Pb, Cd, Mn and others (Pajor, 2005). The main source of contamination from surface storage of tailings are ions of metals and SO_4^{2-} ions which are leached by water flowing through an above-ground tailings storage facility, then infiltrated from over-sedimentary pond to underground waters. Metals, and their compounds, form dust emitted by the open surface of dry sedimentation ponds. Currently, there is not an explicit assessment of the influence of these ponds on the surroundings, but the restoration of the affected area to its appropriate utilization functions is connected with conducting detailed research and working out the method of their safe rehabilitation (Jarosiński and Natanek, 2005; Jarosiński, Żelazny, Nowak and Banach, 2005; Girczys and Sobik-Szołtysek, 1998; Łuszczkiewicz, 2007).

At present, the management of flotation tailings from the Boleslaw Mine and Metallurgical Plant mainly consists in utilizing them (about 60% of the mass of the produced wastes) in order to construct the embankment of an active sedimentation pond. The following directions of tailings recycling are still being investigated:

- as a component of hydraulic filling,
- as a reclamation material for levelling holes and strip pits in post-mining areas,
- in production of building materials,
- in recovery of metals by means of their re-enrichment.

The research into utilization of dolomite, the main component of similar waste from the Trzebionka Mine Plant, has been conducted (Jarosiński and Natanek, 2005; Jarosiński, Żelazny and Nowak, 2005; Jarosiński, Fela and Kozak, 2005; Jarosiński and Madejska, 2005). Dolomite has been investigated as a material for magnesium sulphate(VI) production, which is an important component used in many industrial processes in such industries as paper, textile, dyeing, tanning, building materials and metallurgy. Dolomite has also been examined as a component of artificial fertilizers (as so called magnesium sulphate heptahydrate - $\text{MgSO}_4 \cdot 7\text{H}_2\text{O}$ - epsomite) (Jarosiński, Fela and Kozak, 2005; Jarosiński and Madejska, 2005).

The objective of research was to determine the conditions of acid digestion and neutralization of alkaline components of Zn-Pb flotation tailings from the point of the recovery of magnesium compounds. The influence of the following parameters on the degree of the metal transition in solutions was taken into account: the concentration of sulphuric acid(VI) solution, a ratio of solid phase to liquid phase, temperature, and time. The nature of the research was exploratory and the obtained results form the basis for further work on the possibility of recovery of useful components, for example zinc, from initially acidified flotation tailings, with the application of biometallurgy methods (Pacholewska, Cwalina, Cabała and Sozańska, 2007).

MATERIALS AND METHODS

The flotation tailings from the zinc and lead ores enrichment process from the Boleslaw Mine Plant were digested. The chemical composition of the examined tailings was as follows: 17.37% Fe; 5.13% Mg; 1.71% Zn; 1.63% Pb; and 0.0098% Cd.

The flotation tailings at the temperature of 333 K were dried and leached in glass flasks in the presence of 100 cm³ of 1, 2 and 4 M solutions of H₂SO₄ with the corresponding amounts of tailings at a ratio of solid phase to liquid phase as 1:10, 1:5 and 1:2. The tailings were continuously stirred with a thermostatic shaker. After the sufficient leaching time, the solutions were filtered by means of a vacuum flask. The obtained filtrates were analysed quantitatively and the AAS method was used to determine the metal concentration of Zn, Pb, Cd, Fe and Mg. The phase composition of flotation tailings before and after leaching was determined by a pattern method with a Phillips PW 3710 X-ray diffractometer and X'Pert software.

RESULTS AND DISCUSSION

METAL LEACHING EFFICIENCY FROM Zn-Pb FLOTATION TAILINGS

The efficiency of metal leaching- w was calculated with the following formula:

$$w = \frac{V \frac{c_1}{1000}}{m_0 \frac{c_0}{100}} 100\%$$

- c_0 – the initial metal concentration in the tailings, %,
- c_1 – the metal concentration in the solution after leaching, g/dm³,
- V – the volume of the solution after filtration, cm³,
- m_0 – the initial mass of the tailings, g.

INFLUENCE OF H₂SO₄ CONCENTRATION

The influence of H₂SO₄ concentration on the efficiency of leaching of Pb, Fe, Zn, Cd and Mg is shown in the Table 1 and in Figs 1 - 2. The values of the rate of metal leaching from flotation tailings during 3-hour digestion period at various H₂SO₄ concentrations are presented.

It was found that increasing H₂SO₄ concentration in leaching solutions caused a decrease in the rate of magnesium leaching from flotation tailings (Table 1). As a result, too high H₂SO₄ concentration limits digestion of magnesium compounds, which the results obtained in the research confirm (Jarosiński, Fela and Kozak, 2005).

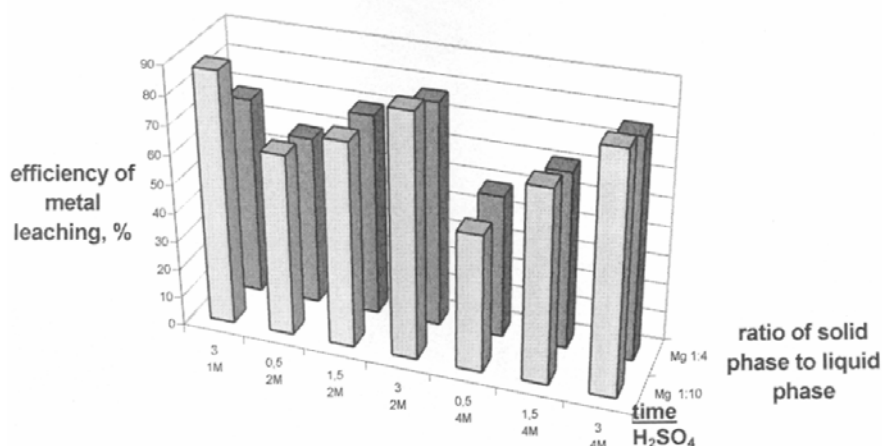
Table 1. Rate of metal leaching at the ratio of phases 1:10, 3 hours

Exp. #	Concentration H ₂ SO ₄ [mol/dm ³]	The efficiency of metal leaching, %				
		Mg	Zn	Cd	Pb	Fe
1	1	87.71	13.34	19.15	0.69	3.46
2	2	84.14	13.17	17.34	0.66	3.66
3	3	82.46	13.97	17.17	0.47	3.99

INFLUENCE OF TIME

In the course of flotation tailings leaching, both foaming of the solutions and emission of gases, connected with the neutralisation of dolomite in the H₂SO₄ solutions were observed.

With the increase in the time of digestion, the increase in the efficiency of metal leaching from flotation tailings was observed. A favourably high rate of magnesium leaching was obtained in particular after three hours of leaching (above 80% for the

Fig. 1. Influence of time, H₂SO₄ concentration, solid phase to liquid phase on the efficiency of magnesium leaching from Zn-Pb flotation tailings

ratio of solid phase to liquid phase 1:10 and around 70% and more for the ratio of phases 1:4). Cd and Zn were also leached at a relatively high rate (13 – 15%), whereas the rate of leaching of Pb and Fe was lower (below 5%) (Figs 1- 2).

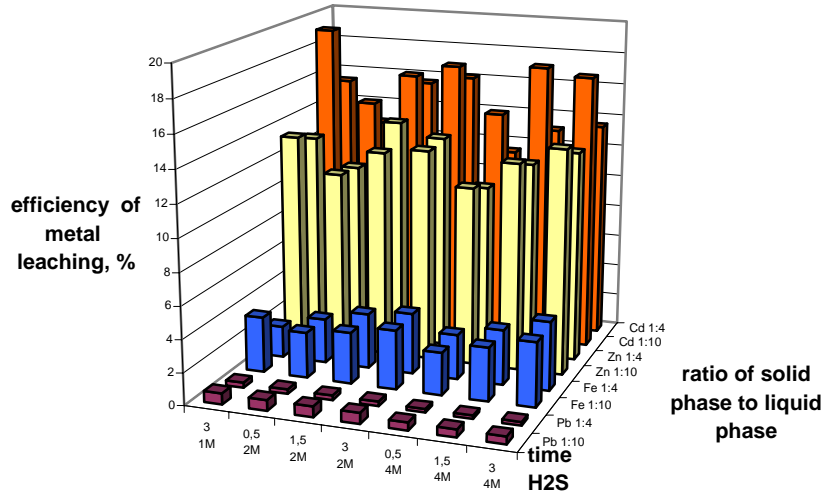


Fig. 2. Influence of time, H₂SO₄ concentration, solid phase to liquid phase on the efficiency of leaching of Cd, Fe, Pb and Zn from Zn-Pb flotation tailings

The metal concentrations (Mg, Zn, Cd, Pb, Fe) in the filtrates after leaching are presented in Table 2.

Table 2. The metal concentrations in solutions after leaching for the ratio of solid phase/liquid phase = 1:10 and 1:4, temperature 293 K

Exp. #	Concentration H ₂ SO ₄ , [mol/dm ³]	Time of leaching, [h]	Concentration of metals				
			Mg [g/dm ³]	Zn [g/dm ³]	Cd [mg/dm ³]	Pb [mg/dm ³]	Fe [g/dm ³]
The ratio of phases 1:10							
1	1	3.0	5.36	0.27	2.23	5.21	0.71
2	2	0.5	3.81	0.22	1.68	4.98	0.58
3	2	3.0	5.08	0.26	1.99	4.89	0.75
4	4	0.5	2.76	0.21	1.61	3.51	0.52
5	4	3.0	5.04	0.28	2.00	3.54	0.83
The ratio of phases 1:4							
6	1	3.0	10.52	0.64	4.48	6.34	1.01
7	2	0.5	8.85	0.55	3.67	5.19	1.41
8	2	3.0	11.70	0.67	4.64	5.45	1.93
9	4	0.5	7.20	0.51	3.18	3.91	1.37
10	4	3.0	11.65	0.66	3.95	4.14	2.21

INFLUENCE OF THE RATIO OF SOLID PHASE/LIQUID PHASE

The influence of the ratio change of the solid-to-liquid phases from 1:10, 1:4 and 1:2 on the metal concentration in the solutions after leaching was investigated. We used either 10g, 25g, 33g or 50g flotation tailings per 100cm³ of H₂SO₄ during 3-hour period at 293 K. The obtained results of metals concentration in the filtrates are shown in Fig.3.

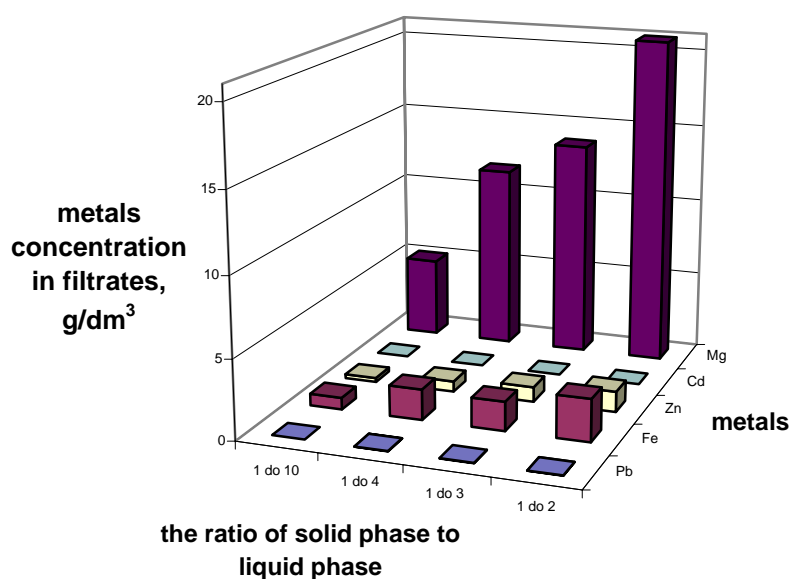


Fig. 3. Metal concentration in the solution at different solid/liquid phases ratios, the temperature of 293 K, 2 M H₂SO₄, 3 hours

It is apparent from the data presented in Fig. 3 that metal concentration in a filtrate increases with the increase in the mass of tailings proportionally to the amount of the leaching solution. The highest magnesium concentration at 20.93 g/dm³ in solutions after the leaching process was observed at the ratio of solid-to-liquid phase 1:2. Under these conditions, Fe concentration was 2.67 g/dm³, Zn concentration 1.31 g/dm³, Pb concentration 12.70 mg/dm³, and Cd concentration 8.99 mg/dm³. It has been found that favourable high magnesium concentration equal to 11.70 g/dm³ in the presence of 2M H₂SO₄ and after 3 hours of leaching was obtained at the ratio of the solid phase to the volume of the solution equal to 1:4 (25g/100cm³). It corresponds with results obtained by Jarosiński et al. (2005) Using lower quantities of wastes, compared to the volume of solutions, does not provide sufficiently high magnesium concentration in the solution.

INFLUENCE OF STIRRING ON FLOTATION TAILINGS LEACHING

The experiment was repeated at stirring speeds 100 and 130 rpm (amplitude 6) respectively, every time using 25g of flotation tailings and 100 cm³ of 2M H₂SO₄. The time of leaching was 1.5 h and the temperature 293 K for all trials. The results of metal concentration in the filtrate after leaching are shown in Table 3.

Table 3. Metal concentration in filtrate after leaching at 293 K with 2M H₂SO₄ for 1.5 hours applying different vibration frequency

Exp.#	The stirring frequency cycle/min (cpm)	Metal concentration in the filtrates				
		Mg [g/dm ³]	Zn [g/dm ³]	Cd [mg/dm ³]	Pb [mg/dm ³]	Fe [g/dm ³]
1	100	9.20	0.66	4.82	8.12	1.20
2	130	10.68	0.71	4.54	5.35	1.77

The results of metal concentration after leaching, shown in Table 3, point to a considerable influence of stirring intensity on the magnesium recovery from flotation tailings.

INFLUENCE OF TEMPERATURE

The influence of temperature on magnesium recovery from flotation tailings during Zn-Pb tailings leaching was also investigated. In each experiment, there was 25 g of flotation tailing and 100 cm³ of 2M H₂SO₄. The time of leaching was 1.5 h and the temperatures were 303 K, 313 K, 323 K, and 333 K.

The results of metal concentration in the solutions after leaching are shown in Table 4 and Fig 4.

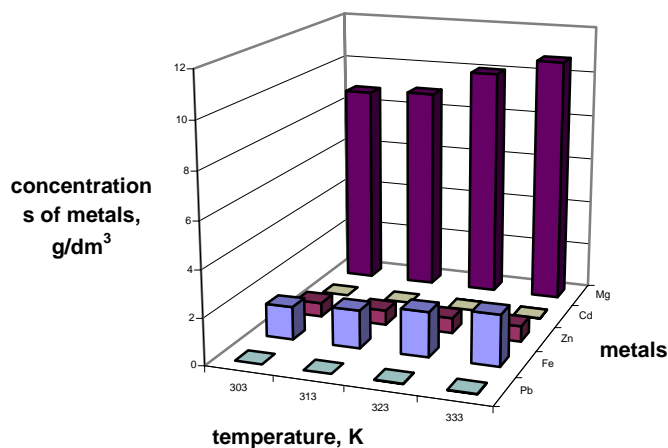


Fig. 4. Influence of temperature on the concentrations of metals in solutions during leaching of the Zn-Pb flotation tailings

The obtained results confirmed that there was an increase in solubility of magnesium compounds in aqueous solution in the examined range of temperatures (Rubisov, 2000; www.phase).

Table 4. Dependence of metals concentration in the filtrates in relation to different temperatures

Exp. #	Temperature of leaching process, K	Metal concentrations in the filtrates				
		Mg [g/dm ³]	Zn [g/dm ³]	Cd [mg/dm ³]	Pb [mg/dm ³]	Fe [g/dm ³]
1	303	8.77	0.61	4.55	9.57	1.42
2	313	8.90	0.63	4.42	10.11	1.63
3	323	10.01	0.66	4.27	13.08	1.94
4	333	10.72	0.67	4.02	13.20	2.19

Figure 5 shows the Arrhenius plot for the reaction rate data k , estimated and calculated from the magnesium leaching experiments shown in Table 4. The activation energy of 6.013 kJ/mol has been calculated from the slope indicating diffusively controlled reaction. Mass transfer may be the rate controlling step.

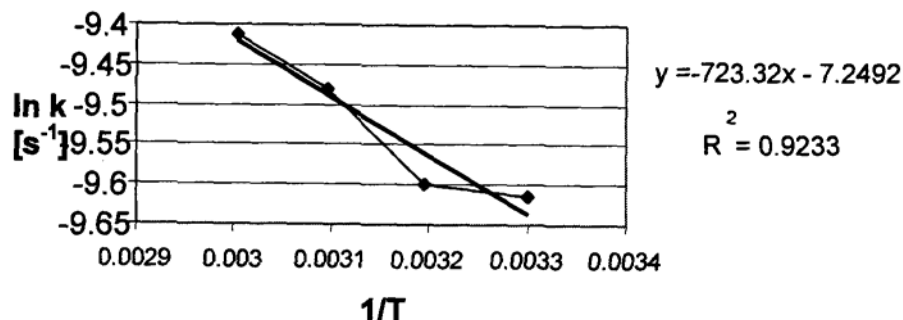


Fig. 5. Arrhenius diagram for determining activation energy

CHARACTERISTICS OF MAGNESIUM SULPHATE FROM THE ACID DIGESTION OF Zn-Pb FLOTATION TAILINGS

Flotation tailings can be used as raw material for production of magnesium compounds (Jrosiński et al., 2005) and a test was conducted for this purpose. The objective of the test was to determine the properties the magnesium sulphate from the Zn-Pb flotation tailings of the Boleslaw Mine and Metallurgical Plant. A 250g sample of the flotation tailings was treated with 1 M H₂SO₄ solution and the pulp was stirred at 293 K for 3 hours and filtered under vacuum. The obtained raw filtrate was subjected to purification from iron compounds with H₂O₂ and, as a consequence, iron(III) compounds precipitated. Next, the solutions were subjected to crystallization with fast water evaporation and drying with a drying evaporator. It was found, on the bases of the thermogravimetric analysis that the obtained product was MgSO₄ · 7 H₂O.

PHASE COMPOSITION OF FLOTATION TAILINGS

The phase composition of the tailings before and after leaching was determined by means of X-ray analysis. The main component of the tailings is ferruginous dolomite, which is accompanied with calcite, quartz, sulphides such as pyrite and marcasite as well as sphalerite. Other minerals constitute admixtures and traces: cerussite, bassanite, smithsonite and feldspar.

As a result of tailings leaching with 1M acid H₂SO₄, mineral components were quantitatively reorganized. It was found that there is bassanite, pyrite with marcasite, sphalerite and quartz as dominating phases, whereas feldspars and cerussite appeared in the form of admixtures. Considerable changes were observed in the tailings leached with 1 M acid, where prevailing component was anhydrite and the remaining phases appeared from between ten and twenty to several per cent by volume. They were pyrite, marcasite, sphalerite, quartz, bassanite, dolomite kizerite, feldspars and calcite.

CONCLUSIONS

On the basis of the research conducted, the following conclusions were drawn:

- increasing H₂SO₄ concentration in leaching solutions causes a decrease in the extraction efficiency of magnesium leaching from flotation tailings (from 87.71 % for 1 M H₂SO₄, to 82.46% for 4M H₂SO₄),
- with the increase in digestion time, the increase in the rate of metal leaching from tailings has occurred. Leaching in 2M H₂SO₄ for 3 hours creates the most favourable magnesium concentrations in the solution equal to 11.70 g/dm³,
- metal concentration in the solution after leaching increases with the increase in the tailings mass in proportion to the amount of the leaching solution. The highest magnesium concentration (20.93 g/dm³) has been observed at the ratio of solid phase to liquid phase 1:2,
- a significant influence of stirring intensity on the demagnetization of tailings has been shown,
- the obtained results concerning the influence of temperature on the digestion of flotation tailings confirm the known relations concerning the increase in the solubility of magnesium compounds with the increase in temperature within the examined range,
- quantitative reorganization of mineral components takes place during leaching and bassanite, pyrite with marcasite, sphalerite and quartz as dominating phases have been found,
- the obtained results will be used for further research on flotation tailings from the Boleslaw Mine in the scope of biohydrometallurgical methods – bioleaching.

ACKNOWLEDGEMENTS

This research work is being financed by funds for science for 2005 - 2008 as Research Sponsored Project PBZ-KBN-111/T09/2004.

REFERENCES

- GIRCZYS J., SOBIK-SZOŁTYSEK J., (1998), *Uwalnianie i eliminacja metali ciężkich w osadnikach odpadów flotacji blendy*, Rudy i Metale Nieżelazne, 8, pp. 371-375.
- JAROSIŃSKI A., FELA K., KOZAK A., (2005), *Magnesium recovery from postflotation tailings*, Instytut Chemii i Technologii Nieorganicznej, Politechnika Krakowska, Materiały Konferencyjne-Recykling odpadów, Kraków, pp.150-155.
- JAROSIŃSKI A., MADEJSKA L., (2005), *Odpady poflotacyjne jako źródło związków magnezu*, Instytut Chemii i Technologii Nieorganicznej Politechnika Krakowska, Materiały Konferencyjne - Zrównoważone zarządzanie obszarami przemysłowymi, Kraków, pp.161-165.
- JAROSIŃSKI A., NATANEK W., (2005), *Niektóre właściwości fizykochemiczne odpadów poflotacyjnych w aspekcie ich utylizacji*, Instytut Chemii i Technologii Nieorganicznej Politechnika Krakowska, Materiały Konferencyjne -Zrównoważone zarządzanie obszarami przemysłowymi, Kraków, pp.166-170.
- JAROSIŃSKI A., ŻELAZNY S., NOWAK A., BANACH M., (2005), *Niektóre własności kompozytów podsadzkowych na bazie odpadów poflotacyjnych*, Instytut Chemii i Technologii Nieorganicznej, Politechnika Krakowska, Materiały Konferencyjne-Zrównoważone zarządzanie obszarami przemysłowymi, Kraków, pp.171-175.
- ŁUSZCZKIEWICZ A., http://www.ig.pwr.wroc.pl/instr_pk/i_flot.html (2007).
- PACHOLEWSKA M., CABAŁA J., CWALINA B., SOZAŃSKA M., (2007), *Środowiskowe uwarunkowania procesów (bio)ługowania metali z odpadów poflotacyjnych rud cynkowo-olowiowych*, Rudy i Metale Nieżelazne, R.52, in print.
- PAJOR G.,(2005), *Gospodarka odpadami poflotacyjnymi w ZGH Bolesław S.A. w Bukowni*, Materiały Konferencyjne-Zrównoważone Zarządzanie Obszarami Przemysłowymi Wyd. Sigma PAN, Kraków, pp.5-19.
- Rozporządzenie Ministra Środowiska z dnia 27 września 2001 r. w sprawie katalogu odpadów (Dz. U. Nr 112, poz. 1206).
- RUBISOV D.H., PAPANGELAKIS U.G., (2000), *Sulphuric acid pressure leaching of laterites-speciation and prediction of metal solubilities "at temperature"*, Hydrometallurgy, vol.58, 1, Nov., pp.13-26.
- Statystyka GUS, (2005), *Ochrona Środowiska*.
www.phasediagram.dk/binary/magnesium_sulfate.htm
- Pacholewska M., Frąckowiak A., Willner J.,** *Wpływ czynników fizycznych i chemicznych na kwasowe roztwarzanie Zn-Pb odpadów poflotacyjnych*, Physicochemical Problems of Mineral Processing, 41 (2007) 167-176 (w jęz. ang.).

W pracy przedstawiono wstępne rezultaty badań kwasowego roztwarzania odpadów poflotacyjnych, pochodzących ze wzbogacania rud Zn-Pb z Zakładów Górniczo-Hutniczych Bolesław S.A., które miały na celu wstępną chemiczną utylizację odpadów na drodze neutralizacji alkalicznych składników skały płonnej oraz odzysk związków magnezu z filtratów. Stała pozostałość po ługowaniu stanowić będzie surowiec w dalszych procesach bioługowania odpadów poflotacyjnych z udziałem mikroorganizmów o charakterze kwasolubnym.

W artykule przedstawiono wyniki badań nad wpływem czynników fizykochemicznych (stężenie H_2SO_4 , czas, temperatura, stosunek f. stałej do f. ciekłej) na stopień wyługowania magnezu, cynku, kadmu, żelaza, ołowiu w procesie kwasowego roztwarzania odpadów poflotacyjnych, oraz charakterystykę stałej pozostałości po ługowaniu i związków magnezu uzyskanych w procesie zateżnienia i krystalizacji filtratu.

Stanisław CHIBOWSKI*, Jan PATKOWSKI*

A RESEARCH ON STABILITY OF SiO₂ IN THE PRESENCE OF POLYETHYLENE OXIDE OF DIFFERENT PURITIES

Received May 10, 2007; reviewed; accepted June 28, 2007

The influence of impurities present in polymer solutions on stability of the suspension of PEO 100 000 with commercial silica was analysed. Stability was measured indirectly, with absorbance measurements of silica and polyethylene oxide suspensions. A XRF method was used to estimate the quality and quantity of impurities in polyethylene oxide solutions.

Impurities left after the polymerisation process, present in polymer solutions can adsorb competitively with macromolecules of the polymer. As a result of that, they block active centres on the surface of the adsorbent thus leaving less surface available for polymer molecules. Purification process is conducted in order to improve the quality of analysed polymer material. Polyethylene oxides used in the presented research were purified by filtration process and fractionation on chromatographic column. Overall, four different samples of PEO were used: commercial of low quality, commercial of high quality, filtrated and fractionated.

The stability of silica is greatly influenced by the presence of polymer of different purities. Silica without adsorbed polymer is stable in the whole period of analysis. An addition of polymer firstly stabilises the suspension but after some time the suspension is suddenly destabilised. The times of stabilisation and destabilisation of the suspensions are different for polymer samples of different purities. It is greatly dependent on the content of impurities and polydispersity index of a polymer.

Key words: polymers, polyethylene oxide, silica, stability, polydispersity index

INTRODUCTION

Adsorption of macromolecules onto oxides is a very complicated process and it varies significantly from the adsorption of small molecules and ions (i.e. inorganic ions). There are many applications for macromolecules adsorption including food, cosmetic, dyer industries and many technological processes used in environment

* Department of Radiochemistry and Chemistry of Colloids, Faculty of Chemistry, UMCS,
pl. Marii Curie-Skłodowskiej 3, 20-031 Lublin, Polska, jpatkows@hermes.umcs.lublin.pl

protection (Fleer et al., 1993; Fleer and Scheutjens, 1993; Markovic, 1996; Pan et al., 2001).

Polymer adsorption also influences the stability of dispersed systems. Low-molecular mass polymers adsorbed onto oxide surface mostly cause strong steric repulsion, i.e. steric stabilisation. This phenomenon is used when stable emulsions and suspensions are required. High-molecular mass polymers cause colloidal systems to flocculate, which is mostly used for utilization of industrial slurries and many other applications. The aspect of stability is the case to study in the presented research.

Commercial polymers, available to purchase, have a fairly high degree of polydispersity as well a content of inorganic impurities, which are left after the polymerisation process. Those substances cannot be used for a model research on polymer's adsorption onto metal oxides with Scheutjen's – Fleer theory application. In order to improve their quality, a filtration process (purification and initial fractionation) as well as fractionation on chromatographic column can be used.

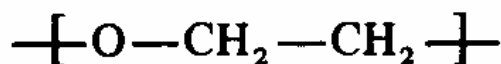


Fig. 1. Example of PEO monomer

Polyethylene oxide was used as a polymer in the presented research. It is a non-ionic, hydrophilic polymer with a very simple structure (Fig. 1). It has many interesting applications including paper industry (sheet formation aid, paper and paper board filler retention aid), glass fibre sizing, construction industry (slurry transport, board extrusion, polymer cement, painting), binder for ceramics, pickup and ending adhesive for paper rolls, mining industry (removal of silica clays, flocculation for phosphatic slimes), suspension polymerization, cosmetics industry (hair care products, skin care products, toothpaste), electronics industry (binder for battery, fluorescent lamp), pharmaceutical industry (controlled-release preparations).

The aim of the presented research was to:

- define the influence of polyethylene oxide on stability of silica;
- define the influence of impurities present in polymer material on the process of stabilisation/destabilisation of silica;
- define the influence of concentration of polymer on stability of silica.

EXPERIMENTAL

SiO₂, used as an adsorbent, was obtained from Aldrich. Silica was washed with doubly distilled water until conductivity of supernatant decreased down to 2 μS/cm. Specific surface of SiO₂ measured by a BET method was 261.7 m²/g. Average size of silica molecules was 157 nm with polydispersity ratio 0.252, which was estimated using Zetasizer 3000 by Malvern Instruments. Similar results for the radius of silica particles were obtained using electron microscopy.

Applied commercial polymers PEO 100 000 and PEO 108 000 were produced by Aldrich and Fluka, respectively. Commercial as well as filtrated and fractionated polymers were used. The aim of a filtration process was to remove both inorganic impurities and macromolecules which molecular weights were much lower than those of the examined polymers. The process was carried out in an ultrafiltrating cell TCF-10 by Amicon. A XM-30 membrane (blocking macromolecules of molecular weight greater than 30 000) was applied for a PEO 100 000. Apart from purification an initial fractionation was also a result of this process because of separation of macromolecules of masses lower than 30 000 from the final solution. A fractionation of the polymers was carried out on a chromatographic column filled with Sephacryl S-300 HR gel by Amersham Biosciences.

A background electrolyte 10^{-2} mole-dm⁻³ NaCl was used. Absorbance was measured with a Specord M42 by Carl Zeiss using a wavelength range from 220 to 400 nm. pH of the measured samples was 6 and the amount of an added oxide equalled a surface of 1.04 m². All measurements were carried out at a constant temperature of 25°C.

RESULTS AND DISCUSSION

Commercial polymers, available to purchase, should be of high purities, which is often not fulfilled. This problem can be solved by purification of the polymers on your own. That is why polymers used in the presented research were purified by filtration process or fractionation on chromatographic column.

Table 1. Conductivity of commercial, filtrated and fractionated PEO solutions [μ S/cm]

PEO 100 000	Conductivity [μ S/cm]
commercial	7.1
filtrated	1.45
fractionated	2.09

Conductivities of water solutions of PEO 100 000 of concentration of 100ppm (commercial, filtrated and fractionated respectively) are presented in Table 1. Presented data clearly show, that commercial polymer solutions are impure in the greatest degree. This fact emerges from not only the variety of ions present in the solution but also its high concentration.

A comparison between conductivities of filtrated and fractionated polymers surprisingly indicate, that solutions of fractionated polymers have higher conductivity compared to filtrated ones. The reason for this fact can be impurities present in chromatographic resins, which were eluted during fractionation process.

Table 2. XRF analysis of researched polymers, content of impurities

	PEO 100 000
commercial	Si 0.9% Ca 0.3% Cu, Zn
filtrate	Si 0.9% Ca 0.3% Cu, Zn
filtrated	Cu, Zn
fractionated	Si 0.2% Cl, K, Cr, Fe, Zn

A XRF analysis of a filtrate, commercial, filtrated and fractionated polymers were additionally conducted. These data, presented in Table 2, are compatible with conductivities of the same solutions (Table 1). According to the expectations, the biggest amount of inorganic impurities is present in commercial polymer solutions. Si content is about 1%, Ca about 0.3%, while Cu and Zn concentration is on the level of ppm, which is the limit of detection for XRF method and cannot be converted into quantity with acceptable accuracy

Both the quality and the quantity of impurities present in the filtrate are comparable with contents of impurities in commercial polymer. It can be concluded that most of inorganic impurities was removed from the solution in the filtration process. Cu and Zn atoms, present in vestigial quantities in filtrated polymer solutions, should not influence its adsorptive and electrokinetical properties.

Impurities content of a fractionated polymer, which was gained by processing a commercial one, is much lower than this observed for the latter. Si content after the fractionation process lowers approximately 4 times. However, other previously absent elements appear: Cl, K, Cr, Fe. The only possible reason for that is the fact of elution of above-mentioned atoms (probably bonded in chemical compounds) from the chromatographic column material. There is a certain probability that these impurities might have an effect on adsorption process and stability of the analysed suspension.

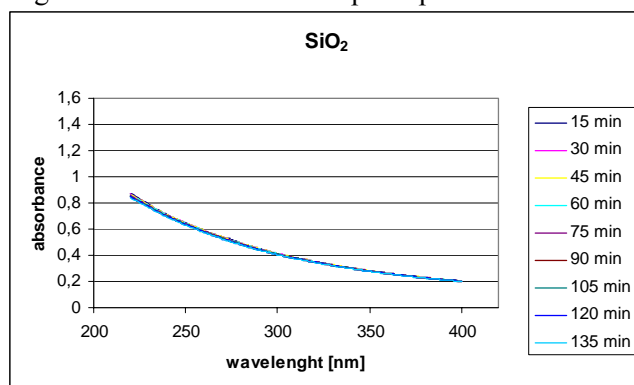


Fig. 2. Absorbance of silica suspension without polymer

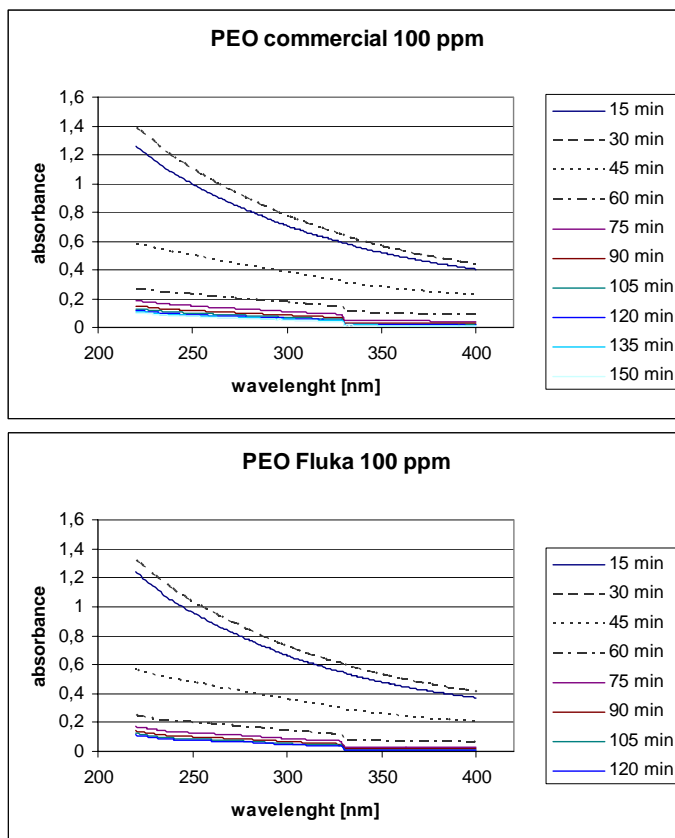


Fig. 3. Absorbance of silica suspension with 100ppm PEO (commercial of low and high quality)

In Figure 2 an absorbance of silica suspension without polymer is presented. The measured range of wavelength is 220-400nm. The change in absorbance of suspension is used as a measure of stability of this suspension. As it can be seen, the absorbance of silica suspension doesn't change in measured period of time. It can be safely stated that over this period of time (over 2h) measured silica suspension is stable.

On the other hand, in Figures 3 and 4 the absorbance of the same silica suspension is presented but with the addition of polyethylene oxide of different purities. Commercial of low quality, commercial of high quality, fractionated and filtrated polymers are being presented respectively. The first thing that can be seen is a distinct change in absorbance of the suspension over measured time for all four polymers analysed. In all cases, the absorbance of the solution increases in the beginning and then decreases suddenly. The increase in absorbance (increase in stability) is caused by the kinetics of the adsorbing polymer. Concentration of the polymer in the solution decreases and concentration on the interface solution/silica increases until equilibrium is reached. This first stage may be considered as a stabilisation of the suspension with

the adsorbing polymer. After the equilibrium is reached, polymer chains adsorbed on separate silica particles start to interact with each other. The result of that interaction is a creation of aggregates. The greater the number of those aggregates, the less stable the suspension is. This second process is seen on absorbance curves as a sudden decrease in absorbance of the analysed solutions.

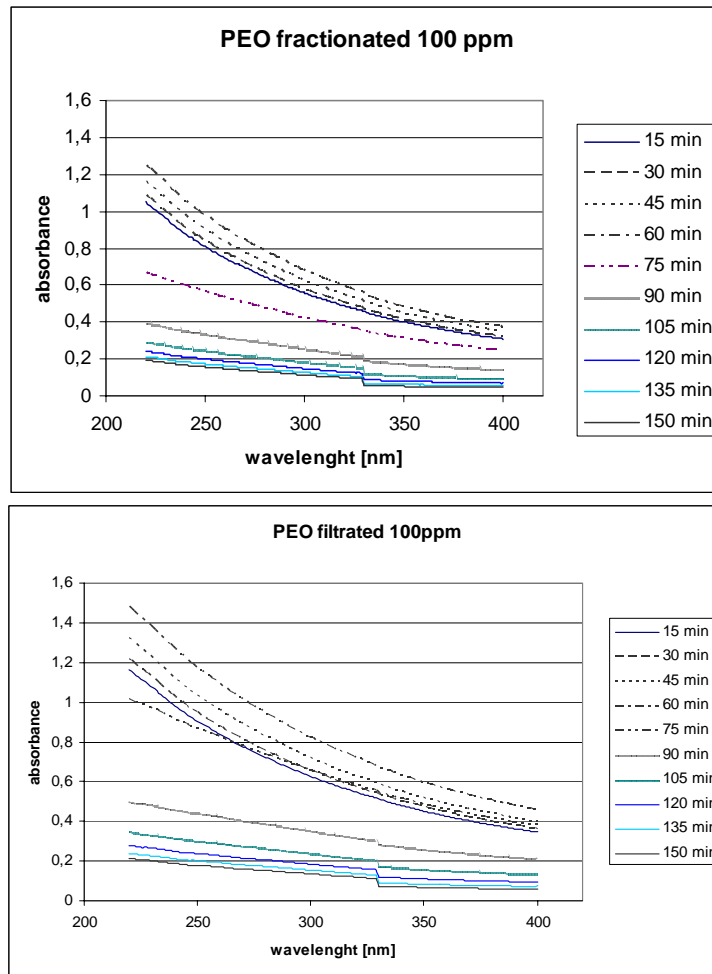


Fig. 4. Absorbance of silica suspension with 100ppm PEO (fractionated and filtrated)

If one compares the rate of establishing of equilibrium, for commercial polymers (both of low and high quality) absorbance increases after 15 and 30 minutes from the start, after that it starts to fall down. For purified polymers (both filtrated and fractionated) absorbance increases up for twice as long (to 60 minutes) and then starts to fall down. This difference in time the absorbance increases is the result of longer establishing of the adsorption equilibrium for purified PEO on SiO_2 . As there are less

impurities in purified polymers, the only molecules that try to adsorb on the surface are the macromolecules of the polymers. Those, being quite large and slow moving, compete together for adsorption sites on silica. The result of that is an increase in time needed to achieve an equilibrium between solution and interface. For commercial polymers the time is shorter, because there are some impurities left after the polymerisation process. Those impurities, being mostly inorganic, are quite fast-moving and adsorb quickly on the silica surface. The result of this is a faster achievement of equilibrium between solution and interface between polymer and impurities molecules.

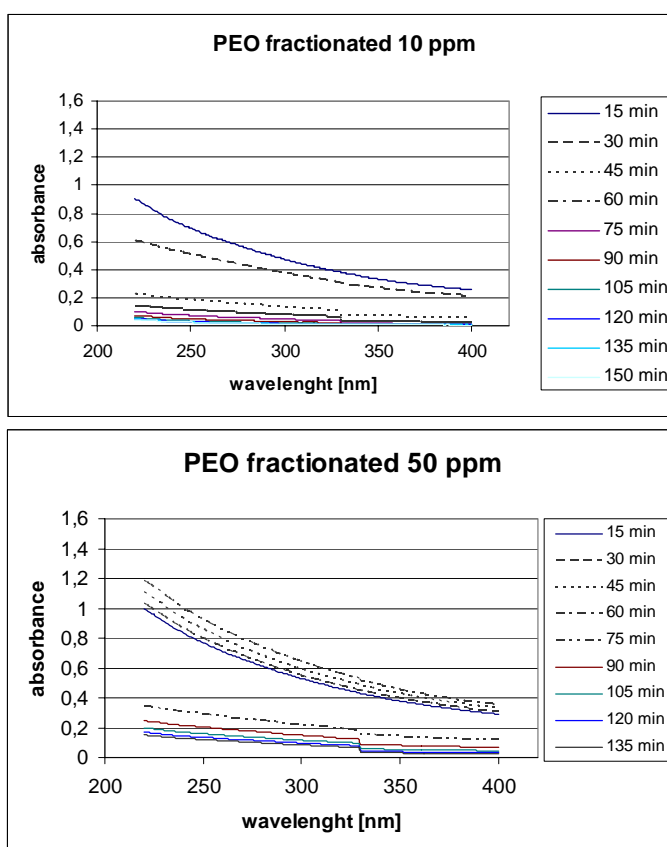


Fig. 5 Absorbance of silica suspension with fractionated PEO (10 and 50ppm)

In Figure 5, a comparison of absorbance of silica suspension with fractionated PEO of different concentrations (10 and 50ppm) is presented. For sample with lower concentration of the polymer an instant decrease in absorbance is observed. This is the result of a very rapid reaching of equilibrium for this system. If the concentration of a polymer is low, there are not so many molecules to adsorb and compete for adsorption

sites so the result is almost immediate adsorption equilibrium. Just after that, a flocculation takes place and suspension starts to destabilise (absorption of the solution decreases).

CONCLUSIONS

1. The stability of silica is greatly influenced by the presence of polyethylene oxide.
2. Silica without adsorbed polymer is stable over the time of at least two hours.
3. An addition of polymer firstly stabilises the suspension but after some time the suspension is suddenly destabilised. The times of stabilisation and destabilisation of the suspensions are different for polymer samples of different purities. It is greatly dependent on the content of impurities and polydispersity index of a polymer.
4. Stability of silica is dependent on concentration of polyethylene oxide used. The greater the concentration of the polymer, the longer time is needed to establish adsorption equilibrium, so the more stable the suspension is.

REFERENCES

- FLEER G.J., COHEN STUART M.A., SCHEUTJENS J.M.H.M., COSGROVE T., VINCENT B., 1993 *Polymers at Interfaces*, Chapman & Hall, London.
- FLEER G.J., SCHEUTJENS J.M.H.M., in: B. Dobias (Ed.), 1993, *Coagulation and Flocculation; Theory and Applications*, Chapter 5, Marcel Dekker, New York.
- MARKOVIC B., 1996, *Adsorption of Polyacrylic Acid on Alumina and Silicon Carbide*, Doctoral Thesis, University of Zagreb, Croatia.
- PAN Z., CAMPELL A., SOMASUNDORAN P., 2001, *Colloids and Surfaces*, 191,(1) 71 – 78.
<http://www.sumitomoseika.co.jp/peo/>

Chibowski S., Patkowski J., *Badanie stabilności SiO₂ w obecności tlenku polietylenu o różnym stopniu czystości*, *Physicochemical Problems of Mineral Processing*, 41 (2007) 177-184 (w jęz. ang.).

Badano wpływ zanieczyszczeń występujących w roztworach polimerów na stabilność suspensji komercyjnej krzemionki w obecności PEO 100 000. Stabilność suspensji mierzono pośrednio, poprzez określanie wielkości absorbancji badanej suspensji krzemionki i tlenku polietylenu. Ilość oraz jakość zanieczyszczeń obecnych w roztworach polimerów określono przy pomocy badania metodą XRF. Zanieczyszczenia obecne w roztworach polimerów będące pozostałością po procesie polimeryzacji, mogą adsorbować się konkurencyjnie z makrocząsteczkami polimeru. W wyniku tego, blokują miejsca adsorpcyjne na powierzchni adsorbentu pozostawiając mniejszą ilość miejsca dostępnego dla makrocząsteczek polimeru. Proces oczyszczania polimeru został przeprowadzony w celu poprawy jakości analizowanego polimeru. Tlenek polietylenu użyty w przedstawianych badaniach został oczyszczony w procesie filtrowania na membranach oraz frakcjonowania na kolumnie chromatograficznej. Użyto czterech próbek polimeru o różnym stopniu czystości i polidispersyjności: komercyjny o niskiej jakości, komercyjny o wysokiej jakości, filtrowany oraz frakcjonowany. Obecność zanieczyszczeń w materiale polimeru w zdecydowany sposób wpływa na stabilność układu krzemionka/roztwór polimeru. Krzemionka bez dodatku polimeru jest stabilna w całym badanym zakresie czasu. Dodatek polimeru początkowo stabilizuje suspensję, która po pewnym czasie jest dość gwałtownie destabilizowana. Czas stabilizacji oraz destabilizacji suspensji jest różny dla próbek polimeru o różnej czystości. Dowodzi to faktu, że stabilność takiego układu wyraźnie zależy od zawartości zanieczyszczeń jak również od stopnia polidispersyjności polimeru.

Filip CIESIELCZYK*, Andrzej KRYSZTAFKIEWICZ*, Teofil JESIONOWSKI*

ADSORPTIVE PROPERTIES OF SYNTHETIC MAGNESIUM SILICATES

Received April 30, 2007; reviewed; accepted 4 June 15, 2007

Studies were presented which were related to formation of a synthetic magnesium silicate in precipitation reaction employing solutions of sodium metasilicate and of appropriate inorganic magnesium salt. The studies aimed at obtaining precipitated products of best adsorptive properties. Both unmodified silicate and magnesium silicates modified with various agents were examined. Adsorptive properties were examined using determined nitrogen adsorption/desorption isotherms.

Key words: synthetic magnesium silicate, surface modification, adsorptive properties

INTRODUCTION

Application potential of the vast group of silicates and silicas to a significant extent reflects their physicochemical properties. The properties are determined, first of all, by parameters of the silicate formation process, including the applied reagents, their quantitative ratios and, possibly, supplementation with surface modifiers (Ciesielczyk 2004, 2005).

Due to the significant role of silicates (both natural and synthetic ones) as polymer fillers and selective adsorbents (Krysztafkiewicz 1996; Harris 2001), their surface activity involves an important problem. The activity is determined first of all by silanol groups ($\equiv\text{Si}-\text{OH}$) and their packing at the silicate surface (Jesionowski 2001). Synthetic magnesium silicates exhibit well developed surface and presence of reactive silanol groups and, thus, they can be included to the group of selective adsorbents.

The process of adsorption on their surface may also be intensified by surface modification of silicates using various agents. The most numerous group of modifiers involves silane coupling agents (Plueddeman 1991). Non-ionic surfactants and quaternary ammonium salts are also frequently used (Jesionowski 2001).

* Poznan University of Technology, Institute of Chemical Technology and Engineering.
pl. M. Skłodowskiej-Curie 2, 60-965 Poznan, Poland, e-mail: Filip.Ciesielczyk@wp.pl

Introduction of a given modifier on the surface of a synthetic magnesium silicate results in the appearance of typical functional groups. The groups significantly affect efficiency of adsorption of various compounds on the silicate surface.

The very process of modification using, e.g., silane coupling agents provides an example of adsorption of the agents on the surface of a synthetic magnesium silicate. Literature of the subject contains mechanisms of silane adsorption on the surface of kaolin. Due to analogies in structure of kaolin, silicas and silicates the modifiers are expected to react in every case in line with the mechanisms (Johansson 1999, Azzopardi 1994).

Adsorptive properties of new products play a very important role in analysis of potential applications of synthetic magnesium silicates. It is assumed that the products may in future be used as selective and very effective adsorbents, particularly for cleaning sewages of heavy metals and the vast group of organic compounds. Therefore, in present study we undertook investigations on production of precipitated magnesium silicates of optimum adsorptive properties.

EXPERIMENTAL

MATERIALS

In the precipitation reaction an advantage was taken of 5% solutions of magnesium sulphate(VI), nitrate(V) and chloride (POCh S.A.), as well as of sodium metasilicate (5% aqueous solution in respect to SiO₂ content). Sodium metasilicate solution manifested the following parameters: Na₂O=8.8 %; SiO₂=28.5 %, density=1.38 g/dm³ and modulus of 3.33 (VITROSILICON S.A.). The following modifying agents were used for surface modification of magnesium silicate: non-ionic surfactants produced by PCC ROKITA S.A. - oxyethylenated unsaturated fatty alcohols, Rokanol K3 and K7, of the general formula RO(CH₂CH₂O)_nH R=C₁₆₋₂₂, where $n_{av}=3$ or $n_{av}=7$, respectively, and the produced by UniSil silane proadhesive compound, U-15 (*N*-2-aminoethyl-3-aminopropyltrimethoxysilane).

METHODS OF STUDIES

At the first stage of the studies magnesium silicate was precipitated using solutions of appropriate magnesium salt and sodium metasilicate. The reaction was conducted in a reactor of 500 cm³ capacity, equipped with a rapidly top stirrer. The reactive system was placed in a thermostat.

The precipitation process was conducted either in the presence or in the absence of non-ionic surfactants (used to induce hydrophobic transformation of the surface). The obtained samples were additionally modified using U-15 aminosilane. The silane was deposited on their surfaces by „the dry technique”.

In order to determine magnesium silicate adsorptive properties their BET specific surface area, pore diameter and pore volumes were estimated using for the purpose nitrogen adsorption/desorption isotherms. The measurements were performed using ASAP 2010 apparatus (Micromeritics Instruments Co. USA).

RESULTS AND DISCUSSION

The nitrogen adsorption/desorption isotherms and pore size distribution of unmodified synthetic magnesium silicate obtained from MgCl_2 and on the surface of silicates precipitated in the presence of 5 wt./wt. of Rokanols K3 and K7 are presented in Fig.1 and Fig.2.

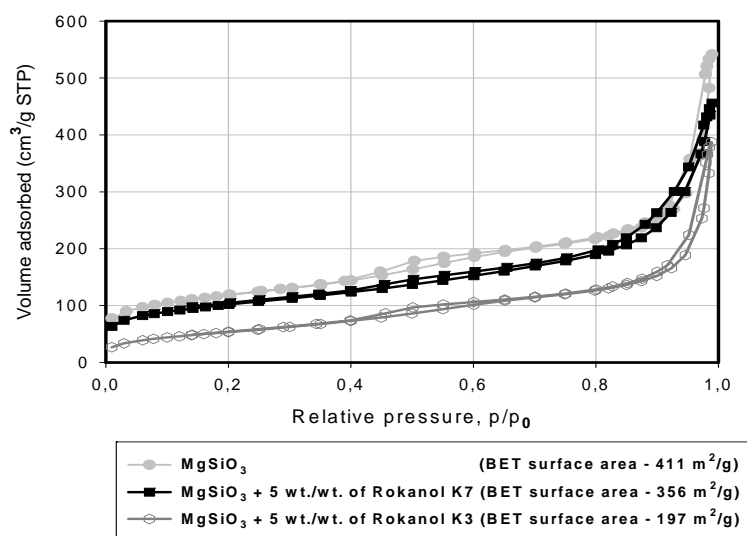


Fig.1. N_2 adsorption/desorption isotherms of the examined magnesium silicates precipitated from MgCl_2 solution

The shape of isotherms representing the modified samples resembled that of the isotherm obtained for the unmodified silicate sample. The amount of adsorbed nitrogen slightly increased until the relative pressure of 0.8 was obtained. At higher values of the relative pressure an abrupt increase was noted in the amount of adsorbed nitrogen. Such course of the isotherms pointed to high activity of the silicates. The adsorbed amount of nitrogen at $p/p_0=1$ reached the value of $543 \text{ cm}^3/\text{g}$ for unmodified silicate, $457 \text{ cm}^3/\text{g}$ for magnesium silicate precipitated in the presence of 5 wt./wt. of Rokanol K7 and $396 \text{ cm}^3/\text{g}$ for magnesium silicate precipitated in the presence of 5 wt./wt. of Rokanol K3. The course of adsorption isotherms indicated that the magnesium silicates belonged to mesoporous sorbents (the amount of adsorbed nitrogen practically did not increase until the relative pressure reached the value of 0.7). On the other hand, significant differences were noted in the amount of adsorbed nitrogen and in values of BET specific surface area. For the unmodified silicate specific surface area amounted to $411 \text{ m}^2/\text{g}$ while for the silicates precipitated in the presence of 5 wt./wt. of Rokanol K3 or K7 the surface amounted to $197 \text{ m}^2/\text{g}$ and $356 \text{ m}^2/\text{g}$, respectively.

Comparison of pore size distribution (Fig.2) indicates that adsorptive forces linked to interaction with pore walls decrease with increasing pore size while molecular interactions introduce increasingly pronounced effects on the adsorption process. Various sizes of the individual pore groups reflect first of all their shape and properties of the adsorbent (Jaroniec 1999). In the case of mesopores their lower limit is sufficiently high to allow multilayered adsorption of adsorbate molecules.

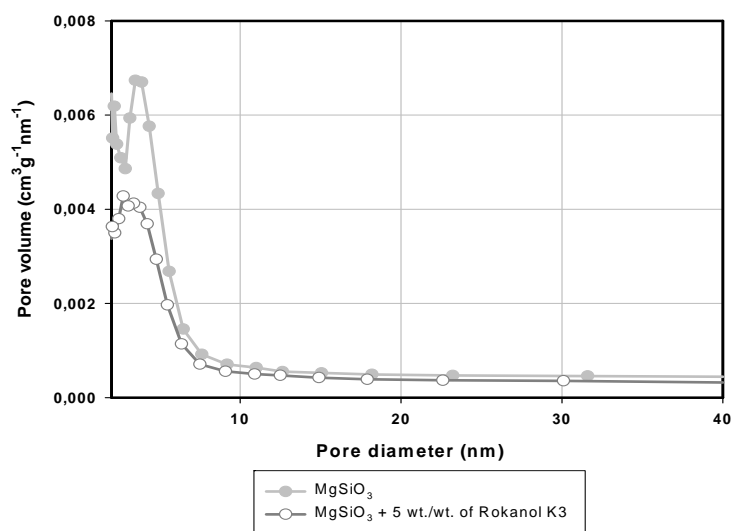


Fig. 2. Pore size distribution (BJH method) of the examined magnesium silicates precipitated from $MgCl_2$ solution

Nitrogen adsorption/desorption isotherms on the unmodified silicate precipitated from $Mg(NO_3)_2$ and for magnesium silicate precipitated in the presence of 5 wt./wt. of Rokanol K3 or K7 are presented in Fig. 3.

The character of isotherms was similar to those presented in Fig. 1. In the case of magnesium silicate precipitated from $Mg(NO_3)_2$ no significant differences were observed in the amounts of nitrogen adsorbed. For magnesium silicates subjected to no hydrophobization and those hydrophobically transformed using 5 wt./wt. of Rokanol K7 the amount was $592 \text{ cm}^3/\text{g}$, but for the magnesium silicate precipitated in the presence of 5 wt./wt. of Rokanol K3 maximum amount of adsorbed nitrogen reached $621 \text{ cm}^3/\text{g}$. In the case when magnesium nitrate(V) was used for precipitation of magnesium silicate the differences in specific surface area were no longer so extensive as those in the case of samples obtained from $MgCl_2$.

In the precipitation process of synthetic magnesium silicate solution of magnesium sulphate(VI) was also used. Isotherms obtained for silicate samples obtained using the substrate are presented in Fig. 4. In this case the lowest differences were observed in the maximum amounts of adsorbed nitrogen and in values of BET specific surface

area. The curves manifested an identical character, pointing to mesoporous structure of the magnesium silicates. The amounts of adsorbed nitrogen ranged from 530 to 580 cm³/g. Remarkably, specific surface area (estimated by BET technique) in cases of silicates precipitated in the presence of 5 wt./wt. of Rokanols K3 or K7 demonstrated higher values (433 cm³/g and 453 cm³/g, respectively) than that noted for the silicate precipitated in the absence of non-ionic surfactants (408 cm³/g).

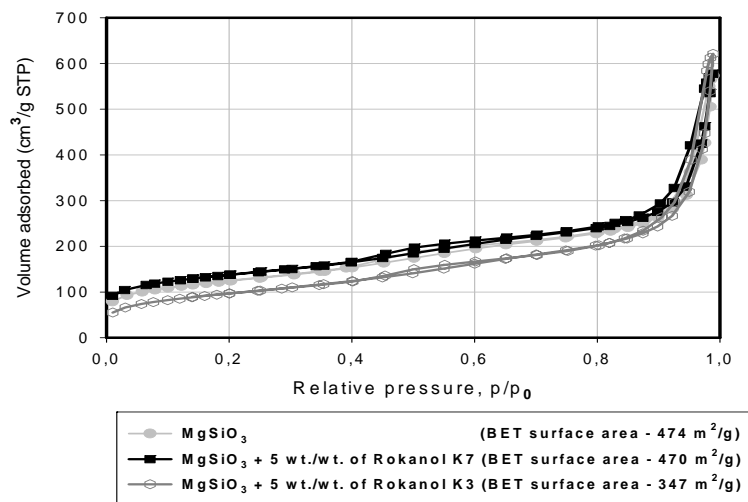


Fig. 3. N₂ adsorption/desorption isotherms of the examined magnesium silicates precipitated from Mg(NO₃)₂ solution

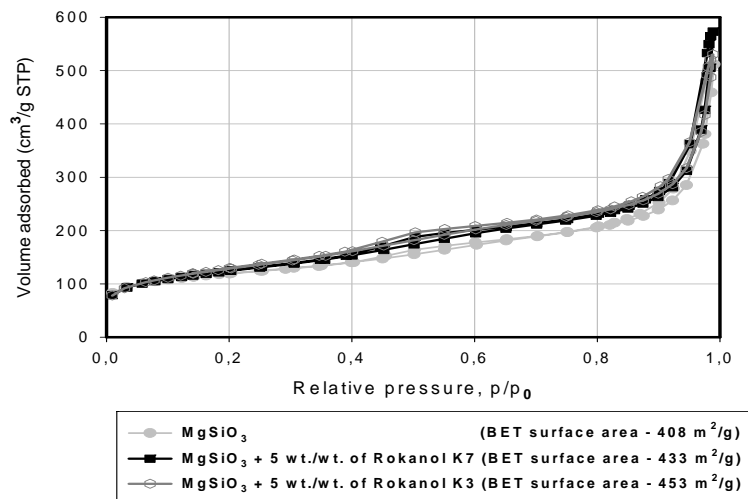


Fig. 4. N₂ adsorption/desorption isotherms of the examined magnesium silicates precipitated from MgSO₄ solution

Application of synthetic magnesium silicate as a selective adsorbent of heavy metals or organic compounds required searches for solutions which would promote the adsorption process. One of such solutions involved introduction to the synthetic magnesium silicate surface of typical functional groups which would freely react with the adsorbed agents. Such groups are contained, e.g., in silane coupling agents and their deposition to the surface of synthetic magnesium silicate was executed by "the dry technique". Nitrogen adsorption/desorption isotherms on the surface of magnesium silicates precipitated using magnesium sulphate(VI) in the presence or in the absence of 5 wt./wt. of Rokanol K3 and, in addition, modified by „the dry technique” with U-15 aminosilane are presented in Fig. 5.

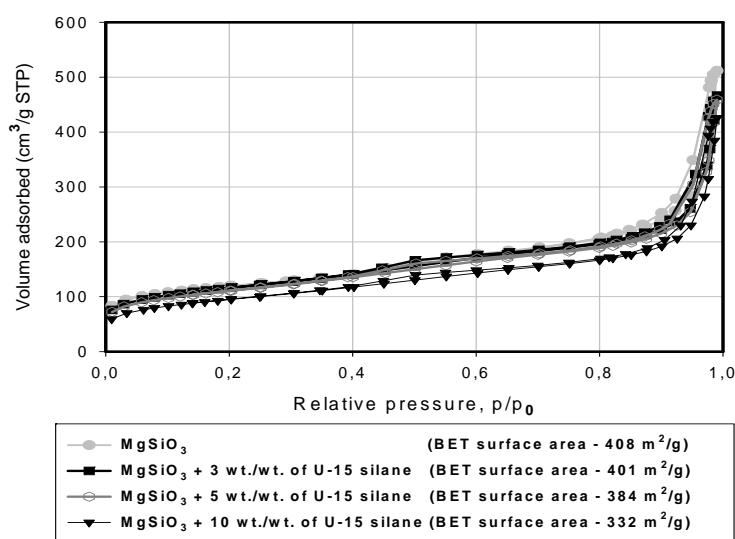


Fig.5. N₂ adsorption/desorption isotherms of the examined magnesium silicates precipitated from MgSO₄ solution modified with aminosilane U-15

Magnesium silicates precipitated in the absence of Rokanol K3 and modified with aminosilane (Fig. 5) manifested very similar course of isotherms of nitrogen adsorption/desorption. The amount of adsorbed nitrogen decreased with increasing amount of applied modifying agent. For the unmodified magnesium silicate the amount of adsorbed nitrogen was 509 cm³/g, while for magnesium silicates modified using 3 or 5 wt./wt. of U-15 aminosilane they reached 477 cm³/g and for magnesium silicate modified with 10 wt./wt. of the aminosilane it was 449 cm³/g. Worth noting, similar tendencies were observed in the case of BET specific surface area. The unmodified magnesium silicate exhibited the highest BET specific surface area (408 m²/g) and magnesium silicate modified with 10 wt./wt. of aminosilane manifested the lowest BET surface area (332 m²/g). This might reflect the fact that binding to the

surface of synthetic silicate the organo-functional silane occupied active centres and in this way decreased surface activity of the precipitated silicate. Additionally, the decreased specific surface area might be caused by steric hindrance produced by hydrocarbon chains of silicate surface adsorbed silanes, which in this way decreased nitrogen penetration to the silicate surface.

Similar relationships were observed in the case when magnesium silicate precipitated in presence of 5 wt./wt. of Rokanol K3 was subjected to aminosilane modification. Specific surface area decreased also with increasing amounts of the applied modifying agent. Again, the lowest BET specific surface area (332 m²/g) was manifested by magnesium silicate modified with 10 wt./wt. of aminosilane.

Principal morphological and structural parameters of precipitated magnesium silicates determined by the nitrogen adsorption/desorption isotherms are listed in Table 1.

Table 1. Physicochemical parameters decided about adsorptive properties of unmodified and modified magnesium silicates

Precipitating agent	Amount of non-ionic surfactants	Modifying agent	Amount of modifying agent (wt./wt.)	Specific surface area BET (m ² /g)	Pore volume (cm ³ /g)	Average pore diameter (nm)
MgCl ₂	-	-	-	411	0.80	5.5
	5 wt./wt. of Rokanol K3	-	-	197	0.67	6.3
	5 wt./wt. of Rokanol K7	-	-	356	0.61	7.9
Mg(NO ₃) ₂	-	-	-	474	0.83	5.5
	5 wt./wt. of Rokanol K3	-	-	347	0.87	6.2
	5 wt./wt. of Rokanol K7	-	-	470	0.98	7.3
MgSO ₄	-	-	-	408	0.73	5.5
	5 wt./wt. of Rokanol K3	-	-	433	0.85	5.6
	5 wt./wt. of Rokanol K7	-	-	453	0.79	5.2
MgSO ₄	-	U-15 silane	3	401	0.68	5.2
	-		5	384	0.67	5.2
	-		10	332	0.63	5.2
MgSO ₄	-	U-15 silane	3	384	0.64	4.8
	5 wt./wt. of Rokanol K3		5	376	0.64	4.9
	5 wt./wt. of Rokanol K3		10	364	0.67	4.8

Among the unmodified samples, the highest specific surface area ($474 \text{ m}^2/\text{g}$) was shown by magnesium silicate obtained from $\text{Mg}(\text{NO}_3)_2$ and the lowest one by the silicate obtained from MgSO_4 . As compared to unmodified samples, samples precipitated in the presence of non-ionic surfactants showed higher value of specific surface area only in the case of magnesium silicate precipitated from MgSO_4 .

Neither the original substrates nor the applied modifying agents significantly affected the remaining adsorptive parameters of precipitated silicates. In all the cases pore volumes and pore diameters demonstrated similar values.

CONCLUSIONS

Formation of synthetic magnesium silicates by precipitation from sodium metasilicate solutions and solutions of various inorganic magnesium salts represents an interesting approach, which yields active, highly dispersed adsorbents and fillers. The precipitated in this way silicates manifest a relatively high value of BET specific surface area, which indirectly points to their high surface activity. The highest values of specific surface area have been shown by magnesium silicate samples obtained from MgSO_4 ($408\text{-}453 \text{ m}^2/\text{g}$) or from $\text{Mg}(\text{NO}_3)_2$ ($470\text{-}474 \text{ m}^2/\text{g}$). Among the three various magnesium salts, magnesium chloride used for magnesium silicate precipitation has proven to be least advantageous. Precipitation of magnesium silicate in the presence of 5 wt./wt. of Rokanols K3 or K7 has resulted in a radically decreased specific surface area, even to $197 \text{ m}^2/\text{g}$ for the silicate precipitated from MgCl_2 in the presence of 5 wt./wt. of Rokanol K3. The situation has been analogous when the surface of synthetic magnesium silicate has been modified using silane coupling agent. Similarly to the effects of non-ionic surfactants, the modification has resulted in marked decrease in specific surface area of precipitated silicates. It is worth stressing that neither the employed substrates nor modifying agents have clearly affected the remaining adsorptive parameters (pore volume and pore diameter).

Summing up, the obtained synthetic magnesium silicates of a relatively high surface activity may find application as selective adsorbents of heavy metals and of selected organic compounds.

ACKNOWLEDGEMENTS

This work was supported by the 6th Framework Programme, Contract No. INCO-CT-2003-003355, within the project of Scientific Network Surfactants and Dispersed Systems in Theory and Practice (SURUZ) and by the Ministry of Science and Higher Education Research Grant No. N205 010 31/0420.

REFERENCES

- AZZOPARDI M.J., ARRIBART H., 1994, *In situ FTIR study of the formation of an organosilane layer at the silica/solution interface*, Journal of Adhesion, 46, 103-115.
- CIESIELCZYK F., KRYSZTAFKIEWICZ A., JESIONOWSKI T., 2004, *Influence of precipitation parameters on physicochemical properties of magnesium silicates*, Physicochemical Problems of Mineral Processing, 38, 197-205.

- CIESIELCZYK F., KRYSZTAFKIEWICZ A., JESIONOWSKI T., 2005, *Influence of surface modification on morphology and physicochemical parameters of synthetic magnesium silicate*, Physicochemical Problems of Mineral Processing, 39, 155-164.
- HARRIS R.G., WELLS J.D., JOHNSON B.B., 2001, *Selective adsorption of dyes and other organic molecules to kaolinite and oxide surfaces*, Colloids and Surfaces A: Physicochemical and Engineering Aspects, 180, 131-140.
- JARONIEC M., KRUK M., OLIVIER J.P., 1999, *Standard nitrogen adsorption data for characterization of nanoporous silicas*, Langmuir 15 (16), 5410-5413.
- JESIONOWSKI T., KRYSZTAFKIEWICZ A., 2001, *Influence of silane coupling agents on surface properties of precipitated silicas*, Applied Surface Science, 172, 18-32.
- JESIONOWSKI T., KRYSZTAFKIEWICZ A., SKRZYPCZAK A., 2001, *Effects of quaternary ammonium chlorides on the surface properties of precipitated silicas*, Tenside Surfactants and Detergents, 38, 158-163.
- JOHANSSON U., HOLMGREN A., FORSLING W., FROST R.L., 1999, *Adsorption of silane coupling agents onto kaolinite surface*, Clay Minerals, 34, 239-246.
- KRYSZTAFKIEWICZ A., RAGER B., MAIK M., WALKOWIAK J., 1996, *Modified sodium aluminium silicate – a highly dispersed polymer filler and pigment*, Colloids and Surfaces A: Physicochemical and Engineering Aspects, 113, 203-214.
- PLUEDDEMAN E.P., 1991, *Silane coupling agents*, 2nd Edition Plenum Press, New York.

Ciesielczyk F., Krysztafkiewicz A., Jesionowski T., *Właściwości adsorpcyjne syntetycznych krzemianów magnezu*, Physicochemical Problems of Mineral Processing, 41 (2007) 185-193 (w jęz. ang.).

Przedstawiono badania dotyczące otrzymywania syntetycznego krzemianu magnezu w reakcji strącania z wykorzystaniem roztworów metakrzemianu sodu oraz odpowiedniej nieorganicznej soli magnezu. Badania zostały ukierunkowane w stronę uzyskania jak najlepszych właściwości adsorpcyjnych strąconych produktów. Przebadano zarówno krzemian niemodyfikowany jak i krzemiany magnezu modyfikowane różnymi czynnikami. Właściwości adsorpcyjne analizowano na podstawie wyznaczonych izoterm adsorpcji/desorpcji azotu na powierzchni syntetycznych krzemianów.

Beata TEPPER*, Teofil JESIONOWSKI*, Andrzej KRYSZTAFKIEWICZ*

COLLOIDAL SILICAS OBTAINED VIA CO-PRECIPIATION METHOD USING CYCLOHEXANE AS AN ORGANIC PHASE

Received April 30, 2007; reviewed; accepted June 4, 2007

The process of obtaining colloidal silicas from the emulsion systems with the use of cyclohexane as the organic phase has been studied and the products obtained have been also characterised. The emulsion systems made of water solutions of sodium metasilicate and hydrochloric acid or alternatively sulfuric acid have been used. Non-ionic surfactants have been used as emulsifiers, while a homogeniser has been a dispersing tool. The optimum compositions of the emulsion systems and the optimum parameters of silicas precipitation have been established. The dispersion character of the colloids obtained has been examined and the shapes, size and morphology of the SiO₂ particles formed have been analysed (including a tendency to agglomerate formation and polydispersity).

Key words: silica, emulsions, non-ionic surfactants, particle size, surface morphology

INTRODUCTION

Highly-dispersed silicas show specific structure and properties making them much desired components in many products of modern technologies. They are used as plastomer and elastomer fillers, carriers of therapeutic substances or herbi- or pesticides, auxiliary substances in toothpastes, media regulating the powder liquidity, or densifying or tixotropic agents in construction materials (Bolt et al., 1997, Mathew et al., 2004, Yatsuyanagi et al., 2001).

A number of obtaining methods of SiO₂ have been proposed differing mainly in the type of substrates used, conditions of the process and properties of the product (Schlomach and Kind, 2004; Utting and Macquarrie, 2002).

Traditional methods are based on combustion of silicon tetrachloride vapours (Galarneau 1998), hydrolysis and polycondensation of alkoxy silanes (Stöber 1968), and precipitation of silicas from the water solutions of alkali silicates by an acidic

* Poznan University of Technology, Institute of Chemical Technology and Engineering,
pl. M. Skłodowskiej-Curie 2, 60-965 Poznan, Poland, btepper@interia.pl,

agent (Chen et al., 2005, Gun'ko et al., 2001). Unfortunately, none of the above methods ensures obtaining strictly monodispersed particles of spherical shape. The need for such products has prompted the search for new preparatory solutions leading to high quality materials of target physicochemical properties.

A wide gamut of materials based on highly-dispersed and powdered substances have been produced by chemical, pharmaceutical, food or processing industries. Among them of great importance have been synthetic silicas that can be produced in a number of processes, one of them being precipitation of silicas from the emulsion systems. The main aim of this study is to obtain highly-dispersed silicas of spherical particles in the reaction of precipitation from the emulsion systems made of water solutions of sodium metasilicate and hydrochloric or sulphuric(VI) acid. The compositions of the emulsion system and the conditions of the process have been optimised with respect to reaching this aim.

EXPERIMENTAL

MATERIALS

The sodium metasilicate ($\text{Na}_2\text{O}\cdot m\text{SiO}_2\cdot n\text{H}_2\text{O}$) used contained 8.50% of Na_2O ; 27.18% of SiO_2 ; silicate modulus of 3.3 and had a density equal 1.39 g/cm^3 (VITROSILICON S.A.). The precipitating agent was a 5% hydrochloric acid or a 3% sulphuric(VI) acid (POCh S.A.). The highly-dispersed silica was obtained by precipitation from the emulsion with the organic phase of cyclohexane (POCh S.A.) and a non-ionic surfactant of oxyethylenate unsaturated fatty alcohol (Rokanol K7) as an emulsifier. The Rokanol K7 formula is $\text{C}_{18}\text{H}_{37}\text{O}(\text{CH}_2\text{CH}_2\text{O})_7\text{H}$ (PCC ROKITA S.A.).

METHODS OF STUDIES

Silicas were precipitated from a water solution of sodium metasilicate by hydrochloric or sulphuric(VI) acid. The process was performed in a system of two emulsions. One of them (E1) contained a solution of sodium metasilicate and cyclohexane, to which the non-ionic surfactant Rokanol K7 (emulsifier) was added. The other emulsion (E2) was made of a selected mineral acid and cyclohexane, to which also Rokanol K7 was added but in a lower amount. For the process of precipitation emulsion E2 was placed in a reactor and vigorously stirred (19.000 rpm), while emulsion E1 was added to E2 at a constant rate of dosing. The resulting product was the emulsion containing the precipitated silica. This emulsion was heated to 80°C to destabilise it, then cyclohexane was distilled off, and the mixture left was filtered under a reduced pressure.

At the first stage of analysis of the silicas obtained the size of their particles was determined, as this parameter is fundamental for evaluation of dispersion of the powders obtained. The particle size distribution was measured by a Zetasizer Nano ZS instrument (Malvern Instruments Ltd.) based on employing the non-invasive back

scattering technique (NIBS). On the basis of the particle size distribution curves also the polydispersity was obtained, which was a measure of homogeneity of a given silica powder. The silica samples were subjected to morphological and microstructural analyses under a scanning microscope SEM (Philips SEM 515). Using a Tensiometer K100 (Krüss) the profiles of sedimentation and wettability in water were determined. The adsorption properties of the silicas were assessed on the basis of nitrogen adsorption/desorption isotherms. The surface area, pore size and volume were measured by an instrument ASAP 2010 (Micromeritics Instruments Co.).

RESULTS AND DISCUSSION

The precipitation of highly dispersed silicas from the emulsion systems was studied for different parameters of the process in order to establish their optimum values. The effect of the amount of the emulsifiers and the type of mineral acid on the physicochemical properties of the final product was tested. Tables 1 and 2 give the quantitative compositions of the emulsions used in the precipitation of silicas with hydrochloric and sulphuric(VI) acid, respectively.

Table 1. The amount of the emulsifier used in precipitation of silicas by hydrochloric acid

Sample No.	Emulsion E1	Emulsion E2	
	Amount of emulsifier Rokanol K7 (g)	Mount of emulsifier Rokanol K7 (g)	Amount of HCl (cm ³)
1	3.0	0.8	33
2	2.5	0.8	33
3	2.0	0.7	33
4	1.5	0.7	33

Table 2. The amount of the emulsifier used in precipitation of silicas by sulphuric(VI) acid

Sample No.	Emulsion E1	Emulsion E2	
	Amount of emulsifier Rokanol K7 (g)	Amount of emulsifier Rokanol K7 (g)	Amount of H ₂ SO ₄ (cm ³)
5	3.0	0.8	33
6	3.0	0.8	70
7	2.5	0.7	390

Figure 1 presents results of the dispersion study of the precipitated silicas for sample 1. The first diagram illustrates the relation between the particles diameter and the intensity, while the other – the relation between the particles diameter and their volume fraction. The curve of particle size distribution in relation to the intensity shows two bands, Fig. 1a. The first corresponds to the silica particles of small diameters ranging from 295 to 459 nm (the maximum intensity of 38.1 corresponds to the diameter of 342 nm). The other band of low intensity corresponds to the presence

of agglomerates of particles covering the range 2300-4150 nm (the maximum intensity of 4.6 corresponds to the agglomerates of the diameter of 3090 nm). The particle size distribution in relation to the volume fraction also shows two bands. The greater volume fraction corresponds to the primary agglomerates (the maximum volume of 22.8 corresponds to the primary agglomerates of the diameter 342 nm).

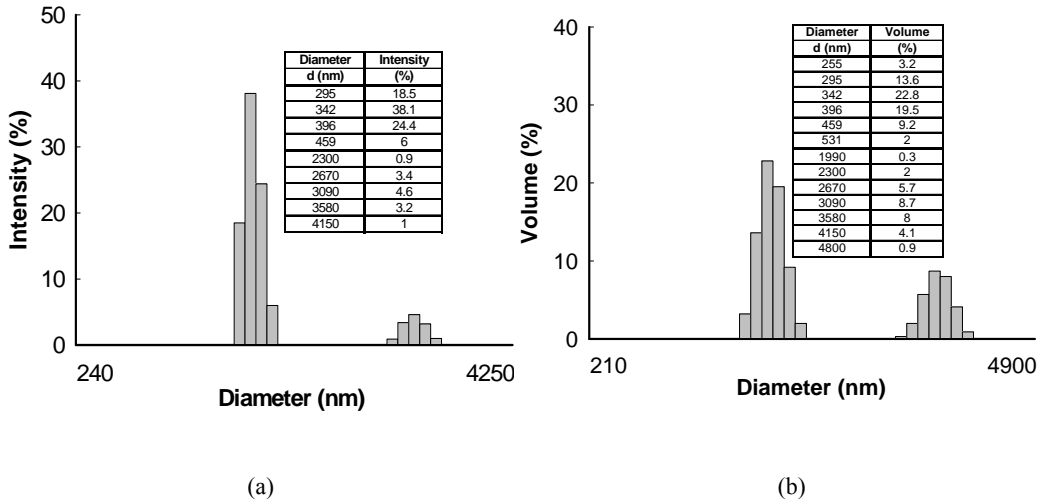


Fig.1. Silica particles size distribution in relation to (a) intensity, (b) volume for silica sample 1

Figure 2 presents the particle size distribution and the SEM photograph of silica sample 2.

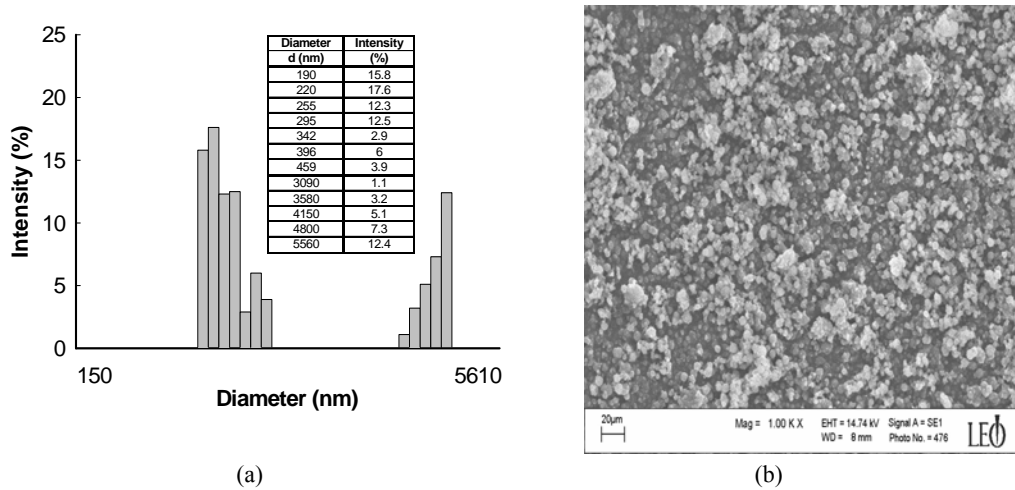


Fig. 2. The particle size distribution in relation to intensity (a) and the SEM photograph (b) for silica sample 2

As follows from Fig. 2a the band assigned to the primary agglomerates (190-459 nm) is dominant and the maximum intensity of 17.6 corresponds to the particles of 220 nm in diameter. The less intense band corresponds to the agglomerates of the diameter from the range 3090-5560 nm and the maximum intensity of 12.4 corresponds to the agglomerates of 5560 nm in diameter. The SEM photo confirms the high quality of the silica sample 2 as the particles are of spherical shape and relatively low polydispersity (0.350). The silica sample 2 is built in 70% of the primary particles whose size varies from 190 to 459 nm.

Figure 3 presents the particle size distribution in relation to volume and the SEM photograph of silica sample 6.

According to the particle size distribution in Fig. 3a, the dominant band corresponds to the primary particles of 164-295 nm in diameter making 67% of the sample. The band corresponding to agglomerates covers relatively narrow range of their diameters from 3580 to 6440 nm and the agglomerates occupy 33% of the sample volume. The polydispersity of silica sample 6 is close to 0.828 and the SEM photo in Fig. 3b (showing the morphology of the particles) attest to the improved quality of this sample.

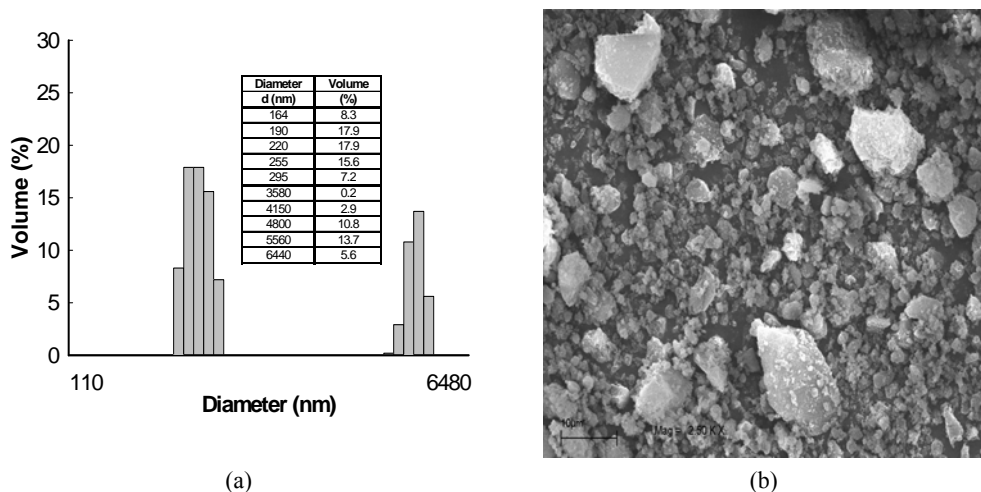


Fig. 3. The particle size distribution in relation to volume (a) and the SEM photo (b) for silica sample 6

Figure 4 presents the particle size distributions in relation to intensity and volume for silica sample 7.

Reduction of the amount of the emulsifier by $\frac{1}{6}$ in emulsion E1 and a considerable increase in the volume of sulfuric acid in emulsion E2 leads to a deterioration of the final product as follows from the volume fraction of the secondary agglomerates being slightly greater than that of the primary particles.

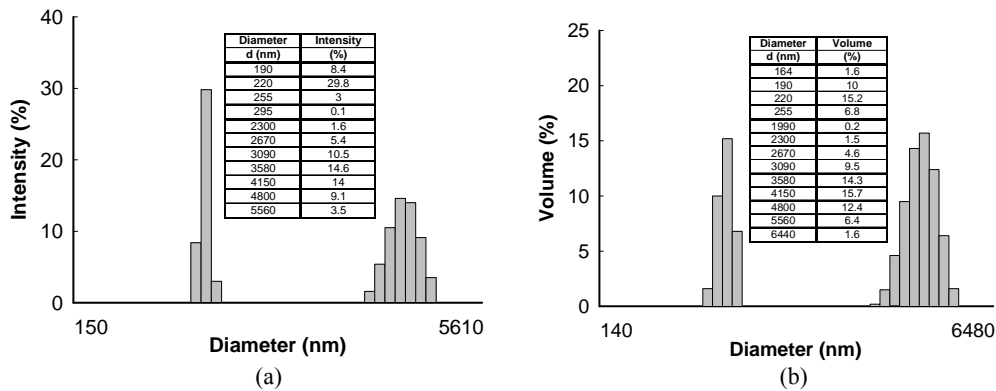


Fig.4. The particle size distribution in relation to intensity (a) and volume (b) for silica sample 7

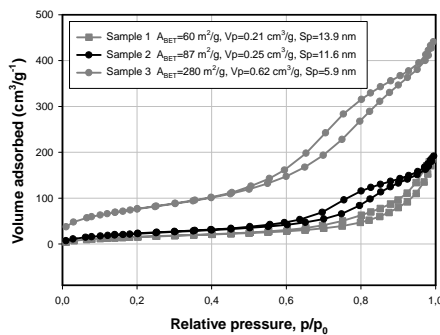


Fig.5. The nitrogen adsorption/desorption isotherms for silicas precipitated from the emulsion system using HCl

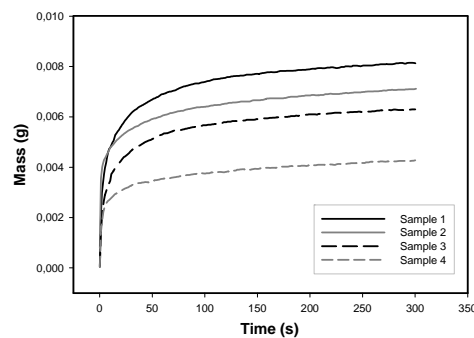


Fig.6. Profiles sedimentation in water for the silicas precipitated applying HCl

Figure 5 presents the nitrogen adsorption/desorption isotherms for silica samples precipitated by a 5% water solutions of HCl in the presence of different amounts of Rokanol K7 in emulsion E1. For samples 1 and 2 starting from low relative pressure the volume of nitrogen adsorbed slightly increases. Starting from the relative pressure of 0.7 the volume of nitrogen adsorbed rapidly increases and reaches a maximum of $200 \text{ cm}^3/\text{g}$ at $p/p_0 = 1$. Sample 3 has a completely different character as indicated by a much greater hysteresis loop. The optimum volume of nitrogen adsorbed of $450 \text{ cm}^3/\text{g}$ (at a relative pressure of $p/p_0 = 1$) indicates that silica sample 3 has the greatest activity. Moreover, the surface area (BET) of sample 3 equal $280 \text{ m}^2/\text{g}$ is significantly greater than those of the other samples. This increase is most probably a result of relatively low content of the emulsifier – close to 2 g – in the alkaline mixture. Despite some differences, each of the samples 1, 2, 3 can be classified as mesoporous on the basis of the nitrogen adsorption/desorption isotherms obtained for them.

Figure 6 presents the profile of sedimentation in water for the silica samples precipitated with the use of hydrochloric acid. The greatest mass increase has been observed for sample 1, characterised by domination of secondary agglomerates over the primary ones. The lowest mass increase has been observed for sample 4, which is characterised by the lowest weight fraction of emulsifiers added to both emulsions E1 and E2, Table 1. A comparison of the results for samples 1, 2, 3 and 4, reveals an inversely proportional relation between the rate of sedimentation and the content of Rokanol K7 in E1, so a decrease in the amount of the emulsifier added to the alkaline emulsion leads to an increase in the rate of sedimentation.

As follows from the plots describing the wettability of silicas precipitated with the use of a 5% water solution of HCl, Fig. 7a, the best wettability has sample 4 obtained from the system with emulsion E1 containing 1.5 g of Rokanol K7, for this sample the total sorption was reached in 1300 seconds. A comparison of the curves presented in Fig. 7a reveals a strict relation between the sample wettability and the amount of the emulsifier in the alkaline emulsion E1; with decreasing amount of Rokanol K7 in E1 the rate of water sorption decreases. Similar conclusions follow from analysis of the wettability curves obtained for the silica samples precipitated using 3% H_2SO_4 (Fig. 7b).

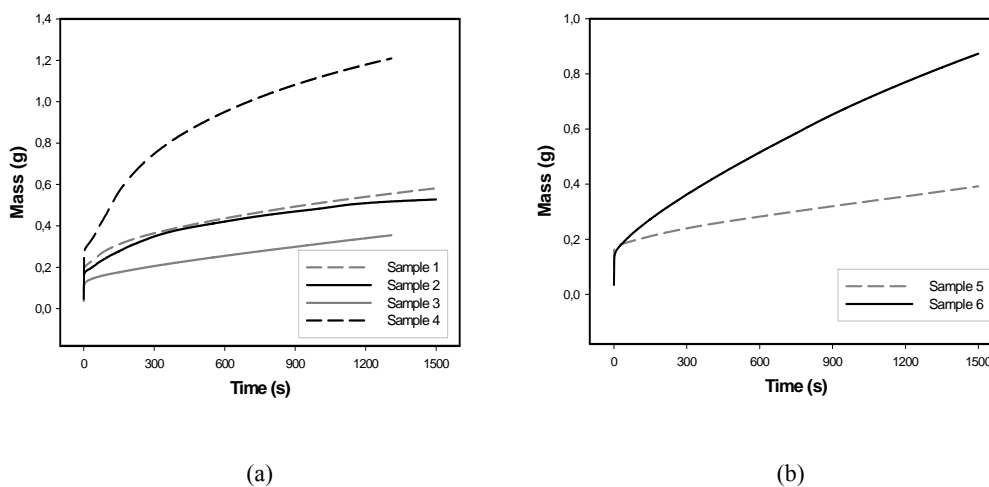


Fig. 7. The wettability of silica samples precipitated from the emulsion system in the presence of (a) HCl and (b) H_2SO_4

Much higher wettability was observed for the silica sample precipitated from the system with a doubled amount of sulphuric(VI) acid in emulsion E2. For this sample a significant increase in the sorption was observed at the end of the measurement (the mass determined reached 1 g).

CONCLUSIONS

The main aim of the study was to obtain highly-dispersed silicas of spherical shape particles and monodisperse nature in the reaction of precipitation from the emulsion systems containing water solutions of sodium metasilicate and hydrochloric or sulfuric acid. As follows from analysis of the silica samples obtained, the precipitation with a 5% solution of hydrochloric acid gives highly-dispersed silicas with particles of spherical shape and homogeneous character. The silica samples precipitated with the use of a 3% sulfuric(VI) acid do not show the characteristics desired. The rate of sedimentation of the silica samples precipitated with a 5% water solution of hydrochloric acid depends on the content of the emulsifier in emulsion E1; the less Rokanol K7 added to E1 the higher the rate. The water sorption by the silica samples precipitated with HCl depends on the weight fraction of Rokanol K7 in emulsion E1. A low content of Rokanol K7 in E1 leads to an increased rate of water sorption, which indicates the hydrophilous character of the samples surface. For the silica samples precipitated with H₂SO₄, the water sorption rate is determined by the presence of the acid in emulsion E2 and a considerable amount of Rokanol K7 in emulsion E2.

ACKNOWLEDGEMENTS

This work was supported by the 6th Framework Programme, Contract No INCO-CT-2003-003355, within the project of Scientific Network Surfactants and Dispersed Systems in Theory and Practice (SURUZ), and by the PUT Research Grant No. 32-115/07-DS.

REFERENCES

- BOLT P.H., BEELEN T.P.M., van SANTEN R.A., 1997, *A small angle X-ray scattering study on high pH silica precipitations*, Colloids Surf. A 122, 183-187.
- CHEN G., ZHOU S., GU G., YANG H., WU L., 2005, *Effects of surface properties of colloidal silica particles on redispersibility and properties of acrylic-based polyurethane/silica composites*, J. Colloid Interf. Sci., 281, 339-350.
- GALARNEAU A., RENZO F.D., FAJULA F., MOLLO L., FUBINI B., 1998, *Kinetics of formation of micelle-templated silica mesophases monitored by electron paramagnetic resonance*, J. Colloid Interf. Sci., 201, 105-117.
- GUN'KO V.M., MIRONYUK I.F., ZARKO V.I., TUROV V.V., VORONIN E.F., PAKHLOV E.M., GONCHARUK E.V., LEBODA R., SKUBISZEWSKA-ZIĘBA J., JANUSZ W., CHBOWSKI S., LEVCHUK YU.N., KLYUEVA A.V., 2001, *Fumed silicas possessing different morphology and hydrophilicity*, J. Colloid Interf. Sci., 242, 90-103.
- MATHEW G., HUH M.-Y., RHEE J.M., LEE M.-H., NAH C., 2004, *Improvement of properties of silica filled styrene-butadiene rubber composites through plasma surface modification of silica*, Polym. Adv. Technol. 15, 400-408.
- SCHLOMACH J., KIND M., 2004, *Investigations on the semi-batch precipitation of silica*, J. Colloid Interf. Sci., 277, 316-326.
- STÖBER W., FINK A., BOHN E., 1968, *Controlled growth of monodisperse silica spheres in the micron size range*, J. Colloid Interf. Sci., 26, 62-69.

UTTING K.A.; MACQUARRIE D.J., 2002, *Formation and evaluation of novel silica supported secondary amines via an effective 'in-situ' reduction of silica supported imines*, Appl. Catalysis A 232, 7-12.

YATSUYANAGI F., SUZUKI N., ITO M., KAIDOU H., 2001, *Effects of secondary structure of fillers on the mechanical properties of silica filled rubber systems*, Polymer, 42, 9523-9529

Tepper B., Jesionowski T., Krysztafkiewicz A., *Otrzymywanie koloidalnych krzemionek metodą strącania w środowisku cykloheksanu jako fazy organicznej*, Physicochemical Problems of Mineral Processing, 41 (2007) 195-203 (w jęz. ang.).

W pracy prowadzono badania ukierunkowane na otrzymywanie cząstek krzemionki z układów emulsyjnych z zastosowaniem cykloheksanu jako fazy organicznej. Badania prowadzono z wodnymi roztworami metakrzemianu sodu i kwasu solnego lub kwasu siarkowego. Stosowanymi emulgatorami były niejonowe związki powierzchniowo czynne. Jako ośrodek dyspergujący zastosowano homogenizator. Ustalono optymalne składy emulsji i parametry strącania krzemionek. Oceniono charakter dyspersyjny otrzymanych koloidów oraz zbadano kształty i morfologię formowanych cząstek SiO₂ (m.in. tendencję do tworzenia aglomeratów, polidispersyjność). Podstawowym celem badań było otrzymanie wysoko zdyspergowanych krzemionek o sferycznych cząstkach i monodispersyjnej naturze w reakcji strącania z układów emulsyjnych zawierających wodne roztwory metakrzemianu sodu oraz kwasu odpowiednio solnego bądź siarkowego(VI).

Katarzyna SIWIŃSKA-STEFAŃSKA*, Andrzej KRYSZTAFKIEWICZ*,
Teofil JESIONOWSKI*

MODIFICATION OF HYDROPHILIC/HYDROPHOBIC CHARACTER OF TiO₂ SURFACE USING SELECTED SILANE COUPLING AGENTS

Received April 30, 2007; reviewed; accepted May 29, 2007

In the studies R-213 titanium white was used, produced by Chemical Works Police S.A. Modification of titanium dioxide surface was conducted in order to alter its physicochemical properties. In this aim for modification organic coupling agents were employed, containing vinyl, amine and metacryloxy functional groups. Effects of concentration of the silane coupling agent (0.5, 1 or 3 weight parts) on dispersive properties and on morphology of TiO₂ particles were examined. In the studies advantage was taken of SEM and NIBS techniques. For the obtained in this way products elemental composition, particle size distribution, BET specific surface area and rate of sedimentation in water were examined. Surface modification changes hydrophilic/hydrophobic character of the obtained preparations, promoting also agglomeration of TiO₂ particles.

Key words: titanium dioxide, surface modification, silane coupling agents, adsorption isotherms, surface morphology, dispersion, particle size

INTRODUCTION

Inorganic pigments, as compared to organic pigments, remain insoluble, chemically neutral, resistant to elevated temperatures and environmental factors such as extreme pH of the environment or chemical agents. They used to manifest augmented resistance to light, higher ability to become dispersed and higher coating potential. Their disadvantages include lower brightness, colour intensity and staining power. Such properties of the pigments are significantly affected by particle shape and size distribution, chemical composition and surface properties of pigment particles (Binkowski 2000, Kohler 1997, Chantrapornchai 2000, Sobolewski 2004).

* Poznan University of Technology, Institute of Chemical Technology and Engineering
M. Skłodowskiej-Curie 2 Sq., 60-965 Poznan, Poland, e-mail: Teofil.Jesionowski@put.poznan.pl

Therefore, the role of inorganic pigments progressively increases, as compared to the role of organic pigments (Krysztafkiewicz 1995, 1999, Endri 1998, Carter 1998).

Apart from carbon black, titanium white belongs to one of the most frequently applied pigments. It used to be applied in paints and varnishes and it finds wide application in staining plastics, first of all due to its excellent coating properties, and in paper industry (Bieniek 2004, Sobolewski 2004). In contrast to colourful pigments (inorganic and organic ones) titanium white absorbs no visible light of any wavelength (Macionga 2005). In the paper studies are described on modification of TiO₂ using selected alkoxysilanes. Moreover, effects of the modification were examined on physicochemical characteristics of titanium dioxide.

EXPERIMENTAL

MATERIALS

TYTANPOL[®]R-213 represents a pigment of a rutile variety, deeply surface processed using compounds of aluminium and silicon (amounting to 4.7% of Al₂O₃ and 8.3% of SiO₂, respectively) and modified with organic compounds of a hydrophilic nature. Principal properties of the pigment, produced by Chemical Works Police S.A. using the sulphate technique are listed in Table 1.

Table 1. Principal properties of the titanium dioxide R-213

Physicochemical parameter	Value
Density (g/cm ³)	3.7
Content of titanium dioxide (wt. %)	82
Content of volatile substances at 105°C (wt. %)	1.5
Content of water soluble materials (wt. %)	0.7
Residue on a sieve of 45 µm mesh (wt. %)	0.02
Brightness	95.5
Shade in a white paste	7.1
Relative scattering ability	86
Ability to tone down the shade	1730
Shade in a gray paste	2.0
pH in water suspension	8.0
Oil absorption number (g/100g pigment)	40

Silane proadhesive compounds produced by PIW Unisil (Tarnów, Poland) were used as the agents capable of modifying titanium white surface. The following organic coupling agents were used: 3-metacryloxypropyltrimethoxysilane (U-511), CH₂=C(CH₃)COO-(CH₂)₃Si(OCH₃)₃, vinyltrimethoxysilane (U-611), CH₂=CHSi(OCH₃)₃ and *N*-2-(aminoethyl)-3-aminopropyltrimethoxysilane (U-15D), H₂N(CH₂)₂NH(CH₂)₃Si-(OCH₃)₃.

METHODS OF STUDIES

The process of modification of titanium white surface was conducted by „the dry technique”: a reactor of 500 cm³ capacity was charged with 40 g titanium dioxide sample to which a solution of the organic modifying agent was dosed. The solution contained silane coupling agent at the amount of 0.5; 1 or 3 wt./wt. of TiO₂ and 10 cm³ of the solvent (mixture of methanol and water at 4:1). The system was mixed for 1 h to assure complete wetting of the titanium white with the solution of modifying agent. Subsequently, titanium white was dried in a stationary drier for 2 h at the temperature of 105°C.

The modified titanium white samples were subjected to morphological and microstructural analysis using scanning electron microscopy (Philips SEM 515). Size of titanium white particles as well as particle size distribution were documented using Zeatasizer Nano ZS instrument (Malvern Instruments Ltd.) employing the technique of non-invasive back scattering (NIBS). Particle size distribution curves permitted also to calculate polydispersity (as a measure of uniform character of the pigment). In order to characterize adsorptive properties of the product nitrogen adsorption/desorption isotherms were determined and parameters such as specific surface area, pore volume, mean pore size were estimated using ASAP 2010 apparatus (Micromeritics Instruments Co.). Moreover, sedimentation profiles for selected TiO₂ using Tensiometer K100 (Krüss) were evaluated.

RESULTS AND DISCUSSION

Particle size distribution, with appropriate attention given to band intensity and volume share, and the respective SEM electron microphotograph of the unmodified titanium dioxide R-213 are presented in Fig.1.

Particle size distribution analyzed in relation to intensity (Fig.1a) demonstrated a single band. The band was linked to the presence of particles of smaller and larger sizes in the range of 220 – 5560 nm (with maximum intensity of 11.2 for the particles of 615 nm in diameter). Polydispersity, representing the scatter of particle diameters, amounted to 0.233. Also in the particle size distribution analyzed by volume share (Fig.1b) a single diffuse band was present. It reflected the presence of particles, primary and secondary agglomerates of 190 – 6440 nm in diameter (with the maximum volume share of 10.2 for the agglomerates of 5560 nm in diameter). The SEM microphotograph (Fig.1c) documented the presence of spherical particles of low diameters, which formed larger aggregates and agglomerates.

Particle size distribution analyzed by band intensity or volume share for titanium dioxide R-213 modified with 3 wt./wt. 3-metacryloxypropyltrimethoxysilane are presented in Fig.2.

The particle size distribution analyzed by intensity (Fig.2a) manifested a single band. The band was linked to the presence of particles, primary and secondary

agglomerates of 190 – 5560 nm in diameter (with maximum intensity of 18.1 for the particles of 396 nm in diameter). The polydispersity amounted to 0.397. The particle size distribution analyzed by volume share showed bimodal character (Fig.2b). It was linked to the presence of particles of lower and higher diameters, ranging from 190 to 6440 nm (with maximum volume share of 13.2 for the particles of 396 nm in diameter).

Particle size distribution for titanium dioxide R-213 modified with 3 wt./wt. of vinyltrimethoxysilane is presented in Fig. 3.

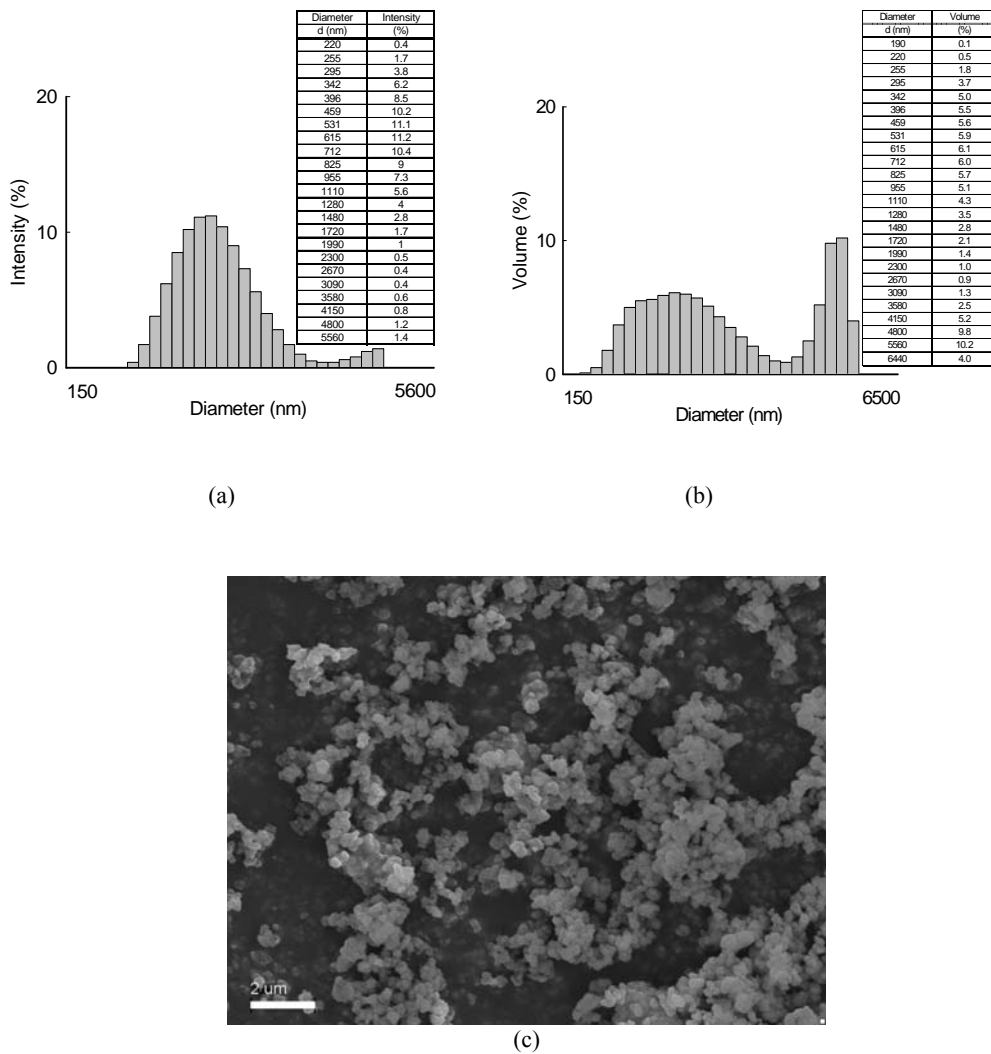


Fig. 1. Particle size distribution: (a) by intensity (b) by volume and (c) SEM image of titanium dioxide R-213

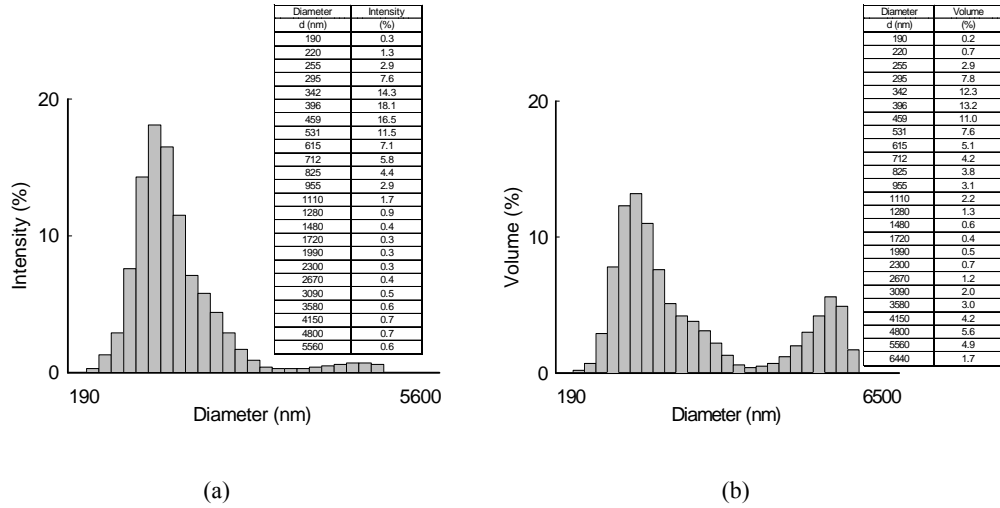


Fig. 2. Particle size distribution: (a) by intensity (b) by volume of titanium dioxide R-213 modified with 3 wt./wt. of 3-metacryloxypropyltrimethoxysilane

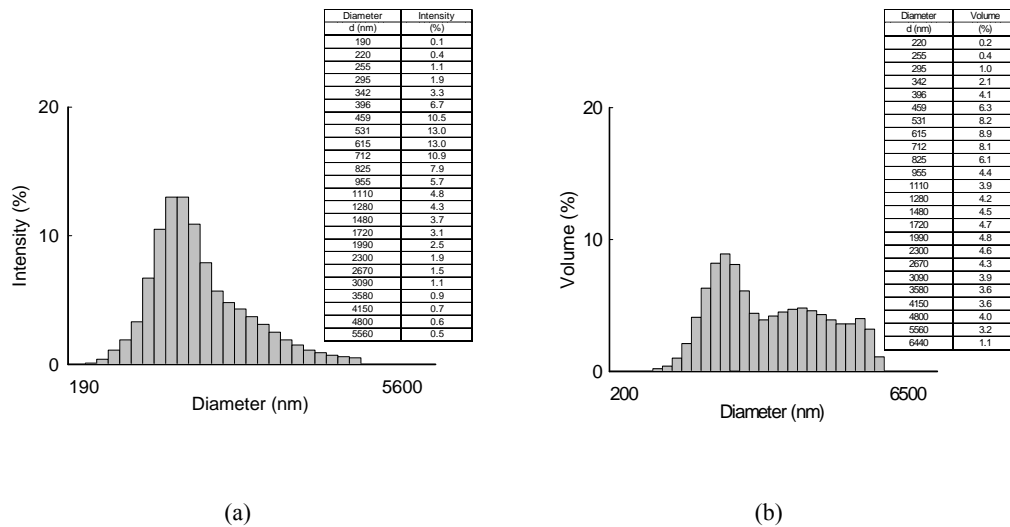


Fig. 3. Particle size distribution: (a) by intensity (b) by volume of titanium dioxide R-213 modified with 3 wt./wt. of vinyltrimethoxysilane

The particle size distribution analyzed by intensity demonstrated a single band (Fig.3a). The band was linked to the presence of primary and secondary agglomerates in the diameter range of 190 – 5560 nm (with maximum intensity of 13.0 for the particles of 531 and 615 nm in diameter). In the particle size distribution analyzed by

the volume share (Fig.3b) also a single band was noted. The band was linked to the presence of particles of smaller and higher diameters, ranging from 220 to 6440 nm (with maximum volume share of 8.9 shown by particles of 615 nm in diameter). Polydispersity of the sample amounted to 0.273.

Particle size distribution analyzed by intensity and by volume share as well as SEM microphotograph of R-213 titanium white modified with 1 wt./wt. of *N*-2-(aminoethyl)-3-aminopropyltrimethoxysilane is shown in Fig.4.

The particle size distribution analyzed in relation to intensity (Fig.4a) demonstrated a single band. The band was linked to the presence of larger and smaller particles within the diameter range of 164 – 5560 nm (with the maximum intensity of 11.7 for the particles of 459 nm in diameter). The polydispersity, reflecting the scatter of particle diameters, amounted to 0.326. Also the particle size distribution analyzed by volume share showed a single band (Fig.4b) which was linked to the presence of primary and secondary agglomerates with diameters ranging from 190 to 6440 nm (with maximum volume share of 19.2 shown by agglomerates of 5560 nm in diameter). The respective SEM microphotograph (Fig.4c) documented presence of spherical particles of a low diameter, which clumped into larger agglomerates.

Titanium white R-213 demonstrated adsorptive capacity with the range of hysteresis loop encompassing relative pressures of 0.6 – 1.0. The BET specific surface area for the R-213 white was 34.7 m²/g, while size and total volume of pores amounted to 9.8 nm and 0.08 cm³/g, respectively. The course of adsorption/desorption isotherms, which did not rise until the relative pressure of 0.6 was exceeded, and pore diameter of 9.8 nm were typical of mesoporous adsorbents. For the titanate white R-213, surface processed using aluminium and silicon compounds (in the amount of 4.7% and 8.3%, respectively), the BET specific surface area proved to be satisfactory due to the presence of higher numbers of surface active centres (silanol and aluminol groups).

Elemental analysis of the titanium white R-213 modified with the applied coupling agents is presented in Fig.5.

Following the conducted modification an increased amount of coupling agent used for the modification was found to be linked to rising elemental contents of carbon, nitrogen and hydrogen. Titanium white samples which were not modified with organic compounds manifested very low contents of carbon and hydrogen (0.1615%C and 0.4395%H). Application of any modifying agents increased contents of carbon and hydrogen, as compared to those in the unmodified titanium white R-213. The amount and the type of the applied coupling agent significantly affected the contents of carbon and hydrogen.

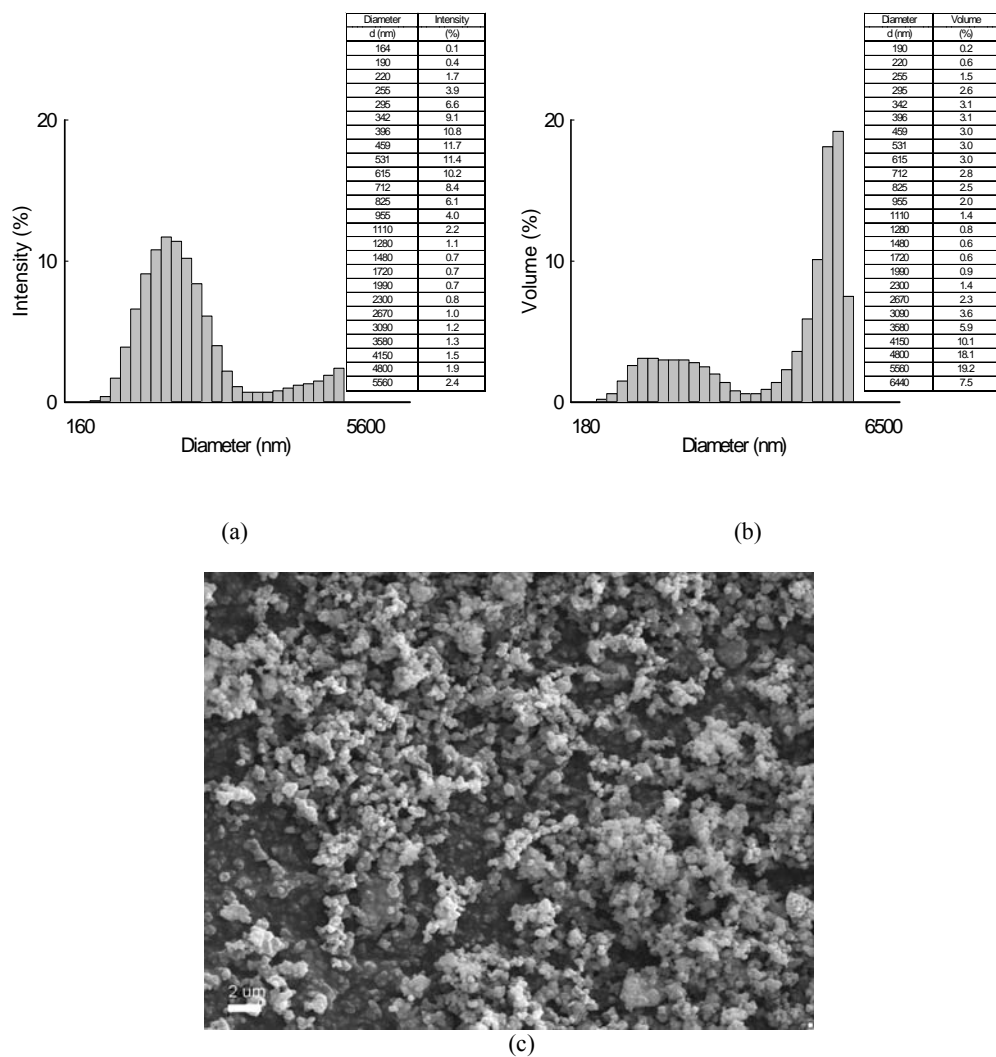


Fig. 4. Particle size distribution: (a) by intensity (b) by volume and (c) SEM image of titanium dioxide R-213 modified with 3 wt./wt. of *N*-2-(aminoethyl)-3-aminopropyltrimethoxysilane

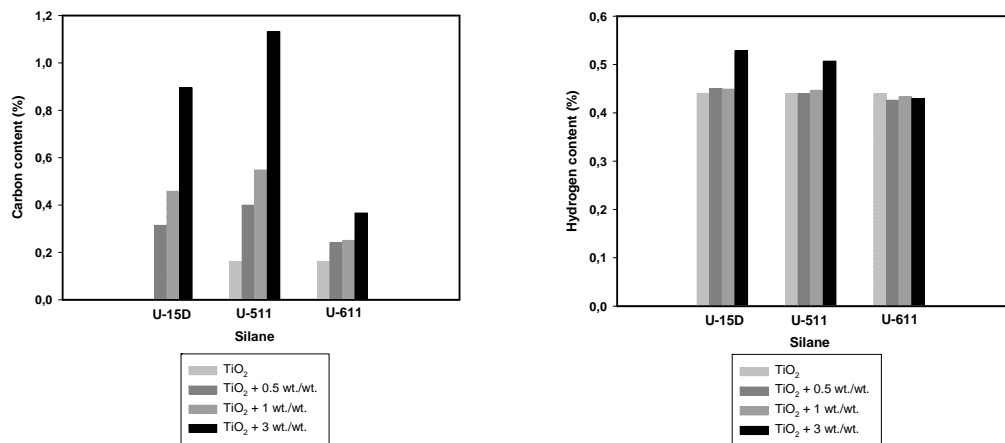


Fig. 5. Elemental content of (a) carbon and (b) hydrogen for titanium dioxide R-213

Water sedimentation profiles for titanium dioxide modified with 1 wt./wt. of the applied proadhesive compounds are presented in Fig. 6.

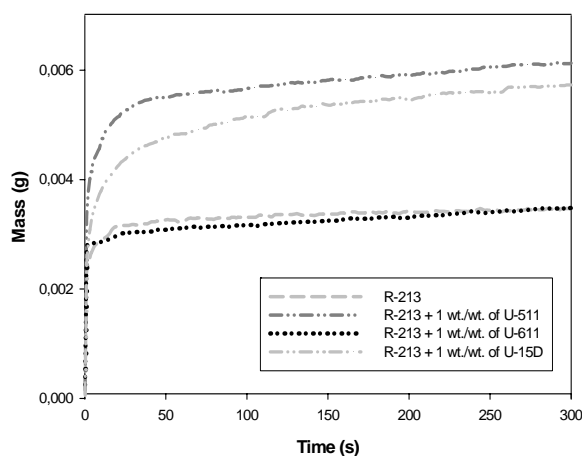


Fig. 6. Profiles of sedimentation in water of titanium dioxide R-213 modified with 1 wt./wt. of appropriate proadhesive compound

The course of curves of sedimentation in water allowed to conclude that the highest time-related increase in sediment weight was demonstrated by titanium dioxide modified with metacryloxysilane, which might be related to C and H contents in the coupling agent, which amounted to 0.548% and 0.4465%, respectively. The lowest

increase in sediment weight in time was manifested by titanium white modified with vinyltrimethoxysilane, the elemental contents of which amount to 0.2505%C and 0.433%H.

CONCLUSIONS

All the titanium white samples subjected to modification with silane coupling agents manifested particles of spherical shape. Thus, we have found that surface modification has not deteriorated morphological and microstructural character of titanium dioxide. Modification of titanium white surface using the applied silanes has promoted changes in polydispersity and in the range of particle diameters. Titanium dioxide modified with 3-metacryloxypropyltrimethoxysilane has manifested particles within a lower range of diameters as compared to the unmodified R-213, and R-213 modified with the two remaining silanes. Nevertheless, independently of the type of employed alkoxysilane modification promotes particle agglomeration which, in a sense, represents an undesirable phenomenon.

The applied for modification titanium white R-213 has demonstrated BET specific surface area of 35 m²/g. It can be included to the group of mesoporous adsorbents. Elemental analysis confirmed efficacy of the conducted modification and may be used for evaluation of the extent to which surface of titanium white is coated with an appropriate modifying agent.

3-Metacryloxypropyltrimethoxysilane has been found to be the best modifier. Titanium dioxide modified with the silane has demonstrated the most pronounced time-related increase in weight of the sediment (as compared to the two other proadhesive compounds used for the modification).

ACKNOWLEDGEMENTS

This work was supported by the 6th Framework Programme, Contract No INCO-CT-2003-003355, within the project of Scientific Network Surfactants and Dispersed Systems in Theory and Practice (SURUZ), and by the PUT Research Grant No. 32-117/07-BW.

REFERENCES

- BINKOWSKI S., JESIONOWSKI T., KRYSZTAFKIEWICZ A., 2000, *Preparation of pigments on modified precipitated silicas*, Dyes Pigm., 47, 247-257.
- KOHLER K., 1997, *Inorganic pigments--a major step in product upgrading*, Paint Ink. Intern., 10, 9-13.
- CHANTRAPORNCHAI, W., CLYDESDALE F.M., MCCLEMENTS D.J., 2000, *Optical properties of oil-in-water emulsions containing titanium dioxide particles*, Colloids Surf. A 166, 123 – 131.
- SOBOLEWSKI W., 2004, *Środki barwiące w budownictwie*, Rynek Chemii Budowlanej, 11, 24-27.
- KRYSZTAFKIEWICZ A., RAGER B., MAIK M., WIECZOREK W., 1995, *Novel aluminosilicate powders and their use as fillers and pigments*, Polish J. Appl. Chem., 39, 73-85.
- KRYSZTAFKIEWICZ A., MICHALSKA I., JESIONOWSKI T., BOGACKI M., 1999, *Zdyspergowane syntetyczne krzemiany cynku, jako przyszłościowe pigmenty ekologicznych farb krzemianowych*, Fizykochem. Problemy Mineralurgii, 33, 83-92.
- ENDRI B H., 1998, *Inorganic Coloured Pigments Today*, Curt R. Vincentz Verlag, Hannover.

CARTER S., BRISTOW D., 1998, *New applications for age old pigments*, Paint Ink. Intern., 11, 15-16.

BIENIEK D., 2004, *Biel tytanowa: mity i fakty*, Rynek Tworzyw, 5, 39-41.

MACIONGA A., 2005, *Blaski i cienie bieli tytanowej*, Rynek Tworzyw, 9, 36-37.

Siwińska-Stefańska K., Krysztafkiewicz A., Jesionowski T., *Zmiana hydrofilowo-hydrofobowego charakteru powierzchni TiO_2 przez modyfikację wybranymi silanowymi związkami wiążącymi*, Physicochemical Problems of Mineral Processing, 41 (2007) 205-214 (w jęz. ang.).

W badaniach wykorzystano biel tytanową R-213 produkowaną przez Zakłady Chemiczne Police S.A. Modyfikację powierzchni ditlenku tytanu prowadzono w celu zmiany jej charakteru fizykochemicznego. W tym celu do modyfikacji zastosowano organiczne związki wiążące z następującymi grupami funkcyjnymi: winylową, aminową i metakryloksy. Badano wpływ stężenia silanowego związku wiążącego (0,5; 1 i 3 cz.wag.) na właściwości dyspersyjne i morfologię cząstek TiO_2 . W badaniach wykorzystano techniki SEM i NIBS. Dla otrzymanych w ten sposób produktów określono skład elementarny, rozkład wielkości cząstek, powierzchnię właściwą BET oraz tendencję do sedymentacji w wodzie. Modyfikacja powierzchni zmienia charakter hydrofilowo-hydrofobowy otrzymanych preparatów, jednocześnie przyczyniając się do aglomeracji cząstek TiO_2 .

Władysław JANUSZ*, Ewa SKWAREK*, Vladimir Iljich ZARKO**,
Vladimir Moiseevich GUN'KO**

STRUCTURE OF ELECTRICAL DOUBLE LAYER AT THE Al₂O₃-SiO₂/ELECTROLYTE SOLUTION INTERFACE

Received March 15, 2007; reviewed; accepted June 4, 2007

The structures of the electrical double layer at the Al₂O₃-SiO₂/NaClO₄ interface with different alumina-to-silica ratios were interpreted using the surface complexation model. The surface charge and potential ζ of the system has been determined as a function of pH for 0.1, 0.01, and 0.001 mol/dm³ solutions of NaClO₄. A significant difference in the pH values of IEP and point of zero charge was observed for Al₂O₃-SiO₂ samples. The ionization and complexation constants have also been determined.

Key words: alumina, silica, electrical double layer, surface charge, zeta potential

INTRUDUCTION

The studies of the surface properties of mixed oxides are important for theoretical and practical reasons, because they imitate better systems that occur in nature (like soils) and technology, than the individual metal oxides. Especially, such mixed oxides are important in catalysis.

The surface charge at a metal oxide/electrolyte interface is formed as result of acid-base reactions of surface hydroxyl groups (-SOH) according to equations:

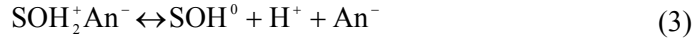


The site-binding theory of the electrical interfacial layer (eil) assumes that the background electrolyte ions play a very important role in the formation of surface

* Department Radiochemistry and Colloid Chemistry Maria Curie Skłodowska University
Pl. M.C. Skłodowskiej 3, 20-031 Lublin, Poland.

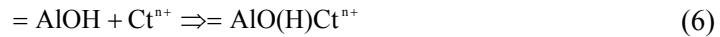
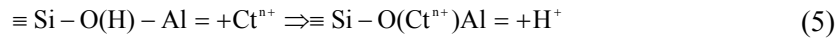
** Institute of Surface Chemistry, 31 Prospect Nuke, 03680 Kiev, Ukraine.

charge due to their specific interactions with surface hydroxyl groups of metal oxide (James and Parks, 1989). This process can be described as follows:



The equilibrium constants of reactions 1 and 2 are denoted as K_{a1} and K_{a2} , whereas those of reactions 3 and 4 as K_{An} and K_{Ct} . These constants may be calculated from the surface charge density or electrokinetic data using different methods.

Structural characteristics of $\text{Al}_2\text{O}_3\text{-SiO}_2$ depends on a synthesis method and composition of the mixed oxide. A different condition of synthesis of mixed oxides leads to changes in distribution of Al_2O_3 across particles and structure. These changes influence chemical properties of mixed oxide surface and consequently adsorption affinity of surface groups to ions from solution. Adsorption of cations on these groups will proceed as follows:



The properties of surface groups at these mixed oxides are not well described because of effect of electrostatic charge accumulation in electron spectroscopic study. For the $\text{Al}_2\text{O}_3\text{-SiO}_2$ system where Al_2O_3 has been deposited by evaporation on a flat SiO_2 surface, electron photoemission parameters such as binding energy (BE) and modified Auger parameter (α) has been analyzed by X-ray Photoemission Spectroscopy (XPS) and Reflection Electron Energy Loss Spectroscopy (REELS) (Reiche et. al., 2000).

Studies of the electrical double layer at the $\text{Al}_2\text{O}_3\text{-SiO}_2/\text{NaClO}_4$ interface and adsorption properties of such system in reference to pure, mixed and composite oxides were reported in literature (Kosmulski, 2001; Schwarz et al., 1983). A comprehensive review of the pH_{PZC} and pH_{IEP} values for such systems was presented by Kosmulski (2001). Schwarz et al. (1983) studied the surface charge density of composite SiO_2 and Al_2O_3 oxides in wide range of composition of solid phase. Their results agree with calculation by means a method suggested by Parks for calculation of the pH_{PZC} of mixed oxide system. The model assumed that each component of the binary oxide system behaves independently and the pH_{pzc} of such a mixed oxide is a linear function of amount of pure oxides. However, to achieve good agreement of calculated values and experimental pH_{pzc} for mixed oxides containing silica, the values of pH_{pzc} of silica has to be taken for calculation is too high. A similar study of the silica alumina system were carried out by Reymond and Kolenda (1999). They found that only when silica

content increases from 0 to 85 wt.%, the mixture pH_{PZC} value changes linearly with silica content. Above this value, the dependence varies as linear extrapolation of pH_{pzc} for pure oxides. Reymond and Kolenda (1999) suggest that in natural and acidic environment, aluminum oxide may dissolve, creating small particles of AlOOH , which precipitate on the SiO_2 surface. When SiO_2 concentration is high (>90%), the surface coverage by AlOOH particles is low and the particle charge is determined by the SiO_2 face. The difference in behavior in both described above systems seems to arise from the difference in the equilibration time of the system. Schwarz et al. (1992) assumed it as 10 min., but Reymond and Kolenda (1999) carried out pH measurements after 24 hours. In such studies, during a long time of equilibration the subsequent dissolution and precipitation of AlOOH process took place in the system. The aim of the paper was to characterize the electrical double layer parameters at the $\text{Al}_2\text{O}_3\text{-SiO}_2/\text{NaClO}_4$. In both papers, the authors in their experiments used magnetic stirrer during titration and this device may grind solid particles, so it is not recommended for potentiometric titration purposes (Janusz, 2000).

The pH_{PZC} measurements for the mixed oxides $\text{Al}_2\text{O}_3\text{-SiO}_2$ which were prepared by a co-precipitation of $\text{Na}_2\text{SiO}_3 + \text{Al}(\text{NO}_3)_3$ in NaNO_3 solution showed, that the pH_{PZC} point shifts to the lower pH value with increase of the SiO_2 concentration in the mixed oxide. For mixed oxide with composition of 50-60% Al_2O_3 the $\text{pH}_{\text{pzc}}=4.5$. For 70% Al_2O_3 $\text{pH}_{\text{pzc}}=5.8$ and for 80% Al_2O_3 the $\text{pH}_{\text{PZC}}=7$ (Kuo and Yen, 1988).

In this paper, some studies on the electrical double layer at mixed silica-alumina oxides/electrolyte solution are presented. Measurements comprise surface charge and zeta potential in the NaClO_4 solutions. The experimental data were used for theoretical calculations of the ionization and complexation constants of reactions of the surface hydroxyl groups. The results of these calculations allowed to estimate the shares of respective surface groups in the surface charge at the mixed silica-alumina oxides/electrolyte solution interface.

EXPERIMENTAL

MATERIALS AND METHODS

The $\text{Al}_2\text{O}_3\text{-SiO}_2$ systems were prepared using the fumed method. The samples of mixed oxide of silica-alumina contain the following amount of Al_2O_3 : 30, 23, 8, 3 and 1% and was described as AS30, AS23, AS8, AS3, AS1, respectively. By means of the nitrogen adsorption-desorption isotherms using a Micrometrics ASAP, the structural characteristics of studied materials were obtained and are collected in Table 1.

S_{BET} (the specific surface area) was calculated according to the BET method (Adamson and Gast, 1997) using adsorption data at relative pressures p/p_o between 0.05 and 0.25, where p and p_o denote the equilibrium pressure. The pore volume V_p was evaluated from the adsorption data using the BJH (Barrett-Joyner-Halenda) method. The R_p (pore radius), S_{BET} , and V_p were utilized to estimate the average specific surface area of mesopores S_K was calculated using the Kiselev equation. The

surface area S_{mes} and volume V_{mes} of mesopores were also calculated using the theory of capillary evaporation by the improved program package described in detail elsewhere (Gun'ko, 1992). The all studied systems contained micropores.

Table 1. Structural AS parameter (Gun'ko et al., 2004)

Sample	AS1	AS3	AS8	AS23	AS30
S_{BET} [m ² /g]	207	188	308	353	239
V_p [cm ³ /g]	0.42	0.39	0.66	0.8	0.57
R_p [nm]	3.7	3.8	3.8	4	4.8
S_K [m ² /g]	158	146	241	283	-
S_{mes} [m ² /g]	90	82	135	158	-
V_{mes} [cm ³ /g]	0.18	0.16	0.26	0.28	-

where:

S_{BET} - the specific surface area;

V_p - the pore volume

R_p - pore radius

S_K - specific surface area was calculated using the Kiselev equation

S_{mes} - surface area was calculated using the theory of capillary

V_{mes} - volume of mesopores

Particle size distribution and electrophoresis study were carried out using a Zetasizer 300 (Malvern Instruments) apparatus based on photo correlation spectroscopy (PCS). The dispersions of silica-alumina oxide (100 ppm of solid) prior electrokinetic and particle size measurements were ultrasonicated for 3 min using an ultrasonic disperser (Sonicator Misonix Inc.). The results of particle size measurements are presented in Table 2. The zeta potential of the Al₂O₃-SiO₂ dispersions was determined by electrophoresis with Zetasizer 3000. The pH values, measured by a precision digital pH meter were adjusted by addition of 0.1 mol/dm³ HClO₄ or NaOH solution.

Table 2. The particle size and factors of polydispersity

Sample	AS1	AS3	AS8	AS23	AS30
Mean particle size, nm	255	259	235	253	244
Factors polydispersity	0.18	0.22	0.17	0.2	0.06

As it can be seen from Table 2 that the values of particle size and polydispersity of samples containing different amount of alumina are similar, so the same formula for zeta potential calculation from electrophoretic mobility had been used.

Surface charge measurements were performed in suspensions having such solid contents to ensure the same surface area to electrolyte volume ratio, to keep identical conditions of the experiments in a thermostated Teflon vessel at 25°C. To eliminate

the influence of CO_2 , all potentiometric measurements were performed under nitrogen atmosphere. pH values were measured using a set of glass REF 451 and calomel pHG201-8 electrodes with Radiometer assembly. Surface charge density was calculated from the difference of the amounts of acid or base added to obtain the same pH value of the suspension as the background electrolyte.

RESULTS AND DISCUSSION

Table 3 presents the values of pH_{PZC} and pH_{IEP} for the studied $\text{Al}_2\text{O}_3\text{-SiO}_2$ oxides/electrolyte solution interface.

Table 3. Values of pH_{PZC} and pH_{IEP} for the $\text{Al}_2\text{O}_3\text{-SiO}_2/\text{NaClO}_4$ solution system

	AS1	AS3	AS8	AS23	AS30
pH_{PZC}	4	4	4	4.4	4.6
pH_{IEP}	<3	<3	<3	<3	<3

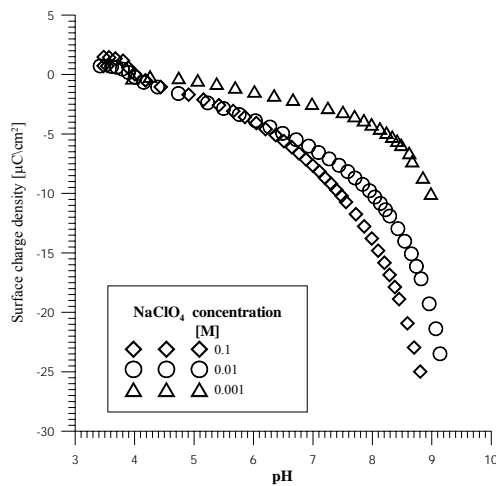


Fig. 1. Surface charge density at the AS1/ NaClO_4 solution interface as a function of pH

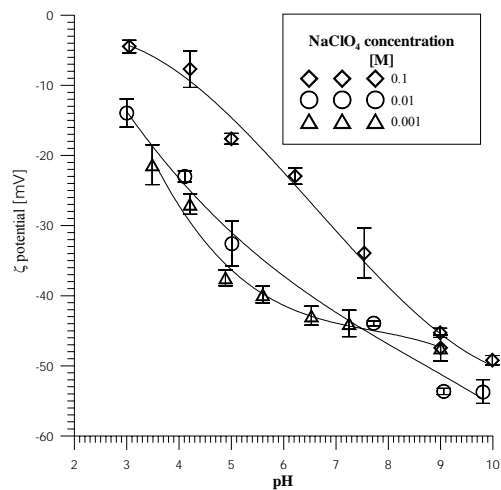


Fig. 2. The ζ potential of AS1/ NaClO_4 solution interface function of pH

Figs 1, 3 and 5 present the surface charge density as a function of pH for three concentrations of NaClO_4 solutions for AS1, AS3 and AS23 samples, respectively. The change of pH_{PZC} with the percentage of Al_2O_3 in the $\text{Al}_2\text{O}_3\text{-SiO}_2$ sample depends of the acid-base properties of the surface hydroxyl groups (that are determined by atoms that surround the oxygen). At low Al_2O_3 concentration, the SiO_2 layer probably covers the oxide surface.

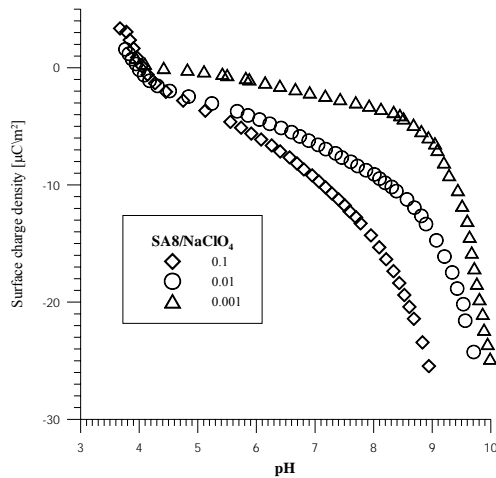


Fig. 3. Surface charge density at the AS3/NaClO₄ solution interface as a function of pH

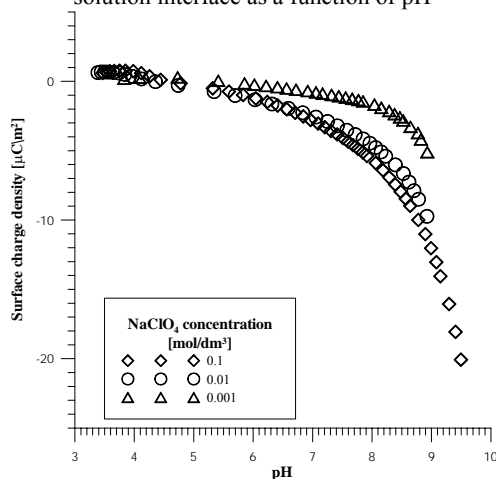


Fig. 5. Surface charge density at the AS23/NaClO₄ solution interface as a function of pH

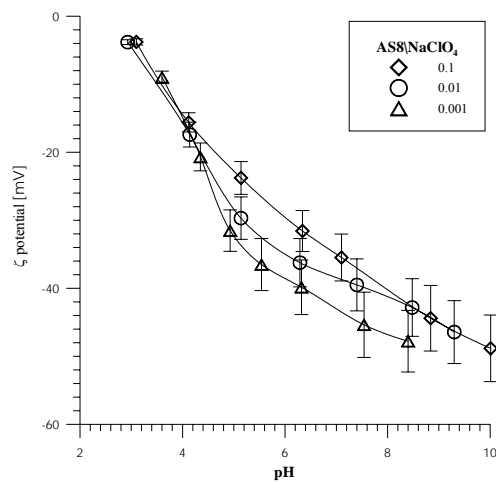


Fig. 4. The ζ potential of AS3/NaClO₄ interface solution function of pH

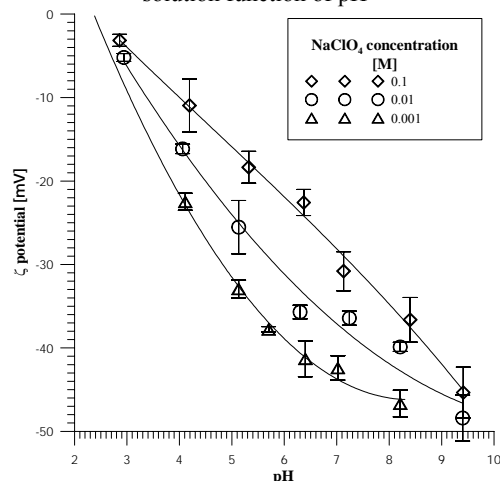


Fig. 6. The ζ potential of AS23/NaClO₄ interface solution function of pH

After exceeding certain aluminum oxide concentration in surrounding of oxygen of surface hydroxyl groups, the Al(III) atoms may appear. That means that the substrate ratio and method of sample preparation influences the subsurface region composition and it may differ from the bulk composition of particle. The surface hydroxyl groups on such oxides may have acidic character (as $\equiv \text{SiOH}$) or totally different basic character (as $= \text{AlOH}$). There may occur also groups of higher coordination level eg. $= (\text{AlO})_3\text{OH}$ or mixed as $\equiv \text{SiO(H)Al}\equiv$ which also have more acidic. According to Sempels and Rouxhet (1976) the last one group has about $\frac{1}{4}$ weaker acidic character than $\equiv \text{SiOH}$.

The ζ potential of AS1, AS3 and AS23 samples in the NaClO_4 solution as a function of pH is presented in Fig. 2, 4 and 6. As it can be seen from these Figs that the ζ potential decreases with the increase of the pH and increases with electrolyte concentration. For all studied samples only negative values of zeta potential were observed. The pH_{IEP} and pH_{PZC} values for all $\text{Al}_2\text{O}_3\text{-SiO}_2/\text{NaClO}_4$ systems are collected in Table 3. A comparison of the pH_{PZC} and pH_{IEP} values is presented in Table 4. The pH_{IEP} values are below $\text{pH}=3$ for all mixed oxide whereas the pH_{PZC} for the mixed oxides of low percentage of alumina are equal to 4 while for higher aluminum oxide concentration the pH_{PZC} shifts to a higher pH value. The difference between pH_{PZC} and pH_{IEP} may arise from different surfaces of oxide accessible in the potentiometric titration and electrophoresis experiments. Since the studied $\text{Al}_2\text{O}_3\text{-SiO}_2$ oxides have mean pores radius about 4 nm, that is almost equal to the electrical double layer thickness for 0.01 mol/dm^3 NaClO_4 solutions, for lower concentration of the electrolyte solutions the double layers from individual walls of pores may overlap. Part of pores may be smaller than 1nm and assuming that the slipping plane is 1.5 nm from the solid surface, such pores maybe blocked during electrophoresis, so the surface properties of this part of the solid will not be active during electrophoresis. A great part of charge may be compensated inside particle pores and only part, created by ionized groups on the oxide surface, is responsible for electrophoretic mobility. The pH_{PZC} and pH_{IEP} values of SiO_2 reported in literature range from 1 to 3 (Jung, 2001; Pickup et al., 1999; Gunawidjaja et al., 2003 and for Al_2O_3 respective values are from 8 to 9 (Parks, 1967). Comparing this to values for the $\text{Al}_2\text{O}_3\text{-SiO}_2$ system, one can see that the SiO_2 surface has decisive influence on the mixed oxide surface properties.

Basing on the potentiometric titration data, the ionization and complexation constants of surface hydroxyl groups were calculated for the electrical interfacial layer on $\text{Al}_2\text{O}_3\text{-SiO}_2/\text{NaClO}_4$ using the TLM theory. The ionization and complexation constants of the surface hydroxyl groups were calculated using the approaches by Davis et al. (1978), Sprycha (1984), the modified Schwarzenbach method (Schwarzenbach and Ackerman, 1948), and a numerical optimization method basing on the surface charge density versus pH and electrolyte concentration data for the AS1/ NaClO_4 system. The calculated values are collected in Table 4. One can see a better agreement of the constants with the values calculated by the Davis et al. method than by the Schwarzenbach method and numerical optimization. Small values of pK_{a1} and pK_{Cl} indicate that positive groups are scarce. The contribution of the particular surface groups in the surface charge of AS1 is depicted in Fig.7. As it can be seen, the calculated concentration of surface charge density with data obtained experimentally shows acceptable consistency for both values (Fig.7). The results for one system only has been presented because of similar tendency for others concentration background electrolyte.

Comparing the constants values of hydroxyl groups for system $\text{Al}_2\text{O}_3\text{-SiO}_2$ with the data from literature for $\text{SiO}_2/\text{NaClO}_4$ ($pK_{a2}=5.7$; $pK_{Na}=7.24$) (Sprycha, 1982) and for

$\text{Al}_2\text{O}_3/\text{NaClO}_4$ ($pK_{a1}=4.45$, $pK_{a2}=8.45$) (Davis et al., 1978), we can see that acid-base character of surface hydroxyl groups bond with Al or Si in mixed $\text{Al}_2\text{O}_3\text{-SiO}_2$ oxide is different than SiO_2 or Al_2O_3 alone. The surface properties of $\text{Al}_2\text{O}_3\text{-SiO}_2$ cannot simply be described by addition of surface properties of hydroxyl groups to the pure SiO_2 or Al_2O_3 .

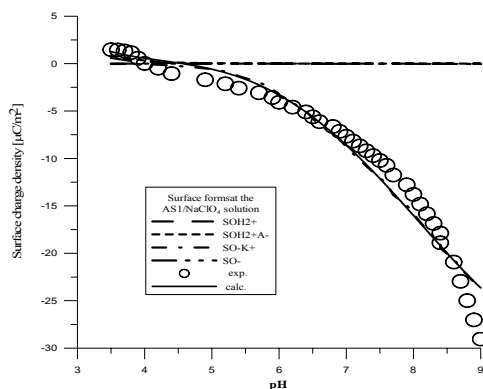


Fig. 7. Model calculation of concentration of surface groups forms at the AS1/0.1 M NaClO_4 solution interface

Table 4. The values of surface ionization and complexation constants for AS/ NaClO_4 system

Constants	Method		
	AS1		
	Davis <i>at al.</i>	Modified Schwarzenbach's	Numerical Optimization
pK_{a1}	1.01	3.63	1.37
pK_{a2}	9.7	6.62	10.99
pK_{Cl}	2.04	5.67	2.07
pK_{Na}	6.7	0	5.96
AS3			
pK_{a1}	2.5	5.74	1.96
pK_{a2}	8.28	8.62	13
pK_{Cl}	-0.29	0	0.004
pK_{Na}	6.96	6.62	6.76
AS8			
pK_{a1}	1.5	2.11	1.82
pK_{a2}	5.71	6.32	6.74
pK_{Cl}	1.9	3.22	3.53
pK_{Na}	6.04	5.15	4.85
AS23			
pK_{a1}	1.34	1.56	2.4
pK_{a2}	7.14	7.72	7.51
pK_{Cl}	2.1	2.71	2.13
pK_{Na}	7.1	7.44	7.3
AS30			
pK_{a1}	5.77	5.23	1.8
pK_{a2}	7.79	8.11	10
pK_{Cl}	0.4	0	1.59
pK_{Na}	7.4	6.85	6.68

One can see a good agreement of the constants with the values calculated by various methods. For example AS1 - Davis et al. method and numerical optimization except pK_{a2} , for AS3 system - Davis et al., then Schwarzenbach's method (without pK_{a1}) and numerical optimization. For AS8 system - Davis et al. method (without pK_{Cl} , pK_{Na}), than Schwarzenbach's method and numerical optimization, and for mixed oxide AS23 and AS30 - Davis et al., then Schwarzenbach's method and numerical optimization (without pK_{a1} , pK_{Na}). Small values of pK_{a1} , pK_{Cl} for all mixed oxide, suggest low number of the concentration of positively charged groups on the surface. Comparing surface hydroxyl groups reaction constants obtained for $\text{Al}_2\text{O}_3\text{-SiO}_2$ systems with literature data for $\text{SiO}_2/\text{NaClO}_4$ ($pK_{a2}=5.7$; $pK_{Na}=7.24$) (Kosmulski, 1997) and for $\text{Al}_2\text{O}_3/\text{NaClO}_4$ ($pK_{a1}=4.45$, $pK_{a2}=8.45$) (Brady, 1994), one can see that the acid-base character of the surface hydroxyl groups bonded to Al or Si atoms in mixed $\text{Al}_2\text{O}_3\text{-SiO}_2$ oxides differs from the one for SiO_2 or Al_2O_3 , without pK_{a2} for AS3 (Davis et al. and Schwarzenbach's method), pK_{a2} for AS8 (Davis et al. method), pK_{Na} for AS23 (Davis et al. then Schwarzenbach's method and numerical optimization). According to above it is rather impossible to describe properties of SiO_2 and Al_2O_3 by simple surface properties summation in the case of the $\text{Al}_2\text{O}_3\text{-SiO}_2/\text{NaClO}_4$ interface.

CONCLUSION

The aim of this paper was to characterize the electrical double layer structure at the $\text{Al}_2\text{O}_3\text{-SiO}_2/\text{NaClO}_4$ interface. The properties of the interface of the mixed oxide/electrolyte solution in a wide range of concentration, mechanism of surface charge creation, and structure of the edl were described. Complex investigations of the mixed oxides/electrolyte interface properties have been carried out for wide concentrations range taking into account the influence of ionic strength on the surface charge generation mechanism and edl composition. The experimental data acquired were used to describe quantitatively the electrical double layer with use of proper models.

1. On basis of the dependences of surface charge density as a function of pH and electrolyte concentration the values of surface ionization and complexation constants for system $\text{Al}_2\text{O}_3\text{-SiO}_2/\text{NaClO}_4$ were calculated. The contributions of the particular surface groups in the surface charge of $\text{Al}_2\text{O}_3\text{-SiO}_2$ were calculated. Calculated concentration of surface charge density shows acceptable consistency with the data obtained experimentally.
2. Parks' theories related to foreseeing the IEP(s) of oxide and Parks' theories modification (Yoon theories and MUSIC) are unable to determine exactly the pH_{PZC} value of mixed oxide because the acid-base surface hydroxyl groups properties are depended on concentration and surface structure.
3. The mixed $\text{Al}_2\text{O}_3\text{-SiO}_2$ oxides with various Al_2O_3 concentrations showed differences between pH_{PZC} and pH_{IEP} value not correlated with oxide composition.

REFERENCES

- ADAMSON A.W., GAST A.P., (1997) *Physical Chemistry of Surface*, 6th ed., Wiley, New York,
- BRADY P., (1994), „*Alumina surface chemistry at 25, 40 and 60 °C*”, *Geochim. Cosmochim. Acta* 58, 1213-1221.
- DAVIS J.A., JAMES R.O., LECKI J.O., (1978), “*Surface ionization and complexation at the oxide / water interface. I Computation of electrical double layer properties in simple electrolyte.*”, *J. Colloid Interface Sci.*, 63, 480 - 491.
- GUN'KO V.M (1989) “*Razczjot Parametrov Mikroporistoj Struktury i Isledovanije Poverchnosti Mesopor Uglerodnych Adsorbentov*”, *Zh. Fiz. Khim.*, 63, 205.
- GUN'KO V.M. ZARKOV.I., MIRONYUK I.F., GONCHARUK E.V., GUZENKO N.V., BORYSENKO M.V., GORBIK P.P., MISHCHUK O.A., JANUSZ W., LEBODA R., SKUBISZEWSKA-ZIĘBA J., GRZEGORCZYK W., MATYSEK M., CHIBOWSKI S., (2004) “*Surface electric and titration behavior of fumed oxides*”, *Colloids Surf., A*, 240, 9-25.
- JAMES R.O., PARKS G. A. (1989), *Characterization of Aqueous Colloids by Their Electrical Double – Layer and Intrinsic Surface Chemical Properties* in. *Surface and Colloid Sci.* vol.12, p.229 Wiley-Interscience New York.
- JANUSZ W., 2000 *Praca habilitacyjna (D.Sc.thesis)*, Wydawnictwo UMCS.
- JUNG M., (2001), “*NMR characterization on the preparation of sol-gel derived mixed oxide materials*”, *Int. J. Inorg. Mater.*, 3, 471-478.
- KOSMULSKI M., (1997), “*The effect of the ionic strength on the adsorption isotherms of nickel on Silics*” *J. Colloid Interface Sci.*, 190, 212-223.
- KOSMULSKI M., 2001, *Chemical Properties of Material Surfaces*, *Surfactant Sci. Series v. 102*, M. Dekker Inc.
- KUO J.F., YEN T.F., (1988), “*Some aspects in predicting the point of zero charge of a composite oxide system*” *J. Colloid Interface Sci.*, 121, 220-225.
- PARKS G.A., (1967), in: *Equilibrium Concepts In Natural Water System*, R.F. Gould Ed., ACS Washington DC p. 121.
- PICKUP D.M., MOUNTJOY G., WALLIDGE G.W., ANDERSON R., COLE J. M., NEWPORT R. J., SMITH M.E., (1999), “*A structural study of (TiO₂)_x(SiO₂)_{1-x}(x=0.18, 0.30 and 0.41) xerogels prepared using acetylacetone*” *J. Mater. Chem.*, 9, 1299 - 1305.
- REICHE R., YUBERO F., ESPINOS J.P., GONZALEZ-ELIPE A.R. (2000), “*Structure microstructure and electronic characterization of the Al₂O₃/SiO₂ interface by electron spectroscopes*” *Surface Sci.*, 457, 199-210.
- REYMOND J.P., KOLENDA F., (1999), *Estimation of the point of zero charge of simple and mixed oxides by mass titration*”, *Powder Technol.* 103, 30-36.
- SCHWARZ J.A., DRISCOLL C.T., BHANOT A.K., (1983), “*The zero point of charge of silica-alumina oxide suspensions*”, *J. Colloid Interface Sci.*, 97, 55-61.
- SCHWARZ J.A., UGBOR C.T., ZHANG R., (1992), “*The adsorption / impregnation of a composite oxide system*” *J. Colloid Interface Sci.*, 121, 220-225.
- SCHWARZ J. A., DRISCOLL C.T., BHANOT A. K., (1994); “*The zero point of charge of silica-alumina oxide suspensions*”, *J. Colloid Interface Sci.*, 97, 55-61.
- SCHWARZENBACH G., ACKERMAN H., (1948), “*Komplexone XII. Die Homologen der Äthylendiamine-tetraessigsäure and Ihre Erdalkalikomplexe*”, *Helv. Chim. Acta*, 31, 1029-1038.
- SEMPELS R., ROUXHET P.G., (1976), “*Infrared study of the adsorption of benzene and acetonitrile on silica-alumina gels: Acidity properties and surface heterogeneity.*”, *J. Colloid Interface Sci.*, 55, 263-273.
- SPRYCHA R., (1982), “*Determination of electrical charge at Zn₂SiO₄/solution interface*” *Colloid Surf.*, 5, 147-157.
- SPRYCHA R., (1984), “*Estimation of surface ionization constants from electrokinetic data*” *J. Colloid Interface Sci.* 102, 173 - 182.

Janusz W., Skwarek E., Zarko V.I., Gun'ko V.M., *Struktura podwójnej warstwy elektrycznej na granicy faz Al₂O₃-SiO₂/roztwór elektrolitu*, Physicochemical Problems of Mineral Processing, 41 (2007) 215-225 w jęz. ang.).

Badania właściwości powierzchniowych tlenków mieszanych są ważne z praktycznego i teoretycznego powodu, ponieważ są szeroko rozpowszechnione w glebach i nowoczesnych technologiach np. jako katalizatory. Struktura podwójnej warstwy elektrycznej na granicy faz Al₂O₃-SiO₂/NaClO₄, z różną zawartością objętościową tritlenku glinu w badanych układach została zinterpretowana przy użyciu odpowiedniego modelu pwe. Określono gęstość ładunku powierzchniowego i wartość potencjału dzeta w zależności od pH dla następujących stężeń elektrolitu 0.1, 0.01 i 0.001 mol/dm³ NaClO₄. Obliczono stałe jonizacji i kompleksowania metodą optymalizacji numerycznej dla poszczególnych układów oraz porównano wartości gęstości ładunku powierzchniowego wyznaczonego metodą miareczkowania potencjometrycznego do wyznaczonego teoretycznie.

Sławomir WIERZBA*, Małgorzata NABRDALIK*

BIODEGRADATION OF CELLULOSE IN BOTTOM SEDIMENTS OF TURAWA LAKE

Received April 25, 2007; reviewed; accepted July 5, 2007

In the presented study the attempt at conducting biodegradation of bottom sediments of Turawa Lake was made. In the research cellulolytic bacteria strains were employed and the biodegradation assumed 19% reduction of the total cellulose content. At the beginning cellulolytic bacteria, originating from the bottom sediments, were isolated and selected. Next step involved evaluation of the cellulolytic activity of bacteria strains and selection of the three most vigorous, to be used in the process of bottom sediments biodegradation. The amount of decomposed cellulose was assessed with the use of anthrone method and changes in bacteria enumeration were determined with the index method. The most efficient group, regarding biodegradation of cellulose, was the mixture of the following bacteria species: *Cytophaga* and *Cellulomonas*. The reduction obtained was equal to 66%, and the bacteria enumeration increased 300-fold, to finally reach the level of the Most Probable Number equal to 10^5 NPL per 1g of the bottom sediment.

Key words: biodegradation, cellulose, bottom sediment, Cytophaga, Cellulomonas

INTRODUCTION

Organic matter, produced in lakes *in situ* in photosynthesis processes by phytoplankton and aquatic higher plants and organic matter deriving from the outer sources delivered by the surface water containing cellulose, is decomposed in aerobic conditions (in water and surface layer of the sediments) as well as in anaerobic conditions (in deeper layers of the water and bottom sediments). Cellulose in its pure form is very rare, and most often it is associated with other polysaccharides and lignin complexes, which has a significant influence on its decomposition rate by microorganisms. Biological decomposition of cellulose and its derivatives requires specific enzymes, which catalyze the reaction of breaking it down to less complicated constituents (disaccharides and monosaccharides), that are easier absorbed by the microorganisms. Bottom sediments, accumulated in Turawa Lake for over 60 years, are mainly sapro-

* Opole University, Chair of Biotechnology and Molecular Biology, ul. Kominka 4, 45-035 Opole, e-mail: slawi@uni.opole.pl

pellic muds containing up to 25% of organic matter. The thickness is varied and fluctuates between ca. 10 cm to almost 2 m, and the capacity is estimated of 4 mln sq metres (Teisseyre 1984). Polysaccharides such as: cellulose, hemicellulose and fibre are the main dominants in the content of organic matter in bottom sediments. Therefore, one of the methods for reducing their amount seems to be biodegradation conducted in natural conditions, by means of carefully selected cellulolytic bacteria strains.

The objective of the study was evaluation of the possibility to biodegrade cellulose in bottom sediments of Turawa Lake with the application of cellulolytic bacteria strains, isolated from the lake water and sediments.

MATERIALS AND METHODS

BOTTOM SEDIMENT

For the investigation, bottom sediment containing ca. 19% of cellulose and pH 6.5 was collected from the north-west part of Turawa Lake, from the depth of 4-5m. It was initially shredded and dried, obtaining 10kg of material for tests.

AUTOCHTHONIC MICROFLORA ISOLATION

Cellulolytic bacteria were isolated in two stages. First, little amount of fresh bottom sediment was placed directly on solid Waksman medium with powdered cellulose (Burbińska et al., 1983) and incubated at 21⁰C, for 7-14 days. In the second stage, typical mucous colonies of cellulolytic bacteria were inoculated into liquid Park medium (Górska and Russel, 1997; Vardavakis 1989) with filter paper discs. The bacteria cultures, prepared as above, were incubated at 21⁰C for 14 days. Only cultures with distinct cellulose decomposition were classified for the further investigation. Strains presence of the following species: *Cytophaga*, *Cellulomonas* and *Bacillus* (Holt and Krieg 1984) was confirmed during microscopic, macroscopic and biochemical identification. Biochemical tests were performed with the use of traditional methods and microanalyser mini API.

EVALUATION OF ENZYMATIC ACTIVITY OF ISOLATED STRAINS

Six isolated bacteria strains marked respectively as: *Cytophaga* C1, *Cytophaga* C2, *Cytophaga* C3, *Cellulomonas* C4, *Cellulomonas* C5 and *Bacillus* C6 were subjected to the cellulolytic activity evaluation. Prior to marking, they were grown in a liquid Park medium with blotting stripes at 21⁰C for 14 days. The evaluation was carried out by analyzing the weight loss in filter paper discs, during 28 days of culturing on Park medium. In order to achieve this, 150 cm³ of Park medium, 250 mg of filter paper discs and 5 cm³ of the cellulolytic bacteria culture were inoculated into a flask of 250 cm³ capacity. The parallel procedure was applied to the 5 remaining isolated strains. Incubation was conducted at 21⁰C on a rotation shaker and the weight loss in the discs was measured every 14 days.

BIODEGRADATION OF BOTTOM SEDIMENT

Biodegradation of the sediment was carried out in a laboratory conditions, in 5 glass containers filled with 2 kg of the bottom sediment and 5 dm³ of the water from Turawa Lake. Each of the three containers was inoculated with 25 cm³ of the one most vigorous cellulolytic bacteria strain. The fourth one contained the mixture of all three strains. Last container was a control treatment. Biodegradation was carried out at 21⁰C, for 6 months and every 2 weeks the microbiological and chemical analysis of the sediment was performed. Water which evaporated from the container was refilled regularly with the lake water.

MICROBIOLOGICAL AND CHEMICAL ANALYSIS OF THE SEDIMENTS

In the microbiological quantitative analysis, the cellulolytic bacteria enumeration was determined with the index method on Park medium with blotting stripes. The Most Probable Number of bacteria (MPN) per 1g of sediment was stated according to the Mc'Crady's tables (Grabińska-Loniewska, 1996). Chemical analysis included determination of cellulose content, with the aide of anthrone method, by stating the amount of liberated glucose after hydrolysis (Kłyszajko-Stefanowicz, 1980).

RESULTS AND DISCUSSION

The results of cellulolytic activity evaluation of the strains isolated from the bottom sediments, are presented in Table 1 and Figure 1.

Table 1. Cellulolytic activity evaluation of isolated strains¹

Bacteria strains	Cellulose weight [mg]		
	1 day	14 days	28 days
<i>Cytophaga</i> C1	250.0	144.2	84.9
<i>Cytophaga</i> C2	250.0	194.2	159.3
<i>Cytopgaha</i> C3	250.0	196.1	111.7
<i>Cellulomonas</i> C4	250.0	201.2	118.6
<i>Cellulomonas</i> C5	250.0	205.1	123.5
<i>Bacillus</i> C6	250.0	218.8	175.4

¹ – cellulolytic activity evaluation was based on the cellulose weight loss in 28 days' strains cultures.

Six identified strains, belonging to the species: *Cytophaga*, *Cellulomonas* and *Bacillus* were subjected to the analysis. In the first 2 weeks the highest enzymatic activity characterised aerobic *Cytophaga* rods, marked as C1. Cellulose reduction amounted 42.32%, and its content was reduced from 250.0 mg to 144.2 mg. The enzymatic activity of the other *Cytophaga* strains (C2 and C3) and *Cellulomonas* (C4 and C5) was

about 2-fold lower. The amount of cellulose ranged between 205.1 mg and 194.2 mg, which corresponded to the reduction level between 17.96% - 22.32%. The lowest cellulolytic activity characterized *Bacillus* strain (C6) and the cellulose decrease amounted 12.48%. After 28 days of cultivation, again the most vigorous strain was C1 of *Cytophaga* species. Recorded cellulose reduction amounted 66.04% and its content dropped to 84.9 mg. Lower activity (by ca. 10%) was stated for C3 strain of *Cytophaga* species – after 4 weeks cellulose content amounted 111.7 mg. It was slightly lower in the bacteria cultures with *Cellulomonas* (C4 and C5) and ranged between 118.6 mg and 123.5 mg, while cellulose reduction was 52.56% and 50.60% respectively. After 28 days (similar to the period of 14 days) the lowest activity characterized the strain of *Bacillus* species (C6). The cellulose content dropped to 175.4 mg, which corresponded to the reduction of 29.84%.

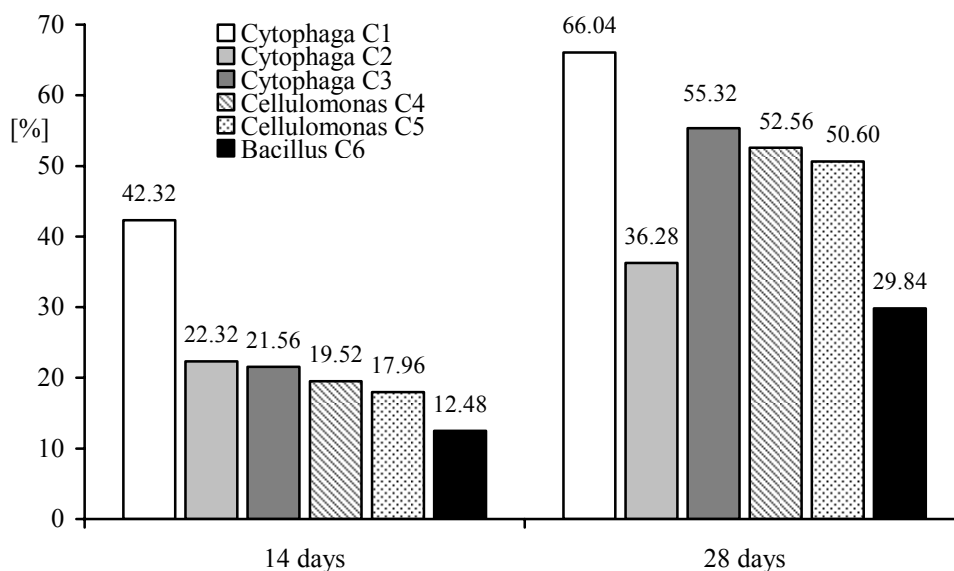


Fig. 1. Reduction of the cellulose content by the strains isolated from bottom sediments

High cellulolytic activity of *Cytophaga* and *Cellulomonas* species was confirmed in many authors' researches (Bujak and Targoński, 1988; Land et al., 2002; Liebert et al., 1984; Trojanowski, 1973) and can be explained by the fact that mentioned bacteria have the ability to synthesize both cellulase and cellobiase enzymes, that perform hydrolysis of cellulose, fibre, starch, chitin and many other polysaccharides. According to Janas et al. (2004) the highest rate of cellulose decomposition takes place in the neutral environment and is stimulated by the presence of Ca^{2+} , Mn^{2+} , Fe^{2+} and Cu^{2+} ions. The authors confirm also inductive influence of the substrate (cellulose) on the biosynthesis of cellulolytic enzymes. In the presented study, enzymatic activity of the

rod bacteria of *Cellulomonas* species was lower after 14 and 28 days when compared to *Cytophaga* strain (C1), by 22-24% and 13-16% respectively. Obtained results are in accordance with the results obtained by Gołębiewska (1992), who noted 50-60% lower activity of *Cellulomonas* strains in the process of cellulose degradation when compared to *Cytophaga*, after 15 and 20 days of cultivation. The author also stated that bacteria *Cellulomonas* do not mineralize cellulose completely, but are able to produce side products, e.g. uronic acid and pigments. *Bacillus* strain (C6) employed in the analysis, was characterized by over 2-fold lower efficiency in the process of cellulose decomposition, when compared to the most vigorous strain. It is commonly known, that cellulose decomposition requires enzymes (among others: endoglucanase, exoglucanase and β -glucosidase) acting together in synergism (Bujak and Targoński, 1988; Górska and Russel, 1997; Land et al., 2002). The researches conducted by Beguin and Aubert (1994) indicate, that most *Bacillus* rods have the ability to synthesize endo- β -1,4-glucanase which is necessary only for decomposition of soluble cellulose derivative, such as: carbomethylcellulose. Decomposition of natural cellulose, which also contains crystallin areas, is catalyzed by exo- β -1,4-glucanase followed by cellobiase. However, disability to synthesize these enzymes restricts the participation of *Bacillus* bacteria in the process of cellulose mineralization.

In the next stage of the research, the attempt at conducting biodegradation of bottom sediments of Turawa Lake was made with the use of the most vigorous strains of isolated cellulolytic bacteria. In many authors' opinion (Gostkowska et. al., 1996; Latała et al., 2004) natural microflora supplemented with the biopreparation containing strains of high enzymatic activity, accelerates the process of biodegradation significantly.

Four prepared experimental combinations were inoculated with the respective bacteria of *Cellulomonas*: *Cytophaga* C1 (combination 1), *Cytophaga* C3 (combination 2), *Cellulomonas* C4 (combination 3), and a mixture of all strains (combination 4). Results of biodegradation are presented in Table 2 and Figure 2.

Table 2. Chemical analysis of the sediment throughout biodegradation process

Type of treatment ¹	Amount of cellulose [g/kg dry matter]			
	1st day	14th day	28th day	42nd day
control treatment	188.00	178.00	171.61	182.51
combination 1	188.00	146.00	120.94	83.99
combination 2	188.00	157.39	136.94	102.79
combination 3	188.00	167.88	161.06	148.65
combination 4	188.00	130.09	99.86	63.84

¹combination 1 – *Cytophaga* C1,
 combination 2 – *Cytophaga* C3,
 combination 3 – *Cellulomonas* C4,
 combination 4 – the mixture of *Cytophaga* C1, *Cytophaga* C3 and *Cellulomonas* C4.

In combinations containing single cellulolytic bacteria strains, cellulose decrease corresponded to their cellulolytic activity. However, the highest cellulose loss was noted in the 4th combination, comprising of *Cytophaga* and *Cellulomonas* strains mixture. It was confirmed in the own research (Latała et al., 2001; Wierzba and Nabrdalik, 2005), as well as by the other authors (Bujak and Targoński, 1988; Gostkowska et al., 1996), that the efficiency of biodegradation process was higher in the case when the microbe mixture was added in contrast to individual strains supplement. After 2 weeks of biodegradation, the decrease amounted 30.80% and cellulose content in sediment dropped to 130.09 g/kg of dry matter. Slightly higher results were recorded in combination 1, with the *Cytophaga* C1 strain – 146.00 g/kg of dry matter which accounted for 22.34% reduction. In combinations 2 and 3 cellulose loss rate shaped within the range of 16.28% to 10.70%. The highest rate was also noted after 28 days in sediment containing the mixture of strains. Cellulose content decreased to 99.86 g/kg of dry matter which accounted for 46.88% reduction.

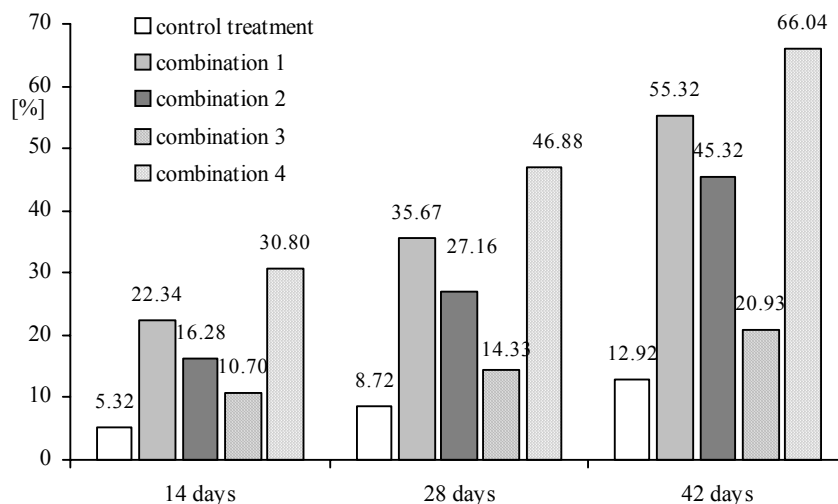


Fig. 2. Cellulose reduction rate throughout biodegradation of bottom sediments

The analysed loss in cellulose content, in the other examined combinations, was of 11.21% (combination 1) to 32.55% (combination 3) lower when compared to combination 4. Finally, the mixture of *Cytophaga* and *Cellulomonas* strains, caused the decrease in cellulose content in bottom sediment to the level of 63.84 g/kg of dry matter, which corresponded to 66.04% reduction. Slightly lower efficiency in cellulose decomposition (55.32%), characterised *Cytophaga* strain C1, employed in combination 2. Lower reduction (about 20%) was recorded in combination 3 with *Cytophaga* C3.

The lowest efficiency in biodegradation was stated for the third combination, containing *Cellulomonas* strain C4. Cellulose loss rate amounted 20.93% and was slightly higher in relation to the control treatment – 12.93% [Tab. 2, Fig. 2].

The same authors' group recorded much lower results during biodegradation of polysaccharides in residual waste with the amendment of biopreparation containing cellulolytic bacteria strains. The most intensive rate of polysaccharides reduction was noted in the first weeks of the experiment, and after 30 days was equal to 39% (Wierzba and Nabrdalik 2005). Also in the own experiments, hydrolysis of cellulose was the most intensive, in combinations 1 and 4, during the first 14 days of biodegradation. It amounted ca. 40% and over 45% of the total content of reduced cellulose, respectively.

The most probable reason for it, could be favourable conditions for the species *Cytophaga* in which cellulose is decomposed: slightly acid pH of waste (6.5) and facilitated oxygen access. According to Bujak and Taragoński (1988) cellulose decomposition is faster in soils of neutral or slightly acidic pH than in strongly acid ones. As many authors report (Eriksson and Pettersson, 1975; Land et al., 2002), the rate of hydrolysis is much higher in aerobic conditions than in nitrogen conditions.

During biodegradation, microbiological quantitative analysis proved growing tendency concerning the Most Probable Number (MPN) of bacteria in all combinations. The highest growth rate of bacteria, similar to cellulose reduction rate, were recorded in the first 14 days, in combination 1 and 4. In comparison to initial rate, bacteria enumeration increased by ca. 19-fold and ca. 35-fold respectively. Finally, after 6 weeks of biodegradation, the highest MPN of bacteria was stated in the combination containing strains mixture. Bacteria enumeration increased by 300-fold in relation to control treatment, and amounted over 10^5 MPN/1 g of sediment [fig. 3].

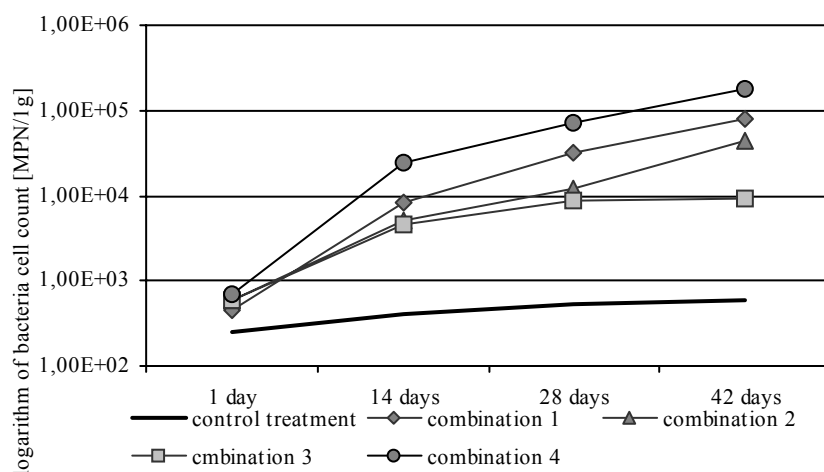


Fig. 3. Changes in bacteria enumeration throughout the biodegradation process of bottom sediments

In the study of the same authors concerning biodegradation of organic waste, slightly lower increase in cellulolytic bacteria enumeration was stated after 60 days of biodegradation, by ca. 240-fold when compared to the initial amount (Wierzba and

Nabrdalik, 2005). Distinct maintaining tendency for the growth of NPL of bacteria in combinations containing *Cytophaga* strains, supports the thesis about favourable conditions for mentioned bacteria growth, during bottom sediments biodegradation. Obtained results suggest, that the effectiveness of cellulose decomposition depended on both quantity and quality of bacteria employed. Also, active process of lignocellulose degradation is guaranteed by the application of the microbes' mixture that possess the ability to synthesise the cellulase complex of advantageous composition. According to Bujak and Targoński (1988), separate applications of two fractions of cellulolytic enzymes, extracted from the cellulolytic bacteria complex, was the reason why the hydrolysis of cellulose occurred at a rate by 2.5-fold slower than in the process of combined activity of both fractions. Many authors (Bujak and Targoński, 1988; Górska and Russel, 1997; Lynd et al., 2002) emphasise the important role played by the β -glucosidases, called cellobiase in biodegradation of lignocellulose. Its deficiency in cellulolytic complex during the process of cellulose hydrolysis, causes cellobiose accumulation, which inhibits endo – and egzoglucanases. The ability to synthesize significant amount of cellobiase were ascertained among bacteria *Cytophaga*.

SUMMARY AND CONCLUSION

Bottom sediments of Turawa Lake contain significant amount of organic matter, including fibre and cellulose, accumulated by the bottom deposition of parts of plants, water animals and contamination that flows with the surface water and groundwater. Presented laboratory results indicate the possibility of polysaccharides decomposition in bottom sediments with the use of specially selected autochthonic microflora. Enzymatic hydrolysis of cellulose is a very complex process and it is performed in presence of the complex of enzymes. Therefore the best results of biodegradation were obtained when the mixture of *Cytophaga* and *Cellulomonas* bacteria were applied. Cellulose decrease rate was 10-45% higher as compared to single strains application and over 33% higher in relation to the control treatment. Biodegradation process was accompanied by significant increase in cellulolytic bacteria enumeration, especially in the combination containing the bacteria mix. Acidic pH of the waste and aerobic conditions of cultivation were favourable for the high enzymatic activity of *Cytophaga* strains.

LITERATURE

- BEGUIN P., AUBERT J.P., 1994, *The biological degradation of cellulose*, FEMS Microbiology Rev., vol. 13 (1), 25-58.
- BUJAK S., TARGOŃSKI Z., 1988, *Mikrobiologiczna degradacja materiałów celulozowych*, Postępy Mikrobiologii, tom XXVII, z. 3, 211-241.
- BURBIANKA M., PLISZKA A., MUSZYŃSKA H., 1983, *Mikrobiologia żywności*, Państwowy Zakład Wydawnictw Lekarskich, Warszawa.
- ERIKSSON K.E., PETTERSSON B., 1975, *Extracellular enzyme system utilized by the fungus*

- Sporotrichum pulverulentum* (*Chrysosporium lignorum*) for the breakdown of cellulose. 1. Separation, purification and physico-chemical characterization of five endo-1,4-beta-glucanases., Eur J Biochem., Feb 3;51 (1):193-206.
- GOŁĘBIEWSKA J., 1992, *Mikrobiologia rolnicza*, PWRiL, Warszawa.
- GOSTKOWSKA K., SZWED A., WYCZÓLKOWSKI A., 1996, *Próba kompostowania odpadów tytoniowych. Cz. III. Wpływ stosowania szczepionki na rozwój mikroorganizmów i niektóre właściwości chemiczne kompostu z odpadów tytoniowych*, Zesz. Prob. Post. Nauk Rol., 437, 159-165.
- GÓRSKA E., RUSSEL S., 1997, *Charakterystyka wyizolowanego z gleby szczepu Bacillus polymyxa. Drobnoustroje w środowisku – występowanie, aktywność i znaczenie*, Wydział Rolniczy AR., Kraków, 195-203.
- GRABIŃSKA-ŁONIEWSKA A., 1996, *Ćwiczenia laboratoryjne z mikrobiologii ogólnej*, Oficyna Wydawnicza Politechniki Warszawskiej, Warszawa.
- HOLT J.G., KRIEG N.R., 1984, *Bergey's manual of systematic bacteriology*, Williams & Wilkins, Baltimore.
- JANAS P., PODGÓRSKA E., MLEKO S., PIELECKI J., 2004, *Biosynteza enzymów proteolitycznych i ich wpływ na aktywność celulaz Trichoderma reesei*, Annales UMCS, Sec. E, 59 (1), 461-469.
- JANAS P., TARGOŃSKI Z., MLEKO S., 2002, *Wpływ wybranych monosacharydów na biosyntezę celulaz, ksylanaz i enzymów litycznych przez mutanta Trichoderma reesei M-7*, Biotechnologia, 1 (56), 195-207.
- KŁYSZEJKO-STEFANOWICZ L., 1980, *Ćwiczenia z biochemii*, PWN, Warszawa.
- LATAŁA A., WIERZBA S., FARBISZEWSKA T., POLACZEK B., BONIEWSKA E., 2004, *Biodegradacja odpadów gospodarczych przy użyciu szczepów bakterii lipolitycznych, proteolitycznych i celolitycznych*, Biotechnologia, 3(66), 202-213.
- LATAŁA A., WIERZBA S., POLACZEK B., 2001, *Uwarunkowania bioutylizacji odpadów tłuszczowych w warunkach laboratoryjnych*, Zesz. Prob. Post. Nauk Rol., 477, 397-403.
- LIEBERT C. A., HOOD M. A., DECK F. H., BISHOP K., FLAHERTY D. K., 1984, *Isolation and characterization of a new Cytophaga species implicated in a work-related lung disease*, Applied and Environmental Microbiology, 48 (5), 936-943.
- LYND, L.R., WEIMER, P.J., VAN ZYL, W.H., PRETORIUS, I. S., 2002, *Microbial Cellulose Utilization: Fundamentals and Biotechnology*, Microbiol. Mol. Biol. Rev., 66, 506-577
- TEISSEYRE A.K., 1984, *Osady denne Jeziora Turawskiego w świetle badań geologicznych*, Geologia Sudetica, 18 (1), 21-60.
- TROJANOWSKI J., 1973, *Przemiany substancji organicznej w glebie*, PWRiL, Warszawa.
- VARDAVAKIS E., 1989, *Seasonal fluctuations of aerobic cellulolytic bacteria, and cellulase and respiratory activities in a soil profile under a forest*, Plant and Soil, vol. 115 (1), 145-150.
- WIERZBA S., NABRDALIK M., 2005, *Biocomposite for organic waste degradation*, Fizykochemiczne Problemy Metalurgii, 39, 249-256.

Wierzba S., Nabrdalik M., Biodegradacja celulozy dennych osadów Jeziora Turawskiego, Physico-chemical Problems of Mineral Processing, 41 (2007) 227-335 (w jęz. ang.).

W pracy podjęto próbę biodegradacji osadów dennych Jeziora Turawskiego, o ok. 19% zawartości celulozy, z wykorzystaniem szczepów bakterii celolitycznych. Na wstępie dokonano izolacji i selekcji bakterii celolitycznych z osadów dennych jeziora. Następnie określono ich aktywność celolityczną i wybrano trzy najaktywniejsze szczepy, które wykorzystano do biodegradacji osadów. Ilość rozłożonej celulozy określano metodą atronową, a zmianę liczebności bakterii metodą miana. Najskuteczniejsza w biodegradacji celulozy okazała się mieszanina szczepów z rodzajów: *Cytophaga* i *Cellulomonas*. Odnotowana redukcja celulozy po 42 dniach trwania procesu wynosiła ok. 66%, a liczebność bakterii zwiększyła się ok. 300-krotnie, osiągając poziom ponad 10^5 NPL/1g osadu dennego.

Piotr WODZIŃSKI*

SCREENS – CLASSIFICATION AND SYSTEMATICS SINGLE-PLANE SCREENS

Received April 2, 2007; reviewed; accepted May 17, 2007

A classification of screens, which covers structures applied in industry, and also new solutions of highly efficient high-tech screens tested in pilot-plant scale is presented in the paper. The last screen classification published in literature comes from Wessel (1963) and is not valid any longer. Therefore, in this paper a new classification of screens is shown which includes the latest achievements in this field and excludes old screens that are not offered by machinery producers any longer.

In the construction of screening machines there are certain design solutions which have been considered the most appropriate now. In the case of screens with a linear flow of screened material through the machine, these are the screens with a drive with two synchronised rotary vibrators. The construction enables different trajectories of riddle vibrations. In the case of spiral flow of screened material on the sieve, there are wobbling caisson screens which actually have dominated this machine class.

Other screening machines constitute small part of all produced screens and complete the two main classes mentioned above. All most important screening machines used in the national economy of a developed country will be presented in this paper.

Key words: sieve, screen, sieve motion trajectory, granular material, particle classification

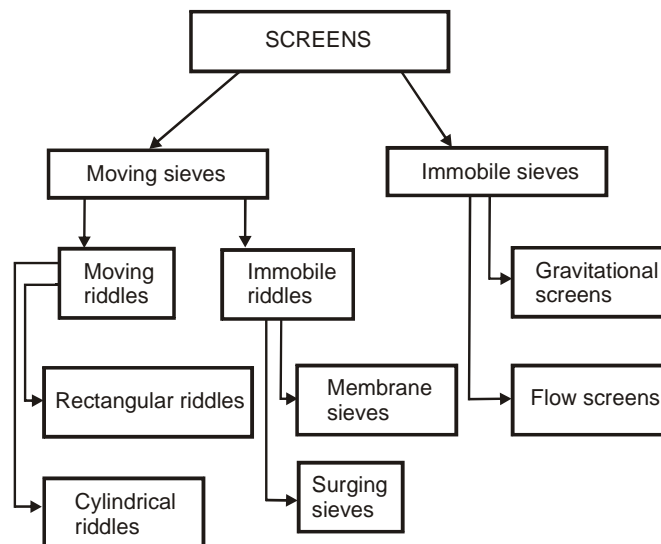
INTRODUCTION

The process of screening granular materials was known most probably in ancient times already. The first published description of this process comes from the 17th century. In the 19th and 20th century a rapid progress of screening techniques and screens was observed [Banaszewski, 1990; Dietrych, 1962; Sztaba, 1993]. The present development of screens is on a stabilised level. In most cases machine building industry produces similar machines on a related technical level. Differences in the structure of individual screens of the same type are small and refer to details. Hence, they do not determine the suitability of particular machines for screening processes.

* Łódź Technical University, W-10; K-101, ul. Wólczańska 175, 90-924 Łódź, Poland.

The main criterion of the presented screen classification was a screen sieve motion. The motion of a vibrating sieve determines the process run, because on this depends the motion of grains in the screened layer and grain transfer through the mesh (Wodziński, 1997). The second important element which characterises a screen is the type of flow of a screened medium through the screen or the trajectory of grains on the sieve. Here, two basic resultant trajectories of grains moving on a sieve surface are distinguished: linear and spiral. The first one refers to the screens with rectangular sieves and cuboid riddle. The second type covers cylindrical sieves and spiral motion of grains from the centre to the sieve edge. There are, however, a few exceptions to this classification.

CLASSIFICATION OF SCREENING MACHINES



The above classification of screens is relatively simple and covers majority (in fact all) machines for industrial screening of granular materials. Further in this study we will discuss subsequent single-plane screens, i.e. such whose riddles along with the sieves perform plane motion in the principal plane of the machine.

SINGLE-PLANE SCREENS

This is undoubtedly the biggest subgroup of screening machines. It is estimated that about 70 to 80% of presently built screens are the single-plane machines. Figure 1 shows possible component motions of the screen with a rectangular riddle. A reference system is the Cartesian system of solid axes (0xyz) (Fig. 1); the centre of the

system overlaps the centre of the riddle mass. Hence, in general, we can distinguish three linear amplitudes, components A_x , A_y and A_z , taken as dislocation along the xyz axis. There are also three torsional amplitudes φ_x , φ_y , φ_z in relation to the axis of the reference system. As it was mentioned, the principal plane of a screening machine π (2 and 3) is the plane on which all plane motions of the riddles occur. These are just single-plane screens. Figures 2 and 3 illustrate these motions, i.e. their trajectories along which the centre of gravity of the screen or other points of the riddle move. This can be a linear, circular, elliptic or complex trajectory characteristic of screens with double frequency (Fig. 4 and 5).

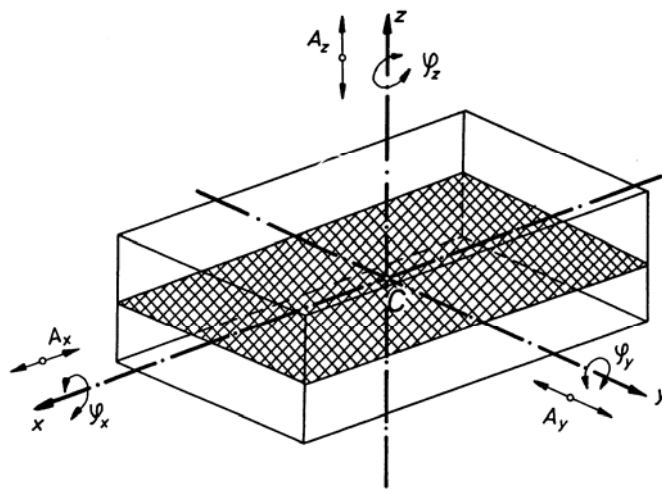


Fig. 1. Component motions of a riddle

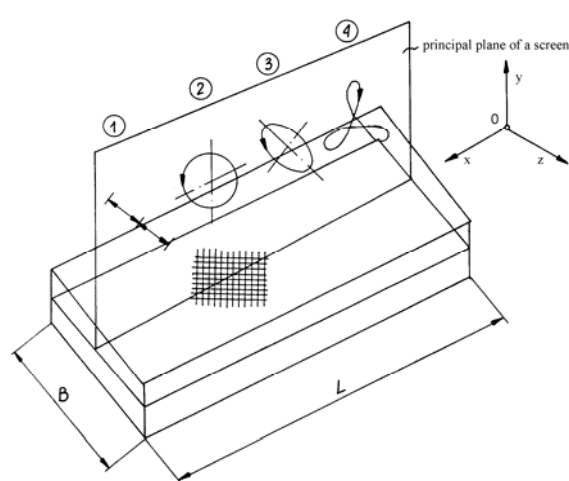


Fig. 2. Principal plane of a rectangular riddle

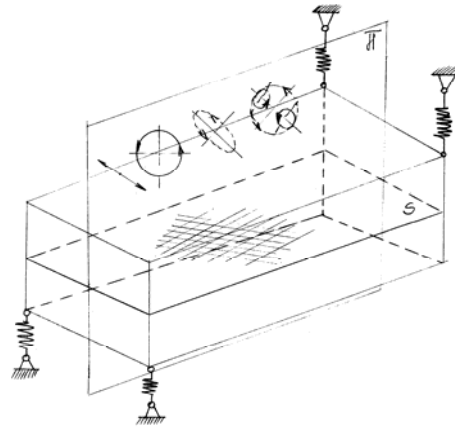
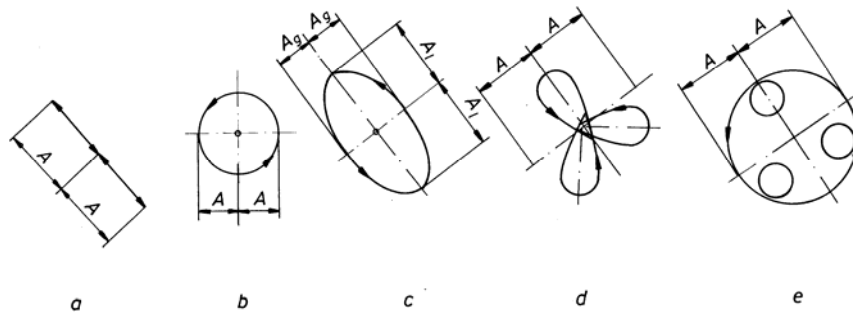
Fig. 3. Sieve-riddle motion trajectories in the principal plane π 

Fig. 4. Single-plane screen trajectories

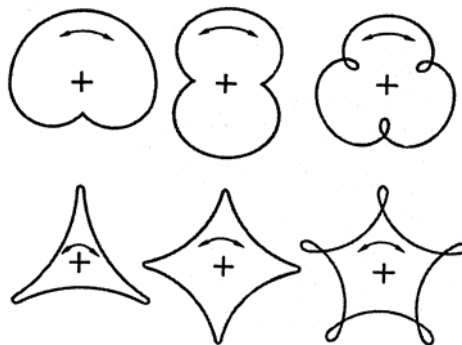


Fig. 5. Trajectories of double-frequency screens

Particular single-plane screens will be discussed, starting with the simplest systems and ending with double-frequency screens.

Figure 6 shows schematically the simplest single-plane screen, i.e. such in which vibrating motion of the sieve and riddle takes place in one plane. The machine is

driven by a rotary vibrator, e.g. unbalanced shaft placed in the riddle centre of gravity. An exciting force is force P (this is the centrifugal force of unbalanced mass rotating at a constant angular velocity ω). The riddle centre of gravity in such a screen moves along a circular or nearly circular trajectory. The riddle beginning and end move along elliptical (oval) trajectories.

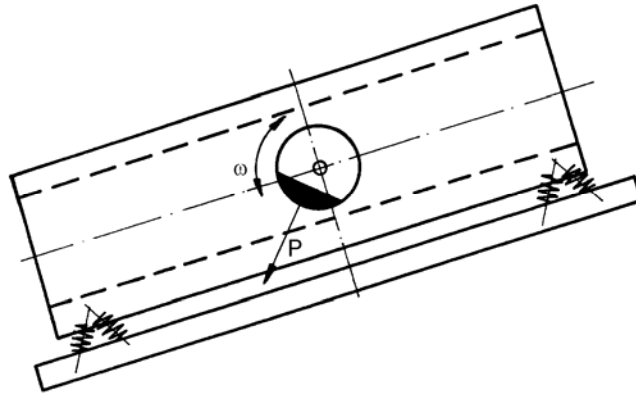


Fig. 6. Single-plane screen driven by a rotary vibrator

Another type of a single-plane screen is shown in Fig. 7. This is a machine driven by an eccentric shaft which comes perpendicular to the principal plane through the riddle in its centre of gravity. The riddle makes a circular motion excited by the size of an eccentric crankshaft shoulder. The beginning and end of the riddle move along trajectories close to circular. Machines of this type find applications in extractive industry and in many other cases.

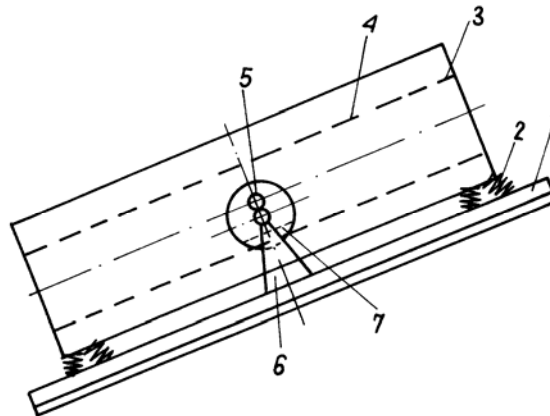


Fig. 7. Screen driven by a crankshaft

Figure 8 shows a single-plane screen similar to the basic machine illustrated in Fig. 6. The screen is driven by an unbalanced shaft 3, on bearings in casing 4, which can move in guides 5. Casing 4 is located elastically along the screen by means of springs

6. It moves cross-wise directly in the guides, without the springs. Such a drive ensures elliptic (or oval) trajectories of machine vibrations on closed-loop trajectories. The machine shown in Fig. 8 is characterised by a pneumatic spring suspension of the riddle, in the form of road wheels 7 to 8. This is an original solution which has significant advantages over the generally used steel coil springs.

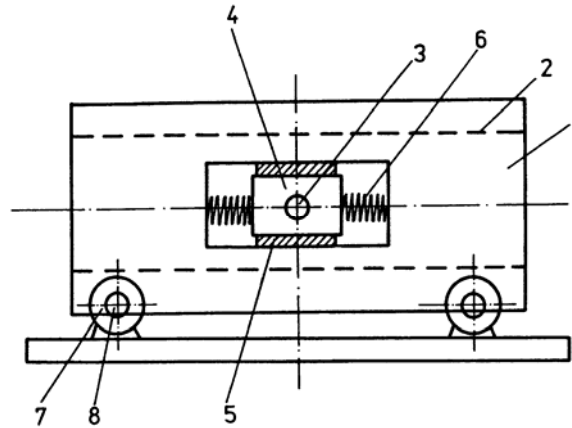


Fig. 8. Screen with a shaft on spring suspension

The next extended construction of the classical single-plane screen with an unbalanced drive shaft placed in the centre of gravity of the riddle, is a machine shown in Fig. 9. Its characteristic feature is an unbalanced shaft 5 with tangent unbalanced mass 6. On both sides the mass is on spring suspensions inside the shaft and can travel perpendicularly to the shaft axis. This solution contributes to smooth passing through resonant frequency and does not cause an increase of the vibration amplitude, particularly during drive system coasting after stopping the feed.

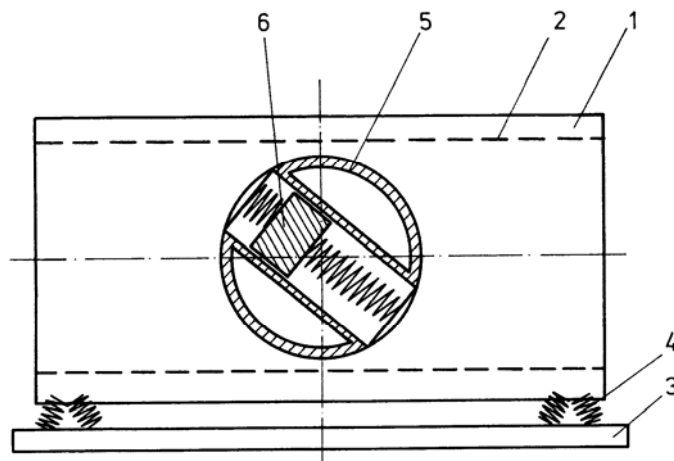


Fig. 9. Screen with a shaft equipped with tangent unbalanced mass

A big group of single-plane screens consists of screens driven by biaxial rotary vibrators. A rotary vibrator is the vibrator with an unbalanced shaft put in uniform rotary motion which induces centrifugal force that is the driving force, i.e. the force which excites vibrations of the riddle. If there are two unbalanced shafts with parallel axes in the drive, then we have a rotary biaxial vibrator. It is important to obtain a synchronised rotary motion of these shafts which can be achieved in three ways:

- using a toothed gear that combines both shafts,
- applying a cogbelt gearing,
- by obtaining the effect of dynamic self-synchronisation of these shafts in the rotary motion.

Figure 10 shows three most popular biaxial drive systems used in screening machine building. Figure 10 a shows a drive placed in the centre of gravity of the riddle composed of two unbalanced shafts rotating in forward direction (concurrent synchronisation), which produces circular motion of the riddle. Figure 10b illustrates two unbalanced shafts placed on the riddle, over the centre of gravity of the mechanical vibrating system, rotating in forward direction (concurrent synchronisation), which ensures elliptic trajectory of the riddle motion, with a characteristic distribution of elliptic trajectories on the riddle. Finally, Fig. 10c shows a rotary biaxial drive when the drive shafts operate in mutual counter-current synchronisation (they rotate in opposite directions) and excite elliptic vibrations of the riddle at uniform distribution of elliptic trajectories of the riddle along its entire length.

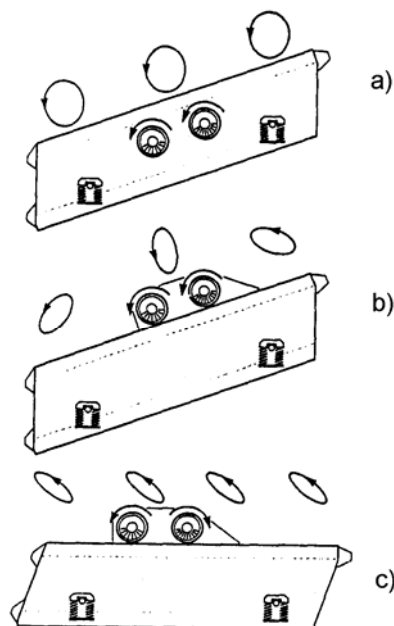


Fig. 10. Screens with two drive shafts (design alternatives)

Figure 11 shows a frequently encountered system of biaxial rotary drive, when the same two unbalanced shafts work in counter-current synchronisation. In such cases the effect of dynamic self-synchronisation is very frequently used. The drive shafts rotate at the same angular velocities ($\omega_1 = \omega_2$) and generate the same exciting forces. The distribution of forces causes linear vibrations of the riddle along the sieve oscillation line (SOL). The line directed to the sieve surface at the angle β , called the angle of sieve trajectory, passes through the centre of screen mass S_0 . In this case the sieve can be horizontal, i.e. the angle of sieve inclination $\alpha = 0$.

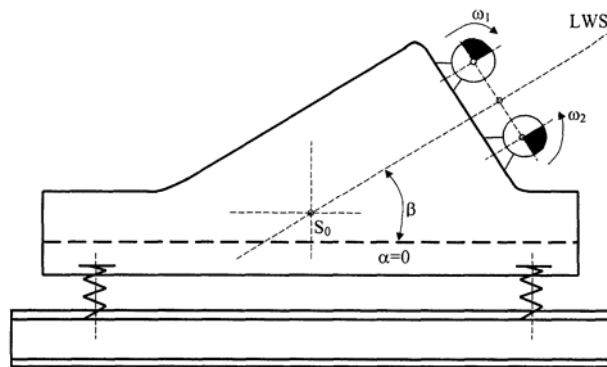


Fig. 11. Screen with a raised riddle and biaxial drive

Another type of a single-plane screen with rotary biaxial drive is shown in Fig. 12. The machine consists of a typical rectangular riddle suspended on springs and located on the machine frame. A drive system is formed by two rotary vibrators with uneven static moments. The shaft with a bigger static moment is placed further from the centre of gravity of the screen. Both drive shafts operate at the dynamic counter-current self-synchronisation. In this screen the riddle motion is elliptic, and by moving the whole drive system along the riddle the trajectory of sieve vibrations can be formed.

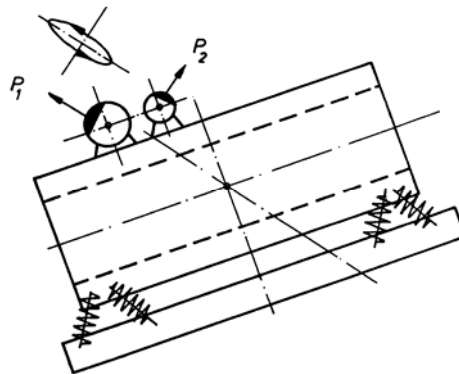


Fig. 12. Elliptic biaxial screen

A representative of the single-plane biaxial screens is also the Mogensen classifier (Fig. 13), which is the only construction of this kind with sieves placed one over the other at subsequently growing angle of inclination. The screen is driven by two rotary vibrators operating at dynamic counter-current self-synchronisation. Hence, sieves of this classifier perform linear vibrations because static moments of the vibrators are the same.

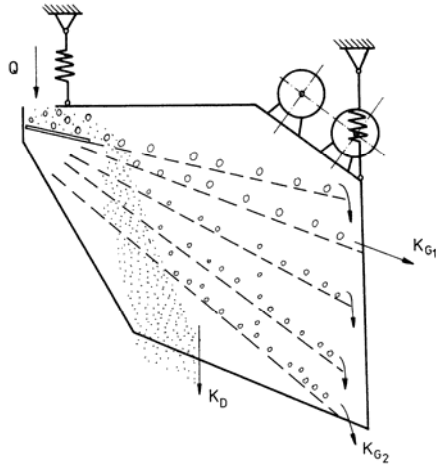


Fig. 13. Mogensen screen

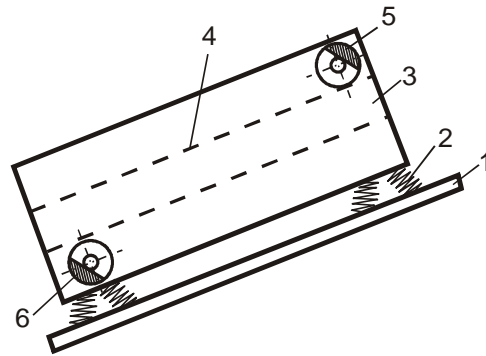


Fig. 14. DF – type screen

The last important class of single-plane screens are double-frequency screens (PD-C). These machines are driven by biaxial vibrators, with unbalanced shafts rotating at different rotational speed. In this way, the trajectory of riddle vibrations consists of two component trajectories formed by the motion excited by various driving forces. This non-linear, complex plane trajectory of the riddle motion is important for segregation of a material layer moving on the sieve. Since it is known that main resistance during screening is on the side of material layer and not the sieve, hence the sieve should be put in such vibrations that it might cause transfer of small particles to the sieve surface to the greatest possible extent. This will enable these particles to get into mesh and to transfer through the sieve. Therefore, a PD-C screen was constructed as the one which offers the most advantageous motion of particles in the screened layer on the sieve.

The oldest known screen of double frequency (DF – type) is shown in Fig. 14. This is a typical single-plane screen driven by two synchronised unbalanced shafts 5 and 6. The shafts rotate at different rotational speeds of the mutual ratio 1:2 or 1:3. Also other values of the speed ratio are possible.

Another DF screen is Cyclorot (Fig. 15), which is also a typical single-plane screen. Its riddle is driven by two unbalanced shafts 5 and 6 of different static moments. Shaft 5 with bigger static moment is situated in the centre of gravity of the riddle, while shaft 6 (of smaller static moment) is over the main shaft, above the

sieves. Depending on the mutual ratio of rotational speeds and concurrency or counter-currency of rotational motion of these shafts, we obtain different trajectories of the machine vibrations.

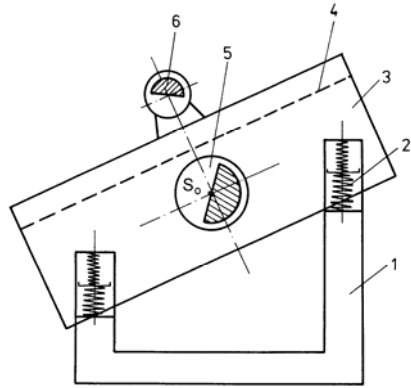


Fig. 15. Cyclorot screen

A relatively new DF screen is a linear-elliptic screen (Fig. 16). This is also a single-plane screen composed of a rectangular riddle suspended on springs and supported by an immobile frame which is also a supporting structure of the whole machine. The machine can be either horizontal or inclined at a certain angle α , however smaller than in the case of typical single-plane screens ($\alpha = 8$ to 10°).

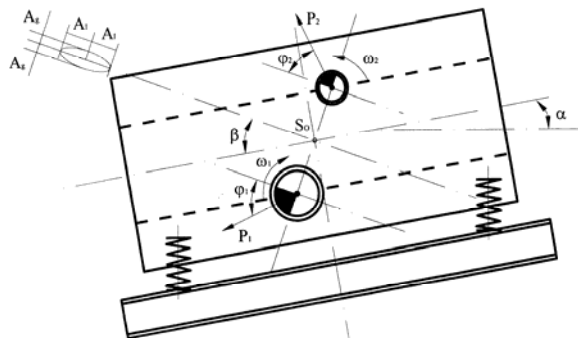


Fig. 16. Linear-elliptic screen

A characteristic feature of the linear-elliptic screen is its drive composed of two rotary vibrators. These are two unbalanced shafts with different static moments, rotating at the same or different rotational speeds. If the shafts rotate at the same speed, we have a single-plane elliptic screen. If, however, they are put in rotary motion at speed ratios 1:2 or 1:3, this is a double-frequency screen. The sieve oscillation line of this screen is inclined to the sieve plane at the angle β which should be in the range $\beta = 45^\circ$ to 60° . It was proved in the industrial practice that the angle of sieve trajectory β should be about $45^\circ = \pi/4$.

The next class of single-plane screens are the screens with electromagnetic drives. Figure 17 shows four different systems of these machines. In the screen driven by an electromagnetic vibrator the sieve and riddle perform a linear motion. The latest design includes 23 c and 23 d machines. The first one has a horizontal sieve and due to the position of an electromagnetic vibrator makes it possible to transport material layer on the sieve. The other machine has an inclined sieve and vibrator situated perpendicularly to the sieve surface. An industrial version of this screen is illustrated in Fig. 18. The screen is equipped with a sieve with pneumatic suspension. The electromagnetic drive has many advantages, one of them being a possibility of smooth control of vibration amplitude in the entire working range of the drive system. This enables removal of blocked grains from the sieves by instantaneous and sudden switching of maximum supply voltage. This means an abrupt increase of sieve vibration amplitudes to the maximum value and a strong shock of the whole riddle and sieves. This causes cleaning of the sieves.

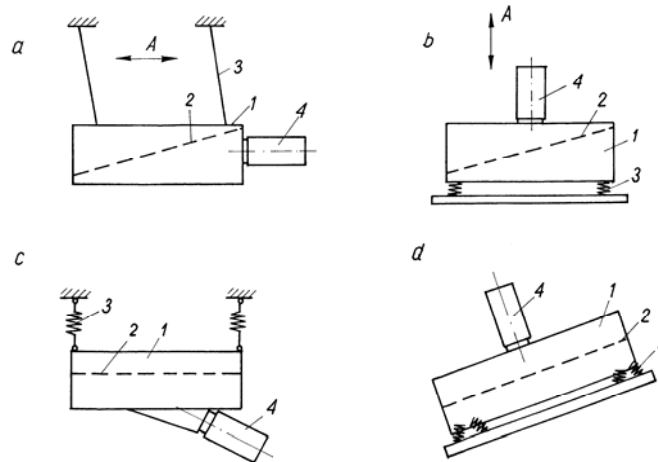


Fig. 17. Schematics of screens with electromagnetic drive

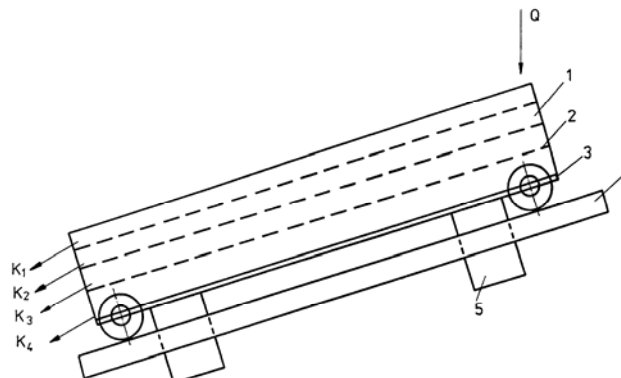


Fig. 18. Multi-deck electromagnetic screen

PROCESS PARAMETERS OF SINGLE-PLANE SCREENS

Process parameters of single-plane screens will be presented and a comparison with membrane screens and cross screens will be made (Table 1). In all cases woven metal sieves (steel, brass and chrome-nickel) were used. These are results obtained by the author.

Figure 19 shows graphically the results of processing various materials in single-plane screens [4] with circular motion:

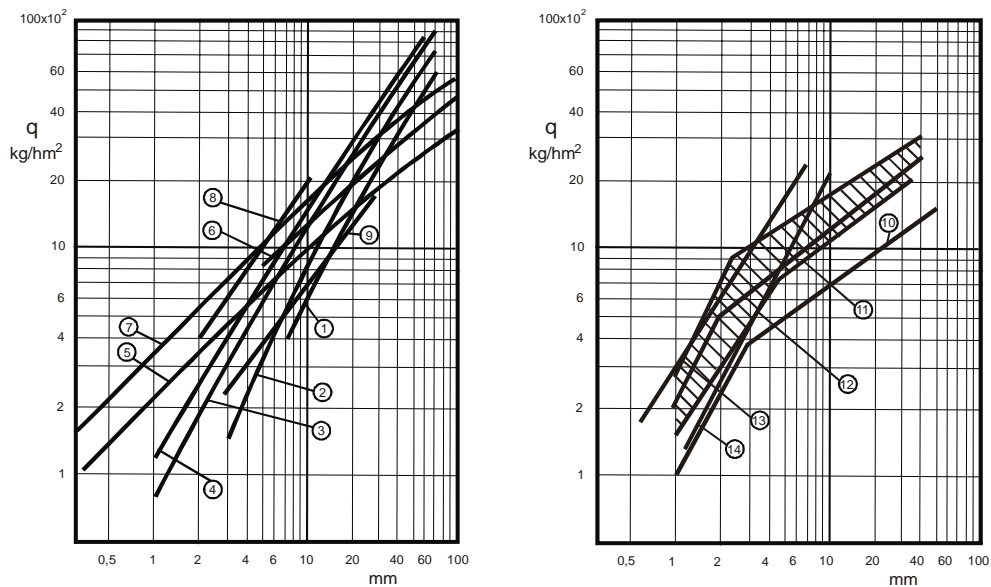


Fig. 19. Process parameters of single-plane screens at circular motion

1 – wet gravel after washing, 2-4 – gravel, 5 – coal, 6 – crushed gravel, 7 – sand, 8 – quartzite, 9 – crushed brick, 10 – coke, 11 – salt, 12 – minerals, 13-14 – gravel mix

Research performed within basic research program in K-101, Łódź Technical University.

REFERENCES

- BANASZEWSKI T., *Screens*, Katowice 1990 (in Polish).
 DIETRYCH J., *The theory and construction of screens*, WGH Katowice 1962 (in Polish).
 SZTABA K., *Screening*, Katowice 1993 (in Polish).
 WESSEL J., *Siebmaschinen, eine Ordnungsstudie der Bauformen und ihrer Eigenarten*, Aufber. – Techn. 1963, s.449-461.
 WODZIŃSKI P., *Screening and screens*, Łódź 1997 (in Polish).

Table 1. Screening of granular materials on different screens

		Circling screen (single-plane)	Electromagnetic screen (single- plane)	Screen with vibrating sieve	Cross screen
Agalite 0-5 mm [kg/m ² s] balls l = 1 mm	q	0.2 – 1.4		1 – 6	1.82 – 3.7
	η [-]	0.6 – 0.8		0.6 – 1.0	0.8 – 1.0
Feldspar m ² s] 0.1 – 0.6 mm l = 0.2 mm	q[kg/		0.219 – 1.281		2.01 – 3.09
	η [-]		0.640 – 0.800		0.500 – 0.800
Grit m ² s] 0 – 10 mm l = 1 mm	q[kg/			1.0 – 8.25	2.0 – 6.13
	η [-]			0.9 – 1.0	0.7 – 0.9
Sugar m ² s] 0 – 3 mm l = 0.71 mm	q[kg/	0.2 – 2.6		1.3 – 7.8	
	η [-]	0.6 – 1.0		0.7 – 1.0	
Superphosphate m ² s] 0 – 10 mm l = 1 mm	q[kg/	1.3 – 2.0		2.1 – 3.9	
	η [-]	0.6 – 0.7		0.8 – 0.9	

Wodziński P., *Sita - klasyfikacja i systematyka przesiewaczy jednopłaszczyznowych*, Physicochemical Problems of Mineral Processing, 41 (2007) 237-249 (w jęz. ang.).

Niniejsza praca jest próbą zbudowania nowej klasyfikacji maszyn przesiewających. Klasyfikacja ta tym różni się od dotychczasowych, iż za główny czynnik decydujący o przynależności do danej grupy maszyn, uznano ruch przesiewacza, albo jego brak. Oprócz tego ten nowy podział przesiewaczy jest prostszy od dotychczas opracowanych. W pracy omówiono szczegółowo przesiewacze jednopłaszczyznowe, które są najbardziej rozpowszechnionymi maszynami przesiewającymi w chwili obecnej. Stwierdzenie to dotyczy zarówno jednostek budowanych przez fabryki budowy maszyn na całym świecie, jak i eksploatowanych w różnych dziedzinach gospodarki narodowej. W końcowej części pracy zamieszczono wyniki procesowe przesiewaczy jednopłaszczyznowych, głównie o ruchu kołowym, które z kolei są najbardziej rozpowszechnione w przemyśle wydobywczym.

V.P. NEBERA, Sai Kyaw Naing Oo*

BIOSORPTION OF METALS FROM GEOTECHNOLOGY SOLUTIONS

Received March 25, 2007; reviewed; accepted June 5, 2007

Different microorganisms studied. As biosorbents emerge different microorganisms: bacteria, micromycetes, fungi, yeasts (baker's, beer and forage), active silts and microalga. As native sorbents studied active carbon and chitines, chitisan. Flotation biomass from the liquid, so named biosorbitive flotation we consider as promising. Scientific and practical urgency of problem consists in revealing an intercoupling between the sorption of non-ferrous metals by the biomass and its floatability, determination of optimum parameters for regulation flotation biomass, loaded by metals. An ability to sorption metals from solutions possess all microorganisms - bonding of metals is realized to the account of different mechanisms (ion exchange, complexing, reducing, formation low soluble compounds). Adsorptive capacity of microorganisms end efficiency of metals recovery determined. For instance, maximum Cu and Ag recoveries were about 100% from 100 ml solutions 1 g/l on 10 g biomass. Floatability of sorbents greatly depends on sorption metals on their surface: mostly metals activated flotation, most of synthetic sorbents displayed pure floatability in ether cases. Biosorbents floated with greater ability. The concentration of metals (or removal toxic inorganic ions) by microorganisms with following flotation can become industrial process both for a cleaning sewages, and for a recovery of metals. There is much reason for making broad study and further development of that field of research with control of metal contents in solution by Ecotest apparatus with ion-selective electrodes on Cu, Ag, Ni, Co etc.; control of both - solution and solids (sorbents, minerals) with Spectroscan G roentgen-fluorescence spectrometer.

Keywords: biosorbents, flotation, parameters, biosorption, metals

INTRODUCTION

Biosorption methods have got sufficiently broad consideration on recent international conferences [Groudev et al., 2003, Matis et al., Volesky 1994]. Their high efficiency is shown on the example of sorptions of precious metals (Table 1) .

* Russian State Geological Prospecting University, vpnebera@msgpa.ru

Table 1. Sorption of precious metals by some microorganisms [Matis et al., 2001]

Metals	Sorbents	Sorption mgg-1
Microalga		
Au	Sargassum natas	420
Au	Micrococcus luteus	30 min - 177 2 hours - 253
Au	Chlorella vulgaris	120
Au	Chlorella pyrenoclosa	140
Pd	Granules of AMT Bioclamtm	462
Pt		102
Fungi		
Au	Aspergillus niger	176
Au	Phizopus arrhizus	100-164
Biopolymers		
Au	Chitosan	150
Ag	Chitosan	100

EXPERIMENTAL WORK

We studied sorption of metals on a number of both synthetic and native sorbents, on biomasses from the classes of fungi, yeasts, actinomycetes, alga. Than the biomasses were flotated by using ordinary laboratory conditions. The flotation characteristics of biomasses were greatly changed after the saturation of biomasses by metals ions. An increase of biomass hydrofobicity allows effectively separate biosorbents from solutions [Nebera, Solozhenkin 2002]. The comparison of synthetic sorbents (AM, AMP, AV 17, ANKB) with others biosorbents has been done. Also, natural sorbents such as: chitin, chitosan, active carbon have been investigated.

Much work is denoted toward native materials: chitines, chitosan, pine barc, sawdust as a sorbent of metals. Pine barc (*Pinus pinaster*, Aiton) after its chemical or biochemical processing was suitable for cleaning effluents from oil products and other organic materials [Skriabina et al., 2002, Sangalov et al., 1999]. From the number of biosorbents studied fungi, alga, bacteria, yeast were frequently used. Their sufficiently high efficiency, often exceeding the capacity of synthetic ion-exchange resins, has been reflected from our work [Taboada et al., 2003]

The strategy of laboratory studies was concluded in mixing a metal ion solution (50 ml) with sorbents (8-10 g) in the conical flasks (100 ml of volume). The flasks were shook (frequency 100 min⁻¹ amplitude 10 mm). The analysis of contents of metal in solution before and after sorptions - have been done using ion-selective electrodes. The instrument Ecotech Akvilon and Spectroscan G for the roentgen-fluorescent analyze of sorbents were used. The sorption isotherms and distribution factors have received, also a sorption kinetic was determined.

RESULTS

The variable values in flotation experiments were: pH and the consumption of flotation reagents (sodium oleate, dodecylammonium chloride (DA)). On the example flotation of sorbents loaded by copper, installed sufficiently high efficiency of biosorbents in the interval pH 5-11 (Fig. 2).

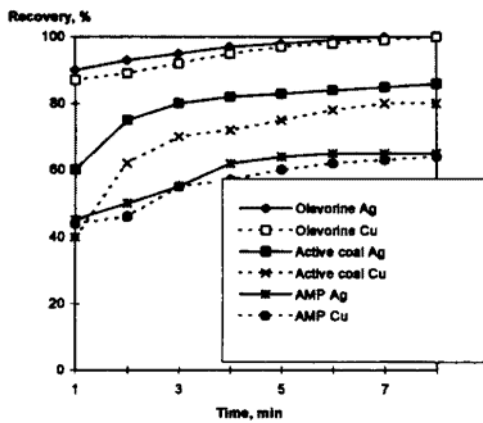


Fig. 1. Comparative sorption of Cu and Ag on different sorbents (AMP – synthetic anionic sorbents)

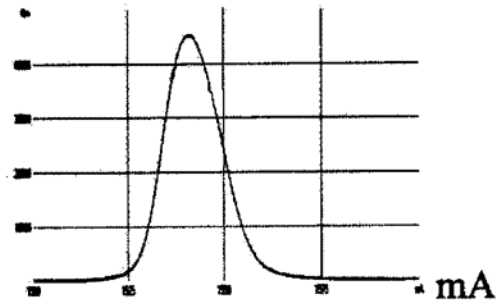


Fig. 2. The results of the analysis of Cu on biosorbent olevorine (20 mg/kg of sorbent, that corresponds to fig. 1 data): "sps" - pulses per sec; mÅ- a wavelength, milliangstrom

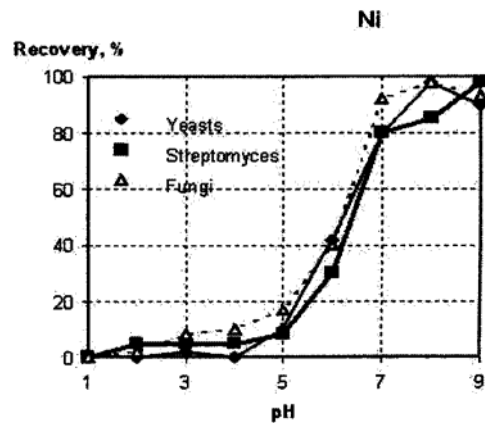
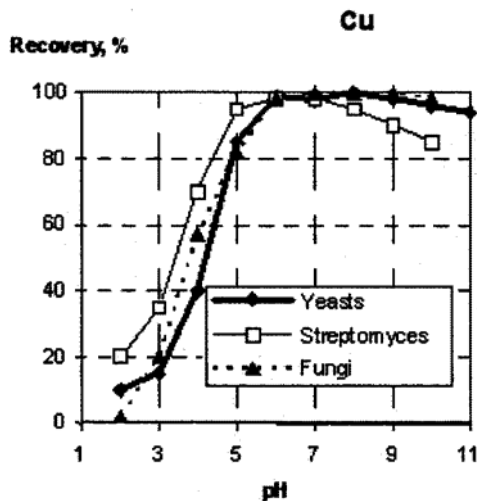


Fig. 3. Biosorbition Cu, Ni at different pH

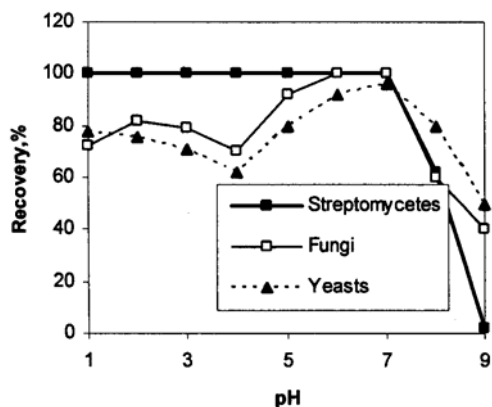


Fig 4. Flotation of biomasses depending on pH with dodecylamines (DA). Concentration of biomass, DA 3x10⁻⁴ M

Fig. 1 data show the unique biosorbitive ability of the oleovorine (bacterial biomass, received from active silt at Mosvodostok firm, responsible for cleaning Moscow effluents [Tcherenkov 2004]) to silver and copper in comparison to the synthetic resins and active coal. Fig.2 presents the possibility selectively separate copper from nickel with different biosorbents under different pH ambiances. Under pH 5 copper adsorbed well and nickel adsorbed more effectively at higher pH (over pH 7).

The adsorptive capacity of microorganisms of different systematic groups in number of events exceeds 40% from the dry weight of biomass. Maximal Au loading on cells *M. luteus* reached 45 % from the dry biomass. High level of Au recovery reached, when using a biomass from departures an different alga biomasses. Sea brown algae *Sargassum natas* sorbed up to 4mg Au/g biomasses in 2 hours. Bacteria *Micrococcus luteus* adsorbs 177 mg Au/g and 253 mgs Au/g biomasses after 30 min. and 2 hours respectively . Granules of AMT Bioclam sorbed 462 mg Pd and 102 mg Pt. *Chlorella vulgaris* accumulated up to 120 mg Au/g masses, *Chlorella pyrenoidosa* - over 140 mg Au/g. Au sorption by *Aspergillus niger* fungi formed 176 mg Au/g, but fungi of *Phizopus arrhizus* sorbed 100-164 mg Au/g. Chitosan can take up 150 mg Au/g from H₂AuCl₄ solution under pH 3.3-4.2 at the recovery up to 99.5 % (Table.1).

The sorption kinetics of metal ions by the cells of microorganisms were high. The ion saturations were obtained at 20-60 min of the time period. Metal ions can convert in the colloidal particles of free metal or its non-soluble compounds (this can be explained uncommonly greater adsorptions values).The biomass of *A. niger* is an adsorption efficient of silver ions from the solutions which the concentration was 2.5 mg/l Ag. The sorption ability was up to 10% silver from the weight of dry biomass. The influence of pH values within 5-7 range do not observed on the silver biosorption. From studied biosorbents oleovorin has shown high efficiency. Oleovorin is a microbial mass isolated from active silt of water filter tank (Fig. 3). Its adsorptive capacity ability exceeded the factors showed by both active carbon and synthetic sorbent AMP.

The heavy metals removing by ion-exchange resins usually sensitive to the presence of Ca²⁺, Mg²⁺ and Na⁺ ions, but fungus biomass, does not adsorbed them

in a good supply. Thereby, the fungi biomass can be more efficient than ion-exchange resins, in the presence of relatively high concentrations of Ca^{2+} , Mg^{2+} and Na^{+} .

The adsorption of metal ion on both non-specific and specific sorbents depends on pH. pH can be influenced on the metal ions accessibility in solution and on the adsorption centers onto the surface.

The acid conditions do not promote cations adsorption. However, the sorption under low pH is connected with the competition of metal cations and H^{+} -ions on the cell surfaces. A significant increase of adsorption of each metal was observed under pH above 7 and it was reached a maximum under pH 10, approximately. In alkaline condition, the metals were precipitated in the form of non-soluble hydroxides onto the surfaces of cells. Interesting example of efficient cleaning of uranium-containing vine waters by driving them through mud ponds with rich vegetation and microflora were a field of studies by Sofia Mining Geological Institute [Groudev, et al., 2003].

The installation for bacterial heap leaching of copper from sulfide ore, belongs to Union Myanmar, works on Kyay Sin Taung deposit. The bioleaching of copper is following the extraction of Cu from the leached solution of copper by the solvent extraction process. This installation reached good results. The practical application of our results could be in cleaning returned solutions from Fe, Ca, Al and other metals.

For the model studied of sorbents, the biomasses containing of protein 58% and baker's yeast (*Saccharomyces cerevisiae*), chitin, chitosan (from "Bioprogress") and chitosan from the Union of Myanmar, active coal, turf, as well as granulated biosorbents (Biochemistries Institute RAS) and oleovorin- a microbial biomass produced from silt of water cleaning were used. The Cu sorption capacity was 47.9 mgg-1 under pH 4 for 5 min contact and 94.9 mgg-1 after 1 hour contact at pH 4.

Table 2. Cu sorption kinetics

Time, min.	Adsorption capacity, mg/g sorbent				
	ANKB-10	SG-10	Chitosan2	Biomass	Yeasts
0	0	0	0	0	0
5	21	10	42	24	12
10	28	14	65	29	19
20	35	16	70	33	22
30	39	18	73	36	26
45	42	20	75	38.9	28.3
60	44	21	76	41.3	31.5

Chitin sorbents can be useful for the cleaning water solution from all heavy metals, radionuclides, bacteria, organic admixtures, and other compounds. High adsorptive features, low ash and cutting prices of chitin and chitosan allow for the application. The potential possibilities of using these sorbents in hydrometallurgical processes for the separations of valuable metals from technological or natural solutions were considered [Mineral proc.,2003, Wodolazov et al. 2000].

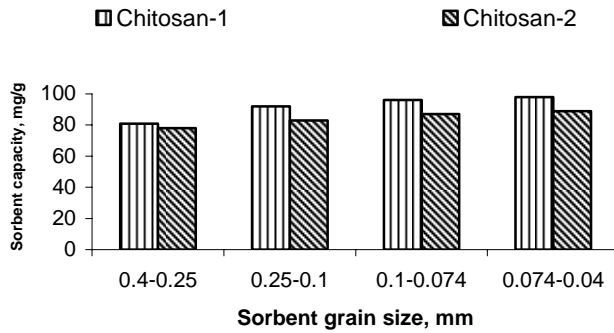


Fig 7. The effect of sorbent grain size on the Cu. sorption capacity

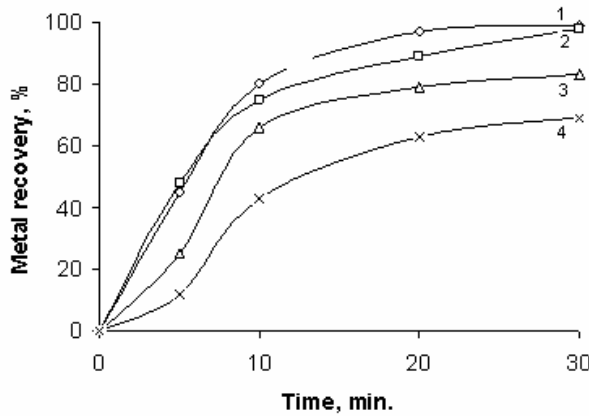


Fig 8. Kinetics of Fe ions adsorption: 1 - AMP; 2 SG - 10; 3-biomass; 4- ANKB-10

The results of calcium adsorption onto sorbents such as KU -2, SG-10, ANKB-10, and turf are presented in Fig. 8. The initial concentration of CaCl_2 was 50 g/l. KU-2 possessed a high capacity 282.8 mgml⁻¹ at a time of mixing 5 min, in contrast to other less efficient sorbents. The biosorbent possesses a high capacity, at the concentrations of Cu ions in an initial solution equals 300 mgml⁻¹ and the time of adsorption of 90 min, it was 41.25 mgg⁻¹, but for yeasts the capacity was 22 mgg⁻¹ under the same conditions. The velocity of Cu sorption on the biosorbent was high. The working capacity of sorbent achieves 14.02 mgg⁻¹ at the recovery equals 93.46%. The influence of pH on the sorption of Cu was important. Under low pH, the sorption on yeasts was satisfy. For this biosorbent, under pH 5 and 3 and the 60 min contact time, the Cu recoveries were 99.0 and 97.7 %, respectively. The adsorptive capacity 14.85 and 14.6 mgg⁻¹ respectively. For comparison, the adsorption capacity of yeasts was 74.3 mgg⁻¹ and the Cu extraction recovery was 74.3% under pH 5. The results of Cu extraction from sewages using both biosorbents, can be used for other plants.

Table 3. Kinetics of Pb sorption

Sorbents (7 ml).	Adsorption capacity mgml-1	Recovery, %.	Time, min.
Active carbon	0.71	4.4	5
Chitosan-2	6.8	42.2	
KU-2	10.14	63.1	
ANKB-10	14.10	87.7	
Turf	15.51	96.5	
Active carbon	3.10	19.33	15
Chitosan-2	8.2	51.0	
KU-2	14.6	91.1	
ANKB-10	16.01	99.6	
Turf	15.8	98.4	
Active carbon	4.14	25.7	30
Chitosan-2	10.9	67.8	
KU-2	14.64	91.1	
ANKB-10	16.07	100.0	
Turf	15.9	99.07	
Active carbon	4.9	30.8	60
Chitosan-2	14.1	87.7	
KU-2	14.64	91.1	
ANKB-10	-	-	
Turf	15.9	99.3	
Active carbon	5.6	34.89	90
Chitosan-2	14.8	92.0	
KU-2	-	-	
ANKB-10	-	-	
Turf	16.07	100.0	

The capacity and kinetics of adsorption depend on the size grains of sorbents, an ambiances pH, and the concentrations of metals in the solutions.

The ion adsorption depends on the grain size of sorbents and the time of mixing (Table 3). The most high capacity 118.57 mgml-1 was observed for -0.5 mm grain size of sorbent and the extraction was 83.0 % at the concentration of solution equals 2 g/l and time of adsorption equals 120 min. A high velocity of adsorptions was observed. The extraction of lead has obtained 100% at the time of mixing of solution with the sorbent, equals 5 min. The high adsorptions velocity was observed at the time period from 0 to 30 min, then the adsorption kinetic was slow.

The influence pH ambiences on the sorption and extraction of lead (II) on the brown coal (size fraction of -0.5 mm) from the solution which the concentration of lead (II) was 2 g/l, are presented in Table 4. The high adsorptive capacities equal 118.57 and 120.0 mg/ml at the time of adsorptions equals 120 min and pH 4 and 5 were obtained. The extraction of lead (II) has been 64.9% and the capacity of sorbent was 92.7 mg/ml under pH of 3.

The results of biosorptive extractions of metals from solutions and cleaning solutions using microorganisms show a possibility for the change the synthetic resins

by biosorbents as well as in steady-state and dynamic conditions. The sufficient time of adsorption falls within 20-30 min. The capacity and kinetics of adsorption depended on pH, the concentrations of metals in solution and others conditions. A perspective using of chitin sorbents, yeasts and others microorganisms for removing Cu and other heavy metals from mine water and an application of sorbents for the conversion of productive geotechnological solution seem more realistic.

ACKNOWLEDGMENT

Our thanks to Shinkareb S M (Bioprogress), Dr War War, Dr Myat Myat Mon (Biotechnological centre, Myanmar) and Ms May Myo Han (REN) for supply samples of chitosan and chitin.

LITERATURE

- Chitin and chitisan - a reception, characteristics and using*. Ed. Skriabina T. G. and others. Science, Moscow, 2002.
- GROUDEV, S. N., 2003, *Bioremediation of polluted waters in an uranium deposit*. Proc. 22-nd International Mineral Processing Congress, Pp.1742-52. Cape Town, South Africa SAMU 5..
- MATIS, K.A., and oth., 2001, *Sorptive flotation for metal ions recovery*. Conference Froth Flotation/Dissolved Air Flotation, University of Nevada, Reno, Nevada, USA.
- Mineral processing in the 21st Century. Proc. X Balkan Mineral Processing Congress, Varna, Bulgaria, 2003
- NEBERA, V.P. SOLOZHENKIN P.M, 2002, *Biosorption and flotation biomass, loaded by precious or toxic metals*. The Europ. J. of Mineral Processing and Environmental Protection, V. 2, 151-157.
- Recycling and waste treatment in mineral and metal processing: technical and economic aspects*, Lulea, Sweden, 2002.
- SANGALOV, A. I., and oth., 1999, *Sorbents for the crude oil on the base of termaly hydrofobised sawdust*. J.Apl. Chem, 72(7), 1276 – 12818.
- TABOADA, EDOLIO, and oth., 2003, *Retention capacity of chitosan for copper and mercury*, J. Chilean Chem. Soc., V.48, No 1.
- TCHERENKOV, A., 2004, Director GUP "Mosvodostok". The big river begins from small. The Moscow Environments, 8(76) p. 2. Interview A. Astafiev.
- VODOLAZOV, L. I., and oth., 2000, *Geotechnology, Heap leaching: Poor mineral sorses*", Moscow, MGGRA.
- VOLESKY, BOYA, 1994, *Biosorption for the next century*, Trans. Internat. Biohydrometallurgy Symposium, Spain.

Nebera V.P., Sai Kyaw Naing Oo, *Biosorpcja jonów metali z roztworów geotechnicznych*, Physicochemical Problems of Mineral Processing, 41 (2007) 251-258 (w jęz. ang).

Szereg mikroorganizmów i naturalnych substancji jest zdolnych do adsorpcji jonów metali z roztworów. Jako naturalne biosorbenty można używać chitynę i chitosan oraz węgiel drzewny. Badania biosorpcji na różnych mikroorganizmach i na równych naturalnych sorbentach zostały przeprowadzone. Na ich podstawie wytypowano szereg biosorbentów jako potencjalny materiał do zastosowania w oczyszczaniu ścieków z hałd mineralnych. Badania przeprowadzono nad flotacją biomasy uzyskanej po biosorpcji jonów metali. Otrzymane wyniki wskazują, że flotacja biomasy po adsorpcji jonów metali była bardzo dobra. Przykładowo, uzyski Cu i Ag były bliskie 100%, prowadząc adsorpcje za pomocą 10g biomasy z 100 ml roztworu tych jonów. Na podstawie przeprowadzonych doświadczeń starano się poznać korelację między wynikami adsorpcji jonów a wynikami flotacji biomasy. Uzyskane w pracy wyniki stwarzają przesłanki dla zastosowania tego procesu dla oczyszczania ścieków przemysłowych i odzysku z nich cennych metali.

Tomasz GROBELSKI*, Jadwiga FARBISZEWSKA-KICZMA*,
Teresa FARBISZEWSKA**

BIOLEACHING OF POLISH BLACK SHALE

Received March 18, 2007; reviewed; accepted July 2, 2007

Heterotrophic pretreatment combined with autotrophic bioleaching of Polkowice black shale were studied. Combination of these two processes was introduced as two-stage process which turned out to be more efficient in the terms of metals extraction. The sequence of preliminary heterotrophic and further autotrophic bioleaching was found as most reliable processing manner, since heterotrophic process provides the material's surface area expansion, and therefore strong influences rate and efficiency of autotrophic leaching. Besides, it was found that tube bioreactors designed specially for hereby research ensure better processing condition than Erlenmeyer flasks in the terms of extraction speed and efficiency.

Key words: heterotrophic bacteria, autotrophic bacteria, bioleaching, black shale, tube bioreactor, copper, silver, leaching

INTRODUCTION

During our studies on bioleaching of sulfide minerals, various experimental conditions were tested. The influence of various parameters (temperature, pH, stirring conditions, leaching medium composition and solid to liquid phase ratio) on bioleaching effectiveness and kinetics were investigated. However, acidophilic bacteria of *Acidithiobacillus* type were the only one considered so far (Farbiszewska et al., 1994, 1996, 2003). Therefore, we have introduced a combination of two processes: autotrophic bioleaching and heterotrophic pretreatment in our latest researches.

We assumed that heterotrophic leaching should provides better extraction of metals ions from organometallic compounds in shale ores. These organometallic compounds cannot be dissolved with autotrophic microorganisms. However, the results of heterotrophic bioleaching in neutral medium, using very active autochthonic bacteria

* Opole University, Faculty of Natural and Technical Sciences, Process Engineering Department, ul. Dmowskiego 7/9, 45-365 Opole, Poland.

** Opole University, Faculty of Natural and Technical Sciences, Biotechnology and Molecular Biology Department, ul. Kominka 4, 45-032 Opole, Poland, gaga@uni.opole.pl.

strains, revealed a marginal role of organometallic compounds in examined mineral materials, thus almost complete lack of biooxidation and poor metal extraction (Farbiszewska-Kiczma et al., 2005). Therefore, alternative two-stage process was taken under consideration. It involves preliminary heterotrophic treatment and further autotrophic bioleaching.

Heterotrophic bioleaching process involves biooxidation of organometallic bonds as well as various organic bonds. This provides mineral's surface area expanding and thus increasing material susceptibility to further autotrophic bioleaching. As a result, great increase of extraction efficiency can be observed (Farbiszewska-Kiczma et al., 2004).

This procedure was introduced in studies on leaching of polymetallic shale ore, called Polkowice black shale. Tube bioreactors designed by our research team were used in these bioleaching experiments (Farbiszewska-Kiczma et al., 2006).

The aims of these researches were:

- evaluate bioleachability of Polkowice black shale ore;
- establish reliable lab-scale pilot operations of process;
- optimize configuration and settings.

MATERIALS AND METHODS

Examined material was black shale ore from Polkowice mine, containing among others 13.94% Cu and 148/t Ag. Particle size was within range of 0.4 to 2 mm. Bioleaching processes were carried out in Erlenmeyer flasks and in tube bioreactors with five beds.

BIOLEACHING IN ERLENMEYER FLASKS

Bioleaching in Erlenmeyer flasks was performed in two ways. First process was 35 days autotrophic bioleaching, while second included 25 days heterotrophic pretreatment and then 35 days autotrophic bioleaching.

In first process to each of three flasks containing 70 g of pretreated black shale ore, 350 dm³ of leaching medium 2 K was added. Before that, leaching medium was inoculated with mixture of autochthonic bacteria strains *Acidithiobacillus ferrooxidans* and *Acidithiobacillus thiooxidans*. Mixture ratio was 1:1. Process was carried out 35 days at temperature 25°C, pH=1.8. Another three control flasks were supplied with thymol – bacteriostatic substance. Both bacterial and control systems were aerated and stirred with magnetic stirrers, pH was regulated daily to value 1.8. At the end of process contents of Cu and Ag in treated ore were examined.

In second process 350 dm³ of mineral solution was added to each of three flasks containing 70g of black shale ore. After that, flasks were inoculated with a mixture of active, autochthonic, non-antagonistic bacteria strains. Thymol was added to control flasks. Process was performed 25 days at temperature 25°C. pH was regulated daily to value 7, and all flasks were stirred with magnetic stirrers. At the end of process, the

contents of Cu and Ag in treated ore were examined. Then, the material was dried and flushed with H₂SO₄ water solution, bringing pH value to 1.8. After that operation, autotrophic bioleaching was started using 2 K medium and autochthonic bacteria strains *Acidithiobacillus ferrooxidans* and *Acidithiobacillus* mixed in the ratio of 1:1. The control flasks were supplied with thymol. All flasks were placed on magnetic stirrers. Bioleaching process was performed 35 days at the temperature 25°C, pH was regulated daily to value 1.8. At the end of process the contents of Cu and Ag in treated ore were examined.

BIOLEACHING IN BIOREACTORS

Process was carried out in tube bioreactors designed by our research team. Each bioreactor contained 1250 g of black shale ore (250 g per bed) and 3750 dm³ of irrigating 2 K medium inoculated with autochthonic bacteria strains *Acidithiobacillus ferrooxidans* and *Acidithiobacillus thiooxidans* mixed in the ratio of 1:1. Control system was supplied with thymol. Bioreactors were aerated with bubbler. Process was carried out 25 days at temperature 25°C. At the end, the contents of Cu and Ag in treated ore were examined.

RESULTS AND DISCUSSION

After 35 days autotrophic bioleaching performed in Erlenmeyer flasks, black shale ore metallization decreased from 13.94% Cu and 148g/t Ag to 8.25% Cu and 132g/t Ag. It means that, 40.82% of Cu and 10.81% of Ag were extracted (Fig.1.). In control systems the contents of Cu and Ag were respectively 12.30% and 141g/megagram (Mg), it means that, 11.77% of Cu and 4,73% of Ag were extracted (Fig. 1.).

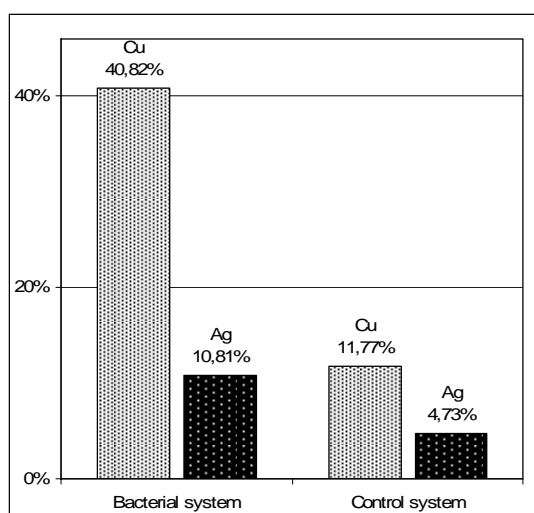


Fig. 1. Percentage of Cu and Ag extracted from ore after 35 days autotrophic bioleaching in Erlenmeyer flasks (process 1: autotrophic bioleaching only)

After 25 days heterotrophic bioleaching in Erlenmeyer flasks black shale ore the metallization decreased to 13.80% and 139 g/Mg of Ag. It means that the contents of Cu and Ag were decreased respectively by 1.0 and 6.08% (Fig.2.). The contents of Cu and Ag in control systems were 13.83% and 142 g/Mg (0.79% of Cu and 4.05% of Ag extracted) (Fig. 2.).

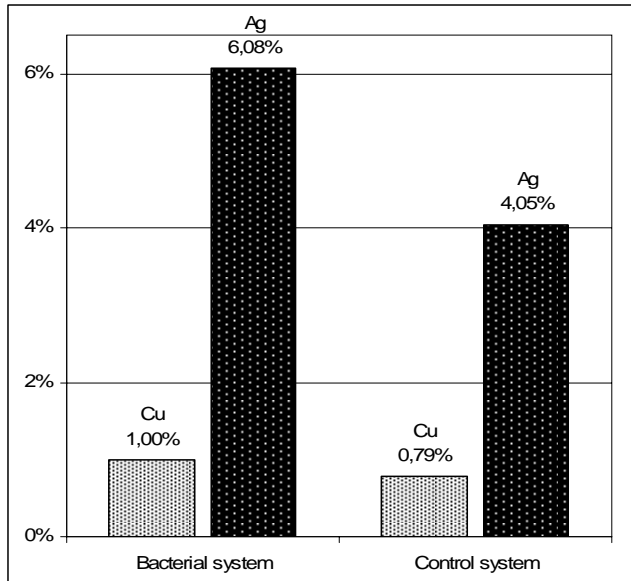


Fig. 2. Percentage of Cu and Ag extracted from ore after 25 days heterotrophic bioleaching in Erlenmeyer flasks (process 2 – stage 1: pretreatment)

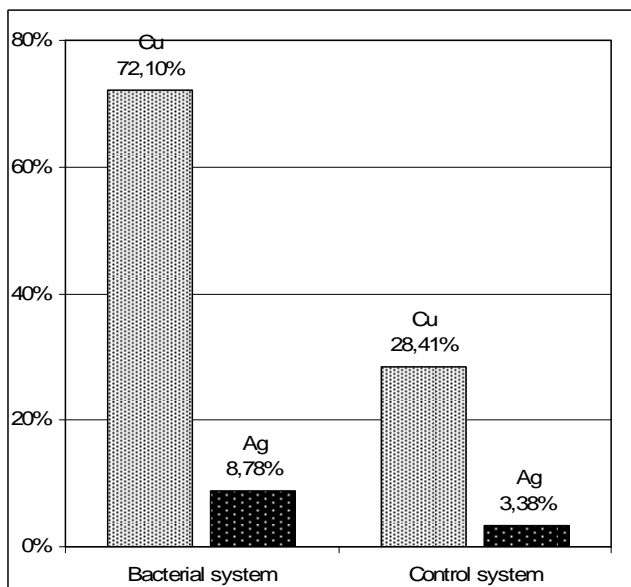


Fig. 3. Percentage of Cu and Ag extracted from pretreated ore (25 days heterotrophic treatment) after 35 days autotrophic bioleaching (process 2 – stage 2: autotrophic bioleaching)

After ore acidification to pH=1.8, further 35-days autotrophic bioleaching in Erlenmeyer flasks was carried out, at the end of bioleaching process 3.75% of Cu and 126g/t of Ag remained in ore. In this process 72.1% of Cu and 8.78% of Ag were extracted (Fig. 3). The contents of Cu and Ag in control systems were 9.87% and 137g/t (that means 28.41% of Cu and 3.38% of Ag were extracted) (Fig. 3.) In total, in both heterotrophic and autotrophic bioleaching experiments 73.1% of Cu and 14.86% of Ag were extracted. The chemical leaching has extracted 29.2% of Cu and 7.43% of Ag.

After 25 days autotrophic bioleaching in bioreactor, the contents of Cu and Ag in shale decreased to 3.33% and 75 g/Mg respectively (13.44% and 133 g/Mg in a control system). Thus, 76.17% of Cu and 49.32% of Ag were extracted in bacterial system, while 3.59% of Cu and 10.14% of Ag in control system (Fig. 4.). Autotrophic bioleaching in tube bioreactor, which lasted 25 days only, was more efficient (3.07% in case of Cu and right up to 34.46% in case of Ag) than two-stage bioleaching in Erlenmeyer flasks. One should notice that process in bioreactor lasted 35 days shorter. The amount of material was 18 times greater and the solid to liquid phase ratio was 1:3 instead 1:5. The percentage of extracted Cu (76.17%) in tube bioreactor was almost two times greater than in flask after 35 days (40.82% - autotrophic bioleaching) and comparable to those in flask after 60 days (73.1% - heterotrophic and autotrophic bioleaching). The percentage of extracted Ag in bioreactor was 4/3 times greater than those in flasks (for autotrophic/autotrophic after heterotrophic bioleaching respectively).

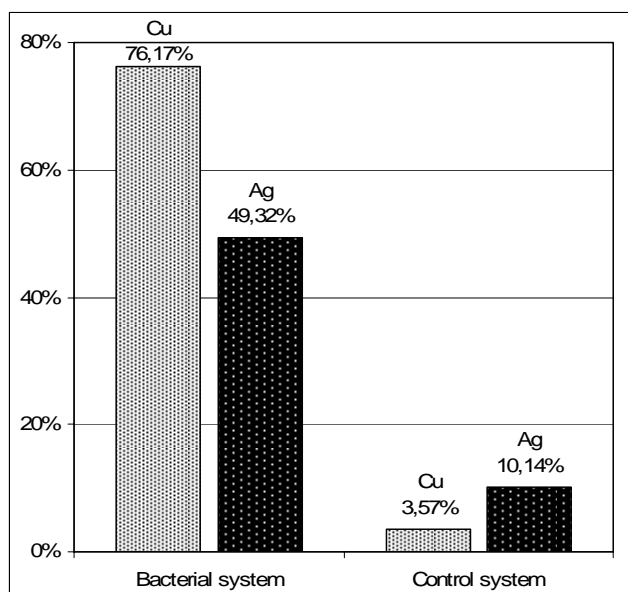


Fig. 4. Percentage of Cu and Ag extracted from ore after 35 days autotrophic bioleaching in tube bioreactors

CONCLUSIONS

1. Black shale ore from Polkowice mine is amenable to bioleaching.
2. Heterotrophic bioleaching of Polkowice ore provides the surface area expansion and an increase of efficiency of autotrophic bioleaching.
3. Bioleaching process runs more effective in tube bioreactors than in Erlenmeyer flasks.
4. The most reliable way to processing Polkowice black shale ore seems to be a two-stage bioleaching process (heterotrophic bioleaching prior to autotrophic) which will be conducted in tube bioreactors.

ACKNOWLEDGEMENT

This work was carried out in the frame of Bioshale (European project contract NMP2-CT-2004 505710). The authors acknowledge the financial support given to this project by the European Commission under the Sixth Framework Programme for Research and Development.

REFERENCES

- FARBISZEWSKA T., CWALINA B., FARBISZEWSKA-BAJER J., Dzierżewicz Z., 1994, *The use of bacterial leaching in the utilization of wastes resulting from mining and burning lignite*, Acta BIOLOGICA CRACOVIENSIA, SERIAS: BOTANICA, 36,1-8.
- FARBISZEWSKA T., CWALINA B., 1996, *Metabolic activity of autochthonous and museum strains of Thiobacillus ferrooxidans*, Acta Biologica Cracoviensia, serias: Botanica, 38, 1-8.
- FARBISZEWSKA T., FARBISZEWSKA-KICZMA J., BĄK M., 2003, *Biological extraction of metals FROM A POLISH BLACK SHALE*, Physicochemical Problems of Mineral Processing, 37, 51-57.
- FARBISZEWSKA-KICZMA J., FARBISZEWSKA T., 2005, *Isolation of bacteria that degrade organometallic compounds from metallic wastes*, Physicochemical Problems of Mineral Processing, 39, 263-267.
- FARBISZEWSKA-KICZMA J., FARBISZEWSKA T., BĄK M., 2004, *Bioleaching of metals from polish black shale in neutral medium*, Physicochemical Problems of Mineral Processing, 2004, 38, p. 273-280.
- FARBISZEWSKA-KICZMA J., FARBISZEWSKA T., GROBELSKI T., KICZMA B., 2006, *Bioleaching in tube reactors for utilization of metallurgical wastes*, Proceedings Central European Conference ECOpole '06, Hradec-Kralove – Jamrozowa Polana, 18-20.
- Grobelski T., Farbiszewska-Kiczma J., Farbiszewska T.,** *Biologowanie polskiego czarnego łupka*, Physicochemical Problems of Mineral Processing, 41 (2007) 259-264 (w jęz. ang.).

Zostały przeprowadzone badania nad wykorzystaniem kombinacji procesów bioprzegotowania z użyciem bakterii heterotroficznych i biolugowania za pomocą bakterii autotroficznych próbek rudy łupkowej otrzymanej z kopalni Polkowice. Kombinacja tych dwóch procesów została przedstawiona jako proces dwu-stadialny, który zapewnia bardziej efektywniejszą ekstrakcję metali z surowca mineralnego. Kolejność realizacji procesu dwu-stadialnego okazała się być bardziej skuteczna, gdyż proces z użyciem heterotroficznych mikroorganizmów powoduje, że powierzchnia surowca staje się bardziej podatna na biolugowanie z użyciem autotroficznych mikroorganizmów. Dodatkowo zostało wykazane, że reaktory rurowe, specjalnie zaprojektowane do tych badań, były lepsze w porównaniu do procesu realizowanego w kolbach stożkowych.

Stoyan GROUDEV*, Irena SPASOVA*, Marina NICOLOVA*, Plamen GEORGIEV*

ACID MINE DRAINAGE CLEANUP IN A URANIUM DEPOSIT BY MEANS OF A PASSIVE TREATMENT SYSTEM

Received April 15, 2007; reviewed; accepted May 15, 2007

Acid drainage waters generated in the Curilo uranium deposit, Bulgaria, were treated by means of a pilot-scale multibarrier with a total volume of 23 m³ and consisting of an alkalizing limestone drain and an anoxic section for microbial dissimilatory sulphate reduction, biosorption and additional chemical neutralization. The waters had a pH in the range of about 2.5 – 4.0 and contained radionuclides (U, Ra), heavy metals (Cu, Zn, Cd, Pb, Ni, Co, Fe, Mn), arsenic and sulphates in concentrations usually much higher than the relevant permissible levels for waters intended for use in agriculture and/or industry. The water flow rate through the multibarrier varied in a large range (approximately from 1 to 17 m³/24 h), reflecting water residence times of about 300 – 18 hours. An efficient removal of pollutants was achieved by the multibarrier during different climatic seasons, even during cold winter days at external air and water temperatures close to 0 °C. However, some essential changes in the composition and properties of the multibarrier arised during the 28 months since the start of its operation.

Key words: drenage, cleanup, uranium, waters

INTRODUCTION

The acid mine drainage waters generated in the Curilo uranium deposit, Bulgaria, are a heavy environmental problem, especially since the end of the mining operations in this deposit sixteen years ago. The fractured ore body and several dumps consisting of mining wastes are, especially after rainfall, the main sources of these waters. The waters have a low pH (usually in the range of 2.5 – 4.0) and contain radionuclides, heavy metals, arsenic and sulphates in concentrations usually much higher than the relevant permissible levels for waters intended for use in the agriculture and/or industry. The solubilization of these pollutants from the residual ore in the deposit is connected mainly with the oxidative activity of the indigenous acidophilic chemolithotrophic bacteria [Groudev et al., 2003].

* University of Mining and Geology “Saint Ivan Rilski”, Sofia, Bulgaria, e-mail: groudev@mgu.bg.

Since the summer of 2004 a portion of the above-mentioned polluted waters is treated by means of a multibarrier constructed in the deposit. The structure of this multibarrier and its work have been described in several papers, the most recent of which are those by Groudev et al., [2006a, 2006b]. The present paper summarizes the data obtained during the 28 months of multibarrier operation and contains the main conclusions based on these data.

MATERIALS AND METHODS

The multibarrier was constructed in a ravine collecting a portion of the acid drainage waters generated in the deposit. The multibarrier was a pond dug into the ground and its bottom and walls were isolated by an impermeable plastic sheet. The multibarrier consisted of two sections: an alkalizing limestone drain and an anoxic section for microbial dissimilatory sulphate reduction, biosorption and additional chemical neutralization. The alkalizing drain had a volume of about 2.5 m³ and was filled by a mixture of crushed limestone and gravel pieces (in a ratio of about 1:2 as dry weight) with a particle size less than 12 mm. The second section of the multibarrier had a volume of about 20.4 m³ (8.0 m long, 1.7 m wide, and 1.5 m deep) and was filled by a mixture of biodegradable solid organic substrates (cow manure, plant compost, straw), crushed limestone and zeolite saturated with ammonium phosphate. This section of the multibarrier was inhabited by a microbial community consisting mainly of sulphate-reducing bacteria and other metabolically interdependent microorganisms (Table 1).

Table 1. Microorganisms in the acid mine drainage and in the effluents from the permeable reactive multibarrier

Microorganisms	In the acid mine drainage	In the multibarrier effluents
	Cells/ml	
Fe ²⁺ -oxidizing chemolithotrophs (at pH 2)	10 ⁴ – 10 ⁷	0 – 10 ²
Aerobic heterotrophs (at pH 2)	10 ¹ – 10 ⁴	10 ¹ – 10 ³
S ₂ O ₃ ²⁻ -oxidizing chemolithotrophs (at pH 7)	0 – 10 ³	10 ¹ – 10 ⁴
Aerobic heterotrophs (at pH 7)	0 – 10 ²	10 ¹ – 10 ⁴
Anaerobic heterotrophs (at pH 7)	0 – 10 ¹	10 ⁴ – 10 ⁷
Sulphate-reducing bacteria	0 – 10 ¹	10 ⁴ – 10 ⁷
Cellulose-degrading microorganisms	ND	10 ³ – 10 ⁶
Bacteria fermenting sugars with gas production	ND	10 ³ – 10 ⁷
Ammonifying bacteria	ND	10 ² – 10 ⁵
Denitrifying bacteria	ND	10 ² – 10 ⁵
Fe ³⁺ -reducing bacteria	ND	10 ³ – 10 ⁶
Methane-producing bacteria	ND	10 ¹ – 10 ⁴

Note: ND = not detected

The quality of the waters was monitored at different sampling points located at the inlet and the outlet of the alkalizing drain and of the section for dissimilatory sulphate reduction and biosorption, as well as at different depths within these two sections of the multibarrier.

The parameters measured in situ included: pH, Eh, dissolved oxygen, total dissolved solids and temperature. Elemental analysis was done by atomic adsorption spectrophotometry and induced coupled plasma spectrophotometry in the laboratory. The radioactivity of the samples was measured, using the solid residues remaining after their evaporation, by means of a low background gamma-spectrophotometer ORTEC (HpGe – detector with a high distinguishing ability). The specific activity of ^{226}Ra was measured using a 10 dm³ ionization chamber.

Elemental analysis of solid samples from the sediments and the plant biomass was performed by digestion and measurement of the ion concentration in solution by atomic adsorption spectrophotometry and induced coupled plasma spectrophotometry. Mineralogical analysis was carried out by X – ray diffraction techniques. The mobility of the pollutants was determined by the sequential extraction procedure [Tessier et al., 1979]. The fraction analysis of the solid organic component in the multibarrier was performed using air dried samples after their prior washing with distilled water to remove the carbonates and the water – soluble organic compounds. The total amount of crystalline polysaccharides (cellulose) and non-crystalline polysaccharides (hemicellulose) was determined by hydrolysis with sulphuric acid [Ryan et al., 1990]. The non-crystalline polysaccharides (hemicellulose) were determined by hydrolysis with hydrochloric acid under anaerobic conditions [Lowe, 1993]. For determination of lignin the samples were initially treated by 1 M HCl for 12 h to remove the solid precipitates from the surface of the organic matrix and to make it well exposed for the subsequent solubilization of the lignin. This solubilization was performed by means of solution containing 2 M NaOH, CuO, Fe(NH₄)₂(SO₄)₂·6H₂O under anaerobic conditions, at 170 °C for a period of 4 h in the Soxhlet apparatus [Kogel & Bochter, 1985]. The suspensions of dissolved organic compounds obtained by the above-mentioned hydrolytic treatments were clarified by centrifugation at 1700 rpm for 30 min. The clarified supernatants were used for determination of the concentration of the respective dissolved organic compounds by their chemical oxidation to CO₂ at high temperature.

The isolation, identification and enumeration of microorganisms were carried out by methods described elsewhere (Karavaiko et al., 1988; Widdel & Hansen, 1991; Widdel & Bak, 1991; Groudeva & Tzeneva, 2001; Hallberg & Johnson, 2001).

RESULTS AND DISCUSSION

An efficient removal of pollutants from the acid drainage waters was achieved by means of the multibarrier (Table 2). The water flow rate through the multibarrier was changed considerably during the operation period (within the range of about 1 – 17

m³/24 h, reflecting water residence times of about 300 – 18 hours). These changes were connected mainly with the activity and permeability of the multibarrier and with the level of pollution of the waters being treated.

Table 2. Data about the acid mine drainage and the effluents from the permeable reactive multibarrier

Parameters	Acid mine drainage	Multibarrier effluents	Permissible levels for waters intended for use in agriculture and industry
Temperature °C	(+1.2) - (+25.1)	(+1.4) - (+27.5)	-
pH	2.42 – 4.25	6.22 – 7.83	6 – 9
Eh, mV	(+290)-(+597)	(-140)-(-280)	-
Dissolved O ₂ , mg/l	1.7 – 6.0	0.2 – 0.4	2
TDS, mg/l	930 – 2972	545 – 1827	1500
Solids, mg/l	41 – 159	32 – 104	100
DOC, mg/l	0.5 – 2.1	51 – 159	20
SO ₄ ²⁻ , mg/l	532 – 2057	275 – 1225	400
U, mg/l	0.10 – 2.75	< 0.05	0.6
Ra, Bq/l	0.05 – 0.50	< 0.03	0.15
Cu, mg/l	0.79 – 5.04	< 0.20	0.5
Zn, mg/l	0.59 – 59.8	< 0.20	10
Cd, mg/l	<0.01 – 0.10	< 0.004	0.02
Pb, mg/l	0.08 – 0.55	< 0.02	0.2
Ni, mg/l	0.17 – 1.49	< 0.03 – 0.10	0.5
Co, mg/l	0.12 – 1.22	< 0.03 – 0.10	0.5
Fe, mg/l	37 – 671	0.5 – 9.5	5
Mn, mg/l	2.8 – 79.4	0.5 – 5.2	0.8
As, mg/l	0.05 – 0.32	< 0.01	0.2

The activity of the multibarrier was based on three main mechanisms participating in the removal of pollutants: chemical neutralization, biosorption and microbial dissimilatory sulphate reduction. The chemical neutralization was performed by the crushed limestone mainly in the alkalizing drain but also in the second, rich-in-organics section. In the alkalizing drain the pH of the polluted waters was increased to values near the neutral point and as a result of this most of the dissolved iron (present as Fe³⁺ ions) was precipitated as ferric hydroxides. Portions of the non-ferrous metals and aluminum (usually about 20 – 40 % and about 70 – 80 %, respectively) were also removed in the drain as a result of hydrolysis and subsequent precipitation as well as by sorption by the gelatinous ferric hydroxides. Portions of uranium and arsenic were also removed in this way (Table 3). The increase in pH in the alkalizing drain facilitated the growth of microorganisms in the second section of the multibarrier. The role of chemical neutralization was essential during the cold winter days when the growth and activity of the microbial community in the multibarrier was inhibited or

completely ceased. The chemical generation of alkalinity steadily decreased in the course of time because the limestone was armored due to the iron precipitates deposited on its surface.

Table 3. A typical example for the changes in the composition of the polluted waters during their treatment in the multibarrier

Parameters	AMD before treatment	Alkalizing drain	Zones in the section for MDSR		
			2 m from the inlet	4 m from the inlet	6 m from the inlet
pH	2.96	5.06	5.63	6.10	6.28
Eh, mV	+ 467	+ 320	+145	- 45	- 214
Acidity, mmol/l	3.8	2.2	0.9	-	-
DOC, mg/l	-	-	135	140	98
Cu, mg/l	50.4	3.73	0.50	0.21	0.05
Zn, mg/l	59.8	13.02	2.62	0.57	0.50
Cd, mg/l	0.04	0.02	0.02	< 0.005	< 0.005
Pb, mg/l	0.16	0.14	< 0.03	< 0.03	< 0.03
Ni, mg/l	1.43	1.35	1.05	0.70	0.008
Co, mg/l	1.10	0.88	1.03	0.24	< 0.005
Fe, mg/l	128	1.81	0.27	0.34	0.55
Mn, mg/l	19.8	20.8	21.5	15.4	5.24
U, mg/l	1.23	0.34	0.07	0.05	0.03
SO ₄ ²⁻ , mg/l	1990	1870	1810	1650	680

Table 4. Content of pollutants in the dead solid plant biomass in the permeable reactive multibarrier

Pollutants	Content, mg/kg dry biomass				
	November 2004	March 2005	August 2005	March 2006	September 2006
Uranium	10 – 32	17 – 71	23 - 88	32 – 114	32 – 122
Radium	5 – 14	10 – 32	15 - 41	21 – 53	23 – 57
Copper	28 – 73	37 – 134	44 - 181	60 – 225	62 – 221
Zinc	14 – 51	28 – 82	37 - 190	51 – 230	59 – 242
Cadmium	2 – 12	6 – 19	6 - 27	8 – 41	8 – 44
Lead	8 – 30	7 – 59	10 - 64	15 – 73	15 – 77
Nickel	8 – 35	9 – 62	9 - 77	15 – 90	19 – 95
Cobalt	5 – 30	11 - 51	14 - 70	17 – 82	16 – 90
Manganese	32 – 109	37 - 135	44 - 190	51 – 210	55 – 233
Arsenic	2 - 14	6 - 23	10 - 31	12 – 44	12 – 51

The biosorption of pollutants by the dead plant biomass present in the second section of the multibarrier was also an essential mechanism in the water clean up during the warmer but mainly during the cold months of the year (Table 4).

Considerable portions of all heavy metals, arsenic and uranium as well as most of the radium were removed in this way. The biosorption, together with the chemical neutralization, was the prevalent mechanism during the first 5 – 6 months since the start of the operation and even later was prevalent in the first 3 – 4 m from the inlet of the anoxic section, especially in the top layers (down to 50 – 70 cm from the surface). The sorption capacity of the dead biomass steadily decreased in the course of time.

The microbial dissimilatory sulphate reduction played an essential role in the water clean up during the warmer months of the year. The anaerobic sulphate-reducing bacteria were a quite numerous and diverse population in the multibarrier (Table 5). The prevalent and most active strains of these bacteria were related to the genera *Desulfovibrio* (mainly *D. desulfuricans*) and *Desulfobulbus* (mainly *D. elongatus*) but representatives of the genera *Desulfococcus*, *Desulfobacter* and *Desulfosarcina* were also well present. As a result of their activity the pH of the waters was stabilized around the neutral point due to generation of hydrocarbonates ions during the microbial sulphate reduction (the role of limestone was also essential as it was mentioned earlier). The non-ferrous metals, iron and arsenic were precipitated mainly as the relevant insoluble sulphides. Uranium was precipitated mainly as uraninite (UO_2) as a result of the prior reduction of the hexavalent uranium to the tetravalent form.

Table 5. Sulphate-reducing bacteria in the effluents from the permeable reactive multibarrier

Sulphate-reducing bacteria	Cells/ml
<i>Desulfovibrio</i> (mainly <i>D. desulfuricans</i>)	$10^4 - 10^7$
<i>Desulfobulbus</i> (mainly <i>D. elongatus</i>)	$10^2 - 10^7$
<i>Desulfococcus</i> (<i>D. postgatei</i>)	$10^2 - 10^6$
<i>Desulfobacter</i> (<i>D. multivorans</i>)	$10^2 - 10^5$
<i>Desulfotomaculum</i> (mainly <i>D. nigrificans</i>)	$10^1 - 10^4$
<i>Desulfosarcina</i> (<i>D. variabilis</i>)	$10^2 - 10^5$
<i>Desulfomonas</i> (non-identified species)	$10^1 - 10^4$

A relatively long period of time (of about 3 – 4 months) was needed for the sulphate-reducing bacteria to establish a numerous and very active population in the multibarrier. The microbial sulphate reduction was the prevalent mechanisms in the deeply located layers and in the back zones in the multibarrier (at distances longer than 4 – 5 m from its inlet). The microbial sulphate reduction was a function of the concentration of organic monomers dissolved in the waters. These monomers were generated as a result of the biodegradation of the solid biopolymers by the different heterotrophs possessing hydrolytic enzymatic activity. This process resulted in a steady decrease in the concentration of the easily degradable solid biopolymers (cellulose and hemicellulose) present in the multibarrier (Table 6). At the same time, precipitation of pollutants caused a negative effect on the permeability of the multibarrier (Table 7). It must be noted that the precipitation of the different pollutants

was not homogenous and the different sites in the multibarrier differed considerably from each other with respect to their chemical and mineralogical composition (Table 8).

Table 6. Exhaustion of the solid organic substrates in the multibarrier after 28 months of treatment

Organic fraction	Initial mixture	Sampling points, distance from the inlet			
		1 m top	1m down	3m top	3 m down
g organic carbon/ 100g solid sample					
Crystalline polysaccharides	8.2	0.5	0.5	0.4	0.8
Non-crystalline polysaccharides	37.4	1.4	1.9	1.7	2.8
Lignin	5.1	4.6	4.8	4.3	4.1

The microbial activity in the multibarrier markedly depended on the temperature and during the cold winter days was negligible. However, at air temperatures about 0 °C and water temperatures close to the freezing point, the temperatures inside the multibarrier, within the deeply located layers, usually were in the range of about 2 – 5 °C. Under such conditions the microbial sulphate reduction still proceeded, although at much lower rates. In any case, the water clean up efficiency of the multibarrier was much higher during the warmer months of the year (Table 9).

Table 7. Data about the changes in the permeability of the main sections of the multibarrier during the treatment of the polluted waters

Section of the multibarrier	Time since the start of the operation, months				
	0 (start)	9	16	22	28
Filtration coefficient, m/h					
Alkalizing drain	110.4	34.6	10.8	4.7	0.08
Zones in the section for MDSR:					
2 m from the inlet	7.2	3.8	1.5	1.4	0.06
4 m from the inlet	7.2	5.7	3.1	2.6	0.07
6 m from the inlet	7.2	6.6	5.6	5.1	0.08

Note: MDSR = microbial dissimilatory sulphate reduction

The effluents from the multibarrier were enriched in dissolved organic compounds and in some cases still contained manganese in concentrations higher than the relevant permissible levels (Table 2). These effluents were treated in a natural wetland where the Mn²⁺ ions were oxidized to Mn⁴⁺ by some heterotrophic bacteria producing peroxide compounds and the enzyme catalase, which degraded the excess of peroxides to molecular oxygen and water. The Mn⁴⁺ ions precipitated as MnO₂. The dissolved organic compounds were efficiently degraded by the different heterotrophs inhabiting the wetland.

The data from the recent monitoring of the multibarrier operation clearly reveal that after a period of twenty eight months since its start it is necessary to replace the armored limestone and the exhausted solid biodegradable organic substrates by fresh batches of these materials.

Table 8. Data about the composition of solid samples from the permeable multibarrier

Parameters	Zones in the section for microbial sulphate reduction					
	2 m from the inlet		4 m from the inlet		6 m from the inlet	
	Time since the start of the operation, months					
	16	28	16	28	16	28
pH (KCl)	5.68	7.06	6.35	7.23	7.43	7.45
Ash content, %	71.0	81.9	62.0	70.7	64.0	72.4
Organic content, %	29.0	18.1	38.0	29.3	36.0	27.6
Cu, mg/kg	1211	1950	482	1466	76.4	212
Zn, mg/kg	587	1488	363	921	135	183
Cd, mg/kg	4.9	15.2	2.9	5.2	0.9	1.0
Pb, mg/kg	46.6	41.9	74.9	68.0	36.9	70.7
Ni, mg/kg	269	1565	249	906	20.2	118
Co, mg/kg	298	890	98.4	495	8.8	59
Fe, mg/kg	6204	6632	6512	6804	6468	7120
Mn, mg/kg	473	895	810	2161	459	783
U, mg/kg	60.3	215	45.3	190	11.1	59.6
As, mg/kg	4.96	0.8	0.4	1.1	1.1	1.4
S total, mg/kg	6612	10087	6239	9111	5520	7050

Table 9. Removal of pollutants from the acid mine drainage by means of the permeable reactive multibarrier during different climatic seasons

Pollutants	Pollutant removed, g/24 h	
	During the warmer months	During the cold winter months (at 0 – 5 °C)
Uranium	2.42 – 19.2	0.35 – 2.27
Copper	9.74 – 80.2	1.52 – 7.20
Zinc	6.44 – 114.4	1.40 – 9.72
Cadmium	0.14 – 1.20	0.03 – 0.19
Lead	1.24 – 5.05	0.28 – 1.34
Nickel	2.71 – 11.35	0.60 – 2.84
Cobalt	1.80 – 7.81	0.41 – 2.08
Manganese	23.5 – 194	4.73 – 25.9
Arsenic	0.95 – 2.71	0.27 – 1.04
Iron	594 – 5481	88.4 – 712

ACKNOWLEDGEMENTS

Parts of this work were financially supported by the European Commission under the project No QLRT – 2001 – 02916 “Multifunctional permeable barriers carrying well-performing microbial biofilms for treatment of mixed polluted plumes” and by the Flemish Government under the project “Improvement of groundwater protection in Bulgaria using advanced environmental impact assessment (EIA) tools” (CO-9004 1755.01).

REFERENCES

- GROUDEV, S.N., GEORGIEV, P.S., SPASOVA, I.I., NICOLOVA, M.V. and DIELS, L., 2006a. *Biological clean up of acid mine drainage by means of a permeable multibarrier*. In: G. Önal et al., (Eds.), Proc. XXIII International Mineral Processing Congress, vol. 3, pp. 2331-2336, Promed Advertising Agency, Istanbul.
- GROUDEV, S.N., SPASOVA, I.I., GEORGIEV, P.S., NICOLOVA, M.V. and DIELS, L., 2006b. *Treatment of acid drainage in a uranium deposit*. Paper presented at the AMIREG Conference, Hania, Greece.
- GROUDEV, S.N., SPASOVA, I.I., KOMNITSAS, K. and PASPALIARIS, I., 2003. *Microbial generation of polluted waters in a uranium deposit*, In: L. Kuzev, I. Niskov, A. Boteva and D. Mochev (Eds.), Mineral Processing in the 21st Century, pp.728-732, Djiev Trade Ltd, Sofia.
- GROUDEVA, V.I. and TZENEVA, V., 2001. *Biodiversity of sulphate-reducing bacteria (SRB) in anaerobic reactor removal of heavy metals polluted water*. In: A. Kujumdzieva (Eds), Vocational Training in Biotechnology and Environmental Protection, Module II – Environmental Protection and Biotechnology, pp.95-120, National Bank of Industrial Microorganisms and Cell Cultures, Sofia.
- HALLBERY, K.B. and JOHNSON, D.B., 2001. *Novel acidophiles isolated from a constructed wetland receiving acid mine drainage*. In: V.S.T. Ciminelli and O. Garcia Jr. (Eds.), Biohydrometallurgy: Fundamentals, Technology and Sustainable Development, Part A, pp.433-441, Elsevier, Amsterdam.
- Karavaiko, G.I., Possi, G., Agate, A.D., Groudev, S.N. and Avakyan, Z.A., (Eds.), 1988. *Biogeotechnology of Metals, Manual*. GKNT International Projects, Moscow.
- LOWE, L.E., 1993. *Total and labile polysaccharide analysis of soils*. In: M.R. Carter (Eds.), Soil Sampling and Methods of Analysis, pp.373-376, Canadian Society of Soil Science, Boca Raton, Florida.
- RYAN, M.G., MELILLO, J.M. and RICCA, A., 1990. *A comparison of methods for determining proximate carbon fractions of forest litter*. Canadian Journal of Forest Research, 20, 166-171.
- WIDDEL, F. and BAK, F., 1991. *Gram-negative mesophilic sulphate-reducing bacteria*. In: A. Ballows, H-G. Trüper, M. Dworkin, W. Harder and K-H. Schleifer (Eds.), The Prokaryotes, vol. IV, 2nd edn., pp. 3352 – 3378, Springer, New York.
- WIDDEL, F. and HANSEN, T.A., 1991. *The dissimilatory sulphate and sulphur-reducing bacteria*. In: A. Ballows, H-G. Trüper, M. Dworkin, W. Harder and K-H. Schleifer (Eds.), The Prokaryotes, vol. II, 2nd edn., pp. 538 – 624, Springer, New York.

Groudev S., Spasova I., Nicolova M., Georgiev P., *Oczyszczanie kwaśnych odcieków ze złoża uranu za pomocą układu pasywnych barier*, Physicochemical Problems of Mineral Processing, 41 (2007) 265-274 (w jęz. ang.).

Kwaśne odcieki, „wytwarzane” przez złożo rudy uranowej zlokalizowane w Curilo (Bułgaria) były oczyszczane w instalacji o skali pilotowej, która składała się z wielu naturalnych barier. Całkowita objętość instalacji wynosiła 23 m³ i składała się ona z drenażowej sekcji alkalinizującej, z sekcji bakteryjnej redukcji siarczków w warunkach beztlenowych oraz z sekcji biosorpcji i dodatkowo, z sekcji chemicznej neutralizacji. Ścieki wykazywały pH w zakresie od 2.5 do 4.0 i zawierały: radionuklidy (U, Ra), metale ciężkie (Cu, Zn, Cd, Pb, Ni, Co, Fe, Mn) oraz arsen i siarczki. Stężenia jonów w ściekach było znacznie

większe niż przewidują to normy zezwalające na wykorzystanie ścieków w rolnictwie i przemyśle. Przepływ cieczy przez układ składający się z wielu barier był zmienny w granicach od 1 do 17 m³/24 godz. Odpowiada to czasowi przebywania roztworu w całej instalacji od 300 do 18 godzin. Wysoka efektywność usuwania zanieczyszczeń przez wielobarierową instalację była niezależna od pory roku. Nawet podczas chłodnej zimy temperatura powietrza i ścieku wahała się w okolicy 0°C. Jednak, pewne istotne zmiany w składzie cieczy i we właściwościach wielobarierowej instalacji miały miejsce podczas pracy instalacji w okresie 28 miesięcy.

Żaklina KONOPACKA* Andrzej ŁUSZCZKIEWICZ* Tomasz CHMIELEWSKI**

EFFECT OF NON-OXIDATIVE LEACHING ON FLOTATION EFFICIENCY OF LUBIN CONCENTRATOR MIDDINGS

Received May 30, 2007; reviewed; accepted June 16, 2007

Mineralogical and petrological properties of black shale occurring in the copper ore deposit of the Foresudetic Monocline have been described. Specific character of the shale layer and its behaviour in the ore processing technology was discussed. A concept of recovery of the black shale from flotation circuits of the Lubin Concentrator by separating a by-product (middlings), which represents the tailings of the first cleaning flotation was presented. It was found that the investigated by-product cannot be practically upgraded using standard xanthate flotation. This is due to a remarkable enrichment in the organic carbon, similarly to the content of carbon in petrographically "pure" black shales. After a comprehensive examination it was assumed that the Lubin middlings can be regarded as a shale concentrate ready for bio- and hydrometallurgical processing. The effect of non-oxidative leaching of middlings with sulphuric acid on further flotation was presented. It was shown that non-oxidative leaching is a selective process, in which calcium and magnesium carbonates decomposition leads to effective liberation of sulphide minerals finely disseminated in hydrophilic gangue. Partial carbonates removal (between 70 and 90% of the total carbonates content) from the middlings resulted in evident liberation of valuable minerals. Consequently, it resulted in an increase of both recovery and the content of metals in concentrates obtained by flotation of shale by-product after non-oxidative leaching.

Key words: copper ores, black shale, flotation, non-oxidative leaching

INTRODUCTION

Black shale fraction in the copper ore deposit of the Foresudetic Monocline is one of the three, next to sandstone and carbonate, copper-bearing lithological layer distinguished in the exploited copper ore in the Legnica-Glogow basin (LGOM). From

* Wrocław University of Technology, Mining Engineering Department, Wrocław, Poland, Teatralny 2, 50-051 Wrocław, zaklina.konopacka@pwr.wroc.pl; andrzej.luszczkiewicz@pwr.wroc.pl

** Wrocław University of Technology, Faculty of Chemistry, Division of Chemical Metallurgy, Wybrzeże Wyspiańskiego 27, 50-307 Wrocław, Poland.

the lithological and geochemical points of view the copper ore is of very specific and unique composition, which require specific technology for processing of the mined ores.

The shale series, called the copper-bearing shale, forms in the deposit layers of thickness from 0.3-0.8 to 1.7 m. It is a heterogeneous material, mainly consisting of bituminous shale, which basic components are clay minerals, carbonate minerals (dolomite and calcite), organic substance (mainly of sapropel origin) and detritic material (Konstantynowicz-Zielinska, 1990). Dark or black color of the shale is considerably related to the presence of carbonaceous organic matter.

In the whole area of the LGOM deposit three shale layers can be distinguished: black clay shale, clay-dolomitic, and dolomitic-clay (Rydzewski, 1996). Shale ore, considering its high copper content (on average from several to a dozen percent) and valuable accompanying metals and compounds, is believed to be the most valuable among all lithological layers of the LGOM deposit. Tomaszewski (1985), calling the shale ore “natural polymetallic concentrate”, estimated that black shale present in the deposit is the carrier of about 25 % of the copper reserves and about 30-40 % of copper accompanying metals. Kijewski and Jarosz (1987) assessed that bituminous shale includes 5-8 % of the ore resource in the deposit. The shale ore is recognized as the most difficult-to upgrade part of mixed ore directed to concentrators in comparison with sandstone and carbonate fraction of the ore. Fine disseminated sulphide minerals present in the clay and clayey dolomitic matter occur as intergrowths with carbonaceous substance. Hard liberation of fine particles of copper minerals during standard grinding process of the shale is the main cause of its upgrading difficulties by flotation.

As a result of the method of exploitation of the deposit, which are currently used, the shale ore is processed in the copper concentrators as a mixture with the remaining two, the sandstone and carbonate lithological layers. Table 1 exhibits an average lithological ore composition, including Cu, Ag and C_{org} contents, which is used as a feed in the processing plants in the 90's of the previous century. In Table 2, similar data for 2004 are put together to emphasize almost double increase of the shale fraction content in the feed of the KGHM Polish Copper S.A. processing plants.

Table 1. Composition of lithological ore layers and content of copper, silver, and organic carbon in feed of the KGHM copper concentrators in nineties (Łuszczkiewicz, 2000)

Ore component	Rudna	Polkowice – Sieroszowice	Lubin
Carbonate ore %	51.0	84.0	38.0
Shale ore, %	5.0	6.0	8.0
Sandstone ore, %	44.0	10.0	54.0
Cu content, %	2.05	1.81	1.36
Ag content, g/Mg	47	34	68
C _{org} content, %	0.64	1.14	1.76

Table 2. Composition of lithological ore layers and content of copper, silver, and organic carbon in feed of the KGHM copper concentrators in 2004 (Luszczkiewicz 2004)

Ore component	Rudna	Polkowice – Sieroszowice	Lubin
Carbonate ore %	33	75	25
Shale ore, %	11	17	15
Sandstone ore, %	56	8	60
Cu content, %	2.23	2.03	1.28
Ag content, g/Mg	53	40	67
C _{org} content, %	1.49	1.66	1.62

A remarkable increase of the black shale content in the mined (up to 27 % for Lubin) ore is currently observed (Kubacz and Skorupska, 2007). In Table 3, results of investigations of samples of the ore taken from one of the mining areas of ZG Lubin in 2004 (Luszczkiewicz 2004) are put together. As it can be seen in the table, when the volumetric distribution of the shale in the ore is 15%, the distribution of copper and silver originating in this shale in the working face is over 45%. For C_{org}, this distribution is about 80%. The C_{org} content in the ore is strictly related to the shale fraction content. C_{org} in the ore mainly originates from the shale fraction, therefore, under particular conditions of upgrading, the product enriched in this component will be of similar character to the shale fraction.

Table 3. Lithological composition and distribution of copper and organic carbon of working face in the Lubin Mine (region G1, Malomice I) (Luszczkiewicz 2004)

Name of the sample	Layers of the thickness m	Volumetric distribution, %	Cu, %		Ag, g/Mg		C _{org} , %	
			Content	distribution	Content	distribution, %	Content	distribution
Dolomitic-clay shale	0.10	5.32	2.96	10.09	134	8.77	6.40	26.05
Clay shale	0.18	9.57	5.74	35.21	293	34.51	7.19	52.67
Boundary dolomite	0.10	5.32	0.75	2.56	42	2.75	0.73	2.97
Grey sandstone	1.50	79.79	1.02	52.14	55	53.98	0.30	18.31
Mixed ore (calculated)	1.88	100.00	1.56	100.00	81	100.00	1.31	100.00
Mixture assay			1.64		83		1.36	

Chemical analysis of the ore samples and lithological layers taken from different mining areas of the KGHM Polish Copper S.A. proved a clear correlation between C_{org} content and metal concentration. The correlation metal content vs. C_{org} content for copper and silver are shown in Figures 1 and 2.

According to claim of technologists, the shale fractions presence in the feed for flotation causes severe difficulties in the technological processes of the mixed ores. The flowsheets became very complex and unit operations very expensive, even though technological systems have recently been modernized. The growing distribution of difficult-to-upgrade shale fraction is also a major reason for the metal losses in the flotation tailings (Luszczkiewicz, 2000).

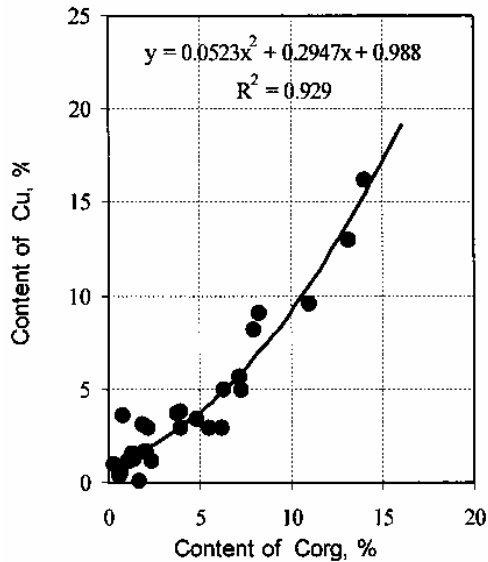


Fig. 1. Cu vs. organic carbon content in shale ore samples from KGHM deposits

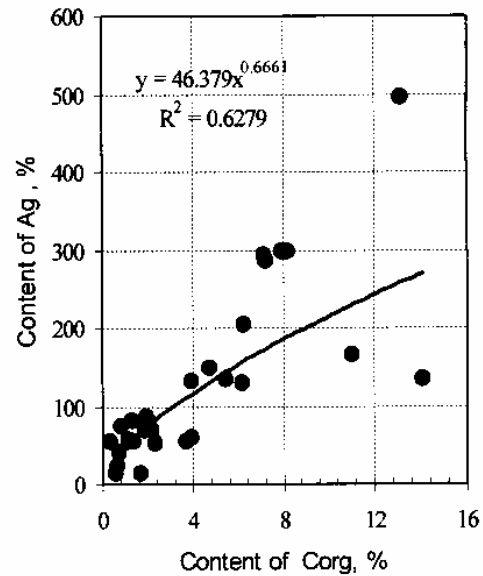


Fig. 2. Ag vs. organic carbon content in shale ore samples from KGHM deposits

During crushing considerable difficulties with liberation of sulphide minerals from the shale layer take place. Simultaneously, a part of clay and organic components, which are easily liberated from the shale, can make the flotation of copper sulphide minerals difficult. The easy-floating fines of clay minerals liberated during grinding and impregnated with organic matter create slime coating on the air bubbles and sulphide minerals hindering flotation. Undoubtedly, apart from very fine granulation of sulphide minerals in the shale, it is one of the most important reasons of difficulties in the flotation process of the feed containing the shale lithological layer.

THE CONCEPT AND AIM OF INVESTIGATION

The aim of the investigation considered in this work was to test the effect of non-oxidative leaching of the by-product (middlings) from the first cleaning operation of the Lubin Concentrator (ZWR Lubin) on flotation effectiveness. The tailing from the 1st cleaning flotation operation at this plant is recognized as the most troublesome product in the existing flotation circuit at the Lubin Concentrator due to a high amount of the difficult-to-treat shale fraction. It was the main reason of choosing it as the material for investigations. Under technological condition at the Lubin Concentrator, this product represents 20-30% of the mass of solids circulating in the whole flotation system, with copper recovery of about 20-25%.

Non-oxidative leaching of shale fraction is a part of the concept to change the technology, which has been developed by the Wrocław University of Technology in the frame of the European Union BIOSHALE project. The concept scheme was shown

in Fig. 3 (BIOSHALE, Deliverable D.4.2, 2006; Chmielewski and Charewicz, 2006). According to the general concept of the project, the difficult-to-upgrade shale fraction should be separated from the existing flotation circuits and applied for further, individual, bio- or hydrometallurgical processing. Using non-oxidative leaching with sulphuric acid solutions is the only chance for successful liberation of the minerals disseminated in the shale carbonate and organic matter as well as for enhance the flotation efficiency.

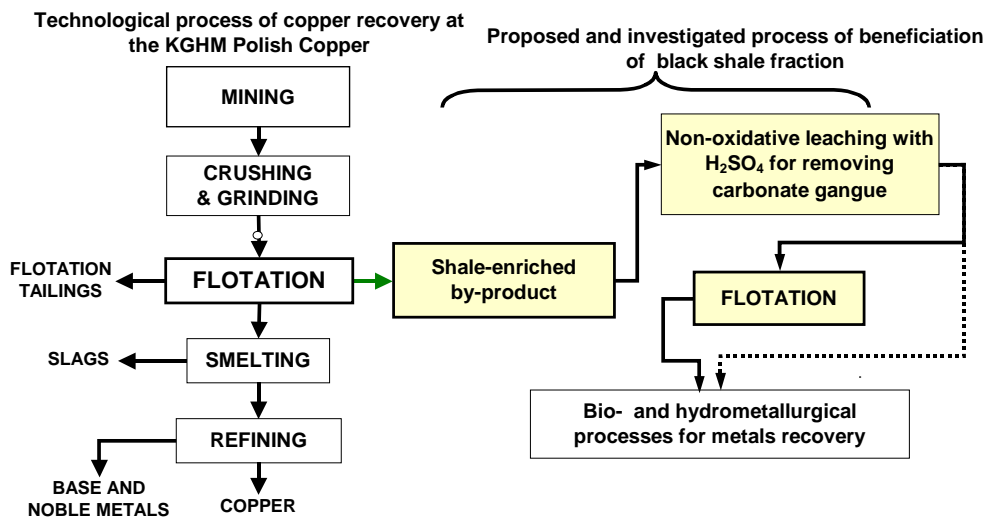


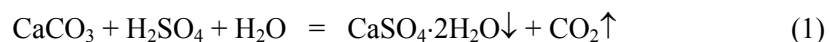
Fig. 3. General BIOSHALE concept of separate processing of black shale ore fraction from Polish copper deposits

EXPERIMENTAL

MATERIALS AND METHODS

Non-oxidative leaching

Non-oxidative leaching of the shale fraction of the copper ore or its processing by-products from the KGHM technological circuits was used as a unit operation which aim was to liberate metal-bearing minerals from carbonate particles. This kind of leaching consists of selective (without breaking sulphides) chemical calcium and magnesium carbonates decomposition by means of sulphuric acid, according to the reactions:



Hydrated calcium sulfate (gypsum) precipitates as a solid reaction product, whereas water-soluble magnesium sulfate and gaseous carbon dioxide are other reaction products. Since particles of middlings are fine, leaching of the carbonate gangue with H_2SO_4 is very rapid and can be performed at ambient temperatures in reactors with mechanical stirring of a simple construction.

The amount of H_2SO_4 applied in the non-oxidative leaching operation directly corresponds to the content of carbonates and must be precisely controlled to maintain the final pH of the pulp at a level enabling its direct transfer either to the flotation circuit without a need for pH correction or to the leaching and bioleaching. Therefore, for further flotation, the amount of sulfuric acid introduced to the leaching operation should always be kept below the analytically determined maximum amount of acid required for the total carbonates decomposition.

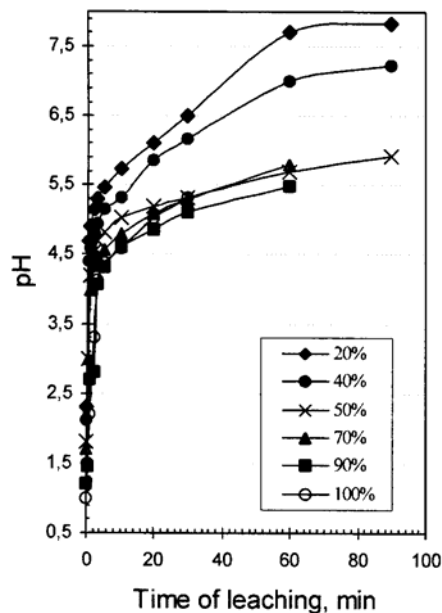


Fig. 4. pH vs. leaching time plots for non-oxidative leaching of Lubin middlings

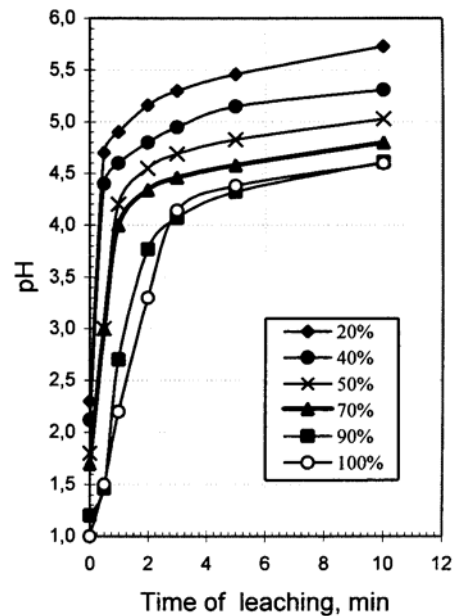


Fig. 5. pH vs. leaching time plots for initial stage of non-oxidative leaching of Lubin middlings

Kinetics of non-oxidative leaching of the middlings from the Lubin Concentrator was investigated for different degrees of carbonates decomposition varying from 20 to 100 %. The key parameter determining the amount of H_2SO_4 required for carbonates leaching is the maximum demand for acid ($z_{\text{H}_2\text{SO}_4}^{\text{max}}$), which is the mass of pure H_2SO_4 necessary for a total decomposition of carbonates in 1 kg of dry solid feed. The $z_{\text{H}_2\text{SO}_4}^{\text{max}}$ parameter should be determined analytically from laboratory tests. H_2SO_4 is introduced to the reactor containing shale slurry at a rate that assures its total

utilization. The maximum demand for sulphuric acid for examined Lubin middlings was 494 g H₂SO₄/kg of dry material.

The process control of non-oxidative leaching is based on pH measurement of leached middlings suspension after introduction of desired amount of sulphuric acid. On the basis of kinetic results for Lubin middlings it was found that the process is very rapid (Figs. 4 and 5) and after about 5 minutes almost entire amount of acid is already used up. The observed further pH changes (up to about 40-60 minutes) correspond to the saturation of the slurry with CO₂.

Non-oxidative leaching is not only very fast but also selective. It does not cause chemical decomposition of metal sulphides under non-oxidative conditions created by the carbon dioxide.

The samples of middlings being the tailings from the 1st cleaning operation at the Lubin Concentrator before and after non-oxidative leaching with sulfuric acid were the material for experiments. The total time of carbonate decomposition in the examined samples was 60 minutes.

Flotation feeds with either 50, 70 or 90 % of carbonate decomposition were used in experiments performed according to the flow-sheet shown in Fig. 6. For comparison, the flotation of raw middling (i.e. non-leached with H₂SO₄) was also carried out. For the flotation experiments a Mekhanobr sub-aeration type laboratory flotation machine equipped with a 1dm³ cell was applied. pH measured during the flotation for the non-leached material was from 7.6 to 8.3, and for the leached samples from 5.5 to 7.0.

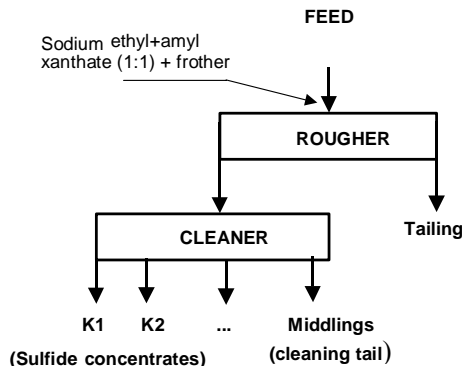


Fig. 6. Flotation experiments

In the standard xanthate flotation of sulfides, 50-60g/Mg of collector (mixture of sodium ethyl+amyl xanthate, 1:1) and 10-20g/Mg of frother (Corflot) were used. The rougher flotation was conducted up to the moment when the flotation froth did not contain useful minerals. The obtained concentrate was subsequently subjected to the cleaning flotation where the following products of flotation were collected at suitable time intervals. The procedures of the flotation experiments were the same, but quantities of the reagents and times intervals of the products collection were different for various examined feed.

Because of the strong frothing properties of the suspension after leaching, experiments were carried out with a minimal air-flow. This caused low yield of the products and resulted in higher selectivity of flotation.

RESULTS AND DISCUSSION

PARTICLE SIZE DISTRIBUTION

Table 4. Particle size distribution of tailing from the 1st cleaning flotation operation at the Lubin Concentrator

(i) Material non-leached – 0% of carbonate decomposition							
(ii) Particle size, µm	Yield γ, %	Cu, %		Ag, g/Mg		C _{org} , %	
		λ	ε	λ	ε, %	λ	ε
>100	6.94	4.20	12.87	268	13.69	8.80	7.43
71 – 100	8.93	3.16	12.45	197	12.93	12.50	13.56
40 – 71	34.13	2.45	36.89	131	32.88	10.30	42.72
25 – 40	17.46	1.83	14.10	103	13.22	6.35	13.47
<25	32.54	1.65	23.69	114	27.28	5.77	22.82
Feed calculated	100.00	2.27	100.00	135.99	100.00	8.23	100.00
50% of carbonate decomposition							
>100	6.57	4.42	10.85	284	11.77	10.80	7.07
71 – 100	9.86	3.28	12.07	188	11.69	14.60	14.33
40 – 71	32.16	2.83	33.98	156	31.65	11.60	37.15
25 – 40	16.20	2.56	15.48	135	13.79	8.16	13.16
<25	35.21	2.10	27.61	140	31.09	8.07	28.29
Feed calculated	100.00	2.68	100.00	158.53	100.00	10.04	100.00
70% of carbonate decomposition							
>100	6.95	4.32	10.73	196	8.16	11.40	7.83
71 – 100	9.93	3.28	11.64	208	12.37	15.10	14.81
40 – 71	29.03	2.94	30.52	174	30.26	12.70	36.43
25 – 40	14.39	2.95	15.18	157	13.54	9.28	13.20
<25	39.70	2.25	31.94	150	35.68	7.07	27.74
Feed calculated	100.00	2.80	100.00	166.93	100.00	10.12	100.00
90% of carbonate decomposition							
>100	5.69	4.46	8.31	296	9.00	11.90	6.21
71 – 100	11.11	3.39	12.34	204	12.11	16.10	16.39
40 – 71	30.08	3.14	30.93	186	29.89	13.20	36.38
25 – 40	12.20	3.40	13.58	175	11.40	10.50	11.73
<25	40.92	2.60	34.84	172	37.60	7.81	29.29
Feed calculated	100.00	3.05	100.00	187.19	100.00	10.91	100.00

γ - yield of fraction in product, %

λ - content of component in fraction, %

ε - recovery of component in fraction, %

Table 4 shows the particle size distribution of the examined raw middlings and samples after non-oxidative leaching. For respective size fractions the contents (λ) of copper, silver, and organic carbon and their distribution (ϵ) are mentioned. It can be seen that the size fraction $<40 \mu\text{m}$ contains 50% of the non-leaching middlings (raw by-product) mass. For the leached materials the content of this fraction increases only several per cent (2-4%).

Therefore, we can say that leaching slightly influences grinding of the material. It is observed that with the increase of carbonates leaching in the investigated sample, there is an increase in useful liberated components in the fractions. The biggest recovery of Cu, Ag and C_{org} was observed in the 0-25 μm and 40-71 μm size fractions, whereas the recovery of the liberated Cu and Ag components of the $<25 \mu\text{m}$ size fraction grows with the increase of carbonates distribution in the sample.

Copper distribution vs. particle size plot for the Lubin middlings is shown in Fig. 7, whereas distribution of Cu, Ag and C_{org} for feed after 70% of carbonate decomposition are given in Fig 8.

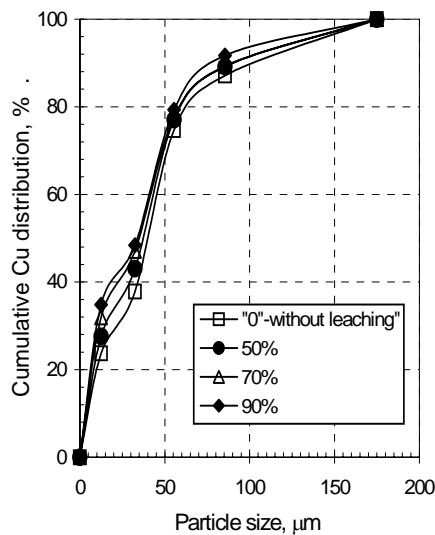


Fig. 7. Copper distribution vs. particle size of Lubin middlings for various carbonates leaching degree

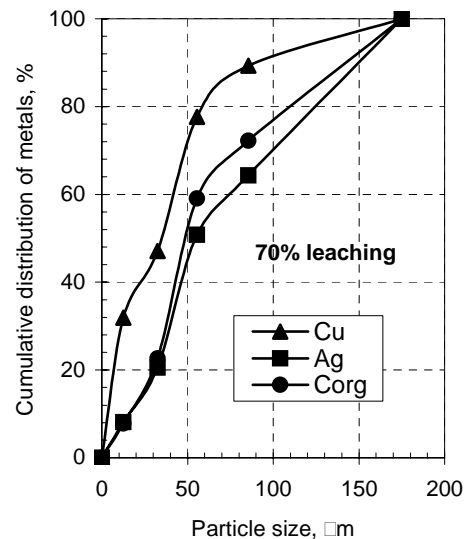


Fig. 8. Cu, Ag and organic carbon distribution vs. particle size of Lubin middlings

The contents of Cu, Ag and C_{org} for the examined middlings feeds after different carbonates leaching degree are shown in Table 5. It is well seen that even partial carbonates leaching with sulphuric acid causes remarkable metal-bearing minerals liberation from carbonates intergrowths. It is revealed by an increase in metal contents in the examined samples.

Table 5. Change of metals and organic carbon content in flotation feed after non-oxidative leaching of various carbonates decomposition degree

% of carbonate decomposition	Cu, %	Ag, ppm	Pb %	C _{org} %	Co, ppm	Ni, ppm	Zn, %	Fe, %
0%	2.27	136	1.27	8.23	505	322	0.114	1.474
50%	2.68	159	1.49	10.04	513	335	0.106	1.459
70%	2.80	167	1.59	10.12	530	348	0.124	1.422
90%	3.05	187	1.83	10.91	564	356	0.111	1.366

RESULTS OF FLOTATION EXPERIMENTS

Table 6 shows the results of flotation experiments with middlings when sodium ethyl+amyl (1:1) xanthate was used as the collector. Flotation of the non-leached material was conducted for comparison with all experiments of this series of tests. The upgrading plots are presented in Figures 9 to 10. They contain the relationship between recovery of valuable components versus their content in the concentrate. It can be seen from Fig. 9 that the increase of the carbonates decomposition degree leads to a remarkably better upgrading of Cu, Ag and C_{org}. It is particularly important for recovery exceeding 80 %.

Figure 10 presents a relationships between recovery of valuable components in concentrate (Cu, Ag, C_{org}) and recovery of a second component (of barren part of the ore) in the tailings. This method of graphical interpretation of upgrading data is referred as the Fuerstenau upgrading curve (Drzymala and Ahmed, 2005). This type of upgrading curve enables to compare enrichment of different components of various ores having different feed composition in one graph. In the plot shown in Fig.10 one can well see an upgrading increase of the examined components taking place with increasing the leaching degree of the carbonates.

Table 6. Results of standard xanthate flotation of middlings. Mixture of sodium ethyl+amyl xanthate (1:1) 50-60g/Mg, frother (Corflot) 10-20g/Mg

Material non-leaching – 0% of carbonate decomposition										
Product	Yield □, %	Cu			Ag			C _{org}		
		□, %	β, %	ε, %	□, g/Mg	β, g/Mg	ε, %	□, %	β, %	ε, %
C1	2.64	5.23	5.23	6.02	283	283.00	5.38	10.35	10.35	3.42
C2	14.15	4.22	4.38	26.06	241	247.60	24.58	10.42	10.41	18.47
C3	12.18	3.09	3.84	16.43	190	223.39	16.68	11.04	10.67	16.84
Cleaning tail	43.26	2.15	2.83	40.58	134	169.86	41.76	8.96	9.65	48.54
Tailing	27.77	0.90	2.29	10.90	58	138.80	11.60	3.66	7.99	12.73
Feed calculated	100.00	2.29		100.00	138.80		100.00	7.99		100.00
Feed assay		2.32			132			8.25		
50% of carbonate decomposition										
continuation: see next page										

continuation from previous page										
Material non-leaching – 0% of carbonate decomposition										
Product	Yield %	Cu			Ag			C _{org}		
		λ, %	β, %	ε, %	λ, g/Mg	β, g/Mg	ε, %	λ, %	β, %	ε, %
C1	3.42	4.34	4.34	6.38	249	249.00	5.87	13.27	13.27	5.21
C2	14.77	3.82	3.92	24.24	223	227.89	22.71	12.83	12.91	21.74
C3	49.84	2.82	3.11	60.39	177	190.61	60.83	11.59	11.94	66.28
Cleaning tail	5.99	1.24	2.96	3.19	96	182.95	3.97	3.57	11.27	2.45
Tailing	25.98	0.52	2.33	5.80	37	145.03	6.63	1.45	8.72	4.32
Feed calculated	100.00	2.33		100.00	145.03		100.00	8.72		100.00
Feed assay		2.34			138			8.40		
70% of carbonate decomposition										
C1	7.75	4.44	4.44	14.25	248	248.00	12.50	13.73	13.73	11.68
C2	16.27	3.88	4.06	26.15	234	238.52	24.76	13.57	13.62	24.25
C3	42.32	2.94	3.35	51.54	188	206.29	51.74	12.47	12.89	57.96
Cleaning tail	8.93	1.18	3.09	4.36	101	193.80	5.86	4.02	11.84	3.94
Tailing	24.72	0.36	2.41	3.69	32	153.80	5.14	0.80	9.11	2.17
Feed calculated	100.00	2.41		100.00	153.80		100.00	9.11		100.00
Feed assay		2.25			141			8.23		
90% of carbonate decomposition										
C1	8.77	4.83	4.83	18.01	393	393.00	17.41	13.71	13.71	13.73
C2	36.31	3.46	3.73	53.45	208	224.42	51.26	14.10	14.02	58.42
C3	19.75	2.74	3.43	23.03	176	209.67	23.60	10.92	13.08	24.62
Cleaning tail	10.02	0.74	3.07	3.15	71	191.11	4.83	1.7	11.56	1.94
Tailing	25.15	0.22	2.35	2.35	17	147.32	2.90	0.45	8.76	1.29
Feed calculated	100.00	2.35		100.00	147.32		100.00	8.76		100.00
Feed assay		2.31			142			8.54		

Comparing the feeds of different carbonate decomposition degree it can be concluded, that flotation of the feed after 90 % of carbonates decomposition leads to high grade concentrates and the lowest losses of the examined components in tailings. This is the consequence of the best material upgrading. It should be pointed out, that even the feed after 50 % of carbonates decomposition can be characterised by evidently better selectivity of the flotation in comparison with the non-leached feed.

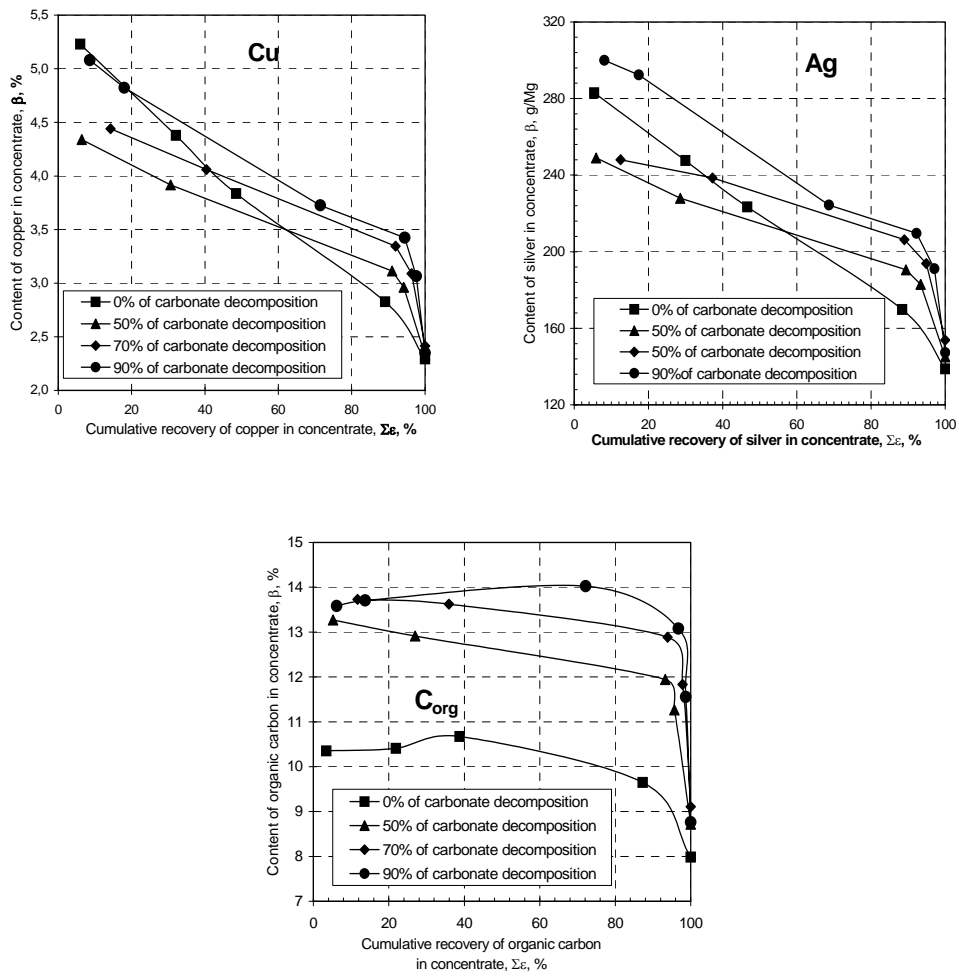


Fig. 9. Recovery – Cu, Ag, C_{org} content upgrading curves of xanthate flotation of middlings of different carbonates distribution degree (50%, 70% and 90%). Based on data from Table 6

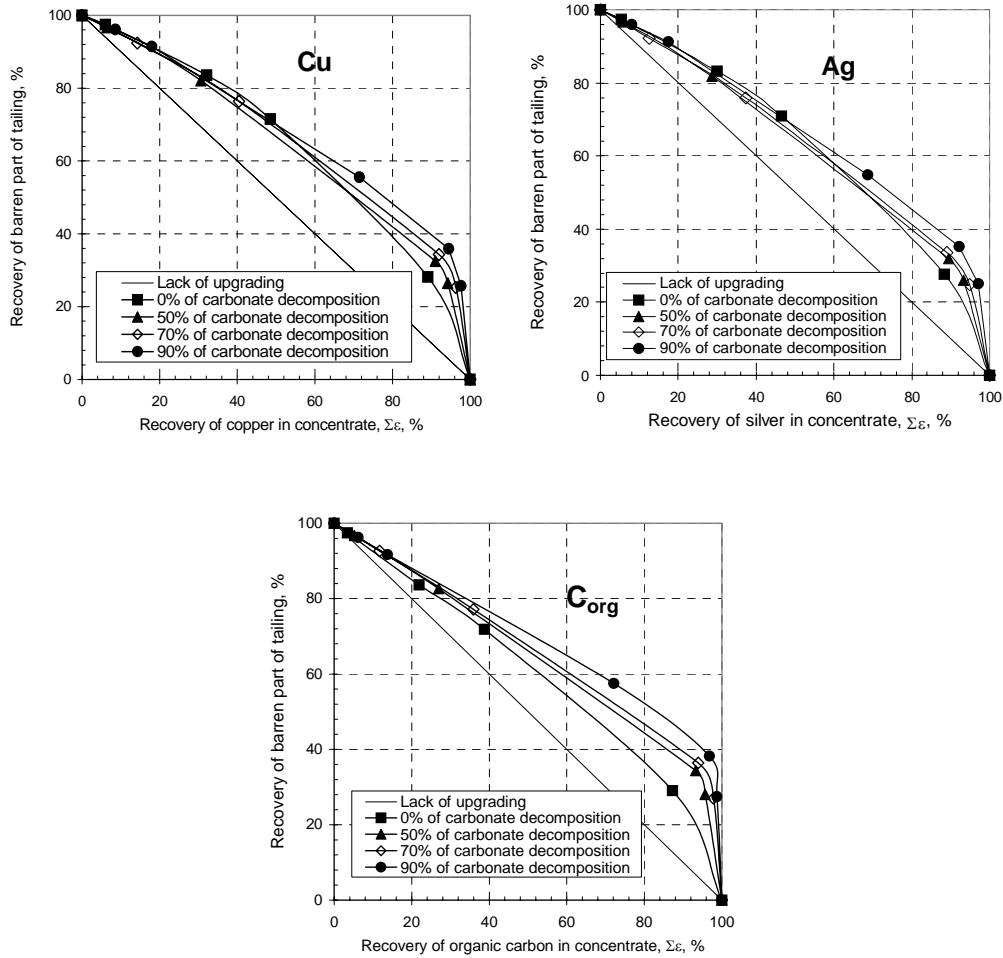


Fig. 10. Comparison of xanthate flotation of 1st ZWR Lubin cleaning middlings for different carbonates leaching degrees for Cu, Ag and C_{org} recovery in concentrate vs. barren part of tailing. Based on data from Table 6

CONCLUSIONS

1. Investigated middlings, being the tailing from the 1st cleaning flotation operation at the Lubin Concentrator is recognized as the most troublesome product in the existing flotation circuit due to a high amount of the difficult-to-treat shale fraction. Fine dissemination of sulfide minerals is the main reason of difficulties in upgrading of the shale fraction. It was the major reason for choosing the middlings as the material for the presented investigations

2. Flotation experiments proved that upgrading the middlings was nearly impossible. Material containing about 2% Cu and 8% of organic carbon provided concentrates containing 3-4% Cu and 8-10% of organic carbon
3. Non-oxidative leaching of Lubin middlings with H_2SO_4 can be used as an effective operation for selective chemical liberation of sulphide minerals before flotation
4. Partial decomposition of carbonates from 50 to 90% remarkably improves the liberation degree of the useful minerals from the hydrophilic intergrowths with carbonate matter
5. Evidently improved flotation of Cu, Ag and C_{org} occurs for leached materials in comparison with direct flotation of untreated raw materials
6. An increase of the carbonates decomposition of the feed results in enhanced recovery and content of the useful components in the concentrate
7. The best results of the flotation parameters (recovery and concentrate grade) were obtained for the feed with the 90 % of carbonate decomposition.

ACKNOWLEDGEMENT

This work was carried out in the frame of Bioshale (European project contract NMP2-CT-2004 505710). The authors acknowledge the financial support given to this project by the European Commission under the Sixth Framework Programme for Research and Development. We also wish to thank our various partners on the project for their contributions to the work reported in this paper.

REFERENCES

- BIOSHALE, Deliverable D.4.2., April 2006, *Technical aspects: Leaching tests. Results with Lubin and Talvivaara Ores.*
- CHMIELEWSKI T., CHAREWICZ W., *Hydrometalurgiczne przetwarzanie półproduktów łupkowych z obiegów technologicznych ZWR Lubin*, Perspektywy zastosowania technologii bioługowania do przerobu rud miedzi zawierających łupki, BIOPROCOOP'06, Lubin 2006, KGHM Cuprum, Wrocław 2006, 125-145.
- DRZYMALA J.; AHMED H.A.M., 2005, *Mathematical equations for approximation of separation results using the Fuerstenau upgrading curves.* International Journal of Mineral Processing, Vol. 76, No. 1-2, April 4, 2005, 55-65.
- KONSTANTYNOWICZ-ZIELIŃSKA J. 1990, *Petrografia i geneza łupków miedzionośnych monokliny przedsudeckiej.* Rudy i Metale Nieżelazne. R.35, Nr 5-6, 128-133.
- KUBACZ N., SKORUPSKA B. 2007. *Estimation of influence of organic carbon on concentration and smelting processes.* Proceed.: VIII International Conference On Non-ferrous Ore Processing, ICNOP'07, 21-23 May, Wojcieszycze, KGHM, IMN, 157-166 (in Polish).
- ŁUSZCZKIEWICZ A. 2004, *Analiza i ocena wzbogacalności rudy o podwyższonej zawartości czarnych łupków.* Sprawozdanie z badań, Archiwum Zakładu Przeróbki Kopalini i Odpadów, Instytut Górnictwa Politechniki Wrocławskiej, Wrocław.
- ŁUSZCZKIEWICZ A., 2000, *Wykorzystanie frakcji czarnych łupków miedzionośnych z rud z rejonu lubińsko-głogowskiego.* W: Współczesne problemy przeróbki rud miedzi w Polsce, Mat. Konf. Polkowice, 16 listopada 2000, Wyd. Komitet Górnictwa PAN i KGHM Polska Miedź S.A., 137-156.

- RYDZEWSKI A., 1996, Litologia skał złożowych. W: Monografia KGHM Polska Miedź S.A., praca zbiorowa pod red. A. Piestrzyńskiego. Wyd. CPBM "Cuprum" Sp. z O.O., Lubin, 137-141.
- TOMASZEWSKI J., 1985, *Problemy racjonalnego wykorzystania rud miedziowo polimetalicznych ze złoża monokliny przedsudeckiej*. Fizykochemiczne Problemy Mineralurgii. Nr 17, 131-141.

Konopacka Ż, Luszczkiewicz A, Chmielewski T. *Wpływ ługowania nieutleniającego na efektywność flotacji półproduktu z i czyszczenia koncentratu z ZWR LUBIN*, Physicochemical Problems of Mineral Processing, 41 (2007) 275-289 (w jęz. ang.).

Opisano mineralogiczno-petrograficzne właściwości czarnych łupków obecnych w złożu rud miedzi Monokliny Przedsudeckiej. Omówiono specyfikę zachowania się warstwy łupkowej w stosowanym procesie technologicznym przeróbki rud. Przedstawiono koncepcję pozyskiwania części frakcji czarnych łupków z urobku kierowanego do zakładu przerobczego ZWR Lubin poprzez wydzielenie produktu pośredniego stanowiącego odpad operacji pierwszego czyszczenia koncentratu. Stwierdzono, że badany produkt pośredni jest materiałem praktycznie niewzbogacalnym, odznaczającym się podwyższoną zawartością węgla organicznego podobną do zawartości w petrograficznie „czystych” czarnych łupkach. Uznano, że produkt ten może być uważany za gotowy koncentrat łupkowy do procesów bio- i hydrometalurgicznych. Przedstawiono wyniki ługowania nieutleniającego H_2SO_4 opisanego półproduktu. Stwierdzono, że ługowanie nieutleniające jest procesem selektywnym, w którym chemicznemu rozkładowi węglanów wapnia i magnezu towarzyszy uwolnienie siarczkowych minerałów użytecznych. Częściowe wyługowanie węglanów (między 70 a 90% całkowitej zawartości węglanów) za pomocą kwasu siarkowego w istotny sposób poprawia stopień uwolnienia minerałów użytecznych. Przejawia się to wzrostem uzysku i zawartości wszystkich metali zawartych w koncentratyach flotowanych z półproduktu łupkowego poddanego ługowaniu nieutleniającemu

Jörg LANGWALDT*, Reijo KALAPUDAS*

BIO-BENEFICIATION OF MULTIMETAL BLACK SHALE ORE BY FLOTATION

Received May 31, 2007; reviewed; accepted June 22, 2007

Within the framework of the EU co-funded Bioshale project the bio-beneficiation of multimetal black shale ore was studied. The EU-co-funded Bioshale project aims to define innovative biotechnological processes for ‘eco-efficient’ exploitation of black shale ores. The ore sample was from the Talvivaara deposit in Finland. In the black shale ore sample, the total amount of sulphides was 31.5% of which the Ni-minerals pentlandite and altered pentlandite is 0.52%. Nickel is distributed into pyrrhotite and oxidized pyrrhotite, 32.5%, and pentlandite and altered pentlandite, 66.0%. Other sulphides are chalcopyrite (Cu), sphalerite (Zn), pyrite (Co) and alabandite (Mn). The ore sample contained 12.3% graphite as a fine mixture with other minerals. In standard flotation, a low grade sulphide concentrate with 0.67 % Ni and nickel recovery of 74 % was obtained from the studied black shale ore. The mass of concentrate was then 34.5% of the ore feed. The recoveries of copper and zinc were 91%, of cobalt 89% and of manganese 53%. The content of carbon in the concentrate was 11.3% as graphite represents a naturally floating harmful mineral in the ore. The bioflotation tests showed that collector chemicals, i.e xanthates, had to be supplied to achieve reasonable flotation results. Out of the three tested bacterial strains, *Staphylococcus carnosus*, *Bacillus firmus* and *Bacillus subtilis*, the minor hydrophobic strain *S. carnosus* yielded the best test results. However, results of bioflotation tests failed to substantially improve the product recovery or grade.

Key words: black shale, flotation, biotechnology

INTRODUCTION

The increasing demand for metals and the decreasing availability of high-grade ores have led to numerous investigations to find better processing techniques and reagents to enable the development of low-grade deposits. Black shale ores can contain significant amounts of base metals, like the Talvivaara deposit in Finland is

* Geological Survey of Finland, Mineral Processing, Tutkijankatu 1, 83500 Outokumpu, Finland,
e-mail: jorg.langwaldt@gtk.fi

the largest known sulphide Ni-deposit in Europe (Loukola-Ruskeeniemi and Heino, 1996). The EU-co-funded Bioshale project aims to define innovative biotechnological processes for "eco-efficient" exploitation of black shale ores. Biobeneficiation processes, i.e. bioflotation and bioflocculation, are generally very fast and have been extensively studied (Das et al., 1999; Santhiya et al., 2001; Sharma, 2001; Smith and Miettinen, 2006; Smith et al., 1993). The separation of minerals in bioflotation is governed by two major factors, the selective adhesion of microorganisms on mineral surface and the interaction of flotation chemicals with biologically pre-conditioned minerals (Sharma, 2001). The selective adhesion of microorganisms on minerals is required to modify the mineral surface properties for mineral separation either by flotation or flocculation.

This study aims to: (i) concentrate base metal containing sulphide minerals from multimetal black shale ore by flotation (beneficiation), (ii) improve the flotation by use of bacteria as activators or depressants (bio-beneficiation).

MATERIALS AND METHODS

PREPARATION OF ORE SAMPLE

An ore sample of 200 Mg (tons), -700 mm, was received from the Talvivaara black shale deposit. The sample was crushed to -80 mm (164 tons) and -12 mm (149 tons). The fine fraction was further crushed to -5 mm and subsequently -1 mm. The latter fraction was used in the bio-beneficiation tests.

CULTIVATION OF BACTERIA

The three bacterial strains *Staphylococcus carnosus*, *Bacillus firmus* and *Bacillus subtilis* were selected for bioflotation studies. The strains *S. carnosus*, *B. firmus* and *B. subtilis* were cultivated in shake bottles and pilot-fermenters (Table 1).

Table 1. Growth conditions and yields

Strain	Fermentation broth, Temperature 30°C				Cell suspension	
	Cultivation time (h)	pH	V (l)	Cell concentration (g d.w./l)	V (l)	Cell concentration (g d.w./l)
<i>S. carnosus</i>	18	>4.8	200	4.8	4	168
<i>S. carnosus</i>	19	>6.0	20	6.4	0.6	213.5
<i>B. firmus</i>	17	>6.8	200	1.9	2	63
<i>B. subtilis</i>	16	6.8	20	2.2	0.2	83
<i>B. subtilis</i>	16	>6.6	20	1.7	0.4	78

FLOTATION TESTS

For flotation tests, a subsample (1 kg) from the -1 mm fine fraction of black shale ore was ground in a stainless steel ball mill (8 kg balls) with 0.7 dm³ water and water glass (500 g/t) for 45 min. The yielded particle size d80 was 78 µm. After grinding the

slurry was placed in a 4-l flotation cell and water was added to make slurry density 25%. All experiments were carried out in Outokumpu cell (4 dm³) with an air flow of 3 dm³/min, stirring speed of 1800 rpm. Freeze dried bacterial cells were used (Table 1 and 2) and conditioned at ambient pH of 6.4-6.6 of tap water. In some of the tests the rougher concentrate (RC) was cleaned by successive 1 to 3 cleaning steps to yield a cleaner concentrate (CC). The chemicals used in the flotation tests are given in Table 3. An overview of the experimental set ups is given in Table 2.

Table 2. Experimental set up of bioflotation and reference flotation (19, 37, 39) tests (RC rougher concentrate, CC cleaner concentrate). Tests without addition of collectors are marked bold. Potassium Amyl Xanthate (KAX), Sodium Isobutyl Xanthate (NaIX)

Test		Bacterial strain (g/t)			Xanthate (g/t)		pH
		<i>Staphylococcus carnosus</i>	<i>Bacillus firmus</i>	<i>Bacillus subtilis</i>	KAX	NaIX	RC/CC
Bio-1	RC	800					4
Bio-2	RC	400			400		4
Bio-3	RC	400					4
Bio-4	RC	400			400		4
Bio-5	RC	800					4
Bio-6	RC	800					4
Bio-7	RC	4000					4
Bio-8	RC	400				150	10.5
Bio-10	RC	800					4
Bio-11	CC	3000			1300		4/5.6-7.7
Bio-12	RC	400				300	10.5
Bio-13	RC	400			300		10.5
Bio-14	RC		400		300		10.5
Bio-15	CC	1600			800		10.5/9.0-9.8
Bio-16	CC		1200		1300		4/5.7-7.6
Bio-17	RC			400	300		10.5
Bio-18	CC			1200	1300		4/5.6-7.3
Bio-19	CC	1200			1300		4/9-10
Bio-20	CC	1200			800		10.5/9.1-9.8
19	CC				750		4/6.2-6.4
37	CC				1300		4/5.9-8.3
39	CC				1300		4/5.2-6.8

Table 3. Chemicals applied in flotation tests

Chemical	Function
Water glass	Dispersant
Sulphuric acid	pH control
Calcium hydroxide	pH control
Copper sulphate	Activator for sulphide minerals
Potassium Amyl Xanthate (KAX)	Collector for sulphide minerals
Sodium Isobutyl Xanthate (NaIX)	Collector for sulphide minerals
Carboxy methyl cellulose (CMC)	Depressant for silicates and graphite
Polyglycol ether (Dow250)	Frother (froth stabilizer)

ANALYSES

The collected concentrates and tailing products of the tests were filtered, dried and weighed. The samples were separated for chemical analyses. The elements Ni, Cu, Co, Zn, Mn and Fe were analyzed with Atomic Absorption Spectroscopy after nitric acid dissolution. Sulphur and carbon were determined with combustion analysis using a Leco analyzer. In addition, X-ray fluorescence was used to determine content of 40 elements in the samples. The masses and analyses of flotation products were used to calculate the feed assay and the recoveries of main elements to flotation products.

The identification of minerals and the mineral composition of the Talvivaara ore sample were determined by using combined Scanning Electron Microscopy (SEM) and Energy Dispersive X-ray analysis (EDAX) with the associated image analysis system of a Mineral Liberation Analysis equipment. The microprobe analyses of sulphide minerals were carried out with a Camexa SX 100 analyzer.

RESULTS AND DISCUSSION

In brief, the geochemical composition of the black shale ore sample was as shown in Table 4. The most abundant mineral group in the ore is formed by different silicates; i.e. quartz 16.7 %, biotite 12.0 % and plagioclase 10.3 %. The total amount of sulphides is 31.5 % of which the Ni-minerals pentlandite and altered pentlandite is 0.52% (Table 4). As much as 32.5 % of nickel is carried by pyrrhotite and 66.0% by Ni-minerals, i.e. pentlandite and altered pentlandite. Other sulphides are chalcopyrite (Cu), sphalerite (Zn) and alabandite (Mn). The ore contains 12.3 % graphite (as a fine mixture with other minerals), the chemical analysis of total carbon results in 7.72 % (Table 4).

The challenges in the beneficiation of this black shale ore are connected with the mineralogical characteristics of the ore. A high grade nickel concentrate cannot be produced with a good recovery because one third of nickel is contained by pyrrhotite. This means that in order to reach a good nickel recovery all sulphides must be recovered to concentrate whereby the grade remains low as the Ni-content of the sulphide phase is 0.845 % only.

Another challenge in the black shale ores is carbon which occurs in the form of graphite in the ore. As a soft mineral graphite forms easily fine slime particles in grinding and in addition to this, graphite is naturally floated without any reagents. Graphite was only partially depressed in flotation and formed one of the major harmful constituents in the concentrates.

The reference flotation tests with standard chemicals indicated that a concentrate containing 0.67 % Ni with a nickel recovery of 74 % was obtained by flotation (Test 39, see Table 5). The amount of concentrate was then 34.5 % of the mass of ore feed (Table 5). The flotation concentrate is a bulk concentrate of all sulphide minerals. The recoveries of copper, zinc and cobalt were about 90 % being thus higher than the recovery of nickel.

Table 4. Major geochemical and mineralogical composition of the black shale ore sample

Element		Chemical analysis		Microprobe analysis of sulphide minerals in total 31.5% of ore (% of element in mineral)						
		Initial	Corrected*	Pyrrhotite+ Oxidized pyrrhotite 19.83% of ore	Pyrite 7.76% of ore	Alabandite 1.79% of ore	Sphalerite 1.05% of ore	Chalcopyrite 0.50% of ore	Altered Pentlandite 0.47% of ore	Pentlandite 0.05% of ore
Ni	%	0.326	0.305	0.44	0.05	0	0.01	0.01	33.97	35.10
Cu	%	0.215	0.228	0	0	0	0	33.89	0	0
Zn	%	0.589	0.589	0.01	0	0.01	53.34	0.19	0	0.01
Co	%	0.033	0.033	0	0.39	0	0	0	1.04	0.83
Fe	%	13.12	13.12	52.46	46.67	3.24	7.52	30.58	20.31	30.02
Mn	%	1.23	0.913	7.46	0.01	58.47	4.14	0.02	0.01	0.07
S	%	13.0	11.0	39.10	52.78	36.43	33.72	34.81	41.67	33.33
C total	%	6.45	7.72							
Distribution of Ni between sulphide minerals (%)				32.5	1.4				59.5	6.5

*Average of feed analysis of 40 flotation tests

Table 5. Comparison of flotation products

	Product	Mass	Ni	Ni-recovery
Flotation		wt-%	%	%
Test 39	Rougher concentrate	65.7	0.436	91.8
	CC1	20.8	0.712	47.4
	CC2	25.8	0.729	60.2
	CC3	34.5	0.672	74.3
Bioflotation				
Test BIO-11	RouQher concentrate	72.6	0.390	93.6
	CC1	52.2	0.484	83.4
	CC2	29.0	0.648	62.1
	CC3	16.8	0.782	43.3
Test BIO-20	Rougher concentrate	64.6	0.451	85.4
	CC1	49.10	0.506	72.7
	CC2	42.00	0.539	66.2
	CC3	25.10	0.756	55.5

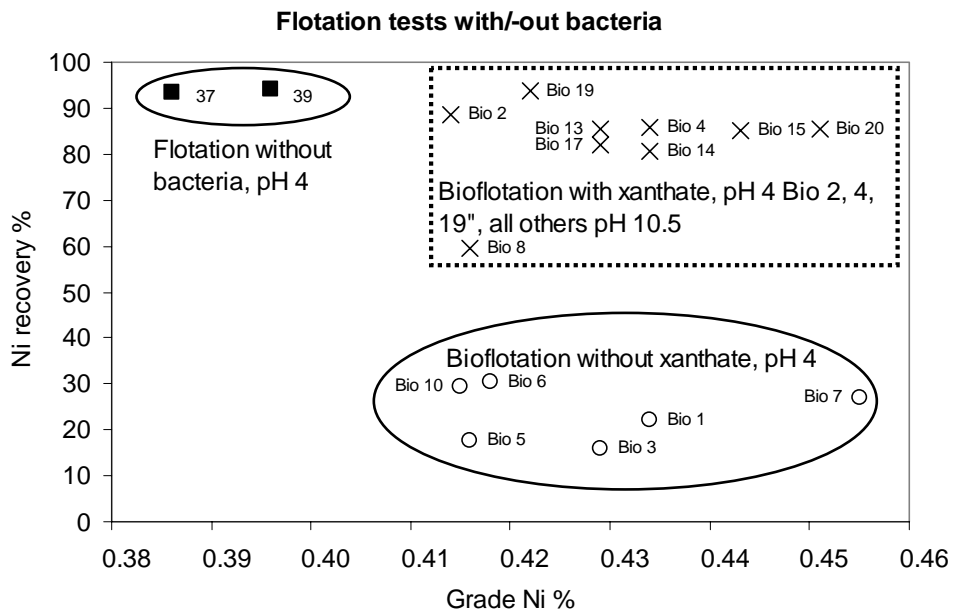


Fig. 1. Ni-recovery and grade in 2nd rougher concentrate during flotation. Experimental conditions see Table 2

CONCLUSIONS

A low grade sulphide concentrate with 0.67 % Ni and nickel recovery of 74 % was floated from the studied black shale ore by using common flotation chemicals. The mass of concentrate was then 34.5% of the ore feed. The recoveries of copper and zinc were 91%, of cobalt 89% and of manganese 53%. The content of carbon in the concentrate was 11.3% as graphite represents a naturally floating harmful mineral in the ore.

The bioflotation tests showed that collector chemicals, i.e xanthates, had to be supplied to achieve reasonable flotation results. Out of the three tested bacterial strains, *Staphylococcus carnosus*, *Bacillus firmus* and *Bacillus subtilis*, the minor hydrophobic strain *S. carnosus* yielded the best test results. However, results of bioflotation tests failed to substantially improve the product recovery or grade.

ACKNOWLEDGEMENT

This work was carried out in the frame of Bioshale (European project contract NMP2-CT-2004 505710). The authors acknowledge the financial support given to this project by the European Commission under the Sixth Framework Programme for Research and Development. We also wish to thank our various partners on the project for their contributions to the work reported in this paper.

REFERENCES

- DAS, A., RAO, K.H., SHARMA, P.K., NATARAJAN, K.A., FORSSBERG, K.S.E. 1999. *Surface chemical and adsorption studies using Thiobacillus ferrooxidans with reference to bacterial adhesion to sulfide minerals*, International Biohydrometallurgy Symposium (IBS) 1999, Spain, Proceeding part B, Chapter 2, 697-708.
- LOUKOLA-RUSKEENIEMI, K., HEINO, T. 1996. *Geochemistry and Genesis of the Black Shale-Hosted Ni-Cu-Zn Deposit at Talvivaara*, Finland. Economic Geology 91:80-110.
- SANTHIYA, D. SUBRAMANIAN, S., NATARAJAN, K.A. HANUMANTHA RAO, K. and FORSSBERG, K.S.E. 2001. *Biomodulation of galena and sphalerite surfaces using Thiobacillus thiooxidans*, Internat. J. Miner. Process. 62: 121-141.
- SHARMA, P.K., 2001. *Surface Studies Relevant to Microbial Adhesion and Bioflotation of Sulphide Minerals* PhD Thesis, University of Lulea, Sweden, 334 p.
- SMITH, R.W. and MIETTINEN, M., 2006. *Microorganisms in flotation and flocculation: Future technology or laboratory curiosity?* Minerals Engineering. 19: 548-553
- SMITH, R.W., MISRA, M. and CHEN, S., 1993. *Adsorption of a hydrophobic bacterium onto hematite: implications in the froth flotation of the mineral*, J. Ind. Microbiol., 11, 63-67.

Langwaldt J., Kalapudas R., Biowzbogacanie poliminerальной rudy łupkowej na drodze flotacji, Physicochemical Problems of Mineral Processing, 41 (2007) 291-299 (w jęz. ang.).

W ramach programu „BIOSHALE”, sponsorowanego przez Unię Europejską, badany był proces biowzbogacania poliminerальной rudy łupkowej. Celem projektu było opracowanie innowacyjnej metody eksploatacji rudy łupkowej w sposób przyjazny dla środowiska naturalnego. Ruda łupkowa pochodziła ze złoża Talvivaara zlokalizowanego w Finlandii. Próby rudy zawierały minerały siarczkowe, których całkowita zawartość wynosiła 31,5%. Nikiel znajdował się w pirytynie 32,5% i w pentlandycie 66,0%.

Inne siarczki jakie występują w rudzie to chalkopiryt (Cu), sfaleryt (Zn), pirotyn (Co) i alabandyt (Mn). Próba rudy zawierała grafit w formie mieszaniny drobnych ziaren z innymi minerałami. W procesie flotacji rudy otrzymywano koncentrat siarczkowy o zawartości 0,67% niklu z uzyskiem 74%.

Zagęszczenie nadawy na flotację wynosiło 34,5 %. Uzyski miedzi i cynku kształtowały się na poziomie 91% i 89%. Uzysk manganu wahał się na poziomie 53%. Zawartość węgla w koncentracie wynosiła 11,3%. Występował on w formie naturalnie flotującego grafitu. Próby bioflotacji pokazały, że kolektor flotacyjny typu ksantogenian musi być zastosowany w celu uzyskania korzystnych wyników. Z trzech testowanych szczepów bakteryjnych: *Staphylococcus carnosus*, *Bacillus firmus* i *Bacillus subtilis* najbardziej hydrofobowym szczepem okazał się być szczep *Staphylococcus carnosus*, który dawał najlepsze wyniki flotacji. Jednakże, wyniki bioflotacji wskazują, że nie udało się w sposób istotny poprawić uzysk i wychód koncentratu flotacyjnego.

Table 4. Major geochemical and mineralogical composition of the black shale ore sample

Element		Chemical analysis		Microprobe analysis of sulphide minerals in total 31.5% of ore (% of element in mineral)						
		Initial	Corrected*	Pyrrhotite+ Oxidized pyrrhotite 19.83% of ore	Pyrite 7.76% of ore	Alabandite 1.79% of ore	Sphalerite 1.05% of ore	Chalcopyrite 0.50% of ore	Altered Pentlandite 0.47% of ore	Pentlandite 0.05% of ore
Ni	%	0.326	0.305	0.44	0.05	0	0.01	0.01	33.97	35.10
Cu	%	0.215	0.228	0	0	0	0	33.89	0	0
Zn	%	0.589	0.589	0.01	0	0.01	53.34	0.19	0	0.01
Co	%	0.033	0.033	0	0.39	0	0	0	1.04	0.83
Fe	%	13.12	13.12	52.46	46.67	3.24	7.52	30.58	20.31	30.02
Mn	%	1.23	0.913	7.46	0.01	58.47	4.14	0.02	0.01	0.07
S	%	13.0	11.0	39.10	52.78	36.43	33.72	34.81	41.67	33.33
C total	%	6.45	7.72							
Distribution of Ni between sulphide minerals (%)				32.5	1.4				59.5	6.5

*Average of feed analysis of 40 flotation tests

Istvan GALFI*, Jari AROMAA*, Olof FORSÉN*

LABORATORY TOOL FOR ELECTROCHEMICAL STUDY OF SULPHIDE MINERALS

Received May 31, 2007; reviewed; accepted June 11, 2007

Sulphide mineral dissolution in aqueous media occurs by different mechanisms. The rate of the overall reaction is controlled by the rate of the slowest reaction step. Most important factor in the anodic dissolution of mineral sulphides is the formation of a reaction product layer, which affects the mass transfer rate, often the rate determining step of the overall reaction. In this work we have used electrochemical tests for evaluating factors affecting sulphide mineral dissolution. As an essential tool, an electrochemical measurement method for leaching behaviour of sulphide minerals has been developed. Development of a graphite paste electrode (GPE) for the electrochemical measurements has made it possible to investigate powdered sulphide mineral samples. This ensures that the measurement conditions are as close as possible to the real leaching conditions. The graphite paste electrode makes it possible to run electrochemical measurements reproducibly and reliably.

Key words: sulphide mineral, dissolution, graphite paste electrode, electrochemical measurement

INTRODUCTION

Measurements were conducted with samples prepared from minerals usually being in solid phase and having a low current resistance. Using of a graphite paste electrode (GPE) for the electrochemical measurements has made it possible to investigate powdered sulphide mineral samples. This ensures that the measurement conditions are as close as possible to the real leaching conditions. The aim of our study was to examine the to use GPE in electrochemical study of sulphide minerals. Special attention was paid on the differences at reaction rates between solid and graphite paste electrodes.

Carbon is available in several forms: amorphous, powder, graphite rods, and diamond. Carbonaceous materials have several properties that have attracted their use in electrodes: good electrical conductivity, acceptable corrosion resistance, availability in high purity, low cost, high thermal conductivity, dimensional and mechanical

* Helsinki University of Technology, PO Box 6200, FIN-02015 TKK; Finland

stability, light in weight and ease of handling, availability in a variety of physical structures and ease of fabrication into composite structures (Kinoshita 2001). The high conductivity of graphite and its good chemical stability are attractive features for its use in electrochemistry.

The first user of carbon powder as paste electrode was Adams and his research group probably in the fifties. The title of carbon paste electrode was mentioned first time in a scientific communication on Analytical Chemistry in 1958 (Adams 1958). In this study powder of graphite was used and the title of graphite paste electrode invented. Graphite paste electrodes have proved to be practically inert in the electrochemical measurements and thereby do not disturb the electrochemical reactions on the powder samples (Ahlberg et al. 1993), (Gerlach et al. 1983), (Rice et al. 1983).

EXPERIMENTAL

The measurements were carried out using two electrochemical workstations: (1) a PAR 273 Potentiostat/Galvanostat controlled by EG&G PAR Model 352 Corrosion Analysis Software 1.00 and (2) Potentiostat/Galvanostat 2000 working together with NF Electronic Instruments 5050 frequency response analyzer (FRA) and NF Electronic instruments 1731 Intelligent/Arbitrary function synthesizer controlled by in-house written software.

A three-electrode AVESTA type electrochemical cell was used for the electrochemical measurements (Figure 1). The cell contained a working electrode, a reference electrode and an auxiliary platinum electrode. To adjust the temperatures between 23-83 °C the cell was thermostatted. In all the measurements the cell was stirred with a mechanical stirrer at 500 rpm.

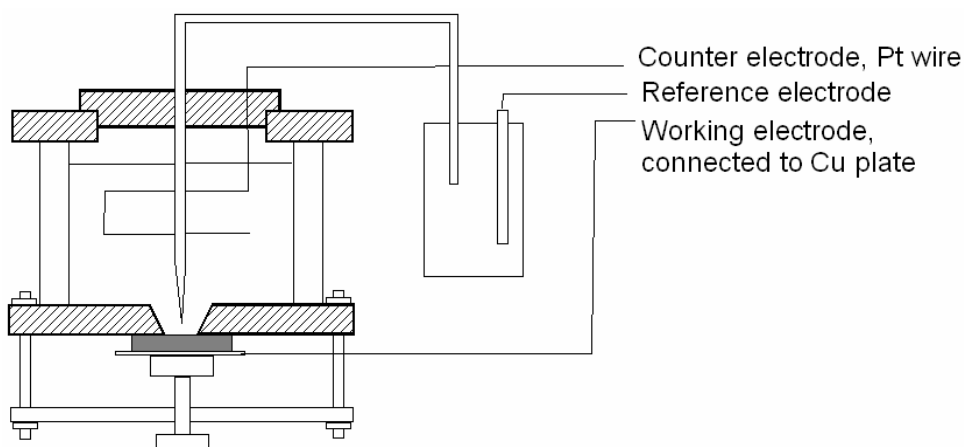


Fig. 1. Simplified diagram of the Avesta cell

The reference electrode used was Hg/Hg₂Cl₂ filled with saturated KCl (trademark: Radiometer analytical, REF 421). The reference electrode was situated in a glass tube (145 mm high, Ø11 mm, Schott Geräte B522), which was filled with a saturated KCl, and KCl salt. On the bottom of the tube there was a platinum gauze. The reference electrode in the glass tube was positioned in an external beaker and connected to the cell with a Haber-Luggin capillary. The composition and the pH of the solution in the beaker were the same as in the cell, but the temperature could not be increased (Figure 2). In consequence of this, the temperature in the beaker was between 21-24 °C during the measurements.



Fig. 2. Modified Avesta cell used in solid sample leaching experiments

The solution used in the electrochemical tests was a saturated solution of calcium sulphate. The solution was made by adding a constant amount (2.41 g) of CaSO₄ into a dm³ of distilled water. The use of calcium salt was to provide hardness salts to the solution to increase conductivity. The temperature and the pH values of the solution were adjusted in each measurement. The temperature was varied between 23 and 83 °C. The pH was monitored in the range of 0.5 to 3.5. The upper pH limit is defined by the formation of ferrous hydroxide, while the lower limit is due to the bacteria activity.

The black shale mineral came from the Talvivaara mine, Finland. The mineral sample was non-homogenous and the composition varied. Solid electrodes were made for the electrochemical measurements. Figure 3. shows a photograph of electrodes.

A set of working electrodes of black shale was made. The most uniform pieces (visually) of the black shale (30x20x20 mm) were chosen (a mineral rich area) and were cut with a diamond cutter. The conductivity of the electrode was tested and it was checked that the resistance of the electrode was 2-5 Ω. The polishing of electrodes

was carried out between every measurement with rotating and wetted abrasive paper. The waterproof abrasive paper used was of grade 800 mesh. The uniformity was inspected visually. After polishing the electrodes were rinsed first with deionised water and ethanol (ETAX Aa, 99.5% ethanol) and then dried with a hairdryer. Some chemical analyses of Talvivaara ore are shown in Table 1.



Fig. 3. Prepared black shale working electrodes with mineral rich area.

The black shale materials contain significant amount of carbonaceous material. Therefore it was decided not to use a former construction of graphite paste electrode (Forsén et. al. 1996). Instead the graphite was mixed with the test material and put in a special holder. The holder was necessary to avoid sample disintegration due to gas evolution. The best graphite paste electrode construction was made by using a mixture of graphite powder (Merck KGaA, Germany, bulk density 20-30 g/100ml), powder samples of Talvivaara black-shale ore, size 1 mm and paraffin oil, Figure 4.

Table 1. Talvivaara black shale analyses

	Fe, ppm	Ni, ppm	Cu, ppm	Zn, ppm	Mn, ppm	Co, ppm	Reference
Black shales Ni < 0,1%	88000	500	600	2600	1600		(Loukola-Ruskeeniemi et. al. 1999)
Black shales Ni ≥ 0,1%	104000	2600	1300	5200	2600		(Loukola-Ruskeeniemi et. al. 1999)
Black schist ore	158000	2800	1400	3900	2900	200	(Riekkola-Vanhanen et. al. 2001)
Bioshale sample	118767	2494	1514	5157	5672	260	(www.talvivaara.com)



Fig. 4. Construction of the graphite paste electrode

RESULTS AND DISCUSSION

POLARISATION CURVES FOR TALVIVAARA ORE

The usability of graphite paste was verified by comparing polarization curves of solid sample to that of powdered sample, Figure 5. The polarization curves of solid and powder samples are close to each other whereas the graphite materials have much lower current densities.

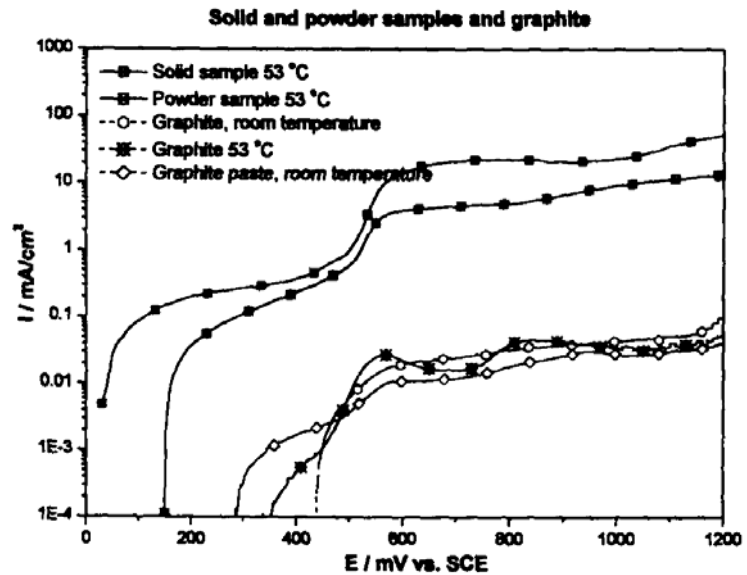


Fig. 5. Anodic polarization curves for solid Talvivaara sample, graphite paste electrode and graphites

At pH below 2 the sample showed clear areas of mineral transformations and sulphide dissolution. At these pH values mineral transformations happen at potentials below 500 mV vs. SCE. Mineral dissolution and release of sulphur, with or without oxidation to sulphate, happens at potentials above 500-550 mV. The beginning of mineral dissolution and sulphur release were observed for rapid current density increase. As the pH increases to 3 or more, the beginning of the mineral dissolution becomes less clear (Riekkola-Vanhanen et al. 2001). This is most likely related to reaction product layer formation (Pourbaix 1966).

Anodic polarization curves for solid and powder samples were measured in the temperature range 23-83 °C and at pH 1. The curve exhibited identical shapes (Figures 6 and 7). There is a clear change between temperatures 43 and 53 °C both for solid and powdered samples. Dissolution starts at lower potentials with increasing temperature and it becomes faster when temperature exceeds 53 °C. The current densities of powdered samples are lower than those of solid samples due to the smaller reactive area of the powdered sample surface. The solid sample has reactive surface of mineral only, whereas the powder sample surface includes also gangue.

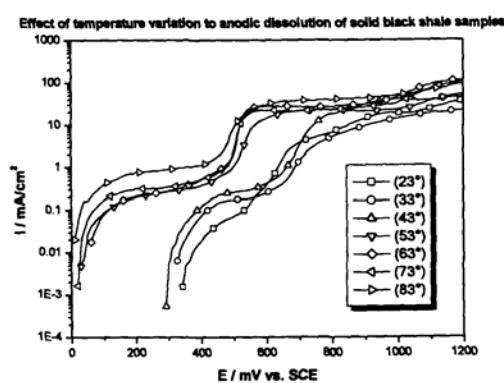


Fig. 6. Anodic polarization curves for solid Talvivaara samples at temperature range from 23 to 83 °C. Solution had $[\text{CaSO}_4 \cdot 2\text{H}_2\text{O}] = 2.41 \text{ g/l}$, pH=1 and scan rate was 0.83 mV/s

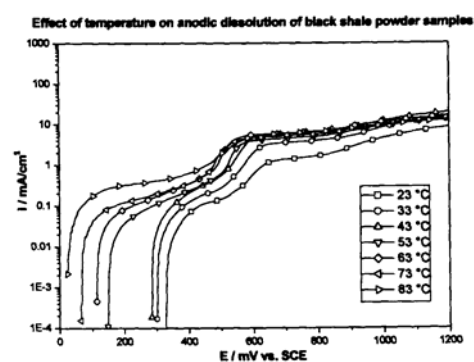


Fig. 7. Anodic polarization curves for powder Talvivaara samples at temperature range from 23 to 83 °C. Solution was in equilibrium with $[\text{CaSO}_4 \cdot 2\text{H}_2\text{O}] = 2.41 \text{ g/l}$, pH=1 and scan rate was 0.83 mV/s

POTENTIOSTATIC MEASUREMENTS WITH TALVIVAARA ORE

The potentials at which the potentiostatic measurements were examined and selected from the anodic polarization curves. Upper potential limit was decided onducted by assumptions on the maximum redox potential that can be reached by common oxidants, such as oxygen or ferric iron. Potentiostatic experiments were in the potential range of 350-950 mV and at temperatures from 23 °C to 53 °C. Figures 8 and 9 show results of long potentiostatic measurements for solid and powdered Talvivaara samples, respectively. At all the chosen potentials it was observed that current density increased slightly with increasing temperature.

Fig. 8. Potentiostatic curves at $T = 43\text{ }^{\circ}\text{C}$. Solution was saturated with CaSO_4 [$\text{CaSO}_4 \cdot 2\text{H}_2\text{O}$] = 2.41 g/l, pH = 1 and the potential range was from 350 to 950 mV

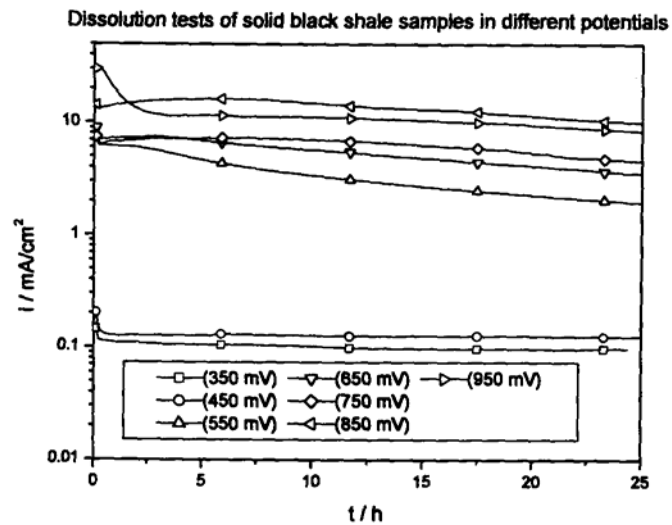
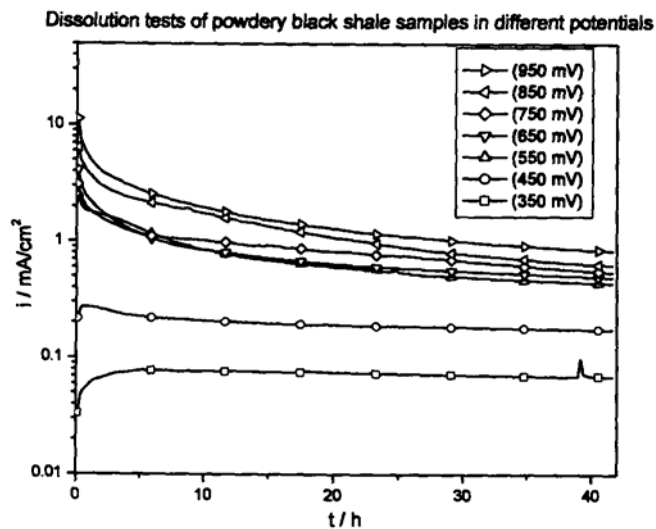


Figure 9. Potentiostatic curves at $T = 43\text{ }^{\circ}\text{C}$. Solution was saturated with CaSO_4 [$\text{CaSO}_4 \cdot 2\text{H}_2\text{O}$] = 2.41 g/l, pH = 1 and the potential range was from 350 to 950 mV



The solutions of potentiostatic tests were analysed by the Geological Survey of Finland in Espoo by using inductively coupled plasma atomic emission spectroscopy (ICP-AES). For the solid samples the metal concentrations indicate that dissolution of iron sulphides increases significantly above 450 mV. Nickel and zinc dissolve slightly faster at potentials above 450 mV, but the effect is not very clear. The analyses were used to model the effect of potential and temperature. Linear regression analysis by using Microsoft EXCEL statistic data analysis package produced relationships shown in equations (1)-(5). The results are calculated separately for Cu, Ni, Fe, Zn and Mn. The functions are of the generic form $\ln[Me] \text{ (g/l)} = a \cdot 1/T \text{ (K)} + b \cdot E \text{ (mV)} + c$.

$$\ln[\text{Cu}] = 110.9 \cdot 1/T - 1.08 \cdot 10^{-3} \cdot E - 3.912 \quad (1)$$

$$\ln[\text{Ni}] = -1988 \cdot 1/T + 3.45 \cdot 10^{-3} \cdot E + 5.517 \quad (2)$$

$$\ln[\text{Fe}] = -1914 \cdot 1/T + 13.2 \cdot 10^{-3} \cdot E + 2.783 \quad (3)$$

$$\ln[\text{Mn}] = -1947 \cdot 1/T + 0.78 \cdot 10^{-3} \cdot E + 5.161 \quad (4)$$

$$\ln[\text{Zn}] = -7657 \cdot 1/T + 5.41 \cdot 10^{-3} \cdot E + 20.41 \quad (5)$$

Statistical testing by F-test revealed that only the equations for iron, nickel and zinc had significance on the 95% confidence level. Further testing by t-test revealed that for these metals only the potential had significance and temperature had effect only for nickel.

The dissolution of powdered black shale samples were studied at potentials 350-950 mV at temperature 43 °C only. Comparison of dissolved metal concentrations (Table 2) indicates that copper dissolution increases by a factor of 3 to 20 at potentials 350-550 mV and by a factor of 50-80 at higher potentials. Dissolution of iron increases by a factor of ten at potentials 350-450 mV but it decreases by 50% at higher potentials. Dissolution of manganese increases by a factor of 10 to 70, but there is no clear potential dependence. The dissolution of nickel is about the same for powder and solid samples. Dissolution of zinc increases by a factor of 10 to 30 at potentials 350-450 mV but there is no clear change at higher potentials.

Table 2. Analyzed metal concentrations after potentiostatic experiments at $T = 43$ °C with powder samples, duplicate tests included. Tests have been done with 1 mm fraction

E (mV)	Cu, ppm	Fe, ppm	Mn, ppm	Ni, ppm	Zn, ppm	
350	0.225	55.9	26.7	3.06	3.06	
350	0.059	42.5	24.5	2.88	2.88	
450	0.245	52.6	26.1	3.04	3.04	
450	0.323	67.7	31.8	3.91	3.91	
450	0.491	76.6	24.5	3.41	3.41	
550	0.584	240	47.8	7.16	7.16	
550	0.613	170	4.4	3.76	3.76	3 mm fraction
650	0.523	191	38.7	6.46	6.46	
750	1.159	236	34.1	6.73	6.73	
850	4.939	332	33.5	8.79	8.79	
950	6.208	348	42.5	9.76	9.76	

Figure 10 shows the final current densities of potentiostatic curves for solid and powder samples. The curve shows the last 10 points at each potential plotted as current densities of powder sample vs. current densities of solid sample. The current densities of powder samples are lower, and the slope of the linear fit is 0.089.

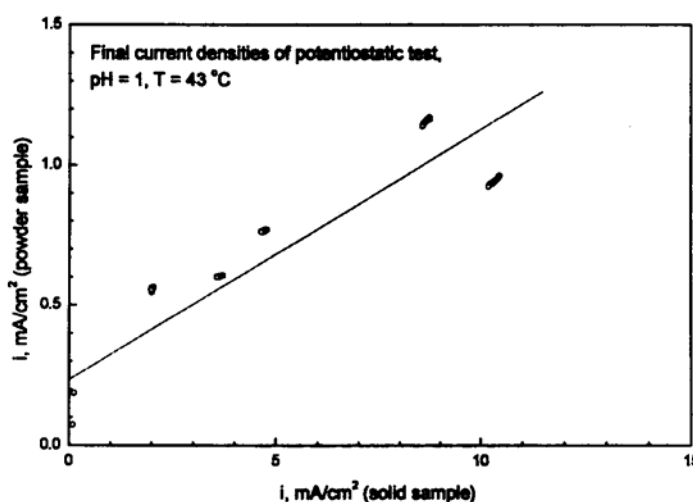


Figure 10. Final current densities correlation of solid and powder black shale samples at $T = 43\text{ }^{\circ}\text{C}$. Solution was saturated with CuSO_4 [$\text{CaSO}_4 \cdot 2\text{H}_2\text{O}$] = 2.41 g/l, $\text{pH} = 1$ and the potential range from 350 to 950 mV

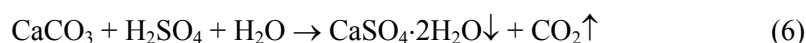
TESTS WITH LUBIN BLACK SHALE ORE AND CONCENTRATE

The powdered samples of Lubin black shale materials were studied using the developed carbon paste electrode. The composition of the material is given in Table 3. The ore contains high Cu contents in thin deposit what results from high percentage of strongly mineralised shale ore. The composition of the Lubin concentrate was not given.

Table 3. The chemical composition of copper ore (shale) in Polish copper deposit (KGHM „Polish Copper”, unpublished data)

Fe, ppm	Ni, ppm	Cu, ppm	Zn, ppm	Mn, ppm	Co, ppm
9330	278	104800	780	947	189

Because the metal sulphides are finely disseminated in the carbonate matter (about 18% CaCO_3) a sulphuric acid treatment was used to enhance dissolution. Acidic non-oxidative leaching of the shale ore or concentrate involves chemical reactions between sulphuric acid and calcium or magnesium carbonates. The reactions (6) and (7) dominate during the non-oxidative leaching:





The leaching of a carbonate gangue with H_2SO_4 is a very fast chemical process and can be performed at ambient temperatures. The consumption of sulphuric acid was followed by looking for the production of carbon dioxide bubbles. Carbon dioxide, evolving in reactions (6) and (7), creates an oxygen-free atmosphere preventing the undesirable dissolution of valuable metals (Cu, Zn, Ni, Co, Mn) from the sulphidic raw material. After the acid treatment desired amount of shale or shale concentrate was crushed and used to prepare GPE for electrochemical examination

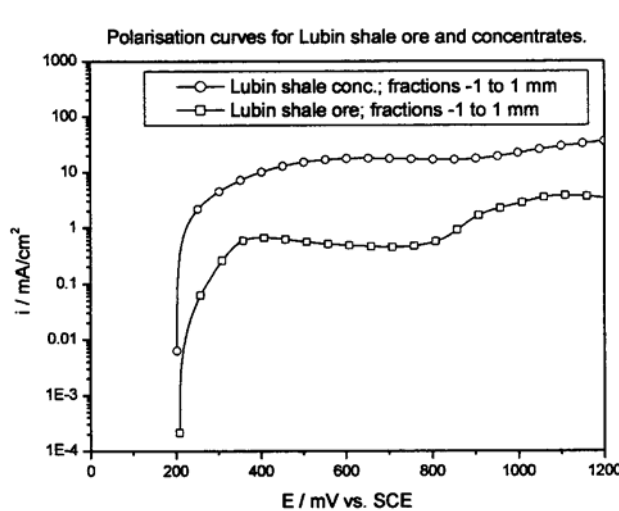


Fig. 11. Anodic polarization curves made at pH 1. Solution composition was $[\text{CaSO}_4 \cdot 2\text{H}_2\text{O}] = 2.41 \text{ g/l}$, $T = 23 \text{ }^\circ\text{C}$ and scan rate was 0.83 mV/s

The dissolution of powdered Lubin shale and shale concentrates samples were studied with polarization curves and potentiostatic tests in the potential range of 500-900 mV and at temperature $23 \text{ }^\circ\text{C}$. Polarisation curves are shown in Figure 11. The dissolution begins almost immediately when the sample potential is increased. The current density does not change much. The same dissolution stages and mechanisms as with Talvivaara ore are not seen. The current densities for Lubin ore are of the same magnitude as for Talvivaara ore, but the current densities of Lubin concentrate are ten times higher. Potentiostatic curves for Lubin ore and concentrate at selected potentials are shown in Figure 12. The current densities for Lubin ore are lower as for Talvivaara ore, but the current densities of Lubin concentrate are slightly times higher. The curves reach fairly soon a steady state indicating formation of a reaction product layer and the controlling mechanism is mass transfer through the layer.

Analyzed metal concentrations after potentiostatic experiments were done by the Geological Survey of Finland in Espoo by using inductively coupled plasma atomic emission spectroscopy (ICP-AES). The analysis results for Lubin ore and concentrate are shown in Table 4. The experiments shown in Table 4 are the same as in Figure 12.

Fig. 12. Potentiostatic curves at $E = 500, 600, 800$ and 900 mV vs. SCE. Solution was saturated with CuSO_4 [$\text{CaSO}_4 \cdot 2\text{H}_2\text{O}$] = 2.41 g/l, pH = 1 and the temperature was 23°

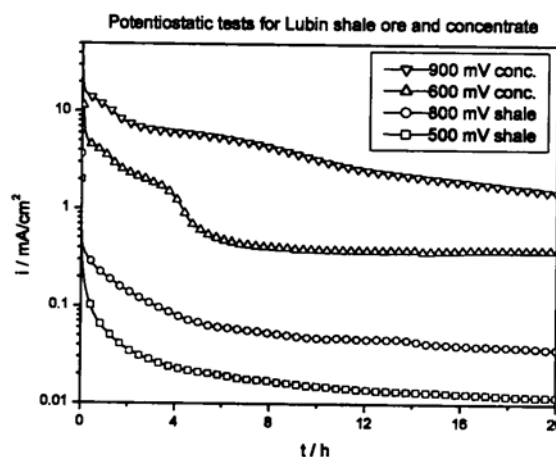


Table 4. Chemical analysis of Lubin ore and concentrate after potentiostatic dissolution tests.

E (mV)	Sample	Cu, ppm	Fe, ppm	Mn, ppm	Ni, ppm	Zn, ppm	Co, ppm
500	shale	34.7	5.9	0.2	15.3	0.53	0.13
800	shale	178	21.7	0.32	1.08	1.13	1.67
600	conc.	293	142	1.47	2.05	3.43	4.97
900	conc.	487	373	2.93	7.65	6.9	9.47

The results in Table 4 indicate that leaching of the concentrate is more efficient than leaching the ore. Improved dissolution rates will be gained by using potentials of 600 mV or more. A possible way to limit iron dissolution is to use ore instead of concentrate and limit the leaching potential.

CONCLUSIONS

The dissolution characteristics of Talvivaara and Lubin black shale minerals were studied with special anode construction, where the powdered samples were mixed with fine particles of graphite and binding components. The sample preparation from powdered mineral has to be done by special procedure in order to obtain reproducible results with respect to solid samples. The electrochemical experiments with Talvivaara ore showed good reproducibility despite the active surface can vary significantly due to its porous character. During electrochemical testing it was noticed that even though the calculated current densities are higher for solid electrodes, the actual dissolved metal contents are higher for powder samples. The metal recoveries from powdered samples were ten times higher than from solid samples. With powder samples the selectivity of valuable metals (other than Fe) was better than with solid samples.

The dissolution of the Lubin black shale and shale concentrate were examined by using the same GPE method as for Talvivaara ore. After an acid treatment a desired amount of shale or shale concentrate sample was used to make a GPE. To verify the

applicability of a newly prepared GPE, potentiodynamic and potentiostatic measurements were carried out. The described method of preparing a graphite paste electrode provides a useful tool for the study of electrochemical dissolution behaviour of sulphide minerals, regardless of their origin.

ACKNOWLEDGEMENT

This work was supported by the European Commission in the frame of Bioshale European project (6th Framework program - NMP2-CT-2004-505710).

REFERENCES

- ADAMS, R.N., 1958, *Carbon paste electrodes*. Analytical Chemistry(Scientific Communications), 1(30): p. 1576.
- AHLBERG, E.A., J., 1993, *Carbon paste electrodes in mineral processing: an electrochemical study of galena*. Hydrometallurgy, 1993(34): p. 171-185.
- FORSÉN, O., ANTILA, E., AROMAA, J., PESONEN, P., 1996, *Evaluation of carbon paste electroactive electrode for the electrochemical characterization of sulphide minerals*. Acta Metallurgica Slovaca 2, 1996(1): p. pp. 7-18.
- GERLACH, J., KÜZECI, E., 1993, *Application of carbon paste electrodes to elucidate hydrometallurgical dissolution processes with special regard to chalcocite and covelite*. Hydrometallurgy, 1983(11): p. 345-361.
- KINOSHITA, K., 2001, *Electrochemical uses of carbon*.
- KUHN, A.T., 1987, *Techniques in Electrochemistry*. Corrosion and Metal Finishing, p. 66 p.
- LOUKOLA-RUSKEENIEMI, K., et al., 1999, *Environmental impact of metalliferous black shales at Talvivaara in Finland, with indication of lake acidification 9000 years ago*. Journal of Geochemical Exploration, 64(1-3): p. 395-407.
- POURBAIX, M., 1966, *Atlas of Electrochemical Equilibria in Aqueous solutions*, ed. P. Press., Bristol. 386.
- RICE, M.E., GALUS, Z. and ADAMS, R. N., 1983, *Graphite paste electrodes. Effect of paste composition and surface states on electron-transfer rates*. Journal of Electroanalytical Chemistry, 1983(143): p. 89-102.
- RIEKKOLA-VANHANEN, M., et al., 2001, *Effect of pH on the biological leaching of a black schist ore containing multiple sulfide minerals*. in *Biohydrometallurgy: Fundamentals, Technology and Sustainable Development*.
- SVANCARA, I., SCHACHL, K., 1999, *Testing of unmodified carbon paste electrodes*. Chemiche Listy, 1999(93): p. 490-499.
- Galfi I., Aromaa J., Forsen O.,** *Laboratoryjne narzędzie do elektrochemicznych badań minerałów siarczkowych*, Physicochemical Problems of Mineral Processing, 41 (2007) 301-312 (jęz. ang.).

Roztworzenie minerału siarczkowego w roztworach wodnych zachodzi na drodze różnych mechanizmów. Szybkość całkowitej reakcji jest kontrolowana przez szybkość najwolniejszego etapu reakcji. Najważniejszym czynnikiem w anodowym rozkładzie minerałów siarczkowych jest tworzenie warstwy produktu reakcji, która wpływa na szybkość wymiany masy na granicy faza stała – roztwór, która jest często etapem kontrolującym proces roztwarzania minerału. W tej pracy użyliśmy elektrochemicznej metody oceny podatności surowców siarczkowych na proces ługowania. Jako podstawowe narzędzie tej metody zastosowaliśmy pomiary elektrochemiczne na elektrodach wykonanych z badanego surowca. Elektrody użyte w pomiarach są wykonane w postaci pasty z udziałem grafitu i drobnopziarnistego materiału siarczkowego. Taka konstrukcja elektrody zapewnia warunki bliskie tym, jakie występują w rzeczywistym procesie ługowania. Grafitowa elektroda w formie pasty zawierającej siarczki metali gwarantuje dużą powtarzalność i niezawodność.

Jari AROMAA*, Petteri PESONEN*

LEACHING MECHANISMS AND KINETICS OF COMPLEX LOW-GRADE SULFIDIC COPPER ORES

Received March 15, 2007; reviewed; accepted May 15, 2007

The aim of the study was to examine the leaching kinetics of powdered chalcopyrite based concentrate and the formation potential of elemental sulphur by means of electrochemistry and chemical analysis. Anodic polarisation curves, cyclic voltammetry and potentiostatic measurements were carried out in 1 N sulphuric acid at temperatures 25-80 °C. The working electrode was a carbon paste electrode, which gives good response to powdered sulphide samples. The dissolved metal ions in the potentiostatic measurements were analyzed using AAS. The leaching of chalcopyrite-based concentrate occurs in two steps. At low overpotentials the reaction is a phase transformation and at higher overpotentials dissolution of the sulphide. The rate-determining step of leaching kinetics was evaluated by calculating the activation energies from the polarisation curves. The formation potential of elemental sulphur is between 500 and 700 mV vs. SCE. Above this potential sulphur is oxidized to sulphate. At room temperature the leaching kinetics is generally controlled by mass transfer and at 60 and 80 °C by charge transfer.

Key words: sulfide ore, copper concentrate, dissolution, sulfur formation, carbon paste electrode

INTRODUCTION

Hydrometallurgy provides numerous advantages for the processing of minerals. Ideally, the hydrometallurgic refining path enables selective dissolution and precipitation of elements in a desired form at a preferred stage of the process. The problems in sulphide leaching are due to iron dissolution and form of sulphur as a reaction product. During chemical or electrochemical dissolution of sulphide minerals, the sulphur may remain in amorphous form enveloping gradually the dissolving particles. Then the dissolution is hindered and the diffusion of ions through the amorphous sulphur layer finally ceases. Sulphur may also be oxidized to sulphate, which increases the consumption of reagents or energy. Iron is practically always present in minerals to be leached and it is an impurity rather than a product. Dissolved

* Helsinki University of Technology, PO Box 6200, FIN-02015 TKK, Finland.

iron, in turn, disrupts the process by consuming reagents and energy and it may also contaminate the products (Doyle 1990), (Gerlach et al. 1983).

One hydrometallurgical process path is the dissolution of sulphide minerals in acid oxidizing media, where the reactions are predominantly of electrochemical nature. The dissolution mechanisms and the kinetics of the dissolution can therefore be examined with electrochemical measurement methods. However, it is essential that the measurements are carried out in conditions that simulate the real circumstances, i.e. the mineral is in powdered form. The application of carbon paste electroactive electrode has been used to allow measurements with powder samples. The material to be studied is mounted on carbon paste. The paste does not take significantly part in the electrochemical reactions, but allows the sulphide material itself to react (Küzeci et al. 1988), (Ahlberg et al. 1994), (Forsén et al. 1996).

A research project concerning the dissolution of sulphide minerals was carried out at the Laboratory of Corrosion and Material Chemistry, Helsinki University of Technology. During the project a method to determine the dissolution characteristics of individual sulphide mineral samples was developed (Forsén et al. 1996). Based on the data obtained in a laboratory scale, the optimum conditions and possibilities of hydrometallurgic refining are estimated prior to pilot plant leaching experiments.

EXPERIMENTAL

The experiments were carried out in a three-electrode cell with electrolyte volume of 200 cm³, Figure 1. The cell was equipped with a jacket connected to a thermobath to maintain electrolyte temperature. The counter electrode was a platinum sheet with dimensions of 20x15 mm. The reference electrode was Radiometer type K 401 saturated calomel electrode (SCE). The SCE was put in Agar-Agar gel in a separate beaker at ambient temperature to protect the electrode. All the potentials in this paper are versus SCE, +242 mV vs. SHE. The electrode potential was measured using Haber-Luggin capillary and liquid junction. A carbon paste electrode was used as a working electrode, Figure 2. A more detailed description of the working electrode and its electrochemical response is given in (Forsén et al. 1996). The electrolyte was 1 N sulphuric acid (Merck 731) solution. The sulfide material studied was a chalcopyrite based powdered mineral. The composition of the material is shown in Table 1.

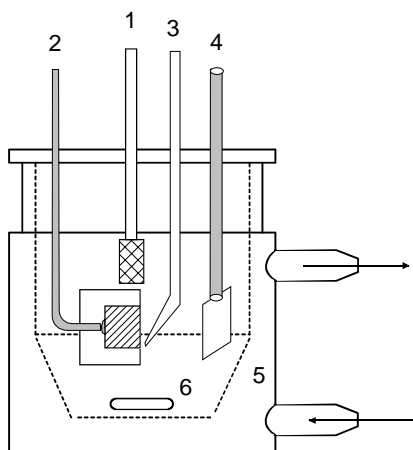


Fig. 1. Electrochemical test cell.
1 - sinter, 2 - working electrode, 3 - Luggin capillary, 4 - counter electrode, 5 - water jacket, 6 - magnetic stirrer

The counter electrode was a platinum sheet with dimensions of 20x15 mm. The reference electrode was Radiometer type K 401 saturated calomel electrode (SCE). The SCE was put in Agar-Agar gel in a separate beaker at ambient temperature to protect the electrode. All the potentials in this paper are versus SCE, +242 mV vs. SHE. The electrode potential was measured using Haber-Luggin capillary and liquid junction. A carbon paste electrode was used as a working electrode, Figure 2. A more detailed description of the working electrode and its electrochemical response is given in (Forsén et al. 1996). The electrolyte was 1 N sulphuric acid (Merck 731) solution. The sulfide material studied was a chalcopyrite based powdered mineral. The composition of the material is shown in Table 1.

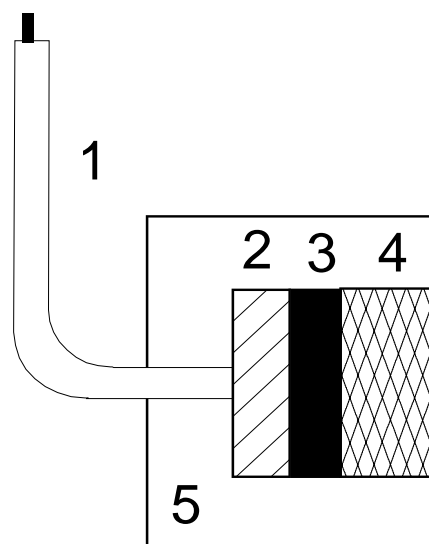


Fig. 2. The carbon paste electrode. 1 - copper wire, 2 - copper backing plate, 3 - carbon paste, 4 - sulfide sample, 5 - epoxy resin housing

The working electrode surface area was calculated geometrically using the radius of the hole. The actual surface area is much larger due to the porous nature of the powder specimen. This gives greater current densities than with the actual surface area in the electrochemical measurements. That also means that possible minor effects can be distinguishable.

Table 1. Mineral distribution of the concentrate

Mineral	Amount [wt-%]
CuFeS ₂	69
FeS ₂	25
ZnS	2.5
(Cu,Fe,Zn) ₁₂ As ₁₄ S ₁₂	1.2
SiO ₂	1.0
PbSO ₄	0.2
Cu ₂ FeSnS ₄	0.2
(Cu,Fe,Zn) ₁₂ Sb ₄ S ₁₃	0.02

The electrolyte was purged with nitrogen (AGA 99.99 % N₂). During the nitrogen purging and the experiments a magnetic stirrer was used. The flow of the electrolyte was kept laminar and constant during all the experiments. The corrosion potentials fluctuated, but after the five minute period the potentials were fairly constant. The electrochemical experiments, which included anodic polarisation, cyclovoltametric and potentiostatic measurements, were carried out with an automatic electrochemical measurement system developed at the Helsinki University of Technology, Laboratory

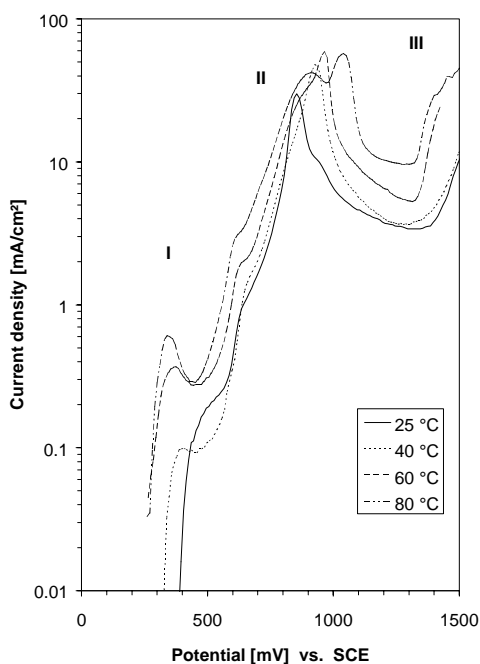
of Corrosion and Material Chemistry (Aromaa, 1988). The iR -drop was corrected after the experiments by using electrolyte resistance measured with electrochemical impedance spectroscopy (EIS) at the corrosion potential. Metal ion contents of the electrolytes in potentiostatic leaching experiments were measured with Perkin-Elmer atom absorption spectrometer (AAS).

RESULTS AND DISCUSSION

The anodic polarisation measurements were carried out to gain general information on dissolution characteristics of the sulphide mineral, the cyclic voltametric measurements gave more detailed information on reaction stages, mechanisms and behaviour of sulphur. The potentiostatic leaching experiments gave detailed data on the kinetics of dissolution.

ANODIC POLARISATION MEASUREMENTS

A general leaching behaviour of the sulphide mineral was examined using anodic polarisation measurements. The activation energy values were calculated from the polarisation curves to define the dissolution rate controlling step of the leaching. Anodic sweeps were started at the corrosion potential and the samples were polarised stepwise at 50 mV/min up to gas evolution region, i.e. 1500 mV vs. SCE.



The polarisation curves are rather uniform (Fig. 3). The dissolution characteristics of the mineral is considered to consist basically of three different reaction stages, i.e. two dissolution reactions of the sulphide including phase transformation (stage I) and decomposition of the sulphide (stage II and III) (Forsén et al. 1996), (Knuutila 1985). At the reaction stage III (Fig. 3) the oxidation of sulphur to sulphate may also occur.

Fig. 3. Anodic polarisation curves of the chalcopyrite based sulphide mineral in 1 N H_2SO_4 , $dE/dt = 50$ mV/min.

Stage I - dissolution by mineral transformations, Stage II - dissolution by oxidation of sulphur to elemental sulfur and Stage III - dissolution by oxidation of sulfur to sulfate

These reactions are followed by oxygen evolution at the anode. The reactions occur at the potential ranges of 300-500 mV (I), 750-950 mV (II) and 1250-1500 mV (III), respectively. This anodic behaviour has been known for a long time (Biegler 1979), (Parker 1981), (Jones 1994). The dissolution was activated considerably when the temperature was increased from 40 to 60°C. The selectivity of dissolution gets also better when the temperature is raised.

The activation energies calculated from the polarisation curves (Table 2) show that at low potentials (400-600 mV) the anodic reaction is controlled by charge transfer and the main reaction is the phase transformation of the mineral. At higher potentials (700-900 mV) activation energies are relatively low. The mineral decomposes and elemental sulphur and sulphate are formed as reaction products. The reaction is controlled by mass transfer in the solution. At 1000 mV a reaction product layer hinders dissolution and the value of the activation energy increases.

Table 2. Activation energies E_a of the chalcopyrite based concentrate calculated from the anodic polarisation curves in 1 N H₂SO₄ electrolyte at the temperature range of 25-80°C

Potential vs. SCE [mV]	E_a [kJ/mol]
400	37.9
500	30.2
600	32.8
700	21.3
800	18.4
900	14.7
1000	29.9

CYCLOVOLTAMETRIC MEASUREMENTS

The cathodic maximum potential in the cyclic voltametric measurements was set to a constant potential of -500 mV and the anodic turning point was altered between +300 and +800 mV, Figures 4 and 5. The measurements were carried out clockwise starting at the corrosion potential of the mineral. The ratio of cathodic reduction charge of sulphur and the anodic charge of dissolution were integrated from the second cycles (steady state).

The elemental sulphur formed in anodic dissolution reaction is reduced to H₂S during the following cathodic sweep. The reduction peak can be seen in the potential range of -100...-400 mV. The charge of both anodic (q^+) dissolution and cathodic (q^- (H₂S)) reaction is integrated from the corresponding peak areas, Figures 4 and 5. It is shown in Figure 6 that at low anodic maximum potentials the ratio of anodic and cathodic charges starts to increase. When the anodic maximum potential is between 500 and 700 mV, the ratio changes only slightly depending on the temperature. At this potential range elemental sulphur is formed as an anodic dissolution product. At higher anodic potentials sulphur is oxidized to sulphate and the $q^+/q^-(\text{H}_2\text{S})$ ratio is increased. The effect is the most distinguishable at ambient temperature.

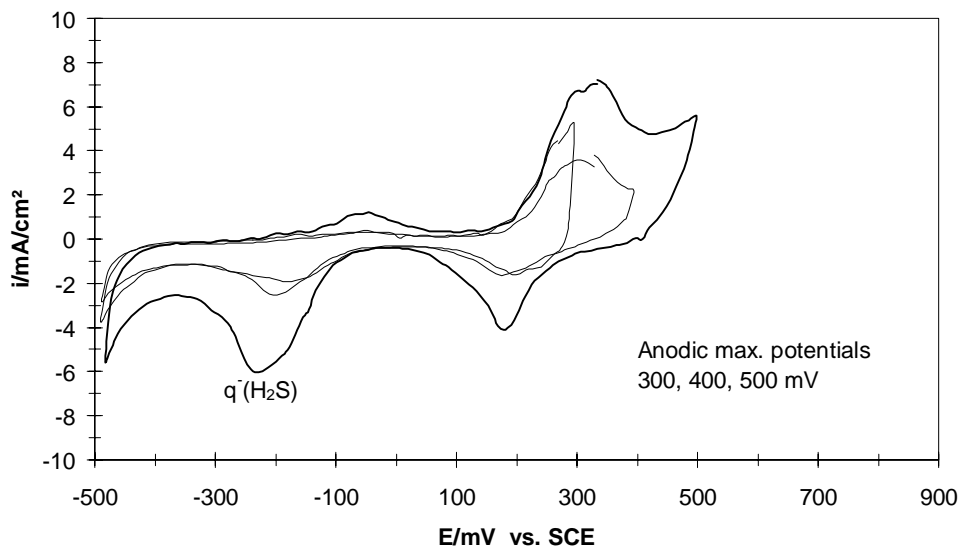


Fig. 4. Cyclic voltammograms of chalcopyrite based sulphide mineral in 1 N H₂SO₄, $T = 25\text{ }^{\circ}\text{C}$, $dE/dt = 20\text{ mV/s}$, second cycles, anodic max. potentials 300, 400 and 500 mV

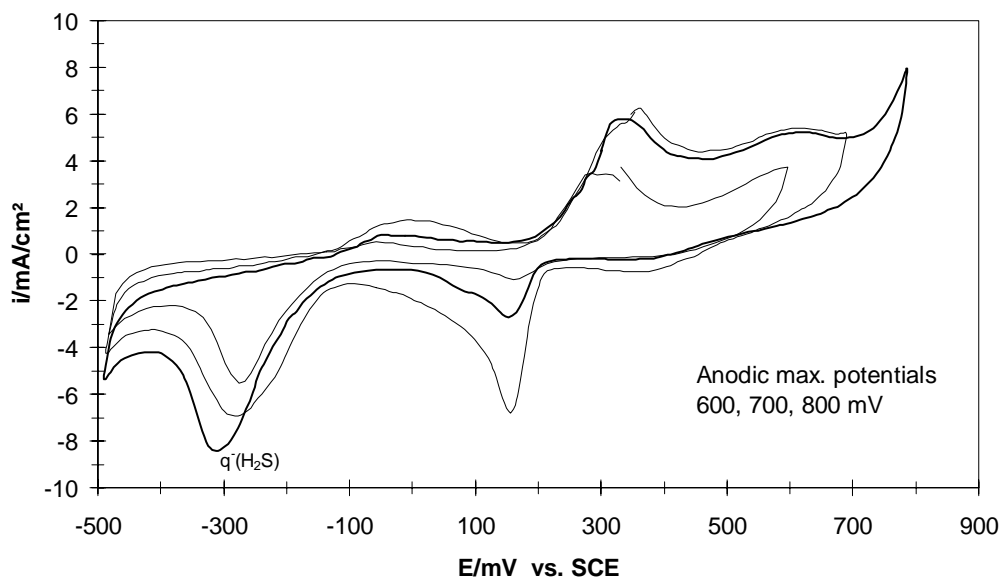


Fig. 5. Cyclic voltammograms of chalcopyrite based sulphide mineral in 1 N H₂SO₄, $T = 25\text{ }^{\circ}\text{C}$, $dE/dt = 20\text{ mV/s}$, second cycles, anodic max. potentials 600, 700 and 800 mV

POTENTIOSTATIC MEASUREMENTS

Electrochemical leaching experiments were carried out at 500 and 600 mV. According to the polarisation measurements anodic leaching reactions can be observed at these potential ranges. The potentiostatic curves at 500 mV are shown in Figure 7. Solution samples were taken at 5, 10, 50 and 100 min for the AAS analysis. Leaching kinetics of the chalcopyrite based concentrate was examined by analysing the copper and iron ion concentration as a function of the leaching time.

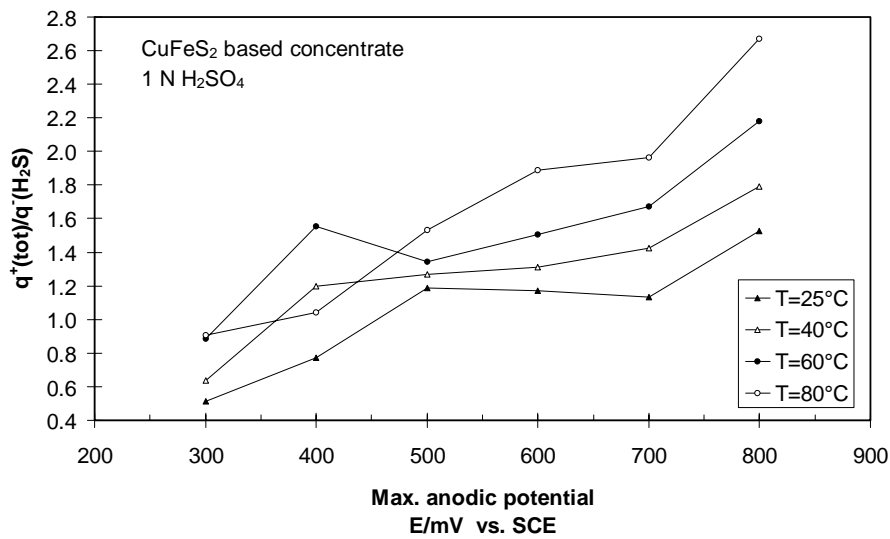


Fig. 6. The ratio of anodic and cathodic charges as a function of anodic maximum potential

Table 3. Relative leaching rates of copper at 500 and 600 mV

Electrolyte temperature [°C]	E = 500 mV	E = 600 mV	E_{600}/E_{500}
25	1	1	1.05
40	1.71	1.39	0.86
60	2.21	1.69	0.81
80	2.69	2.15	0.84

Parabolic and logarithmic leaching kinetics (Cottrell 1985) were compared with each other. Usually the index of correlation R^2 was 0.97-0.99. Both models fit as well with the following two exceptions. The logarithmic fit did not give good index of correlation at low potential and low temperature. The parabolic fit did not give good index of correlation at high potential and high temperature. In Table 3 are shown the proportional leaching rates at 500 and 600 mV. The relative rates are calculated using copper concentration versus time at the first linear range, Figure 8.

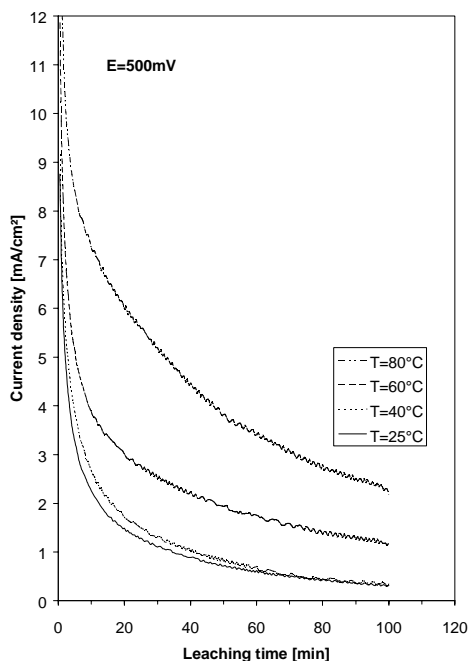


Fig. 7. Potentiostatic curves of the sulphide dissolution, $E = 500 \text{ mV}$, $1 \text{ N H}_2\text{SO}_4$

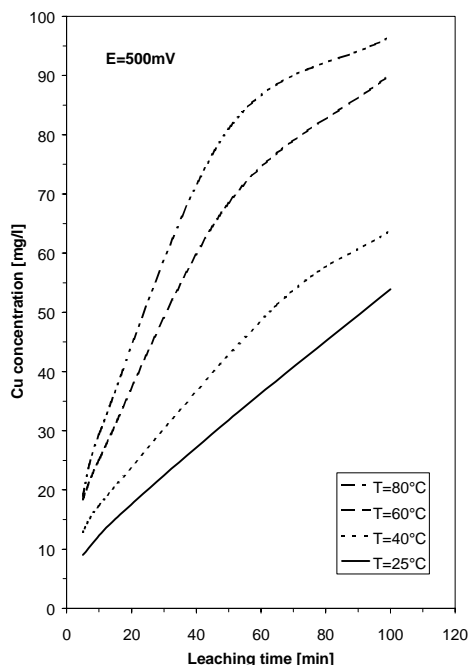


Fig. 8. Cu concentration as a function of the leaching time, $E = 500 \text{ mV}$, $1 \text{ N H}_2\text{SO}_4$

The tendency would be that at low temperatures, i.e. 25 and 40 °C, the parabolic leaching kinetics is dominating. At 60 °C the difference between the two models is negligible and at 80 °C logarithmic leaching model is slightly more accurate than the parabolic one. This means that the leaching mechanism could change. Mass transfer is the rate determining step with the parabolic model and charge transfer with the logarithmic model. Parabolic leaching kinetics has been found appropriate also in chemical leaching (Havlik et al. 1995), (Buttinelli et al. 1992), (Dutrizac et al. 1974).

Dissolved iron concentration was also measured and the dissolving behaviour was similar to that of copper. The ratio of dissolved copper and iron was between 1.09 and 1.37 depending on the temperature and the leaching potential (Table 4).

Table 4. Cu/Fe ratio in the potentiostatic experiments

Electrolyte temperature [°C]	Cu/Fe ($E=500\text{mV}$)	Cu/Fe ($E=600\text{mV}$)
25	1.17	1.23
40	1.09	1.25
60	1.13	1.37
80	1.09	1.27

The Cu/Fe ratio of the concentrate (Table 1) is approx. 0.75 and for chalcopyrite (CuFeS_2) the ratio is approx. 1.17. The electrolyte analysis show that at temperatures and potentials used mainly chalcopyrite was dissolved. Pyrite (FeS_2) is known to be more noble sulphide mineral and does not dissolve at the potentials examined.

CONCLUSIONS

Anodic polarisation curves show that the anodic current increases considerably when the electrolyte temperature is increased from 40 to 60 °C. At the potential range of phase transformation the leaching rate is rather low but the current efficiency is good. At higher potential i.e. when the sulphide decomposes the reaction rate is high but the current efficiency is low. Cyclovoltammetric measurements show that the formation of sulphur occurs between 500 and 700 mV. The rate of leaching increases when either temperature or leaching potential is increased. Both parabolic and logarithmic models of the leaching kinetics are suitable. Parabolic kinetics suits well at moderate temperature and potential. Logarithmic kinetics gets slightly dominant at high temperature and high potential. Based on the solution analysis mainly chalcopyrite was dissolved at the potential range examined by potentiostatic measurements.

REFERENCES

- AHLBERG, E., ÁSBJÖRNSSON, J., 1994, *Carbon Paste Electrodes in Mineral Processing: and Electrochemical Study of Sphalerite*, Hydrometallurgy, 36, 19.
- AROMAA, J., 1988, *Automatization of Electrochemical Experiments Using a Microcomputer*, Lic.Tech. Thesis, Helsinki University of Technology, 115 p. (in Finnish).
- BIEGLER, T., SWIFT, D.A., 1979, *Anodic electrochemistry of chalcopyrite*, J. Applied Electrochem., 9, 545.
- BUTTINELLI, D., LAVECCHIA, R., POCETTI, F., GEVECI, A., GURESIN, N., TOPKAYA, Y., 1992, *Leaching by Ferric Sulphate of Raw and Concentrated Copper-Zinc Complex Sulphide Ores*, Int. J. Miner. Process. 36, 245.
- COTTRELL, A., 1990, *An Introduction to Metallurgy*, Second Edition, Edward Arnold, London 1985, 556 p.
- DOYLE, F.M., *The Aqueous Processing of Minerals and Materials*, The Journal of The Min., Met.&Mat.Soc., 42, 52.
- DUTRIZAC, J.E., MACDONALD, R.J.C., 1974, *The Kinetics of Dissolution of Covellite in Acidified ferric Sulphate Solutions*, Can. Met. Quart., vol 13, 3, 423.
- FORSÉN, O., ANTILA, A.E., AROMAA, J., PESONEN, P., 1996, *Evaluation of Carbon Paste Electroactive Electrode for the Electrochemical Characterization of Sulphide Minerals*. Acta metallurgica Slovaca, 1, 7.
- GERLACH, J., KÜZECI, E., 1983, *Application of Carbon Paste Electrodes to Elucidate Hydrometallurgical Dissolution Processes with Special Regard to Chalcocite and Covellite*, Hydrometallurgy, 11, 345.
- HAVLIK, T., SKROBIAN, M., BALAZ, P., KAMMEL, R., 1995, *Leaching of Chalcopyrite Concentrate with Ferric Chloride*, Int. J. Miner. Process. 43, 61.
- JONES, D.A., PAUL, A.J.P., 1994, *Galvanic Interactions Between Alloys and Minerals in Sulfuric Acid*, Corrosion, 50, 516.

- KNUUTILA, K., 1985, *Electrochemical Dissolution of Sulphide Minerals*, Lic. Tech. Thesis, Helsinki University of Technology, 144 p. (in Finnish).
- KÜZECI, E., KAMMEL, R., 1988, *Anodische Auflösung von Kupferkieselektroden in Schwefelsauren Lösungen*, Metall, 42, 780.
- PARKER, A.J., 1981, *Electrochemistry of the Oxidative Leaching of Copper from Chalcopyrite*, J. Electroanal. Chem., 118, 305.

Aromaa J., Pesonen P., *Mechanizmy i kinetyki ługowania ubogich siarczkowych rud miedzi*, Physicochemical Problems of Mineral Processing, 41 (2007) 313-322 (w jęz. ang.).

Celem pracy były badania kinetyki ługowania koncentratu o przeważającej zawartości chalkopirytu oraz wyznaczenie potencjału tworzenia elementarnej siarki w oparciu o pomiary elektrochemiczne połączone z chemiczną analizą roztworu. Krzywe polaryzacji anodowej, pomiary voltametrii cyklicznej i pomiary potencjostaticzne prowadzono w 0.5 M roztworach kwasu siarkowego w temperaturach w zakresie 25-80 °C. Elektroda badaną była elektroda w postaci pasty grafitowej zawierającej badany siarczek, która gwarantuje powtarzalność i niezawodność pomiarów. Stężenie jonów metali roztwarzanych w eksperymentach potencjostaticznych było analizowane przy pomocy spektroskopii AAS. Ługowanie koncentratu zawierającego chalkopiryt zachodzi dwuetapowo. Dla niskich nadpotencjałów obserwuje się przemiany fazowe siarczku, natomiast dla wyższych wartości obserwuje się jego roztwarzanie. Najwolniejszy etap reakcji określano na podstawie wartości energii aktywacji wyznaczonych z krzywych polaryzacji. Potencjał tworzenia elementarnej siarki był w zakresie 500 – 700 mV (NEK). Powyżej 700 mV siarczek utlenia się do rozpuszczalnych siarczanów. W temperaturze otoczenia proces kontrolowany jest na etapie transportu masy, natomiast w temperaturach 60 i 80 °C najwolniejszym etapem jest wymiana ładunku.

Tomasz CHMIELEWSKI*

NON-OXIDATIVE LEACHING OF BLACK SHALE COPPER ORE FROM LUBIN MINE

Received May 18, 2007; reviewed; accepted June 15, 2007

The beneficial effect of leaching of carbonate gangue of flotation middlings (tailings from 1st cleaning at Lubin Concentrator) with sulfuric acid prior to their final flotation, leaching or bioleaching has been presented. The leaching of flotation feed with sulfuric acid decomposes selectively the carbonate gangue and leads to liberation of sulfide minerals and enhanced flotation or leaching results. It was shown, that after decomposing of 50-70% of carbonates in flotation feed, both flotation recovery and concentrate grade increased considerably versus the results observed for unleached feed. Products of acidic leaching comprise gypsum, soluble magnesium sulfate and gaseous carbon dioxide. Carbon dioxide evolving during the reaction creates the non-oxidizing atmosphere in the pulp during leaching and therefore effectively prevents the digestion of metals from sulfide minerals. The beneficial effect of acidic leaching on flotation was evidently confirmed in pilot tests performed on several feed materials. The application of sulfuric acid leaching of flotation feed produced an enhancement of flotation results (metal recovery and concentrate grade) and provided a rational use of H₂SO₄, which becomes a troublesome and difficult-to-sale product of copper metallurgy. Non-oxidative leaching has to be unquestionably applied prior to the atmospheric, pressure or bio-leaching in acidic conditions.

Key words: copper ores, black shale, non-oxidative leaching

INTRODUCTION

Sedimentary nature of Polish copper deposits (LGOM - Legnica-Glogow Copper Basin, SW Poland) results in the presence of three ore fractions: dolomitic, sandstone, and shale. Most of sulphidic ores require exceptionally fine milling for efficient liberation of sulphide particles prior flotation. This is due to dissemination of fine metal sulfides in carbonate matter and in black shale-clay rocks that form the majority of the gangue. Dissemination of fine copper sulfides in carbonate matrix reduces considerably the susceptibility of the ore to effective liberation of metal-bearing

* Wrocław University of Technology, Faculty of Chemistry, Division of Chemical Metallurgy, Smoluchowskiego 23, 50-370 Wrocław, tomasz.chmielewski@pwr.wroc.pl.

minerals. A relative increase of fraction of shale-clays and carbonates in flotation feeds, which are known as mostly hard-to-treat in flotation circuits, is currently observed in Polish copper industry.

The genesis, lithology, geochemistry, mineralogical composition and observed properties of black shales in flotation circuits of Polish copper industry are unique with regard to carbonate and sand fractions (Konstantynowicz, 1990; Rydzewski, 1996). Black shale ores are mostly non-uniform material and the thickness of their layers in a deposit changes from 0.3 – 0.6 to even 1.7 m (Tomaszewski, 1985). The shale ore is composed of clay-dolomitic matter saturated with organic matter and with finely dispersed sulphide mineral particles. Black shale layers are the thinnest in the deposit but they represent on average 11 % of the ore in Rudna deposit, 17 % of Polkowice-Sieroszowice and 15 % of Lubin with growing tendency (Table 1). According to the latest data (Kubacz and Skorupska, 2007) the content of shale fraction in Lubin copper deposit has already reached 27 % and became the major problem in effective ore processing. The content of shale in Polish copper ores has almost doubled within last four years. Almost 64 % of all valuable metals and 60 % of their potential value are placed in shale fraction. It is interesting to mention that a high percentage of minor metals (above 75%) are concentrated in shale fraction.

Table 1. Distribution of the lithological ore layers and content of copper, silver, and organic carbon in feed of the KGHM copper concentrators in 2004 (Łuszczkiewicz 2004, Chmielewski, et al., 2007)

Content of ore fraction or component	Mine		
	Rudna	Polkowice - Sieroszowice	Lubin
Carbonate ore, %	33	75	25
Shale ore, %	11	17	15
Sand ore, %	56	8	60
Cu content, %	2.23	2.03	1.28
Ag content, g/Mg	53	40	67
TOC, %	1.49	1.66	1.62

The tendency of increase in the content of black shales in Polish copper ores is expected to be continued in forthcoming years. It is also known that with the shale content of 15 % for Lubin deposit, the share of copper and silver in the shale fraction was as high as 45 %. Near 80 % of organic carbon in the ore is concentrated in shale fraction. The content of organic carbon (TOC) in solids in flotation circuits is considered as a measure of shale concentration.

Complex mineralogical structure and chemical composition of Polish copper ores mined from sedimentary deposits are the principal reasons for rather high losses of copper, silver and other metals to flotation tailings. This additionally creates serious technical, economical and ecological issues. The selective liberation of these fine

particles would be the only way to enhance metal recovery. However, it appears to be either inefficient or very costly by physical methods in the existing milling circuits. Consequently, the hydrophilic gangue-sulphide intergrowths greatly reduce both flotation selectivity and the metal grade in the concentrate, particularly at Lubin Concentrator.

Table 2. The comparison of chemical composition of three lithological copper ore fractions: sandstone, shale, and dolomite in Polish copper deposits (KGHM, unpublished data)

Chemical component	Sandstone	Shale	Dolomite
SiO ₂ , %	69.82	30.63	19.03
Al ₂ O ₃ , %	4.22	10.01	6.18
CO ₂ , %	6.50	9.90	29.16
CaO, %	7.34	7.94	21.93
MgO, %	2.19	4.05	11.76
Na ₂ O, %	0.25	0.32	0.29
K ₂ O, %	1.11	2.18	1.34
C _{org} , %	0.40	8.04	0.72
S _S , %	0.82	2.64	0.71
S _S O ₃ , %	2.91	1.81	1.68
FeS ₃ , %	0.19	0.66	0.54
FeO, %	0.62	0.49	0.48
Fe ₂ O ₃ , %	0.53	1.01	0.74
MnO ₂ , %	0.16	0.15	0.29
Cu, %	2.67	10.48	2.10
Zn, %	0.04	0.078	0.03
Pb, %	0.05	0.41	0.14
Ag, g/Mg	29	186	58
Ni, g/Mg	46	278	60
Co, g/Mg	19	189	40
V, g/Mg	59	1204	120
Mo, g/Mg	40	255	30

Due to presently observed and forecasted unfavourable changes in mineralogical composition of the ore, the increase in grade of copper concentrates can be only accomplished by lowering the copper recovery. Therefore, it can be concluded that beneficiation technologies currently applied to Polish copper ores have already reached the limit of their technical efficiency. The only way to considerably reduce

observed losses of copper, silver, and other metals to the flotation tailing is a recognition and application of an entirely novel approach, involving major changes in the flotation circuits (Łuszczkiewicz, et al., 2006; Łuszczkiewicz and Chmielewski, 2006). This approach primarily involves the separation of the most troublesome shale fraction and application of hydrometallurgical and/or biometallurgical processes to its alternative, efficient processing. Such idea is the base of process alternatives suggested by BIOSHALE project partners (Chmielewski and Charewicz, 2006) and was recently seriously considered and discussed at ICNOP Conference (Grotowski, 2007).

Copper shale fraction exhibits substantially elevated concentrations of organic fraction, sulphidic sulphur, copper, silver and other metal values (Ni, Co, V, Mo, Pb, Zn) (Table 2). From the chemical analyses of numerous geological samples of shale ore we have found that the higher content of the organic matter implies the higher metal content in the shale (Chmielewski, et al., 2007). Separation of the organic shale rich fraction and its bio- or hydro-metallurgical processing seems to be the only reasonable way of effective recovering of all valuable metals from shale and reducing the observed metal losses.

Currently applied methods of ore mining and processing do not respect specific properties of the shale fraction, which is mined, comminuted and floated together with dolomitic and sand fractions. The presence of shale fraction in the flotation circuits creates serious technical troubles and leads to hardly acceptable metal losses to flotation tailings (Łuszczkiewicz, 2000). Copper recovery at Lubin Concentrator has been remarkably decreasing for several years reaching some 86-87 % with a concentrate grade less than 17 %. Similar unfavorable effect has also been observed for silver.

Table 3. Value of metals in 1 tone of Lubin middlings (metals prices of 30 April 2007)

Metal	Content	Price, US\$	Value, US\$
Cu	2,7 %	7 820 US\$/t	211.1
Ni	373 g/t	50 100 US\$/t	18.7
Co	569 g/t	30 US\$/lb	37.4
Pb	1,52 %	2 000 US\$/t	30.4
Ag	180 g/t	13 US\$/oz	81.0
Zn	1200 g/t	4 300 US\$/t	4.4

Due to both elevated content of copper (several times higher than in the ore) and presence of significant amounts of valuable metals (Ag, Pb, Ni, Co, Zn, V, Mo...) shale fraction is considered to be the most significant and valuable fraction among

three lithological layers of Polish copper ores. This fraction, as a hardly upgradable, is concentrating during the flotation in the middlings - tailings of 1st cleaning at Lubin Concentrator. The comparison of market values of copper and accompanying metals contained in this shale enriched fraction indicates nearly equal magnitudes (Table 3). The value of copper is about US\$ 211 whereas value of other metals (Ag, Ni, Co, Zn, Pb) is US\$172, considering the metal prices at the end of April 2007. Therefore, shale middlings from Lubin Concentrator is a polymetallic material which requires modern and specific methods of treatment for successful recovering of metals.

Chemical analyses of samples of copper ore collected from various mining areas of KGHM indicate good correlation between the total organic carbon (TOC) content and the content of metals: Cu, Ag, Ni, Co (Figs 1-4) (Chmielewski, et al., 2007).

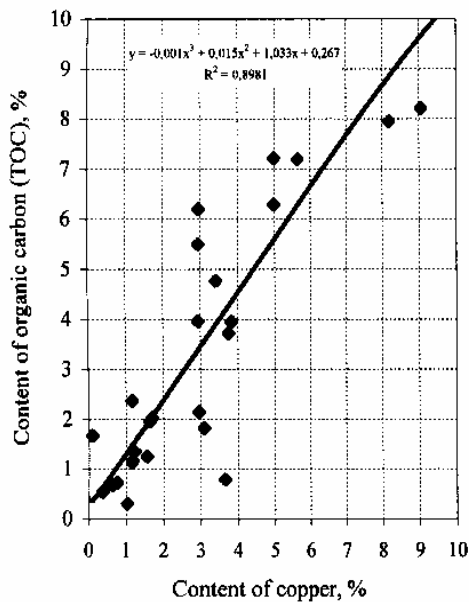


Fig. 1. Organic carbon vs. Cu content in ore samples from KGHM deposit.

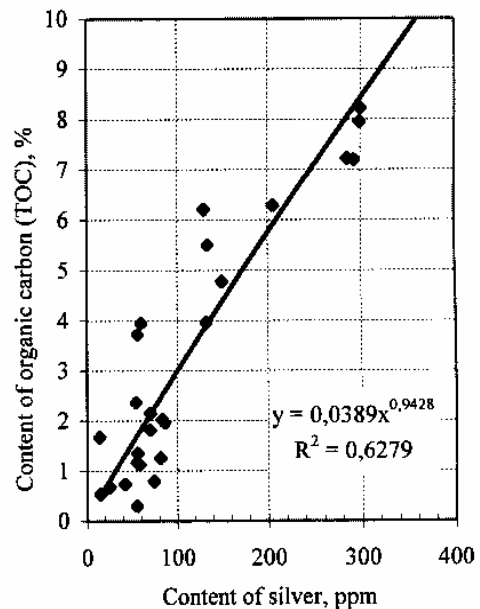


Fig. 2. Organic carbon vs. Ag content in shale ore samples from KGHM deposits

While grinding a low liberation of metal-bearing minerals finely disseminated in shale gangue is observed. Moreover, the flotation of liberated particles became difficult due to slimes of hydrophilic shale components. These two phenomena create significant troubles in effective flotation of shale.

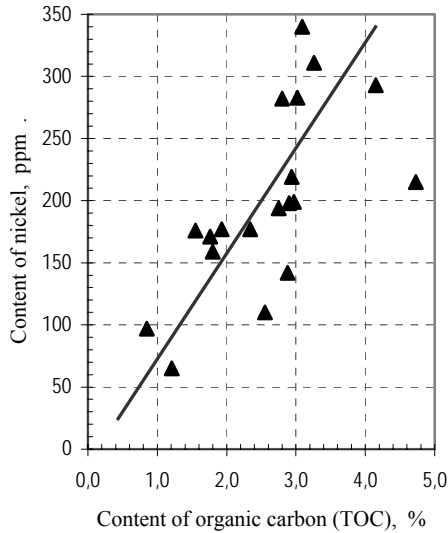


Fig. 3. Ni vs. organic carbon content in shale ore samples from KGHM deposits

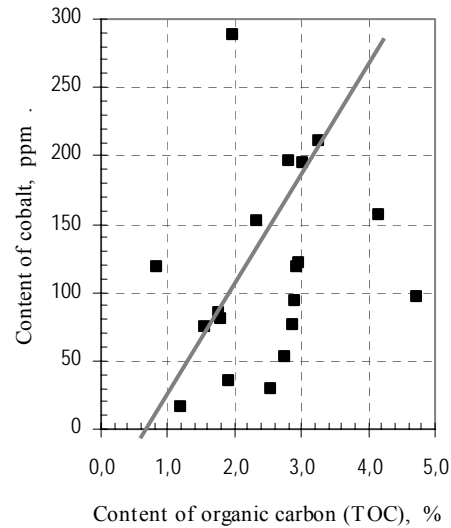


Fig. 4. Co vs. organic carbon content in shale ore samples from KGHM deposits

GENERAL CONCEPT OF SHALE PROCESSING AT LUBIN CONCENTRATOR

The concept of separation and further hydrometallurgical and/or biometallurgical processing of middlings (shale fraction) from existing flotation circuit at Lubin Concentrator (tailings from 1st cleaning) was elaborated during the investigations performed within the BIOSHALE project founded by European Commission (European project contract NMP2-CT-2004 505710). The process was initially suggested and is currently investigated at Wrocław University of Technology (PWR) (Chmielewski, et al., 2007). Its idea was presented in Fig. 5 (Chmielewski and Charewicz, 2005, 2006). The idea accepts an introduction of novel processes with the necessity retaining the existing flotation circuits, which are the only source of final concentrates for metallurgical plants.

The Lubin middlings, exhibiting remarkably elevated concentration of shale fraction, will be initially directly applied or alternatively upgraded by non-polar flotation, leached in non-oxidative conditions with H₂SO₄ for decomposition of carbonates, and finally processed by atmospheric leaching, pressure leaching or bioleaching. The leaching pregnant solutions will be subsequently purified and metals will be separated using standard methods – mainly SX/EW. Alternatively, the pregnant solutions can also be processed in existing technological circuits at KGHM. The Ag, Pb, Au and PGM containing solid leaching residue will be additionally processed by flotation or leaching procedures for recovering of metals (Fig. 6).

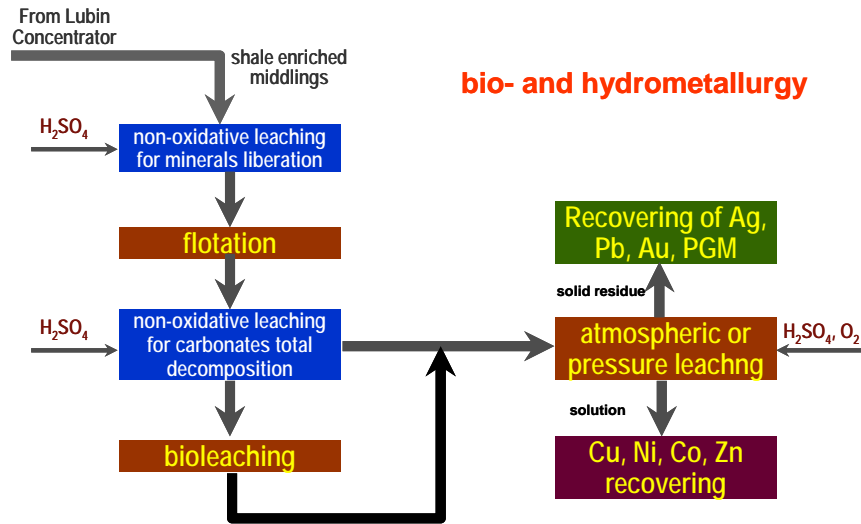


Fig. 6. General concept of bio- & hydrometallurgical processing of shale middlings from Lubin Concentrator and the role of non-oxidative leaching

EXPERIMENTAL AND MATERIAL

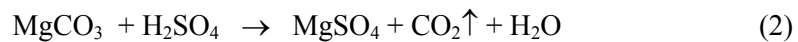
The feed material used in laboratory experiments on non-oxidative leaching was shale containing by-product (middlings) – tailings from 1st cleaning flotation 1st technological circuit at Lubin Concentrator (ZWR Lubin). Chemical composition of the solid was given in Table 4. The content of organic carbon was very high (about 9 %) and confirmed that the middlings can be actually recognized as a shale concentrate. The content of carbonates in the middlings was very high and corresponded to utilization of 497 g H_2SO_4 /kg of dry solid for total decomposition of carbonates. Therefore, the application of any leaching or bioleaching unit operation taking place in acidic conditions requires previous non-oxidative leaching with acid in order to totally decompose of acid consuming components.

Table 4. Chemical composition of Lubin middlings (tailings of 1st cleaning)

CONTENT					
(I) Cu, %	Fe, %	Ni, g/t	Co, g/t	(b) Pb, %	As, %
2,72	1,76	374	572	1.51	0.09
CONTENT					
Ag, g/t	Zn, g/t	S _c , %	SsO ₄ , %	C _{total} , %	C _{org} , %
190	1 200	2.95	1.45	14.30	8.96

PRINCIPLES OF NON-OXIDATIVE LEACHING

Acidic non-oxidative leaching of the shale copper fraction is based on the chemical reactions between sulfuric acid and calcium or magnesium carbonates. These carbonates are the main component of the hydrophilic solid which forms intergrowths and impregnations with copper sulfides or creates hydrophilic ultra-fine slimes on the surface of metal sulfides. Small diameter of the leached solid particles is beneficial for a high rate of heterogenic leaching. The following chemical reactions describe the leaching:



Hydrated calcium sulfate (gypsum) is as a solid reaction product, whereas water-soluble magnesium sulfate and gaseous carbon dioxide are two other products. Due to fine particle distribution of middlings the leaching of carbonate gangue with H_2SO_4 is very rapid and can be performed at ambient temperatures in reactors with mechanical stirring of a simple construction.

The amount of H_2SO_4 applied in the non-oxidative leaching directly corresponds to the content of carbonates and must be precisely controlled to maintain the final pH of the pulp at a level enabling its direct transfer either to the flotation circuit without pH correction or to the leaching and/or bioleaching. Therefore, for the further flotation, the amount of sulfuric acid introduced to the leaching operation should be always kept below the analytically determined maximum amount of acid required for total decomposition of carbonates.

The key parameter determining the amount of H_2SO_4 required for leaching of carbonates is the maximum demand for acid, ($z_{\text{H}_2\text{SO}_4}^{\text{max}}$), which is the mass of pure H_2SO_4 necessary for the total decomposition of carbonates in 1 kg of a dry solid feed. The $z_{\text{H}_2\text{SO}_4}^{\text{max}}$ parameter should be determined analytically from laboratory tests. H_2SO_4 is introduced to the reactor containing shale slurry at a rate that assures its total utilization. Usually, 70-80 % of determined $z_{\text{H}_2\text{SO}_4}^{\text{max}}$ was applied in leaching, maintaining the final pH of the slurry about 5 or higher. This is the pH level enabling direct transfer of the slurry either to the flotation circuit without pH correction or to the leaching and/or bioleaching. If the solid is used for further atmospheric leaching, pressure leaching or bioleaching the amount of sulphuric acid adequately exceeds the maximum demand to maintain pH at the required, acidic level.

Carbon dioxide, evolving in reactions (1) and (2), creates the favorable oxygen-free atmosphere in the leached slurry and prevents the undesirable digestion of sulphides of valuable metals (Cu, Pb, Zn, Ni, Fe). This minimizes the metal losses to the solution and remarkably simplifies the entire process. Therefore, saturation of a slurry with

CO₂ assures the selectivity of carbonate leaching. This was confirmed by the chemical analyses of the wastewater during numerous laboratory tests.

A selective chemical decomposition of non-floatable carbonate-sulfide intergrowths is schematically shown in Figure 7. The diagram indicates that the change of composition of solid takes place while the reaction proceeds. Selectivity of carbonate leaching from flotation feed is according to the proposed method particularly beneficial and secures a high chemical stability of metal sulfide minerals. Noticeably beneficial effects of the preleaching with H₂SO₄ on flotation of copper ores were observed during comprehensive laboratory investigations and several pilot plant tests with various flotation feeds from Lubin and Polkowice concentrators.

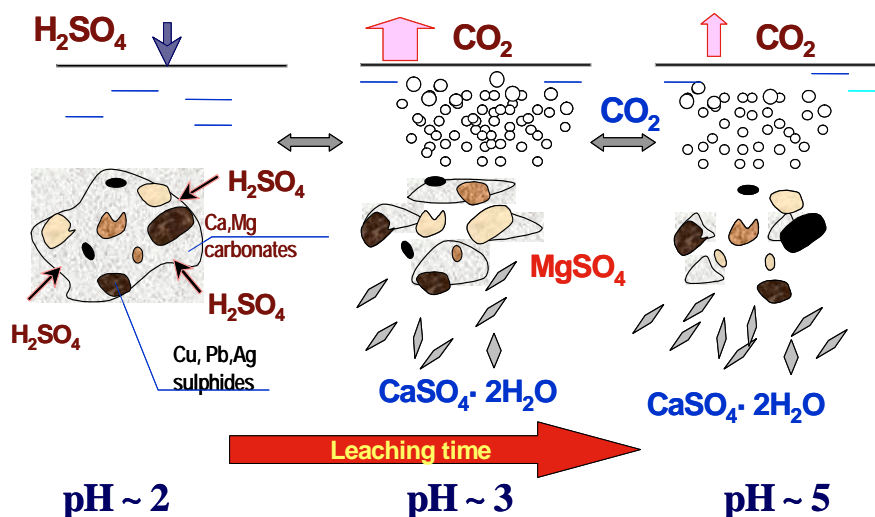


Fig. 7. A selective chemical decomposition of carbonate-sulfide intergrowths during the non-oxidative leaching of a shale feed with sulphuric acid

Another advantage of the non-oxidative leaching is the benefit of the heat effect ($\Delta H_r < 0$). According to the calculations, by means of the HSC Chemistry ver. 2 (Outokumpu), 0.262 kWh/kg CaCO₃ and 0.150 kWh/kg MgCO₃ is created during leaching with H₂SO₄. As a consequence, an increase of pulp temperature to about 30 °C was observed during leaching. This higher pulp temperature increased the reaction rate and favourably improved the rejection of CO₂ after leaching. This heat effect can be particularly beneficial for plants operating under cold climatic conditions.

The acidic non-oxidative leaching of the carbonate-containing flotation feed resulted in the apparent decomposition of solid particles by means of chemical, selective process which precisely and economically liberated sulfide minerals. Under oxygen-free conditions all metal sulfides remain chemically stable and susceptible for

flotation. This selective “chemical grinding” is very efficient particularly for fine intergrowths, which can not be disintegrated with typical mechanical milling. High selectivity and low energy consumption are, therefore, additional beneficial factors of this process. We also believe that an application of leaching on industrial scale would remarkably simplify milling circuits or even eliminate some milling operations, leading to the further reduction of processing costs.

KINETICS OF NON-OXIDATIVE LEACHING

Kinetics of non-oxidative leaching of shale middlings from Lubin Concentrator was investigated at various degree of carbonate decomposition – from 20 to 100 %. The analytically determined content of acid-consuming minerals (carbonates) corresponded to maximum sulphuric acid consumption, $z_{H_2SO_4}^{max} = 497$ g/kg.

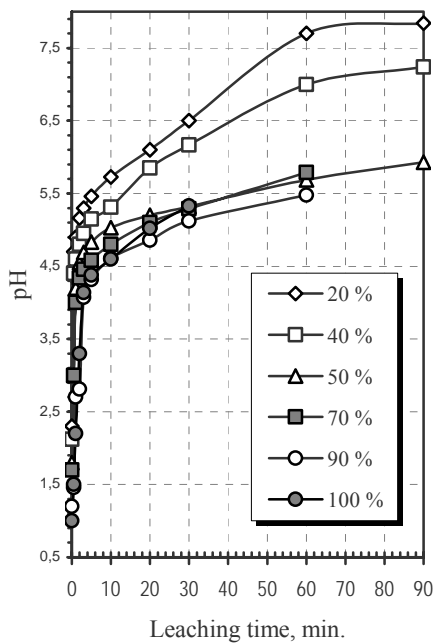


Fig. 8. pH vs. leaching time for non-oxidative leaching of Lubin middlings

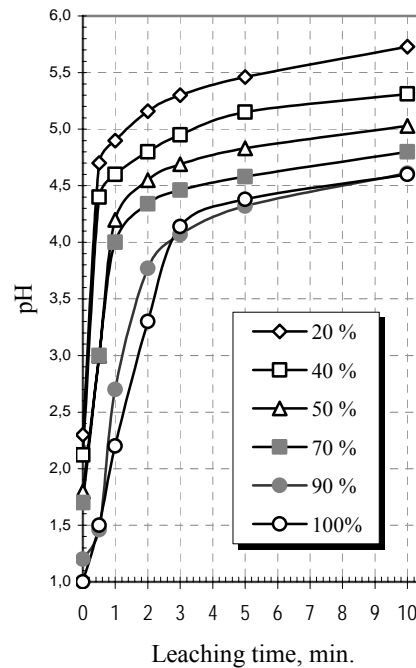


Fig. 9. pH vs. leaching time for initial stage of non-oxidative leaching of Lubin middlings

The process control of non-oxidative leaching is based on pH measurement of leached shale suspension after introduction of desired amount of sulphuric acid. On the basis of kinetic results for Lubin middlings (Figs 8 and 9) it was found that leaching is very rapid and after about 5 minutes almost entire amount of acid is already used up. The observed further pH changes (up to about 40-60 minutes) results from saturation of the slurry with CO_2 .

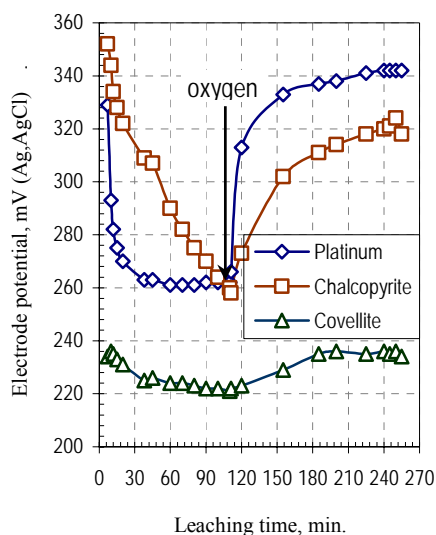


Fig. 10. Potential of platinum, chalcopyrite and covellite electrodes during non-oxidative leaching of Lubin shale by-product and after introduction of oxygen

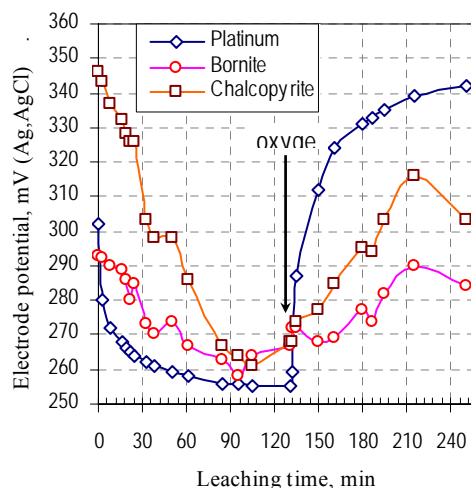


Fig. 11. Potential of platinum, chalcopyrite and bornite electrodes during non-oxidative leaching of Lubin shale by-product and after introduction of oxygen

The presence of carbon dioxide in the middlings leaching system allows for maintaining the low red-ox potential and preventing the digestion of metals. According to Figs 11 and 12 potential of platinum, chalcopyrite, covellite and bornite electrodes decreases to the region, where electrochemical liberation of metal ions to the solution can not be achieved. This was additionally confirmed by chemical analysis of solutions after various R_w - leaching grade of carbonates (Table 5). Introduction of gaseous oxygen under atmospheric pressure leads to remarkable increase in potential of all electrodes and to liberation of metals to the solution.

Table. 5. Concentration of metal ions in the solution from non-oxidative leaching of the Lubin middlings with H_2SO_4

Sample symbol	Carbonates decomposition, R_w , %	Leaching time, min.	Concentration of metal ion in solution, mg/dm^3				
			Cu	Fe	Ni	Co	As
NL-3/1	20	90	0.179	0.005	0.066	0.065	0.007
NL-3/2	40	90	0.216	0.025	0.099	0.097	0.006
NL-3/3	50	90	0.136	0.048	0.275	0.259	0.118
NL-3/4	70	60	0.194	0.020	0.191	0.248	0.023
NL-3/5	90	60	0.171	0.028	0.295	0.358	0.208
NL-3/6	100	60	0.114	0.027	0.271	0.325	0.205
NL-3/7*	100*	-	78.2	92.1	0.737	0.906	1.98

*) Analyzed after 24 hours from the termination of leaching (open to the atmosphere).

CONCLUSIONS

In order to reduce the growing losses of metals observed in the flotation circuits of Lubin Concentrator, the significant alteration has to be introduced into the existing flotation system.

The shale by-product (middlings), the most troublesome material in the flotation, has to be separated from the flotation circuits at Lubin Concentrator and alternatively processed by means of non-oxidative, atmospheric and/or pressure leaching. High content of acid-consuming minerals (calcium and magnesium carbonates) and dissemination of fine metal-bearing sulphides in dolomitic and shale host unquestionably require an application of non-oxidative leaching with sulphuric acid prior to the atmospheric or pressure leaching if acidic conditions are to be preferably applied. Total decomposition of carbonates is recommended to avoid hardly controlled acid consumption during the oxidative leaching.

Non-oxidative leaching of shale rich middlings appeared to be a very rapid (30 – 60 minutes) and selective process, exhibiting the remarkable pH changes as a process controlling parameter. Rapid liberation of carbon dioxide during the reaction of sulphuric acid with carbonate gangue creates beneficially non-oxidative conditions, preventing the leaching of copper, nickel, cobalt and zinc from their sulphides.

Partial and selective liberation of metal sulfides leads to enhanced liberation of metal-bearing minerals, what remarkably improves their floatability, while total decomposition of carbonates makes further atmospheric and pressure leaching more efficient. This has confirmed in additional, detailed investigations.

ACKNOWLEDGEMENTS

This work was carried out in the frame of Bioshale (European project contract NMP2-CT-2004 505710). Author acknowledges the financial support given to this project by the European Commission under the Sixth Framework Programme for Research and Development. I also wish to thank my various partners on the project for their contributions to the work reported in this paper.

REFERENCES

- CHMIELEWSKI T., CHAREWICZ W., 2006, Hydrometallurgical processing of shale by-products from beneficiation circuits of Lubin Concentrator, *In: Perspectives for applying bioleaching Technology to process shale-bearing copper ores*, BIOPROCOOP'06, Lubin 2006, KGHM Cuprum, Wrocław 2006, 125-145 (in Polish).
- CHMIELEWSKI T., ŁUSZCZKIEWICZ A., KONOPACKA Ż., *Separation and concept of processing of black shale copper ore from Lubin mine*, Proc. VIII International Conference on Non-ferrous Ore Processing, Wojcieszycze (Poland), May 21-23, KGHM Cuprum, Wrocław 2007, 171-184 (in Polish).
- CHMIELEWSKI T., CHAREWICZ W.A., 2006, *Technical aspects: Leaching tests. Results with Lubin and Talvivaara Ores*, BIOSHALE, Deliverable D.4.2, 2006.
- GROTOWSKI A., *Possibilities and perspectives for implementation of hydrometallurgical methods in KGHM Polska Miedz S.A.*, Proc. VIII International Conference on Non-ferrous Ore Processing, Wojcieszycze (Poland), May 21-23, KGHM Cuprum, Wrocław 2007, 29-46 (in Polish).
- KONSTANTYNOWICZ-ZIELIŃSKA J. 1990, *Petrography and Genesis of copper-bearing shales from Foresudetic Monocline. Rudy i Metale Nieżelazne*. R.35, Nr 5-6, 128-133.

- KUBACZ N., SKORUPSKA B. 2007, *Evaluation of influence of organic carbon on concentration and smelting processes*. Proc. VIII International Conference on Non-ferrous Ore Processing, Wojcieszycze (Poland), May 21-23, KGHM Cuprum, Wrocław 2007, 157-166.
- ŁUSZCZKIEWICZ A., 2000, *Application of copper-bearing-black shales from Lubin-Glogow region*, in: Proceedings of "Modern problems of copper ore processing in Poland", Conference. Polkowice, 16 November 2000, Komitet Górnictwa PAN / KGHM Polska Miedź S.A., 137-156, (in Polish).
- ŁUSZCZKIEWICZ A. 2004, *Analysis and evaluation of beneficiation of the ore with elevated content of black shales*, Report of investigations, Archiwum Zakładu Przeróbki Kopalini i Odpadów Instytut Górnictwa Politechniki Wrocławskiej, Wrocław, October 2004, (in Polish).
- ŁUSZCZKIEWICZ A., CHMIELEWSKI T., 2006, *Technology of chemical modification of by-products in copper sulphidic ore flotation systems*, Rudy i Metale Nieżelazne, R-51, Nr.1, pp. 2-10 (in Polish).
- ŁUSZCZKIEWICZ A., KONOPACKA Ż., DRZYMAŁA J., 2006, *Flotation of black shales from Lubin copper ores*, In: Perspectives for applying bioleaching Technology to process shale-bearing copper ores, BIOPROCOP'06, Lubin 2006, KGHM Cuprum, Wrocław 2006, 29-47(in Polish)..
- RYDZEWSKI A., 1996, *Lithology of deposit rocks*, in: Monography of KGHM Polska Miedź S.A., A. Piestrzyński (Ed.). CPBM "Cuprum" Sp. z O.O., Lubin, 137-141(in Polish)..
- TOMASZEWSKI J., 1985, *Problems of a rational utilization of copper-polymetallic ores from the Foresudetic Monocline deposits*. Physicochemical Problems of Mineral Processing, Nr 17, 131-141(in Polish).
- CHAREWICZ W., CHMIELEWSKI T., 2005 et al, Deliverable BIOSHALE - D 4.1., *Process variant selection options and test work programme*, Tecnicas Reunidas, March 2005.

Chmielewski T., *Ługowanie nieutleniające czarnego łupka miedzionośnego ze złoża lubińskiego*, Physicochemical Problems of Mineral Processing, 41 (2007) 323-335 (w jęz. ang).

Omówiono korzystny wpływ nieutleniającego ługowania węglanów za pomocą kwasu siarkowego z półproduktu flotacji (odpad I czyszczenie I ciągu technologicznego ZWR Lubin). Ługownie nieutleniające stosowano jako operację poprzedzającą flotację, ługowanie atmosferyczne, ługowanie ciśnieniowe lub bioługowanie. Proces kwaśnego ługowania nadawy do flotacji prowadzi do selektywnego rozkładu węglanów wapnia i magnezu i zapewnia uwolnienie siarczków metali z ich hydrofilnych wzrostów z węglanami. Efektem tego jest wyraźne podwyższenie wskaźników flotacji w porównaniu z nadawą nieługowaną oraz umożliwienie skutecznego, utleniającego ługowania metali w roztworach kwasu siarkowego. Wykazano, że po chemicznym rozkładzie 50 – 70 % węglanów zawartych w nadawie do flotacji następuje wyraźny wzrost uzysku oraz jakości koncentratu w porównaniu z flotacją materiału nieługowanego.

Produktami ługowania nieutleniającego są gips ($\text{CaSO}_4 \cdot 2\text{H}_2\text{O}$), rozpuszczalny w wodzie siarczan magnezu (MgSO_4) oraz gazowy ditlenek węgla (CO_2), który wytwarza korzystnie nieutleniającą atmosferę w ługowanej zawieszynie. Zapewnia to chemiczną stabilność siarczków metali, które nie ulegają roztwarzaniu w warunkach procesu. Korzystny wpływ procesu ługowania nieutleniającego na flotację został wcześniej potwierdzony dla innych flotowanych półproduktów i koncentratów miedzi. Zastosowanie kwasu siarkowego do ługowania nadawy do flotacji prowadzi nie tylko do podwyższenia wskaźników wzbogacania, ale również umożliwia racjonalne wykorzystanie kwasu, który staje się kłopotliwym i trudno zbywalnym odpadem procesu metalurgicznego. Ługowanie nieutleniające jest operacją, która musi być stosowana przed ługowaniem atmosferycznym, ługowaniem ciśnieniowych lub bioługowaniem w warunkach kwaśnych.

Tomasz Chmielewski*

ATMOSPHERIC LEACHING OF SHALE BY-PRODUCT FROM LUBIN CONCENTRATOR

Received June 11, 2007; reviewed; accepted June 26, 2007

The results of non-oxidative leaching with sulphuric acid followed by atmospheric leaching with oxygenated H₂SO₄ have been presented for shale containing middlings (tailings from 1st cleaning flotation) from Lubin Concentrator. It was found that all leaching or bioleaching processes performed in acidic media has to be preceded by non-oxidative decomposition of acid-consuming carbonate components to liberate finely disseminated metal-bearing minerals. Atmospheric leaching appeared to be very efficient process for recovering Cu, Ni and Co from Lubin middlings due to favorable mineralogical composition and fine diameters of leached particles. Maximum recovery of Cu, Ni and Co after 5 hours leaching was observed for experiments at 90 °C in the solutions containing 15 – 30 g/dm³ of Fe(III). Solid residue after atmospheric will be further processed by flotation or chloride leaching to recover Ag, Pb and precious metals.

Key words: shale ore, atmospheric leaching, copper

INTRODUCTION

Polish copper deposits (LGOM - Legnica-Glogow Copper Basin, SW Poland) exhibit unique, sedimentary nature (Rydzewski, 1996, Konstantynowicz, 1990). These results in the presence of three ore fractions: dolomitic, sandstone, and shale. From those three ore fractions shale fraction reveals two exceptional, opposite properties. It contains the highest concentrations of copper and accompanying metals (Ag, Ni, Co, Zn, Pb, V, Mo...) and simultaneously is the most troublesome in the flotation circuits (Tomaszewski, 1995). In the case of shale fraction observed is the dissemination of fine metal sulfides in the carbonate matter and in black shale-clay rocks that form the majority of the gangue. Such a fine dissemination of copper sulfides in carbonate-organic matrix considerably reduces the susceptibility of the ore to both effective liberation and flotation. A relative increase of quantity of shale-clay and carbonate

* Wrocław University of Technology, Faculty of Chemistry, Division of Chemical Metallurgy, Wybrzeże Wyspińskiego 27, 50-307 Wrocław, Poland, tomasz.chmielewski@pwr.wroc.pl.

fractions in flotation feeds, which are known as mostly hard-to-treat in flotation circuits, is currently observed. According to the latest data (Kubacz and Skorupska, 2007) the content of shale fraction in Lubin deposit has already exceeded 25 % and is expected to increase in coming years.

Complex and unique mineralogical structure as well as chemical composition of Polish copper ores mined from sedimentary deposits is the principal reasons for copper, silver and other metals losses to flotation tailings (Łuszczkiewicz 2000, 2004). The presence of shale creates additional technical, economical and ecological issues. The selective liberation of fine metals-bearing particles from the host matrix would be the only way to enhance metals recovery. However, it appears to be ineffective by physical methods in the existing milling circuits. Consequently, the hydrophilic gangue-sulphide intergrowths seriously reduce both flotation selectivity and the metal grade in the concentrate (Łuszczkiewicz, et al., 2006). Therefore, it can be concluded that the existing beneficiation technologies currently applied to Polish copper ores have already reached the limit of their technological efficiency (Chmielewski and Charewicz 2006, Łuszczkiewicz and Chmielewski 2006, Chmielewski, et al., 2007).

The application of modern hydro- or biometallurgy, well known and approved in the world for copper recovering, becomes an urgent necessity in Polish copper industry to reverse unfavorable trends in flotation results, particularly at Lubin Concentrator (Grotowski, 2007). The application of atmospheric leaching has to be considered as a complimentary process for processing of shale flotation by-product which is hardly to beneficiate using existing techniques. This approach, presented by author within the research program of BIOSHALE (Chmielewski and Charewicz, 2005, 2006a) primarily involves the separation of the most troublesome ore fraction (shale containing middlings) and introduction of hydrometallurgical methods for their alternative, effective processing

EXPERIMENTAL AND MATERIAL

In the concept of separation and individual processing of shale-containing by-product from Lubin Concentrator two alternatives were initially considered (Fig. 1). First one was the shale flotation from run-of-mine ore by means of non-polar collectors, second was the flotation or separation of middlings – tailings from 1st cleaning in 1st flotation circuit. The comprehensive investigations of both alternatives resulted in elimination of the first approach and in an approval the Lubin middlings as a shale concentrate suitable for hydrometallurgical treatment.

The feed material applied for laboratory experiments on non-oxidative leaching followed by atmospheric leaching in oxygenated sulphuric acid was shale containing by-product (middlings) – tailings from 1st cleaning flotation 1st technological circuit at Lubin Concentrator (ZWR Lubin). Chemical composition of the solid was given in Table 1. The content of organic carbon was very high (about 9 %) and confirmed that the middlings can be actually recognized as a shale concentrate. The content of carbonates in the middlings corresponded to the utilization of 497 g H₂SO₄/kg of dry

solid for total decomposition of carbonates. Therefore, the application of atmospheric leaching taking place in acidic conditions required previous non-oxidative leaching with acid in order to decompose totally the acid consuming components, mainly calcium and magnesium carbonates (Łuszczkiewicz and Chmielewski, 2006) Chmielewski, et al., 2007). The non-oxidative leaching was performed before each atmospheric leaching experiment.

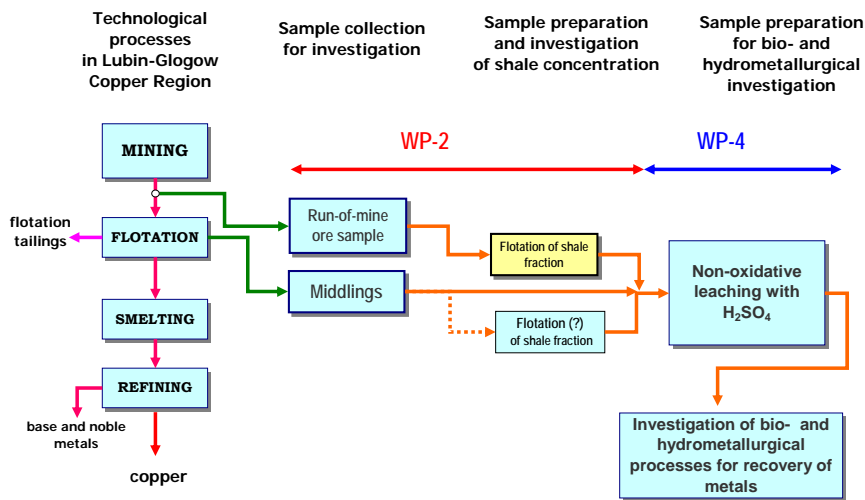


Fig. 1. PWR general concept of separate processing of shale ore from Lubin Concentrator by means of hydro- and bio-metallurgy

Table 1. Chemical composition of Lubin middlings (tailings of 1st cleaning) applied for atmospheric leaching

Content					
Cu, %	Fe, %	Ni, g/t	Co, g/t	Pb, %	As, %
2,72	1,76	374	572	1.51	0.09
Content					
Ag, g/t	Zn, g/t	S _c , %	S _{so4} , %	C _{total} , %	C _{org} , %
190	1 200	2.95	1.45	14.30	8.96

Middlings from Lubin Concentrator (Table 1) exhibit elevated contents of copper, silver and other base metals, which are present in the solid as sulphides. Solubilisation of metals from their sulphidic minerals is only possible when oxidation agent is added to the leaching system. Gaseous oxygen and iron(III) ions were selected for this purpose, taking into account technical, economical and ecological aspects. Laboratory tests were performed at various temperatures (25, 60, 80, 90 °C), sulphuric

acid (20, 50, 120 g/dm³) and iron(III) (0, 7, 15, 30 g/dm³) concentration. Analysed were the concentration – leaching time relationships for Cu, Fe, Ni, Co, and As. Solid residue were examined for metals content and mineralogical SEM observation were conducted to assess the liberation of remaining metals (Ag, Pb, Au, PGM...) for further recovery.

Polish copper ores, in contrast to majority of world copper chalcopyrite - deposits, exhibit very favourable mineralogical composition with regard to hydrometallurgical and biometallurgical processing. Chalcocite (Cu₂S) and bornite (Cu₅FeS₄) are the dominating minerals while chalcopyrite (CuFeS₂) and covellite (CuS) are the minor copper minerals. Detailed mineralogical analysis of Lubin middlings, performed by BRGM in the frame of BIOSHALE project (Auge et al., 2007) unexpectedly revealed, that practically only chalcocite/digenite and bornite are dominating copper minerals in Lubin middlings with traces of chalcopyrite and covellite – most refractory copper minerals. Consequently, we could expect quite high recovery of copper and other base metals from middlings even at mild conditions. The presence of finely dispersed grains of copper sulphide in shale-dolomitic middlings gangue is additional beneficial factor, particularly after their liberation by non-oxidative leaching.

Separation of organic fraction along with shale-containing middlings has an additional beneficial effect leading to the reduction of organic carbon in the feed, what is particularly significant for the flash smelter at Głogów II metallurgical plant. Presently observed elevated content of organic carbon in concentrates already exceeds about 9 % and is the main reason for undesirable, significant decrease in smelter throughput (Kubacz, 2007).

RESULTS AND DISCUSSION

EFFECT OF CONCENTRATION OF H₂SO₄

According to Cu concentration – leaching time plots for atmospheric leaching of Lubin middlings in oxygenated sulphuric acid (Fig. 2) the process of copper solubilisation starts only when oxygen was introduced to the leaching system. It means that there is no oxidized copper in the solid subjected to leaching in sulphuric acid solution. Copper is present in the middlings exclusively in the sulphidic form and requires an oxidant to be solubilised. In contrary, iron digestion was observed to leach even in not oxygenated acidic solution. It was the evidence of presence of iron in the oxidized form. Additional increase in iron concentration following the oxygen introduction, can be explain by the solubilisation of Cu-Fe sulphides, mainly bornite – Cu₅FeS₄, one of the dominating copper sulphides in the Lubin middlings.

Very fine copper mineralization in the Lubin middlings and exceptionally beneficial mineralogical composition of the leaching feed, resulted in superior leachability of middlings even at ambient conditions. About 40 % of Cu was observed to leach out in experiments conducted at 21 °C. The concentration of Cu in the leaching pregnant solution was about 1.6 g/dm³ after 6 hours of leaching at s/l = 1:5.

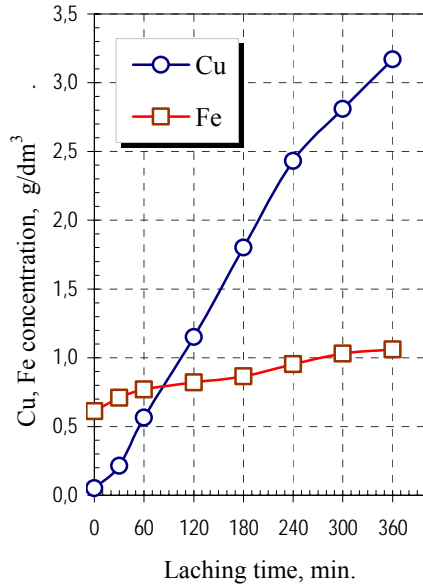


Fig. 2. Cu, Fe concentration – time plots for atmospheric leaching of Lubin middlings in 50 g/l H_2SO_4 solution at 90 °C (s/l = 1:5, oxygen – 30 l/h)

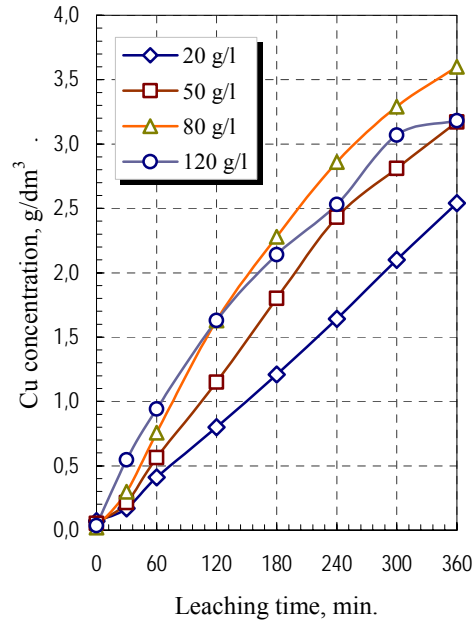


Fig. 3. The effect of concentration of H_2SO_4 on the copper atmospheric leaching from Lubin middlings. (temp. – 70 °C, s/l = 1:5, oxygen – 30 l/h)

The effect of concentration of sulphuric acid was examined on atmospheric leaching of Lubin middlings at various temperatures (25-90 °C) at solid/liquid ratio from 1:5 to 1:4 and at the oxygen flow rate of 30 l/h. The concentration of copper vs. leaching time plots at 70 °C (Fig. 3.) indicates the favorable effect of acid concentration between 20 g/dm³ and 50 g/dm³. Further increase in H_2SO_4 concentration was rather less significant. Similarly, minor effect of concentration of sulphuric acid was observed for Ni, Co and As leaching. Therefore, the H_2SO_4 concentration was kept at the level of 50 g/dm³ for all leaching experiments.

EFFECT OF TEMPERATURE

The effect of temperature was examined on atmospheric leaching of Lubin middlings with solutions containing 50 g/dm³ H_2SO_4 at s/l ratio of 1:4. Leaching tests were conducted at 25, 60, 80, and 90 °C. Results for Cu, As, Co and Ni are given in Figs. 4 – 7.

Temperature appeared to be the essential parameter for atmospheric leaching of middlings. Copper concentration after 5 hours of leaching (s/l = 1:4) increased from about 2,8 g/dm³ to 9,0 g/dm³ when temperature grew from 25 to 90 °C (Fig. 4).

The temperature was also evidently the most advantageous parameter for leaching of arsenic, cobalt and nickel (Figs. 5, 6 and 7).

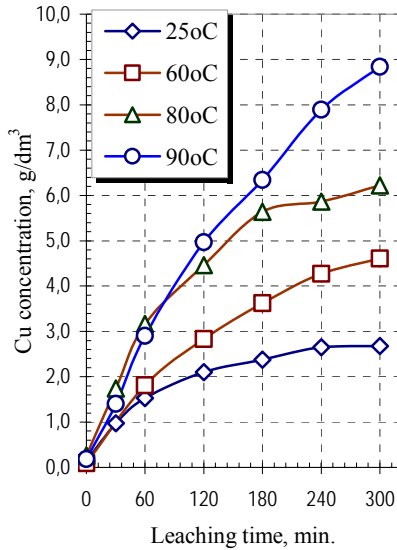


Fig. 4. The effect of temperature on the atmospheric leaching of copper from Lubin middlings. ($s/l = 1:4$, oxygen – $30 \text{ dm}^3/\text{h}$, $\text{H}_2\text{SO}_4 - 50 \text{ g}/\text{dm}^3$)

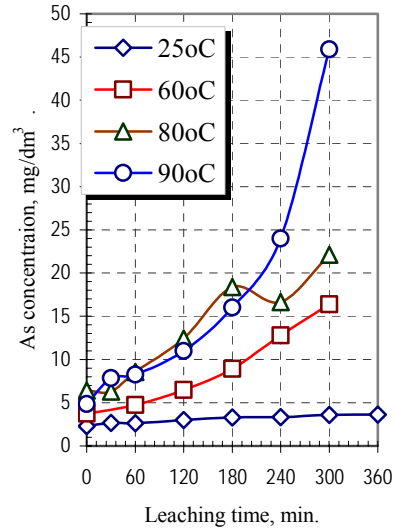


Fig. 5. The effect of temperature on the atmospheric leaching of arsenic from Lubin middlings. ($s/l = 1:4$, oxygen – $30 \text{ dm}^3/\text{h}$, $\text{H}_2\text{SO}_4 - 50 \text{ g}/\text{dm}^3$)

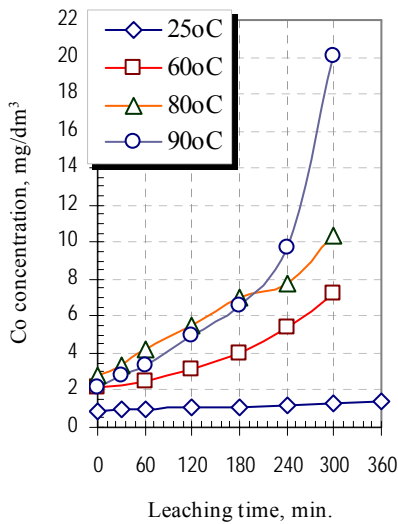


Fig. 6. The effect of temperature on the atmospheric leaching of cobalt from Lubin middlings. ($s/l = 1:4$, oxygen – $30 \text{ dm}^3/\text{h}$, $\text{H}_2\text{SO}_4 - 50 \text{ g}/\text{dm}^3$)

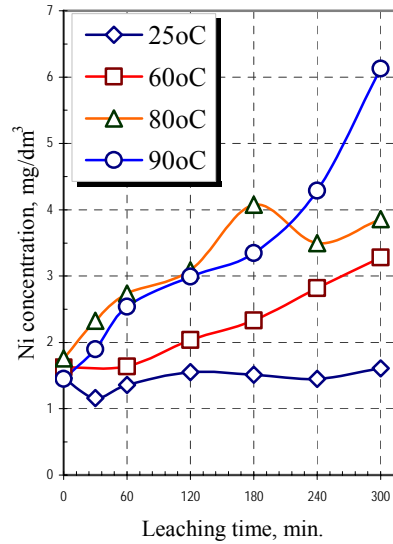


Fig. 7. The effect of temperature on the atmospheric leaching of nickel from Lubin middlings. ($s/l = 1:4$, oxygen – $30 \text{ dm}^3/\text{h}$, $\text{H}_2\text{SO}_4 - 50 \text{ g}/\text{dm}^3$)

EFFECT OF Fe(III) CONCENTRATION

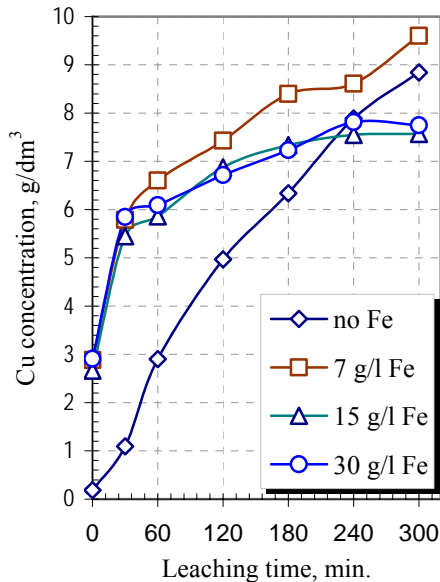


Fig. 8. The effect of Fe(III) on the atmospheric leaching of copper from Lubin middlings. (90 °C, s/l = 1:4, oxygen – 30 dm³/h, H₂SO₄ – 50 g/dm³)

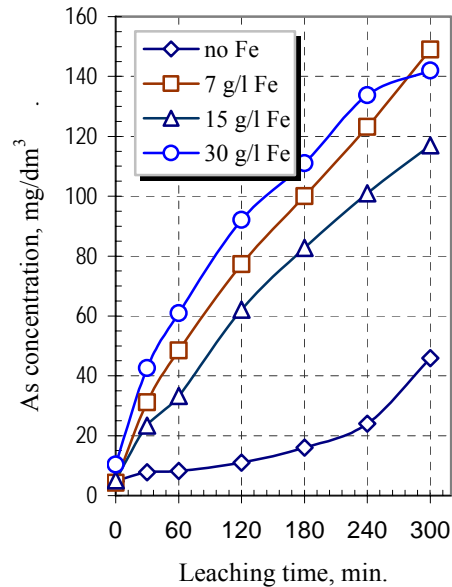


Fig.9. The effect of Fe(III) on the atmospheric leaching of arsenic from Lubin middlings. (90 °C, s/l = 1:4, oxygen – 30 dm³/h, H₂SO₄ – 50 g/dm³)

The addition of Fe(III) to solutions of atmospheric leaching of Lubin middling resulted in significant increase of copper, nickel, cobalt and arsenic leaching rate. The presence of Fe(III) created apparently higher copper leaching rate, particularly in its first period (Fig. 8). More pronounced effect of iron(III) was observed in Ni, Co, and As leaching (Figs. 9, 10, 11). Final concentrations of Co and Ni in solutions from atmospheric leaching with Fe(III) were about 5 times higher than those observed after leaching with oxygenated H₂SO₄ without Fe(III). Concentrations of Ni and Co after 5 hours of atmospheric leaching of Lubin middlings were 27 and 100 mg/dm³, respectively. Unfortunately, the addition of Fe(III) resulted in remarkably high arsenic leaching. The presence of As in leaching liquors has to be considered in forthcoming solutions purification steps.

Comparing the atmospheric leaching results presented in Figs. 9 – 11 on the basis of middlings analysis we may see a high leaching recovery of Cu, Co and As, while the recovery of nickel was the lowest among the considered metals. The leaching results in oxygenated sulphuric acid without Fe(III) for Ni, Co and As were correlated as a function of copper concentration in the leaching solution (Fig. 12). It is well seen that process of leaching exhibits acceleration as copper is being leached out from the middlings. This acceleration is most pronounced for arsenic while the least for nickel.

The presented correlations can be an evidence that Ni, Co and As are partially disseminated in copper sulphides (which dissolve at first) and partially form their own phases.

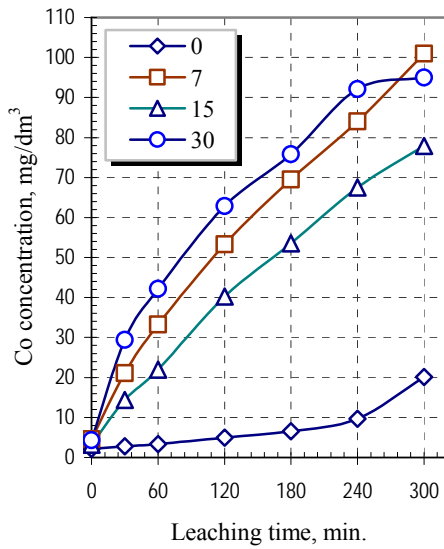


Fig. 10. The effect of Fe(III) on the atmospheric leaching of cobalt from Lubin middlings. (90 °C, s/l = 1:4, oxygen – 30 dm³/h, H₂SO₄ – 50 g/dm³)

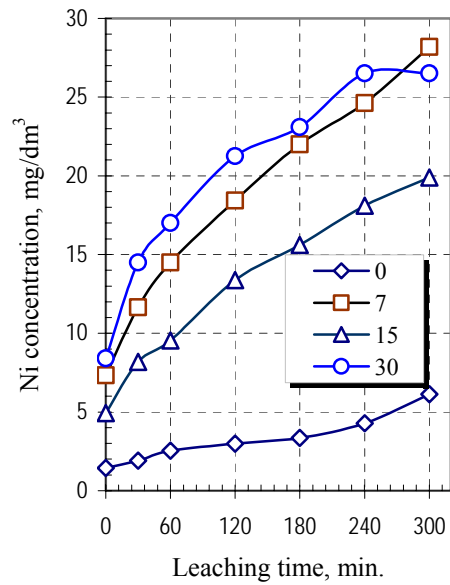


Fig. 11. The effect of Fe(III) on the atmospheric leaching of nickel from Lubin middlings. (90 °C, s/l = 1:4, oxygen – 30 dm³/h, H₂SO₄ – 50 g/dm³)

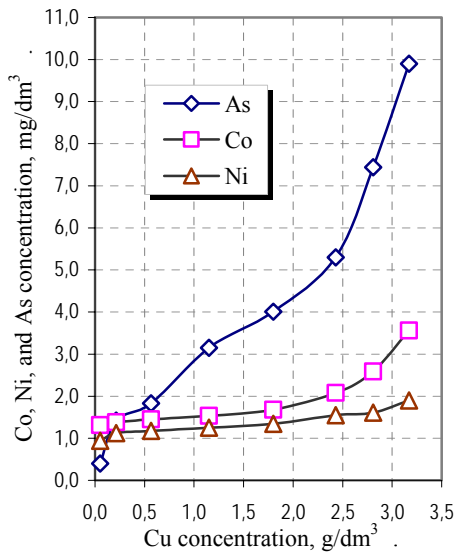


Fig. 12. Correlation between concentration of Cu and other metals during atmospheric leaching of Lubin middlings at 70 °C, H₂SO₄ – 50 g/dm³

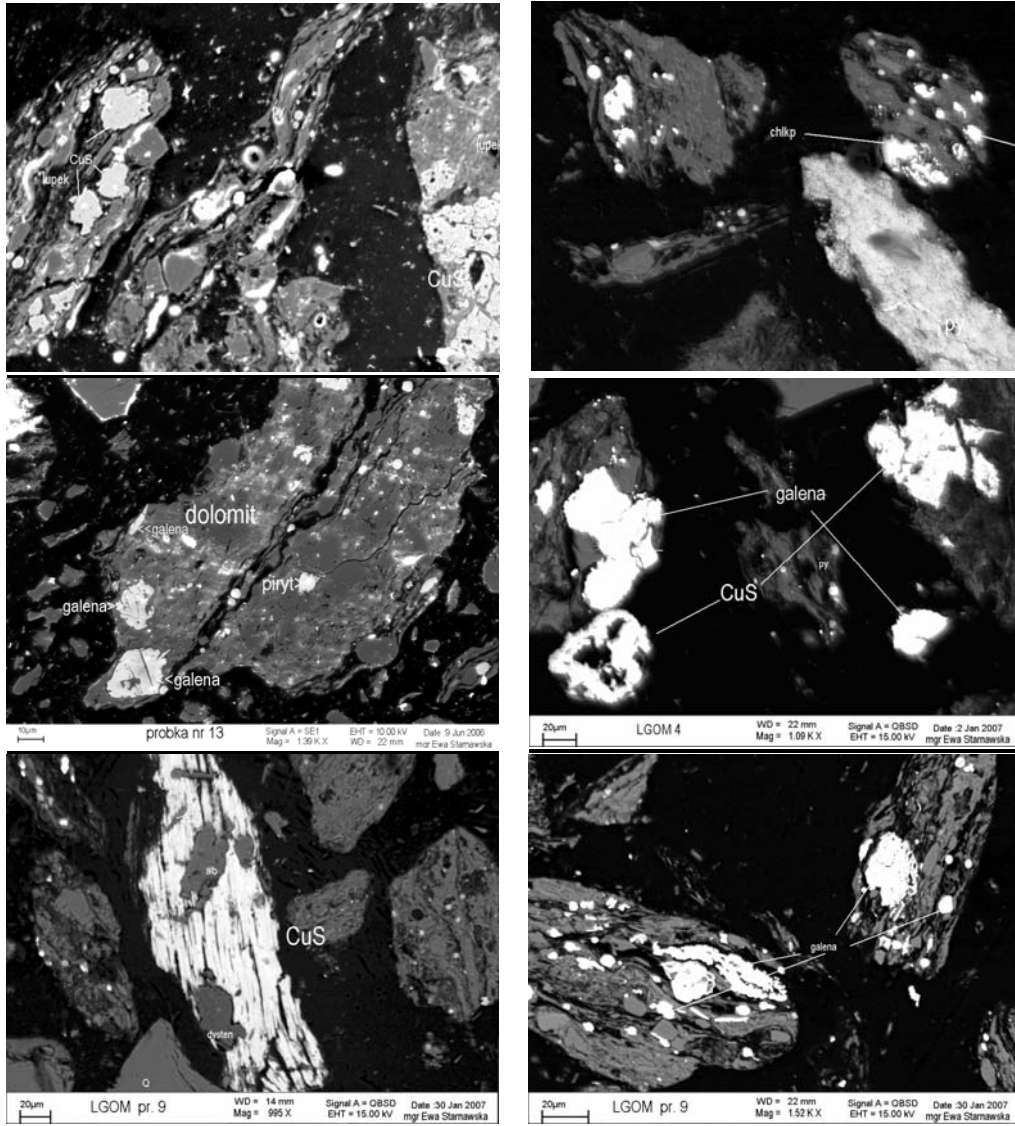


Fig. 13. SEM mineralogical analyses of Lubin middlings before (A, B, C) and after atmospheric leaching(C, D, E)

SEM MINERALOGICAL ANALYSIS OF SOLID RESIDUE AFTER LEACHING

Mineralogical SEM analysis of middlings before and after atmospheric leaching (Fig.13) indicated very fine dissemination of metals-bearing sulphides in carbonate and shale matter (Fig. 13 A, B, C). This is the major reason for observed elevated, growing and hardly accepted loses of metals in flotation tailings, particularly at Lubin

Concentrator. Liberation of metals-bearing sulphide particles from complex carbonate- or shale-based intergrowths presented in Fig.13 A, B, C can not be accomplished by mechanical milling in existing technological circuits. Consequently, only small part of metals from such a material can be recovered to the flotation concentrate. The application of novel approach, using bio- or hydrometallurgy is the only chance to solve the technical issues and to reduce the metals losses.

Solid residue after the atmospheric leaching performed for various experiment parameters (Fig. 13 C, D, E) exhibited the presence of residual amounts of most refractory copper minerals (covellite and chalcopyrite) requiring either more reactive leaching parameters (temperature) or longer leaching time for higher copper recovery. In the solid residue after the atmospheric leaching we could not observe the presence of the sulphide-carbonate intergrowths, which were chemically decomposed during the non-oxidative preleaching. Dominating are the fine disseminated minerals in organic matter, which was only partially decomposed at the atmospheric leaching parameters. The organic shale particles contain both fine particles of copper residual minerals and minerals not leached in sulphate solution (galena, silver minerals).

CONCLUSIONS

Shale-containing by-product from flotation circuits at Lubin Concentrator (which exhibited remarkably elevated content of organic carbon) can be efficiently processed hydrometallurgically, using non-oxidative leaching with sulphuric acid followed by atmospheric leaching in oxygenated H_2SO_4 and in the presence of iron(III). High carbonate content, a specific and unique feature of Polish copper ores, and fine dissemination of metal-bearing minerals (predominantly sulphides) in carbonate and shale matter unquestionably require a chemical pretreatment of the shale solid prior the atmospheric leaching in oxygenated solutions of sulphuric acid.

Non-oxidative leaching of Lubin middlings (Cu – 2,7 %, Pb – 1,52 %, Ni – 374 ppm, Co – 572 ppm, Ag – 170 ppm) and Lubin shale concentrates is quite rapid, selective, and relatively simply-controlled process. Selective liberation of metal sulphides in non-oxidative leaching remarkably improves their flotability while total decomposition of carbonates makes further atmospheric or pressure leaching more efficient.

Atmospheric leaching in oxidized sulphuric acid can be applied to recover Cu, Ni, Co and As from Lubin middlings and from shale concentrates. Leaching results were very satisfactory predominantly due to advantageous mineralogical compositions of Lubin copper minerals, with chalcocite and bornite as principal components. The most advantageous parameters for atmospheric leaching are: concentration of H_2SO_4 – 50 g/dm³, solid/liquid ratio, s/l = 1:4, temperature – 90 °C, concentration of Fe(III) – 30 g/dm³, and percolating oxygen as an oxidizing agent. Atmospheric leaching of Lubin middlings leads to about 9 g/dm³ Cu in leaching solution after about 5 hours of one-stage leaching. Concentrations of Ni, Co, and As are 27 mg/dm³, 100 mg/dm³,

and 140 mg/dm³, respectively. Lead, silver, and precious metals remain unleached in the leaching solid residue and will be recovered by means of flotation or leaching in downstream operations. Large part of organic matter was not subjected to decomposition after the atmospheric leaching and still contained the fine particles of metals-bearing minerals.

ACKNOWLEDGEMENTS

This work was carried out in the frame of Bioshale (European project contract NMP2-CT-2004 505710). The authors acknowledge the financial support given to this project by the European Commission under the Sixth Framework Programme for Research and Development. We also wish to thank our various partners on the project for their contributions to the work reported in this paper.

REFERENCES

- AUGE T., et al., 2007, BIOSHALE, Deliverable D.5.2., *Product behavior during the hydro- and bioprocesses (T12-30)*, March 2007.
- CHAREWICZ W., CHMIELEWSKI T., 2005 et al, Deliverable BIOSHALE - D 4.1., *Process variant selection options and test work programme*, Tecnicas Reunidas, March 2005.
- CHMIELEWSKI T., CHAREWICZ W., 2006, BIOSHALE, Deliverable D.4.2., *Technical aspects: Leaching tests. Results with Lubin and Talvivaara Ores*, April 2006.
- CHMIELEWSKI T., CHAREWICZ W., 2006a, Hydrometallurgical processing of shale by-products from beneficiation circuits of Lubin Concentrator, *In: Perspectives for applying bioleaching Technology to process shale-bearing copper ores*, BIOPROCOP'06, Lubin 2006, KGHM Cuprum, Wrocław 2006, 125-145.
- CHMIELEWSKI T., ŁUSZCZKIEWICZ A., KONOPACKA Ż., *Separation and concept of processing of black shale copper ore from Lubin mine*, Proc. VIII International Conference on Non-ferrous Ore Processing, Wojcieszycze (Poland), May 21-23, KGHM Cuprum Wrocław 2007, 171-184.
- GROTOWSKI A., *Possibilities and perspectives for implementation of hydrometallurgical methods inKGHM Polska Miedz S.A.*, Proc. VIII International Conference on Non-ferrous Ore Processing, Wojcieszycze (Poland), May 21-23, KGHM Cuprum Wrocław 2007, 29-46.
- KONSTANTYNOWICZ-ZIELIŃSKA J. 1990, *Petrography and Genesis of copper-bearing shales from Foresudetic Monocline. Rudy i Metale Niezależne*. R.35, Nr 5-6, 128-133.
- Kubacz N., Skorupska B. 2007, *Evaluation of influence of organic carbon on concentration and smelting processes*. Proc. VIII International Conference on Non-ferrous Ore Processing, Wojcieszycze (Poland), May 21-23, KGHM Cuprum Wrocław 2007, 157-166.
- ŁUSZCZKIEWICZ A. 2004, *Analysis and evaluation of beneficiation of the ore with elevated content of black shales*. Report of investigations, Archiwum Zakładu Przeróbki Kopalini i Odpadów Instytut Górnictwa Politechniki Wrocławskiej, Wrocław, October 2004
- ŁUSZCZKIEWICZ A., 2000, *Application of copper-bearing-black shales from Lubin-Glogow region*, in: Proceedings of "Modern problems of copper ore processing in Poland", Conference. Polkowice, 16 November 2000, Komitet Górnictwa PAN / KGHM Polska Miedz S.A., 137-156
- ŁUSZCZKIEWICZ A., CHMIELEWSKI T., 2006, *Technology of chemical modification of by-products in copper sulphidic ore flotation systems*. Rudy i Metale Niezależne, R-51(2006)2-10.
- ŁUSZCZKIEWICZ A., KONOPACKA Ż., DRZYMAŁA J., 2006, *Flotation of black shales from Lubin copper ores*. In: Perspectives for applying bioleaching Technology to process shale-bearing copper ores, BIOPROCOP'06, Lubin 2006, KGHM Cuprum, Wrocław 2006, 29-47.
- RYDZEWSKI A., 1996, *Lithology of deposit rocks*, in: Monography of KGHM Polska Miedz S.A., A. Piestrzyński (Ed.). CPBM "Cuprum" Sp. z O.O., Lubin, 137-141.
- TOMASZEWSKI J., 1985, *Problems of a rational utilization of copper-polymetallic ores from the Foresudetic Monocline deposits*. Physicochemical Problems of Mineral Processing, Nr 17, 131-141.

Chmielewski T. *Ługowanie atmosferyczne półproduktu łupkowego z obiegów ZWR Lubin*, Physicochemical Problems of Mineral Processing, 41 (2007) 337-348 (w jęz. ang.).

Przedstawiono wyniki badań nad ługowaniem nieutleniającym za pomocą kwasu siarkowego i ługowaniem atmosferycznym w natlenionym roztworze H_2SO_4 i w obecności jonów Fe(III) półproduktu flotacji (odpad I czyszczenia ZWR Lubin). Badany półprodukt stanowił materiał o wysokiej koncentracji frakcji łupkowej i został uznany za koncentrat tej frakcji. Wykazano, że procesy ługowania utleniającego lub bioługowania prowadzone w warunkach kwaśnych muszą być bezwzględnie poprzedzone procesem nieutleniającego rozkładu składników węglanowych w celu uwolnienia bardzo drobno rozproszonych minerałów metalonośnych. Ługowanie atmosferyczne okazało się procesem bardzo efektywnym w odniesieniu do badanego półproduktu łupkowego. Proces zapewnia skuteczne odzyskanie do roztworu Cu, Ni, Co dzięki korzystnemu składowi mineralogicznemu frakcji łupkowej. Maksymalny stopień wylugowania metali, po 5 godzinnym procesie, obserwowano w doświadczeniach prowadzonych w temperaturze 90 °C i obecności jonów Fe(III) o stężeniu w zakresie 15-30 g/dm³. Pozostałość stała po ługowaniu atmosferycznym będzie poddawana procesowi flotacji lub ługowaniu chlorkowemu dla odzyskania srebra, ołowiu i innych metali szlachetnych

Jerzy WÓDKA*, Tomasz CHMIELEWSKI*, Bogumił ZIÓŁKOWSKI*

PRESSURE LEACHING OF SHALE ORE IN OXYGENATED SULPHURIC ACID

Received June 16, 2007; reviewed; accepted July 3, 2007

The effect of initial temperature, sulphuric acid concentration and oxygen partial pressure on pressure leaching of shale fraction of copper ore is presented. Leaching was performed in the autoclave in the temperature range of 100 -180 °C using oxygen as an oxidizing agent. Tailings from 1st cleaning of Lubin Concentrator (ZWR Lubin) were used as a shale material exhibiting elevated contents of metals and organic carbon. Process was performed at sulphuric acid concentration from 20 to 50 g/dm³. The high efficiency of pressure leaching for copper, cobalt, nickel, iron and zinc from polymetallic shale middlings of the Lubin Concentrator was revealed.

Key words: pressure leaching, shale ore, copper

INTRODUCTION

Pressure hydrometallurgy has an extensive application, particularly in processing of zinc, nickel, and copper sulphides and in pretreatment of refractory gold ores, in which gold is finely dispersed in sulphidic lattice. Especially, the pressure hydrometallurgy is widely used in nickel recovering from laterite ores.

Currently, the tests are undertaken to apply hydrometallurgy for process of byproducts and wastes of copper refining (anode slimes) and for recovery of metals from ores and raw materials of the specific properties and composition, making difficulties in their treatment by pyrometallurgy (black shale ores, tailings).

Pressure hydrometallurgy exhibits numerous advantages creating intensive investigation of it at industrial scale. The main advantages of application of pressure leaching processes are:

- high rate of reaction
- elimination of SO₂, other gases and dust emission

* Wrocław University of Technology, Faculty of Chemistry, Division of Chemical Metallurgy,
Wybrzeże Wyspiańskiego 27, 50-307 Wrocław, Poland, jerzy.wodka@pwr.wroc.pl

- high selectivity of pressure leaching
- possibility of arsenic utilization or stabilization (as a low – solubility scorodite)
- total recovery of noble metals
- no restriction of the scale production.

Pressure leaching can be applied in a large scale - to teragram (millions ton) per year of refractory gold ores or to produce several tons of nickel and cobalt from their sulphidic or laterite raw materials.

In the sulphidic copper ores originated from Polish deposits (LGOM - Legnica - Glogow Basin, SW Poland) the content black shale fraction has been increasing systematically, particularly in recent years (Kubacz and Skorupska, 2007). The black shale ores exhibit unique properties. They contain more copper, base metals and noble metals than sandstone or carbonate fraction. The elevated carbonate and organic coal content as well as the metals-bearing minerals dissemination occurring in the black shale ore make significant difficulties in the flotation and causes remarkable metals losses, which has to be limited (Grotowski, 2007).

During the comprehensive investigations on application of bio- and hydrometallurgy for alternative processing of black shale fraction the non-oxidative leaching, atmospheric leaching in oxygenated sulphuric acid, acidic leaching under oxygen pressure and bioleaching have been considered as optional processes for recovering of copper and base metals from shale by-product (middlings) of Lubin Concentrator (Chmielewski and Charewicz, 2006; 2006a). Tailings of 1st cleaning were selected as a shale concentrate for further alternative, hydrometallurgical treatment.

The pressure leaching in H₂SO₄ solution, at elevated temperatures and in the presence of pressurized oxygen. Sulphuric acid is produced at KGHM smelters as a by-product during the processing of copper sulphide concentrate by pyrometallurgy and is the most suitable, cheap and easy-accessible leaching agent.

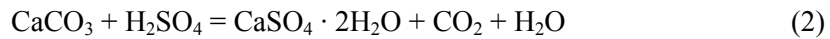
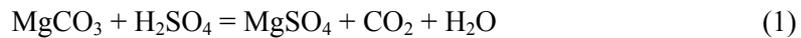
The tailings of the first cleaning flotation (middlings) of the first circuit at Lubin Concentrator (ZWR Lubin) were selected for the laboratory investigations as a shale concentrate. This material can not be effectively upgraded by flotation and creates serious issues in copper ore flotation, predominantly at Lubin Concentrator. It appears, that the separation of the middlings from the flotation circuit and utilisation for leaching purposes is quite easy. Moreover, the middlings have an enormously advantageous composition with regard to pressure hydrometallurgy. Bornite and chalcocite, the most easy leachable copper sulphides, are dominating copper minerals. Moreover, the tailings contains up to 9 % of organic carbon and some 30 % of carbonates that must be decomposed by sulphuric acid prior to pressure leaching.

The effect of initial temperature, sulphuric acid concentration and oxygen partial pressure on pressure leaching of shale fraction of copper ore has been investigated to evaluate the leaching ability of the shale fraction (middlings) separated as tailing of 1st cleaning from Lubin Concentrator. Pressure leaching examinations were performed in the 2 dm³ autoclave in the temperature range from 100 to 180 °C using oxygen as an

oxidizing agent. The pressure leaching was always preceded with non-oxidative acidic pretreatment of the feed in order to totally decompose the acid-consuming components, predominantly carbonates.

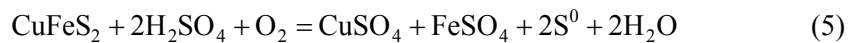
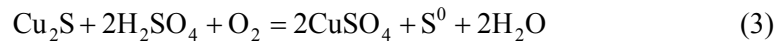
THEORETICAL ASPECTS

The decomposition of carbonates during the non-oxidative treatment preceding pressure leaching follows the reactions:



The carbonate acidic decomposition is a necessary selective process in which the evolving gaseous carbon dioxide leads to hindering of the metals leaching from their sulphide minerals. Magnesium sulphate formed during the carbonates decomposition is easily soluble, whereas calcium sulphate precipitates as a crystalline gypsum $\text{CaSO}_4 \cdot 2\text{H}_2\text{O}$.

The leaching mechanism of the sulphide metals in the sulphuric acid solutions under oxygen pressure depends on temperature range, sulphuric acid concentration and oxygen pressure. At temperatures below 150 °C the major amount of sulphide sulphur is oxidized to elemental sulphur during the leaching according to the following reactions:

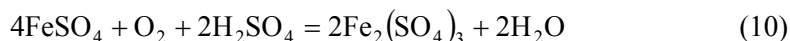


The chalcocite dissolution takes place by forming covellite as intermediate product whereas chalcopyrite may form during bornite dissolution.

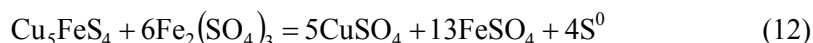
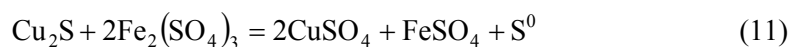
At the temperatures above 150 °C mechanism of leaching changes remarkably and sulphates are forming as products of sulphide oxidation:



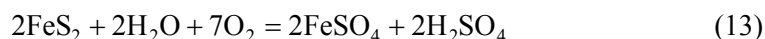
Ferric ions, present in the pressure leach solution, can precipitate as a goethite or jarosite depending on sulphuric acid concentration and temperature. Iron, existing in the ore is initially solubilised as Fe(II) ions and next oxidized by oxygen to Fe(III) ions:



The Fe(III) compounds formed during leaching can also act as a oxidizing agent:



If the ore contain pyrite it will undergo digestion with oxygen, forming sulphuric acid:



Dissolution of nickel, cobalt and zinc sulphides in sulphuric acid solution at elevated temperature under oxygen pressure proceeds in the similar way.

FEED MATERIAL CHARACTERISATION

The feed material applied for laboratory experiments on non-oxidative leaching followed by pressure leaching in sulphuric acid and under oxygen pressure was shale containing by-product (middlings) – tailings from 1st cleaning flotation 1st technological circuit at Lubin Concentrator (ZWR Lubin). Chemical composition of the solid was given in Table 1. The content of organic carbon was very high (about 9 %) and confirmed that the middlings can be actually recognized as a shale concentrate for individual processing.

The content of carbonates in the middlings corresponded to the utilization of 497 g H₂SO₄/kg of dry solid for total decomposition of carbonates. Therefore, the application of pressure leaching in acidic conditions strictly required previous non-oxidative leaching with acid in order to decompose totally the acid consuming components, mainly calcium and magnesium carbonates (Łuszczkiewicz, Chmielewski, 2006) Chmielewski et al., 2007). The non-oxidative leaching was therefore performed before each atmospheric leaching experiment.

Table 1. Chemical composition of Lubin middlings (tailings of 1st cleaning) applied for pressure leaching as a shale concentrate feed

CONTENT					
Cu, %	Fe, %	Ni, g/t	Co, g/t	Pb, %	As, %
2,72	1,76	374	572	1,51	0,09
CONTENT					
Ag, g/t	Zn, g/t	S _c , %	Sso ₄ , %	C _{total} , %	C _{org} , %
190	1 200	2.95	1.45	14.30	8.96

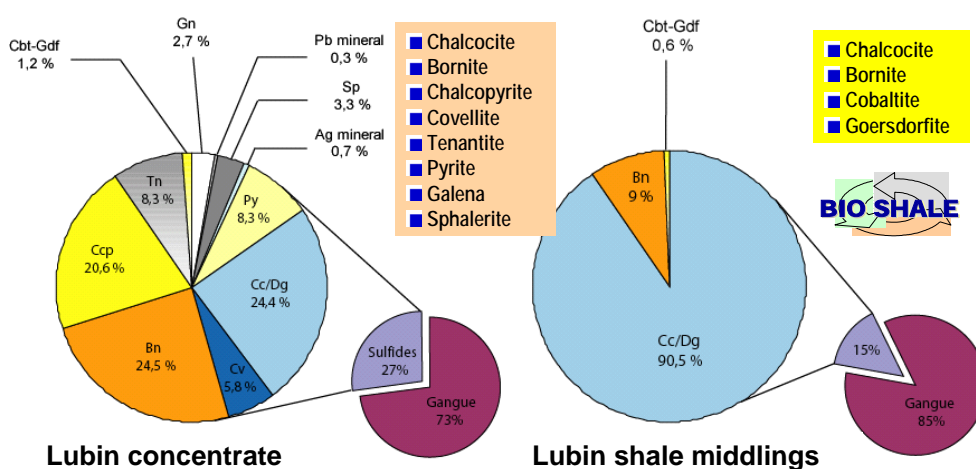


Fig. 1 . Mineralogical composition of Lubin copper sulphide concentrate and shale middlings tailings of 1st cleaning flotation (BRGM data, Auge et al., 2007)

Figure 1 presents mineralogical composition of the Lubin copper sulphide concentrate and the tailings of 1st cleaning (middlings), respectively. The differences in composition are clearly visible.

Lubin flotation copper concentrate, similarly to concentrates from Polkowice and Rudna, contains chalcocite and bornite as dominating copper sulphides. Some 30 % of copper is however in the form of chalcopyrite and covellite – most refractory minerals. Such a mineralogical composition of Lubin concentrate makes this material favorable for hydrometallurgical treatment.

During the flotation of copper ore in Lubin Concentrator observed is a specific segregation of some copper sulphides in the middlings shale fraction. The shale middlings exhibit chalcocite as the predominant (above 90 %) and the most leachable copper sulphide mineral. Bornite (some 9 %) is the second dominating and easy leached copper mineral in middlings. Chalcopyrite and covellite, the most refractory copper sulphides are represented in middlings as minor, trace components. Therefore,

the mineralogical composition of middlings seems to be almost ideal for application as a feed for oxidative leaching, including pressure leaching in oxygenated sulphuric acid.

The sample of Lubin middlings was collected for about 14 days to get the most representative material. It was stored in the form of slurry (58.4 % of solids) in sealed containers to avoid the effect of oxygen.

Fig. 2 presents SEM cross-section of middlings grains. The dissemination of minerals (white areas) and gangue (grey areas) are clearly visible.

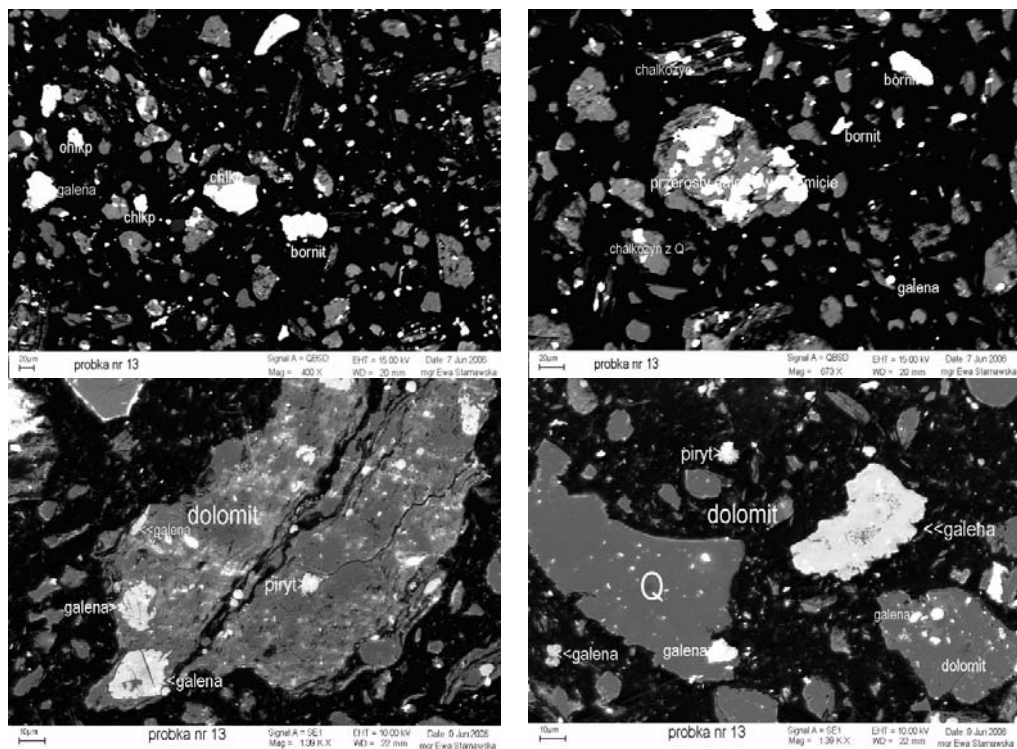


Fig. 2. SEM pictures of untreated samples of Lubin middlings exhibiting fine dissemination of metals-bearing minerals in carbonate and shale matter

The separation of shale fraction in the form of middlings and subsequent treatment by means of hydrometallurgical method was proposed during extensive research in the frame of BIOSHALE project program. Hydrometallurgy (or biometallurgy) are expected to be satisfactory methods for recovering of copper, base metals and silver, which concentration is very high (Tab. 1) Concentration of copper is in ore is 2.72 % and concentration of silver is 190 g/t. Taking into account the market value of metals in Lubin middlings (Table 1), this material has to be recognized as a polymetallic.

EXPERIMENTS

The effect of the temperature, oxygen partial pressure and sulphuric acid concentration on the kinetics and efficiency of pressure leaching of Lubin middlings have been investigated. All experiments were carried out at temperatures between 100 and 180 °C and under oxygen pressure within the range of 0.25 – 1.0 MPa.

The experiments were performed in 2.0 dm³ autoclave having the internal equipment made of teflon. The following experimental procedure was used: A teflon beaker containing 1.0 dm³ of solution of the required concentration of sulphuric acid and the required amount of the middlings was introduced into the autoclave. The liquid to solid phase ratio (s/l) was kept 1:10 in all experiments. The stirring was switched on when the decomposition of carbonates with H₂SO₄ begun prior to the main leaching. After carbonates decomposition (ca. 60 min.) autoclave lid was installed, and the slurry was purged two times with nitrogen. The heating was switched on and as the temperature rose to 100 °C the nitrogen was removed from the autoclave.

After the temperature reached the require level the solution “zero sample” was drawn off for chemical analyses. Subsequently, the mixture of 50 % of oxygen and 50 % of nitrogen was introduced into the autoclave to establish the required oxygen partial pressure. During the experiments samples of the solution were taken periodically to determine metals concentration (Cu, Zn, Ni, Co, As). Metals concentration was analyzed at Quality Investigation Center (CBJ) in Lubin by ASA spectrometry.

Solid samples of middlings before and after each pressure leaching test were examined by mineralogical SEM microscopy to evaluate the composition of the solid and to assess the effectiveness of applied leaching parameters range.

RESULTS AND DISCUSSION

EFFECT OF TEMPERATURE ON PRESSURE LEACHING OF THE SHALE MIDDLLINGS

Pressure leaching of Lubin middlings was examined at elevated temperatures from 100 to 180 °C while concentrations of Cu, Fe, Ni, Co and As were analysed in the samples taken during the leaching. Experimental results are shown in Figs. 3 for Cu, Fe, and Co, respectively. The observed effect of temperature was quite complex and the following observations have been done:

- leaching of copper in oxygenated sulphuric acid at 100 °C required about 120 min. of activation time. This was most likely due to the formation of H₂S observed at the initial stage of the process. Remarkable acceleration of the process was subsequently detected after 120 min. of activation
- unexpectedly, at 120 °C no copper leaching was detected. This might be most likely explained as a hindering effect produced by the presence of elemental sulphur at its melting point

- at temperatures exceeding 140 °C the leaching appeared to be very rapid, although some decrease of Cu concentration was observed at 160 and 180 °C versus 140 °C. Co-precipitation of iron compounds or sorption on organic matter are the only explanation of observed effects
- the rate of leaching of Fe from Lubin middlings increases with temperature up to 120 °C, then iron concentration slightly drops as the result of precipitation of iron(III) oxide (Fe_2O_3) or goethite (FeOOH). The appearance of soluble iron in leaching solution results from leaching of Cu-Fe sulphides, mainly bornite – Cu_5FeS_4 and chalcopyrite – CuFeS_2 .

Pressure leaching of cobalt was practically not observed at temperatures 100 and 120 °C with detected concentration of cobalt about 5 mg/dm³. Remarkable acceleration of leaching of Co was observed at temperatures above 140 °C and detected concentration of cobalt grown-up to 40 – 50 mg/dm³.

Quite complex kinetic curves for nickel (not presented here) indicated that at 120 °C the highest leaching recovery was observed with the final Ni concentration of about 180 mg /dm³. At temperatures exceeding 140 °C the leaching rate of nickel decreases, which are hard to explain at this stage of investigation and require detailed analysis of post-leaching residues from the leaching process, particularly the mineralogical forms of metals.

The concentration vs. leaching time relationships for leaching of arsenic was similar to those of cobalt. Pressure leaching of arsenic was nearly not observed at temperatures 100 and 120 °C when detected concentration of As was about 10 mg/dm³. Significant increase in leaching rate of As was observed at temperatures above 140 °C while concentration of arsenic grown-up to 70 – 90 mg/dm³.

From results of pressure leaching it is well seen, that very effective recovery of metals from Lubin middlings can be observed for experiments performed at temperatures exceeding 140 °C. At 140 °C observed were the highest Cu, Co and As recoveries. It was also detected that at temperatures exceeding 180 °C iron control became possible as a result of precipitation of FeOOH or Fe_2O_3 . Arsenic, a harmful contaminant, will require a removal procedure prior to recovering of copper, nickel and cobalt. Precipitation of crystalline scorodite – $\text{FeAsO}_4 \cdot 2\text{H}_2\text{O}$ at temperatures above 180 °C could be taken into consideration.

The relationship presented in Fig. 3 are characterized by rapid copper, iron and cobalt leaching during the initial 60 minutes. Subsequently, a slower increase in copper, iron and cobalt concentration is observed. The first, very rapid step of leaching, lasting 30 to 60 minutes is, most likely due to initial fast leaching of easy leachable copper minerals - bornite and chalcocite, the once existing in the shale ore originated from Lubin. The second, slow step is probably due to leaching of chalcopyrite and covellite the most refractory copper minerals. The fact that concentration of ferrous ions in the solution before introduction of oxygen is 1.0 g/dm³ suggest that ferric partly occurred as a oxides in the shale ore. Maximum recovery of copper (97 %) and cobalt (80 %) was observed at 140° C and above 90 % for Fe at 160

°C. However, in the investigated range of temperatures nickel did not leach well. Nickel leaching recovery rarely exceeded 10 % in most experiments. Neither lead nor silver was detected in the solution.

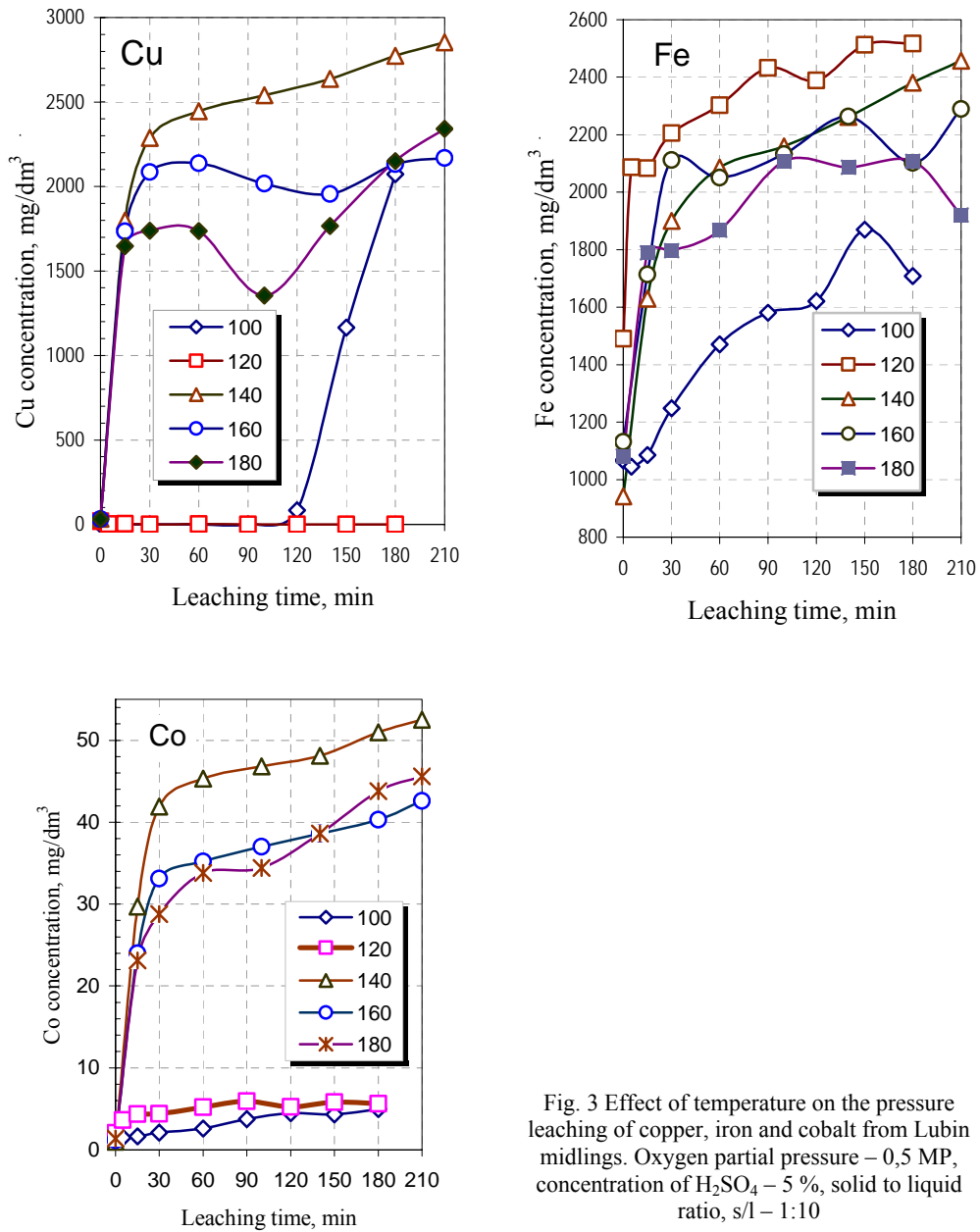


Fig. 3 Effect of temperature on the pressure leaching of copper, iron and cobalt from Lubin midlings. Oxygen partial pressure – 0,5 MP, concentration of H₂SO₄ – 5 %, solid to liquid ratio, s/l – 1:10

EFFECT OF INITIAL SULPHURIC ACID CONCENTRATION ON THE COPPER, FERRIC AND COBALT LEACHING

The effect of sulphuric acid concentration on the metals leaching was investigated in the range of 20 to 50 g/dm³ at temperature of 140 °C and oxygen partial pressure 0.5 MPa. Fig. 4 presents concentration – leaching time relationships for copper and cobalt at different sulphuric acid concentrations. Copper doesn't leach before introduction of oxygen and course of copper leaching resembles those observed during investigations of the effect of temperature.

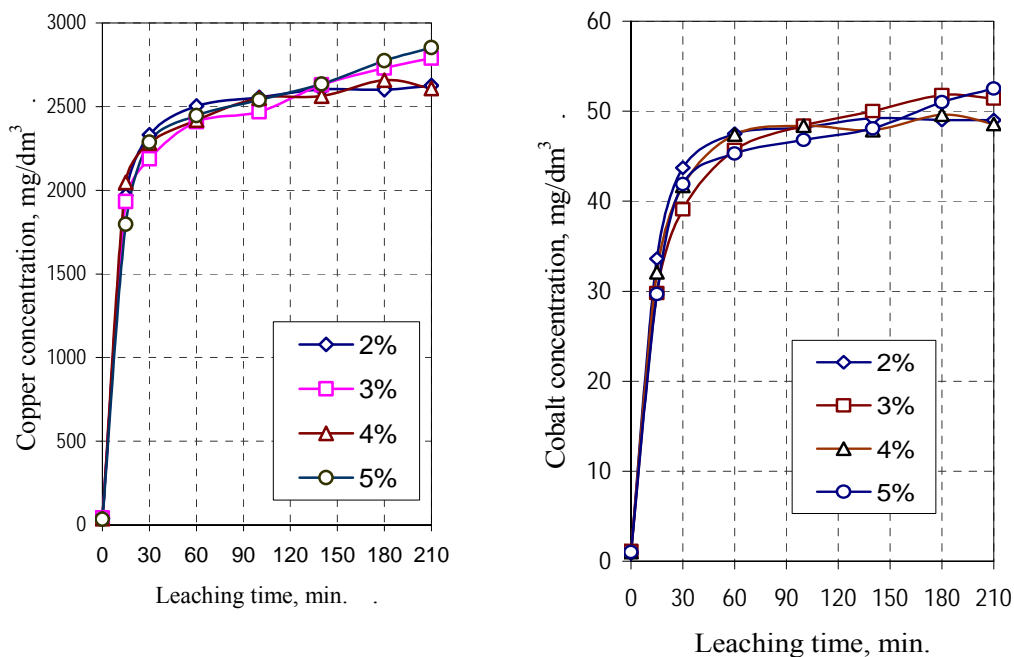


Fig. 4. Effect of sulphuric acid concentration on copper and cobalt pressure leaching (temperature – 140 °C, oxygen partial pressure 5.0 atm (0.5 MPa), liquid - solid phase ratio 10 : 1, rate of mixing 400 rpm.)

Only for concentration of sulphuric acid 30 g/dm³ a highest leaching rate and highest concentration of copper in the solution was observed. There are two steps of pressure leaching. The ferric ion starts to leach sulphidic minerals before the oxygen introduction. There were also observed some differences in ferric concentration depending on sulphuric acid concentration. For 20 g/dm³ of H₂SO₄ the concentration of ferric ions in solutions was 680 mg/dm³ and for 50 g/dm³ of H₂SO₄ the concentration of ferric raised to 940 mg/dm³.

Generally, sulphuric acid concentration was found to have an effect on middlings ferric leaching. For concentration of sulphuric acid below 20 g/dm³ the precipitation of ferric compounds have occurred after 60 minutes of leaching. There were also two

leaching steps for 30, 40, and 50 g/dm³ concentrations of sulphuric acid, similarly to copper leaching. The highest concentration of ferric ions in solution has been reached for sulphuric acid exceeding 30 g/dm³. Kinetic curves observed for Cu and Co leaching at acid concentrations above 30 g/dm³ were almost identical.

There was no cobalt leaching detected before introduction of oxygen. The course of cobalt leaching resembles the copper leaching i.e. there were observed two steps. The first step, in which the rate of cobalt dissolution was found high and the second one with evidently slow cobalt dissolution rate.

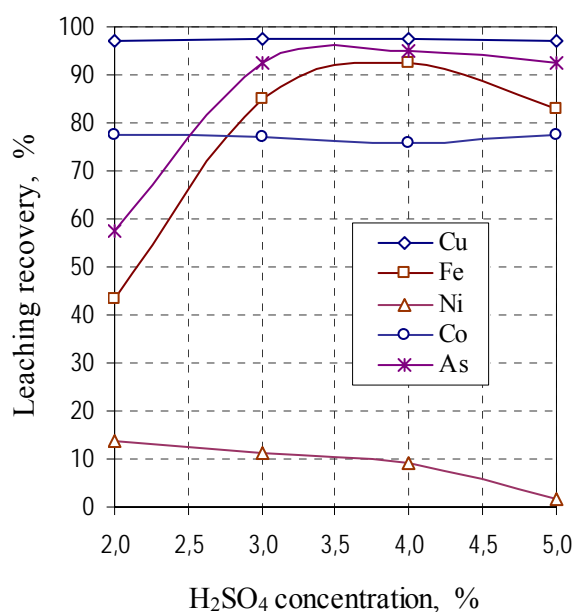


Fig. 5. Effect of sulphuric acid concentration on metals recovery by pressure leaching from Lubin middlings

Generally, a little effect of sulphuric acid concentration on cobalt and copper leaching have been found from H₂SO₄ concentrations above 3 % (Fig.6). A 97 % of leaching recovery of copper and 80 % of leaching recovery of cobalt recovery was reached regardless to sulphuric acid concentration. The highest iron recovery occurred for 30 g/dm³ of H₂SO₄. Presented results suggest that high recovery of copper with simultaneous partial precipitation of ferric compounds is possible. However, it was evident, that at the lowest H₂SO₄ concentration (2 %) the precipitation of Fe(III) from the solution was observed, most likely as FeOOH and Fe₂O₃ and the concentration of Fe in solution decreased to about 1.3 g/dm³. This precipitation of Fe was not detected at higher acid concentration (3-5 %). Iron control in the leaching solution at elevated temperature can be useful as a method of purification from the excesses of Fe prior the recovering of metals. His effect will be further investigated in details.

THE EFFECT OF OXYGEN PARTIAL PRESSURE ON CU, FE AND CO LEACHING

The effect of oxygen partial pressure was investigated in the range from 2,5 to 10 MPa. The leaching temperature (140 °C), sulphuric acid concentration (50 g/dm³) and liquid/solid ratio ratio (10 : 1) were kept constant. Figure 6 presents concentration – leaching time relationships for copper and cobalt. Two steps of leaching courses were found, similarly to the other experiments. Effect of oxygen partial pressure on leaching recovery of Cu, Fe, Ni, Co and As were collected in Fig. 7. Lead and silver were not solubilised during pressure leaching.

On the basis of results presented in Fig. 7 it can be seen that pressure leaching is a very efficient process. Oxygen partial pressure has a noticeable effect on copper, cobalt, arsenic and ferric solubilization. The highest recovery of metals was detected at oxygen partial pressure of 7.5 MPa. Solubilisation of nickel was highly reduced most likely due to the dissemination of Ni in pyritic phase, according to mineralogical examinations (Auge et al., 2007).

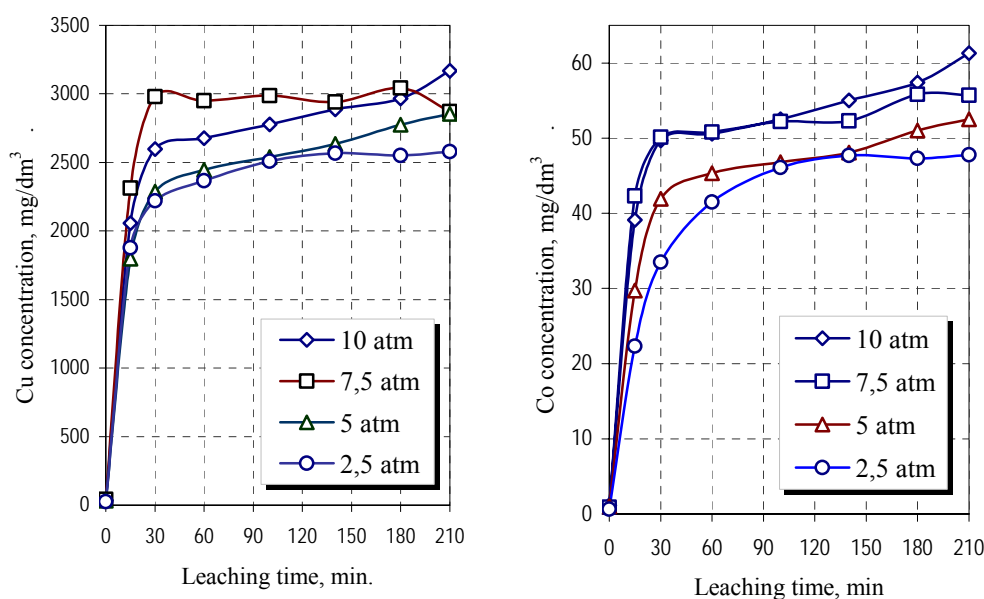


Fig. 6. Effect of oxygen partial pressure on Cu and Co leaching rate for the pressure leaching of Lubin middlings. Temperature 140 °C, Concentration of H₂SO₄ 5 %, Liquid/solid ratio 10:1

Table 2 summarises the pressure leaching experiments for Cu, Co, Ni, As and Zn on the basis of solid residue analysis. According to the presented data, only nickel leaching recovery was observed to be as low as 30-40 %. Copper, cobalt and zink can be easily leached out from the examined Lubin middlings. Pressure leaching can be therefore considered as an efficient alternative for processing of Lubin middlings.

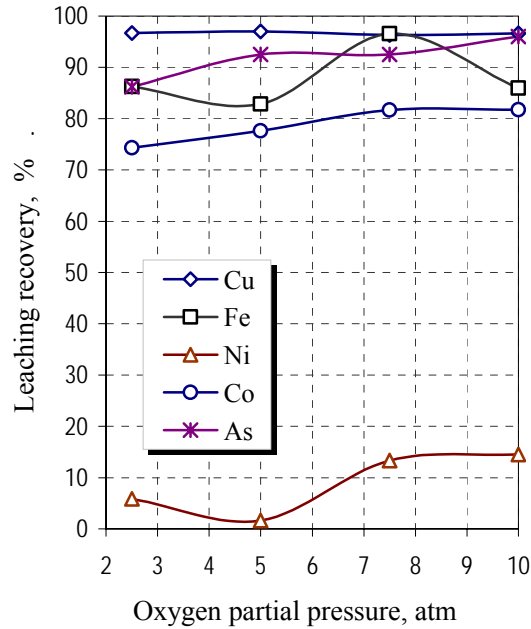


Fig. 7. Effect of oxygen partial pressure on metals recovery from Lubin middlings. Temperature 140 °C, H₂SO₄ 50 g/l, s/l 1:10 (1 atm = 0.101 MPa)

Table 2. Recovery of metals during pressure leaching of Lubin middlings In oxygenated sulphuric acid

Sample	Temperature, °C	Oxygen partial pressure, atm	H ₂ SO ₄ concentration, %	Leaching recovery, %					
				Cu	Co	Fe	Ni	As	Zn
PL/1/10	100	5	5	68.8	8.1	6.6	6.2	8.1	87.5
PL/2/10	120	5	5	38.1	33.6	12.6	27.2	30.7	88.3
PL/7/09	140	5	5	98.8	80.3	70.3	28.2	50.3	97.5
PL/8/09	140	10	5	98.7	81.7	77.3	22.7	41.9	97.4
PL/9/09	140	7.5	5	98.9	82.5	83.6	36.2	50.5	97.4
PL/10/09	140	2.5	5	97.9	77.5	82.6	30.4	48.5	96.8
PL/11/09	140	5	2	98.2	82.9	38.5	39.3	44.0	96.7
PL/12/09	140	5	3	98.4	81.2	70.0	33.2	50.4	97.4
PL/13/09	140	5	4	98.6	79.3	79.5	32.8	51.5	97.2
PL/14/09	160	5	5	83.4	71.7	86.4	25.5	48.4	98.1
PL/15/09	180	5	5	89.8	78.6	69.4	29.1	45.8	98.2
PL/17/09	140	5	5	98.8	81.2	61.2	31.3	47.1	97.2
PL/18/09	140	5	5	98.3	80.2	78.5	26.8	52.8	96.6

CHARACTERIZATION OF PRESSURE LEACHING RESIDUE BY SEM MINERALOGICAL EXAMINATIONS

Solid residue after pressure leaching was examined by SEM (Fig. 8). It can be seen that unleached metal-bearing minerals (mostly covellite, chalcopyrite, pyrite and galena) are disseminated in shale organic matter (Figs. 8 B,C and D), which was practically not decomposed neither during non-oxidative nor pressure leaching. To liberate these particles for further metals recovering require is either further intensification of pressure leaching or additional milling to reduce particle size of unleached solid grains.

Some unleached minerals (CuS , CuFeS_2) remain in the solid as quite coarse, spongy structure requiring either longer leaching time or more intensive leaching parameters (Fig. 9 A).

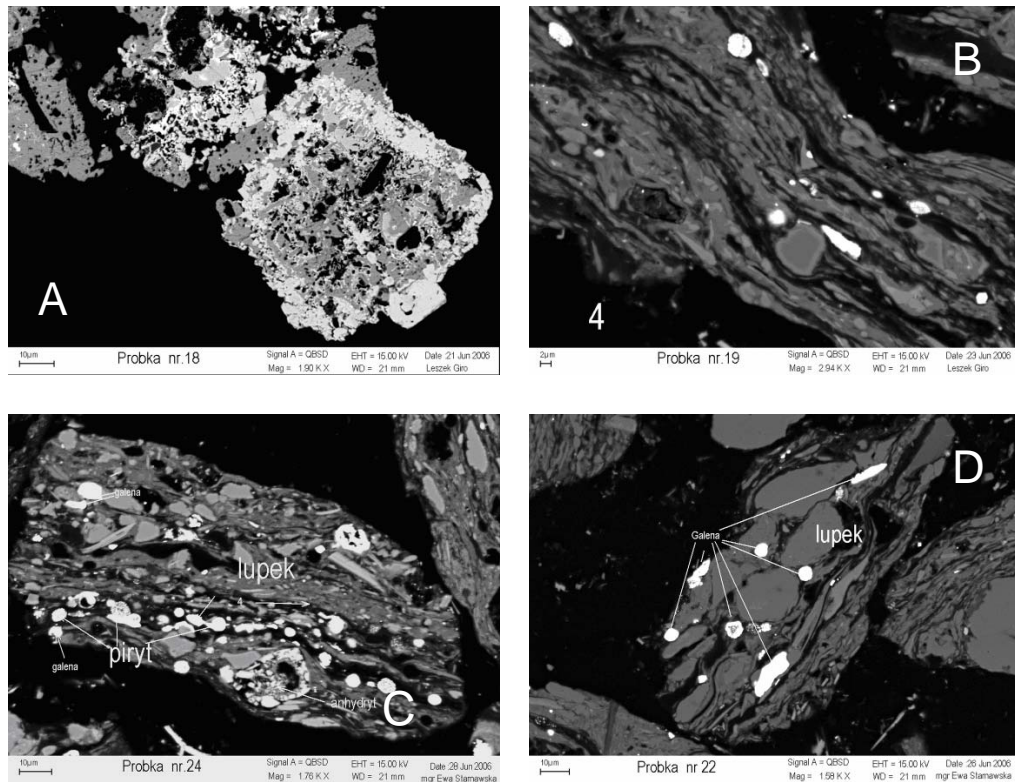


Fig. 8. SEM pictures of pressure leached samples of Lubin middlings exhibiting fine dissemination of metals-bearing minerals in shale matter

CONCLUSIONS

Shale-containing by-products (middlings) - tailings of 1st cleaning from flotation circuits at Lubin Concentrator, which exhibited remarkably elevated content of organic carbon, can be efficiently processed hydrometallurgically by non-oxidative leaching followed by pressure leaching. High carbonate content, a specific and unique feature of Polish copper ores, and fine dissemination of metal-bearing minerals (predominantly sulphides) unquestionably require a chemical pretreatment of the shale feed with H₂SO₄ prior the atmospheric and pressure leaching in oxygenated solutions of sulphuric acid.

Non-oxidative leaching of Lubin middlings (Cu – 2,7 %, Pb – 1,52 %, Ni – 374 ppm, Co – 572 ppm, Ag – 170 ppm) is a very rapid, selective, and relatively simply-controlled process. Selective liberation of metal sulphides improves their flotability while total decomposition of carbonates makes further pressure leaching more efficient.

Pressure leaching of Lubin middlings revealed, that the process is remarkably fast and efficient for recovering of Cu, Fe, Co and As with much lower recovery of Ni. To accomplish maximum recovery of metal, pressure leaching has to be conducted at temperatures above 140 °C and under oxygen pressure exceeding 5 atm. From pressure leaching experiments performed at temperatures 120 – 180 °C, under oxygen pressure 2.5 – 10 at H₂SO₄ concentrations 2 – 5 %, and at solid/liquid ratio 1:10 it results that about 96 – 97 % of Cu, 96 % of Fe 96 % of As, and 82 % of Co can be recovered after about 2 hours of leaching. Much lower leachability of nickel (30-40 %) can be explain in terms of its dissemination in pyrite. It was also observed that at temperatures exceeding 160 °C precipitation of Fe as goethite or hematite commences, which can be applied as an iron control process for solution purification.

Pressure leaching with oxidized H₂SO₄ solutions was not efficient to leach of Ag, Pb, and precious metals. The solid residue after leaching must be either upgraded by flotation or subjected to leaching in chloride solutions to recover remaining metals.

REFERENCES

- AUGE T., et al., 2007, BIOSHALE, Deliverable D.5.2., *Product behavior during the hydro- and boprocess (T12-30)*, March 2007.
- CHMIELEWSKI T., CHAREWICZ W., 2006, BIOSHALE, Deliverable D.4.2., *Technical aspects: Leaching tests. Results with Lubin and Talvivaara Ores*, April 2006.
- CHMIELEWSKI T., CHAREWICZ W., 2006, Hydrometallurgical processing of shale by-products from beneficiation circuits of Lubun Concentrator, *In: Perspectives for applying leaching Technology to process shale-bearing copper ores*, BIOPROCOP'06, Lubin 2006, KGHM Cuprum, Wrocław 2006, 125-145 (in Polish).
- CHMIELEWSKI T., CHAREWICZ W., 2006a, Hydrometallurgical processing of shale by-products from beneficiation circuits of Lubun Concentrator, *In: Perspectives for applying leaching Technology to process shale-bearing copper ores*, BIOPROCOP'06, Lubin 2006, KGHM Cuprum, Wrocław 2006, 125-145.

- CHMIELEWSKI T., ŁUSZCZKIEWICZ A., Konopacka Ż., *Separation and concept of processing of black shale copper ore from Lubin mine*, Proc. VIII International Conference on Non-ferrous Ore Processing, Wojcieszycze (Poland), May 21-23, KGHM Cuprum, Wrocław 2007, 171-184 (in Polish).
- GROTOWSKI A., *Possibilities and perspectives for implementation of hydrometallurgical methods in KGHM Polska Miedz S.A.*, Proc. VIII International Conference on Non-ferrous Ore Processing, Wojcieszycze (Poland), May 21-23, KGHM Cuprum Wrocław 2007, 29-46.
- KUBACZ N., SKORUPSKA B. 2007, *Evaluation of influence of organic carbon on concentration and smelting processes*. Proc. VIII International Conference on Non-ferrous Ore Processing, Wojcieszycze (Poland), May 21-23, KGHM Cuprum Wrocław 2007, 157-166.

Wódka J., Chmielewski T., Ziółkowski B., *Ługowanie ciśnieniowe rudy łupkowej w natlenionych roztworach kwasu siarkowego*, Physicochemical Problems of Mineral Processing, 41 (2007) 349-364 (w jęz. ang.).

Przedstawiono badania wpływu temperatury, stężenia kwasu siarkowego i ciśnienia parcjalnego tlenu na ciśnieniowe ługowanie frakcji łupkowej rudy miedzi. Ługowanie prowadzono w autoklawie, pod ciśnieniem tlenu i w temperaturach od 100 do 180 °C. Nadawę do ługowania ciśnieniowego stanowił odpad I czyszczenia i ciągu technologicznego ZWR Lubin, który jest materiałem łupkowym o podwyższonej koncentracji metali i węgla organicznego. Proces ługowania prowadzono w roztworach kwasu siarkowego o stężeniu od 20 do 50 g/dm³. W badaniach wykazano wysoką skuteczność procesu dla ługowania miedzi, kobaltu, niklu, żelaza i cynku z półproduktu łupkowego ZWR Lubin.

Katarzyna ROTUSKA*, Tomasz CHMIELEWSKI*

SOLVENT EXTRACTION OF VALUABLE METALS FROM PREGNANT LEACH SOLUTIONS OF CUPRIFEROUS SHALE

Received June 4, 2007; reviewed; accepted June 25, 2007

The pregnant solution after atmospheric leaching of cupriferous shale (middlings from Lubin Concentrator) with sulphuric acid and/or with sulphuric acid containing Fe(III) in the presence of oxygen were applied for solvent extraction experiments with several extractants. The solutions containing soluble sulphates of Cu(II), Zn(II), Ni(II), Co(II), Fe(II), Fe(III) and As as a contaminant. Aromatic hydroxyoximes, LIX 84, LIX 612 and LIX 984, were investigated as copper(II) extractants to evaluate their extraction and reextraction abilities. From the copper free raffinate Zn(II) was next extracted with di-(2-ethylhexyl)phosphoric acid (D2EHPA). Additionally, cobalt(II) and nickel(II) were separated from the zinc-free raffinate with di-(2,2,4-trimethylpentyl)phosphinic acid (Cyanex 272). Industrial aromatic hydroxyoximes used for copper(II) extraction were not sufficient selective and other metal ion species present in leach solutions were also transferred to the organic phase. The extractive recovery of Cu(II), Co(II) and Ni(II) was better for the solutions obtained from acidic leaching of shale in the absence of Fe(III) salts. The recovery of valuable metals was not satisfactory and further experiments are necessary to establish the optimal conditions of extraction and reextraction processes.

Key words: shale ore, atmospheric leaching, solvent extraction

INTRODUCTION

Polish copper deposits (LGOM - Legnica-Glogow Copper Basin, SW Poland) exhibit unique, sedimentary nature with three ore fractions: dolomitic, sandstone, and shale. Shale fraction indicates the highest concentrations of copper and accompanying metals (Ag, Ni, Co, Zn, Pb, V, Mo...) and simultaneously is the most troublesome in the flotation circuits, creating serious technical and ecological issues (Łuszczkiewicz, 2000, 2004).

* Wrocław University of Technology, Faculty of Chemistry, Division of Chemical Metallurgy, Wybrzeże Wyspiańskiego 27, 50-307 Wrocław, Poland.

In the case of shale fraction observed is the dissemination of fine metal sulfides in the carbonate matter and in black shale-clay rocks that form the majority of the gangue. Such a fine dissemination of copper sulfides in carbonate matrix considerably reduces the susceptibility of the ore to the effective liberation. A relative increase of quantity of shale-clay and carbonate fractions in flotation feeds, which are known as mostly hard-to-treat in flotation circuits, is currently observed. According to the latest data (Kubacz and Skorupska, 2007) the content of shale fraction in Lubin deposit has already exceeded 25 % and is expected to increase in coming years.

Complex mineralogical structure and chemical composition of Polish copper ores mined from sedimentary deposits are the principal reasons of copper, silver and other metals losses to flotation tailings. The presence of shale creates serious technical, economical and ecological issues. The selective liberation of these fine particles would be the only way to enhance metal recovery. However, it appears to be ineffective by physical methods in the existing milling circuits. Consequently, the hydrophilic gangue-sulphide intergrowths greatly reduce both flotation selectivity and the metal grade in the concentrate.

Due to presently observed unfavourable changes in the ore mineralogical composition, the desired grade of copper concentrates can only be accomplished by lowering the copper recovery. The problem will undoubtedly increase in the next future due to forecasted increase in shale fraction content, which now reached 27 % for Lubin ore (Kubacz and Skorupska, 2007). Therefore, it can be concluded that the existing beneficiation technologies currently applied to Polish copper ores have already reached the limit of their technological efficiency. The only way to reduce significantly losses of copper, silver, and other metals to the flotation tailing is the application of an entirely innovative approach involving major change in the flotation circuits (Grotowski, 2007). This approach primarily involves the separation of the most troublesome ore fraction (shale containing middlings) and introduction of hydrometallurgical and/or biohydrometallurgical methods of their alternative, effective processing. The concept is currently analysed by BIOSHALE Consortium in the frame of comprehensive investigations conducted by several institutions (Chmielewski and Charewicz, 2005, 2006, 2006a). Atmospheric leaching in oxygenated sulphuric acid, pressure leaching and bioleaching, as an alternatives, appear to be very promising and effective.

Leaching and bioleaching in oxygenated solutions of sulphuric acid lead to solubilisation of most valuable (Cu, Fe, Ni, Co, Zn) and toxic (As) metals. Pregnant leaching solutions have to be subjected to purification and separation of metals, using solvent extractions an alternative. The preliminary studies of copper(II), cobalt(II) and nickel(II) recovery from the pregnant leach solutions by means of solvent extraction were performed in this work.

EXPERIMENTAL

The initial composition of pregnant leach solution applied for preliminary investigations of copper(II), cobalt(II) and nickel(II) recovery by means of solvent extraction is indicated in Table 1. The solution was a pregnant liquor from atmospheric leaching of Lubin shale fraction (middlings) – tailings from 1st cleaning at Lubin Concentrator (Chmielewski, 2007).

Table 1. The initial composition of pregnant leach solution

Component	Concentration, ppm
Copper	4324
Nickel	4.74
Cobalt	8.65
Iron	2061
Zinc	115
Arsenic	13.50

The solvent extraction was used for the recovery of copper(II), cobalt(II) and nickel(II) from the pregnant solutions after leaching cupriferous shale with sulphuric acid in the absence and presence of Fe(III) salts. Aromatic hydroxyoximes, LIX 84, LIX 612 and LIX 984, were investigated as copper(II) extractants to check their extraction and reextraction abilities. From the copper free raffinate Zn(II) was extracted with di-(2-ethylhexyl)phosphoric acid (D2EHPA). Subsequently, cobalt(II) and nickel(II) were separated from the zinc free raffinate with di-(2,2,4-trimethylpentyl)phosphinic acid (Cyanex 272). All extractants were dissolved in kerosene. Sulphuric acid of different concentration (1 or 3 M) was used as a stripping solution. All experiments were performed at a room temperature. The phases were shaken at 140 r.p.m. in a shaker bath for 1 hour.

The extraction experiments were carried out varying the volume phase ratio of aqueous (A) to organic (O) phases (A/O = 1:1, 2:1, 1:2 and 1:5). The concentration of Cu, Co, Ni, Fe, Zn and As in aqueous phases were determined by spectrometric ICP-OES method. The concentrations of metals in the organic phase were determined from mass balance.

The pregnant solution obtained from leaching of shale with sulphuric acid was neutralized with Lubin middlings to pH around 2 and then was used as an initial aqueous phase for copper(II) extraction with 20 or 30 % (v/v) of aromatic hydroxyoxyme solution in kerosene. The raffinate from Cu(II) extraction was used for further extraction of Zn(II) by D2EHPA. After zinc(II) extraction, the resulting raffinate was purified from Fe(III) and compounds of arsenic by neutralization with ammonia to pH around 5.5. After phase separation, ferrous and arsenic free solution was used for extraction recovery of Co(II) and Ni(II) with Cyanex 272.

The pregnant solutions obtained from the acidic leaching of shale with Fe(III) salts were neutralized with ammonia to precipitate Fe(III). Except of Zn(II) which was

omitted in this case, the subsequent extraction of Cu(II), Co(II) and Ni(II) from purified solutions was carried out in a similar way as described above. Copper(II) was extracted with 30 % (v/v) LIX 84 or LIX 984 solutions in kerosene.

RESULTS AND DISCUSSION

PREGNANT SOLUTION FROM LEACHING WITHOUT Fe(III)

It was shown that considered copper(II) extractants were very effective and the yield of extraction above 85 % was obtained. The best extraction power exhibited LIX 984 since 99.4 % of Cu(II) was removed from initial solution at A/O 1:1. Under the same conditions LIX 84 appeared to be less effective. In each case the increase of extractant concentration in the organic phase increases yield of copper(II) extraction (Fig. 1).

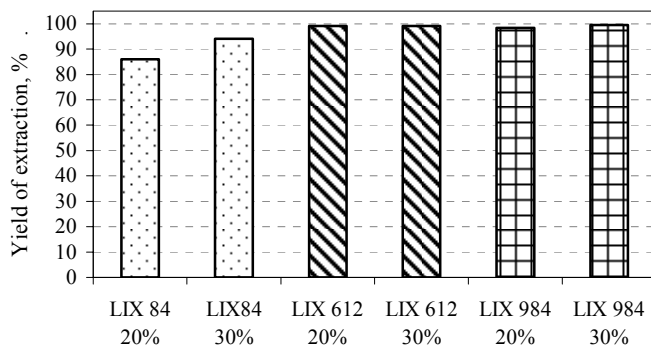


Fig. 1. Yield of Cu(II) extraction for different copper extractants at A/O = 1:1

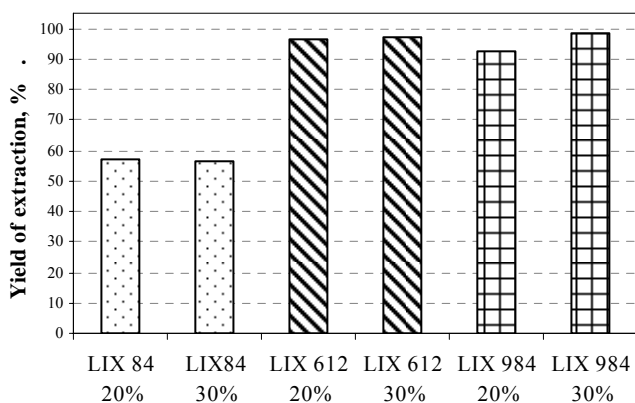


Fig. 2 Yield of Cu(II) extraction for different copper extractants at A/O = 2:1

When A/O ratio was equal to 2:1 the yield of extraction was lower for LIX 84 (around 57 %) but still high for LIX 612 and LIX 984, respectively (Fig. 2).

Moreover, it was found that examined Cu(II) extractants are not enough selective, because copper(II) was extracted together along with other metals present in the initial solution (Fig. 3).

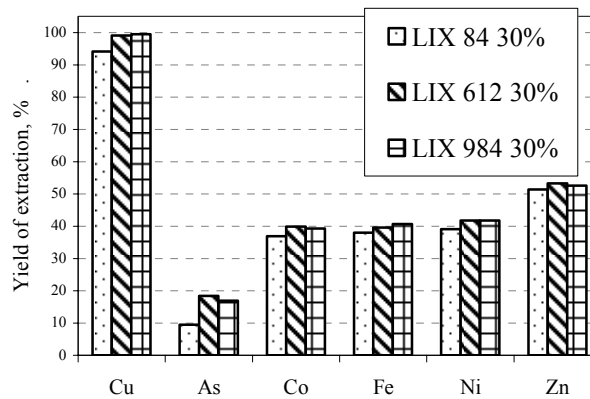


Fig. 3. Comparison of different extractants and their selectivity during copper separation from other metals present in the aqueous phase

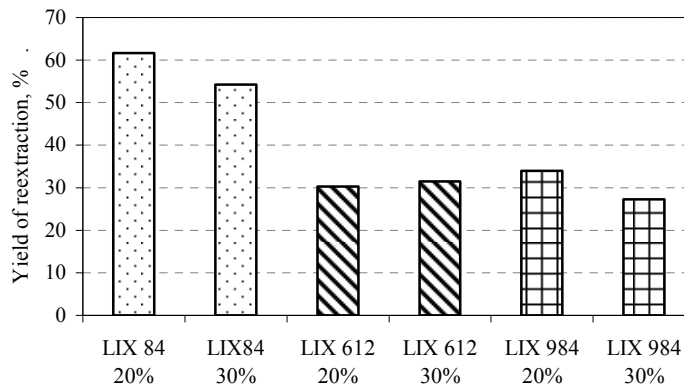


Fig. 4. Yield of Cu(II) reextraction for various copper extractants

The main purpose of this work was to investigate whether the recovery of valuable metals from pregnant leach solutions is possible or not. Therefore, the second step - reextraction of metals from the organic phase is always significant. The obtained results of copper(II) reextraction in one stage with 1 M sulphuric acid were not satisfying since the fraction of Cu(II) remaining in the organic phase was still high (Fig. 4). Probably, the higher concentration of H₂SO₄ in strip solution would affect a higher yield of metal reextraction.

The reextraction of copper(II) can be facilitated by addition to the organic phase an appropriate quantity of modifier, eg. tridecanol or nonylphenol. However, the effect of such modifiers on copper(II) extraction and reextraction from pregnant solutions of shale middlings leaching should be studied in additional experiments.

PREGNANT SOLUTION FROM LEACHING WITH Fe(III)

The pregnant solutions obtained from the atmospheric leaching of shale middlings with Fe(III) salts were neutralized with ammonia to precipitate Fe(III) as ferric hydroxide. The composition of the purified solution was found to be 0.024 ppm As, 2.91 ppm Co, 2707 ppm Cu, 0.172 ppm Fe, 1.47 ppm Ni and 15 ppm Zn.

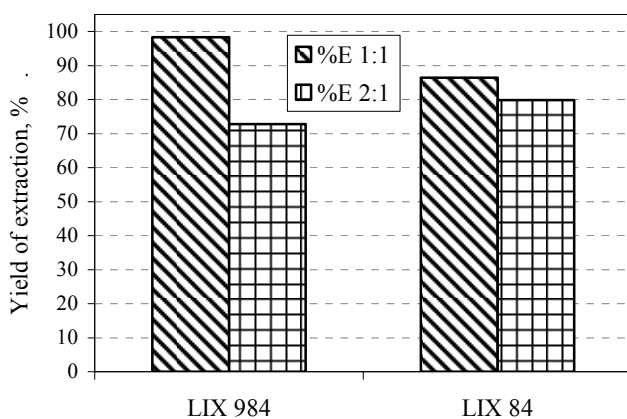


Fig. 5. Yield of Cu(II) extraction for different copper extractants at A/O = 1:1

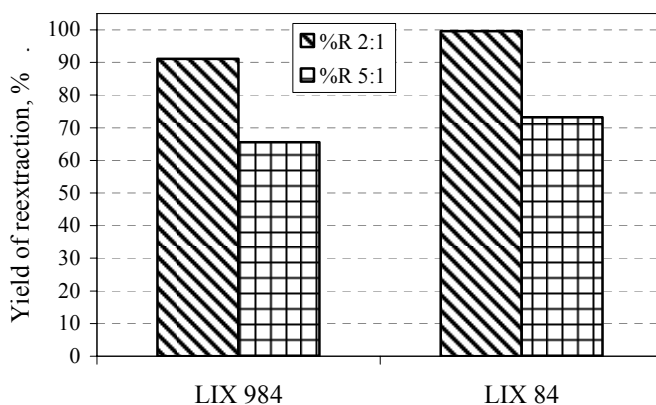


Fig. 6. Yield of Cu(II) extraction for different copper extractants at A/O = 2:1

The observed yield of Cu(II) extraction for LIX 984 and LIX 84 confirmed earlier results which indicated that the LIX 984 was evidently better for Cu(II) extraction than LIX 84 (Fig. 5). As a stripping phase 3 M H₂SO₄ was used. The comparison of reextraction abilities of both extractants exhibited that higher Cu(II) recovery was accomplished from the organic phase containing LIX 84 (Fig. 6).

Using the acidic chelating extractants for cobalt and nickel recovery can give satisfactory results. The selectivity series undergoes changes within the series phosphoric, phosphonic and phosphinic acids as shown below:

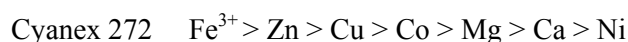
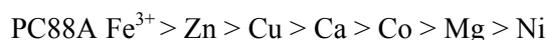
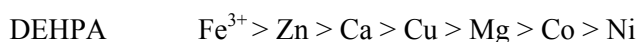


Table 2. Results of cobalt(II) and nickel(II) extraction and reextraction in the system with Cyanex 272

Metal	Yield of extraction, %		Yield of reextraction, %
	A/O 1:1	A/O 2:1	A/O 1:1
Co	16.5	13.0	36.9
Ni	14.3	12.2	28.4

Unlike DEHPA, which requires concentrated HCl to strip any co-extracted ion, Cyanex 272 can be readily stripped with relatively diluted (1,5 M) H₂SO₄ (Flett, 2004). However, in our experiments the yields of Co(II) and Ni(II) extraction from pregnant acid leaching solution with Fe(III) salts with Cyanex 272 (Table 2) were not satisfying and lower than those obtained for solutions from acidic leaching of shale in the absence of Fe(III) salts.

CONCLUSIONS

The solvent extraction technique is one of the most versatile methods used for the removal, separation and concentration of metallic species from aqueous media. Our results on solvent extraction of metals from pregnant leach solutions after atmospheric leaching of shale middlings demonstrated, that application of aromatic hydroxyoximes for copper(II) extraction can give satisfying results. However, these extractants were not enough selective and other metal ion species present in leach solutions were also transferred to the organic phase. Furthermore the extractive recovery of Cu(II), Co(II) and Ni(II) was better for the solutions obtained from acidic leaching of shale in the absence of Fe(III) salts.

The recovery of valuable metals was not high and further experiments are necessary to establish the optimal conditions of extraction and reextraction processes.

ACKNOWLEDGEMENTS

This work was carried out in the frame of Bioshale (European project contract NMP2-CT-2004 505710). Author acknowledges the financial support given to this project by the European Commission under the Sixth Framework Programme for Research and Development. I also wish to thank my various partners on the project for their contributions to the work reported in this paper.

REFERENCES

- CHAREWICZ W., CHMIELEWSKI T., 2005 et al, Deliverable BIOSHALE - D 4.1., *Process variant selection options and test work programme*, Tecnicas Reunidas, March 2005.
- CHMIELEWSKI T., CHAREWICZ W., 2006, BIOSHALE, Deliverable D.4.2., *Technical aspects: Leaching tests. Results with Lubin and Talvivaara Ores*, April 2006.
- CHMIELEWSKI T., CHAREWICZ W., 2006a, Hydrometallurgical processing of shale by-products from beneficiation circuits of Lubin Concentrator, *In: Perspectives for applying bioleaching Technology to process shale-bearing copper ores*, BIOPROCOP'06, Lubin 2006, KGHM Cuprum, Wrocław 2006, 125-145.
- CHMIELEWSKI T., 2007, *Atmospheric leaching of shale by-product from Lubin concentrator (this Journal)*.
- FLETT D.S., 2004, *Cobalt - Nickel Separation in Hydrometallurgy: a Review*, Chemistry for Sustainable Development, 12, 81-91.
- GROTOWSKI A., *Possibilities and perspectives for implementation of hydrometallurgical methods in KGHM Polska Miedz S.A.*, Proc. VIII International Conference on Non-ferrous Ore Processing, Wojcieszycze (Poland), May 21-23, KGHM Cuprum Wrocław 2007, 29-46.
- KUBACZ N., SKORUPSKA B. 2007, *Evaluation of influence of organic carbon on concentration and smelting processes*. Proc. VIII International Conference on Non-ferrous Ore Processing, Wojcieszycze (Poland), May 21-23, KGHM Cuprum Wrocław 2007, 157-166.
- ŁUSZCZKIEWICZ A. 2004, *Analysis and evaluation of beneficiation of the ore with elevated content of black shales*,. Report of investigations, Archiwum Zakładu Przeróbki Kopalini i Odpadów Instytut Górnictwa Politechniki Wrocławskiej, Wrocław, October 2004.
- ŁUSZCZKIEWICZ A., 2000, *Application of copper-bearing-black shales from Lubin-Glogow region*, in: Proceedings of "Modern problems of copper ore processing in Poland", Conference. Polkowice, 16 November 2000, Komitet Górnictwa PAN / KGHM Polska Miedz S.A., 137-156.

Rotuska K., Chmielewski T. *Ekstrakcja metali użytecznych z roztworów po ługowaniu miedzionośnej rudy łupkowej*, Physicochemical Problems of Mineral Processing, 41 365-372 (2007) (w jęz. ang.).

Roztwory kwasu siarkowego po ługowaniu atmosferycznym półproduktu łupkowego (odpad I czyszczenia I ciągu ZWR Lubin) w obecności tlenu i żelaza(III) zastosowano do ekstrakcji metali przy użyciu różnych ekstrahentów. Roztwory zawierały rozpuszczalne siarczany Cu(II), Zn(II), Ni(II), Co(II), Fe(II), Fe(III) i As jako składnika niepożądanego. Aromatyczne hydroksyoksyminy: LIX 84, LIX 612 i LIX 984 były stosowane jako ekstrahenty Cu(II). Z roztworu rafinatu pozbawionego Cu(II) ekstrahowano Zn(II) za pomocą kwasu di-(2-etylohexylo)fosforowego (D2EHPA). Ponadto, kobalt(II) i nikiel(II) były wydzielane z wolnego od cynku rafinatu za pomocą kwasu di-(2,2,4-trimetylopentylo)fosfonowego (Cyanex 272). Przemysłowe hydroksyoksyminy aromatyczne użyte do ekstrakcji miedzi okazały się mało selektywne i obserwowano przenoszenie jonów innych metali do fazy organicznej. Odzysk ekstrakcyjny Cu(II), Ni(II) i Co(II) okazał się znacznie lepszy dla roztworów po ługowaniu pozbawionych obecności Fe(III). Odzysk metali użytecznych okazał się niezadowalający i potrzebne są dalsze systematyczne badania nad optymalizacją procesów ekstrakcji i reekstrakcji.

Patrick d'HUGUES, Paul R. NORRIS, Barrie JOHNSON, Andrzej GROTOWSKI,
Tomasz CHMIELEWSKI, Andrzej ŁUSZCZKIEWICZ, Zygmunt SADOWSKI,
Aleksandra SKŁODOWSKA, Teresa FARBISZEWSKA*

PRESENTATION OF THE FP6 EUROPEAN PROJECT BIOSHALE: EXPLOITATION OF BLACK SHALE ORES USING BIOTECHNOLOGIES - POLISH CASE STUDIES

Received May 31, 2007; reviewed; accepted June 14, 2007

The Bioshale project, involving 13 partners throughout Europe, is co-funded by the European Commission under the FP6 program. The main objective of this project (which started in October 2004) is to identify and develop innovative biotechnological processes for "eco-efficient" exploitation of metal-rich, black shale ores. Three extensive deposits have been selected for R&D actions. These are: (i) a site (in Talvivaara, Finland) that, at the outset of the project, had not been exploited; (ii) a deposit (in Lubin, Poland) that is currently being actively mined, and (iii) a third site (in Mansfeld, Germany) where the ore had been actively mined in the past, but which is no longer exploited. The black shale ores contain base (e.g. copper and nickel), precious (principally silver) and PGM metals, but also high contents of organic matter that potentially handicap metal recovery by conventional techniques.

The main technical aspects of the work plan can be summarized as: (i) evaluation of the geological resources and selection of metal-bearing components; (ii) selection of biological consortia to be tested; (iii) assessment of bioprocessing routes, including hydrometallurgical processing; (iv) techno-economic evaluation of new processes from mining to metal recovery including social, and (v) assessing the environmental impacts of biotechnological compared to conventional processing of the ores. An overview of the main results obtained to date are presented, with special emphasis on the development of bioleaching technologies for metal recovery that can be applied to multi-element concentrates and black shale ores from Poland.

Key words: bioleaching, biotechnology, mineral processing

INTRODUCTION

The natural ability of microbes to degrade minerals was already used in the Roman times for copper recovery, without awareness of the role of micro-organisms. In the last 30 years, extensive research has been carried out on biooxidation and bioleaching

* BRGM- Mineral Resources Division 3, avenue Claude Guillemin BP 36009, 45060 Orleans, France.

processes. As a consequence, and where circumstances are favourable, biohydrometallurgy emerged as an industrial reality and a alternative for the treatment of some minerals (sulphides, oxides) and the recovery of metals such as copper, gold and cobalt (Rawlings and Johnson, 2007). There could be applications of "biomining" technologies for the recovery of other metals, such as rare and precious metals (PGM), or for processing other type of mineral targets, such as black shale ores but these would need significant technical and scientific engineering advances.

Since 2004, two consortia of industrial and research organisations, supported by the European Commission in the Sixth Framework Programme for Research and Development, have attempted to contribute to the transformation of the mineral industry towards cleaner, safer and more environmentally friendly production methods. These projects are BIOSHALE, a targeted project that aims at developing the potential of biotechnology for exploitation of "black shale - Kupferschiefer" ores for base and rare metals production, and BioMinE, a large integrated project that will allow the integration of innovative biotechnology based processes for recovery or removal of metals from primary European resources (ores and concentrates) and secondary materials (Morin et al., 2006).

All aspects concerning this project, including the Finish case study and the main results were recently presented at the Minerals Engineering conference that was held in Falmouth, UK in May 2007 (d'Hugues et al., 2007). This paper presents an overview of Bioshale project, with a special emphasis on both the biotechnological aspects of the project and the Polish case studies.

CONTEXT AND GENERAL DESCRIPTION OF THE PROJECT

European deposits of black shale ores contain considerable reserves of base and highly valuable rare and precious metals (including Cu, Ni, Zn, Pb, Ag, Zn, Co, Au, Pt, Pd), of which Europe is a main consumer. The black shale ores are typically poly-metallic ores with a variable proportion of sulphide components. In particular, the "Kupferschiefer" is a lithological formation that extends over 600,000 km² from England to Poland, but of which exploitable Cu reserves represent only 0.2% of the total area, notably at the southern edge of the Zechstein Basin. To date, more than two million tons of copper have been produced from this geological formation, along with noble and rare metals, extracted as by-products but often with a poor recovery. In Poland, the Lubin ore deposit which is currently being exploited belongs to this type of geological formation and evaluation of potentially more efficient and environmentally sensitive processing routes is of strategic importance for the Polish copper industry. In Finland at Talvivaara, the potential exploitation of a large, low-grade black shale ore deposit containing Ni, Cu and Zn was under evaluation when the Bioshale project started. The Mansfeld/Harz site in Germany has large amounts of black shale ore residues resulting from many years of mining activities in the area.

These three sites, at three different stages of development, were targeted to support the studies of innovative ways of processing black shale ores. Two major difficulties restrict the exploitation of such abundant resources. The first is the low efficiency of the conventional technical means for recovering valuable metals, from mining extraction to metallurgical processing. The second is the environmental impact of the application of the conventional techniques, even with the goodwill of the mining and metallurgy industries on this matter. From the processing point of view the black shale ores have specific features within a variable morphology: the metal-bearing compounds are dispersed as small-size particles and the valuable metals may be trapped in organic matter in the ore or in slimes. This explains the limited recovery of the metals and the problems encountered in the processing and management of the tailings.

The research and development challenge in this respect is two-fold. The first is to transpose the existing know-how in the treatment of sulphidic ores to black shale ores, and the second is to investigate new processing ways for beneficiation of the shales, among which could be the biotreatment of the organic components and the use of bioflotation for improving the production of concentrates. Therefore, natural biological activity in ore deposits and mining wastes stockpiles has been screened in a search for new bioprocessing reagents and in order to assess its influence on the environmental impact of the present and future mining activities.

OVERVIEW AND OBJECTIVES OF THE BIOSHALE PROJECT

“Bioshale” is a Specific Targeted Research Project co-funded by the European Commission in the frame of the FP6 programme (contract - NMP2 - CT - 2004 505 710), with a total budget of 3.4 M€ (EC contribution 2.3 M€).

The project duration is 3 years, and it began on 1st October 2004. In order to take up the scientific and technical challenges of the project, a multidisciplinary partnership (Table 1), working complementarily on the different case studies was implemented. The work was broken down in 6 Work packages-WP (Fig. 1).

The main goal of the Bioshale project is to define an innovative biotechnological processes for the “eco-efficient” exploitation of black shale ores for metals production. The main tasks involved are : (i) evaluation of the geological resources (geological modelling); (ii) selection of metal-bearing materials and biological consortia to be tested; (iii) assessment of bioprocessing methods and determination of complementary hydrometallurgical processing routes for metals recovery; (iv) risk assessment relative to wastes management of the new processing routes; (v) techno-economic evaluation of new processes from mining to metal recovery, including social and environmental impacts.

Three large-scale black shale deposits, of various stages of exploitation, were selected at the outset of the project. There were:

- (i) an un-mined deposit, located in Talvivaara, Finland;

- (ii) a deposit that is actively mined (and which accounts for the largest point production of copper in Europe) located at Lubin, Poland,
- (iii) and a post-mining deposit (Mansfeld, Germany). The social and economic benefits of this project aim to extend the exploitation life of European mining sites in operation (Lubin) and to allow exploitation of new resources with considerable reserves (Talvivaara). The site of Mansfeld in Germany was chosen to illustrate and support the evaluation of the Environmental Impact of exploiting black shale ores.

Table 1. Description of the Bioshale consortium

Participant Name	Country	Role
Bureau de Recherches Géologiques et Minières	France	Project coordination / WP5 leader - R&D activities in microbiology, biotechnology, geology, mineralogy & socio-economy
KGHM CUPRUM sp. z o.o. CBR	Poland	WP2 leader- Topic leader (technology/Engineering) R&D activities in geology, mineral processing and environmental impacts - sample provider
Wroclaw University of Technology	Poland	R&D activities in mineral processing, biotechnology and hydrometallurgy
University of Opole	Poland	R&D activities in microbiology & mineral processing
University of Warsaw – Faculty of Biology - CEMERA	Poland	Topic leader (environmental impacts) - R&D activities in microbiology, biotechnology & environmental impacts
Geological Survey of Finland	Finland	WP6 leader - R&D activities in mineral processing, biotechnology, mineralogy, environmental impacts & socio-economy - sample provider
Helsinki University of Technology	Finland	R&D activities in geology, mineralogy, electrochemistry & environmental impact
Técnicas Reunidas	Spain	WP4 – leader - R&D activities in mineral processing, hydrometallurgy and socio-economy
University of Wales, Bangor	UK	WP3 leader - R&D activities in microbiology and biotechnology
University of Warwick, Biological Science	UK	Topic leader (microbiology) - R&D activities in microbiology and biotechnology.
G.E.O.S. Freiberg, Ingenieurgesellschaft mbH	Germany	R&D activities in geology & environmental impacts
University of Mining and Geology “Saint Ivan Rilski”, Sofia	Bulgaria	R&D activities in mineral processing, microbiology, biotechnology and environmental impacts
Czech Geological Survey	Czech Republic	R&D activities in geology & mineralogy

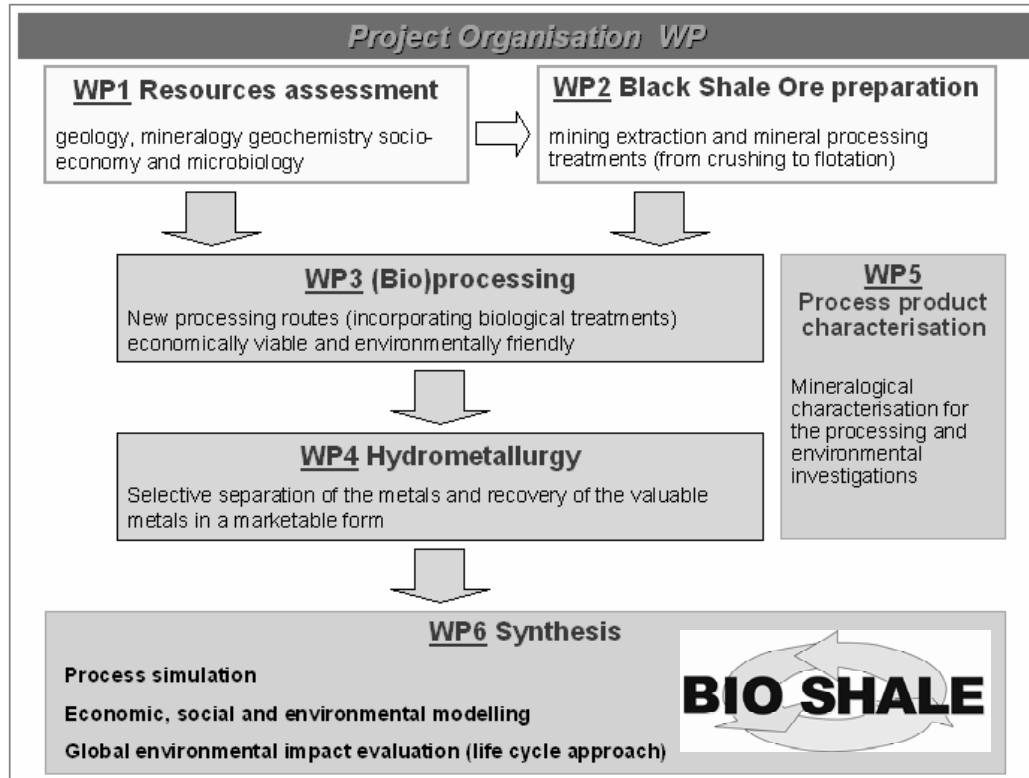


Fig. 1. Overview of the Bioshale project structure

BIOHYDROMETALLURGY AS A POTENTIAL OPTION

In order to evaluate the potentiality of bioprocess alternatives, regarding technical, environmental and economic criteria, a global analysis was carried out to better understand the real position of bio-technologies in comparison with alternative ones. This general study was mainly focused on copper of which production is ensured through a large variety of processes.

In biohydrometallurgy, two types of techniques exist and are proved as being reasonable technical and industrial options. The first one, and most simple, is the bioheap leaching technology. The crushed ore or the agglomerated concentrate/ore is placed in heaps and irrigated. The pregnant solution obtained by percolation through the heap is either recycled or used for downstream processing steps and metal recovery by hydrometallurgical routes. This technology is mainly applied for the treatment of copper ores. Some operation for pre-treatment of gold-bearing ores were also implemented. There are currently several bioheap-leach operations world-wide processing copper sulphide ores (Rawlings et al, 2003; Watlings, 2006). Two among them are treating primary sulphide (chalcopyrite) ore at pilot scale. Many bioheap

processes have targeted extraction of marginal ores not suitable for concentration and smelting.

The main operators are: Newmont Mining, Phelps Dodge, BHP Billiton, RioTinto, Mintek, and Codelco. The critical reasons for selecting bioheap over other techniques can be summarised as follows:

- low capital and operating cost, easy to operate, mainly inert wastes
- flexible in size, remoteness of the mine and cost for transportation
- less sensitive to impurities in the feed material (“dirty” concentrates with high impurities levels are charged with penalties by smelters)
- metal production can be applied on site.

Nevertheless this technology presents the following drawbacks and weak points:

- necessity of large surface for implementation
- relatively slow and limited recovery of some metals.

The second biotechnology that can be applied for metal recovery is known as the stirred tank technology. A bioreactor is continuously fed with a finely milled mineral suspension. The pulp is agitated and aerated in the tank where the main key operating parameters can be monitored and controlled. There are currently more than 14 plants in operation at industrial or demonstration scale for gold, Co, Cu and Ni (Rawlings et al, 2003). The main designers & operators are: BHP Billiton, Bactech, Mintek, BRGM, Gold Fields, and Codelco.

The principal reasons for selecting the stirred tank technology over other type of alternatives can be summarised as follows:

- attractive capital and operating costs and short construction and starting-up period
- relatively cheap environmental requirements (stable wastes)
- robust and simple process
- production on site of pure metal directly saleable on market
- on the other hand, this technology presents some weak points:
- limitation of the recovery on certain type of minerals
- energy requirements for mixing and oxygen.

Some extended and complete reviews were recently published concerning the role of biotechnology in the mining industry in general, and more specifically in the copper industry (Clark et al., 1995 ; Crundwell, 2005 ; Watlings 2006).

From a general point of view and in the case of copper extraction technologies, the choice of the best technology is driven by both the metal grade in the ore and the total amount of resource. Nevertheless, the main conclusion of the macro economic study (Pelon, 2006) is that the feasibility of a process on a given resource is strongly dependent on many site/resource specific factors.

Pyrometallurgy remains the main technology for metal recovery in general and especially for copper extraction. Nevertheless, there are more and more potential niches for application of biohydrometallurgy. Nowadays, biohydrometallurgy is taking an important place in the mining industry of non-ferrous metals either in competition or in complement of classical technologies. It is definitely offering to the mining

operators an alternative development option with inherently attractive economics. But although these technologies are used commercially in many countries, there have been relatively very limited developments in Europe. It remains to be clearly demonstrated that these technologies can:

- be used on a wider range of mineral resources, including metal-bearing wastes of the mining industries
- be economically viable and technically robust, with reasonable energy and water consumption and acceptable waste production
- help to reduce the environmental impact of the mining industry
- benefit from an expansion of the knowledge base, especially of microbiological aspects.

MAJOR ACHIEVEMENTS (PROCESS OPTIONS AND ACADEMIC R&D)

In terms of process development, the work carried out in the frame of Bioshale is focused on two case studies, involving two contrasting “black shale” deposits located in Poland (Lubin Mine) and in Finland (Talvivaara deposit). The most likely successful process options operations were developed early on in the project. In both cases, the work on process options assessment took into account the current situation on the target sites.

In the case of Lubin, there is an existing concentrator plant combined with a smelter that extracts mainly copper and silver. A copper concentrate is produced there, along with an “enriched shale fraction” (or “middlings”) which causes trouble in the flotation circuits. A second mine (Polkowice) located close to Lubin produces a similar concentrate, but which is more enriched in PGEs. Lubin ore contains disseminated sulphidic particles, closely associated with organic matter.

The most valuable metal in the Talvivaara deposit is Ni, while Co, Zn and Cu are also present in significant quantities. Currently a large-scale industrial project evaluating heap leaching technology to recover metals from the Talvivaara ore is under evaluation. The Talvivaara black shale is a metamorphosed black shale that contains mainly graphite.

LUBIN ORE/CONCENTRATE PROCESS OPTIONS

Many bioshale process options were considered by the consortium during the first two years of the project (Table 2). Cu and Ag recovery would be expected downstream of all of the Polish material options, except primary bioheap leaching of the ore which would not facilitate Ag extraction.

Bioleaching tests showed that the Lubin black shale middlings and concentrate fractions were amenable to bioleaching, with extraction of up to 98% of the copper (options 2 and 3). A variety of microorganisms from different phylogenetic groups

were used successfully at widely different temperatures, ranging from 30°C with mesophiles and 45°C with moderate thermophiles to 78°C with thermophiles. This leaching at low pH by acidophilic chemolithotrophic bacteria involved significant consumption of sulfuric acid.

Table 2. Bioshale process options (Polish case study)

Bioshale Process Options	General Description
Option 1: Bioheap leaching of Lubin run-of-mine ore	Classical bioheap leaching of Cu using agglomerated Lubin ore
Option 2: Leaching of Lubin middlings after pre-treatment	Bioleaching (or atmospheric chemical leaching) using middlings after acid pre-treatment for carbonate decomposition
Option 3: Bioleaching of Lubin concentrate (after pre-treatment)	Bioleaching using Lubin concentrate (after acid pre-treatment for carbonate decomposition)
Option 4: Selective flotation of Lubin run-of-mine ore + (Bio)leaching	Selective flotation of Lubin RoM to produce an enriched shale concentrate further treated using acid leaching for carbonate decomposition and bioleaching
Option 5 - Selective flotation of Lubin middlings + bioleaching	As option 4, but with middlings in place of ore
Option 6 - Selective mining + bioleaching	Selective mining of the deposit to separate the shale fraction. The enriched shale fraction would be treated using bioleaching

Although a range of heterotrophic microorganisms as well as some basophilic chemolithotrophs were able to leach copper from black shales, the results were far inferior to those obtained with chemolithotrophic acidophiles. Biodegradation of the organic matrix of black shales (Lubin ores and concentrates) was more difficult to achieve. No evidence of biodegradation was found with acidophilic heterotrophic bacteria. Experiments with neutrophilic microorganisms were more successful, but their positive impact on metal recovery efficiency remains to be demonstrated and quantified at larger scale.

Bioleaching using the Lubin concentrate after acid pre-treatment for carbonate decomposition was selected during the initial bioprocess selection (Fig. 2). This option is not yet of direct interest in the context of the current industrial process with the Lubin concentrator. It could become an option in the case of 'capacity shortage' in the smelter, or production of a 'dirty' concentrate (e.g. presence of arsenic).

Following successful batch culture tests with the pre-treated materials, processing in continuous conditions is necessary to determine the specifications for the application of the stirred tank technology to a sulphide concentrate from black shale ores. The work carried out on the downstream processing is also a technical challenge and more specifically the recovery of silver from the bioleached residues. Preliminary

results showed that more than 90% of the copper and more than 85% of the silver respectively can be extracted using the continuous stirred tank technology. Better performances are expected to be obtained following optimisation steps.

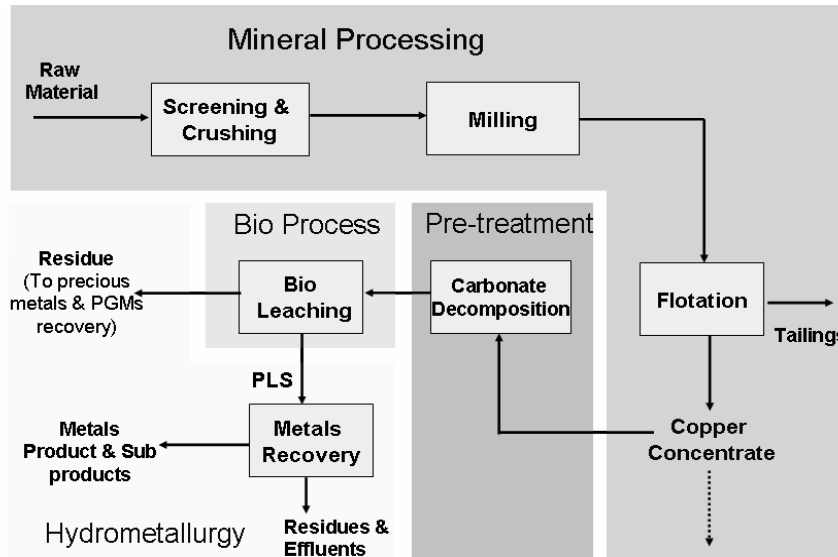


Fig. 2. Bioshale process option N°3 - Bioleaching of Lubin concentrate (after pre-treatment) (From TR - F. Sánchez and J. Palma ; From BRGM - D. Morin and P. d'Hugues)

Several process options concerning the Lubin middlings (Fig. 3) were considered.

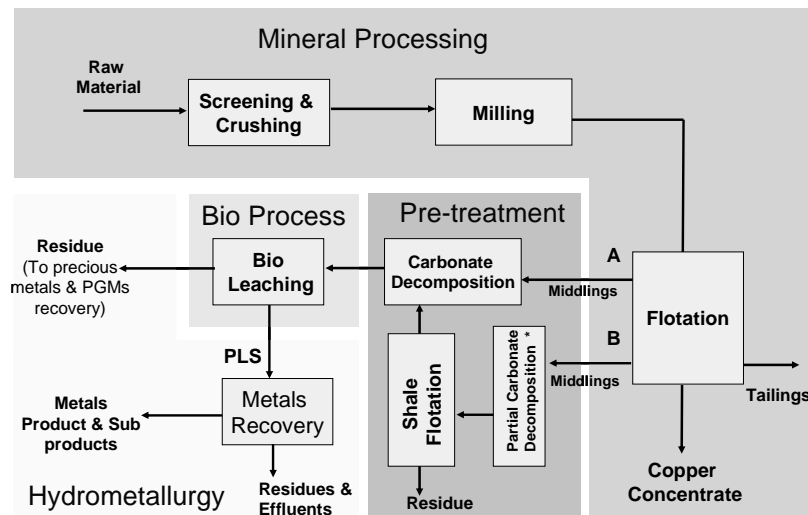


Fig. 3. Bioshale process option N°2 and N°5 - Bioleaching of Lubin middlings (From TR - F. Sánchez and J. Palma and PWR - A. Luszczkiewicz and T. Chmielewski)

This material has very similar properties to the shale ore. It was estimated that with the operation of the Lubin concentrator, the tailings of the first cleaning flotation represent 20-30% of the mass of solids in the whole flotation system, with copper recovery about 20-25%. Although it was demonstrated at laboratory scale that the material is relatively easy to bioleach, and its use could reduce the material flow in, and improve the total efficiency of, the flotation circuit, a direct (bio)leaching of the middlings does not look like economically viable because of the low copper grade. Agglomeration of this very fine material would be necessary prior to an alternative, bioheap treatment, and, although technically difficult, could be considered further.

Selective shale flotation (including bioflotation) of the Lubin Middlings (option 5) was tested. The flotation experiments proved that upgrading middlings is very difficult. It is necessary to produce enough high copper grade concentrate for further bioleaching before this option can be considered further. In conclusion, the technical and economical viability of any process on Lubin middlings remains very uncertain. The real consequences of bleeding the middlings stream are still not perfectly known and difficult to evaluate.

Two stage bioleaching of Lubin middlings (option 7) was also considered (Fig. 4) in case it was demonstrated that shale organic matter degradation was necessary to recover rare and noble metals. Biodegradation of organic matter, extracted from the shale, and synthetic metallo-organic complexes (metallo-porphyrins), were examined at neutral pH. So far, any added value of the neutral leaching stage was not demonstrated. The preliminary results indicate that this option is not applicable in the context of Lubin mine, but might be of interest with black shale samples enriched with rare and noble metals encapsulated in the organic matter.

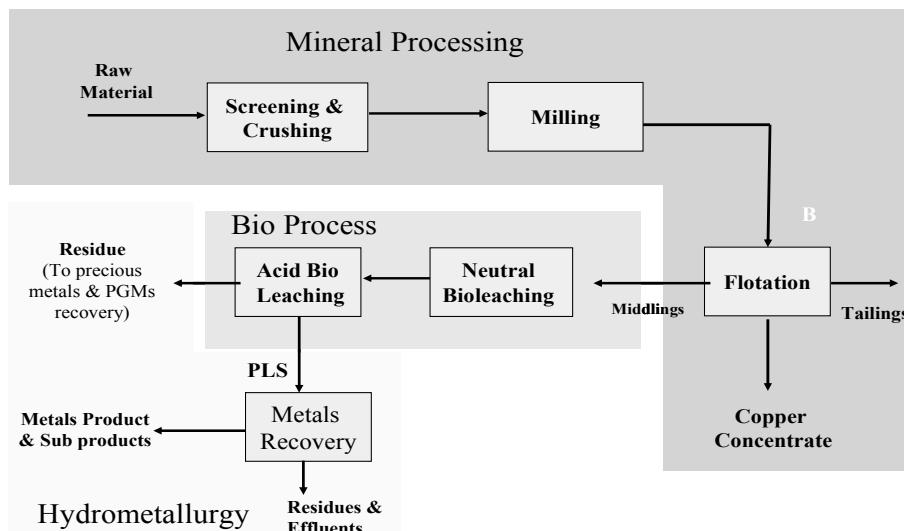


Fig. 4. Bioshale process option N°7 – Two stages bioleaching of Lubin middlings (From PWR and UO - Z. Sadowski and T. Farbiszewska)

ACADEMIC ASPECTS

In addition to the development of bioprocess options, some more academic scientific research has been carried out during the first two years of the Bioshale project.

1. Production of new scientific data on noble metals occurrence (PGE,...) in black shales.
2. Research into the identification of noble metal carriers in metal rich shales in order to explain the mechanism of the origin of noble metals in various black shales worldwide.
3. Participation in the development of bioleaching technologies for copper recovery that can be applied to multi-element (metals) concentrates and black shale ores.
4. Optimisation of silver recovery from residues after bioleaching. Demonstration of the ability to bioleach metals from black shale ores that contain organic matter.
5. Study of phenomena governing bacterial adhesion, role of cell surface properties in adhesion and bioflotation processes.
6. Bioprospecting at all three sites for (novel) bioleaching microorganisms.
7. Study of the microbial ecology of the TVK heap using molecular biology tools. Modelling and simulation of heat transfer using data from both pilot operations (GTK and TVK).

The reports that were produced by the Bioshale consortium since the beginning of the project are presented in Table 3. All these reports are confidential, but abstracts are available on the Bioshale web site (<http://bioshale.brgm.fr>) and the main results will be freely disseminated during and after the final year of the project.

CONCLUSIONS

Between 2003, the preparation phase of the project, and the beginning of 2007, the project's final year, some changes occurred and some adjustments were made to the original programme. The beginning of the project coincided with a spectacular rise in worldwide commodity prices. Non-ferrous metals all witnessed a strong price increase over 2005 and early 2006, that was sustained over 2006 (Lips, 2006). This phenomenon was notably observed on copper, nickel and zinc, and the Talvivaara mine project became a likely commercial reality. Chemical analysis of samples from the Lubin area did not show any high concentration of rare/strategic metals or PGE in the organic matter. The technical issues related to the accumulation of shale fractions (middlings) in the flotation circuit of the mineral processing step at Lubin was clearly identified as an important target for the project. The consequence of all these issues on the Bioshale project was that the recovery of base metals (Cu, Ni, Zn) from black shale ores became the main priority over the challenge of the recovery of valuable minor metals (PGE, V, Re, etc.) potentially trapped in organic matter. The (bio)processing R&D actions on Polish ores and concentrates from Lubin Area have

been focused mainly on copper and silver recovery. The various process options presented in this paper have been investigated or are still under investigation. The most promising ones will be assessed against technical, economic and environmental criteria. The results of these pre-feasibility studies will be presented at the end of the project.

ACKNOWLEDGMENT

This work was carried out in the frame of Bioshale (European project contract NMP2-CT-2004 505710). The authors acknowledge the financial support given to this project by the European Commission under the Sixth Framework Programme for Research and Development. We wish to thank H. Karas (president of KGHM Cuprum) and D. Morin (BRGM) who initiated this project in 2004 and TVK and KGHM Polska Miedź S.A. for their support during the project.

We also wish to thank the representatives of our various partners and the members of the executive board for their contributions to the work reported in this paper: Thierry Auge and Dominique Morin (BRGM); Jan Pasava and Anna Vymazalova (CGS) Barbara Pakulska (Cuprum); Franz Glombitza and Jana Pinka (GEOS); Jorg Langwaldt and Lasse Ahonen (GTK); Kirsti Loukola-Ruskeeniemi and Olof Forsen (HUT); Witold Charewicz (PWr.), Jesus Palma and Francisco Sanchez (TR); Stoyan Groudev and Irena Spasova (UMGS); Jadwiga Farbiszewska-Kiczma (UO); Kevin Hallberg (UWB); Renata Matlakowska (UW-FB); and all our colleagues from the different organisation who participated to this project.

This paper is published with the permission of BRGM as scientific contribution No 5057

REFERENCES

- CLARK, M.E., BATTY, J., VAN BURREN, C., DEW, D., EAMON, M., 2006. *Biotechnology in minerals processing: Technological breakthroughs creating values*. Hydrometallurgy 83 (1-4), 3-9.
- CRUNDWELL, F. *The economics of process selection in the copper industry*, 2005. In Harrison, S.T.L., Rawlings, D.E., Petersen, J. (Eds.), Proceedings of the 16th International biohydrometallurgy symposium. pp105-114.
- d'HUGUES, P., NORRIS P.R., HALLBERG, K., SÁNCHEZ F., LANGWALDT, J., GROTOWSKI, A., CHMIELEWSKI, T., GROUDEV, S., Bioshale consortium., 2007. *Bioshale FP6 European project: exploiting black shale ores using biotechnologies?*, In Proceedings of BioHydrometallurgy 07 (CD-Rom), MEI Conference, Falmouth, May 1-2 2007.
- LIPS, A.L.W., 2006. *A review of non-ferrous mineral deposits in Europe - finalised initial database on primary and secondary resources for biotechnological metal extraction*. BioMinE Deliverable DI.3, Final Report (BioMinE Integrated Project, IP NMP2-CT-2005-500329), report BRGM/RP - 54957-FR, 30pp.
- MORIN, D., LIPS, A., PINCHES, T., HUISMAN, J., FRIAS, C., NORBERG, A., FORSSBERG, E., 2006. *BioMinE – integrated project for the development of biotechnology for metal-bearing materials in Europe*. Hydrometallurgy, 83, 69-76.
- PELON, R., 2006. *Economic background of copper biohydrometallurgy*, Personal communication participation to Deliverable D6.1. of Bioshale project.
- RAWLINGS, D.E., DEW, D.W., and Du PLESSIS, C.A., 2003. *Biomineralization of metal-containing ores and concentrates*. Trends in Biotechnology, 21, 38-43.
- RAWLINGS, D.E., JOHNSON, D. B. (eds.) (2007) *Biomining*. Springer, Heidelberg
- WATLING, H.R., 2006. *The bioleaching of sulphide minerals with emphasis on copper sulphides - A review*. Hydrometallurgy 84 (1-2), 125-264.

d'Hugues P., Norris P.R., Johnson B., Grotowski A., Chmielewski T., Łuszczkiewicz A., Sadowski Z., Skłodowska A., Farbiszevska T., *Europejski Projekt BIOSHALE, Eksploatacja rud łupkowych z użyciem biotechnologii – Polska część badań*, Physicochemical Problems of Mineral Processing, 41 (2007) 373-385 (w jęz. ang.).

Projekt BIOSHALE, obejmujący 13 partnerów z Europy, jest sponsorowany przez Unię Europejską w ramach programu FP6. Głównym przedmiotem badań w tym projekcie, który rozpoczął się w październiku 2004r., jest znalezienie i opracowanie innowacyjnego procesu biotechnologicznego, który umożliwi eksploatację w sposób ekologiczny rud łupkowych bogatych w metale. Badaniem poddane zostały trzy istniejące złoża. Są nimi: (i) złoże Talvivaara w Finlandii, które w momencie rozpoczęcia projektu nie było eksploatowane, (ii) złoże Lubińskie w Polsce, które jest obecnie eksploatowane, (iii) trzecim miejscem były okolice miejscowości Mansfeld w Niemczech, gdzie została zakończona eksploatacja i pozostały hałdy odpadów. Rudy łupkowe zawierają metale takie jak: miedź, nikiel, metale szlachetne (głównie srebro) oraz metale z grupy platynowców (PGM), a także duże ilości substancji organicznej, która uniemożliwia odzysk tych metali w sposób konwencjonalny.

Głównymi aspektami pracy w projekcie są:

1. opis zasobów geologicznych i wydzielenie składników (rud) bogatych w metale,
2. wybór konsorcjum bakteryjnego dla prowadzenia procesu bioługowania,
3. ocena procesu bakteryjnego ługowania łącznie z procesem hydrometalurgicznym,
4. opracowanie założeń techniczno-ekonomicznych nowego procesu odzysku metali,
5. ocena ryzyka zagrożenia środowiska naturalnego przez wprowadzenie procesu bazującego na biotechnologii w porównaniu do istniejących procesów.

W pracy został dokonany przegląd najważniejszych wyników ze szczególnym wyróżnieniem technologii bioługowania w celu odzysku metali. Technologie tę można będzie zastosować do przerobu wieloskładnikowych koncentratów i rud łupkowych w Polsce.

Zygmunt SADOWSKI*, Agnieszka SZUBERT*

COMPARISON OF KINETICS OF BLACK SHALE BIOLEACHING PROCESS USING STATIONARY AND AGITATED SYSTEMS

Received March 15, 2007; reviewed; accepted May 15, 2007

In the study, the kinetics of black shale ore bioleaching process, carried out in small column and tank reactor, was investigated. During all experiments the concentration of Cu^{2+} ions in the leaching solution was determined as a function of leaching time. Based on the results obtained, kinetics of bioleaching processes in the agitated tank reactor and column reactor were compared. The rate of bioleaching in column was similar to that in agitated tank. For the experiments in column, two different types of packing materials (plastic bullets and sawdust) were tested in order to improve the bed porosity. The results showed that sawdust was the best packing material used in this study.

Key words: bioleaching, tank, column, black shale, packed bed, sawdust, plastic support, kinetic

INTRODUCTION

There are two fundamental mechanical systems using for bioleaching processes: dispersed (agitated) and stationary solid beds. The stationary solid bed can be applied for beds of a good porosity and permeability for the solvent. For the fine minerals particles agitated systems are more suitable.

The heap leaching process may be considered as heterogeneous fixed bed reactor, where the leaching solution circulates through the ore bed. The fractional void space occupied by the leaching solution depends on the particle size. During the bioleaching process, the bacteria diffuse from the leaching solution into porous medium and react with sulfide particles.

According to Lizama, (2004) the mechanics of heap leaching systems includes a particle size, particle composition and fluid flow phenomena inside the column. The fluid flow through the particle bed is important for the heap leaching operation. The

* Wrocław University of Technology, School of Chemistry, Department of Chemical Engineering, Wybrzeże Wyspiańskiego 27, 50-370 Wrocław, POLAND, zygmun.sadowski@pwr.wroc.pl

leaching kinetics are proportional to the irrigation rate divided by heap height (Lizama et al., 2005).

Under these conditions, an important parameter is the effective external area of the solid particles wetted by the leaching solution and colonized by bacteria cells. The kinetic analyses of bioleaching data were interpreted according to the colonization shrinking core model (Lizama et al., 2005).

Bioleaching in column with recirculation of the leaching liquid is a lab-scale simulation of heap bioleaching processes (Long et al., 2004).

Understanding of the liquid flow phenomena inside the packed bed is important to enhance the bioleaching performance. The milli-Ct scanner has been used to determine the pore structure of the packed column before and after bioleaching. The application of this sophisticated technique give an opportunity to establish a fundamental relationship between pore microstructure and effective transport coefficient (Lin et al. 2004, 2005).

The purpose of this article is to compare the kinetics of bioleaching processes using stationary solid bed and dispersed solid systems. The paper considers also the effect of different materials (shavings, plastic) added to the mineral bed on the column bioleaching kinetic.

EXPERIMENTAL

MATERIALS AND MICROORGANISMS

The materials obtained from Lubin mine were fine powder with the mean particle size of 34.1 (sample A) and 43.3 μm (sample B). The particle size distribution for two black shale samples are presented in Fig. 1 and Fig 2. The chemical analysis has revealed that copper grade in these materials were 7.04 % and 2.32 % sample A and sample B, respectively.

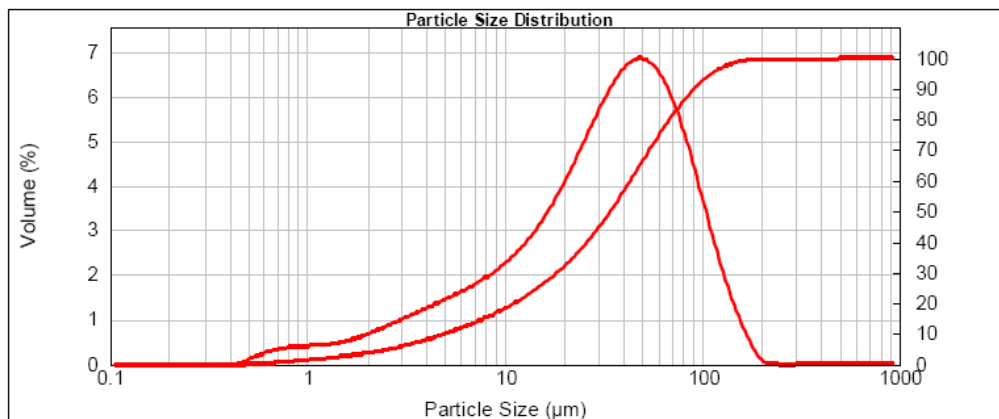


Fig. 1. Particle size distribution of black shale sample "A"

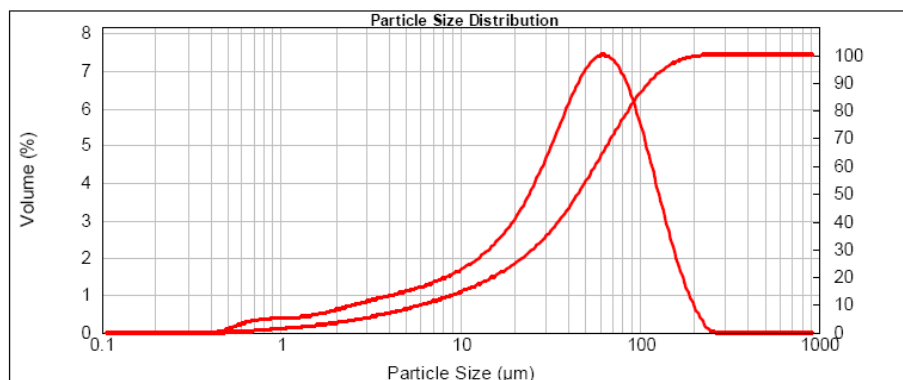


Fig. 2 Particle size distribution of black shale sample "B"

Support materials

The support materials used in this study were polyethylene spheres (3 mm in diameter) and wood sawdust (size range of 2-10 mm).

Bacteria strains

Microorganisms used in both column and tank leaching experiments can be classified as heterotrophic and autotrophic bacteria. The culture of *Streptomyces setonii* purchased from ATCC. The Actinomycetes *Streptomyces setonii* is known to degrade some types of coal organic compounds. The culture of chemolithotrophic bacteria such as *Acidithiobacillus ferrooxidans*, isolated from water samples taken from Zloty Stok old arsenic mine, was used to bioleaching procedure. The culture was adapted to grow with the high As and Cu ions concentration.

APPARATUS

Column bioleaching

Column leaching experiments were conducted in small column (37cm/5.0cm). The column was charged with 70 g of black shale material. The charges for column experiments when a support was used, were prepared by mixed 70 g of sawdust and 70 g of shale powder or 13.5 g of plastic bullets and 70 g of shale sample. The leaching solution (200 cm³) was pumped from the feed container to the top of the column. Also, the gas (air) was introduced at the top of column, where a layer of leaching solution was created during the leaching tests.

Tank bioleaching

The leaching experiments were carried out in 8-dm³ tank bioreactor with one propeller. The temperature and pH of the solution in the bioreactor were monitored and maintained at the designated pH by the addition of concentrated sulfuric acid. The temperature of the process was maintained at 30⁰ C, using the circulating water bath.

Parameter measurement

The particle size distribution has been obtained by powder analysis using a laser diffractometer Mastersizer 2000 (Malvern Instruments G.B). During the experiments Cu^{2+} , Fe^{2+} , Fe^{3+} ions and protein concentrations, as well as pH and Eh have been measured.

Two stage bioleaching process

The residues obtained in the heterotrophic leaching stage were treated with H_2SO_4 in order to remove carbonate minerals. The residues were then bioleached with autotrophic bacteria with fresh nutrient medium and new inoculum.

RESULTS

In black shales, the fine metal sulfide particles are dispersed in the carbon-organic matter. The role of heterotrophic microorganisms is biodegradation of organic matter compounds in order to release metals and metal sulphides from it.

TANK BIOLEACHING

The initial stage of the study was consisted in evaluation of effectiveness of the two stages bioleaching process, conducted in tank reactors, for two shale samples (A and B). The results of bioleaching by heterotrophic bacteria *Streptomyces setonii* are presented in Fig 3.

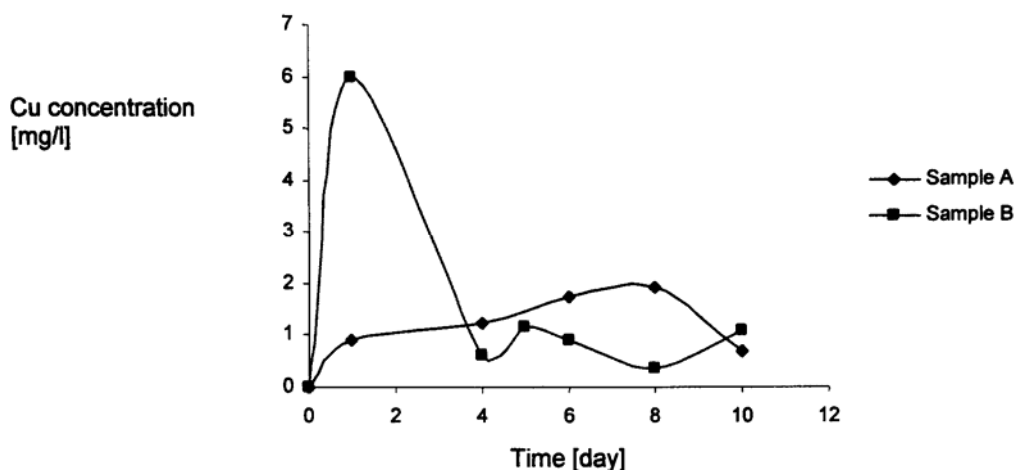


Fig. 3. Heterotrophic bioleaching of black shale samples

As can be seen, a low concentration of copper ions in the leaching solution resulted in a strong biosorption of Cu^{2+} ions by microbial cells.

The second stage of bioleaching procedure was preceded by carbonates neutralization with sulphuric acid (partially atmospheric leaching). From this reason the initial copper concentrations were much higher, then it was after heterotrophic bioleaching.

As can be seen from Fig. 4, a continues increase of copper concentration was observed during two weeks autotrophic bioleaching. The differences in the yield of the process of the two samples is due to various content of copper in them.

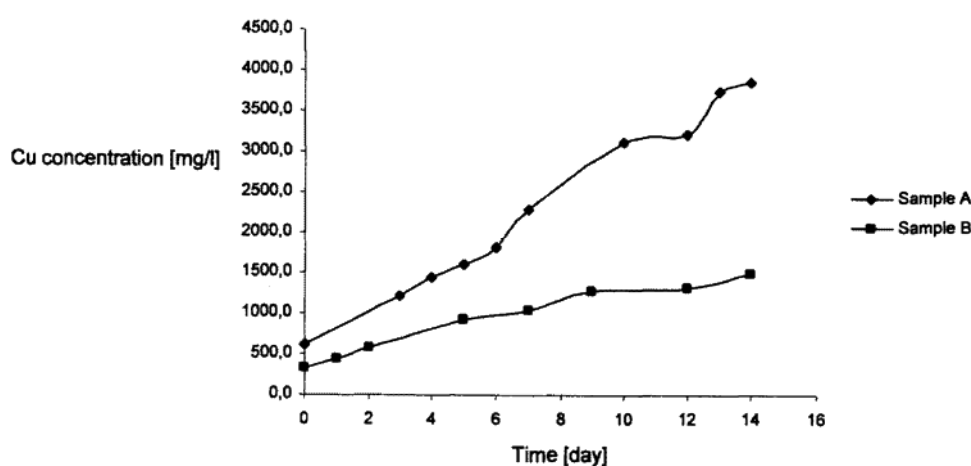


Fig. 4. Autotrophic bioleaching of black shale samples

COLUMN BIOLEACHING

The bed permeability is an essential process parameter, in the case of column bioleaching. The particle size distributions of shale samples (Fig. 1 and 2) showed that both materials contain a lot of fine particles. The amount of fine particles is a key parameter. It was recommended that the fine fraction should be less than 10 % (Lin et al., 2004, 2005).

The present work shows the influence of two supports (plastic and sawdust) on the bioleaching kinetics of shale samples in the trickle packed bed reactor (TBR).

It was observed that bioleaching rate rapidly increased with a sawdust as the support. This fact is connected with an immobilization of bacterial cells onto the sawdust surface. The decrease in the end of bioleaching can be connected with iron salts precipitation on the mineral surface and the occlusion of copper ions.

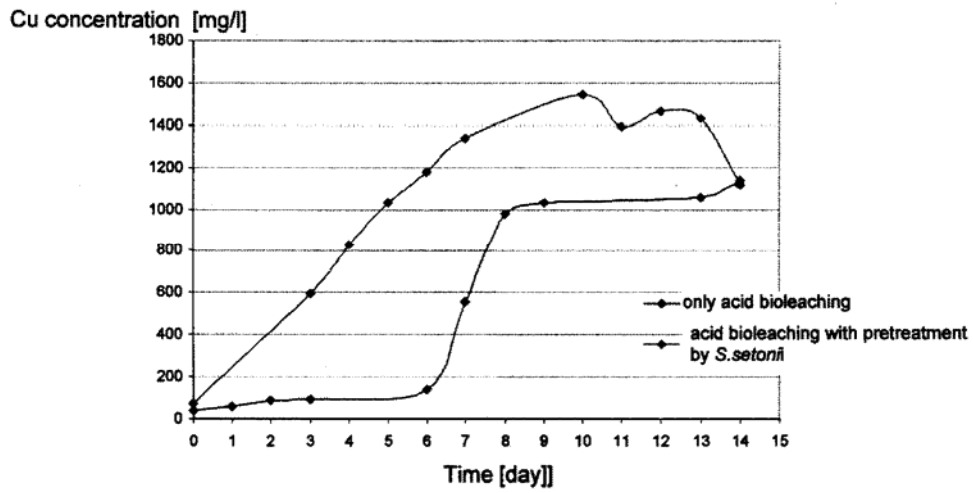


Fig. 5. Comparison of autotrophic bioleaching with or without heterotrophic leaching

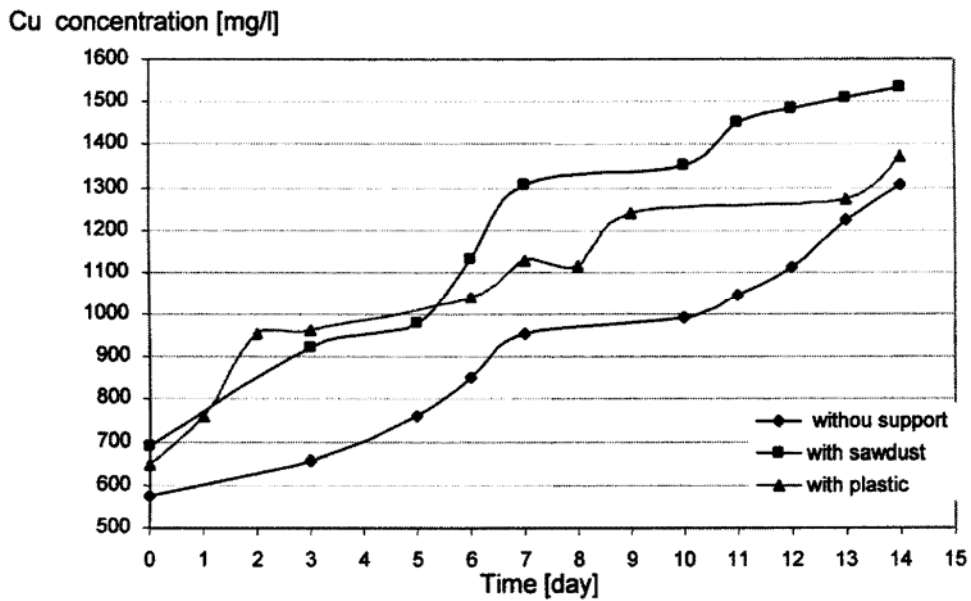


Fig. 6. Comparison of acid, autotrophic leaching with or without support for sample A

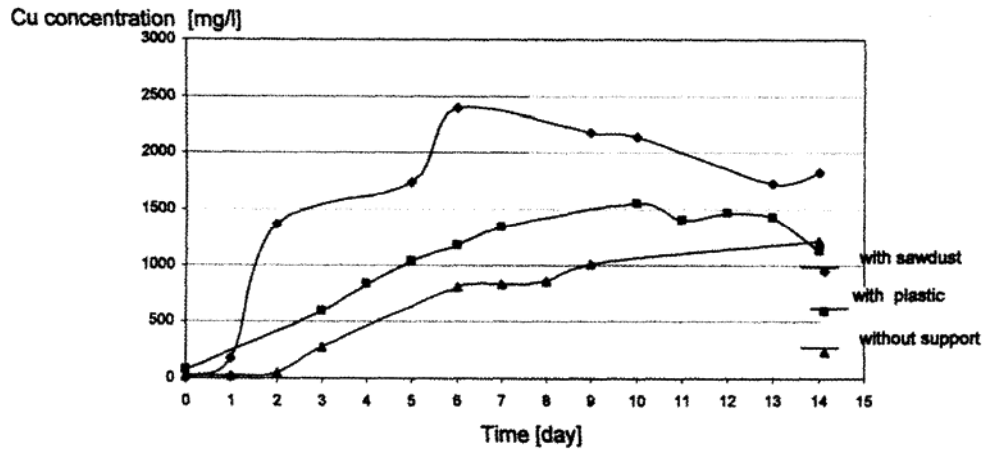


Fig. 7. Comparison of acid, autotrophic leaching with or without support for sample B

DISCUSSION

The bioleaching efficiency of the mineral particles in the column can be considered as a function of Reynolds number of the leaching solution flows through the bed. In the heap leaching practice, it is advisable to crush the mineral down to diameter of about 3 cm. The reduction of particles size can cause the plugging and channeling of the leaching solution. The porosity decrease influences an increase of the resistance of an internal mass transfer and an increase of bioleaching time considerably. (Bartlett, 1992) suggested a porosity range of 0.02 to 0.08 for typical minerals processed by heap leaching.

During the heap leaching the solution circulates from the top of the heap. At the steady state the liquid content in the bed becomes constant. The liquid flow is constant and was measured for each bead (Table 1).

Table 1. Leaching liquid flow through the column

Filler	Leaching liquid flow [cm ³ /60s]	
	Shale sample "A"	Shale sample "B"
Without filler	12.37	11.86
Plastic spheres	13.58	13.34
Sawdust	17.3	17.1

The natural tendency of *Acidithiobacillus ferrooxidans* to grow on the solid surface makes it a potential microorganism able to be immobilized. Several solid supports have been used for cellular immobilization, including agar, polyurethane foam, glass beads, activated coal, sand and polyvinyl chloride. The immobilization of

microbial cells offers significant advantages over the processes where the free cells are used (Giro et al., 2006).

An inhibitory effect of high ferrous ion concentration on the activity of immobilized *A. ferrooxidans* cells was observed (Long et al., 2004). In this work, a good effect of immobilization of *A. ferrooxidans* cells on the bioleaching of shale ores was achieved. On the other hand, the effect of the flow rate on the shale bioleaching was limited. As the flow rate increases, the mass transfer between the solid particles and the solution increases. In contrast, when the flow rate increases, the mean residence time of the solution in column decreased, resulting in relatively low bacteria cells in solution. The bioleaching of shale samples decreased.

CONCLUSIONS

The results of comparative tank and column tests using heterotrophic and autotrophic cultures indicate that bioleaching rates are similar in both cases. However, the bioleaching results of black shale samples indicated, that the column reactor with sawdust support for microbial cells immobilization, exhibited more suitable conditions for the metal leaching. The bacteria (*Acidithiobacillus ferrooxidans*) attached to the sawdust surface play a significant role in the bioleaching of shale samples. A higher copper recovery, for two investigated fillers, may be obtained for the shale sample mixed with wood shavings. The capillary model based on the hydraulic radius concept (Petersen et al., 2006) seems to adequate for the flow in porous media description.

ACKNOWLEDGMENTS

This work was carried out in the frame of Bioshale (European project contract NMP2-CT-2004 505710). The authors acknowledge the financial support given to this project by the European Commission under the Sixth Framework Programme for Research and Development. We also wish to thank our various partners on the project for their contributions to the work reported in this paper.

REFERENCES

- BARLETT W.R., 1992, *Simulation of ore heap leaching using deterministic models*, Hydrometallurgy, 29, 231-260.
- FOUCHER S., BATTAGLIA-BRUNET F., D'HUGUES, CLARENS M., GODON J.J., MORION D., 2003, *Evolution of the bacteria population during the batch bioleaching of a cobaltiferous pyrite in a suspended-solid bubble column and comparison with a mechanically agitated reactor*, Hydrometallurgy 71,5-12.
- GIRO A.E.M., GARCIA O., JR., ZAIAT M., 2006, *Immobilized cells of Acidithiobacillus ferrooxidans in PCV strands and sulfite removal in a pilot-scale bioreactor*, Biochemical Eng. J., 28, 201-207.
- LIN C.L., MILLER D.J., 2004, *Pore structure analysis of particle beds for fluid transport simulation during filtration*, Int.J.Miner. Process., 73,281-294.
- LIN C.L., MILLER D.J., GARCIA C., 2005, *Saturated flow characteristics in column leaching as described by LB simulation*, Minerals Engineering, 18, 1045-1051.
- LIZAMA M.H., 2004, *A kinetic description of percolation bioleaching*, Minerals Engineering, 17, 23-32.

- LIZAMA M.H., Harlamovs R.J., McKay J.D., Dai Z., 2005, *Heap leaching kinetics are proportional to the irrigation rate divided by heap height*, Minerals Engineering, 18, 623-630.
- LONG Z., Huang Y., Cai Z., Cong W., Ouyang F., 2004, *Kinetics of continuous ferrous ion oxidation by Acidithiobacillus ferrooxidans immobilized in poly(vinyl alcohol) cryogel carries*, Hydrometallurgy 74, 181-187.
- NEMEC D., LEVEC J., 2005, *Flow through packed bed reactors: 1. Simple-phase flow*, 2005, Chemical Eng. Sci., 60, 6947-6957.
- PETERSEN J., DIXON G.P., 2006, *Competitive bioleaching of pyrite and chalcopyrite*, Hydrometallurgy, 40-49.
- SANCHEZ-CHACON E.A., LAPIDUS T.G., 1997, *Model for heap leaching gold ores by cyanidation*, Hydrometallurgy, 44, 1-20.

Sadowski Z., Szubert A., *Porównanie bioługowania rudy łupkowej w kolumnie ze stacjonarnym wypełnieniem i mieszalnikowym bioreaktorze*, Physicochemical Problems of Mineral Processing, 41 (2007) 387-395 (w jęz. ang.).

W pracy przedstawiono wyniki doświadczeń przeprowadzonych na dwóch próbkach rudy łupkowej o zawartości miedzi 7,04 % (próbka A) i 2,32 % (próbka B). Obie próby materiału do badań zostały dostarczone przez Centrum Badawczo-Rozwojowe KGHM Cuprum. Przeprowadzone doświadczenia miały za cel porównanie procesu bioługowania próbek rudy łupkowej, który był prowadzony z bioreaktorze z mieszaniami i w kolumnie ze złożem stacjonarnym. W przypadku bioługowania w kolumnie użyto dodatkowo dwóch wypełniaczy, to jest plastikowych kulek i wiórów drewnianych. Bioługowanie prowadzono z wykorzystaniem bakterii heterotrofowych (*Streptomyces setoni* i mieszanka C) i autotrofowych (*Acidithiobacillus ferrooxidans*). Otrzymane wyniki sugerują, że kinetyka procesu bioługowania w bioreaktorze był lepsza od kinetyki procesu w kolumnie. Procesy, prowadzone w kolumnach z wypełnieniem, były korzystniejsze w porównaniu z procesami bez użycia wypełnienia. Z zastosowanych dwóch materiałów wypełniających, trociny okazały się być lepszym wypełniaczem. Może to być spowodowane bardziej porowatą strukturą materiału w kolumnie, o czym świadczy większa szybkość przepływu medium ługującego.

Marian BROŻEK*, Agnieszka SUROWIAK*

EFFECT OF PARTICLE SHAPE ON JIG SEPARATION EFFICIENCY

Received May 15, 2007; reviewed; accepted July 4, 2007

Settling velocity of particles, which is the main parameter of jig separation, is affected by physical (density) and the geometrical (size and shape) properties of particles. The authors worked out a calculation algorithm of particles falling velocity distribution for monosized spherical and irregular particles assuming that the density of particles, their size and shape constitute random variables of fixed distributions. The distributions of falling velocity of irregular particles of a narrow size fraction were calculated utilizing industrial experiments. The measurements were executed and the histograms of distributions of projection diameter, as well as volume and dynamic shape coefficient, were drawn. The separation accuracy was measured by the change of process imperfection of irregular particles in relation to spherical ones, resulting from the distribution of particles settling velocity.

Key words: spherical particles, irregular particles, settling velocity, imperfection, enrichment, jig, random variable distribution

INTRODUCTION

Enrichment in jigs occurs during vertical pulsating motion of the suspension containing particles. After some time of such motion, the particles are stratified into groups differing in physical (density) and geometrical (particle size and shape coefficient) properties. According to Mayer's potential theory (Mayer, 1964) the separation runs towards minimizing the potential energy of the system. If the material were separated into densimetric fractions and each densimetric fraction into size fraction and the size fractions arranged from the largest to the smallest, then the porosity of the layer after separation would be larger than before separation (Kuprin et al, 1983). Consequently, the potential energy of the system after separation would be larger than before separation. This is in contradiction with the principle of least action according to which the processes run towards the minimization of potential energy.

* AGH University of Science and Technology, Department of Mineral Processing and Environment Protection, Al. Mickiewicza 30, 30-065 Kraków, Poland, brozek@agh.edu.pl, asur@agh.edu.pl.

The decrease of porosity will occur when the voids between larger particles are replaced by smaller ones. It will happen in the situation when smaller particles of higher density will be transferred to the higher sub-layer of larger particles of lower density. Such a stratification means that in consecutive layers, for ideal separation, there are particles of the same value of terminal settling velocity. Thus, it can be stated that terminal settling velocity is this property (separation argument) according to which, for ideal separation, the stratification of the material into respective subsets of the same value of separation argument occurs.

In industrial separation processes, as a result of particles dispersion resulting from interactions between particles, the fouling of respective subsets with particles of neighboring layers occurs, and these are characterized by different, for a given layer, values of settling velocity. This phenomenon is characterized by the partition curve and its mathematical representation, i.e. the partition function while numerically it is estimated by the so-called probable error and imperfection parameters. These indicators are a measure of separation efficiency which determines the quality of separation machinery. Respectively, for every separator the representative measure of separation efficiency should be applied, corresponding to the real separation argument in the separator. Since the settling velocity of an irregular particle depends on the particle shape, this paper presents the method of evaluation of the effect of particle shape on separation efficiency. To achieve this, the authors calculated the distributions of settling velocities of spherical and irregular particles according to the empirical data for a narrow 8-10 [mm] size fraction.

TERMINAL SETTLING VELOCITY OF IRREGULAR PARTICLES

Terminal settling velocity of a particle is the value of velocity which is obtained by a particle which moves uniformly in the medium. It is calculated from the particle motion equation. The following forces act on irregular particles moving in water under the force of gravity for Reynolds numbers greater than $5 \cdot 10^2$:

$$1) \text{ gravity force: } Q = \rho V g \quad (1)$$

$$2) \text{ buoyancy force: } F_w = \rho_o V g \quad (2)$$

3) medium dynamic resistance force, determined by Newton's formula:

$$P = -\psi_z \frac{1}{2} \rho_o v_t^2 S, \quad (3)$$

where: V - particle volume, v_t - momentary velocity of particle motion, ψ_z - drag coefficient for a particle, S - particle projection area on the plane perpendicular to the motion direction, ρ - particle density, ρ_o - medium density, g - acceleration due to

gravity, $Re = \frac{\rho_0 v_t r}{\eta}$ – Reynolds number, r – particle radius, η – dynamic viscosity coefficient of the medium. The expression $\frac{1}{2} \rho_0 v^2$ represents the liquid hydrodynamic pressure. Respectively, the equation of particle motion in a vertical direction will be as follows:

$$\rho V \frac{dv}{dt} = (\rho - \rho_0) V g - \psi_z \frac{1}{2} \rho_0 v_t^2 S \quad (4)$$

Equation (4), after transformation, takes the form:

$$\frac{dv}{dt} = a - b v_t^2 \quad (5)$$

where $a = \frac{\rho - \rho_0}{\rho} g$, $b = \frac{\psi_z \rho_0 S}{2 \rho V}$.

Formula (5) is known as Riccati's equation (Leja, 1971). This equation can be solved by quadratures and its solution is as follows (Ponomariev, 1973):

$$v_t = \sqrt{\frac{a}{b}} \operatorname{tgh}(\sqrt{ab} t) = \sqrt{\frac{2(\rho - \rho_0) V g}{\psi_z \rho_0 S}} \operatorname{tgh}\left(\sqrt{\frac{\psi_z \rho_0 (\rho - \rho_0) g S}{2 \rho^2 V}} t\right) \quad (6)$$

The following limit:

$$\lim_{t \rightarrow \infty} v_t = \sqrt{\frac{2(\rho - \rho_0) V g}{\psi_z \rho_0 S}} = v \quad (7)$$

presents the general formula for the terminal settling velocity of a particle. Its detailed form, with respect to irregular particles, must consider particle shape, characterized by shape coefficient and the value of drag coefficient. In Eq. 7, the particle drag coefficient ψ_z , particle volume V and particle projection area S occur. The following measures of particle size are used to characterize these values:

- equivalent diameter d_z , which is the diameter of a sphere of the volume equal to the particle volume V according to the dependence:

$$d_z = \sqrt[3]{\frac{6V}{\pi}} \quad (8)$$

- projection diameter d_p , which is equal to the diameter of a circle of the area equal to the particle projection area S , i.e.

$$d_p = \sqrt{\frac{4S}{\pi}} \quad (9)$$

The particle drag coefficient is connected with the sphere drag coefficient in the Newtonian range of Reynolds number by the following dependence (Thomson and Clark, 1991, Ganser, 1993):

$$\psi_z = k_2 \psi_k \quad (10)$$

where: k_2 is the dynamic or Newtonian coefficient of particle shape.

For the sphere, the drag coefficient is $\psi_k = 0.46$ (Abraham, 1970, Concha and Almendra, 1979).

Thus:

$$\psi_z = 0.46 k_2 . \quad (11)$$

Therefore, the particle drag coefficient depends on the particle shape and more irregular particles provide higher resistance forces. Ganser (1993) gave the following statistical dependence of dynamic shape coefficient upon the particle sphericity coefficient ϕ :

$$k_2 = 10^{1.148 (-\log \phi)^{0.5743}} . \quad (12)$$

Equation 12, according to Ganser, can be applied to particles of any shape while the sphericity coefficient as the particle measure is defined as follows (Wadell, 1933, according to Heiss and Coull, 1952):

$$\phi = \left(\frac{d_z^2}{d_k^2} \right) = \left(\frac{A_s}{A} \right)_v \quad (13)$$

where: d_k – diameter of a sphere of the area equal to the particle area, A – particle area, A_s – area of a sphere of the volume equal to the particle volume.

Due to the difficulties in measuring the particle area, Wadell proposed an approximation of the sphericity coefficient by the circularity coefficient, calculated from measurements on the plane and defined as follows:

$$\phi \cong k_c = \left(\frac{C}{C_z} \right)_s \quad (14)$$

where: C_z – perimeter of the particle projection area, C – perimeter of the circle of the area equal to the area of the particle projection area.

If appropriate expressions of formulas in Eqs 11, 8, and 9 are substituted for ψ_z , V and S into formula in Eq.7, the following expression for irregular particle settling velocity is obtained:

$$v = 5.33\sqrt{x} \frac{\sqrt{d_z^3}}{d_p \sqrt{k_2}} \quad (15)$$

where : $x = \frac{\rho - \rho_0}{\rho_0}$ – reduced particle density.

For the spherical particle $d_z = d_p = d$ and $k_2 = 1$, thus the settling velocity is expressed by the formula:

$$v = 5.33\sqrt{x} \sqrt{d} \quad (16)$$

Heywood (1937, according to Heiss and Coull, 1952) proposed to determine the particle volume by the volume shape coefficient k_{1H} , according to the formula:

$$V = k_{1H} d_p^3 \quad (17)$$

In this paper the volume shape coefficient k_1 was determined from the analogical expression:

$$V = k_1 \frac{\pi d_p^3}{6} \quad (18)$$

After substituting ψ_z , S and V with the expression from Eq. 11, 9, and 18 for irregular particle settling velocity into Eq.7, the following formula is obtained:

$$v = 5.33\sqrt{x} \sqrt{d_p} \sqrt{\left(\frac{k_1}{k_2}\right)} \quad (19)$$

Equations 16 and 19 will be applied further in this paper to determine the distributions of settling velocities of spherical and irregular particles.

DISTRIBUTION OF SETTLING VELOCITY FOR A SAMPLE OF MONOSIZED SPHERICAL PARTICLES

Let R , X , D_p , K_1 , and K_2 determine random variables of particle density, reduced density, particle projection diameter, particle volume shape coefficient and particle dynamic shape coefficient, respectively. For spherical particles $k_1 = k_2 = 1$, $d_p = d_o$ where d_o – size of feed particles. In this situation particle settling velocity v_{ms} is expressed by the formula:

$$v_{ms} = 5.33\sqrt{x}\sqrt{d_o} \quad (20)$$

Reduced density x is connected with particle density by the dependence:

$$x = \frac{\rho - \rho_o}{\rho_o} \quad (21)$$

from which:

$$\rho = \rho_o x + \rho_o = \rho(x) \quad (22)$$

Let the random variable R have the distribution determined by the probability density function of density $f_\rho(\rho)$. Then, the random variable X has the distribution of density (Gerstenkorn and Śródka, 1972):

$$f(x) = f_\rho[\rho(x)] \left| \frac{d\rho(x)}{dx} \right| \quad (23a)$$

$$f(x) = \rho_o f_\rho(\rho = \rho_o x + \rho_o) \quad (23b)$$

After introducing a new random variable:

$$Y_1 = X^{1/2} \quad (24)$$

from which $x = y_1^2 = x(y_1)$.

The settling velocity is:

$$v_m = 5.33\sqrt{d_o} y_1 \quad (25)$$

The distribution of the random variable Y_1 , analogically as above, is as follows:

$$f_1(y_1) = f[x(y_1)] \left| \frac{dx(y_1)}{dy_1} \right| \quad (26a)$$

$$f_1(y_1) = 2y_1 f(x = y_1^2) \quad (26b)$$

The following random variable $Y_2 = 5.33 Y_1$ ($y_1 = \frac{y_2}{5.33} = y_1(y_2)$) has the probability density function:

$$f_2(y_2) = f_1[y_1(y_2)] \left| \frac{dy_1(y_2)}{dy_2} \right| \quad (27a)$$

$$f_2(y_2) = f_1\left(y_1 = \frac{y_2}{5.33}\right) \cdot \frac{1}{5.33} \quad (27b)$$

After the transformations the settling velocity as a random variable is expressed by the following formula:

$$V_{ms} = \sqrt{d_o} Y_2 \quad (28)$$

Consequently, the settling velocity of the set of monosized spherical particles has the frequency function:

$$h(v_{ms}) = f_2[y_2(v_{ms})] \left| \frac{dy_2(v_{ms})}{dv_{ms}} \right| \quad (29a)$$

$$h(v_{ms}) = f_2\left(y_2 = \frac{v_{ms}}{\sqrt{d_o}}\right) \frac{1}{\sqrt{d_o}} \quad (29b)$$

DISTRIBUTION OF SETTLING VELOCITY FOR MONOSIZED IRREGULAR PARTICLES

It was assumed that the sample of particles have the same value of the projection diameter $d_p = d_o$ while the particle shape coefficients constitute the random variables K_1 and K_2 of the frequency functions $w_1(k_1)$ and $w_2(k_2)$, respectively. Then, the frequency function of the random variable $Z = \frac{K_1}{K_2}$ is expressed by the following formula (Gerstenkorn and Śródka, 1972):

$$p_1(z) = \int k_2 w_2(k_2) w_1(zk_2) dk_2 \quad (30)$$

The following random variable $A = Z^{1/2}$ ($z = a^2 = z(a)$) has the frequency function determined by the formula:

$$p_2(a) = p_1[z(a)] \left| \frac{dz(a)}{da} \right| \quad (31a)$$

$$p_2(a) = 2ap_1(z = a^2) \quad (31b)$$

The random variable of settling velocity of monosized irregular particles, after the above transformations, is :

$$V_{mn} = V_{ms} \cdot A \quad (32)$$

As it can be seen from Eq. 32, the random variable of settling velocity of irregular particles is the product of the random variable of settling velocity of monosized spherical particles and the random variable being the function of particle shape coefficients. Consequently, the function of distribution density of settling velocity of monosized irregular particles is (Gerstenkorn and Śródka, 1972):

$$h(v_{mn}) = \int_{v_{s \min}}^{v_{s \max}} h(v_{ms}) p_2 \left(a = \frac{v_{mn}}{v_{ms}} \right) \frac{1}{v_{ms}} dv_{ms} \quad (33)$$

EXPERIMENTAL

A narrow 8-10 mm size fraction was fed into the Allmineral jig. In this sample the densimetric analyses were performed. Moreover, by means of the image analysis, the distribution of projection diameter was determined as well as the distributions of volume and dynamic shape coefficients. In order to calculate the dynamic shape coefficient, the photographs of particles were taken with a digital camera in the most stable position. Next, using the image analysis software, the projection areas and perimeters of individual particles were calculated. Applying Eq. 14, the sphericity coefficients ϕ and projection diameters d_p were fixed, according to Eq. 9. The dynamic shape coefficient k_2 was calculated using dependence shown in Fig. 12. The volume shape coefficient k_1 was determined according to the volumetric method, consisting in the measurement of density of individual particles with a pycnometer and in calculating their volumes. The shape coefficient k_l was calculated using Eq. 18.

MEASUREMENT RESULTS AND DISCUSSION

DISTRIBUTION OF PARTICLE DENSITIES

The cumulative distribution function of particle density, according to the dispersive particle model (Brożek, 1995), is expressed by a two-parameter function of gamma distributions family. As it will be shown further, that it is the Weibull distribution which cumulative distribution function and frequency function are as follows:

$$F_\rho(\rho) = 100 \left\{ 1 - \exp \left[- \left(\frac{\rho}{\rho_c} \right)^{k_n} \right] \right\} \quad (34)$$

$$f_\rho(\rho) = \frac{100k}{\rho_c^{k_n}} \rho^{k_n-1} \exp \left[- \left(\frac{\rho}{\rho_c} \right)^{k_n} \right] \quad (35)$$

where: ρ_c – characteristic density ($F_p(\rho = \rho_c) = 63.21\%$), k_n – non-homogeneity coefficient.

On the basis of empirical data on the densimetric analysis, the coordinates of the cumulative distribution function of density were calculated and, next, Weibull's distribution was fitted to the empirical data. Distribution parameters ρ_c and k_n were obtained from this fitting. Figure 1 presents the model dependence with marked empirical values. The compatibility of the model with the experiment was estimated, calculating the index of curvilinear correlation. Its high values ($R > 0.99$) prove a good compatibility of the model distribution function with the empirical data.

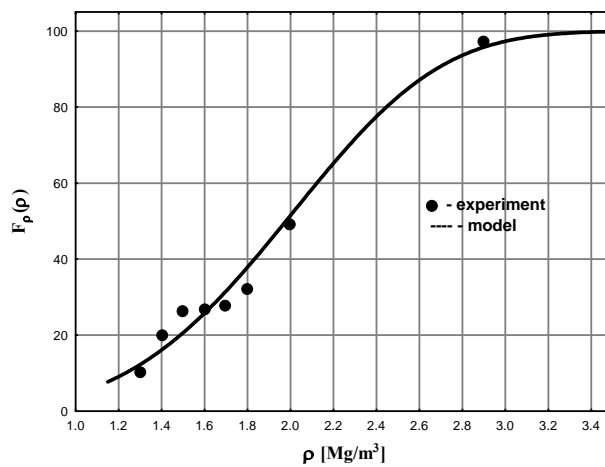


Fig. 1. Distribution of particle densities for size fraction 8 – 10 [mm], $\rho_c = 2170$ [kg/m³]; $k_n = 3.97$

DISTRIBUTION OF PROJECTION DIAMETER

Figure 2 presents the histogram of distribution of projection diameter.

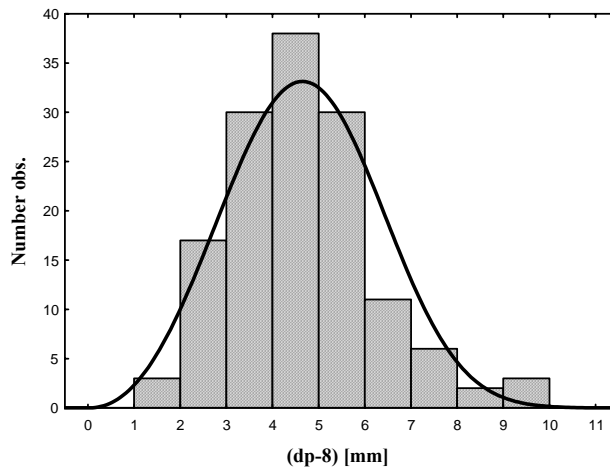


Fig. 2. Histogram of distribution of projection diameter of 8 -11 [mm] size fraction: $d_{cp} = 13.2$ [mm]; $k_p = 3.17$; $b_p = 8$ [mm]; $\bar{d}_p = 12.8$ [mm]

By means of the Statistica program the frequency function of projection diameter was fitted to the histogram. The best fitting was obtained for Weibull's distribution in the form:

$$g_p(d_p) = \frac{100k_p}{d_{cp}^{k_p}} d_p^{k_p-1} \exp \left[- \left(\frac{d_p - b_p}{d_{cp} - b_p} \right)^{k_p} \right] \quad (36)$$

where: d_c – characteristic value of projection diameter, k_p – non-homogeneity coefficient, b_p – value of shift of random variable.

For the description of Fig. 2 the parameters of Weibull's distribution together with the value of shift of random variable b_p are given. The average value of projection diameter is calculated from the following formula (Gerstenkorn and Śródka, 1972):

$$\bar{d}_p = d_{op} \Gamma \left(\frac{1}{k_p} + 1 \right) + b_p \quad (37)$$

The average value $\bar{d}_p = 12.8$ mm was assumed as the size of spherical particle in calculating the distribution of settling velocity of spherical particles.

DISTRIBUTION OF SHAPE COEFFICIENTS

Figures 3 and 4 show the histograms of distributions of random variables K_1 and K_2 .

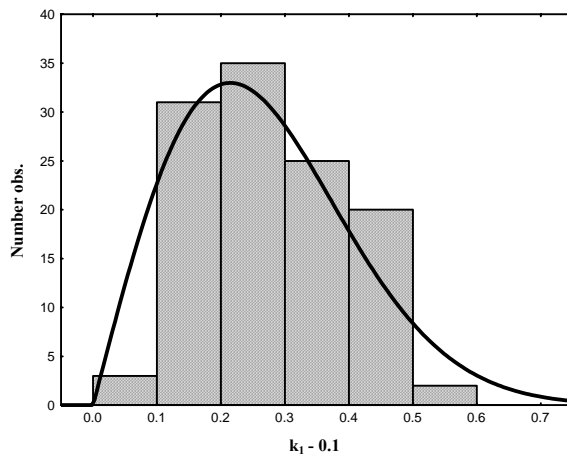


Fig. 3. Histogram of distribution of volume shape coefficient $k_1, \lambda_1 = 11$

The investigations of other authors indicate that the distributions of shape coefficients are of the gamma type (Hodenberg, 1998; Stark and Muller, 2005). Because of this, Rayleigh's and Weibull's distributions were fitted to these histograms. The statistical evaluation of compatibility of model distributions with

empirical data was the same for both distribution types and, consequently, Rayleigh's distributions of shape coefficients were accepted and used in further considerations. Their general equations are as follows:

$$w_1(k_1) = 2\lambda_1 k_1 \exp(-\lambda_1 k_1^2) \tag{38}$$

$$w_2(k_2) = 2\lambda_2 k_2 \exp(-\lambda_2 k_2^2) \tag{39}$$

where λ_1 and λ_2 are distribution parameters.

The values $\lambda_1 = 11$ and $\lambda_2 = 0.015$ for distribution parameters were obtained from the fitting to empirical distributions with the Statistica program.

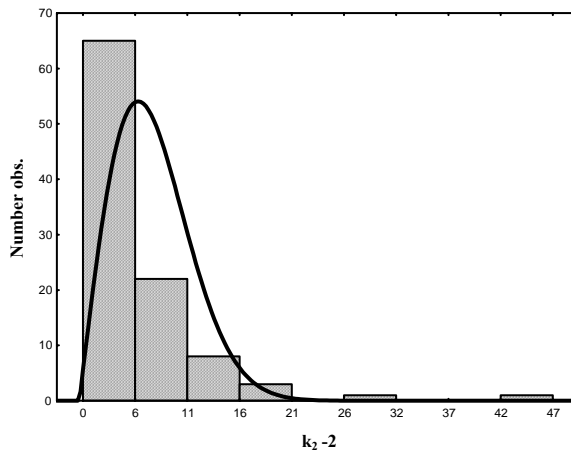


Fig. 4. Histogram of distribution of dynamic shape coefficient $k_2, \lambda_2 = 0.015$

DISTRIBUTION OF SETTLING VELOCITY OF SPHERICAL PARTICLES

Applying the Eq. 29 and the algorithm of chapter 3, the frequency function and the cumulative distribution function of settling velocity of spherical particles were calculated.

$$h(v_{ms}) = \frac{200k_n}{(v_{msc}^2 + 28.41d_o)^{k_n}} v_{ms} (v_{ms}^2 + 28.41d_o)^{k_n - 1} \times \exp\left[-\left(\frac{v_{ms}^2 + 28.41d_o}{v_{msc}^2 + 28.41d_o}\right)^{k_n}\right] \tag{40}$$

$$H(v_{ms}) = 100 \left\{ 1 - \exp\left[-\left(\frac{v_{ms}^2 + 28.41d_o}{v_{msc}^2 + 28.41d_o}\right)^{k_n}\right] \right\} \tag{41}$$

where: $d_o = \bar{d}_p = 12.8$ mm – diameter of sample particles, while v_{msc} is:

$$v_{msc} = \sqrt{d_o} y_{2c} = 5.33 \sqrt{d_o \frac{\rho_c - \rho_o}{\rho_o}} \quad (42)$$

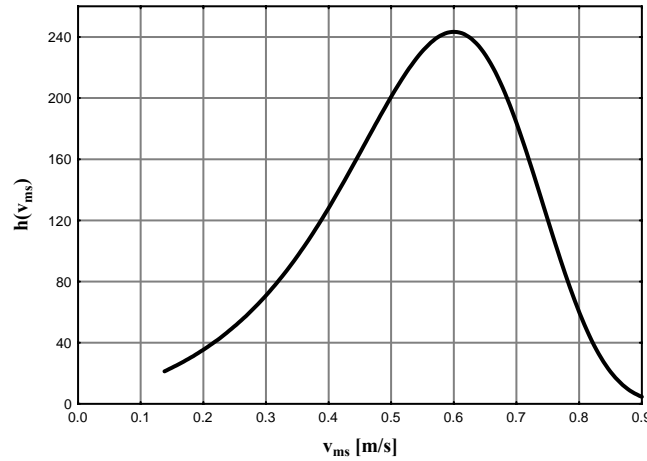


Fig. 5. Frequency function of particle settling velocity for size fraction 8 -10 [mm]

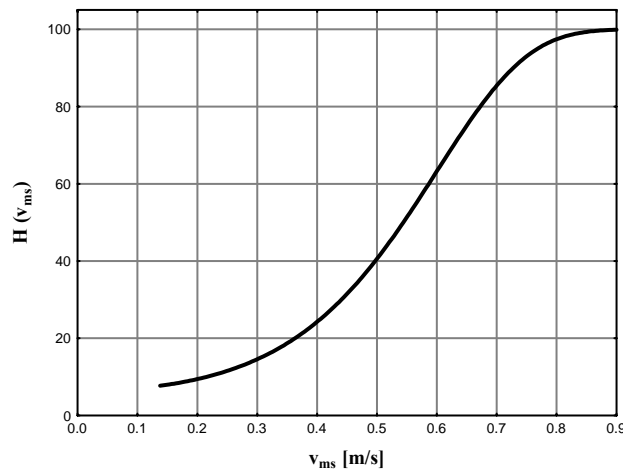


Fig. 6. Cumulative distribution function of settling velocity of particles for size fraction 8 -10 mm,
 $v_{msc} = 0.599$ m/s, $k_n = 3.97$

As it can be seen from Eq. 41 – 42 that the distribution of settling velocity in this case is expressed by the parameters of distribution of particles density and their diameter. Analogically as for the density distribution, this is also Weibull's distribution. The parameters of settling velocity distribution are constituted by non-

homogeneity coefficient k_n and characteristic velocity v_{msc} , calculated according to Eq. 42. The density ρ_o of liquid, occurring in this formula, which is transferred to the jig chamber, is higher than water density and equals $\rho_o=1093 \text{ kg/m}^3$ because it is recirculated from Dorr's settling tank. Figures 5 and 6 present the frequency and cumulative distribution function of settling velocity, respectively, in the sample of spherical particles.

DISTRIBUTION OF SETTLING VELOCITY OF IRREGULAR PARTICLES

According to Eq. (33) and the algorithm of chapter 4 the frequency function of settling velocity of irregular particles is expressed by the following formula:

$$h(v_{mn}) = 1941 \int_0^{0.88} (v_{ms}^2 + 0.36)^{2.97} \exp\left[-\left(\frac{v_{ms}^2 + 0.36}{0.72}\right)^{3.97}\right] \frac{v_{mn}^3 \cdot v_{ms}^5}{(0.015v_{ms}^4 + 11v_{mn}^4)^2} dv_{ms} \quad (43)$$

As it results from Eq. 43 that the distribution of settling velocity is openly dependent on the distribution of particle shape coefficients. Because of complexity of that integral, integration was performed by the numerical method. Figures 7 and 8 present, respectively, the frequency and cumulative distribution function of settling velocity of irregular particles. The comparison of both graphs indicate that, after considering the distribution of shape coefficients, the shape of the frequency function changes (distribution asymmetry changes from negative to positive), the values of the most probable velocity decreases from 0.6 m/s to 0.084 m/s and also the maximum value of settling velocity decreases from 0.88 m/s to 0.4 m/s. Consequently, the flat particles of higher density than the analogical particles of lower density and lower asymmetry will be grouped in the light product. This conclusion is in agreement with the observed experimental facts (Ferrara et al., 2000; Ociepa and Mączka, 2000).

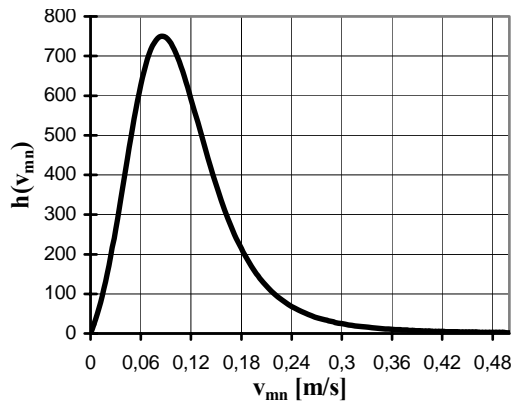


Fig. 7. Frequency function of settling velocity of irregular particles

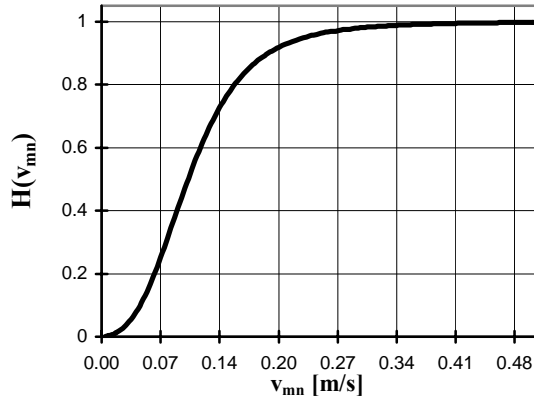


Fig.8. Cumulative distribution function of settling velocity of irregular particles

EFFECT OF PARTICLE SHAPE UPON SEPARATION EFFICIENCY

The indicators based on the partition curves, i.e. probable error and imperfection, are the most popular and most often applied indicators of evaluation of separation efficiency. Belugu (1959, according to Samylin et al., 1976) gave the following empirical dependence to evaluate the effect of distribution of particle density in the feed:

$$I = I_o + 0.021tg\alpha \quad (44)$$

where: I_o – value of imperfection, characteristic for a given jig, $tg\alpha = k_I \frac{\Delta\gamma(\Delta\rho)}{\Delta\rho}$, k_I

– coefficient of scale, $\Delta\rho = \pm 100 \text{ kg/m}^3$ – range of density around partition density, $\Delta\gamma(\Delta\rho)$ – content of particles in the feed of the density range ($\rho_r - \Delta\rho, \rho_r + \Delta\rho$) in %. To estimate the effect of shape coefficients distribution upon separation efficiency the authors used the dependence analogical to dependence in Eq. 44 in relation to settling velocity as the argument of separation:

$$\Delta I_{mn} = I_{mn} - I_o = a tg\alpha_{mn} \quad (45)$$

where: ΔI_{mn} – change of imperfection, I_o and a – constants, $tg\alpha_{mn} = \frac{\Delta\gamma_{mn}(\Delta v)}{\Delta v}$,

$\Delta\gamma_{mn}(\Delta v)$ – content of particles in the feed of the settling velocity range ($v_r - \Delta v, v_r + \Delta v$), $\Delta v = \pm 0.04 \text{ m/s}$ – range of settling velocity around the partition velocity.

The width of Δv range was selected by analogy to the width of density range $\Delta\rho = \pm 100 \text{ kg/m}^3 \cong \frac{1}{8}(2000 - 1250) \text{ kg/m}^3$ which Belugu proposed in Eq. 44. According to Fig. 8 $\Delta v = \frac{1}{8} \cdot 0.32 \text{ mm}$.

Analogically to Eq. 45, for the separation of spherical particles the equation can be written as:

$$\Delta I_{ms} = I_{ms} - I_o = a \operatorname{tg} \alpha_{ms} \quad (46)$$

And the values of this equation have a similar interpretation as in Eq. 45 only in relation to spherical particles. Dividing by sides Eq. 45 by Eq. 46 we obtain:

$$\frac{\Delta I_{mn}}{\Delta I_{ms}} = \frac{\operatorname{tg} \alpha_{mn}}{\operatorname{tg} \alpha_{ms}} = \frac{\Delta \gamma_{mn}(\Delta v)}{\Delta \gamma_{ms}(\Delta v)} \quad (47)$$

From Eq. 47, having the distributions of settling velocities of irregular and spherical particles in the feed, it is possible to calculate the relation of process imperfection changes during the separation of irregular and spherical particles in the same conditions. For the separation velocity determined from the equation of partition curve for waste of 8-10 mm size fraction the following value was obtained (Surowiak, 2007): $v_r = 0.159 \text{ m/s}$. Respectively, from Fig. 8. $H(v_{mn} = 0.159) \cong 82\%$ and $\Delta \gamma_{mn}(\Delta v) \cong 28\%$. Next, for spherical particles, according to Fig. 6. for $H(v_{ms}) = 82\%$, velocity $v_{ms} = 0.68 \text{ m/s}$. The content of spherical particles of velocity range $(0.68 - \Delta v; 0.68 + \Delta v)$ in the feed is $\Delta \gamma_{ms}(\Delta v) \cong 16\%$. Respectively, from Eq. 47:

$$\frac{\Delta I_{mn}}{\Delta I_{ms}} = \frac{28}{16} = 1.75 \quad (48)$$

According to the obtained results, it can be stated that in the case of the tested coal sample the irregular shape of particles results in about 70% larger change of process imperfection on average than in the case of separation of a sample of monosized spherical particles under the same conditions, which is connected with the decrease of separation efficiency of irregular particles. This increase results from the decrease of difference of settling velocity of irregular particles in relation to the difference of settling velocity of spherical particles.

CONCLUSIONS

- The frequency function of settling velocity in the sample of monosized spherical particles is Weibull's distribution of negative asymmetry. On the other hand, however, in the case of monosized irregular particles (particles of the same projection diameter and distribution of shape coefficients), the asymmetry is positive. The irregular particles shape decreases the value of settling velocity. This increases the probable error as a result of the decrease of the non-homogeneity rate of velocity distribution in the sample.
- The irregularity of particle influences the separation efficiency measured by the imperfection change. The difference in particle settling velocity decreases with the growth of the particle irregularity rate (increase of dynamic shape coefficient and decrease of volume coefficient). This narrows the range of variation of settling velocity of irregular particles in relation to the analogical range for spherical particles, causing the increase of particles content in the range of settling velocity around partition velocity and, automatically, also the increase of imperfection.

ACKNOWLEDGEMENTS

This work was supported by a grant of the National Research Committee No. 4 T12A 006 29.

REFERENCES

- ABRAHAM F.F., (1970), *Functional dependence of drag coefficient of a sphere on Reynolds number*. Phys. Fluids, 13, 2194-2195.
- BELUGU P., DANNIEL G., POZETTO L., (1959), *Upgrading of fine coal in jigs*. Proc. III ICPC, pp. 19-34, (in Russian).
- BROŻEK M., (1995), *The distribution of selected physical properties in the crushed material*. Arch. Min. Sci., 40, 83-100.
- CONCHA F., ALMENDRA E.R., (1979), *Settling velocities of particulate systems, I. Settling velocities of individual spherical particles*. Int. J. Mineral Processing, 5, 349-367.
- FERRARA G., BEVILACQUA P., LORENZI L.D., ZANIN M., (2000), *Influence of particle shape on dynamic DMS processes*. Proc. XXI IMPC, Rome, P.A7, pp. 95-104.
- GANSER G.H., (1993), *A rational approach to drag prediction of spherical and non-spherical particles*. Powder Technology, 77, 143-152.
- GERSTENKORN T., ŚRÓDKA T. (1972), *Kombinatoryka i rachunek prawdopodobieństwa*, PWN, Warszawa.
- HEISS J.F., COULL J., (1952), *On the settling velocity of non-isometric particles in a viscous medium*. Chemical Engineering Progress, 48, 133-140.
- HEYWOOD H., (1937), *Chemistry and Industry*, 56, Part.2, 149.
- HODENBERG M., (1998), *Gravimetric and optical particle analysis of mixed particle samples*. Aufbereitungs Technik, 39, 461-466.
- KUPRIN A.I., KLESZNIN A.A., FEDORENKO G.I., (1983), *Effect of porosity on efficiency of jigging*. Izv. VUZ Gornyj Zurnal, no 4, 129-132, (in Russian).
- LEJA F., (1971), *Rachunek różniczkowy i całkowy*. PWN, Warszawa.
- MAYER F.W., (1964), *Fundamentals of a potential theory of the jigging process*. Proc. VII IMPC, New York, pp. 75-86.

- OCIEPA Z., MAĆZKA W., (2000), *Badanie wpływu kształtu ziarn na wyniki rozdziału w procesach wzbogacania grawitacyjnego*. Gospodarka Surowcami Mineralnymi, 16, 59-75.
- PONOMARIEV K.K., (1973), Group of differential equations. Izd. Vyshejszaja Shkola, Minsk, (in Russian).
- SAMYLIN N.A., ZOŁOTKO A.A., POZINOK V.V., (1976), *Otsadka*. Izd. Nedra, Moskva.
- STARK U., MULLER A., (2005), *Effective methods for measurement of particle size and shape*. Aufbereitungs Technik, 45, 6-16.
- SUROWIAK A., (2007.), *Wpływ rozkładu właściwości fizycznych i geometrycznych ziaren na dokładność rozdziału w osadzarce na przykładzie węgla*. Ph.D. Thesis, Biblioteka Główna AGH, Kraków, Poland
- THOMPSON T.L., CLARK N.N., (1991), *A holistic approach to particle drag prediction*. Powder Technology, 67, 57-66.
- WADELL H., (1933), *Volume, Shape and Roundness of Rock Particles*, Journal of Geology, 40.

Brożek M., Surowiak A., *Wpływ kształtu ziaren na dokładność rozdziału w osadzarce*, Physicochemical Problems of Mineral Processing, 41 (2007) 297-413 (w jęz. ang.).

Na prędkość opadania ziaren, będącą argumentem rozdziału w osadzarce, wpływają właściwości fizyczne (gęstość) oraz geometryczne (wielkość i kształt) ziaren. W artykule opracowano algorytm wyliczania rozkładu prędkości opadania ziaren w monodispersyjnej próbce ziaren sferycznych i nieregularnych przy założeniu, że gęstość ziaren, ich wielkość i kształt stanowią zmienne losowe o określonych rozkładach. W oparciu o eksperyment przemysłowy wyliczono rozkłady prędkości opadania ziaren nieregularnych w wąskiej klasie ziarnowej. Wykonano pomiary i wykreślono histogramy rozkładów średnicy projekcyjnej, objętościowego i dynamicznego współczynnika kształtu. Dokładność rozdziału mierzono zmianą imperfekcji procesowej ziaren nieregularnych w stosunku do ziaren sferycznych wynikającą z rozkładu prędkości opadania ziaren.

Our books are available in *Tech* bookstore
plac Grunwaldzki 13
50-377 Wrocław, D-1 PWr, tel. (071) 320 32 52
Orders can also be sent by post

ISSN 0137-1282
Physicochemical Problems of Mineral Processing, 41 (2007)